BOEING

Solar Power Satellite System Definition Study

Volume II
Phase I, Final Report
Systems Analyses and Tradeoffs
D180-25037-2

NASA CR-
160371

BOEING
GENERAL ELECTRIC
GRUMMAN
Arthur D Little, Inc
TRW

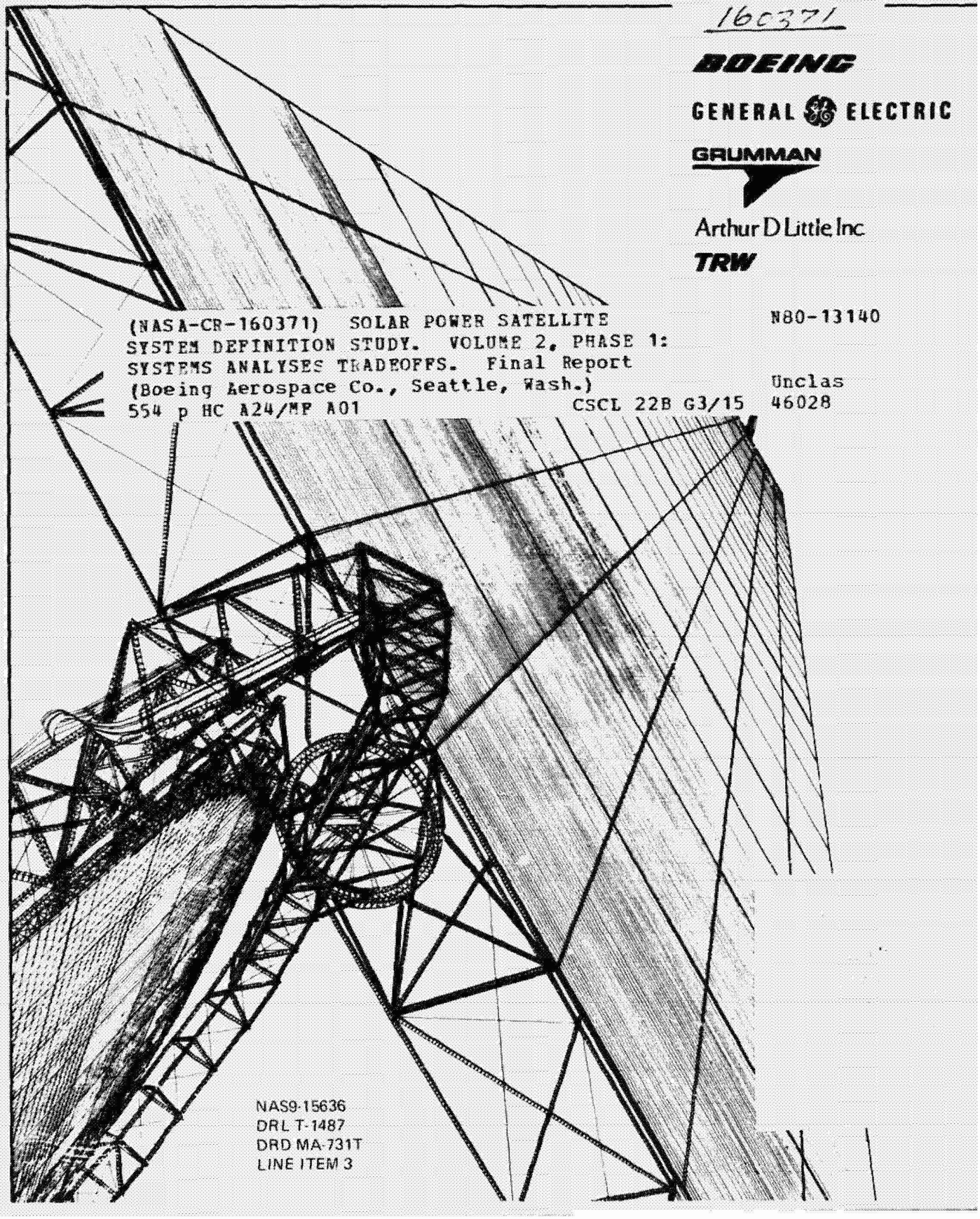

NAS9-15636
DRL T-1487
DRD MA-731T
LINE ITEM 3

Solar Power Satellite
System Definition Study
Conducted for the NASA Johnson Space Center
Under Contract NAS9-15636

Volume II
PHASE I, FINAL REPORT
Phase I Systems Analyses and Tradeoffs
D180-25037-2

March 1, 1979

Approved By: G R Woodcock

G. R. Woodcock
Study Manager

Boeing Aerospace Company
Ballistic Missiles and Space Division
P.O. Box 3999
Seattle, Washington 98124

FOREWORD

The SPS System Definition Study was initiated in June of 1978. Phase I of this effort was completed in December of 1978 and is herewith reported. This study is a follow-on effort to an earlier study of the same title completed in March of 1978. These studies are a part of an overall SPS evaluation effort sponsored by the U. S. Department of Energy (DOE) and the National Aeronautics and Space Administration.

This study is being managed by the Lyndon B. Johnson Space Center. The Contracting Officer is Thomas Mancuso. The Contracting Officer's representative and Study Technical Manager is Harold Benson. The study is being conducted by The Boeing Company with Arthur D. Little, General Electric, Grumman, and TRW as subcontractors. The study manager for Boeing is Gordon Woodcock. Subcontractor managers are Dr. Philip Chapman (ADL), Roman Andryczyk (GE), Ronald McCaffrey (Grumman), and Ronal Crisman (TRW).

This report includes a total of seven volumes:

I - Executive Summary
II - Phase I Systems Analyses and Tradeoffs
III - Reference System Description
IV - Silicon Solar Cell Annealing Test
V - Phase I Final Briefing Executive Summary
VI - Phase I Final Briefing: SPS and Rectenna Systems Analyses
VII - Phase I Final Briefing: Space Construction and Transportation

In addition, general Electric will supply a supplemental briefing on rectenna construction.

Key team members that contributed in the various disciplines were the following:

Subject	JSC-Management Team	Contractor Team
Structures	Bob Reed	Rich Reinert (Boeing) M. Romanelli (Grumman)
Power Distribution	R. Kennedy; M.E. Woods	J. Gewin
Power Transmission	R.H. Dietz	Erv Nalos
RF-DC Conversion	L. Leopold	E. Nalos
Phase Control	J. Seyl	W. Lund
Fiber Optic Phase Distribution	J. Seyl	G.E. Miller
Solid State Design	L. Leopold	G.W. Fitzsimmons B.R. Sperber
Array Analysis	Dr. D. Arndt	S. Rathjen
Information & Communications	R.H. Dietz, J. Kelley	Tom Walter (TRW)
Space Construction Operations	L. Jenkins	K. Miller (Boeing) R. McCaffrey (Grumman)
Space Transportation	H. Davis E. Crum	Eldon Davis
Ground Receiving Station		R. Andryczyk (GE)
Siting	H. Roberts	D. Gregory (Boeing)
Power Collection	R.H. Dietz	P. Foldes (GE)
Grid Interface	L. Monford	B. Kaupang (GE)
Constuction	H. Roberts	J. Chestik (GE)
Mission Ops & Control	B. Wolfert	K. Miller (Boeing) R. Crisman (TRW)
Industrial Infrastructure	J. Poradek	P. Chapman (A.D. Little)

CONTENTS

1.0 INTRODUCTION AND BACKGROUND

1.0.1 HISTORY

Solar power has long been recognized as an ideal source of energy for mankind. It is naturally available and plentiful, does not disturb the environment, e.g., by creation of wastes, and is itself free.

About ten years ago, a way of utilizing solar energy to generate electricity on a 24-hour continuous basis was proposed by Peter Glaser of A. D. Little. His proposal was to place the solar collectors in space, where they can collect sunlight continuously, can readily be aimed at the sun, and where very large collector areas can be obtained with relatively little investment in material resources. Energy collected by these solar power satellites (SPS's) would be transmitted to Earth by electromagnetic means. The original Glaser proposal, and most of the subsequent studies, have assumed the use of radio frequency systems in the microwave frequency range. Recently, the possibility of laser beaming has also been recognized.

The solar power satellite principle is illustrated in Figure 1.0-1. In a geosationary orbit 36,000 km above the Earth's equator, each SPS would be illuminated by sunlight over 99% of the time and be in continuous line-of-sight contact with its ground receiving station. Electrical power produced on the satellite by photovoltaic or heat engine conversion of the sunlight would be converted to electromagnetic energy at high efficiency, and formed into a narrow beam precisely aimed at the SPS ground stations. The ground station receiving antennas would reconvert the energy into electricity for distribution. Solar power satellites are intended to serve as producers of baseload electricity for utility service. SPS's are seen not as a substitute for other solar energy options, but as a complement that would allow solar energy to more completely serve humanity's energy needs.

Dr. Glaser's original proposal was published in 1968 in Science magazine. In 1971 and 1972 a small contractor study team was formed including Arthur D. Little, Grumman, Raytheon and Spectrolab. This team was awarded a study contract through the NASA Lewis Research Center to investigate basic technical feasbility of the SPS concept. The conclusions of that study were that the system is

technically feasible and could provide baseload electricity from solar power for use on Earth. Additional studies and experiments, partly funded by NASA over the period 1973 to 1975, established the feasibility of efficient energy transmission at microwave frequencies. In 1975 a demonstration conducted at JPL transmitted more than 30 kilowatts over a distance greater than a mile with a reception and conversion efficiency of 82 percent.

In the 1975 to 1977 time period, NASA conducted a technical assessment of SPS and began inhouse studies at the Johnson and Marshall Space Center. The Department of Energy conducted its own assessment; SPS was discussed in congressional hearings. These activities led to development of an SPS Development and Evaluation Program Plan jointly spnsored by DOE and NASA. The principal milestones in this plan are:

Reference System Definition Report, Oct. 1978 (Complete)
Preliminary Program Recommendations, May 1979
Updated Program Recommendations, Jan. 1980
Final Program Recommendations, June 1980

(Also during this period, NASA-funded space transportation system studies indicated that the high traffic volumes required to support an SPS program could lead to cost reductions far below those projected for the space shuttle. The potential for such cost reductions was seen as significant to the economic practicality of SPS.)

As a result, plans were formulated by NASA to conduct solar power satellite system definition studies in 1977 in order to support the first milestone of the DOE/NASA evaluation plan. These would increase by roughly an order of magnitude the degree of depth of design and cost definition for SPS systems. One such study was awarded to Boeing through the Johnson Space Center; the other study was awarded to Rockwell through the Marshall Space Flight Center. These studies created reference system designs including the solar power satellites, ground receiving stations, space transportation systems, space construction systems and other support systems. The results indicated that SPS's could be built by the year 2000 with a likelihood of economic benefit. The principal findings of these studies might be summarized as follows:

78-474

- Satellites are positioned in high-intensity, nearly continuous sunshine; unaffected by night and weather, they provide baseload electricity.
- Hundreds of satellites can be installed above equator over Pacific Ocean.

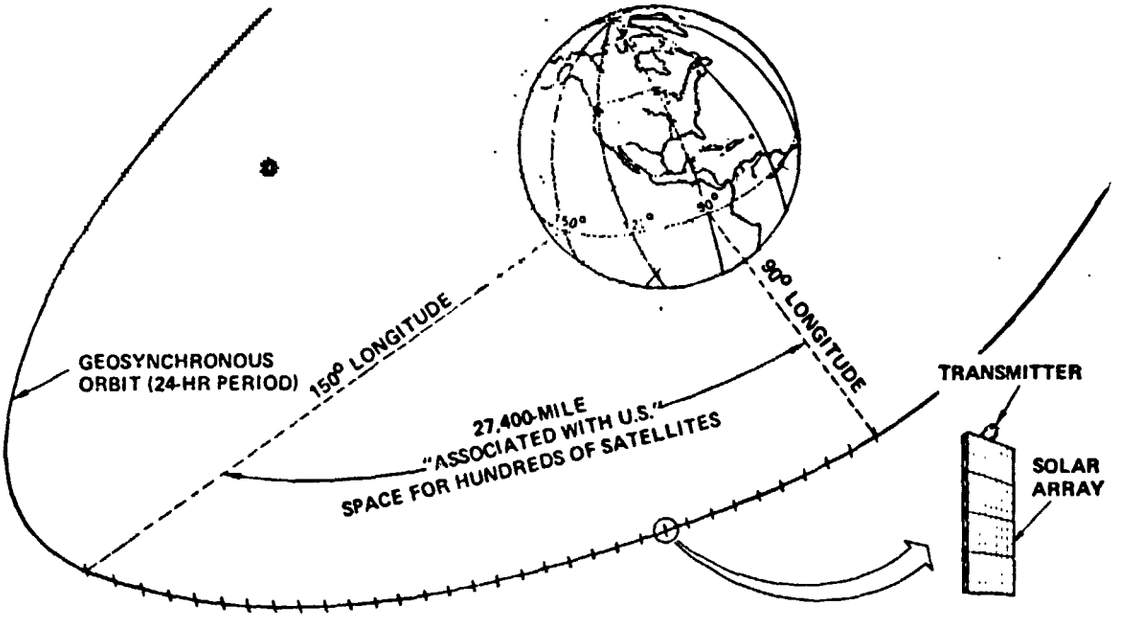

Figure 1.0-1. Solar Power Satellites: The Principle

1. Examination of energy conversion options led to a preference for silicon photovoltaics in the Boeing study, and gallium arsenide photovoltaics in the Rockwell study. (Both studies suggested thermal engine SPS designs as a hedge against the possibility that expected cost reductions in photovoltaics mass production might not be achieved.) The silicon photovoltaic system offers less risk with a more mature technology but an energy conversion system roughly 40 percent more massive than gallium arsenide.

2. Analyses of the power transmission system confirmed the basic feasibility indicated by the earlier studies and detailed microwave link error analysis confirmed attainability of adequate efficiencies. Integrated power transmission system conceptual designs were developed considering RF, electrical, mechanical, and thermal factors.

3. Space transportation systems were designed to accomplish the SPS transportation operations at acceptable cost.

4. Space construction approaches and construction base designs were developed for construction of 10,000 megawatt SPS's in geosynchronous orbit at a rate of approximately 1 per year.

The principal system elements from that study were the point of departure for the current study. The preferred SPS defined by Boeing is illustrated in Figures 1.0-2 through 1.0-6.

1.0.2 OBJECTIVES

The overall intent of the systems definition studies, past and present, may be summarized as follows:

1. Assess the technical feasibility of solar power satellites based on forecasts of technical capability in the various applicable technologies. Select the most appropriate technological paths leading to the most environmentally benign and economically practical systems. Define the areas of high leverage research.

2. Define the characteristics of SPS systems that may be derived if a development were to proceed. Assess performance, cost, operational characteristics,

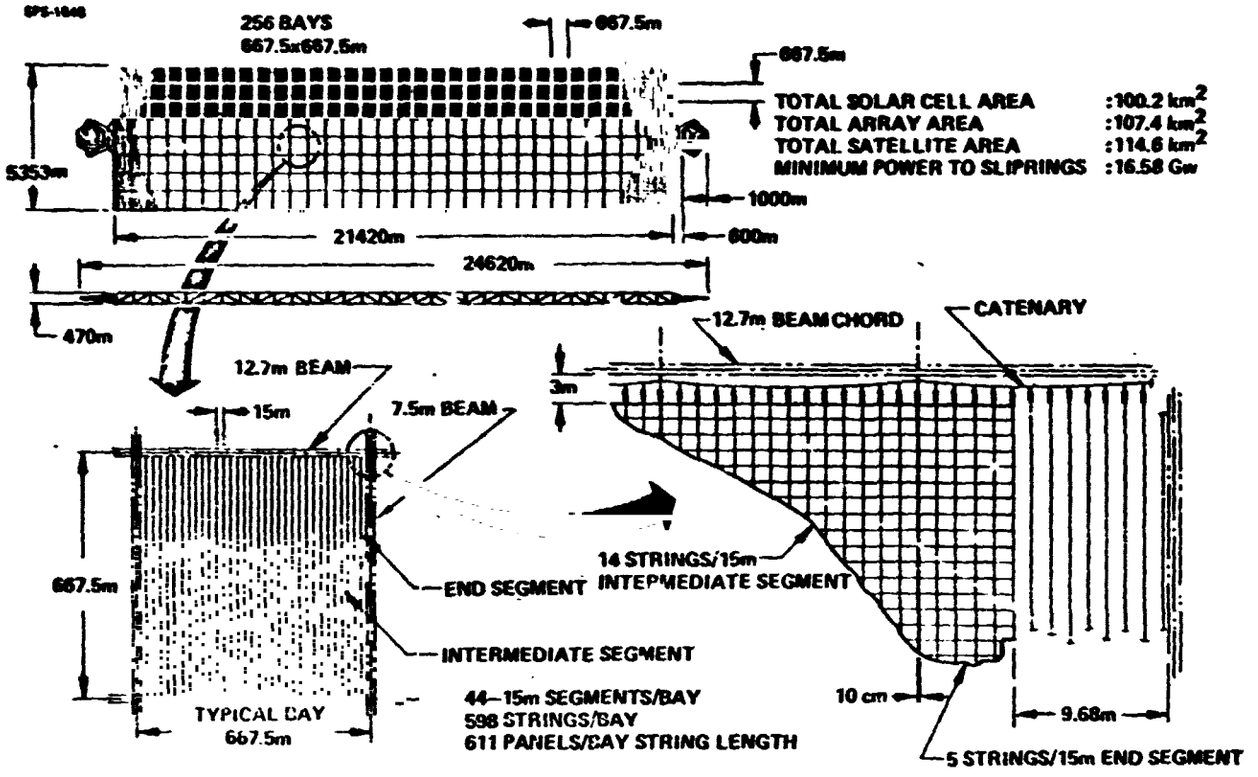

Figure 1.0-2. Reference Photovoltaic System Description

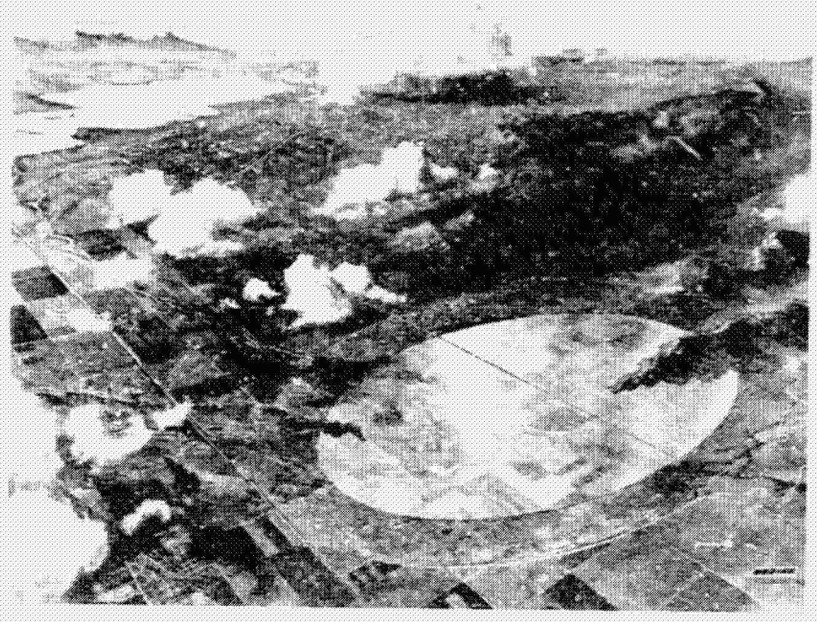

Figure 1.0-3 Ground Rectenna

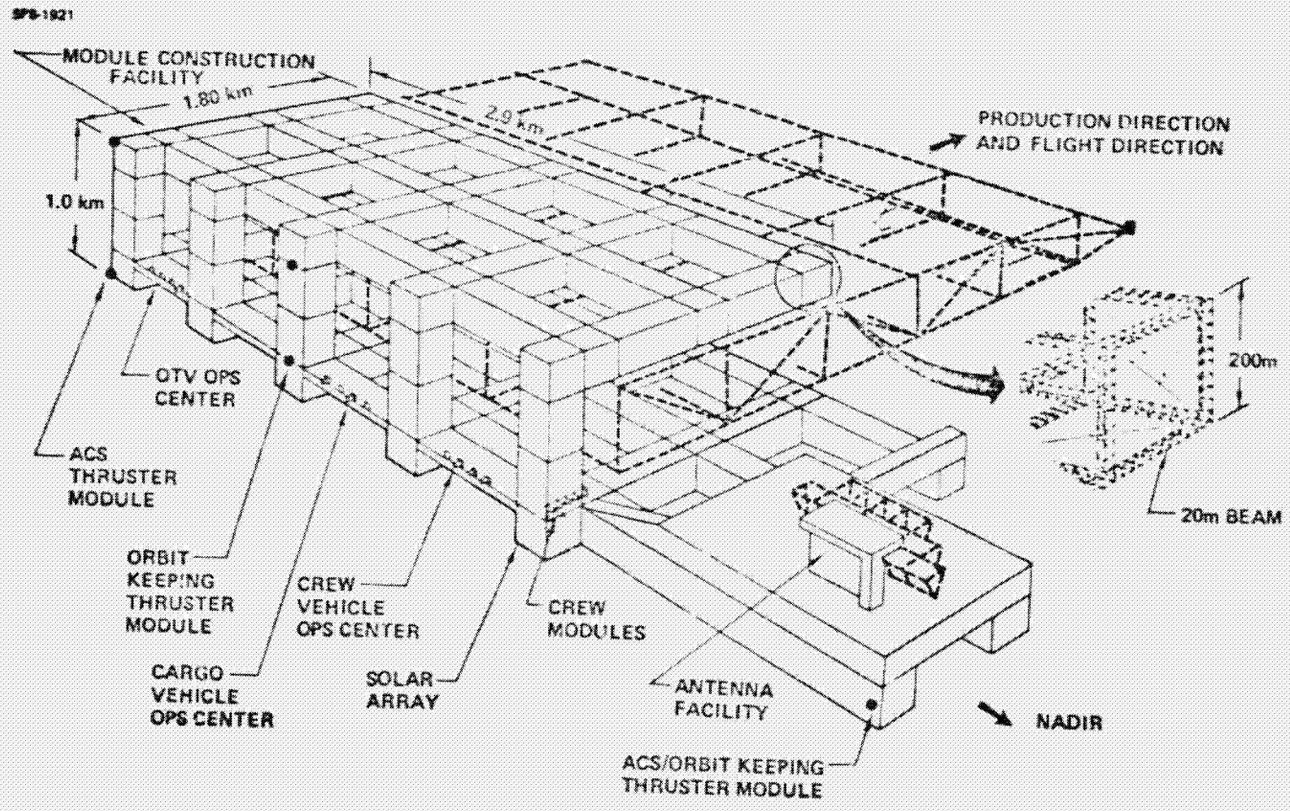

Figure 1.0-4 LEO Construction Base—Photovoltaic Satellite

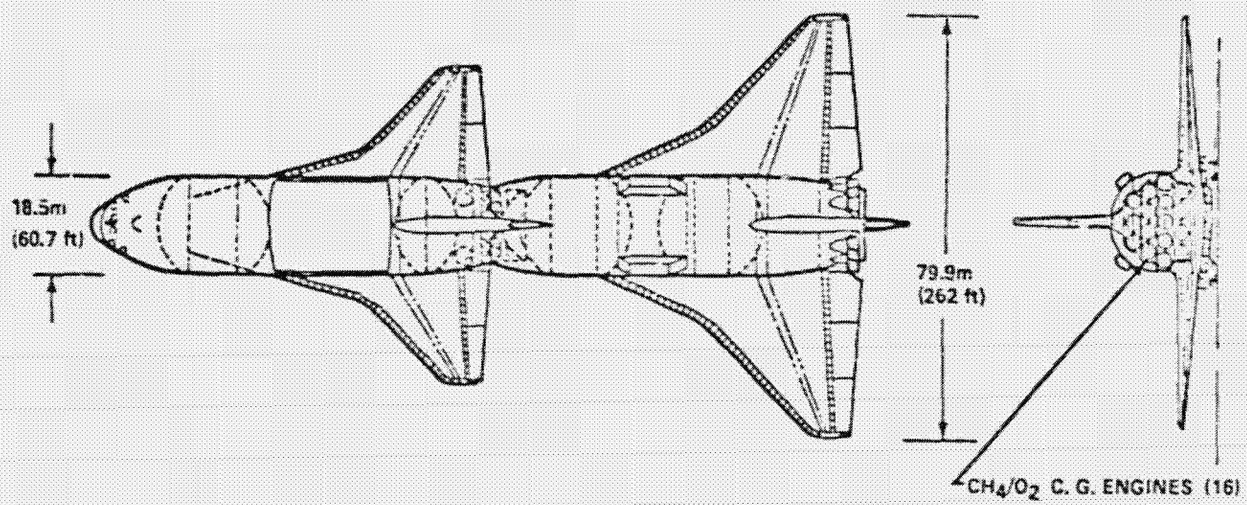

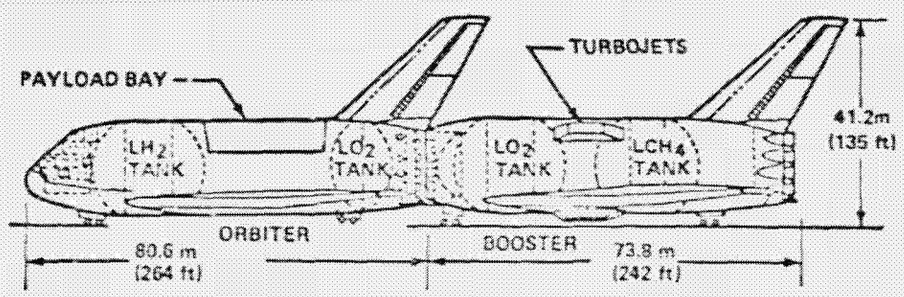

HLLV (Fully Reusable Cargo Carrier)

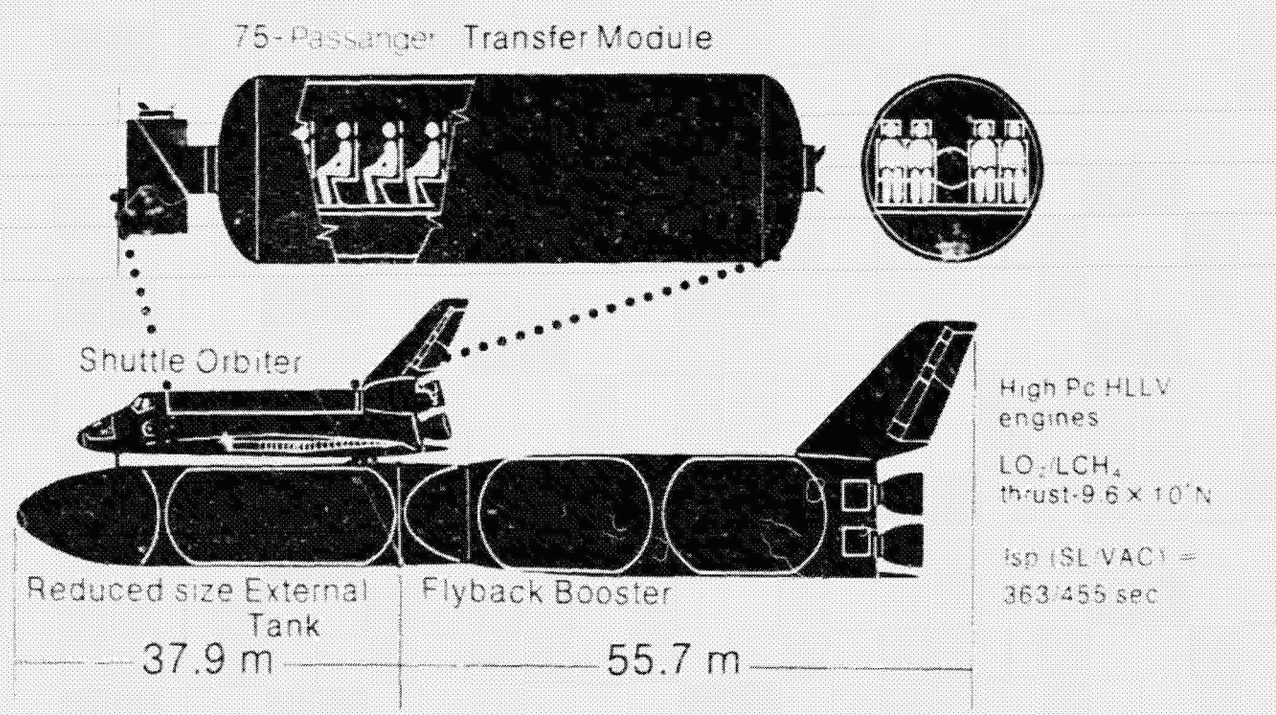

PERSONNEL LAUNCH VEHICLE

Figure 1.0-5 SPS Launch Vehicles

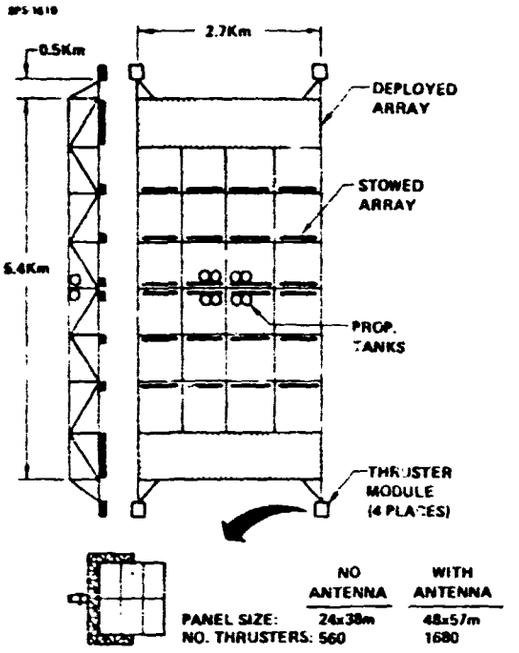

GENERAL CHARACTERISTICS

- 5% OVERSIZING (RADIATION LOSS)
- TRIP TIME = 180 DAYS
- ISP = 7000 SEC

MODULE CHARACTERISTICS	NO ANTENNA	WITH ANTENNA
• NO. MODULES	6	2
• MODULE MASS (10^6KG)	8.7	23.7
• POWER REQ'D (10^6Kw)	0.3	0.81
• ARRAY %	13	36
• OTS DRY (10^6KG)	1.1	2.9
• ARGON (10^6KG)	2.0	5.6
• LO_2/LH_2 (10^6KG)	1.0	2.8
• ELEC THRUST (10^3N)	4.5	12.2
• CHEM THRUST (10^3N)	12.0	5.0

Self Power Configuration for Orbit-to-Orbit Delivery of Photovoltaic Satellite

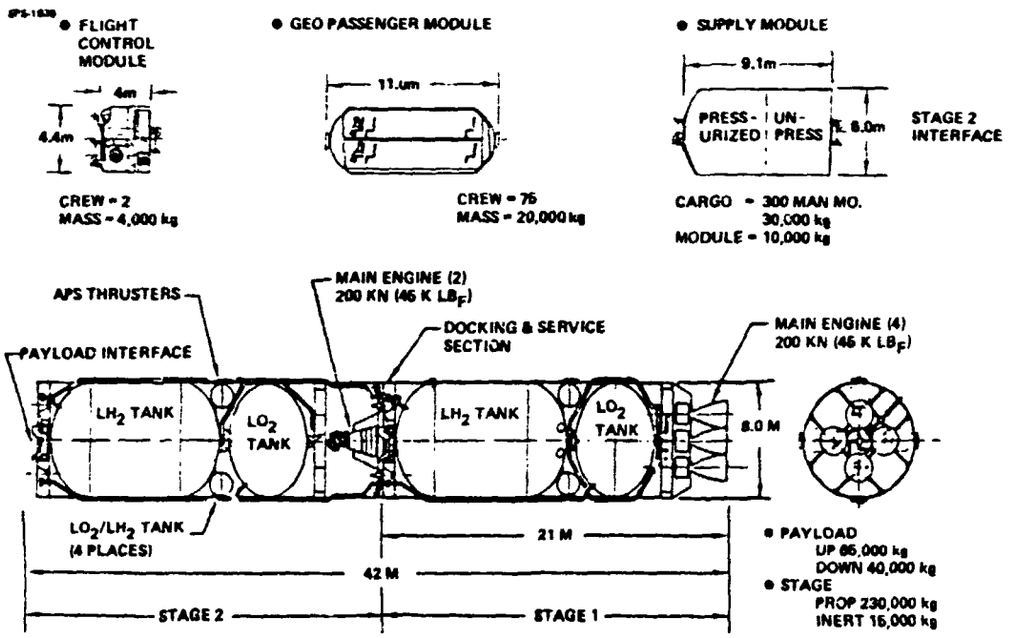

Chemical (LO_2/LH_2) Orbit Transfer Vehicle for GEO Crew/Supply Delivery

Figure 1.0-6 Orbit-to-Orbit Transportation

reliability, and the suitability of SPS's as power generators for typical commercial electricity grids.

3. Assess the uncertainties inherent in the system characteristics forecasts, based on technological uncertainties, on cost estimating uncertainties, and on uncertainties that arise from incompleteness in the data base.

4. Define the most economically prudent path to minimizing these uncertainties to the point that confident decisions can be made to proceed or not to proceed with development of this energy system.

The specific objectives of the present study are:

(1) to verify, maintain and update the presently-defined elements of the system,
(2) complete the definition of the total system, and
(3) prepare a series of plans required for technology advancement and SPS program implementation

Phase I of the present study, reported herewith, has concentrated on the first two objectives. Phase II will emphasize end-to-end operations analyses and the third objective. These objectives and the timing of the study are designed to support the NASA program recommendations in fulfillment of the DOE/NASA evaluation plan.

1.0.3 STUDY APPROACH AND STUDY TEAM

The JSC/Boeing and MSFC/Rockwell SPS system definition studies of 1977 and early 1978 proceeded largely independently of one another and developed system concepts with a number of significant differences. NASA then developed a refernece SPS system description based on NASA inhouse studies as well as on Boeing and Rockwell contract results.

The present study is divided into two phases. The first lasted 7 months and the second will last 9 months. Phase I accomplished additional analyses of the options and issues identified by NASA in developing the reference system report, beginning with a thorough critique of the JSC/Boeing reference system followed by analyses of options and critique items. The reference design was updated at the end of Phase I. The overall schedule is shown in Figure 1.0-7.

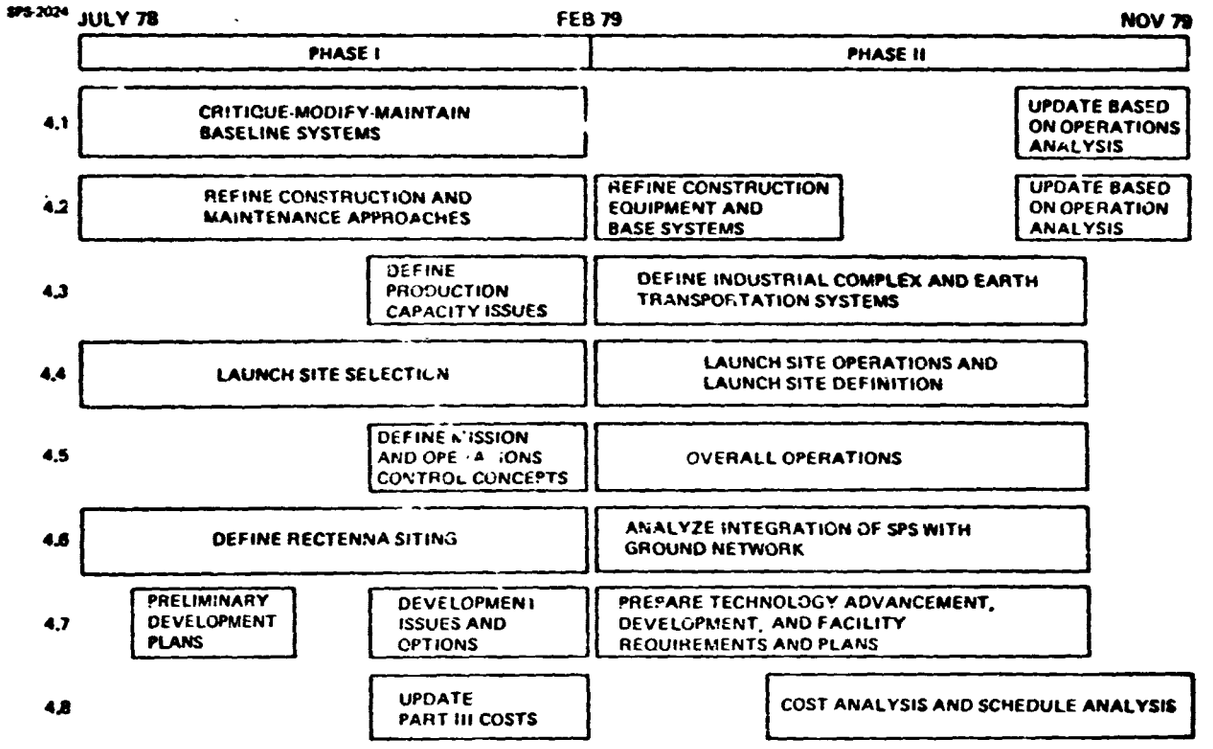

Figure 1.0-7. Study Plan Overview

The Study Contract Team included Boeing as prime contractor and General Electric, Grumman, Arthur D. Little, and TR as subcontractors. Principal task areas and the study team leaders for each contractor are shown in Figure 1.0-8.

1.0.4 SYNOPSIS OF STUDY RESULTS

A major part of the phase I activity was directed to review, critique and modification of the baseline system. Additional analysis was invested in some parts of the baseline system for which definition was incomplete. Finally, an evaluation of technology, objectives and development planning in general was conducted.

Results of the major trade-off studies were as follows:

1. A review of the annealing concept was conducted with confirmation of the feasibility of the principle. Additional tests of directed energy annealing of solar cells were conducted. Recovery of 50 micron silicon solar cells degraded by proton radiation was demonstrated. The solar blanket design was updated to reflect the use of shunting diodes on each solar array blanket panel to protect the sollar array from shadowing.

2. An alunminum structure option for the solar array support system was analyzed. It was found to be a feasible design but would be about 25 percent heavier than the composite design. Analysis of aluminum structure for the transmitter antenna indicated that excessive thermal deformation would occur. Thus, aluminum transmitter structure would require active compensation for thermal deformation affects. The use of aluminum waveguides was also examined. Detuning of the waveguides due to thermal expansion introduces an additional 1 percent loss in the microwave power transmission system efficiency. It was therefore recommended that a suitable composites material be developed for the waveguides.

3. Analysis of solid state power amplifiers indicated that potentially useful efficiencies could be achieved but that the solid state transmitter will be limited by thermal effects to lower power systems in the range of 2500 megawatt per RF link.

4. A review of the Lincom phase conbtrol system approach indicated that this approach was satisfactory baseline phase control system.

SPS-2200

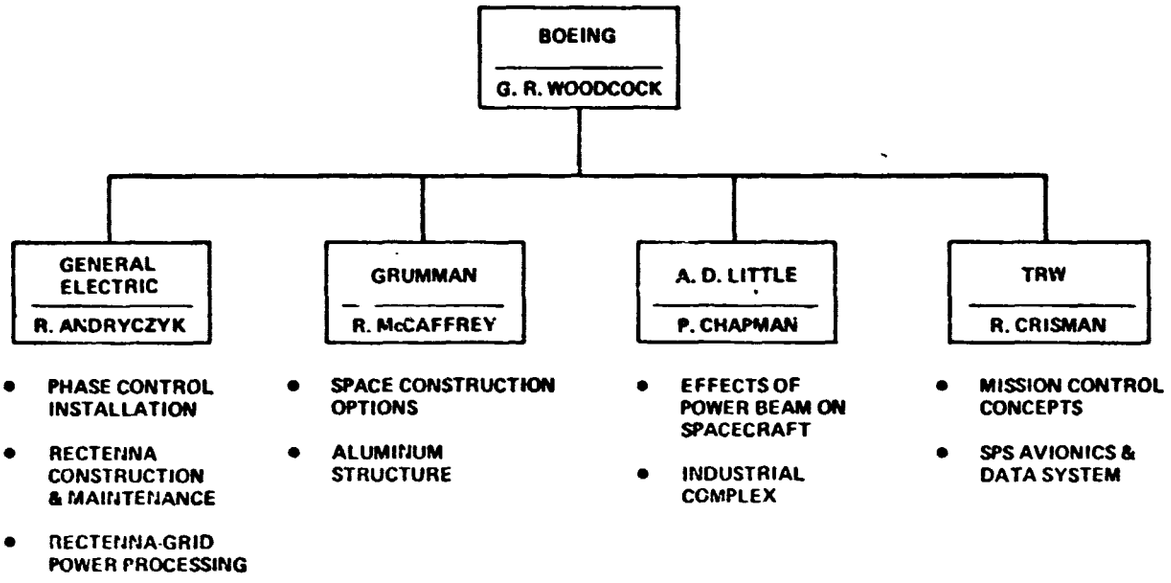

Figure 1.0-8. Study Contract Team Organization (Phase I Tasks Shown)

5. A failure and maintenance rate analysis was conducted indicating a potential availability of SPS energy of approximatelly 90%. Improvements in this figure could be achieved by minor changes in the power transmitter design or by changes in maintenance philosophy.

6. Studies of smaller SPS's indicated that power per microwave link as low as 2500 megawatts could be achieved with modest cost penalties. Solid state power transmitters were identified as potentially desirable for these reduced power levels because of improved packaging for the power transmitter subarrays.

7. A major analysis of orbit transfer and construction location options was conducted. The earlier study had indicated a preference for low earth orbit contruction. Electric propulsion would be employed to move SPS modules to geosynchronous orbit. This was based on a comparison with chemical propulsion system for obit-to-orbit transportation for geosynchronous orbit construction. The current study reviewed the self-power option, made some minor configuration changes, and evaluated this option relative to an independent electric orbit transfer vehicle for geosynchronous orbit construction. The cost comparison showed essentially equal fully amortized transportation costs for these options. The independent electric OTV option exhibit a higher front end cost due to the need for investment in the orbit transfer vehicle fleet. The self-power system is more of a "pay as you go" option.

8. A major analysis of construction techniques and construction base options was conducted. Six alternatives were evaluated and narrowed down to two preferred options - a platform type facility and an endbuilder facility. The comparison between these two options was relatively close. The platform exhibits somewhat lower design and operational risk, and the end builder exhibits somewhat lower cost and higher productivity.

9. A study of equatorial launch sites exhibited no particular cost preference for the equatorial option. Cost savings due to space transportation performance improvements turned out to be relatively minor because the electric propulsion options are insensitive to the delta V difference between inclined orbits and low inclination orbits. Trajectory suppression studies indicated that launch trajectories could be held below 100 kilometers altitude, thus

reducing and probably eliminating concern for effects of launch vehicle effluent on the upper atmosphere.

10. A mission control concept for SPS mission operations was developed and an SPS avionics data and communication system concept appropriate to this mission control approach was defined.

11. A preliminary analysis of the industrial intrastructure required to support SPS operations indicated that only the production of solar cells blankets represented a major industrial challenge.

The baseline system description selected by NASA for the Phase II of the present effort is described in Volume III of this report.

Development planning analysis identified 4 major program phases subsequent to the present system definition and evaluation phase. These are:

1. Technology Research
2. Engineering Technique Development
3. Prototype SPS
4. Commercialization

A detailed plan for the technology/research phase is in the process of formulation. The current version of this plan was provided to JSC for information, but is not regarded as a recommended plan at this stage of analysis.

1.1 SATELLITE

Four subjects are reported at this WBS level: the SPS critique; SPS size and configuration effects; SPS internal EMI; and interactions of SPS power beams with other spacecraft.

1.1.0.1 REVIEW OF CRITIQUE RESULTS

The following discussion summarizes the results of the critique:

1. At the program level, although the materials list for approximately 90% of the mass of an SPS have been identified, concern was expressed that certain exotic materials, even if used only in trace quantities, could represent a materials availability problem. This applies, for example, to materials used in the electronics and RF power systems.

2. The second item identified several concerns associated with the large unit size of the reference design SPS. This issue is being addressed in the current study.

3. The third item dealt with the space debris issue. Collisions between the SPS's and other space junk have been addressed in earlier studies and means identified to minimize the risk of such collisions. This critique item, however, also identified a potential issue with creation of debris by the construction process, and concern with outgassing or emission of particulates (e.g. graphite fibers) as a result of extended exposure of the SPS's to the combined space environment.

4. A related concern was expressed about the long-term suitability and stability of graphite fiber composites in the space environment. The issues raised included creep and micro-cracking.

5. A relative lack of definition exists for the flight control and onboard computing systems. This issue is being addressed in the current study phase.

6. Definition of detail is needed in the antenna yoke and turntable. This system provides the mechanical motion between the antenna and the SPS solar array. Mechanical isolation is necessary to minimize dynamic effects on the transmitting antenna. The solar array electric power must be delivered across this coupling.

Although a reasonable definition of the electrical slip rings exists, comparable definition of bussing on both sides of the slip rings and the flexible electric connection between the antenna yoke and the antenna itself has not been provided.

7. Plasma interactions may occur with the high voltage solar array. In particular, this item singled out the problem of plasmas produced by the electric thrusters. A careful analysis could shed some light on this issue but an adequate resolution will require experiments in space.

8. This item addressed solar blanket details and recommended that experimental samples of the lightweight annealable solar array be built and tested to verify annealability as well as survivability of the rest of the array under annealing conditions; also the interconnect techniques and compatibilities of all materials contemplated for use.

9. This item addressed solar blanket installation details. One concern was the lack of definition of a repair and replace concept. A second concern regarded details of the jumper installations between blankets across the structural members, in particular the relatively high voltage potential that will exist between the structure and the jumpers. Also, the change from bi-axial to uni-axial tensioning of the solar blanket left some inconsistencies in structural arrangement and installation details that need to be corrected. This latter item is discussed below.

10. Power Distribution System: Better definition is needed of the details of installation of the main power busses on the SPS and their interconnection through switchgear to the solar array. Concern was also expressed over the production of wear particles in the slip ring assembly and the possibility that these wear particles could "track" high voltage insulators causing arcing and damage to the slip ring assembly or nearby components. Also, concern was expressed regarding the arrangement of the power supply hookup to the klystrons. Each power processor feeds about 400 klystrons; the potential fault currents that could arise from a high voltage arc at one klystron could involve the entire power supply current. Also, for the klystron power that is provided directly from the solar array busses, a fault could theoretically short the entire bus to ground. In addition to the problem of very large fault currents, the electrical and magnetic

forces caused by severe transients could easily cause major mechanical damage to the SPS. A residual concern was also expressed that power supply faults frequently cause failures in other parts of an electronic system. Means of predicting, minimizing, isolating and correcting such failures need to be developed.

11. This item concerned the thermal environment on the transmitter antenna and recommended further thermal analysis. A problem was identified with the effective sink temperature for the power processing subsystem radiators. In the present configuration, the sink temperature created by the klystron thermal rejection system appears to exceed the temperature at which it is desired to reject heat from the solid state components on the power processor system. Several avenues are available to correct this deficiency. A thorough trade study is needed to select the best approach. Options include the use of refrigeration cycles, use of higher temperature components (such as gallium arsenide transistors or vacuum tube diodes), relocation and reorientation of thermal control radiators, and increases in overall transmitter aperture combined with decreases in overall power. Also, the possibility of alternative RF power amplifiers such as amplitrons, injection-locked magnetrons, or solid state systems, should not be overlooked.

12. The use of plated composite waveguides in the power transmission system was addressed. Thermal cycling or age deterioration could cause cracking of the plating in these waveguides, resulting in reduction of efficiency and increases in radio frequency interference from the power transmission system. This issue is being addressed in the current study by examination of an all-metal-waveguide backup design. In addition, testing of plated composite waveguides was recommended.

13. It was recommended that additional integrated analysis of the antenna array and phase control system be conducted. This item is being worked in the current study as well as in a separate JSC contract with the Lincom Corporation.

14. Concern was expressed regarding damage of sensitive communications equipment on other satellites whose flight paths intersect the SPS microwave power beam. This issue is being addressed in the current phase of study.

15. This item concerns the power transmitter antenna structural configuration. In particular, the issue was raised that the secondary structure in effect forms a part of the primary structure. An analysis of this problem is included in the present report.

16. Concern was expressed that the power processor high-voltage transformer life may be too short for SPS application due to failures caused by a-c corona within the windings. This item is being addressed in the current study.

17. This item expressed concern that high voltage, high power transistors (used in power processors) are not radiation resistant and that the space radiation environment would result in short life for these devices. Shielding was suggested as a possible fix.

18. Concern was expressed regarding design of, and materials for, high voltage insulators and cable insulation for use in the space environment.

19. This addressed the actual performance of the microwave power transmission phase control, phase distribution, and RF power distribution systems. The general nature of the concerns was such that a test program would be required to accomplish resolution.

20. This item expressed concern about the RF power amplifier design. First, that other kinds of d-c/RF conversion may be superior to klystrons; secondly, concerns over klystron efficiency, klystron tuning over the thermal range that is expected, and klystron or thermal control failures and life.

21. It was noted that in space checkout of the SPS modules, the integrated SPS, and its operation with the ground system has not been adequately defined.

22. This item expressed concern over radiation of harmonics by the rectenna. This subject was discussed in reports prepared as a part of the previous contract (Part III effort of Contract NAS9-15196).

This summary has omitted a number of minor critique items that were primarily concerned with lack of adequate definition detail or uncertainties in masses and costs. A detailed critique package was provided to JSC at the orientation briefing.

1.1.0.2 TRW CRITIQUE OF THE BASELINE MICROWAVE

POWER TRANSMISSION SYSTEM

The task assigned to TRW was to provide a critique of the SPS baseline Microwave Power Transmission System and Phase Control System. The purpose of the critique is to identify:

a. Design concept concerns
b. Areas requiring additional analysis
c. Inconsistencies and/or integration problems
d. Potentially more attractive options from a cost/mass and a technology/schedule risk standpoint.

An additional review category, i.e., identification of areas requiring additional technology advancement, which is part of another task, has also been included.

For purposes of the critique the Microwave Power Transmission System was reviewed in two sections, the power distribution section from the slip-rings to the klystrons and the rf section from the klystrons through the antenna. For each section the critique results are presented in the categories requested, however, categories (a) and (c) have been combined. As will be seen, a single item may fit more than one category, however, it is only included in one.

POWER DISTRIBUTION

This section is principally concerned with power distribution on the antenna side of the slip rings, however, the power distribution aspects of the solar array as it relates to power quality and distribution were also included where necessary.

Design Concept Concerns

In general, the system redundancy in the slip rings and other major power system busses are of some concern. Our review indicates that a single failure on "B" bus would prevent power from being radiated from either antenna. In addition, other slip rings will be required for control of power, fluids, and probably, critical energy storage circuits.

The insulation provisions on the solar array busses may not be adequate for the required level of voltage (nominally up to 44 KV). Considerably more spacing may be

required for successful isolation. Plasma effects, those naturally occurring at synchronous altitude plus the effects of ion engines, and other propulsion engines as well as the potential or discharge of environmental oxygen or other ionizable gasses introduce the need for corona suppression concerns. Argon gas is one of the most easily ionized gasses and is presently the baseline stationkeeping ior engine gas selection.

The main solar array busses were interpreted to be oriented in a plane perpendicular to the main array surface. The method of accommodating the thermal expansion was explained for the axial growth. The method of transitioning to these flatplate conductors from the array segments was not covered in sufficient detail to permit analysis. The problem of threading the array to main array bus connections would require three dimensional insulation support. The force on each conductor by interaction of the self-induced magnetic field when carrying current in opposite directions is substantial and accumulative for each unit of conductor length. The formula for parallel bus bars is presented below to show the magnitude of these forces. This does not apply to edge oriented bus bars. A new constant is required for this geometry.

$$F = \frac{2 \times 10^{-7} \times I_1 \times I_2}{9.81 \times d} = \text{force in kilograms per meter of length}$$

I_1 and I_2 are the respective currents and d is the distance between conductors in meters. This formula was adapted from Rudenberg's Transient Performance of Electrical Power Systems.

In considering the forces from current, the worst-case short circuit current, not the normal current should be used to analyze the forces induced. The worst-case current is the sum of all the sources tied together, plus the pump back current from loads and commutating devices. If it were possible to size circuit breaker commutation requirements, all the circuit breakers connected to the circuit would have an additive contribution to the fault current as would the dc to dc converters that are used to supply the klystrons. For example, TRW's TDRS satellite has a nominal total load of 1.5 kW. The capacitors in the input terminals of the traveling wave tubes and two power processors approximates 10,000 microfarads. In the SPS the sources are large, but with these large dc to dc converters, the collective current delivered to a fault could exceed the system nominal nameplate current by a substantial margin.

Suggested Areas of Additional Analysis

A review of the assessment of technology readiness as related to dc to dc converters which relates switching frequency, efficiency and converter size is recommended. The optimum frequency does not necessarily go up to 30 kHz when large (hundreds of kilowatt) units are considered. It is a distribution problem. As the distance between power components goes up, the length of connecting conductors goes up also, hence the inductance increases in the interconnections. The voltage drop increases as a function of frequency. Co-axial type interconnections for multiphases and the proper control of their distance to the ground plane becomes impractical. Lower dc to dc efficiencies and increased weight should be assumed until actual units of comparable size are built.

The current density in the sheet aluminum conductors should be checked for the criteria of $100^{o}C$ as this density appears to be high even when radiating to a black body. The method of conductor support from and to the slip rings was not specified and could add substantially to the weight due to insulators and collector terminations. In reviewing the I^2R loss as tabulated, the return conductor losses were apparently not added to the loss for dc to dc converter input or klystron collector 4 and 5 connections in computing the heat loads. The negative conductor would generate significant voltages in the shared conductor and would, if connected as diagrammed, present interractions in unrelated circuits that would make it impossible to deliver the voltage of the quality specified. The method of busing all of those interconnected wires requires definition. In fact high voltage splices, connectors or attachment provisions for conductors would be expected to have a significant weight. In past utility practice using dc grid systems, the ground connection was always made at the source and at the source only. The report does not address the point as to the planned usage, grounded or ungrounded. The absence of a single ground complicates fault detection relaying for system protection. Further analysis on grounding and its relation to plasma neutralization and static buildup on insulated system components is recommended.

The capability of interrupting an arc in a klystron by applying a modulating anode clamp in microseconds requires further analysis or testing. Clamping does stop the rf output, but the arc may make a plasma of the collector material and sustain the arc until the dc to dc converter is turned off and the stored energy of its output dissipated.

As indicated later it is recommended that the weight analysis of the commutation components required for dc switching be reassessed after the components have been identified and sized.

Areas of Technology, Requiring Additional Development

Circuit breakers that can handle the power levels of the SPS in the 10 microseconds stated as the requirement require development. Terrestial units that rely on the assistance of convection currents induced by gravity are expected to have significant derating if applied in space. The report cites utility success in use of high voltage dc as evidence of technology readiness. However, it is our understanding that all such dc link switching is accomplished on the ac side (input and output) and the capability to switch dc at any power level approaching the ones proposed for the SPS will require appreciable development. Every switch has to have enough energy stored with it to commutate off the collective short circuit capacity. Commutation is normally accomplished by the combination of capacitors and inductors. We are not aware of any suitable capacitors for use on a 40 kV multi-megawatt dc system. Electrolytic capacitors, which probably have the least size for the kVa required, will require considerable development to achieve sufficient reliability for 30 years service in space in a critical nonredundant circuit breaker application. The wet slug tantalum capacitor is in a similar situation for this application. In addition, vacuum interrupters do not perform as well at zero G as they go at one G. The energy snubber circuits and the commutation components may weigh much more than the circuit breaker weight budget tabulated, and it is recommended that this area be evaluated.

The Hughes dc switch as presented in the literature is a krypton gas cathode anode that acts as a gas tube when it conducts. It was sized for 1,000 amperes at 100 kV. It operated in 50 to 60 milliseconds with the aid of two mechanical contactors and large energy absorbing resistor grids. One of its insulated bushings may weigh as much as the stated budget cited in the report for main bus circuit breakers. The report identifies "A" bus units as 620 amperes and 6200 ampere momentary current. Methods of calculating the short circuit current capability of the system which would become the rupture requirement of those circuit breakers, also require development.

Potential Options

In our review, diodes were assumed for each parallel string of solar cells. Use of a large power diode on the main solar array circuit breaker circuit is also recommended

as the short circuit requirement of this circuit breaker is thus reduced to that of its own group of cells. This makes the selection of the commutating capacitors and other devices more practical by reducing the stored energy for commutation requirement determined by worst-case short circuit current and the speed selected for the circuit breaker operation.

The report suggests the use of on-array switching of individual strings for voltage regulation. Use of this capability to clip the excess voltage that occurs due to B.O.L. to E.O.L. decay and the initial overvoltage that is induced by occulation would reduce the excess power that must be dissipated on the antenna. The power quality could be thus held to even closer tolerance from the array than those selected in the report. It is recognized the temperature of the solar array would elevate whenever any load is turned off.

It is suggested that the use of ac rather than dc should be reconsidered even from a solar array, as the ac technology is readily at hand even if space rated hardware is not. It is not obvious what the optimum frequency should be for such a large system, but experience indicates it might be 60 or 120 Hz as an approximation. The resistance losses of major feeders would be a critical sizing parameter not just transformer weight as has been concluded in previous studies. Ac systems would not require as large a plasma neutralizing provision as would a dc system because the net current flow, based on the electrode spacing could average out to nearly zero.

For ac or dc systems for use in space, all circuit breaker, relays, contactors, fuses and fuse holders should be redesigned for cold-plate cooling to permit reduced weight and size and for installation in power junction boxes for mechanical and personnel protection. Electrical and electronic equipment has always required a benign environment for good reliability; and therefore, it is anticipated that liquid or gas cooling loops will often be required, especially for high power equipment.

The energy storage for this SPS electrical system should be redundant with the possible exception of the klystron heaters. The energy storage subsystem would result in a larger solar array penalty than stated in the report especially if nickel hydrogen batteries are used. They are expected to have roughly a 6% loss each day, and would have to be recharged even on days that no occulation occured. Low rates of battery charging are the least efficient, therefore additional penalty should be

estimated for this subsystem. Due to the large spatial relationship of the loads to each other, dispersed energy storage locations are indicated. It is possible that an energy storage electrical grid system could reduce the amount of batteries or other electrical energy storage components by avoiding some of the redundant capacity at all critical load locations. When large dc storage systems using batteries are considered, the recommended distribution is use of inverters and ac so that commutation switches may be designed to isolate the battery from the bus without added fault contribution from other things connected to the output bus.

RF GENERATION AND TRANSMISSION

This section is primarily concerned with rf generation and transmission by the Spacetenna.

Design Concept Concerns

The estimated overall system efficiency assumes very precise phase control. Present techniques for determination of relative phase over large apertures and control of the phase have relatively large errors. It is suggested that projection of measurement capabilities to the MPTS time freame should be made to provide a more conservative estimate of phase determination and control.

Thermal stress may produce large scale distortion errors in both the subarrays surface and the total array surface. The retrodirective concept corrects for deviations from the plane but does not correct for beam peak alignment shifts, i.e., if a subarray is sufficiently distorted so that its pattern is skewed, the conjugate phase technique will correct the phase of its radiation in the direction of the Rectenna, but will not realign its beam peak in that direction. Extension of the thermal distortion analysis is needed to evaluate the magnitude of associated pattern changes of the subarray and total array.

Suggested Areas of Additional Analysis

The present rationale for the Spacetenna aperture distribution is based on a controlled amplitude taper which achieves high efficiency combined with sidelobe level well below the present U.S. safety standards. However, the sidelobe levels are significantly above the USSR safety standards. On the basis of the assumption that the latter are derived from health problems encountered in operations; studies of the antenna sizes, and Spacetenna aperture distribution should be extended to determine the impact of these significantly lower safety levels on the MPTS.

The slight mismatch of the Rectenna elements will produce coherent scattering of a small portion of the incident field by each element. Despite the fact that the Rectenna functions as a scalar system, i.e., no array pattern; this scattered field will closely resemble the pattern that would be realized if it did function as a vector array. This will occur at the carrier frequency and the potential for sidelobe scattering from atmospheric disturbances should be investigated as to potential interference with terrestrial communications.

Areas of Technology Requiring Additional Development

On-board alignment measurement to determine distortion of the antenna and its subarrays, and attitude control of the antenna and subarrays to minimize pointing errors and to compensate for large-scale, ordered error in the antenna.

Long term aging properties of realizable phase reference distribution implementations are not well established at present. Error growth with time in the phase reference distribution network is a real possibility. A study is needed to develop concepts for autonomous phase-reference distribution calibration throughout the entire array and subsequent compensation of error.

Potential Options

Reduction of diffraction perturbation of illumination by use of passive techniques.

It is feasible by use of passive complementary, line-sources on the Rectenna panel edges to readily adjust the Sommerfeld diffraction to produce a near uniform illumination. These techniques have been used in the past with considerable success.

1.1.0.3 SPS SIZE AND CONFIGURATION EFFECTS

PARAMETRIC INVESTIGATIONS

SPS baselines have generally used a 5,000 megawatt power transmission link. This power rating may be uncomfortably large for some applications and it is natural to raise the question, "How much smaller could SPS's be made?" Shown in Figure 1.1-1 is a joint optimization of transmitter diameter and power level holding the rectenna size constant at the optimum value. This result was developed on the earlier contract, and did not nclude packaging density considerations. As the system power level is reduced, it is possible to employ somewhat larger transmitting antennas without violating the

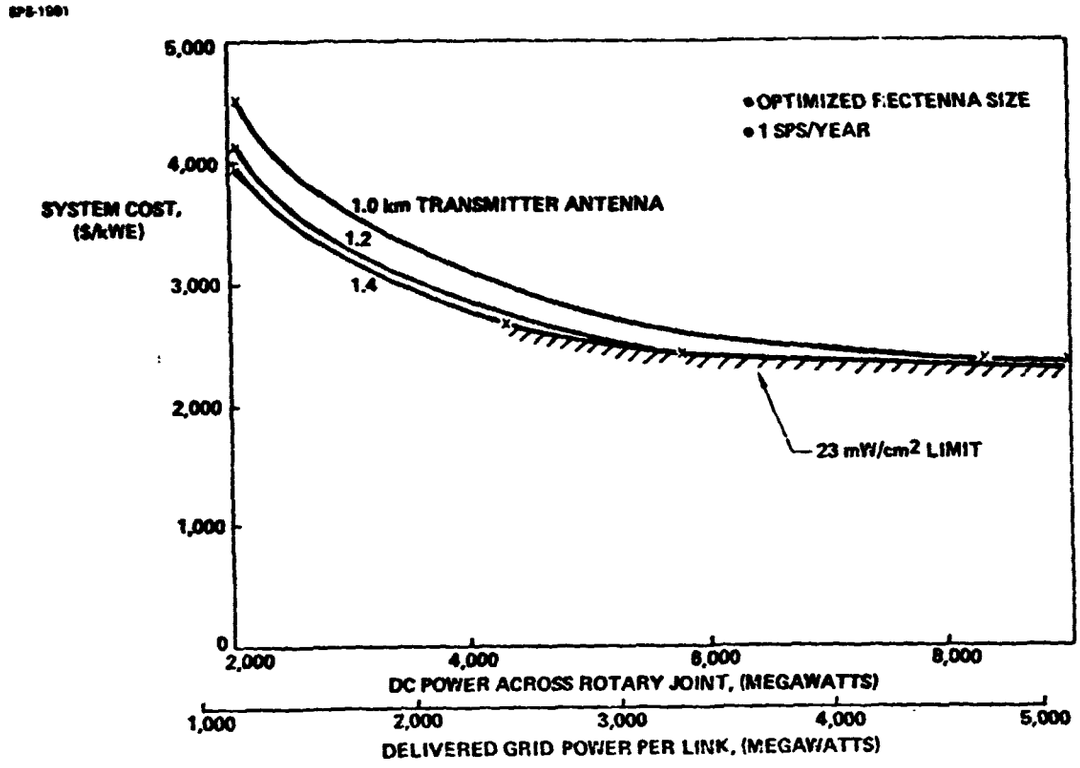

Figure 1.1-1 Size Sensitivity Analysis Power Level and Transmitter Diameter

23 mw/cm^2 limit. Transmitter diameters larger than 1.4 kilometers do not pay off; the minimum system cost in dollars per kilkowatt follows along the 23 mw/cm^2 limit to about 2,500 megawatts and then follows up the 1.4 kilometer transmitter curve. Note that comparatively little cost penalty is incurred going down as low as 3,000 megawatts of grid power. Below 3,000 megawatts, the system cost in dollars per kilowatt begins to turn up rapidly.

The present study expanded on these earlier results to consider packaging and specific configuration effects arising from asymmetric configurations. Three smaller SPS configurations are compared to the original 10 gigawatt baseline in Figure 1.1-2. The first of the three shown is the present NASA 5 gigawatt baseline with one transmitting antenna. Analysis of the control requirements for this asymmetric configuration determined that because of the overriding importance of solar pressure compensation in the control thrust scheme, no propellant penalties were incurred by the lack of symmetry. Also, no packaging differences have been identified that would arise from dividing the original configuration into two equal halves. Therefore, the only consequence of this alternative to the original baseline is the requirements for more positions in geosynchronous orbit to effect a given total installed generating capacity.

The next alternative shown is also a 5 gigawatt system, but the power is transmitted through two power transmission links each rated at 2½ gigawats. In order to minimize land use and rectenna costs, it is desirable when reducing the link power to increase the transmitter aperture, in turn reducing the receiving station area. This design option, however, has approximately four times as many transmitter subarrays as the single-transmitter 5 gigawatt satellite. As a result, it incurs a significant payload packaging problem because of the low packaging density of completely assembled transmitter subarrays. The packaging density situation appears to be much improved through use of a solid state transmitter. In the solid state option, all of the active functions are included in a planar sheet only about 2 centimeters thick (including the resonant cavities). Thus, a much higher packaging density per unit of aperture area can be achieved.

The final option shown, like the second option, results from effectively dividing a symmetric configuration in half. As for the other case, no penalties were determined for this design option excepting the use of more geosynchronous orbit space.

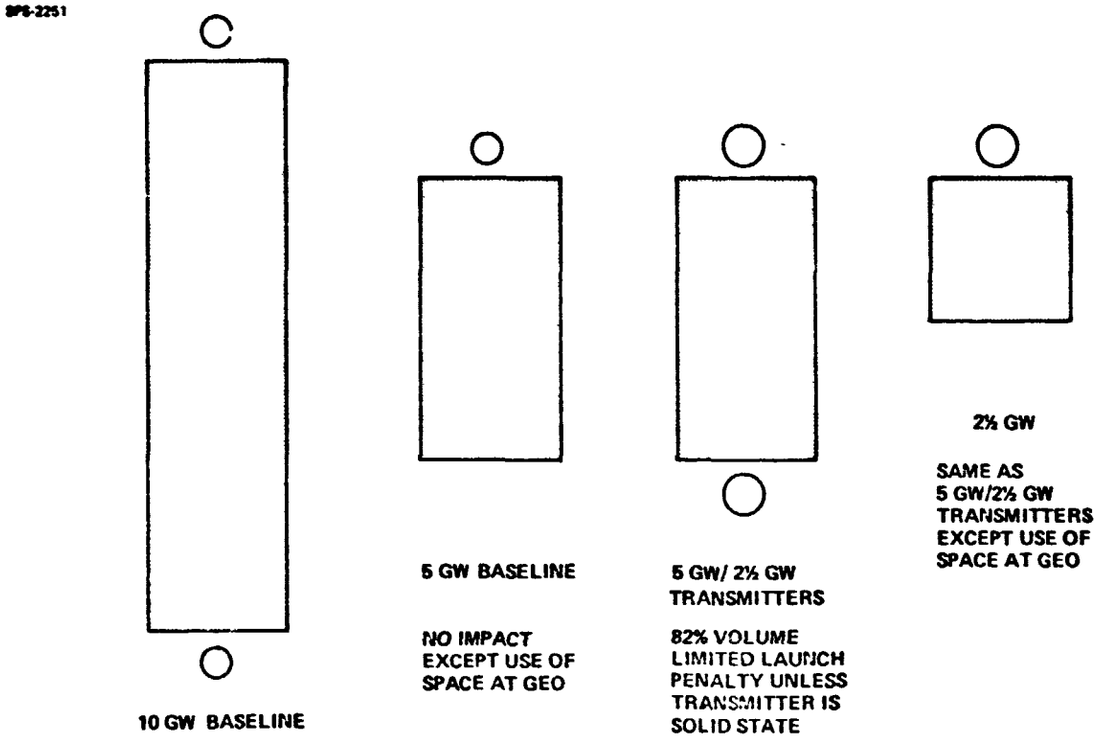

Figure 1.1-2 Small SPS's

Because of the potential problems with packaging smaller SPS's, an update of the earlier packaging studies was performed. This packaging update is summarized in Table 1.1-1. It includes allowances for orbit transfer hardware and orbit transfer propellants (both of which package relatively densely), thus density determined for the 10 gigawatt reference configuration has increased somewhat from earlier estimates. Nonetheless, a significant problem is identified for the systems of the reference type with 2½ gigawatt transmitter links. The problem is much alleviated in the solid state transmitter case.

ASYMMETRIC CONFIGURATIONS

The configuration considered is the Photovoltaic Reference Configuration, cut in half so that the north-south dimension of the array is reduced from 21,280m to 10,640m. A sketch appears in Figure 1.1-3.

It is assumed that the vehicle remains oriented perpendicular to the orbit plane (POP) and tracks the sun to the extent possible with a single degree of rotational freedom (about the orbit normal). Thruster clusters are assumed at the four corners of the array.

There are two significant disturbance sources—solar radiation and gravity gradient. Solar radiation generates a force normal to the panel at all times except during occultation. The force varies seasonally as the sun moves about and below the orbit plane. There is also a north-south force component, tangential to the array, which is a function of surface reflectivity. These forces are shown in Figure 1.1-4. Because the center of mass and center of solar pressure are separated in this asymmetric configuration, the solar forces generate disturbance torques.

Gravity gradient torques are produced whenever the principal axes of inertia are rotated out of alignment with the local vertical and local horizontal. The major contribution arises from the rotation of the array about the axis perpendicular to the orbit plane. This leads to a sinusoidal torque with a half-orbit period, Figure 1.1-5. A gravity gradient torque also occurs about the hinge line when the antenna points off the equator but the magnitude is negligibly small.

North-south the east-west stationkeeping are not considered, but it is assumed that the solar force must be continually compensated to prevent distortion of the orbit.

SPS-2336

Table 1.1-1 SPS Packaging Estimates

	PACKAGING DENSITY	HLLV FLIGHTS TO DELIVER SPS	VOLUME-LIMITED PENALTY, %
10 GW, REF. DESIGN	125 kg/m^3	415	0
5 GW, REF. DESIGN	125 kg/m^3	208	0
2.5 GW, ONE ANTENNA	42 kg/m^3	207	82%
5 GW, TWO ANTENNAS	42 kg/m^3	414	82%
2.5 GW, ONE ANTENNA, SSPA	77 kg/m^3	111	0
5 GW, TWO ANTENNA SSPA	77 kg/m^3	222	0

PACKAGING DENSITY INCLUDES SPS AND APPLICABLE ORBIT TRANSFER HARDWARE

SPS-2579

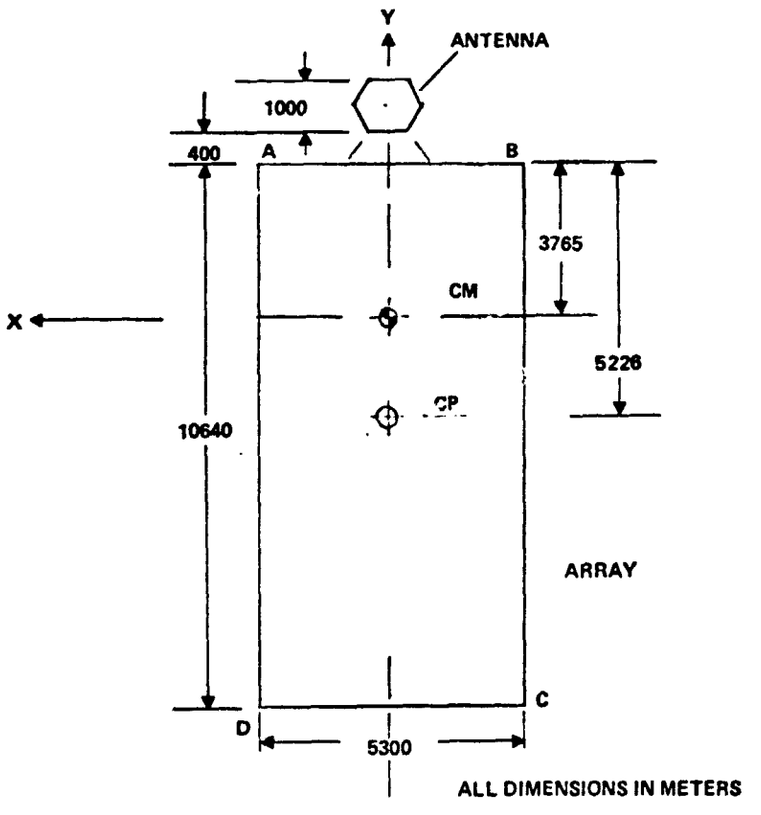

Figure 1.1-3 Spacecraft Geometry

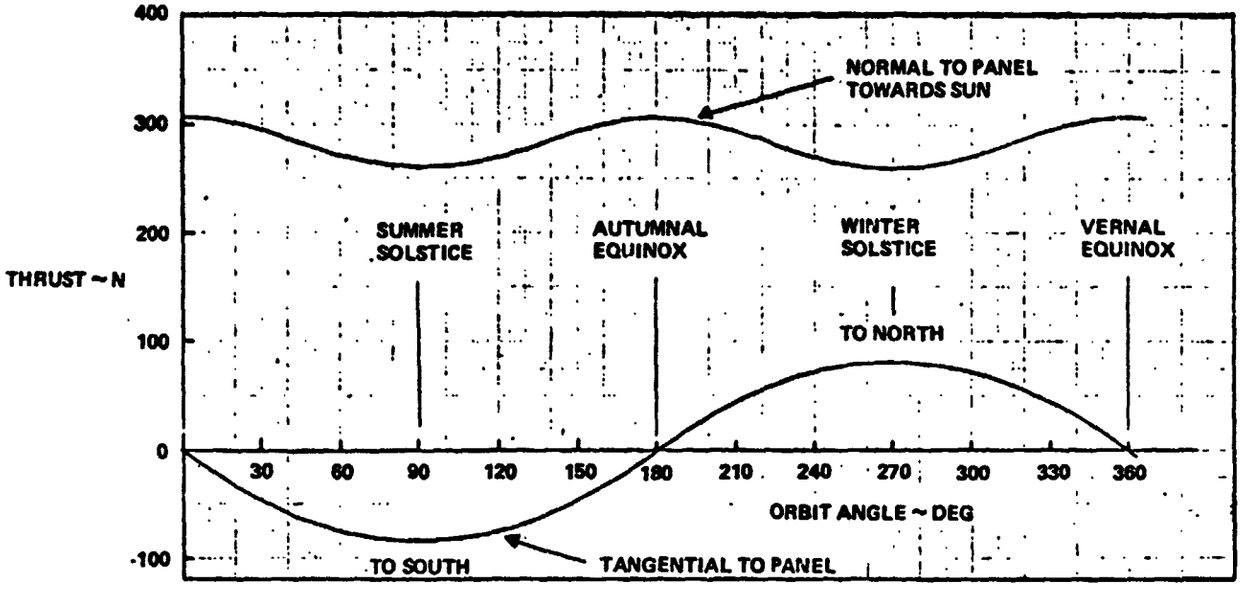

Figure 1.1-4 Seasonal Thrust Variation

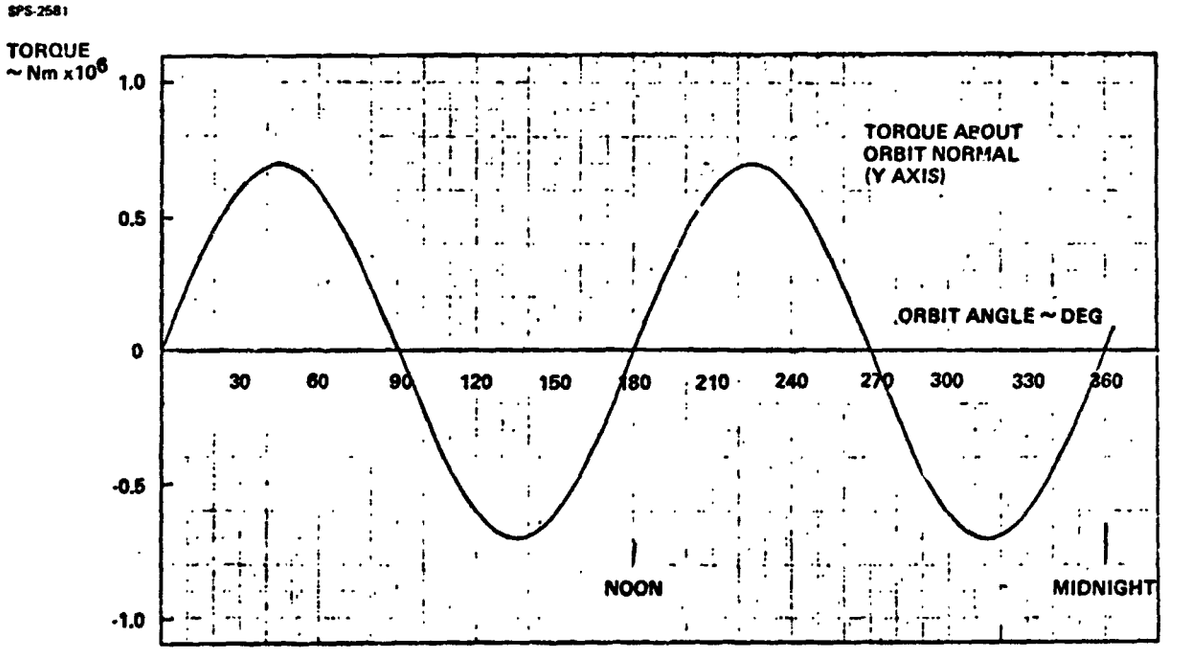

Figure 1.1-5 Daily Gravity Gradient Torque Variation

If this is done, it follows that no additional propellant is needed for attitude control. Control torques can be generated by increasing the thrust on one side of the vehicle and reducing it on the other while maintaining the total thrust equal and opposite to the solar force.

If the thruster clusters are designated A B C D, as was shown in Figure 1.1-3, the required thrusts are:

Normal to the array

A: $78.25 \cos^2 \quad + 65.70 \sin \frac{t}{6}$ N

B: $78.25 \cos^2 \quad - 65.70 \sin \frac{t}{6}$

C: $75.55 \cos^2 \quad - 65.70 \sin \frac{t}{6}$

D: $75.55 \cos^2 \quad + 65.70 \sin \frac{t}{6}$

Where $= 23.5 \sin \frac{2D}{365}$ deg.

D is the number of days from the vernal equinox, and

t = the local time in hours.

Maximum and minimum values of A and B are 143.95 and 0.11 N and of C and D, 141.25 and -2.16 N.

The mean thrust normal to the array is 282.7N and the mean thrust tangent to the array, 55.2N. The total yearly impulse is 1.066×10^{10}N sec which requires 54,330 Kg of propellant assuming a specific impulse of 20,000 sec.

Thrust values depend on the panel reflectivity. Coated cells have a generally accepted range of 0 to 0.3 and a value of 0.15 has been used above. Zero reflectivity would reduce the impulse to 0.980×10^{10}N sec (49,650 Kg of propellant) while a value of 0.3 would require 1.151×10^{10}N sec (58,700 Kg of propellant).

1.1.0.4 GENERAL SPS FLIGHT CONTROL STUDIES

Solar Power Satellite Control

Solar Power Satellite control encompasses a wide range of vehicle configurations with varying control requirements during the construction, transportation, and operation mission phases.

There are two basic control modes: (a) powered flight when thrust is being applied to produce a velocity increment (v) either for the purpose of maintaining orbit altitude, or changing from one orbit to another or for achieving and maintaining a specific location in a given orbit; (b) coasting flight which includes all other flight regimes.

The control requirements and criteria for each mission phase are discussed below. Included are a description of the currently preferred control concept and a comparison with other candidate approaches which were considered.

Altitude and Velocity Control During Construction

During the coasting periods, the construction base must be maintained in a stable attitude to permit rendezvous and docking of supply vehicles and to minimize internal forces which would result if the vehicle were allowed to tumble. Also, a constant relative earth orientation and a regular sun orientation will provide improved working conditions over those which would exist on a randomly rotating vehicle. Because a specific orientation is required during orbit-keeping operations, attitude maneuver propellant and time can be eliminated if this desired attitude is also maintained during coasting flight. The criteria for selecting a preferred attitude are listed below:

a. Aerodynamic drag should be minimized in order to reduce orbit make-up propellant.

b. Disturbance torques should be minimized in order to reduce attitude control propellant.

c. The orientation should be compatible with the selected orbit-keeping approach.

d. The orbit mechanics forces between the construction base and the module should be minimized to simplify the indexing mechanism design (minimize size, weight, and cost).

Edgewise orientation (that is with the plane of the collector module parallel to the orbit plane) is the obvious choice for one of the two alignment axes, because it minimizes drag, and it is a gravity-gradient stable orientation. The other alignment (module down or module forward) is not as easily determined. Items a) and b) do not provide a conclusive choice because the resulting preferred orientation changes during the construction process and also because the minimum drag orientation is not always the one which results in minimum gravity-gradient disturbance torque. Mutual compatibility with the orbit keeping concept is the major factor in selecting the preferred orientation and is discussed in the next paragraph.

The requirement and criteria for control during orbit-keeping ΔV operations are listed below:

a. The construction base must be capable of orbit-keeping by itself (when module-mounted thrusters are not available).

b. Even when module-mounted thrusters are available, it is preferable that orbit-keeping be achieved using facility-mounted thrusters only.

c. Plume impingement on the structure should be minimized.

d. To maximize efficiency (and minimize propellant requirements), a large component of thrust should be in the direction of the orbital velocity.

e. A fixed orientation of the thrusters is favored over gimbaling for reasons of improved cost, weight, and reliability.

f. Continuous burn is favored over pulsing operation if multiple starts have adverse effects on thruster failure rates. However, for non-gimbaled thrusters, on-off operation is required for attitude control unless there is a throttling capability.

g. An acceleration of 10^{-4} g is assumed. This value is based on a reasonable burn time.

Figure 1.1-6 shows the vehicle configuration for seven stages of construction. It is recognized that the configuration changes continuously during construction. The ones shown have been selected because they represent some of the extremes of configuration parameters such as mass, moment-of-inertia unbalance, c.g., location, principal axis orientation and aerodynamic drag. The selected concept must be capable of controlling all of these configurations.

A matrix of possible control approaches using fixed and gimbaled thrusters with fixed (module down and module forward) and variable attitudes is shown in Figure 1.1-7. Typical thruster locations and orientations are shown for each concept. Also shown are the c.g. locations taken from the seven representative configurations. Concept A shows the use of separate attitude control thrusters to offset the ΔV thruster unbalanced moment. This approach is not acceptable because the required attitude control thrust and propellant, for some c.g. locations, can exceed those for the ΔV thrust. In the module-forward attitude shown in Concept B, the ΔV thrusters can be located so that both positive and negative control moments can always be generated regardless of c.g. location. Furthermore, all of the propellant expended contributes to a positive velocity increment. This is the only fixed-attitude concept which does not have a large wasted side component of thrust. Concept C shows the approximate thruster location and orientation required to accommodate all predicted e.g., locations for the module-down orientation. Concepts E and F illustrate the large gimbal angles (and consequent inefficiency) for thrust vector control with a fixed vehicle attitude. Concepts D, G, and H show how efficiency is improved by rotating the vehicle so that the thrust vector, when pointing through the vehicle c.g. is also aligned with the orbital velocity vector. However, the time and propellant required to rotate the vehicle to the required attitude make this approach unacceptable.

Figure 1.1-8 shows the selected approach to attitude and velocity control of the construction base and spacecraft components during the LEO construction phase of the mission. Included are the design features and advantages of the concept. The average orbit-keeping propellant required is 1200 kg per day for this configuration (assumed I_{sp} = 400 sec).

Figure 1.1-9 is a summary of the computed orbit maintenance parameter values and resulting propellant requirements. Burn times for both constant thrust and constant acceleration modes are given.

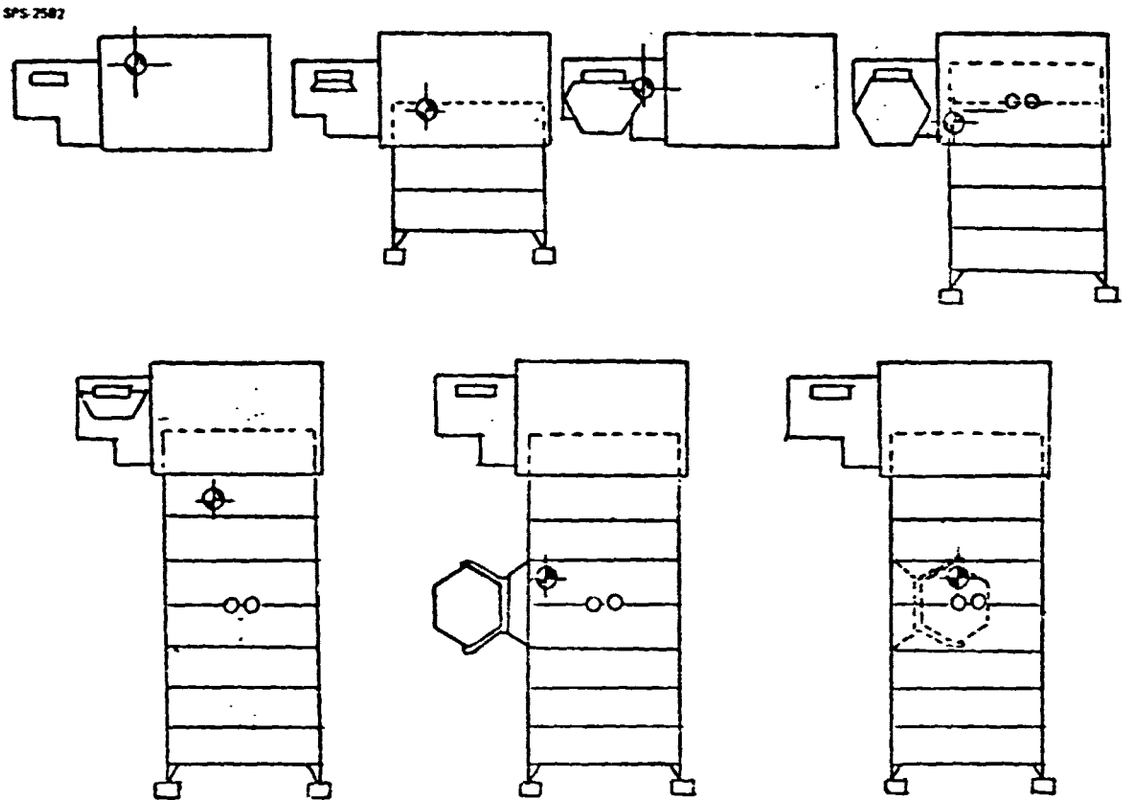

Figure 1.1-6 Typical Construction-Phase Configurations

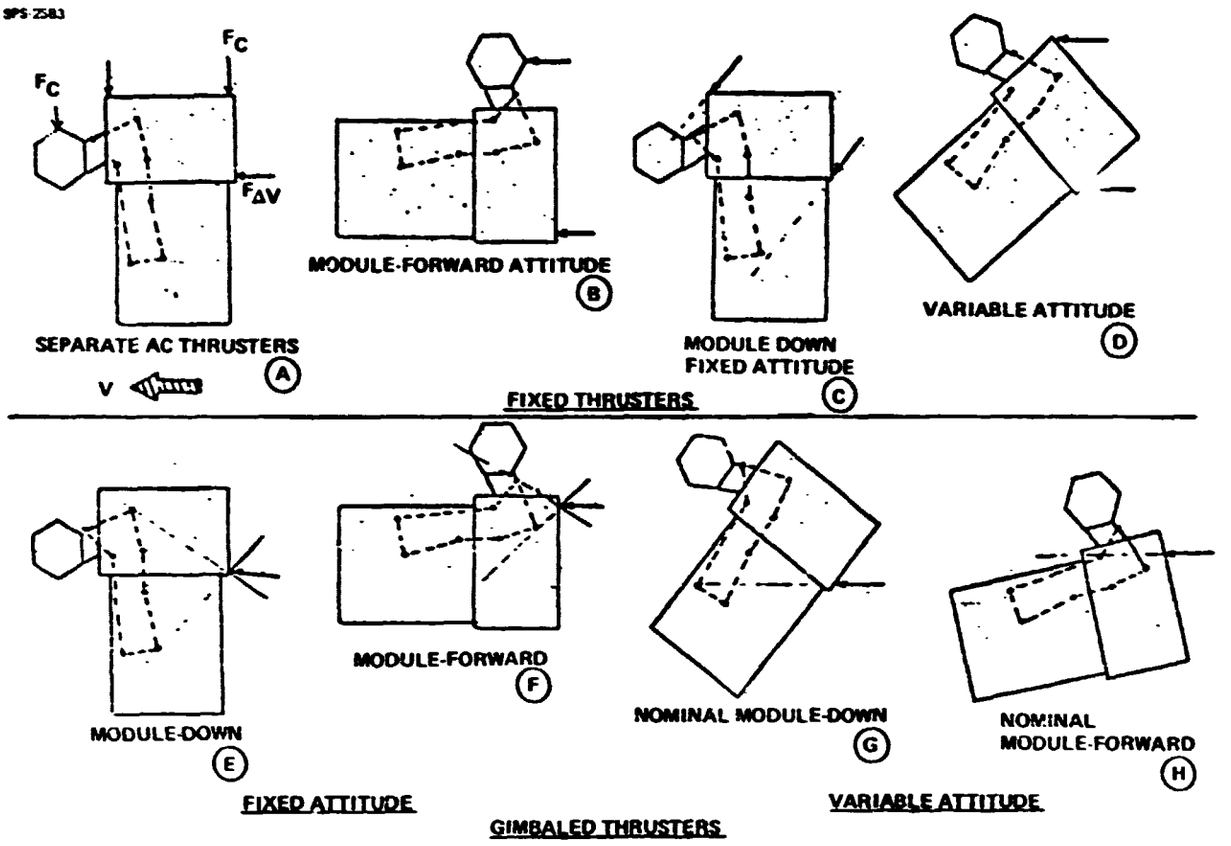

Figure 1.1-7 Orbit-Keeping Control Using Facility-Mounted Thrusters Only

SPS-2584

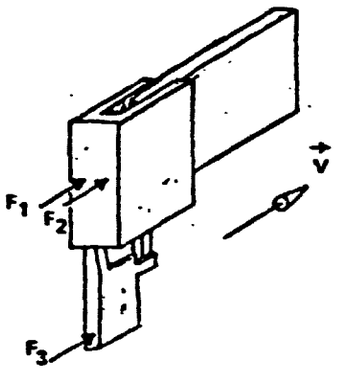

NOTES:
- LATERAL LOCATION OF F_1 & F_2 SELECTED TO MINIMIZE BASE STRUCTURAL DEFLECTIONS
- VERTICAL POSITION AND/OR THRUST MAGNITUDE BASED ON PREDICTED CG LOCATIONS

ADVANTAGES OF SELECTED DESIGN

- 100% EFFICIENT ΔV THRUSTING
- NO THRUST GIMBALING REQUIRED
- GRAVITY-GRADIENT STABILITY:
  - UNCONDITIONALLY STABLE ≈ 2/3 OF TIME
  - UNSTABLE EQUILIBRIUM ≈ 1/3 OF TIME
- LOWEST DRAG FOR HEAVY CONFIGURATIONS
- POSSIBLE COMMON LOCATION FOR ATTITUDE CONTROL AND ΔV THRUSTERS
- ATTITUDE CONTROL PROPELLANT CONTRIBURES TO POSITIVE ΔV
- ORBIT MECHANICS FORCES BETWEEN BODIES MINIMIZED
- "VELOCITY VECTOR" APPROACH CAN BE USED FOR DOCKING OF SUPPLY VEHICLES

Figure 1.1-8 Orbit-Keeping ΔV Approach

SPS-2585

CONFIG	MASS (kg)	M/A (kg/m^2)	$\partial R/\partial t$ (kg/day)	$\partial V/\partial t$ (m/sec/day)	Wp PER DAY (kg) ▷	CONSTANT THRUST (5690 N)		CONSTANT ACCEL. (10^{-4} g)	
						ACCEL. (g)	BURN TIME (min)	THRUST (N)	BURN TIME (min)
I	5.8×10^6	15.8	0.95	.528	780	1×10^{-4}	9	5690	9
II	14.4×10^6	28.9	0.525	.292	1072	$.4 \times 10^{-4}$	12.3	14 126	5
III	24.6×10^6	34.3	0.44	.245	1536	$.24 \times 10^{-4}$	17.7	24 133	4.2
IV	38.2×10^6	65.3	0.233	.129	1256	$.15 \times 10^{-4}$	14.4	37 474	2.2
V	41.5×10^6	58	0.257	.143	1512	$.14 \times 10^{-4}$	17.3	40 712	2.43
VI	41.5×10^6	58	0.257	.143	1512	$.14 \times 10^{-4}$	17.3	40 712	2.43
VII	17.2×10^6	46.9	0.345	.192	841	$.337 \times 10^{-4}$	9.7	16 873	3.3

$\frac{\partial V}{\partial r}$ = .556 m/sec/km at h = 478 km ▷ ASSUMES THRUSTING ALONG $\vec{V}$ AND I_{SP} = 400 SEC.

Figure 1.1-9 Orbit Maintenance Parameters

Orbit Transfer

The required velocity increment must be provided while maintaining a sun orientation for self-power. During the early part of this phase, the offsetting of gravity-gradient disturbance torques requires a large portion of the available thrust. Chemical propulsion is used during occultation periods. The control loop design must provide safe stability margins for structural coupling effects. Such techniques as multiple sensors, multiple thrusters, and digital signal processing will be used in control algorithm development.

Geosynchronous Orbit Operations

Velocity control is required to maintain orbit station by offsetting solar pressure and orbital drift toward the neutral point. Attitude control is required to provide Sun orientation of the collector and high accuracy Earth rectenna pointing of the two antennas. In addition to countering the gravity-gradient disturbance torques, the control concept must avoid unstable interaction of the antenna and collector control loops and the structural flexibility effects. The current baseline approach for collector control makes use of multiple thrusters providing a total force equal to the solar pressure. Individual thrusters are modulated above or below their bias level to provide the control torques needed to offset gravity-gradient disturbance torques. In essence, there is no additional propellant penalty for collector attitude control. The basic features of this concept are illustrated in Figure 1.1-10. Single axis (pitch) rigid body control only is shown. Thruster location will be at the nodal points of one of the lower modes to minimize excitation of that particular flexible mode. Active damping of other modes will be achieved by superimposing additional thrust modulation signals on the attitude control thrust level commands. These signals are derived from the outputs of multiple rate sensors which are processed to isolate the rigid body and lower bending mode components of motion.

Because of the fine pointing requirement, the antenna is controlled in free-floating gimbals as if it were a separate body. The conventional approach of gimbal torqueing would result in undesirable coupling of the antenna and the collector (rigid body and flexible) motions through the rigidized gimbals. The selected approach also avoids gimbal torquer design and reliability problems. To point toward rectennas in the Northern Hemisphere requires an antenna boresight pointing offset of as much as 8.6 degrees from nadir. This results in a continuous, unidirectional gravity-gradient disturbance torque on the antenna about the elevation gimbal axis. In adition, if

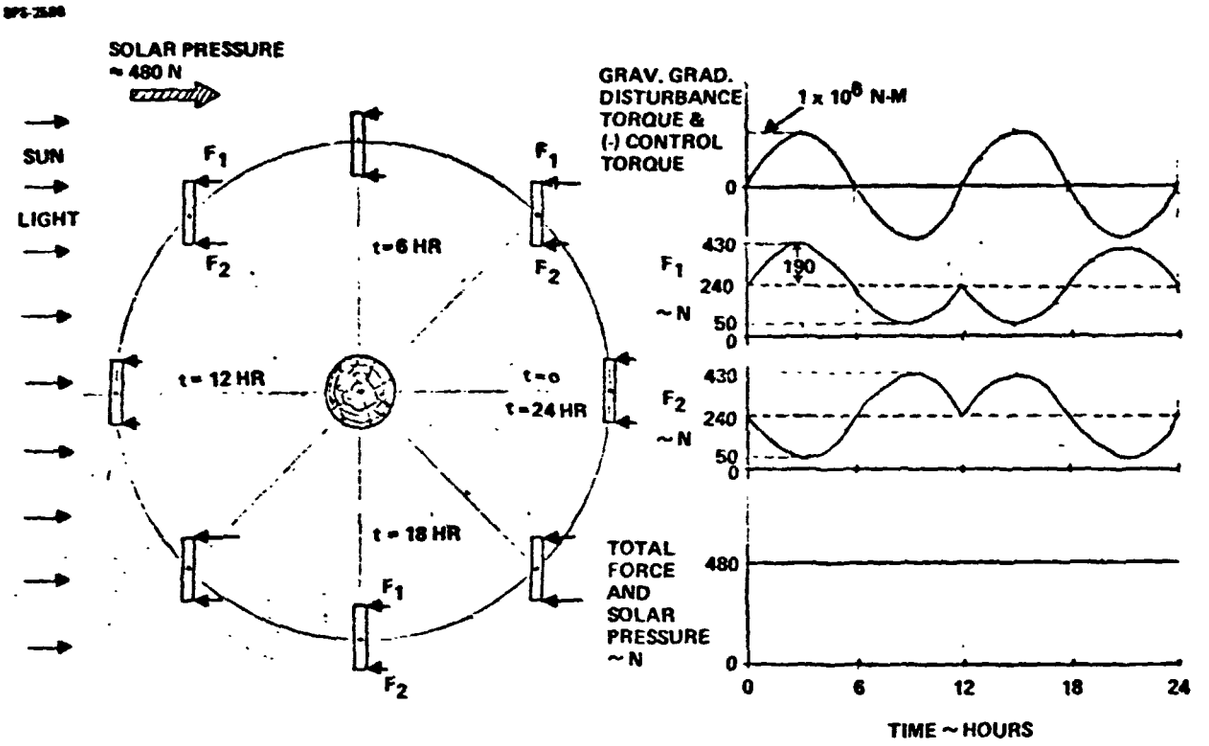

Figure 1.1-10 Operational (GEOSYNC) Orbit– Combined Attitude and Station Control

there is a requirement to point toward rectennas at different longitudes, a similar torque is experienced about the azimuth gimbal axis. The gravity-gradient torque can be reduced or eliminated by mass balancing to make all three principal moments of inertia equal. A large mass mounted on a long boom parallel to the boresight axis (out the back side of the antenna) is required. If the boom length (or tip mass) is further increased and the boom angle made adjustable, the gravity-gradient torque can be used for positive active attitude control. However, the boom length and tip mass required are very large. Other candidate concepts for antenna control are: ion propulsion reaction control, reaction wheels, control-moment gyros (cmg's) and electromagnetic torquing against the Earth's magnetic field. The current baseline uses cmg's because of their fine resolution, high reliability (for redundant systems) and long life. Because of the unidirectional torques, the cmg's will eventually become saturated. Periodic desaturation is accomplished by gimbal torquing against the collector.

The antenna and collector control loops are coupled through the gimbal bearing and slip-ring friction and by the inertial reaction resulting from any antenna cg offset from the gimbal axes. Design requirements should specify the smallest practical values for these parameters. Computer simulations will be required for design analysis and verification of the control concepts. The effects on stability margins of off-nominal values of design parameters must be assessed. Figure 1.1-11 is a simplified block diagram which illustrates how the structural flexibility modes are coupled to the rigid body control loop through the control sensors. It also shows how the antenna control loop is coupled through the mass unbalance and gimbal friction effects.

SPS Antenna Control

Antenna gimbal torquing results in a reaction moment on the collector even for a perfectly balanced antenna. If the antenna c.g. is offset from the gimbal axis, there is an additional reaction force at the gimbal point. These forces and moments excite the collector structural modes and appear as disturbances to the collector attitude control. This coupling can be reduced significantly by using "free floating" gimbals and generating the control torques within the antenna itself. (However the antenna mass unbalance reaction forces will not be eliminated.) Trades of control-moment gyros (cmg's), inertia wheels, reaction control thrusters and geo-magnetic torquing have resulted in the tentative selection of multiple, antenna-mounted cmg's to generate control torques. Because of the unidirectional gravity-gradient disturbance torque,

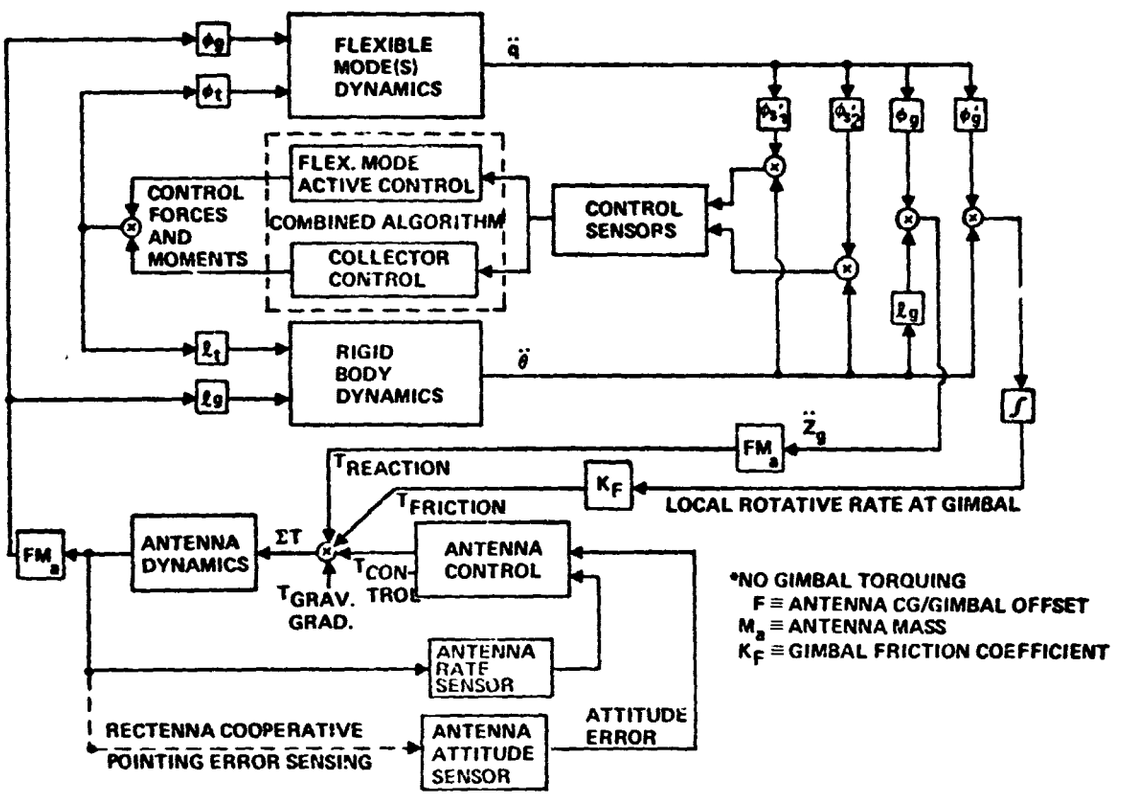

*Figure 1.1-11 Collector and Antenna Attitude Control Simplified Block Diagram (Free-Floating, Self-Controlled Antenna)**

the cmg's will, in time, become saturated. It is proposed that periodic or continuous cmg desaturation be accomplished by antenna gimbal torquing against the collector. A scheme for accomplishing this while retaining the decoupling feature, to the maximum extent possible, is described in the paragraphs which follow.

The baseline hybrid control concept shown in Figure 1.1-12 uses antenna-mounted control-moment gyros (cmg's) for fine resolution, high frequency control and uses antenna gimbal torquing against the collector to desaturate the cmg's. The gimbal torquing mechanism, in effect, counteracts the steady unidirectional gravity-gradient torque while the cmg's compensate for base motion effects caused by structural flexibility, and collector attitude stabilization. The block diagram shows how these two torque-producing elements can be combined to provide the desired control characteristics.

The antenna gimbal servo loop is not closed directly with the antenna pointing error but indirectly with a cmg "degree-of-saturation" signal. The optional switch can be included if continuous desaturation is not desired. The non-linear gain characteristic and the low-pass filter prevent the gimbal actuator from responding to small-amplitude, high-frequency antenna oscillations caused by structural flexiblity effects. This decoupling of the antenna pointing control, collector attitude stabilization and collector flexibility effects enhances system stability and is a key feature of this approach. The system will settle at an operating point on the gain curve where the antenna gimbal torque just balances the gravity-gradient disturbance torque.

The cmg loop features "proportional-plus-integral" control. By including the integral of the pointing error in the control torque command signal, the system can produce a torque to offset the disturbance without requiring a "hang-off" attitude error. This allows the attitude error to go to zero, a condition which could otherwise be realized only by making the position gain ($K_{\ }$) infinitely large.

A similar arrangement can be used for antenna azimuth control. In addition to the gravity-gradient disturbance torque which results when offset pointing from nadir is required, there is a continuous unidirectional brush/slip-ring torque to be overcome.

The discussion thus far has considered the antenna as a rigid body. The baseline design, consisting of a deep structure of graphite epoxy composite material provides

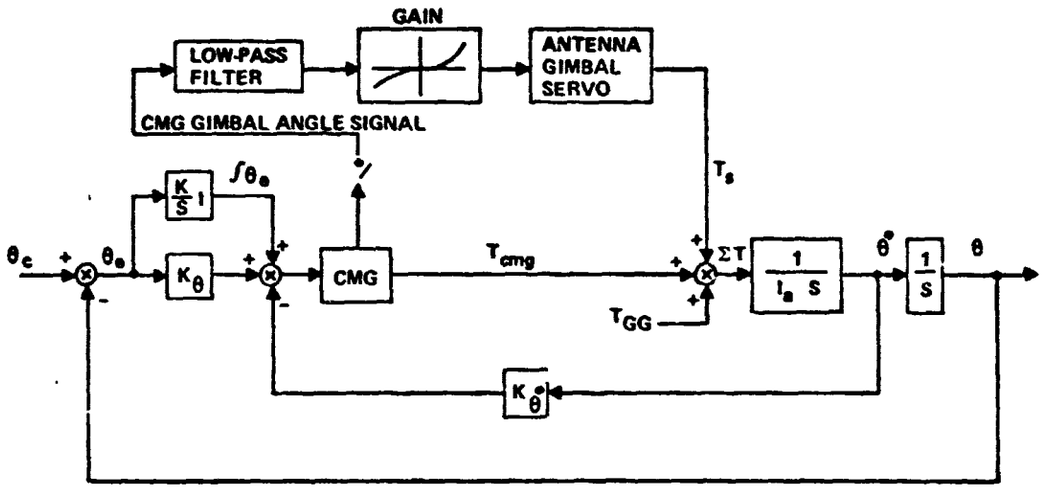

Figure 1.1-12 SPS Antenna Pointing Control

a stiff configuration with minimal thermal distortion. Active control of the antenna figure, therefore, is not considered to be required at this time. The control/structural coupling interaction is minimized in the selected control approach because the high frequency torques are produced by multiple cmg's distributed throughout the antenna structure, and gimbal torques are applied very gradually. This results in smaller control-induced structural deflections. The problems of sensor location and signal processing to provide adequate control-loop stability margins will be analyzed when antenna structural properties are more clearly defined.

1.1.0.5 SPS INTERNALLY-GENERATED ELECTROMAGNETIC INTERFERENCE

Examination of the SPS configuration resulted in the following as the most probable internal sources of high EMI:

High voltage switch gear	Inrush currents
Slip rings	70 KW klystrons
Corona effects	DC/DC converters

Very preliminary consideration of these sources in order to select one for analysis indicated that the corona effects and inrush current were likely to be less severe sources than the others. The high voltage switch gear was not selected since there will be no disconnect operations on energized lines. The slip rings and 70 KW klystrons were not selected because of lack of data on equipment of the size under consideration for SPS.

The 5.5 megawatt DC/DC converters were selected for analysis since some information is available on their design, they are a continuous as opposed to intermittent source and it was considered that extrapolation of data from a 3 KW converter was reasonably valid since the same switching techniques will probably be used.

The following information and assumptions were used for this assessment:

- Input Voltage = 38.2 KW
- Input Current = 135 A
- Switching Frequency = 20 KHz
- Filters will limit ripple to 1%
- Switching will be by SCR's

- Power busses are made of 1 mm thick aluminum sheets of different widths and lengths
- The satellite structure is of graphite epoxy
- Converters connected to the same bus will be synchronized such that their switching pulses are not coincident with each other.

Photographic data currently available shows that the current waveform is a series of cosine pulses and that the voltage waveform is a series of irregular pulses that can be crudely approximately by a triangular pulse. These data do not show the attenuation effects of a power line filter; however, EMI test data shows that spectral line amplitudes are generally less than 1% of the rated input current. Using this as a basis for the emissions from a 5.5 megawatt converter, the following assumptions result:

- The current spectrum will be spectral lines having an amplitude of 1.35 A at 20 KHz, declining in amplitude at a rate of 40 dB per decade for even harmonics, with suppressed odd harmonics.

- The voltage spectrum will be spectral lines having an amplitude of about 380 volts at 20 KHz, declining in amplitude at a rate of 40 dB per decade for odd harmonics, with suppressed even harmonics.

These values were used to calculate the E- and H-fields near the power bus conductors. Since the current distribution across the bus at high frequency is only known very generally, a very simplified approach was taken, whereby the 5-meter and 17-meter sheets were replaced by imaginary conductors separated by 18.9 meters (a circular arc with a radius equal to half the distance between the centers of the conducting sheets). The voltage difference was taken as 1% of the bus voltage, i.e., 380 volts. The mean electric field at a distance of 6 meters (the approximate radius of the arc) would then be approximately 20 volts/meter at 20 KHz, declining at higher frequencies. Current equipment must be designed for 10 volts/meter from 14 KHz to 35 MHz.

In a similar manner (i.e., greatly simplified) the mean magnetic field at a distance of 6 meters is approximately 36 milliamperes/meter at 20 KHz, declining at higher frequencies. The current requirement on equipment is 2.6 microamperes per meter.

The common resistance interference effects were not calculated due to lack of detailed information on the power distribution system lumped resistances configurations.

These EMI effects will result in modulation of the power beam baseband signal unless appropriate measures are taken in the design of the transmitter and power supply systems.

1.1.0.6 SPS EQUIPMENT FAILURE MODES, RATES, AND EFFECTS ANALYSIS

An analysis was performed to 1) define SPS hardware failure modes, 2) predict equipment filaure rates, and 3) determine the effects on SPS system operation and ground power output. Table 1.1-2 presents the results of the analysis.

FAILURE RATES

Previous reliability analysis performed during the study effort of contract NAS-15196 showed that a potential reliability problem existed with the solar blanket design. The problem occurred because lengthy series-parallel strings (4 parallel by 130,000 in series) would experience total string failure if, for any of the 130,000 sets of 4 parallel cells, two of the four cells failed causing the remaining two cells to be reversed biased with their subsequent failure. The revised blanket design of fourteen cells in parallel allows for failure of 4 of the 14 cells to fail without total string failure. As a result, the expected total number of cell string failures for a ten gigawatt satellite is approximately 0.01 per year. With a mean time between failures (MTBF) of 10^8 hours for the solar cell/interconnect combination, approximately 0.3% of the cells are predicted to fail over a thirty year period, but with no predicted total string failures.

The power generation portion of the satellite contains large numbers of identical components such as solar cells, blanket tensioning devices, blanket support cables, and conductors for connecting the solar arrays between bays. When predicting total failures using the traditional exponential reliability predictions, and predicted number of annual failures is quite large. Annual failure rates for non-series elements were computed

$$N_F = N(1-e^{t})$$

where

N_F = number of equipment item failures per year

N = total number of the equipment items on the SPS

= 1/mean time between failures (hours)

t = 8766 hours/year (365.25 x 24)

The mean time between failures data was obtained from Boeing's Experience Analysis Center which provides a data bank of reliability and maintenance information from aircraft, missiles, spacecraft, ships, and ground equipment. The predicted number of failures for the power generation portion of the satellite is large but has negligible effects on the power output because of redundance and/or satellite oversizing. Table 1.1-2 summarized the SPS elements which will have the highest total number of failures Table 1.1-3 provides a detailed listing. The primary failure mode of the blanket tensioning devices is breakage of the tensioning spring. However, the device is designed to have a positive stop in the event of a spring failure so that attachment of the array blanket is not totally lost.

The effects of satellite failures on the ground output power are summarized in figure 1.1-3. The primary contributors to power loss due to failures are the antenna mounted DC to DC converter switchgear and RF to DC converters. Though not shown in this sumary, there are certain failures of satellite systems which can cause total loss of an antenna power output. Amoung these are certain rotary joint failures which would prohibit antenna rotation. For the mechanical portion of the rotary joint redundant drive systems are provided as well as provisions for disabling frozen drive systems. Redundance in the electrical slip ring assembly is provided by multiple brush assemblies operating at low (approximately 10 amperes per square centimeter) current densities. In addition, provisions for retracting the brush assembly are provided.

Table 1.1-2 SPS Satellite Failure Summary—10 GW SPS

WBS	NOMENCLATURE	QUANTITY/SPS	FAILURES/YR.
1.1	ENERGY CONVERSION		
1.1.1.1.4	BLANKET TENSIONING DEVICES	337,920	325
1.1.1.3.2	BLANKET MECHANICAL ATTACHMENT	337,920	658
1.1.1.4.5	CELL STRING BLOCKING DIODES	19,072	7
1.1.2	POWER TRANSMISSION		
1.1.2.2.1	RF/DC CONVERTER MODULE	203,104	7,934
1.1.2.3.2	SWITCHGEAR	912	9
1.1.2.3.3	DC/DC CONVERTER	456	24
1.1.2.3.4	DISCONNECT SWITCHES	912	3
1.1.2.4.2	DC/DC CONVERTER THERMAL CONTROL	456	4
1.1.2.5	PHASE CONTROL	203,568	
1.1.2.5.1	RECEIVERS	203,568	4
1.1.2.5.2	DIPLEXERS	203,568	2
1.1.2.5.3	PHASE TRANSMITTERS	220,408	29
1.1.2.5.4	PHASE RECEIVERS	220,408	4
1.1.2.5.5	CONJUGATORS	203,568	33
1.1.2.5.6	CABLING	218,888	25

Table 1.1-3 SPS Satellite Failure Analysis—Detailed Results

WBS ELEMENT	EQUIPMENT NOMENCLATURE	FAILURE MODE	POWER LOSS PER FAILURE (KW)	MTBF (HRS)	QUANTITY PER SPS	TOTAL FAILURES PER YEAR	ANNUAL POWER LOSS (KWH)	COMMENTS
1.0	SOLAR POWER SATELLITE							
1.1	SATELLITE							
1.1.1	ENERGY CONVERSION							
1.1.1.1	STRUCTURE							
1.1.1.1.1	PRIMARY STRUCTURE							
1.1.1.1.2	SUPPORT STRUCTURE							
1.1.1.1.3	BLANKET SUPPORT CABLES				22,528			
1.1.1.1.4	BLANKET TENSIONING DEVICES	SPRING FAILURE	NEG	9.1×10^6	337,920	325	NEG	
1.1.1.1.5	POWER DISTRIBUTION SUPPORT							
1.1.1.2	CONCENTRATORS							
1.1.1.3	SOLAR BLANKET							
1.1.1.3.1	BLANKET PANELS	NO CELL STRING OUTPUT		[1]	19,072	0.01		[1]
1.1.1.3.2	BLANKET MECHANICAL ATTACHMENTS	BROKEN	NEG	4.5×10^6	337,920	6.58	NEG	
1.1.1.3.3	INTERBAY JUMPER WIRES	OPEN		2.0×10^9	190,720	1	NEG	
1.1.1.4	POWER DISTRIBUTION AND SWITCHGEAR							
1.1.1.4.1	MAIN POWER BUSES	OPEN		2.0×10^9	6	–	NEG	
1.1.1.4.2	ACQUISITION POWER BUSES	OPEN		2.0×10^9	768	–	NEG	
1.1.1.4.3	SWITCHGEAR	FAILURE TO OPERATE		8.7×10^5	206	2	NEG	[2]
1.1.1.4.4	DISCONNECT SWITCHES	INTERMITTENT OR OPEN		2.3×10^6	412	2	NEG	[2]
1.1.1.4.5	BLOCKING DIODES	OPEN		2.3×10^7	19,072	7	NEG	[3]
1.1.1.4.6	INTERCONNECT CABLING	OPEN		2.0×10^9	768	–	–	
1.1.1.4.7	DC/DC CONVERTERS	FAIL TO REGULATE OR NO OUTPUT	NEG	1.62×10^5	14	1 2	NEG	
1.1.1.4.8	ENERGY STORAGE							
1.1.1.5	THERMAL CONTROL							
1.1.1.5.1	SWITCHGEAR THERMAL CONTROL				768			
1.1.1.5.2	CONDUCTOR THERMAL CONTROL							
1.1.1.5.3	DC/DC CONVERTER THERMAL CONTROL	FAIL TO OPERATE	NEG	1.1×10^6	14		NEG	[4]
1.1.1.5.4	THERMAL CONTROL SURFACES							
1.1.1.5.5	ATTITUDE CONTROL SYSTEM THERMAL CONTROL				14			
1.1.1.5.6	AVIONICS THERMAL CONTROL							
1.1.1.6	MAINTENANCE							
1.1.1.6.1	SOLAR ARRAY ANNEALER				8			
1.1.1.6.2	MAINTENANCE GANTRY				8			
1.1.1.6.3	GANTRY TRACKS							
1.1.1.6.4	CREW PROVISIONS							
1.1.1.6.5	CARGO HANDLING							
1.1.1.6.6	DOCKING SYSTEMS							
1.1.2	POWER TRANSMISSION							
1.1.2.1	STRUCTURE							
1.1.2.1.1	PRIMARY STRUCTURE							
1.1.2.1.2	SECONDARY STRUCTURE							
1.1.2.1.3	SUPPORT STRUCTURE							
1.1.2.1.4	SUBARRAY POSITIONING	FAIL TO OPERATE						
1.1.2.1.5	POWER DISTRIBUTION SUPPORT							

Table 1.1-3 SPS Satellite Failure Analysis—Detailed Results (continued)

WBS ELEMENT	EQUIPMENT NOMENCLATURE	FAILURE MODE	POWER LOSS PER FAILURE (KW)	MTBF (HRS)	QUANTITY PER SPS	TOTAL FAILURES PER YEAR	ANNUAL POWER LOSS (KWH)	COMMENTS
1.1.2.2	TRANSMITTER SUBARRAYS				14,440			
1.1.2.2.1	DC/RF CONVERTER MODULE	FAIL TO OPERATE		2.2×10^5	203,104	7,934	3,424	5
1.1.2.2.2	DISTRIBUTION WAVEGUIDE				406,208			
1.1.2.3	RADIATING WAVEGUIDE				1,732,800			
1.1.2.4	THERMAL CONTROL				14,440	–		
1.1.2.5	WIRING HARNESS	OPEN IN A CONDUCTOR		2×10^9	14,440			
1.1.2.6	CONTROL CIRCUITS				203,104			
1.1.2.7	STRUCTURE							
1.1.2.3	POWER DISTRIBUTION AND CONDITIONING							
1.1.2.3.1	POWER CONDUCTORS	OPEN		2.0×10^9	54			
1.1.2.3.2	SWITCHGEAR	FAIL TO OPERATE		8.7×10^5	912	9	1,730	5
1.1.2.3.3	DC/DC CONVERTERS	FAIL TO REGULATE OR NO OUTPUT		1.62×10^5	456	24	4,614	
1.1.2.3.4	DISCONNECT SWITCHES	INTERMITTENT OR OPEN CONTACT		2.3×10^6	912	3		
1.1.2.3.5	ENERGY STORAGE		NEG	2.1×10^6				
1.1.2.4	THERMAL CONTROL							
1.1.2.4.1	THERMAL CONTROL SURFACES							
1.1.2.4.2	POWER PROCESSING THERMAL CONTROL	FAIL TO OPERATE		1.1×10^6	456	4	769	5
1.1.2.4.3	INSULATION							
1.1.2.4.4	CONTROL CIRCUITS THERMAL CONTROL							
1.1.2.4.4	CONTROL CIRCUITS THERMAL CONTROL							
1.1.2.4.5	MECHANICAL POINTING THERMAL CONTROL				24			
1.1.2.5	CONTROL							
1.1.2.5.1	RECEIVERS	FAIL TO OPERATE		5×10^8	203,568	4	2	5
1.1.2.5.2	DIPLEXERS	FAIL TO OPERATE		1×10^9	203,568	2	1	
1.1.2.5.3	PHASE TRANSMITTERS	NO OUTPUT		6.7×10^7	220,408	29	13	
1.1.2.5.4	PHASE RECEIVERS	FAILS TO RECEIVE		5×10^8	220,408	4	2	6
1.1.2.5.5	CONJUGATORS	NO OUTPUT		5.4×10^7	203,568	33	14	
1.1.2.5.6	CABLING	OPEN/SHORTED		7.8×10^7	218,888	25	11	
1.1.2.5.7	POWER DIVIDER	FAIL TO OPERATE		1×10^9	7,643	–	43	
1.1.2.5.8	SWITCHES	FAIL TO OPERATE		5×10^7	1,180	–		
1.1.2.6	MAINTENANCE							
1.1.2.6.1	MAINTENANCE GANTRIES				44			
1.1.2.6.2	GANTRY TRACKS							
1.1.2.6.3	DOCKING PORTS				4			
1.1.2.6.4	CARGO HANDLERS				4			
1.1.2.6.5	CREW BUSES							
1.1.2.6.6	CREW WORK STATIONS							
1.1.2.7	ANTENNA MECHANICAL POINTING							
1.1.2.7.1	CMG'S		NEG		24			
1.1.2.7.2	CMG DRIVES	NO DRIVE TORQUE	NEG	4.8×10^5	24	–	–	
1.1.2.7.3	CMG CONTROL CIRCUITS	NO DRIVE CONTROL	NEG		24			
1.1.3	INFORMATION MANAGEMENT AND CONTROL							
1.1.3.1	TRANSDUCERS							
1.1.3.2	SIGNAL CONDITIONERS							
1.1.3.3	DATA ACQUISITION/ MANAGEMENT							

Table 1.1-3 SPS Satellite Failure Analysis—Detailed Results (continued)

WBS ELEMENT	EQUIPMENT NOMENCLATURE	FAILURE MODE	POWER LOSS PER FAILURE (KW)	MTBF (HRS)	QUANTITY PER SPS	TOTAL FAILURES PER YEAR	ANNUAL POWER LOSS (KWH)	COMMENTS
1.1.3.4	CENTRAL COMPUTERS				3			
1.1.3.5	CONTROL CIRCUITS							
1.1.3.6	SIGNAL ROUTING							
1.1.3.7	SOFTWARE							
1.1.3.8	INTRA-SATELLITE VOICE							
1.1.4	ATTITUDE CONTROL AND STATION KEEPING							
1.1.4.1	SENSORS	NO OUTPUT	NEG					
1.1.4.2	ELECTRIC PROPULSION							
1.1.4.2.1	THRUSTERS	NO THRUST	NEG	1.5×10^7	160			7
1.1.4.2.2	PROPELLANT							
1.1.4.2.3	TANKAGE				4			
1.1.4.2.4	PROPELLANT DELIVERY				4			
1.1.4.2.5	CONTROLS							
1.1.4.3	CHEMICAL PROPULSION							
1.1.4.3.1	THRUSTERS/ENGINES	NO THRUST	NEG					
1.1.4.3.2	PROPELLANTS							
1.1.4.3.3	TANKAGE				4			
1.1.4.3.4	PROPELLANT DELIVERY				4			
1.1.4.3.5	CONTROLS							
1.1.4.4	GIMBALS				4			
1.1.5	COMMUNICATIONS							
1.1.5.1	SATELLITE TO EARTH							
1.1.5.1.1	RECEIVERS	NO OUTPUT	NEG	1.1×10^5	3	–		
1.1.5.1.2	TRANSMITTERS	NO OUTPUT	NEG	1.1×10^5	3	–		
1.1.5.1.3	ANTENNAS	SHORT OR OPEN	NEG		6			
1.1.5.1.4	SIGNAL INTERFACE	NO DATA TRANSFER	NEG	7.8×10^5	3			
1.1.5.1.5	CABLING	OPEN	NEG	2.0×10^9				
1.1.5.2	GEO OPERATIONS COMMUNICATIONS							
1.1.5.2.1	RECEIVERS	NO OUTPUT	N/A	1.1×10^5	3	–		
1.1.5.2.2	TRANSMITTERS	NO OUTPUT	N/A	1.1×10^5	3	–		
1.1.5.2.3	ANTENNAS	SHORT OR OPEN	N/A		6			
1.1.5.2.4	SIGNAL INTERFACE	NO DATA TRANSFER	N/A	7.8×10^5	3			
1.1.5.2.5	CABLING	OPEN	N/A					
1.1.6	INTERFACE (ENERGY CONVERSION/POWER TRANSMISSION)							
1.1.6.1	STRUCTURE							
1.1.6.1.1	PRIMARY STRUCTURE							
1.1.6.1.2	SUPPORT STRUCTURE							
1.1.6.1.3	CABLES				24			
1.1.6.2	MECHANISMS							
1.1.6.2.1	MECHANICAL [illegible]ARY JOINT				2			
1.1.6.2.1.1	DRIVE RING				2			
1.1.6.2.1.2	DRIVE MECHANISMS	NO DRIVE	NEG		24			8
1.1.6.2.1.3	DRIVE MOTORS	NO DRIVE TORQUE	NEG	1.1×10^6	24	–		9
1.1.6.2.1.4	DRIVE CONTROL CIRCUITRY	NO DRIVE CONTROL		1.1×10^5	24	2		10
1.1.6.2.2	ELEVATION JOINT							
1.1.6.2.2.1	ELEVATION DRIVE				4			
1.1.6.2.2.2	DRIVE MECHANISMS	NO DRIVE	NEG		4			
1.1.6.2.2.3	DRIVE MOTORS	NO DRIVE TORQUE	NEG	1.1×10^6	8	–		9
1.1.6.2.2.4	DRIVE SUSPENSION				2			
1.1.6.2.2.5	DRIVE CONTROL CIRCUITRY	NO DRIVE CONTROL	NEG	1.1×10^5	8	1	NEG	10

Table 1.1-3 SPS Satellite Failure Analysis—Detailed Results (continued)

WBS ELEMENT	EQUIPMENT NOMENCLATURE	FAILURE MODE	POWER LOSS PER FAILURE (KW)	MTBF (HRS)	QUANTITY PER SPS	TOTAL FAILURES PER YEAR	ANNUAL POWER LOSS (KWH)	COMMENTS
1.1.6.2.3	POWER DISTRIBUTION							
1.1 6.2.3.1	SLIP RINGS				6			
1.1.6 2.3.2	BRUSH ASSEMBLIES	NO CURRENT FLOW	NEG	5.8×10^5	80	1	NEG	
1.1.6.2.3.3	FEEDERS	OPEN	NEG	2.0×10^9	96	–		
1.1.6.2.3.4	INSULATORS	SHORTED			272	–		
1.1.6 2.3.5	POWER BUSES	OPEN			18			
1.1.6.2.4	THERMAL CONTROL							
1.1.6.2.4.1	MECHANICAL ROTARY JOINT THERMAL CONTROL				24			
1.1.6.2.4.2	ELEVATION JOINT THERMAL CONTROL				8			
1.1.6.2.4.3	SLIP RING THERMAL CONTROL							
1.1.6.2.4.4	THERMAL CONTROL SURFACES							
1.1 6.2.4.5	INSULATION							

COMMENTS

1. NOT NORMAL FAILURE DISTRIBUTION—14 PARALLEL CELLS
2. ARRAY OVERSIZED
3. ARRAY SHIFTS OPERATING POINT
4. HOUSEKEEPING AND ATTITUDE CONTROL
5. POWER LOSS FACTOR = 2
6. USE KLYSTRON POWER
7. DOES NOT INCLUDE WEAROUT (15,000 OPERATING HOURS)
8. REDUNDANT DRIVE MECHANISMS
9. REDUNDANT DRIVE MOTORS
10. REDUNDANT DRIVE CONTROLS

The power distribution system was re-designed to provide multiple power buses to limit potential fault currents and to reduce the probability of loss of the total antenna power output due to failures in the main power bus system. The multiple bus power distribution system does increase the complexity of the bus and installation system and the electrical slip ring, but offers a significant reduction in fault currents and increase in overall system reliability.

One of tne objectives of this analysis was to recommend design modifications to assure graceful failure degradation modes. Based on the results shown in figure 1.1-13 the folowing modifications are recommended:

1. Switchgear - The antenna mounted switchgear controls power to 228 individual power sectors per antenna. Loss of a single switchgear results in the loss of approximately 0.5% of the ground power output. The installation of redundant switchgear for antenna power sector control will significantly improve system operating time. In addition, failures can occur on individual subarrays which will require removal of all input power to the subarray. With the present design the loss in ground power is equivalent to an antenna power sector (0.5% since tnis is the lowest switchgear control level). Improvements in power sector availability can be made with the addition of switchgear at the subarry level.

2. DC to DC Converters - Failures of antenna mounted DC to DC converters, which supply most of the various voltages required by the klystrons, are the largest source of predicted SPS ground power loss. A significant reduction in ground power loss can be realized by installing redundant DC to DC converters on the antenna. The predicted number of antenna power sector output losses due to converter failures decreases from 12 (with no redundance) to 0.6 (with redundance) per antenna. By installing redundant converters on the antenna the increase in operating revenues is significant. The mass penalty would be approximately 10 metric tons per converter including the thermal control system for the converter.

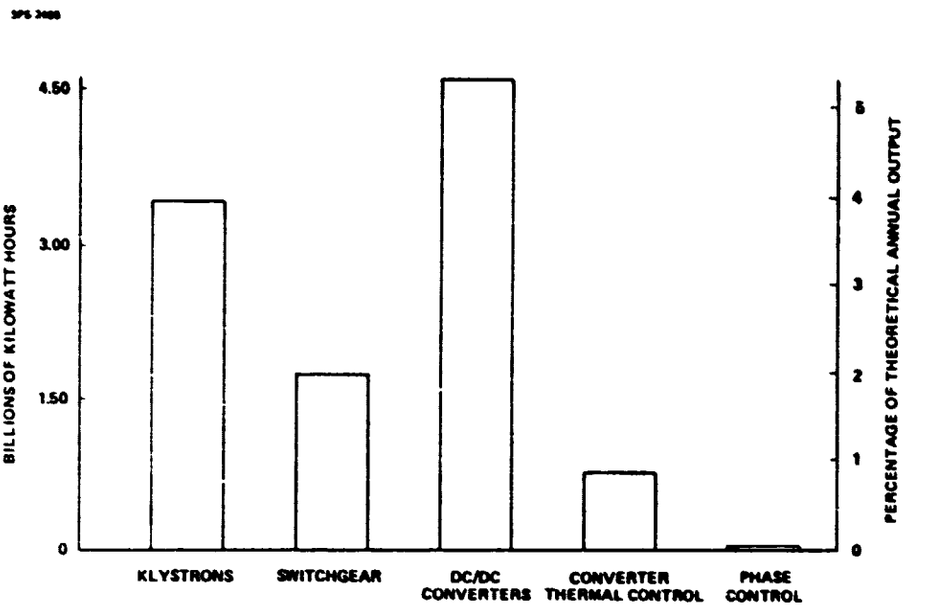

Figure 1.1-13 Annual Power Loss Due To Failures

1.1.0.7 Analysis of Power Transmission System Availability and Maintenance Requirements by General Electric

Maintenance Requirements

Maintenance of Space Antenna Power Transfer System

On the basis of the previously assumed failure rates, applicable component numbers and half yearly maintenance periods the expected number of failures and their estimated repair time requirements can be calculated. The results are exhibited in Table 1.1-4

Table 1.1-4

Number of Failures and Associated Maintenance Time Requirements in the Space Antenna Power Transmission System

Item	f / .5 year p	N	F	Hrs. Repair m	Total Repair Time
DC Convertor	.075	456	34.2	4	136.8
DC Vector Line	.00594	228	1.35	12	16.2
Subarray Line	.000315	101784	32.06	4	128.2
SW_1 Output	.01859	60	1.11	8	8.9
2nd B_{19} Output	.006048	380	2.29	6	13.8
B_{mm} Output	.005246	7220	37.87	2	75.7
Klystron Input	.007626	101784	776.2	.75	582.1
Klystron and Drive	.025	101784	2544.6	1	2544.6
Total			3429.68		3506.3
Man hours for two man team					7012.7

From these results it is calculated that if 1 man produces 42 hours in an 84-hour maintenance period then an 84-man team is required to maintain the space antenna.

Maintenance of the Rectenna DC Power Collection System

According to the maintenance philosophy of the rectenna the panels containing the dipoles and diodes are designed for 30 years life without scheduled maintenance. The rese of the system, including DC bus lines, switch gear and circuits will be maintained on a continuous basis without discontinuing the overall operation of the rectenna. Thus maintenance work will require shut down of panel strings or unit to group lines only.

The failure number calculations and total repair time requirements are displayed in Table 1.1-5

Table 1.1-5

Number of Failures and Associated Maintenance Time Requirements in the Rectenna DC Power Collection System

	$\frac{f}{.1 \text{ year}}$ p	N	F	$\frac{\text{Hrs}}{\text{Repair}}$ m	Tot. Repair Hrs. Per Maintenance Cycle	Man Hours
Panel String	.0063	87240	549.6	5 (2 man)	2748	5496.1
Unit to Group Center Lines	.00315	784	2.47	18 (6 man)	44.4	266.4
				Total		5762.5

From these results it may be estimated that if one man provides 200 hours within the .1 year maintenance cycle, then 30 men are required for the maintenance operations. On the average 15.1 failures are to be repaired daily. It must be emphasized that the above numbers are order of magnitude indications only, because failure rates and repair times are highly dependent on the detailed component design of the rectenna.

Maintenance of Rectenna AC Power Collection System

Introduction and Definitions

The maintenance requirements will be discussed in two separate categories. The normal or scheduled maintenance requirements will be defined as being inspections and performance tests causing either no curtailment of power or performed during periods in which the power generation from the rectenna system is zero for other reasons than rectenna AC Power Collection System maintenance.

The unscheduled maintenance or failure repair will be defined as all other maintenance. This would include restoring power output which was lost due to a failure, as well as component repair or replacement following a failure when redundant design prevented a loss of power.

Since the scheduled maintenance of the devices in this part of the rectenna system is typically on a yearly or multi-annual basis as well as of very short durations (hours) it is reasonable to assume that scheduled maintenance will never cause power curtailment from the rectenna.

Unscheduled Maintenance Requirements

The values for repair time given in the failure rate and effects analysis will be used as a basis for developing the unscheduled maintenance requirements. Table 1.1-6 shows the mean time to repair for the components in the system. The values used are typical electric industry statistical data. The values for the SPS rectenna system may be considerably lower than the values shown due to availability of specially trained maintenance personnel and a well-stocked replacements parts supply. Particularly in the area of transformer maintenance the value of a sufficient number of spares would be quite significant. The values in the table assume available spares for the transformers.

Table 1.1-6

Unscheduled Maintenance Requirements

Component	Mean time to Repair-hours	Repair time hours/year
DC Switchgear	8	1.600
DC/AC Converters	10	3.300
Converter Transformer	75	.225
AC Cable	16	.054 (per 1000 ft)
Synchronous Condenser	112	56
AC Switchgear	3.8	.067
Step-up Transformer	72	.936

In Table 1.1-7 the number of components present in each of the designs are listed, with Table 1.1-8 showing the expected values of failures per year calculated as Repair time (hrs/yr) x number of components/ 8760 hrs/yr = Expected value of failures in a year.

Table 1.1-7

Number of Components

	Part III Baseline	Low Current Design	Low Voltage Design
DC Breakers	10,500	15,512	16,108
D/A Converter	125	544	784
Converter Transformer	125	544	784
AC Cable	125	544	784
Synch. Condenser	25	25	25
AC Switchgear	400	225	225
SU Transformer	10	8	8

Table 1.1-8

Expected Values of Failures/Year

	Part III Baseline	Low Current Design	Low Voltage Design
DC Breakers	1.917	2.833	2.942
D/A Converters	.047	.205	.295
Converter Transformer	.003	.014	.020
AC Cable	.004	.017	.024
Synch. Condenser	.16	.16	.16
AC Switchgear	.00?	.002	.002
SU Transformer	.001	.0008	)08

Scheduled Maintenance Requirements

The scheduled maintenance requirements for the components in the rectenna AC power collection system are quite nominal. There are few standard practices in this area in electric utility systems, since each user would tailor the maintenance practices to fit with his specific situation. Contamination from particles and chemicals, the impact of weather and duty cycles and manufacturers specifications would all be variables in determining frequency and maintenance activities.

Based on available survey results of maintenance activities the data given in Table 1.1-9 show scheduled maintenance in terms of manhours per year for the components in the rectenna AC system. Depending on the number of the various devices for a given rectenna AC layout, increased effectivity in performing this maintenance could reduce the manpower requirements.

Table 1.1-9

Scheduled Maintenance Requirements

	Manhours/year/device
DC Switchgear	2
DC/AC Converters	16
Converter Transformer	16
AC Cable	2
Synchronous Condenser	40
AC Switchgear	20
Step-up Transformer	16

Table 1.1-10 summarizes the "unscheduled" and scheduled maintenance requirements for the AC power collection system for a 1/10 year period. The total hours can be provided by a 35 man team. The total AC-DC crew is 64 people.

Table 1.1-10

Summary of Maintenance Hours Requirements for the AC Power Collection System

	Hrs.
Unscheduled	495.7
Scheduled	6450
	6945.7

Failure Modes and Effects Analysis

Space Antenna DC Power Distrubution System

The input to the space antenna DC power distribution system is defined at the output terminal of the flexible DC cables through the elevation angle yoke. The output of the DC power distribution system is at the power connector of the klystron. It is assumed that the availability of the low power level distribution system is much higher then the high power system and it is neglected in the following claculations.

The availability of the system will be calculated by using the binomial probability function. In order to do this the following quantities have to be defined:

λ = number of failure for a given component

T = period of time during which λ failure occurs

$\frac{\lambda}{T}$ = failure rate

r = mean time necessary to remove a failure (mean time to repair)

$p = \frac{\lambda}{T} r$ = probability of failure for a given failure rate and mean time to repair

Using the definition given above the probability of x failure is

$$P(x) = \frac{N!}{x!\ (N-X)!}\ p^X\ (1-p)^{N-X}$$

For large N it is more practical to use the following recursive formula

$$P(x) = \begin{cases} (1-p)^N & \text{for } x = 0 \\ \frac{N-X+1}{x}\ \frac{p}{1-p}\ P\ (x-1) & \text{for } x \neq 0 \end{cases}$$

The mean value of expected failures

$$E(x) = pN.$$

The DC power distribution system can be divided into two parts for the purpose of availability calculations: 1) Sector lines, 2) Subarray lines.

Sector Lines

This system consists of N = 228 separate main DC buses, each carrying a nominal of 35 Mw DC power at a nominal 40 kV and 875A using approximately 35 mm diameter

aluminum conductors. At the end of a typical line there is a switchgear unit. Part of the power (5.44 MW) goes through a DC to DC converter with 218 kw loss and there is a nominal 446 way power divider at the output of the converter station.

The following failure rates are assumed for an individual DC to DC converter:

$$\frac{\lambda}{T} = .15 \frac{\text{failure}}{\text{year}}$$

$$r = .5 \text{ years}$$

$$p = .075$$

For all space antenna availability calculations .5 year repair time is selected. Assuming double redundancy (N = 2) and using the above given recursive formulas the probability of failure, p = P(2) for the system of 2 redundant converters is shown in Table 1.1-11.

Table 1.1-11

Calculation of the Probability of Failure for Two Redundant DC to DC Converters

n	P(n)	$\overline{P} = \sum_{k=0}^{n} P(k)$
0	.855625	.855625
1	.138750	.994375
2	p = .005625	1

The failure rates for the complete sector lines system:

	P
Redundant DC to DC converter	.005625
Main DC bus	.000315
Resultant sector lines	.00594

One line carries $a = \frac{1}{228} = .4385\%$ part of the total power. The available power if n failure occured ised is

$$A = (1 - an)$$

part of the full power. A is the availability of power. Table 1.1-12 shows the calculation of A as a function of

$$P = \sum_{o}^{n} P(k) \text{ for } N = 228 \text{ and } p = .00594.$$

Table 1.1-12

Calculation of Availability for the DC Sector Lines of the Space Antenna
(N = 228, p = .00594)

n	P(n)	$\bar{P} = \sum_{o}^{n} P(k)$	A%
0	.25708247	.2571	100
1	.35025244	.6073	99.56
2	.25757473	.8449	99.12
3	.10693304	.9518	98.68
4	.03594250	.4876	98.24
5	.00962188	.9974	97.81
6	.00213692	.9995	97.37
7	.00040496	.9999	96.92

Figure 3.1-1 shows the availability vs. probability for the space antenna DC sector lines for .075 and .166 failures per half year in the individual DC to DC converters. It can be seen that even with the lower failure rates and double redundancy the availability is only 99.5% in not less than 66% of the time ($\bar{P}$ = 66%). (The 66% probability corresponds approximately to the average, thus system failures on the average cause .5% reduction of output power).

Subarray Lines

This system consists of the lines between the output from the end of the main bus to the individual klystrons. These lines go either directly to the klystrons (about 446 lines from each converter) or first to subarrays (on the average approximately 31 lines from each converter) and then from subarray centers via an additional junction point to the klystrons (on the average approximately 14 lines).

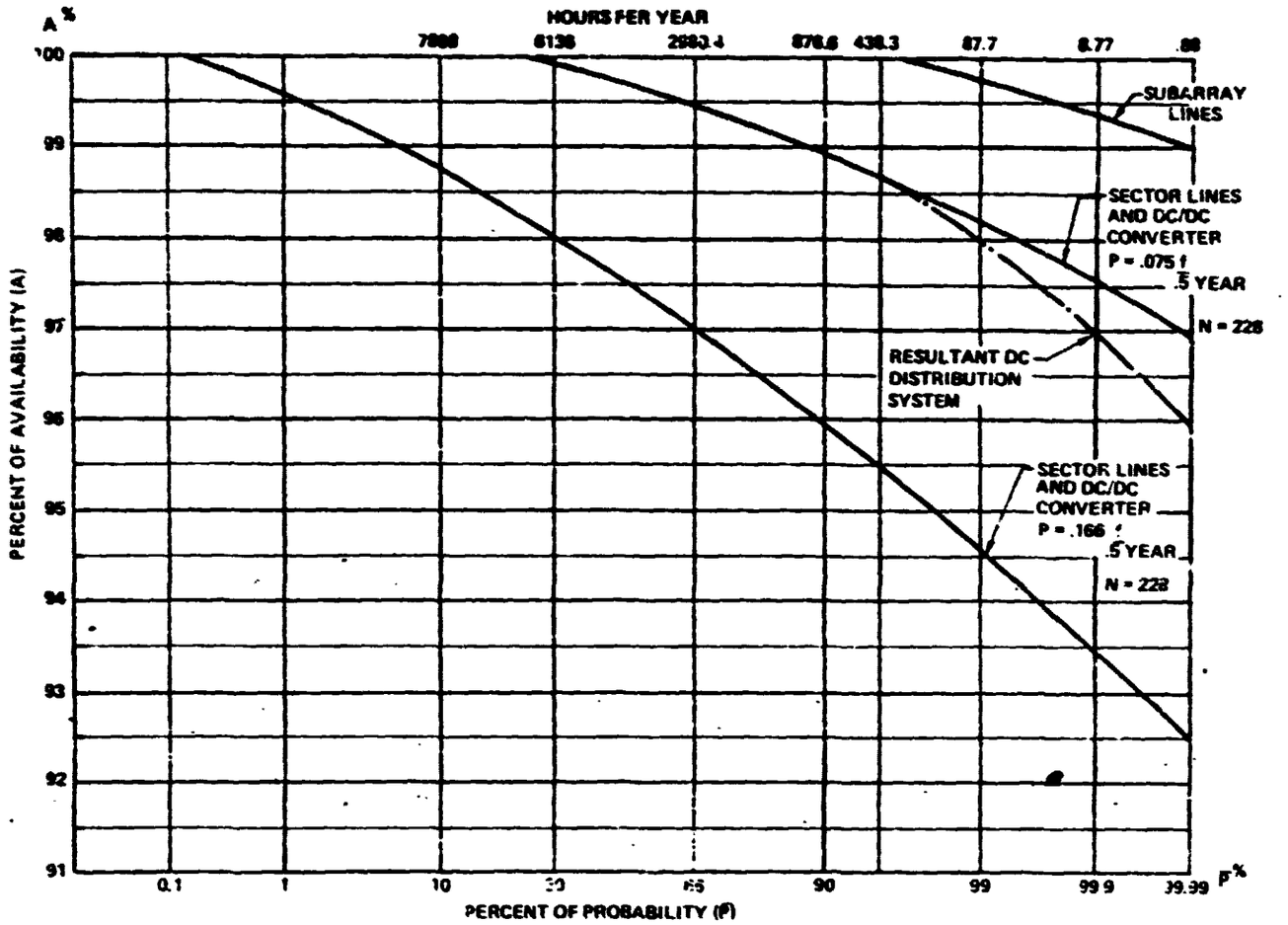

Figure 1.1-14 Availability Vs. Probability for Space Antenna DC Distribution System From Output of Elevation Flexible Joint to Klystron Input.

For availability calculation the direct connection is assumed. For the DC bus p = .000315 and N = 446. The end result is shown in Figure 1.1.-14. The same figure shows also the resultant availability of the complete DC power distribution system, assuming that the converter with $\frac{\lambda}{T}$ = .15 failure/year is selected. The resultant availability is the product of the availability of the sector and subarray lines. It can be seen that the availability of this part of the SPS system is limited by the failure rate of the DC to DC converters.

Space Antenna Phase Control System

The input to the space antenna phase control system is defined at the aperture of the receive antenna element. (There are three redundant antennas). The output of the phase control system is at the input terminal of the driver for the klystron. It is assumed that the ground pilot station has a much better availability then the space antenna phase control system, thus it is neglected in the present calculations.

The block diagram of the phase control system for availability calculation purposes is shown on Figure 1.1.15. This figure also exhibits the failure rates in one failure per 10^6 Hrs. units for each component. Since the phase control network is a four layer tree, it is practical to calculate the availability for each layers separately. The definition of the interfaces:

Part 1. Input of phase control system to output of switches SW_1

Part 2. Output of switches SW_1 to output of 2nd B_{19} power dividers

Part 3. Output of 2nd B_{19} power dividers to output of B_{mn} power dividers

Part 4. Output of B_{mn} power dividers to input of Klystron drives

Part 1

The following failure rates are selected:

Reference antenna	.0005	$f/10^6$ hours
Filter	.0010	$f/10^6$ hours
Receiver	.0800	$f/10^6$ hours
B_{20} power divider	.0100	$f/10^6$ hours
Phase transmitter	.0150	$f/10^6$ hours
1st layer cable	.0129	$f/10^6$ hours
SW_1 switch	.0200	$f/10^6$ hours
Resultant	$\frac{\lambda}{T} = .1414$	$f/10^6$ hours

$$p = \frac{\lambda}{T} r = .0185925$$

The first layer is triple redundant (N = 3 parallel branch). For this case the probability of failure for the system of three redundant first layer lines is shown in Table 1.1-13.

Table 1.1-13

Calculation of the Probability of Failure for Three Redundant First Layer Circuit

n	P(n)	$\overline{P} = \sum_{o}^{n} P(k)$
o	.94525300	.94525300
1	.05372278	.99897578
2	.00101776	.99999354
3	p = .00000646	1

Thus the resultant probability of failure is p = .00000646 for the redundant braches and there are N = 20 lines at this (sector). The probabilities of availability is shown in Table 1.1-14.

Table 1.1-14

Calculation of the Probability for the Phase Control Network Sector Layer (Part 1)

n	P(n)	$\overline{P} = \sum_{o}^{n} P(k)$	A%
0	.99987080	.99987080	100
1	.00012918	.99999998	95

A vs $\overline{P}$ for Part 1 of the system is shown on Figure 1-16. It can be seen that this type of system failure affects the system availability for very small times only, but for this part of the probability range it varies very rapidly. (Once a single failure occurred it affects a relatively large, 5% part of the antenna system power output.)

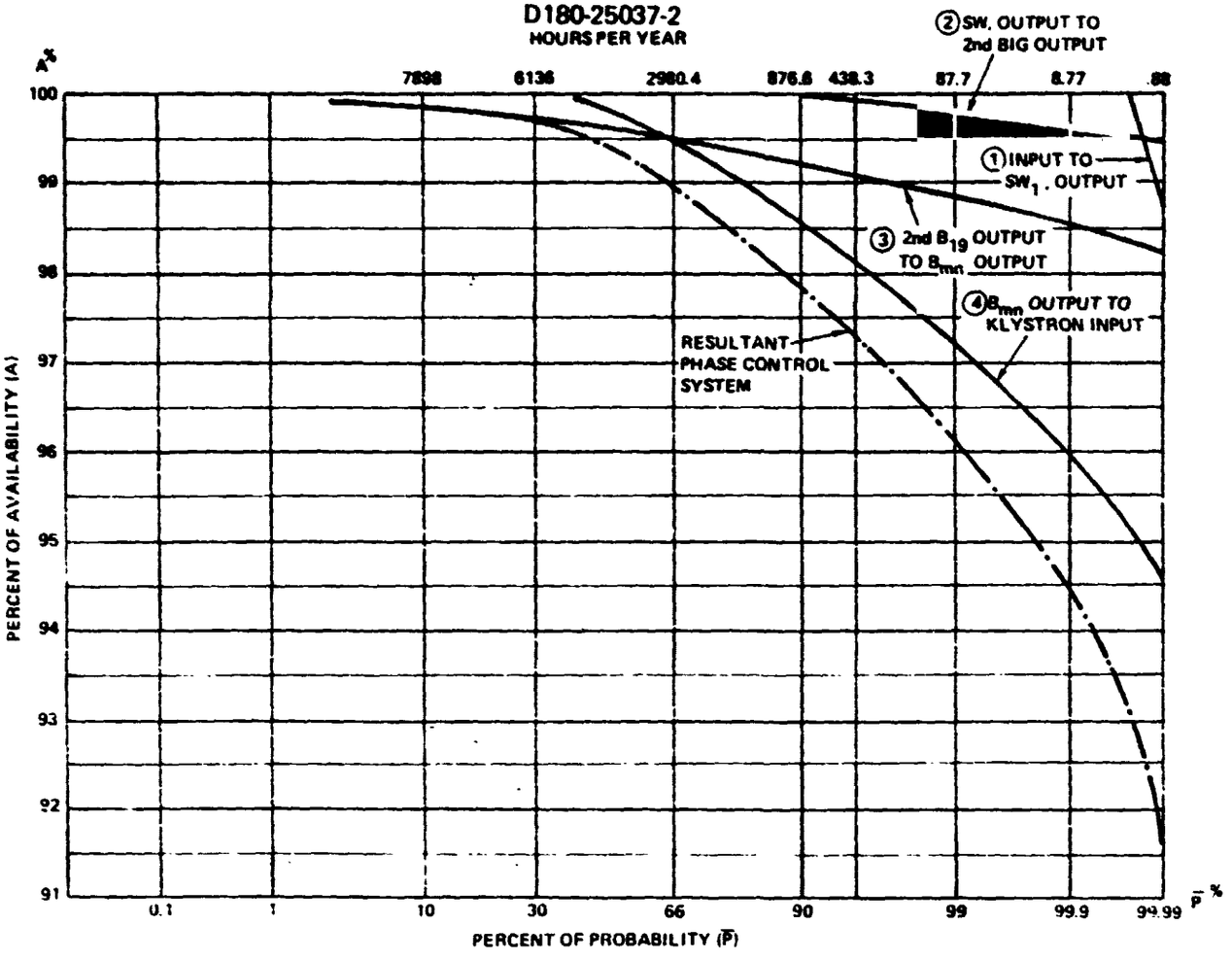

Figure 1.1-16. Availability Vs. Probability for Space Antenna Phase Control System from Input of Pilot Receive Antenna to Klystron Drive Input.

Part 2

The following failure rates are selected:

SW_2 switch	.0200	$f/10^6$ hours
B_{19} power divider	.0100	$f/10^6$ hours
Phase transmitter	.0150	$f/10^6$ hours
H_3 hybrid	.0010	$f/10^5$ hours
Resultant	$\frac{\lambda}{T}$ = .0460	$f/10^6$ hours

$$p = \frac{\lambda}{T} r = .00604849$$

This layer is double redundant (N = 2 parallel branch). For this case the probability of failure is shown in Table 1.1-15

Table 1.1-15

Calculation of the Probability of Failure for Two Redundant Second Layer Circuit

n	P(n)	$\overline{P} = \sum_{o}^{n} P(k)$
0	.98683434	.98683434
1	.01303536	.99986970
2	p = .00013030	1

The failure rates for the remaining portion of this layer to its output interface:

2nd layer cable	.0129	$f/10^6$ hours
SW_4 switch	.0200	$f/10^6$ hours
Phase receiver	.0020	$f/10^6$ hours
H_4 hybrid	.0010	$f/10^6$ hours
B_{19} power divider	.0100	$f/10^6$ hours
Resultant	$\frac{\lambda}{T}$ = .0459	$f/10^6$ hours

$p = \frac{\lambda r}{T} \cong .00604849$ as for the first portion of Part 2.

Table 1.1-16

Calculation of the Probability of Failure for the Phase Control Network Group Layer (Part 2, Input Portion)

n	P(n)	$\overline{P}$	A%
0	.95168879	.95168879	100
1	.04712806	.99881685	99.73
2	.00116383	.99998068	99.47
3	.00001911	.99999979	99.20

Thus the resultant probability of failure is p = .0001303 for the redundant branches. There are N = 380 lines at this (group) layer. The probability of availability is displayed in Table 1.1-16.

The resultant values for the complete Part 2 are therefore the same as in Table 1.1-16 except the numbers in the Column A have to be squared. The results are also displayed in Figure 1.1-16.

Part 3

The following failure rates are selected:

Phase transmitter	.0150	$f/10^6$ hours
3rd layer cable	.0129	$f/10^6$ hours
Phase receiver	.0020	$f/10^6$ hours
B_{mn} power divider	.0100	$f/10^6$ hours
Resultant	$\frac{\lambda}{T}$ = .0399	$f/10^6$ hours

$$p = \frac{\lambda}{T}r = .00524640$$

There is no redundancy and there are N = 7220 lines in this (subarray) layer. Since N is very large the A versus P function converges to its assymptatic value very slowly. (n ~ 130 would be needed to reach $\overline{P} > .9999$.) Adequate accuracy can be obtained by reducing the size of the system by an order of magnitude by selecting $N' = \frac{N}{10} = 722$. In this case n = 1 corresponds to 10 failures instead of 1. The probability of availability is shown in Table 1.1-17.

Table 1.1-17

Calculation of the Probability of Failure for the Phase Control Network Subarray Layer (Part 3)

n	P(n)	$\overline{P}$	A%
0	.02241842	.0224	100
1	.08536662	.1077	99.86
2	.16230773	.2700	99.72
3	.20544532	.4755	99.58
4	.19476502	.6703	99.44
5	.14750651	.8178	99.30
6	.09296617	.9107	99.16
7	.05015170	.9609	99.03
8	.02364000	.9845	98.89
9	.00989120	.9944	98.75
10	.00371950	.9982	98.61
11	.00126974	.9994	98.48
12	.00039678	.9998	98.33
13	.00014291	.9999	98.20

The results of the above table are also plotted in Figure 1-1-16.

Part 4

The following failure rates are selected:

Phase transmitter	.0150	$f/10^6$ hours
4th layer cable	.0129	$f/10^6$ hours
Phase receiver	.0020	$f/10^6$ hours
Conjugator	.0186	$f/10^6$ hours
Receiver	.0080	$f/10^6$ hours
Filter	.0010	$f/10^6$ hours
Radiating element	.0005	$f/10^6$ hours
Resultant	$\frac{\lambda}{T} = .0580$	$f/10^6$ hours

$P = \frac{\lambda}{T} r = .00762635$

There is no redundancy and there are N = 101784 lines in this (klystron) layer. $N' = \frac{N}{101.784} = 100$ scale reduction is selected thus n = 1 corresponds to 101.784 failure causing 1% of output power loss from the antenna.

The probability of availability is shown in Table 1.1-18.

Table 1.1-18

Calculation of the Probability of Failure for the Phase Control Network Klystron Layer (Part 4)

n	P(n)	$\overline{P}$	A%
0	.46507391	.4651	100
1	.35740736	.8225	99
2	.13595970	.9584	98
3	.03413159	.9925	97
4	.00636077	.9989	96
5	.00093854	.9998	95
6	.00011420	.9999	94

The results of the above table are also shown in Figure1.1-16, together with the resultant availability for the complete phase control system.

The following conclusions can be drawn from Figure 1.1-16.

1. The effect of first layer failures are completely negligible except for loss which occurs in less than 1 hour per year. However, if the redundancy would be reduced to double from the baseline triple redundancy the loss of space antenna output power becomes noticeable for several hours per year.

2. At rms (66%) probability level the nonredundant part of the system causes about 1% loss of output power from the space antenna. This would be recoverable by extending the double redundancy to the Klystron level and thereby increasing the cost of the phase control system by approximately a factor of 2.

3. In the probability region corresponding to about 100 hours per year the availability is limited by the 4th layer, which within this time range causes about 3% power loss. Most of the associated failures are attributable to the conjugator and last phase transmitter. If the specifications of these units can be improved without redundancy, then this limitation can be removed.

4. It must be emphasized that all output power losses in the space antenna cause twice as much reduction of power into the rectenna, because the associated unused aperture area of space antenna causes also a reduction of antenna gain.

Klystrons

The achievable failure rate for a 70 kw output power klystron in space is one of the key parameters of the whole SPS system. At the moment no hard numbers are available, but there are speculations that the presently achieved one failure/two years rate can be extended by an order of magnitude. In the following this desirable failure rate will be assumed in order to compare the resultant availabilities with the rest of the system.

For this case

$$\frac{\lambda}{T} = \frac{1 \text{ failure}}{20 \text{ years}} = .05 \frac{\text{failure}}{\text{year}}, \quad r = .5 \text{ year}$$

There are N = 101784 klystrons. A scale reduction of 379.791 is selected, which results N = 268, a large enough group for adequately accurate calculations. For this condition n = 1 corresponds to 379.791 failure and a loss of a = 1/268 = .37313% in the output from the space antenna.

The probability of availability is displayed in Table 1.1-18.

The results of the above table are also shown in Figure 1.1-17. It can be seen that on the average (p = 66%) the klystrons cause 2.5% of output power reduction, while at p = 99.9% probability (.867 hours/per year) the output power loss may be as high as 6.4%. The loss to the rectenna is twice of these values because at the same time the corresponding antenna area is also lost. It may be noted that the probability distribution shown on Figure 1.1-17 remains unchanged until the $\frac{\lambda}{T}$ p product is the constant. For instance a similar availability can be achieved with a 10 year life time klystron if the maintenance is due in every three months instead of every six months. The total space maintenance hours per year of course would be increased for this case. Alternatively, with the 20 year life time klystron and four yearly maintenance period half of the lost energy can be recovered.

If the value of a kw Hr. is .03$, then the value of the recovered energy is 32.8M$ yearly. For this recovery the cost of the additional maintenance time associated to the more frequency replacement of failed klystrons has to be traded off.

Table 1.1-18

Calculation of the Probability or Failure for the Klystron and Driver Circuit

n	P(n)	$\overline{P}$	A%
0	.00113041	.0011	100
1	.00776796	.0190	99.62
2	.02659033	.0456	99.25
3	.06045324	.1061	98.88
4	.10269302	.2088	98.50
5	.13903054	.3478	98.13
6	.15626082	.5041	97.76
7	.14996460	.6540	97.38
8	.12545116	.7795	97.01
9	.09292678	.8724	96.64
10	.06171291	.9341	96.26
11	.03711406	.9712	95.89
12	.02038101	.9916	95.52
13	.01029100	.9965	95.14
14	.00480624	.9986	94.77
15	.00208681	.9995	94.40
16	.00084609	.9998	94.02
17	.00032159	.9999	93.65

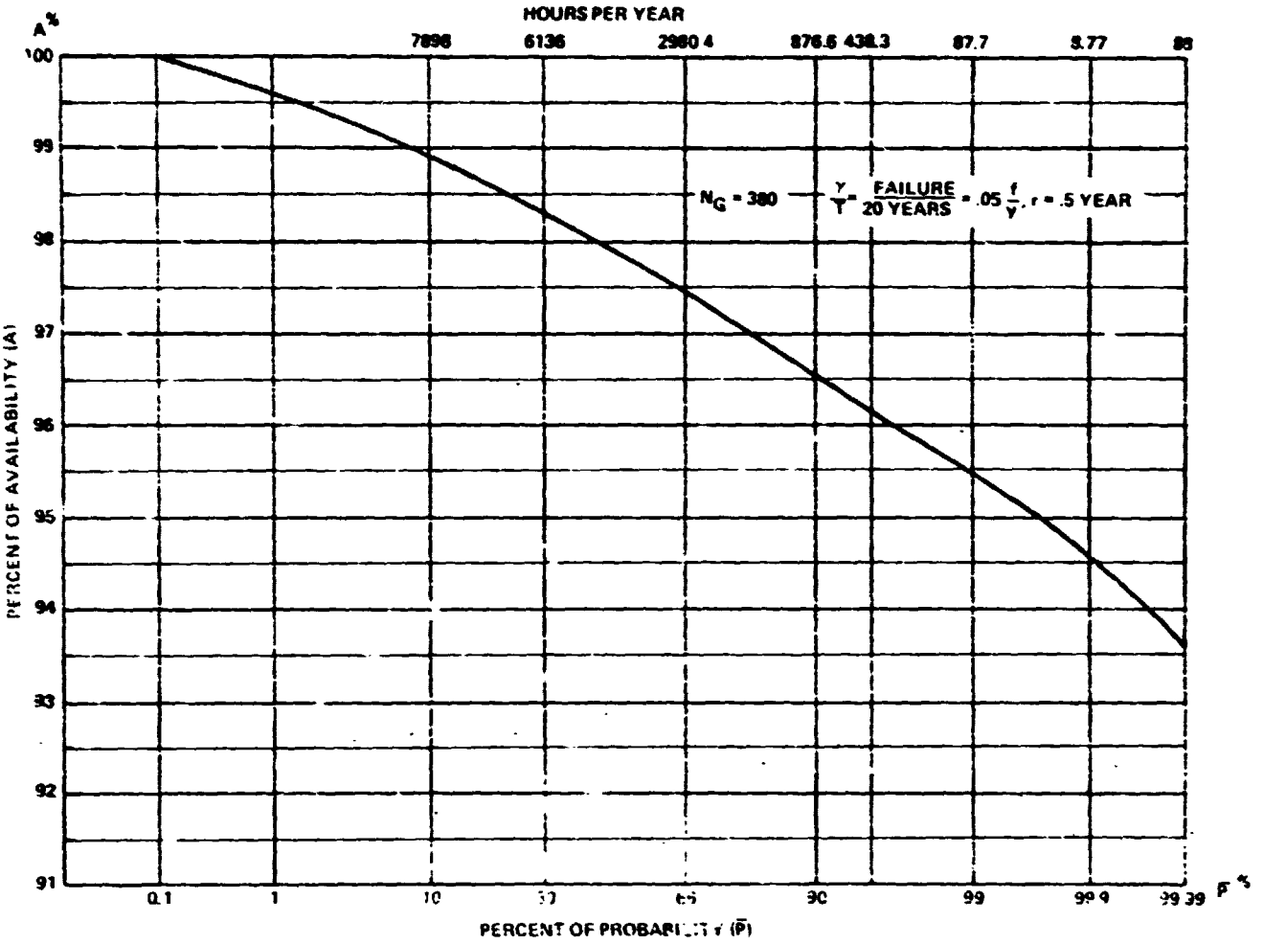

Figure 1.1-17. Availability Vs. Probability for Klystrons With Their Drive, Based on a Group of 380 Klystrons.

Availability Reduction Associated with Space Segment System Operation and Propagation Effects

Figure 1.1-18 shows 4 types of random effects which are not associated with failure modes, but their effect on availability produces a similar distribution to the effect of failures. These effects are:

- Random phase errors in the aperture of the SPS space antenna
- Random amplitude errors in the aperture of the SPS space antenna
- Atmospheric attenuation
- Faraday rotation

The rms and peak value of the random amplitude and phase errors have been calculated during Part III of the study and are included in Part III final report. The peak errors were taken as 3ϵ values for Figure 1.1-18. The random amplitude error was taken on the basis of assuming that the subarrays are aligned within $\Delta\theta_S$ = .05° peak angular accuracy.

The atmospheric attenuation value was taken for a typical East Coast U.S. site, thus it is pessimistic for the assumed Texas location of the rectenna. Note that the atmospheric attenuation value does not converge to 100% availability, thus it represents about 1% constant loss on the average relative to vacuum.

The Faraday rotation effect is negligible most of the time, except for the January period of the worst years of the sunspot cycle. When the associated loss vs % of time is calculated and averaged for the 30 year life time of SPS the loss is about 1.5% for 1 hour/year.

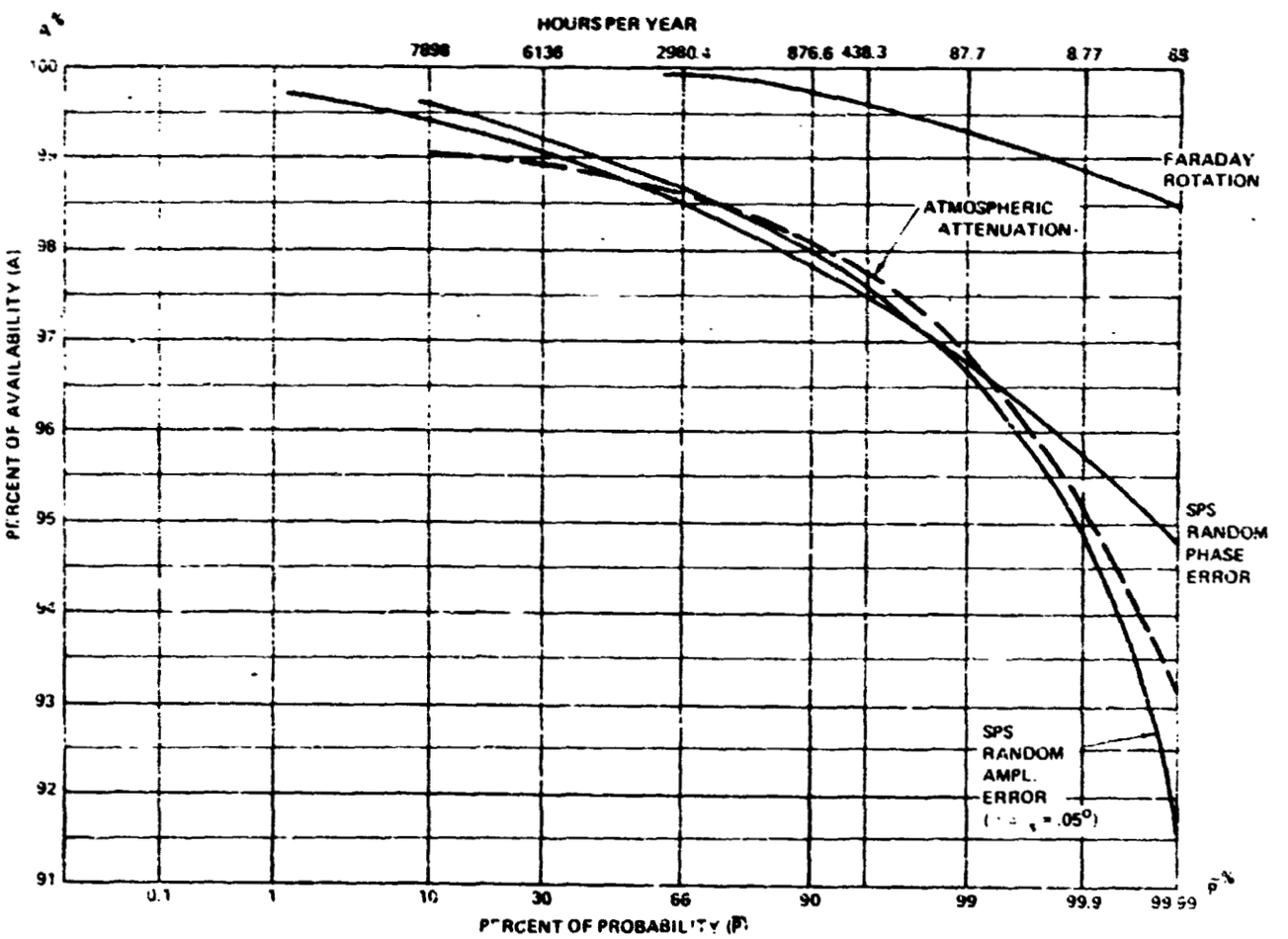

Figure 1.1-18. Availability of Effective Antenna Gain of Space Antenna Vs. Probability Due to Random Aperture Distribution Errors and Propagation Conditions in Media.

Rectenna DC Power Collection System

According to the overall DC power collection layout of the rectenna as it is described in Section 2 the availability of the DC system can be calculated in four portions:

1. String of 43 diodes
2. Panel covering 43^2 = 1849 diodes
3. String of panels
4. Unit to group center lines

These main failure modes are recognized: diode open circuit, panel string line short circuit, group center line short circuit. The diode cannot fail as a short circuit because of its build in fuse.

The basic maintenance philosophy is that the failed diodes and panels are not replaced over the 30 year period, but the DC bus line failures are repaired continually as soon as they are detected.

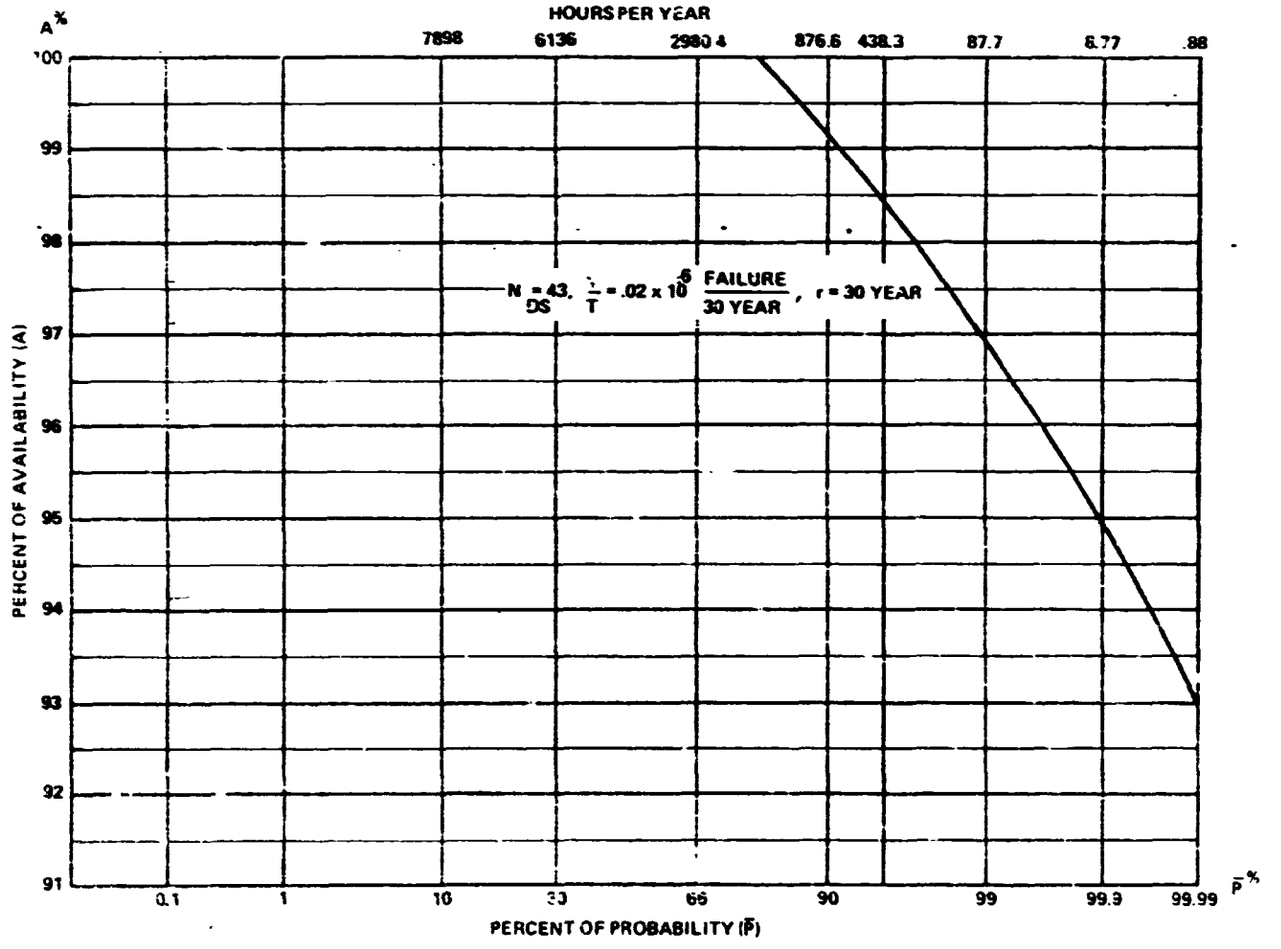

Figure 1.1-19. Availability Vs. Probability of a String of 43 Paralliel Diodes in Rectenna.

1. String of 43 Diodes

These diodes are parallel connected. The assumed failure rate is

$$\frac{\lambda}{T} = .02 \times 10^{-6} \frac{\text{failure}}{\text{Hr}} = 5.2596 \times 10^{-3} \frac{\text{failure}}{30 \text{ year}}$$

The above failure rate is about a factor of 2 better than present state of art. If the repair time is r = 30 year

$$p = .0052596.$$

The probability or availability is shown in Table 1.1-19 and Figure 1.1-19

Table 1.1-19

Calculation of the Probability of Failure for a String of Parallel Diodes (N = 43, p = .0052596)

n	P(n)	$\overline{P}$	A%
0	.797098	.7971	100
1	.181227	.9783	97.67
2	.020123	.9985	95.35
3	.001454	.9999	93.02

2. Panel of 1849 Diodes

p = .0052596, N = 1849. The results are shown in Table 1.1-20

Figure 1.1-20 shows availability values as calculated in Table 1.1-20 but also includes the data for

$$10^6 \frac{\lambda}{T} = .03$$

and also .04. It may be noted that the availability values refer to the end of the 30 year lifetime of the rectenna. For

$$10^6 \frac{\lambda}{T} = .02$$

the failures cause on the average (66% probability) .56% power loss. If the rectenna is refurbished with new diodes after 15 years .28% power can be recovered, which is a very small value compared to the required refurbishing effort.

Table 1.1-20

Calculation of the Probability of Failure for a Panel
(N = 1849, p = .0052596)

n	P(n)	$\bar{P}$	AZ
0	.0000582	.0000	100
1	.0005691	.0006	99.94
2	.0027804	.0034	99.89
3	.0090509	.0124	99.83
4	.0220854	.0345	99.78
5	.0430898	.0776	99.72
6	.0700208	.1476	99.67
7	.0974759	.2451	99.62
8	.1186697	.3638	99.56
9	.1283494	.4921	99.51
10	.1248690	.6170	99.45
11	.1105790	.7273	99.40
12	.0893910	.8169	99.35
13	.0667886	.8837	99.29
14	.0463116	.9301	99.23
15	.0299555	.9602	99.18
16	.0181551	.9786	99.12
17	.0103503	.9889	99.07
18	.0055699	.9945	99.02
19	.0028381	.9973	98.96
20	.0013730	.9987	98.91
21	.0006322	.9993	98.85
22	.0002778	.9996	98.80
23	.0001667	.9998	98.75
24	.0000469	.9999	98.69

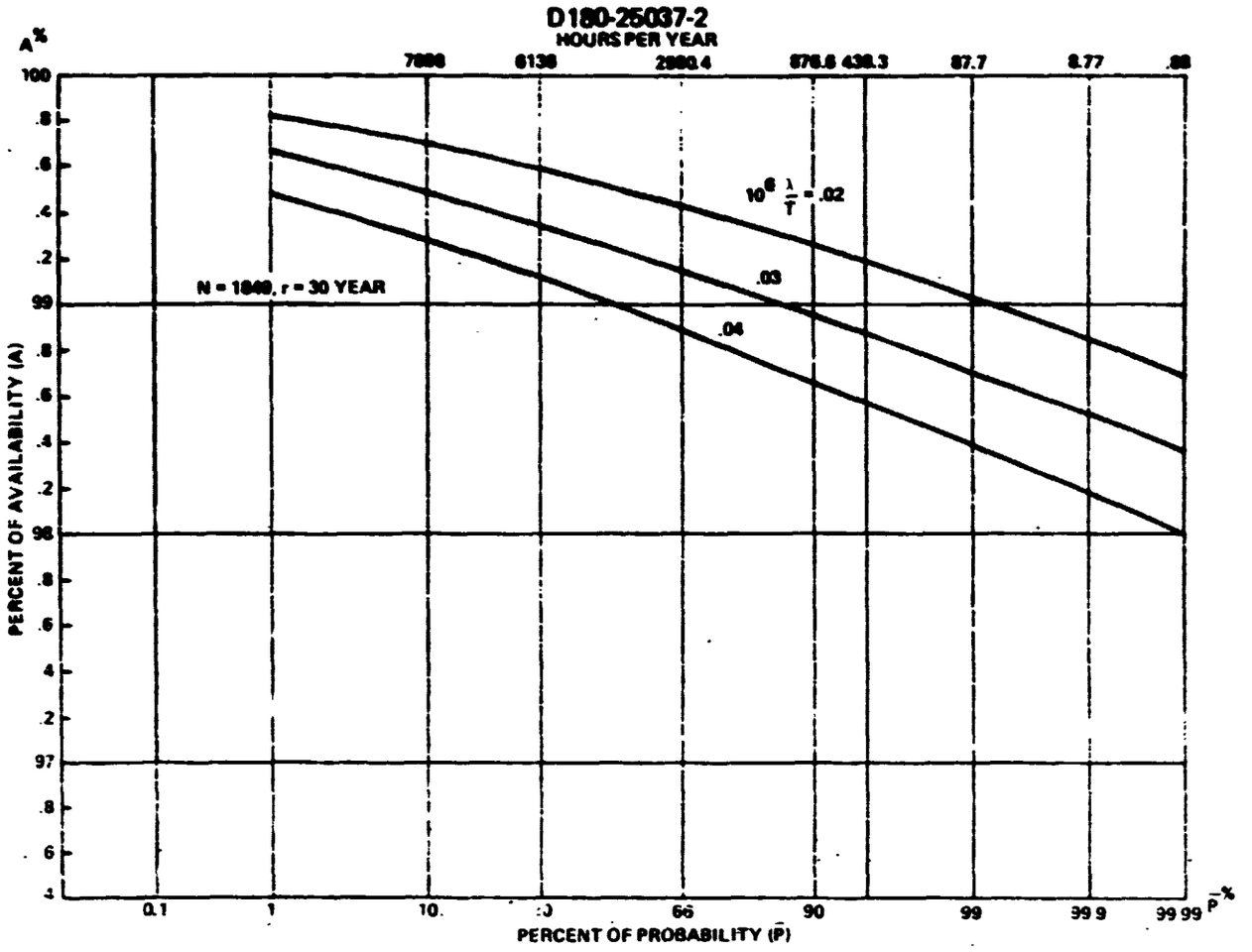

Figure 1.I-20 Availability Vs. Probability of a Typical Rectenna Panel Containing 1849 Diodes.

3. Panel Strings

There are approximately N_{ps} = 87240 panel strings in the rectenna. For simplicity the calculations are done for a 100 times reduced scale, where

$$N'_{ps} = \frac{N_{ps}}{100} \sim 872$$

failure/year, r = 876 hours mean time to repair and m = 15.93 hour/failure actual repair time. (See Table 1.1-21.)

These conditions yield p = 6.3 x 10^{-3}. However, Figure 1.1-21 also shows the availability for r = 1752 hours repair time. The relatively large mean time to repair times are assumed to allow the use of a comparatively small repair crew.

For λ/T = 6.3 x 10^{-2} f/y the total number of failures are 5496 f/year or 54.96 f/876 hour. If one repair takes 5 hours then a crew of 14 men is needed.

Table 1.1-21

Calculation of the Probability of Failure for a Panel String (N_{ps} = 872, p = 6.3 x 10^{-3}, r = 876 Hrs)

n	P(n)	$\overline{P}$	AX
0	.004042	.0040	100
1	.022346	.0264	99.88
2	.061700	.0881	99.77
3	.113441	.2015	99.65
4	.156248	.3578	99.54
5	.171969	.5297	99.42
6	.157544	.6873	99.31
7	.123569	.8108	99.20
8	.084707	.8955	99.08
9	.051555	.9471	99.97
10	.028208	.9753	98.85
11	.014014	.9893	98.74
12	.006375	.9957	98.62
13	.002673	.9984	98.51
14	.001040	.9994	98.39
15	.000377	.9998	98.28
16	.000128	.9999	98.16

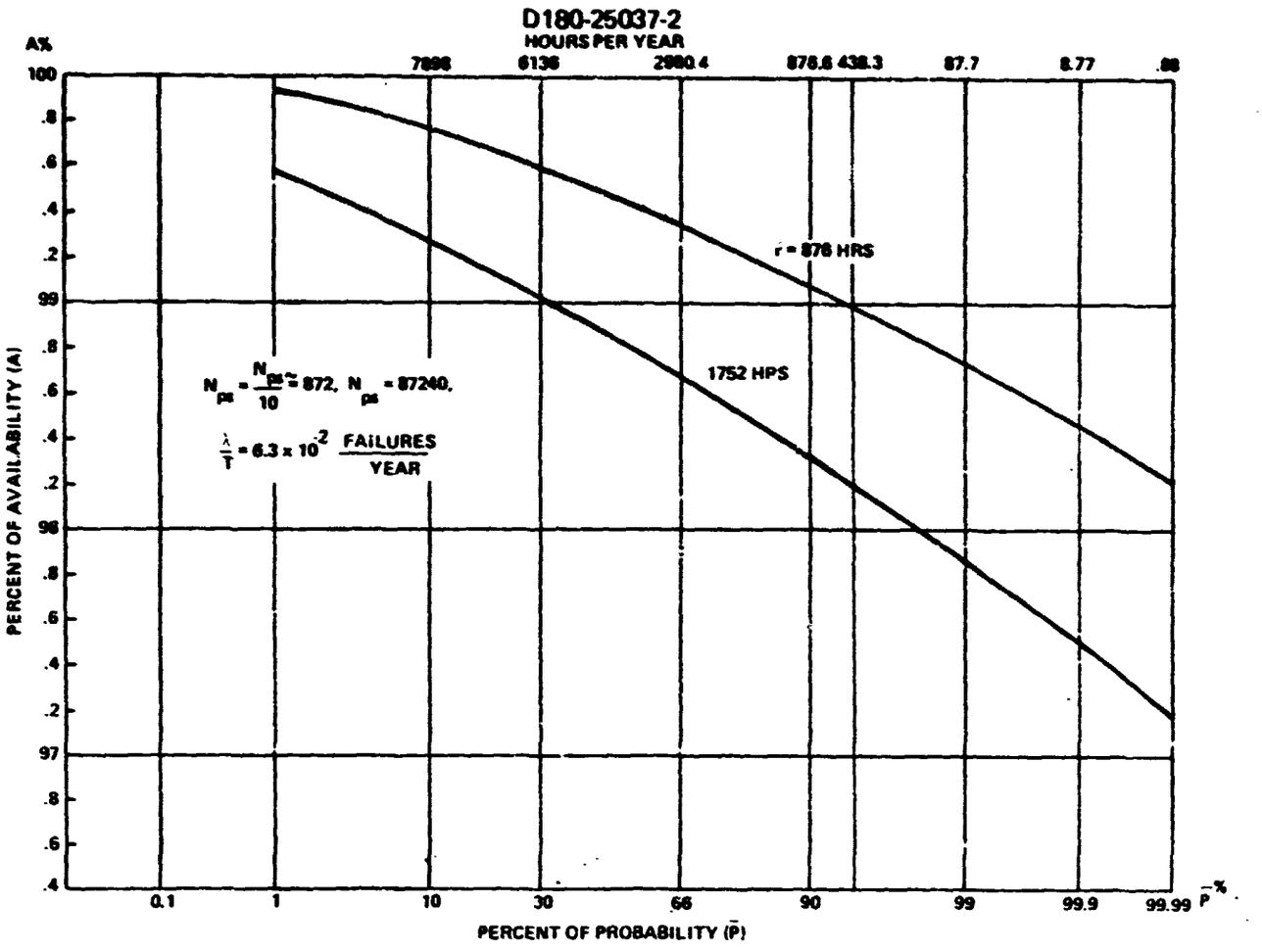

Figure 1.1-21. Availability Vs. Probability of a Typical Rectenna Panel String Containing 872 Panels.

Group Center Lines

There are N_G = 784 groups in the rectenna, each carrying approximately .2175% of the total power. Their failure mode is short circuit on the lines going from unit to group center, where the DC to AC converters are located. The DC bus line failure rate assumption is λ/T = .0315 failure/year.

This is a factor of 2 better than the panel string lines. The improvement is considered reasonable on the basis of running these lines as clearly separated elevated high power conduits. The total number of yearly failures for the group lines is 24.69 or 2.469 within the assumed r = 876 hours maintenance period. The calculated failure probabilities are displayed in Table 1.1-22 and in Figure 1.1-22.

Table 1.1-22

Calculations of the Probability of Failure for the Group Center Lines
(N_G = 784, p = .00315, r = 876 Hours)

n	P(n)	$\overline{P}$	A%
o	.08428	.0843	100
1	.20879	.2931	99.87
2	.25830	.5514	99.75
3	.21276	.7641	99.62
4	.13127	.8954	99.49
5	.06471	.9601	99.36
6	.02654	.9866	99.23
7	.00932	.9960	98.10
8	.00310	.9991	98.98
9	.00075	.9998	98.85
10	.00017	.9999	98.72

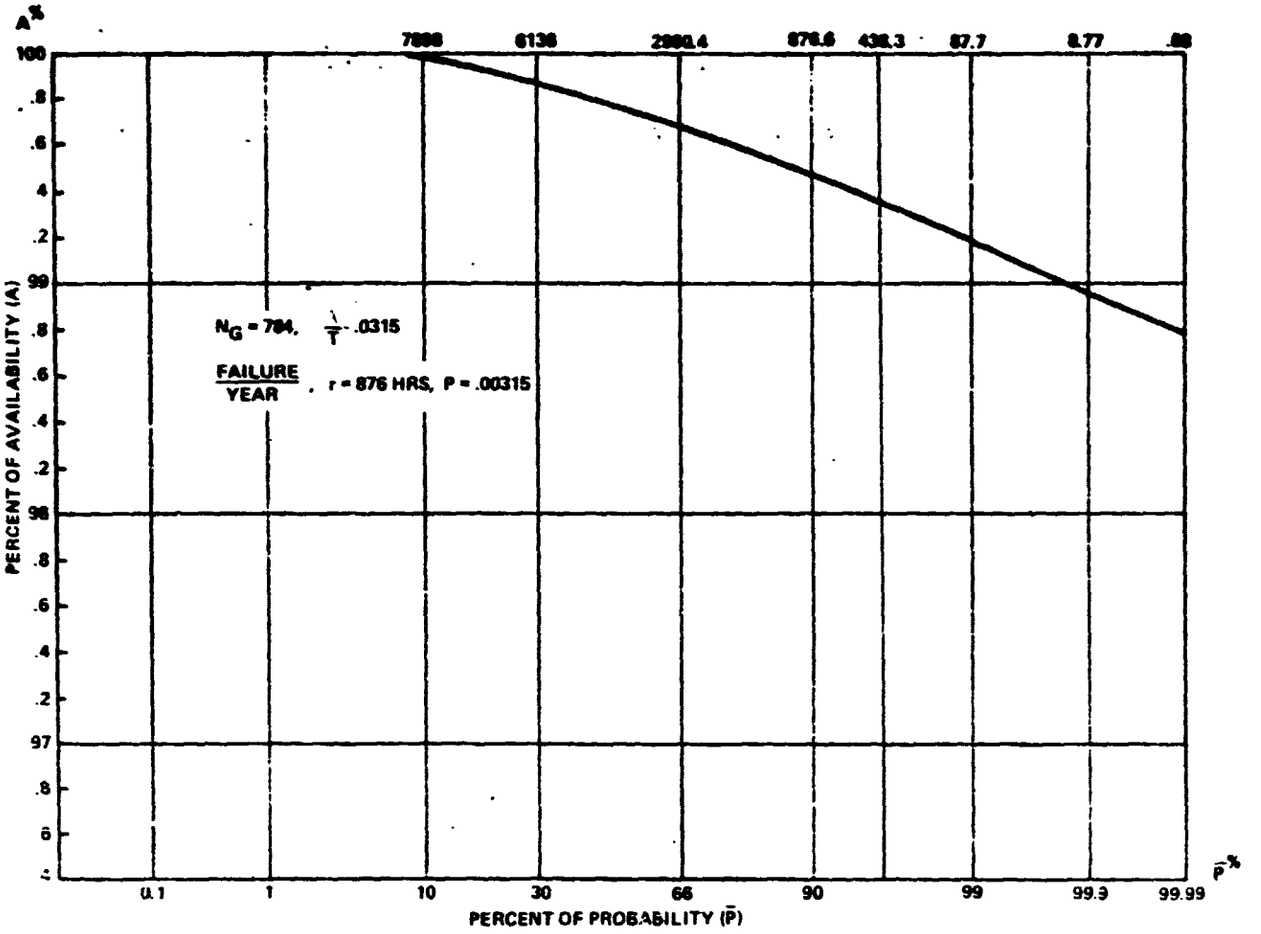

Figure 1.1-22. Availability Vs. Probability of Rectenna Unit to Group Center Lines for 784 Lines.

Resultant DC Power Collection System

On the basis of the previous calculations the resultant availability of the DC power collection system is shown in Figure 1.1-23 for the different combinations of failure characteristics. The four cases are defined in the table as Figure 1.1-23. It can be seen that for the best combinations of failure characteristics (Case 1) the DC system causes an average power loss of 1.55% after 30 years of operation. The most effective way to improve this figure is by decreasing the mean time to repair, which can be achieved by increasing the size of the ground maintenance crew.

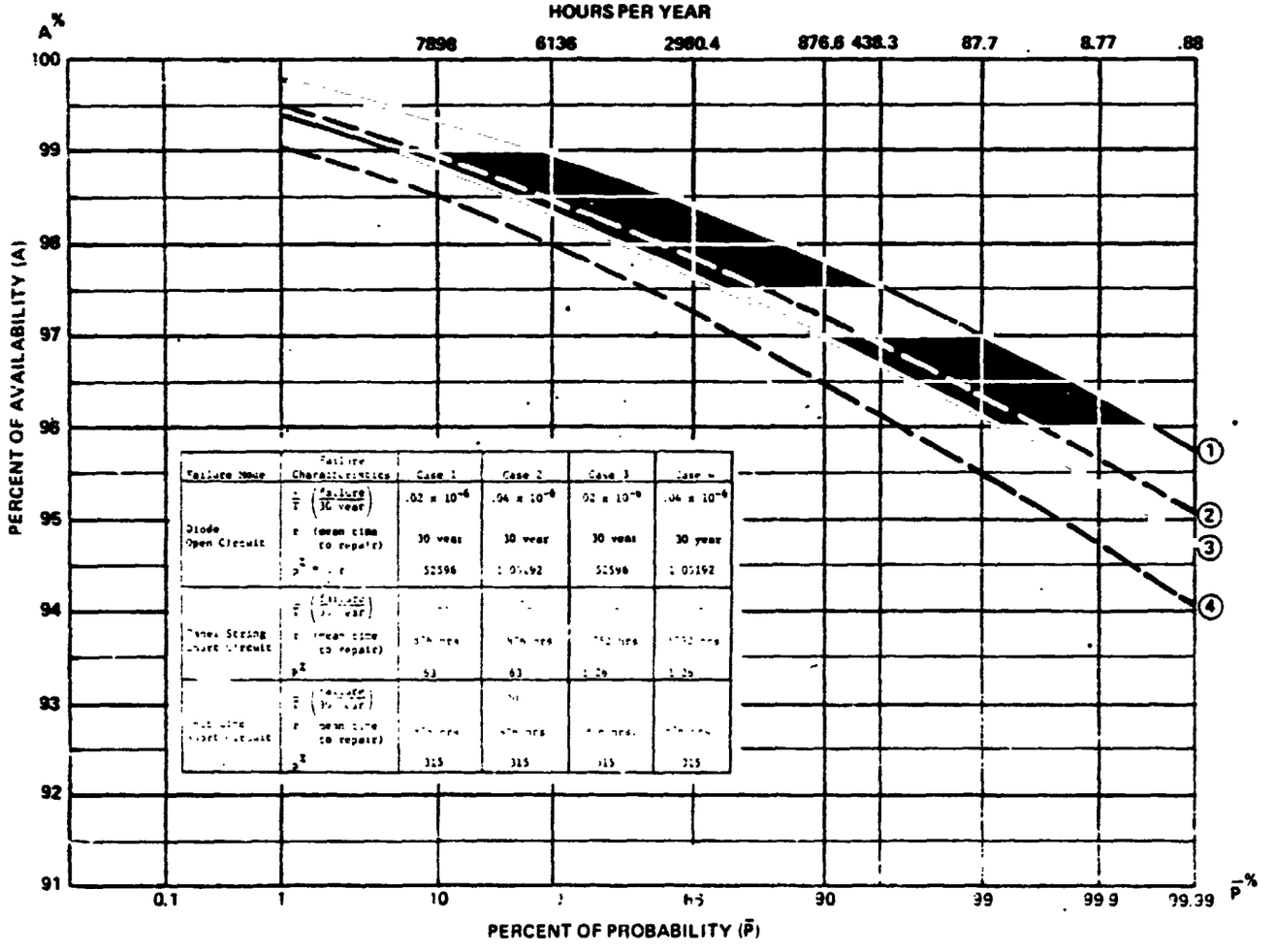

Failure Mode	Failure Characteristics	Case 1	Case 2	Case 3	Case 4
Diode Open Circuit	$\frac{1}{T}\left(\frac{\text{failure}}{30 \text{ year}}\right)$	$.02 \times 10^{-6}$	$.04 \times 10^{-6}$	$.02 \times 10^{-6}$	$.04 \times 10^{-6}$
	r (mean time to repair)	30 year	30 year	30 year	30 year
	$p^2 = \cdot r$	52596	1.05192	52596	1.05192
[illegible] String Short Circuit	$\frac{1}{T}\left(\frac{\text{failure}}{30 \text{ year}}\right)$	[illegible]	[illegible]	[illegible]	[illegible]
	r (mean time to repair)	[illegible] hrs	[illegible] hrs	[illegible] hrs	[illegible] hrs
	p^2	63	63	1.26	1.26
[illegible] Short Circuit	$\frac{1}{T}\left(\frac{\text{failure}}{30 \text{ year}}\right)$	[illegible]	[illegible]	[illegible]	[illegible]
	r (mean time to repair)	[illegible] hrs	[illegible] hrs	[illegible] hrs.	[illegible] hrs.
	p^2	315	315	315	315

Figure 1.1-23 Availability Vs. Probability of Overall Rectenna DC Power Collection System for Various Failure Mode Characteristics.

Rectenna AC Power Collection System

There is no technological problem to achieve any desired availability in the AC part of the rectenna and the availability figures are strictly limited by cost.

Figure 1.1-24 shows the circuit layout selected for availability calculations. This layout does not match exactly the DC power output format of the rectenna but the necessary practical deviations do not affect the availability numbers significantly.

The assumed failure characteristics for the various components are shown in Table 1.1-23.

Table 1.1-23

Assumed Component Failure Characteristics in the AC Power Collection System

Component	$\frac{\lambda}{T}$ $\frac{\text{failure}}{\text{year}}$	$\frac{\lambda}{T}$ $\frac{\text{failure}}{\text{Hr}}$	r_{Hrs}	p
1MW breaker	.2	.00002281	8	.0001824
DS bus	.00063	7.1868×10^{-8}	13	.0000009
20 MW breaker	.2	.00002281	8	.0001824
Converter station	.33	.00003764	10	.0003764
20 Mw transformer	.0041	4.6772×10^{-7}	219	.00010242
200 MW switchyard	0	0	-	0
200 MW transformer	.0041	4.6772×10^{-7}	219	.00010242
Synchronous condenser	.5	5.7038×10^{-5}	112	.006388
1000 MW switchyard	0	0	-	0
1000 MW transformer	.0041	4.6772×10^{-7}	219	.00010242
500 KV transmission	2	.0002281	8	.001825

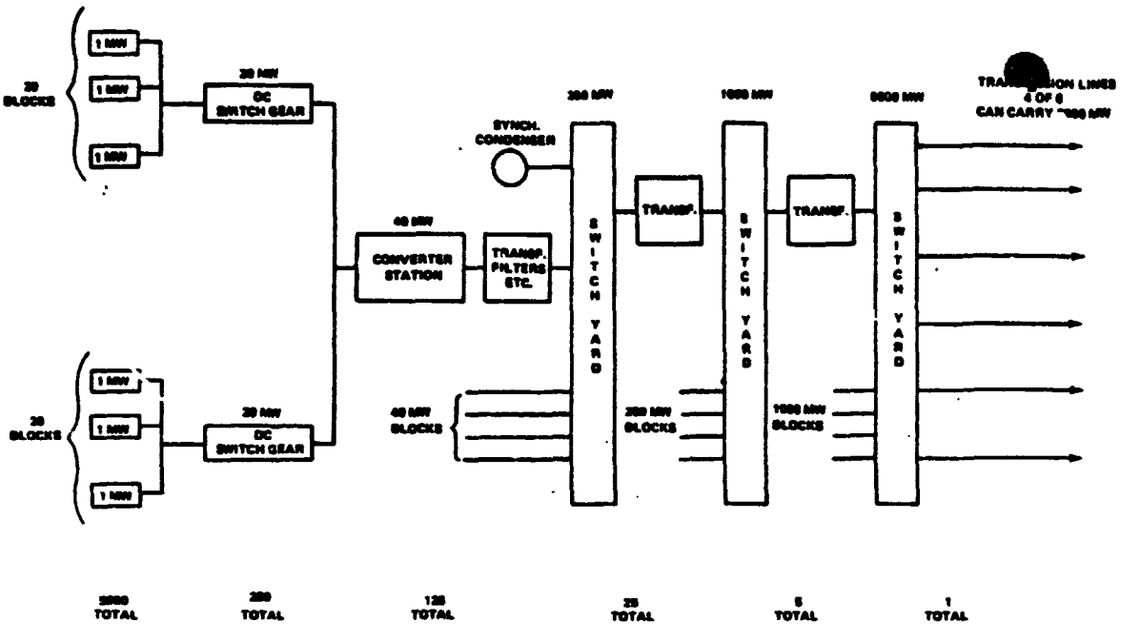

Figure 1.1-24. Block Diagram of Rectenna AC Power Collection System for Availability Calculations.

There are five layers in the AC power combining three, representing the 1, 20, 40, 200 and 1000 MW levels. The resultant p values can be obtained on the basis of Figure 1.1-24 and Table 1.1-23. The applicable N numbers are summarized in Table 1.1-23.

Table 1.1-24

P and N Values Applicable in the DC Power Collection

Unit (MW)	N	p
1	5000	.0003652
20	250	.004030
40	125	.000479
200	25	.0001025
1000	5	.0001025

Tables 1.1-25, 1.1-26, 1.1-27, 1.1-28 and 1.1-29 show the availability calculations for the various power levels of the network.

Table 1.1-25

Calculations of the Probability of Failure for the 1MW Level Network

(N' = 500, p = .003652)

n	P(n)	$\bar{P}$	A%
0	.83307358	.8331	100
1	.15217339	.9852	99.8
2	.01387058	.9991	99.6
3	.0008417	.9999	99.4

Table 1.1-26

Calculations of the Probability of Failure for the 20 MW Level Network

(N = 250, p = .00403)

n	P(n)	$\bar{P}$	A%
0	.36438817	.3644	100
1	.36725499	.7316	99.6
2	.18433189	.9160	99.2
3	.06143195	.9812	98.8
4	.01529307	.9964	98.4
5	.00303335	.9994	98.0
6	.00049934	.9999	97.6

Table 1.1-27

Calculations of the Probability of Failure for the 40 MW Level Network

(N = 125, p = .00479)

n	P(n)	$\bar{P}$	AZ
0	.94186875	.9419	100
1	.05642142	.9983	99.2
2	.00167641	.9999	98.4

Table 1.1-28

Calculations of the Probability of Failure for the 200 MW Level Network

(N = 25, p = .001025)

n	P(n)	$\bar{P}$	AZ
0	.99744065	9974	100
1	.00255619	.9999	96

Table 1.1-29

Calculations of the Probability of Failure for the 1000 MW Level Network

(N = 5, p = .0001025)

n	P(n)	$\bar{P}$	AZ
0	.99948760	.9995	100
1	.00051228	.9999998	80

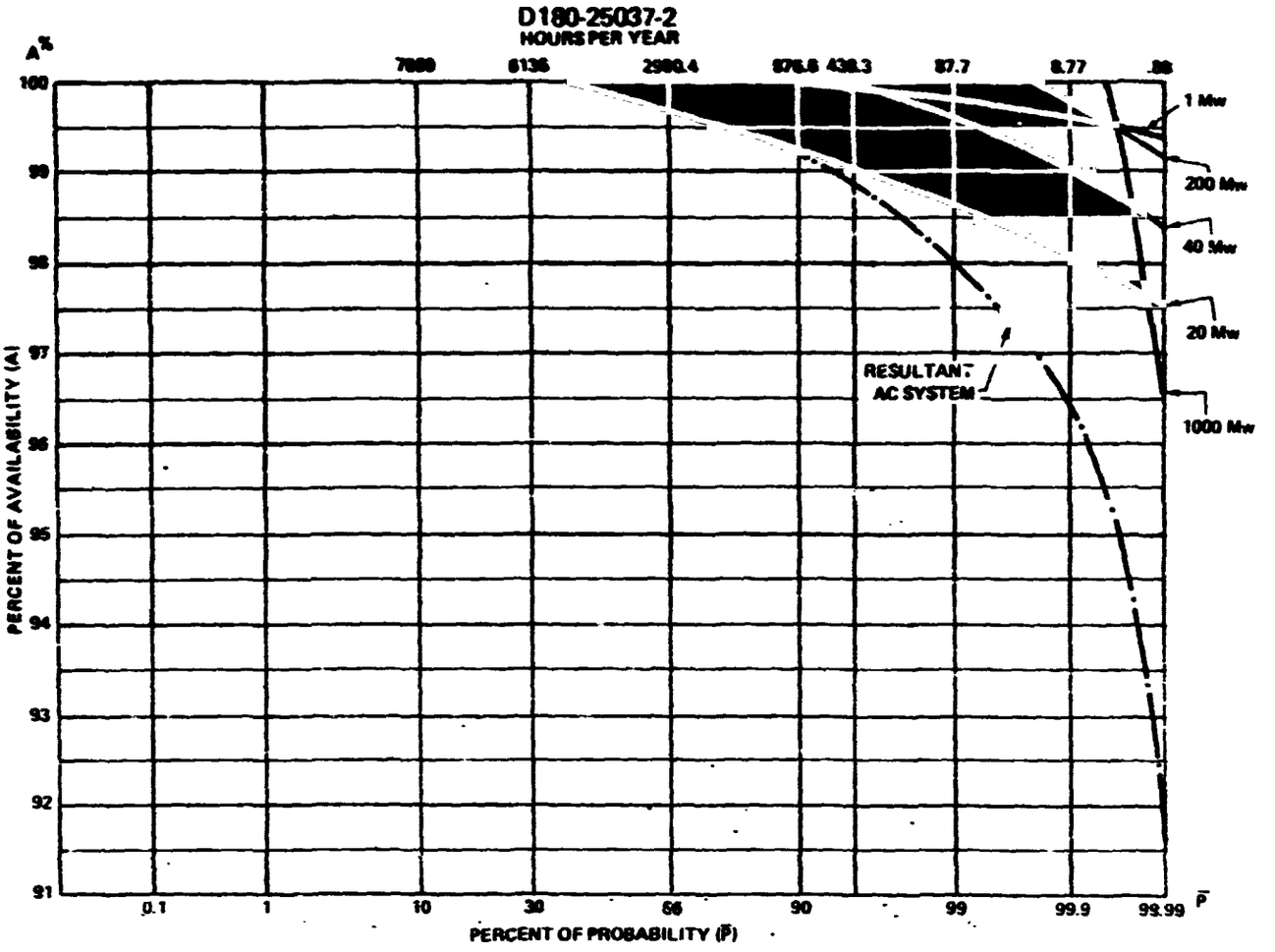

Figure 1.1-25. Availability Vs. Probability of Overall Rectenna AC Power Collection System.

The components and the resultant availability curves for the AC power collection system are displayed in Figure 1.1-25. It can be seen that the effect of the AC system is very small on the overall availability of the SPS system except for a few hours per year.

The above calculations were completed for the somewhat idealized AC system, developed during Part III of the study. The sensitivity of these calculations system availability was checked by repeating it for interfacing with the so-called "low voltage" and "low current" AC power collection system. The block diagram for these availability calculations were done on the basis of failure rates shown in the block diagram of Figure 1.1-26. The applicable component counts are displayed in Table 1.1-30. The corresponding availability profiles are shown in Figures 1.1-27, 28, and 29.

Table 1.1-30

NUMBER OF ELEMENTS IN RECTENNA AC POWER COLLECTION SYSTEM

	Baseline Design	Low Current Design	Low Voltage Design
DC Breakers	10,000	14,424	14,540
Bus Connections (Approx.)	11,000	14,700	14,800
DC Converter Breakers	500	1,088	1,568
DC/AC Converter	125	544	784
Converter Transformer	125	544	784
AC Cable	125	544	784
69/230 Transformer	25	0	0
69/500 Transformer	0	8	8
230/500 Transformer	10	0	0
500 kV AC Circuit Breakers	12	12	12

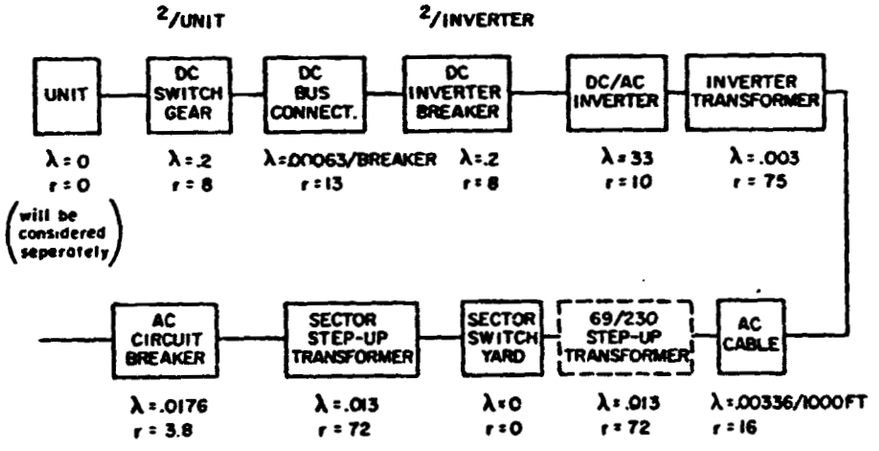

Figure 1.1-26 Block Diagram of Rectenna AC Power Collection System for Availability Calculations

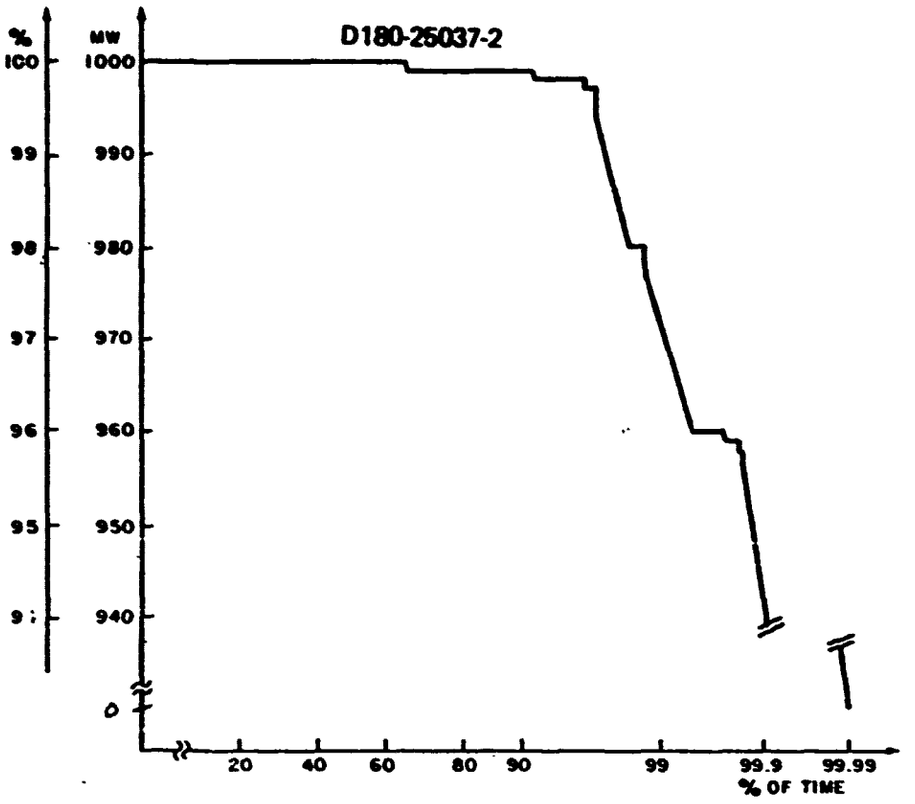

Figure 1.1-27 Availability Vs. Time for 1 Gw Sector AC Assuming Part III Study Rectenna Layout

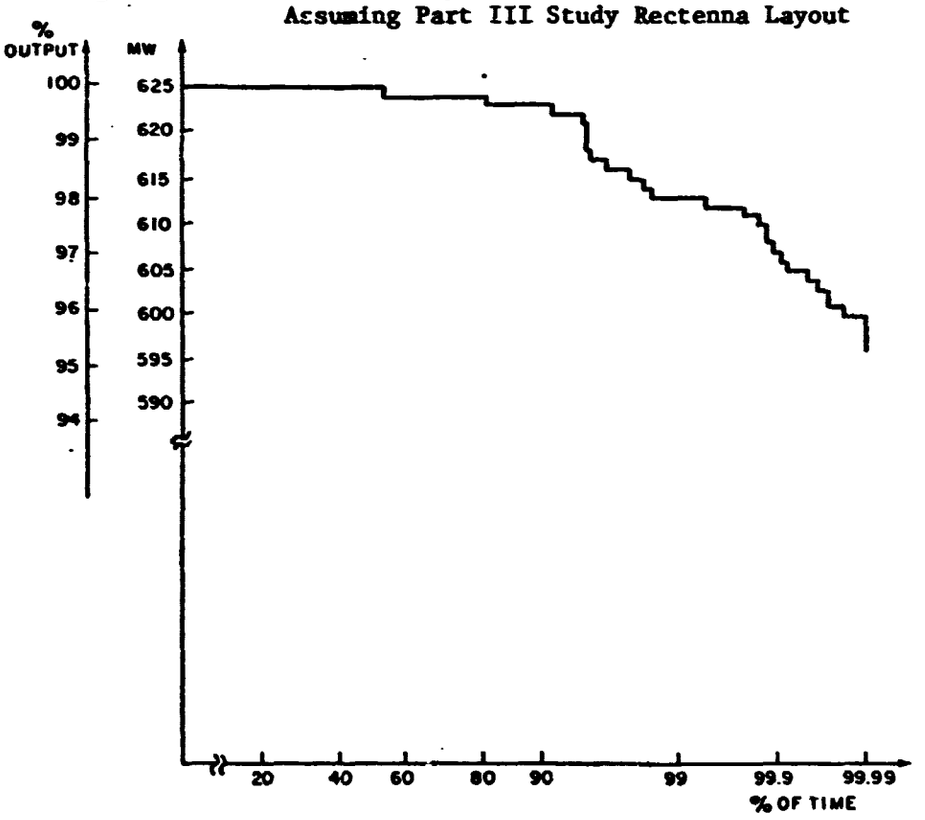

Figure 1.1-28. Availability Vs. Time for 625 Mw Sector AC Assuming Low Current Rectenna Layout

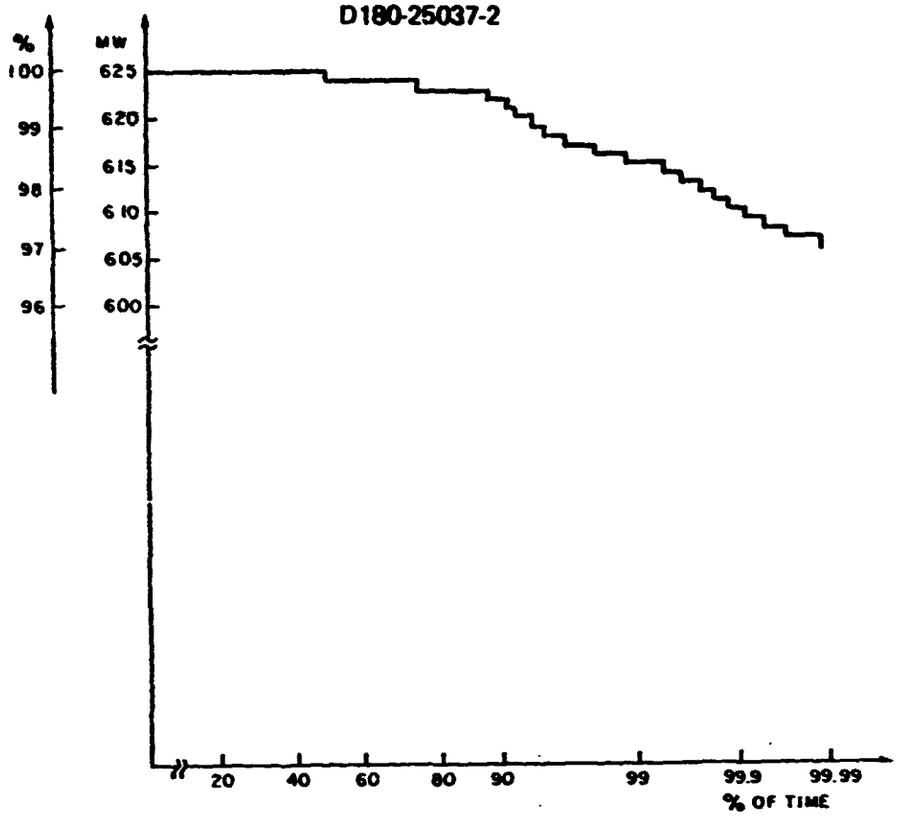

Figure 1.1-29. Availability Vs. Time for 625 Mw Sector AC Assuming Low Voltage Rectenna Layout

Resultant Availability of the Microwave Power Transmission System

From the availability calculations presented in the previous sections the resultant availability of the complete microwave power transmission system can be calculated. These results are summarized in Table 1.1-31. It must be emphasized that the equipment availability calculated previously is related, but not identical to the availability of power at the output terminal of the system, which is the interface to the power grid.

The resultant equipment availability for a given probability value P can be calculated approximately by simply multiplying the corresponding A values of the components in the series connected chain. However, when a power producing component in the space antenna fails, then at the same time the corresponding part of the space antenna aperture area is also lost. Thus in Table 1.1-31 the A values related to the DC distribution, phase control and Klystron of the space antenna must be entered twice in the resultant power availability product. The A values shown for the random phase and amplitude error effects were already calculated on the basis of their influence on antenna gain reduction.

On the basis of the power transfer efficiency values estimated by GE* for an SPS without failure and the power availability caused by failures the resultant efficiency probabilities can be calculated. This is shown in Table 1.1-32. The same table shows the actually available power. The absolure value of output power is 5% higher if a corresponding improvement in the resultant RF to DC conversion in the rectenna diode circuit is assumed.

*GE estimates of rectenna RF-DC conversion efficiency appear to be highly conservative inasmuch as higher values have been measured in laboratory tests - GW.

Figure 1.1-30 is a graphical presentation of the equipment and power output availability.

Table 1.1-31
Summary of Equipment and Power Availability Calculations

$\overline{P}^{\%}$	10	66	80	90	99	99.9	99.99
Hrs/Year	7889	2980	1753.2	876.6	87.66	8.766	.8766
A. Space Antenna	97.75	93.20	91.56	89.59	84.12	78.62	71.28
1 DC Distribution	100.00	99.50	99.22	98.95	98.00	97.00	95.95
2 Phase Control	99.84	98.92	98.44	97.83	96.10	94.40	91.30
3 Klystron	98.90	97.50	97.02	96.55	95.48	94.58	93.60
4 Random Phase	99.40	98.50	98.20	97.82	96.80	95.75	94.80
5 Random Amp.	99.60	98.60	98.40	98.00	96.65	94.90	91.70
B. Propagation	99.05	98.54	98.28	97.84	96.24	94.17	91.77
6 Attenuation	99.05	98.62	98.40	98.10	96.90	95.20	93.15
7 Faraday Rotation	100.00	99.92	99.98	99.74	99.32	98.92	98.52
C. Rectenna	98.38	98.13	97.61	97.03	95.06	92.96	87.65
8 DC power Collection	99.38	98.45	98.15	97.81	97.00	96.38	95.80
9 AC Power Collection	100.00	99.68	99.45	99.20	98.00	96.45	91.50
Total Power Transmission System Equipment Availability	96.22	90.12	87.78	84.99	76.96	68.88	57.33
Power Availability at Power Grid Interface Relative to Equipment Without Failure	95.00	85.85	83.19	79.43	69.20	59.65	47.01

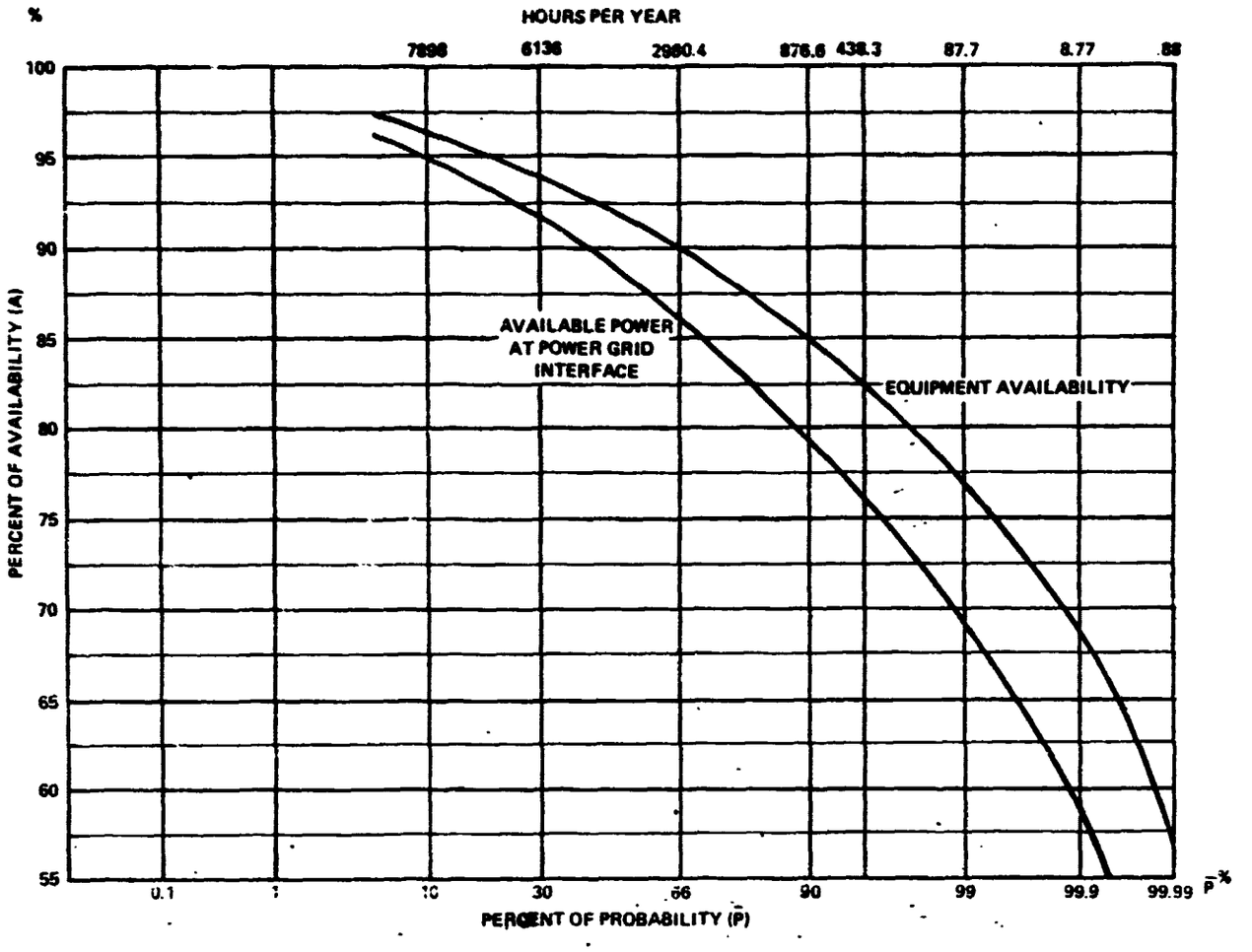

Figure 1.1-30. Equipment and Power to Utility Grid Availability of Overall SPS System Between Elevation Flexibile Joint of Space Antenna and Power Grid Interface.

Table 1.1-32

Availability of Efficiency and Power Into Power Grid

$\bar{P}$ %	10	66	80	90	99	99.9	99.99
Hrs/Year	7889	2980	1753.2	876.6	87.66	8.766	.8766
Available Efficiency %	63.33	57.23	55.46	52.29	46.13	39.76	31.34
Available Power MW	4513.3	4078.6	3952.3	3773.6	3287.6	2833.9	2233.4

An interesting characteristic is the rms power availability at the input of the rectenna. This can be obtained from Table 1.1-31 by taking the product of A of the space antenna, A related to the propagation media and sub-items 1, 2 and 3 at $\overline{P}$ = 66%. This yields

$$A = (.932)(.9854)(.995)(.9892)(.975) = .8858.$$

The above factor reduces the ideal value of RF power density in the middle of of the rectenna from the given 24.3 mw/cm^2 (see Section 2.1) to 21.52 mw/cm^2 on the average. Thus if 23 mw/cm^2 is allowable, the output from the space antenna can be increased by a factor of 1.068 or .29 dB. This would bring the available output power 4355.9 MW at the power grid interface. This is the maximum possible average power into the utility grid, compatible with the 23 MW/cm^2 specifications for the assumptions of the above presented (baseline) availability calculations.

The results in Table 1.1-32 are relatively pessimistic but it has to be judged from a proper perspective. With the exception of the klystron failure rate, no drastic reliability or diode efficiency improvements were considered and the assumed redundancies were not excessive. The calculations should not be taken as final result for an optimum system but merely a tool, by which the weak spots of the system can be detected. On the basis of these calculations reliability improvements can be implemented in such areas of the system where its cost impact is minimum. Alternatively some redundancies may be removed or maintenance requirements reduced in areas where their impact or cost is high, but their effect on availability is second order.

The cost senitivity of these variations relative to the assumed system can be demonstrated on the following simple model.

Assume that the relative cost distribution of the baseline SPS system is the following:

		%
①	Rectenna (Panel assembly: 7.15%, balance of system: 7.15%)	14.3
②	Space Antenna	14.3
③	Klystrons	7.1
④	Structure, solar cells, DC distribution, attitude control	50.0
⑤	Phase control	3.6
⑥	Control-monitor, misc.	10.7
	Total SPS capital investment	100.0
	Capital investment to cover yearly space maintenance cost	4.28
	Capital investment to cover yearly rectenna maintenance cost	.7

On the basis of the above assumption Table 1.1-33 shows the impact of various output power increasing options on output power and cost increase.

Table 1.4-33

Effect of Deviation From Baseline SPS on Relative Output Power

Option	A % Increase of Output Power	B % Increase of System Cost	B/A
A. Increase 4 and 3 by 1.068 for 23 mw/cm^2 max. Received Power Desnity	6.8	3.88	1.75
B Increase 4 and 3 by 1.1 Reduce 2 by 1.1 Increase 1 by 1.1	10.0	5.71	1.75
C. Increase 1 by 1.1211 for 96.77% beam efficiency	1.5	1.73	.87
D. Implement klystron Maintenance in Every 3 Months	2.5	1.58	1.58
E. Make Last Layer of Phase Control System Fully Redundant	.4	3.0	.13
F. Refurbish Rectenna Panel Asssembly After 15 Years	.58	3.57	.16
G. Reduce r to 438 Hours on Panel String Maintenance	.37	.35	1.06
All the above options are implemented. Average Power Output	23.88 (5052 MW)	26.50	.901
Only Cost Effective Options A, B and D are Implemented Average Power Output	20.42 (4911.4 MW)	11.50	1.77

It may be noted that the availability profile of the output power as shown in Table 1.1-33 is quite favorable in comparison to present day utility systems. If the average power of the system is rated at 4078.6 MW, then it falls to 80% of that level in less than 87.7 Hrs (1%) yearly.

The above availability number include only random failures. On the top of that during eclipse and biyearly maintenance period the system will be closed down completely on a scheduled basis.

Considering only the two 84 hours scheduled shut down and neglecting eclipse and the shut down and start up times Figure 1.1.31 shows the resultant available power, including scheduled maintenance.

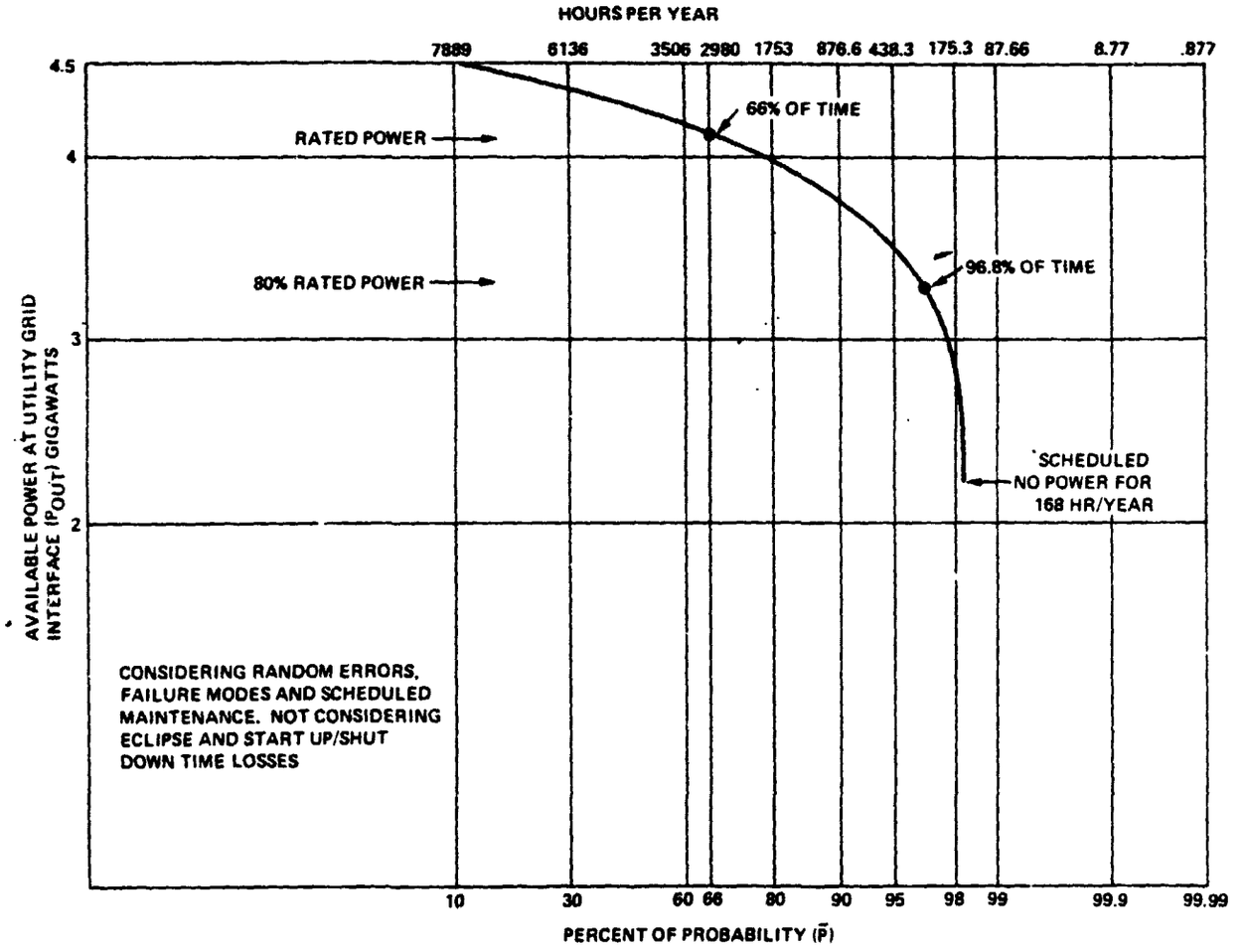

Figure 1.1-31. Available SPS Power to Utility Grid Considering Random Errors and Failure Modes and Scheduled Maintenance, But Neglecting Eclipse and Start Up/Shut Down Time Losses.

1.1.0.8 Command & Data Handling System Failure Modes and Effects Analyses (Provided by TRW)

A preliminary failure modes and effects analysis was conducted at the system level for both the CDHS and the communication subsystem. The status of the design is such that it was not considered productive to attempt an analysis at any lower hardware levels.

For the communication subsystem, one of the major recommendations was the use of earth coverage antennas instead of utilizing one of the techniques involving the MPTS antenna for this purpose. The concern was loss of communication in the event of a relatively small attitude control or antenna pointing error when the MPTS beam is deliberately despoiled. A second recommendation was use of separate communication links for the spacecraft and the MPTS antenna due to the magnitude of the requirements and concern over the ability to transmit high data rates across the slip rings.

For the CDHS, recommendations were made for several system areas:

A. System Redundancy

1) The RTU's should be non-redundant, however, the telemetry data should be distributed among the RTU's such that information concerning one component is divided among two or more RTU's. For example if one RTU monitors the on/off switch position of an electrical component, another RTU can be used to monitor the component temperature. Thus if one of the RTU's indicates a failure, the next level controller can check the output of the other RTU to verify the failure. If there is disagreement between the RTU's the next level controller can also check the status of the RTU's to determine both of these are operating properly.

2) The RTU's should be configured such that failure of one does not propagate to others or to the next level controller. An example of this would be local isolation of each RTU power supply.

3) One-for-one standby redundancy is recommended for the CPU's and the next lower level processors (module controllers) because of the relatively small number required and the importance of their functions.

4) For intermediate level processors (between the RTU's and the module controllers) it was concluded that a bank of spares would be satisfactory. Each of these spares would be such that it could be activated to replace a failed processor.

B. Data Bus

1) The use of fiber optics was recommended for the same reasons outlined in the information management section of volume 3, however, a concern was expressed over the degradation of the optical conducting material during the required 30 year lifetime.

2) The use of a parallel, redundant data bus between the module controller and the CPU is also recommended.

1.1.1 Satellite Energy Conversion

Three subjects are covered in this section: Solar Array Support Structure Analyses (WBS 1.1.1.1), Solar Blanket Analyses (WBS 1.1.1.3), and Solar Blanket Maintenance (Annealing; WBS 1.1.1.6). There were no analyses to report under WBS numbers 1.1.1.2, 1.1.1.4, or 1.1.1.5.

1.1.1.1 Structural Analyses

A loads analysis which resulted in a structural resize was performed during this contract period. The results of the loads analysis, including initial assumptions, and the new structural configuration and member sizes will be discussed. Also, Grumman analyzed an aluminum solar array support structure.

A. Loads Analysis

The loads analysis was performed on one module of the solar power satellite (4x8 bays). The maximum load condition was determined to be that of a satellite module, with one antenna payload, undergoing self-powered orbit transfer from LEO to GEO. For the loads analysis the maximum acceleration of the module was assumed to be 10^{-4}g. The acceleration of the satellite module is achieved by using electric thrusters mounted at each corner.

The basic configuration of the module used for the loads analysis is shown in figure 1.1.1-1. The antenna would be installed on the back of the module (opposite the solar array) attached to the geometric center of that face.

The structural cell (bay) configuration shown in the part III documentation was revised to provide a suitably stable unit. Figure 1.1.1-2 illustrates the original and revised structural concepts. In the original system the edge cells of each of the eight modules making up the entire SPS used the configuration illustrated. The interior cells employed an absolute minimum of structure. Further analysis indicated that the edge cells were not stable with the result that the entire system was not stable. Further, the 7½ meter beams were not adequate for solar blanket tension when the solar blanket tension was changed to uniaxial. As a result, the system was revised to the configuration indicated for solar blanket tension support and all cells incorporating the structural concept shown. The lower-deck-to-uppper-deck diagonal provides structural stability.

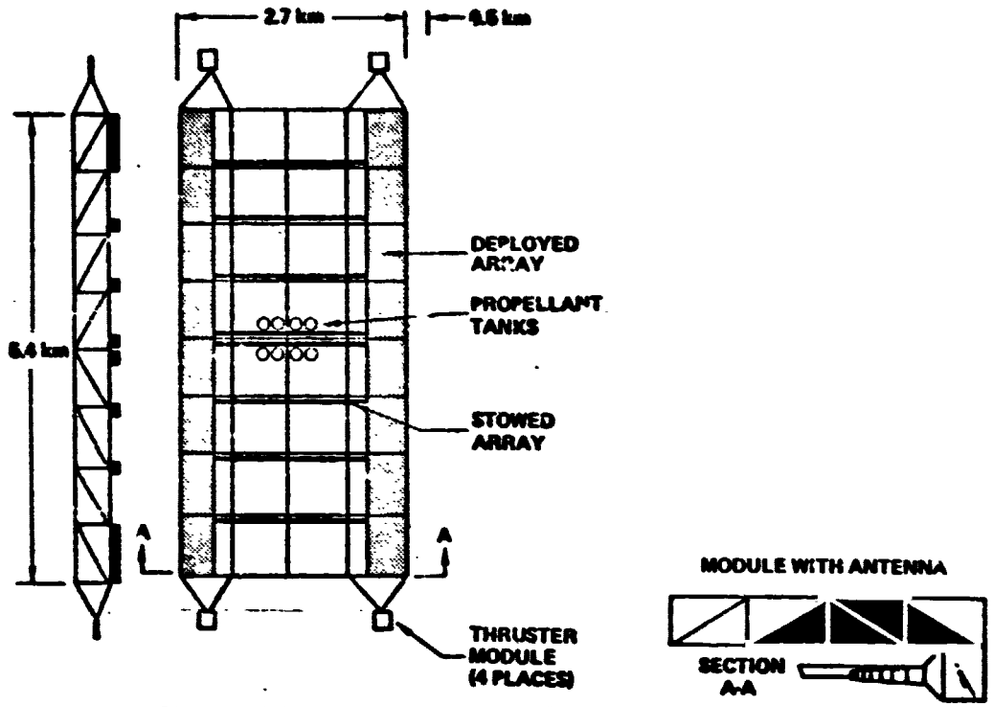

Figure 1.1.1-1 SPM Configuration for Loads Analysis

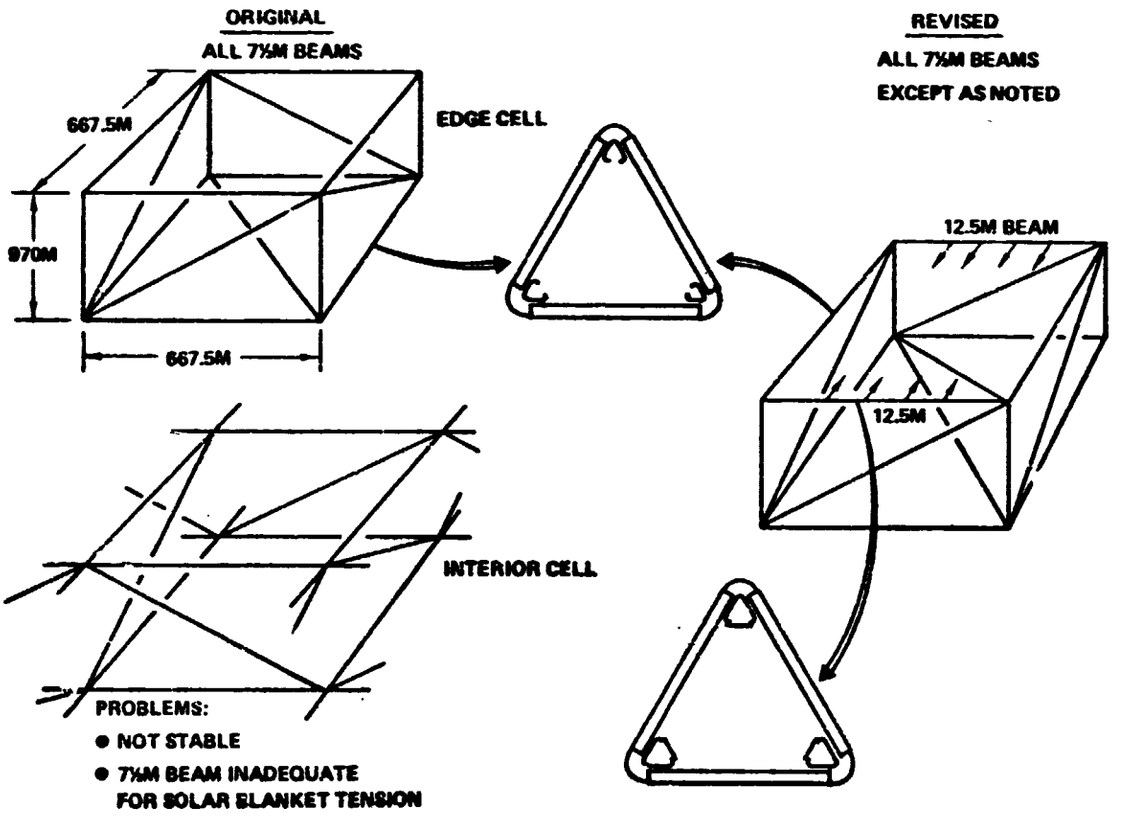

Figure 1.1.1-2 Solar Array Support Structure Evolution

The maximum acceleration condition (10^{-4}g) results in a thrust per corner on the module of 6100N. This thrust was reacted into the module structure to determine the member loads on the short edge (four bay side) and the long edge (eight bay edge). Figure 1.1.1-3 illustrates the results of the loads analysis on the satellite module with the maximum loads summarized in table 1.1.1.-1. The maximum loads in the table were used to resize the structural members.

B. Revised Structural Configuration and Member Sizing

The revised bay configuration including an index of the location and types of beams used in a typical bay is shown in figure 1.1.1-4. The loads analysis resulted in the selection of three types of beams for the satellite structure. For construction purposes, type B and C beams differ only in their batten spacing. This will allow the use of only two types of beam machines in the construction facility.

Type A beams are designed for accommodating the bending load resulting from blanket pretension. A bending load of 4.285 N/m resulted from the necessity to achieve a blanket first mode frequency of 0.0024 Hz, two times the system first mode frequency. To react this bending load a 12.7 meter beam width and a 15.0 meter batten spacing was selected. The beam characteristics are shown in table 1.1.1-2.

Type B beams are designed for all satellite lateral beams to accommodate the maximum column loads that result from the 10^{-4}g orbit transfer acceleration.

Type C beams are designed for all other satellite beams to accommodate the lower column loads shown previously in table 1.1.1-1. The majority of the beams in the baseline system are type C beams.

The structural mass of the satellite (without the MPTS or support) was calculated to be 9728.7 MT. Figure 1.1.1-5 and table 1.1.1-3 summarize the new module configuration, dimensions and structural mass breakdown.

The reference system selected for Phase 2 is a 5-gigawatt satellite (one antenna) to be constructed in geosynchronous orbit. For this system, all type B beams can be changed to type C, as orbit transfer loads are not a design factor. Also, the duplicate structure inherent in the modular design is eliminated. The resulting structure mass is 3198 metric tons, about 35% less massive per unit SPS area than the LEO construction structure.

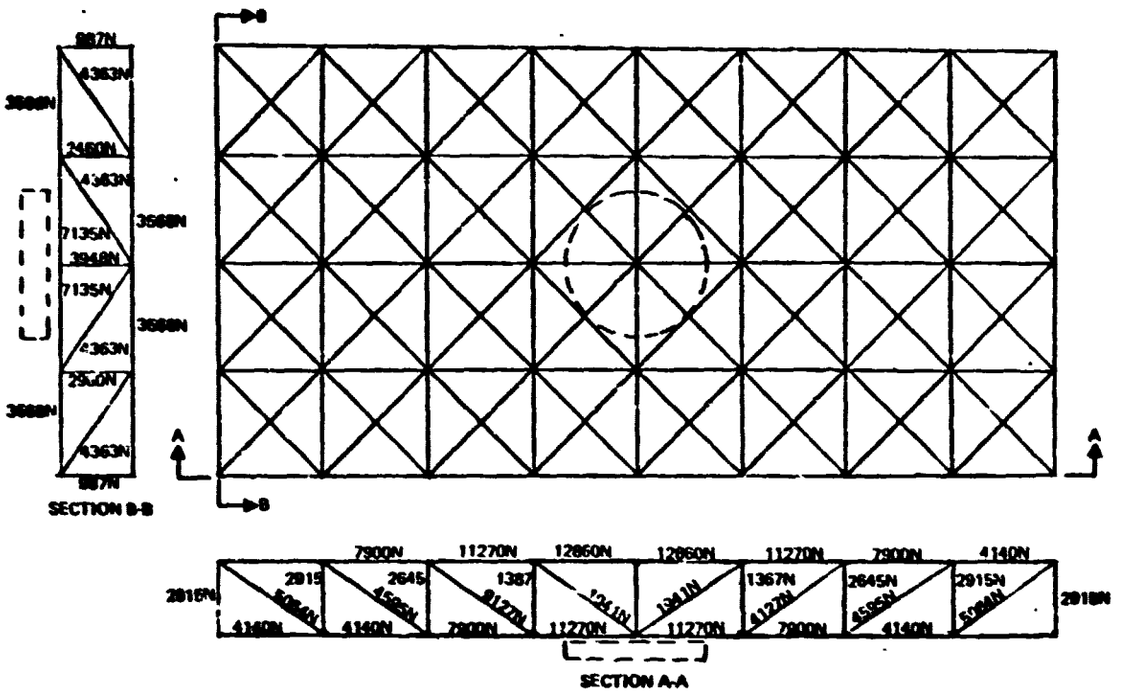

Figure 1.1.1-3 Loads Analysis Results

Table 1.1.1-1 Loads Summary

Element	Column	Bending	Comment
Posts	4000N		
Diagonals	5064N		
Longitudinal Beam	3568N		Module Transport
Longitudinal Beam	333N	4.285 N/m	Array Pretension
Lateral Beam	13000N		

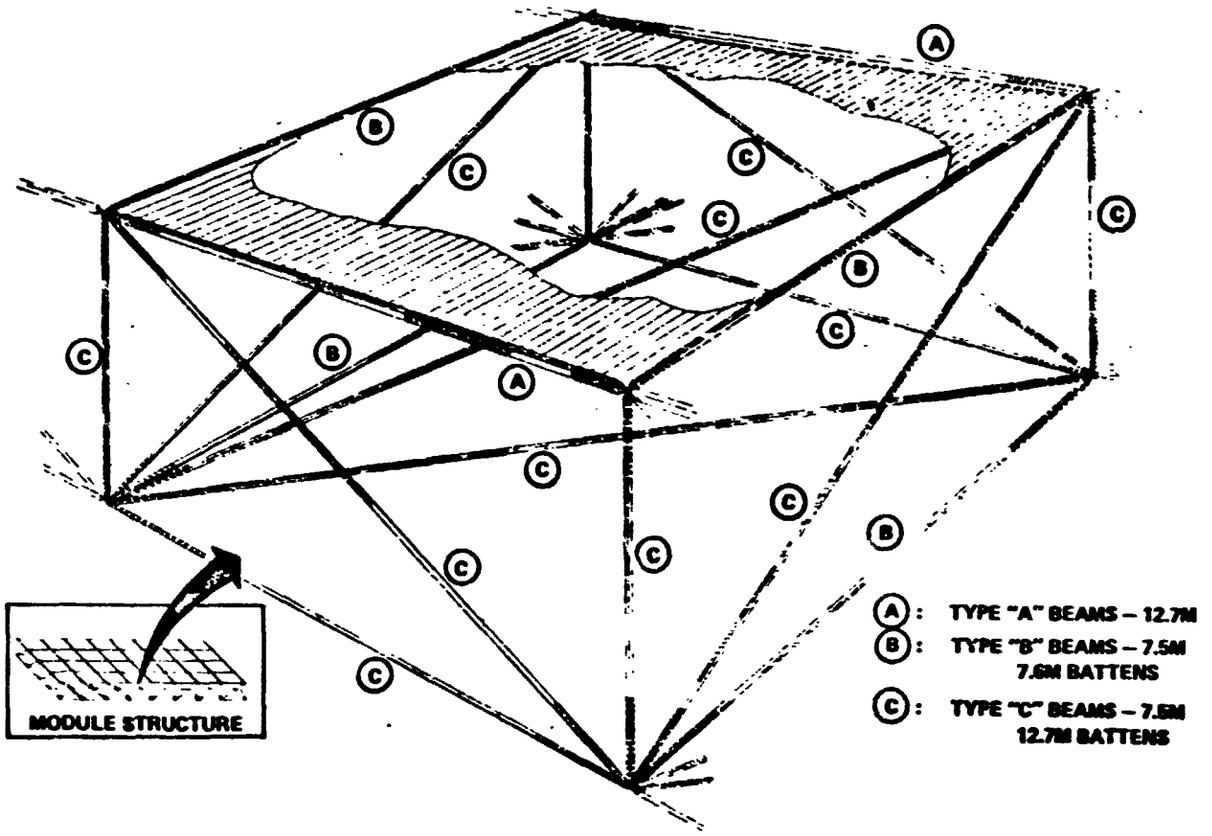

Figure 1.1.1-4 Solar Power Satellite Structural Bay Configuration

Table 1.1.1-2 Solar Power Satellite Structural Update Beam Configurations

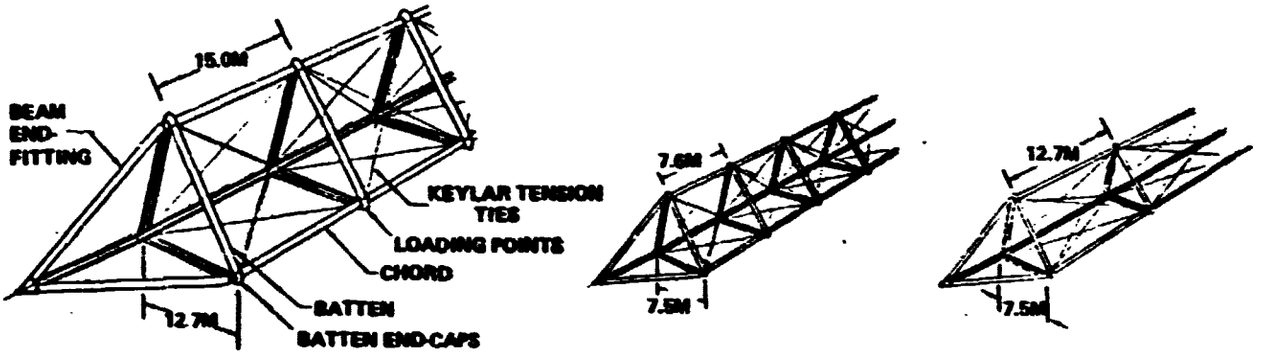

ITEM	TYPE A UPPER SURFACE LONGITUDINAL BEAM	TYPE B UPPER AND LOWER SURFACE LATERAL BEAM	TYPE C BEAM USED IN ALL OTHER LOCATIONS
SECTION	CLOSED	OPEN	OPEN
REF. SIDE LENGTH	38 CM	38CM	38CM
MAT'L THICKNESS	0.86 MM	0.71 MM	0.71 MM
EI_X	3.30 E8 N/CM^2	1.80 E8 N/CM^2	1.80 E8 N/CM^2
BEAM WIDTH	12.7M	7.5M	7.5M
BATTEN SPACING	15.0M	7.6M	12.7M
CRITICAL LOAD	17480N (CRIP. CHORD)	19000 N (BUCK. BEAM)	7080 N(BUCK BEAM)
MASS/LENGTH	7.48 KG/M	5.12 KG/M	4.11 KG/M

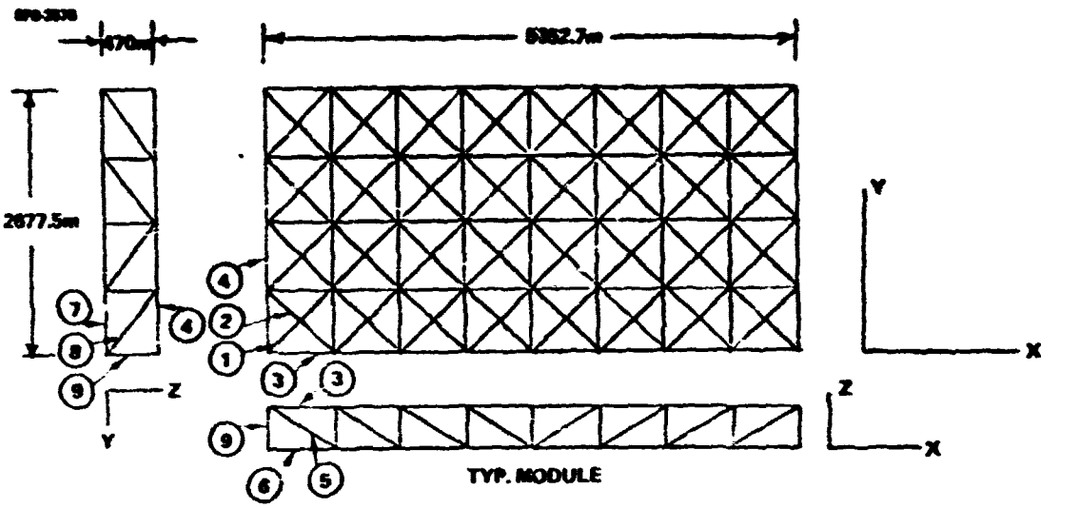

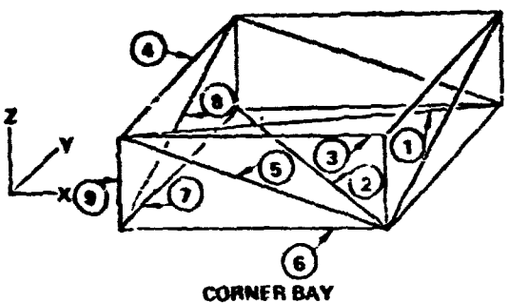

1 BODY DIAGONAL – 1054.5m

2 LOWER SURFACE CROSS-BAY DIAGONAL – 944.0m

3 UPPER SURFACE LATERAL – 667.5m

4 UPPER SURFACE LONGITUDINAL – 667.5m

5 LATERAL INTERSURFACE DIAGONAL – 816.4m

6 LOWER SURFACE LATERAL – 667.5m

7 LOWER SURFACE LONGITUDINAL – 667.5m

8 LONGITUDINAL INTERSURFACE DIAGONAL – 816.4m

9 CORNER POSTS – 460.2m

LATERAL/LONGITUDINAL DEFINED FOR ASSEMBLED (8x32) SPS.

Figure 1.1.1-5 Module Mass Calculations

Table 1.1.1-3 Structural Mass Summary

BEAM TYPE	CONF. TYPE	NO. OF BEAMS MODULE	TOTAL LENGTH MODULE (m)	MASS (kg) LENGTH m	MASS MODULE (MT)
1	C	32	33744	4.106	138.55
2	C	32	30288	4.106	124.03
3	B	40	28700	5.122	136.76
4	A	36	24030	7.476	179.65
5	C	40	32656	4.106	134.09
6	B	40	26700	5.122	136.76
7	C	36	24030	4.106	98.67
8	C	36	32656	4.106	134.09
9	C	46	18408	4.106	75.58
BEAM MASS/MODULE				–	1158.18 MT
5% MASS FOR JOINTS				–	57.91 MT
TOTAL MASS/MODULE				–	1216.09 MT
TOTAL STRUCTURAL MASS/SATELLITE (NO MPTS OR SUPPORT) [PRIMARY STRUCTURE]				–	9728.7 MT

ALUMINUM SOLAR ARRAY STRUCTURE

During Phase I, Grumman also performed preliminary studies on the feasibility of using aluminum alloys for the basic solar array structure of the SPS. Practical thermo/structural design solutions were found for minimizing the effects of thermal transients in orbit. The results of this analysis are compared with Boeing's advanced composite SPS structure.

This study was focused on the design conditions for Boeing's 10GW SPS, which is fabricated in low earth orbit. As shown in Fig. 1.1.1-6, this satellite consists of eight attached solar array modules and two microwave antennas. Each solar array module, 2678 m by 5348 m, is self transported to geosynchronous orbit using thrusters mounted at each of four corners. Two of the modules are coupled with antennas. The complete satellite is assembled in GEO.

Estimates of design loads were made for the critical design conditions; stiffnesses were calculated and used to estimate the natural frequency of the complete satellite. Several thermal design conditions were selected for evaluation to assess the response of the aluminum structure to the thermal environments. The very limited studies carried out, particularly in the thermo/structural area, indicate that the use of aluminum is feasible. However, a considerable amount of design and analytic effort must be done to reach a more definitive conclusion.

The major conclusions derived from this task are as follows:

- Roll formed closed section aluminum structures can be automatically fabricated in orbit.
- Design load requirements for LEO constructed SPS module are satisfied - aluminum 23% (2.82×10^5 Kg) heavier than composite but maybe lower in cost.
- 10 GW SPS natural frequency with aluminum (AR 4) is 65 times orbital frequency - instead of 100 times.

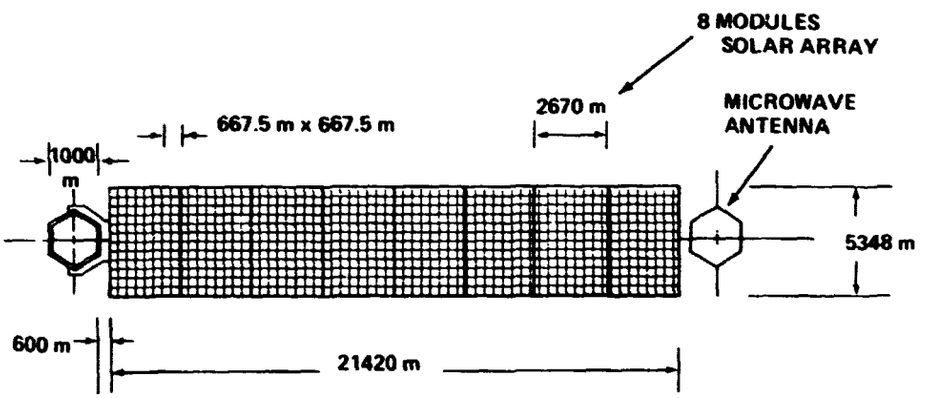

Figure 1.1.1-6 10 GW Solar Power Satellite

2955-002V

- Estimated natural frequency is adequate for satellite control system stability; further analysis required to verify.
- Based on initial studies, thermal stresses are within capability of aluminum design.
- Satellite deflections are within acceptable limits (2°).
- LEO thermal cycle effect may alter basic aluminum beam length (667.5m) by as much as .9m. Further study required on assembled structure response, and thermal design options.
- GEO construction approach can avoid LEO thermal cycle problem by not fabricating during biannual occultation periods.
- Open issues (aluminum vs. composite trade)
  - LEO vs. GEO construction approach
  - Satellite and construction base requirements for overall stiffness alignment and local rigidity constraints
  - Equipment structural designs
  - Comparable costing (ground prep and delivery to orbit).

It is recommended that the aluminum solar array structure be investigated further in Phase II. The aluminum structure design should be updated for the current SPS baseline. Specific areas to be emphasized include:

- Broaden thermostructural analysis
- Investigate interface loads and interactions between satellite and construction base
- Verify satellite control system feasibility
- Analyze space fabrication requirements and costs
- Define advanced technology requirements.

DESIGN REQUIREMENTS AND LOADS

The basic design data and requirements supplied by Boeing for the study are shown in Fig. 1.1.1-7. The thrust to weight ratio is applied to the 4 bay by 8 bay modules for self transport to LEO. The SPS structure natural frequency of 1.2×10^{-3} hz (4.32 cph) which is 100 times orbital frequency in GEO is used to assess the aluminum structure frequency and also used to establish the solar array blanket pretension after increase by a factor of 2.0 to 2.4×10^{-3} hz.

- MASS DATA

SOLAR ARRAYS	5.178×10^7 kg
MW ANTENNAS	2.521×10^7 kg
WT GROWTH	2.051×10^7 kg
TOTAL	9.75×10^7 kg

- SOLAR ARRAY BLANKET UNIT WEIGHT – 0.427 kg/m^2
- T/W IN TRANSPORT FROM LEO TO GEO – 0.0001
- SPS NATURAL FREQUENCY INCLUDING SOLAR CELLS & ANTENNAS – 0.0012 Hz
- SOLAR BLANKET NATURAL FREQUENCY – 0.0024 Hz
- SOLAR BLANKET PRELOAD NEEDED TO OBTAIN FREQUENCY = 4.285 N/m (0.0245 LB./IN.)
- FACTOR OF SAFETY – 1.4
- 30 YEAR SERVICE LIFE

2955-004V

Figure 1.1.1-7 Design Data

- SOLAR BLANKET PRE-LOAD
- TRANSPORT ACCELERATION TO GEO
- TEMPERATURES & THERMAL GRADIENT TIME HISTORIES
- ATTITUDE CONTROL & STATION KEEPING TORQUES
- STIFFNESS
- INTERFACE LOADS BETWEEN MODULE & CONSTRUCTION BASE? BEAM HANDLING

Figure 1.1.1-8 Design Conditions

2955 003V

The 30 year service life, when increased by an appropriate scatter factor, is used to evaluate time dependent failure modes such as fatigue, flaw growth, creep and environmental degradation effects. It is expected that low stress levels may permit aluminum to satisfy the life requirements.

The more significant structural loading conditions shown in Fig. 1.1.1-9 currently are the solar array blanket preload and loads caused by transport of the 4 bay x 8 bay module to GEO. The first condition causes a high local cap load in the 7.5 meter beam; the second induces the highest column compression load in the 7.5 m by 667.5 m beam. Inasmuch as aluminum has a coefficient of thermal expansion greater than the advanced structural composites, the effect of gradients on distortions, stresses etc., are evaluated. Thermal control features are incorporated in the design to minimize thermal/structural response. These include thermal coatings, incorporation of lightening holes in members, etc. Loads induced during fabrication and handling will also require assessment in later phases of this program. The stiffness requirements are used to define the loads on the beams supporting the solar array blanket and to evaluate the overall SPS natural frequency in GEO.

Further discussion on loads due to orbital transfer and solar array preload are provided below.

Loads - Orbital Transfer Condition

Figure 1.1.1-9 shows the 4 bay by 8 bay module which is constructed in LEO and transported to GEO for assembly into the full size SPS. Eight of these modules are joined together to make up the 21420 m x 5348 m satellite. The thrusters are supported on four outrigger structures. At each end of the module solar array blankets are deployed to provide power during transport. This arrangement defines the two basic design conditions which are critical for the primary solar array structure. The thrust forces balanced by inertia forces induce bending and shear in the truss; the larger member loads occur in the 5348 meter direction. These loads are the largest column loads on the 667.5 meter beam. The solar blanket preloads on each of the two end bays cause the maximum local cap compression load.

Figure .1.1.-10 shows the module with thruster loads applied to the combined module and antenna mass; the antenna is supported at points A, B, C and D. A dynamic magnification factor of 2.0 and a safety factor of 1.4 were used to obtain ultimate design loads in the truss.

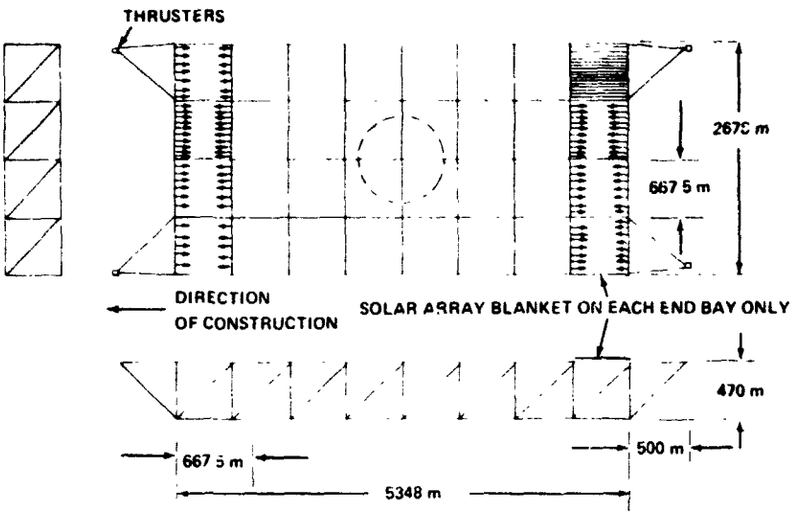

2955 005V

Figure 1.1.1-9 4 Bay by 8 Bay Module

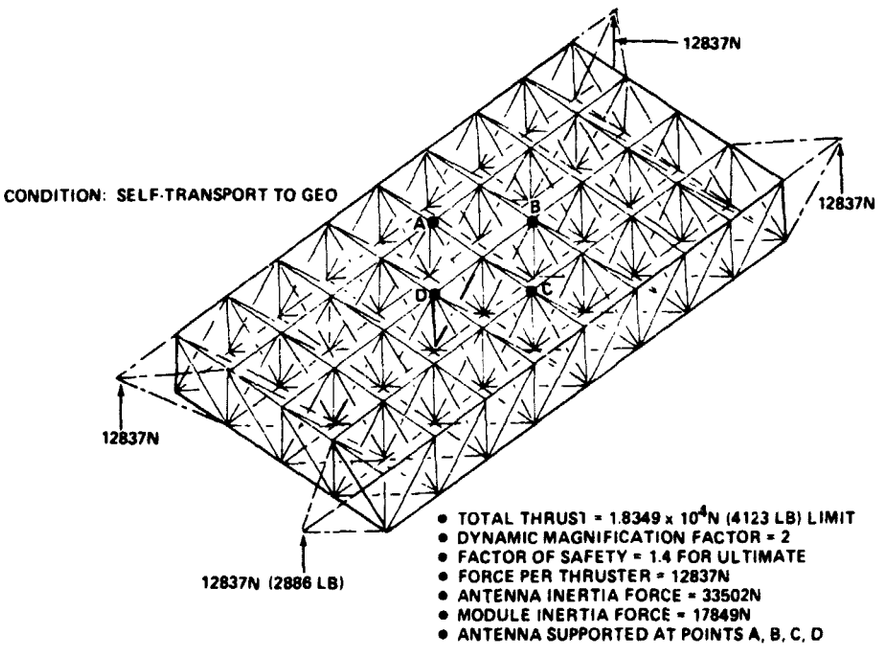

Figure 1.1.1-10 Design Loads on Module

2955 006V

The summary of critical member loads for the truss are shown in Fig. 1.1.1-11 for the module plus antenna transport condition. The loads are based on the required thrust to weight ratio of 10^{-4}. The maximum load condition for the 667.5 meter beam was used to analyze the member as a lattice column; the results show the member has a 10% margin of safety.

Loads - Solar Array Preload

The LEO baseline configuration utilizes a four bay wide construction base to fabricate the 4 bay by 8 bay module. During module construction, the 15 meter wide solar array blankets are installed on the two end bays of the 8 bay length as shown in Fig. 1.1.1-12. The 15 meter arrays are interconnected along their lengths and uniaxially pretensioned such that the blanket natural frequency is 8.64 cph. Bending moments, caused by the pretension result in high axial compression loads in the caps of the 667.5 m beam. This condition gives the critical load in the cap of the 7.5 meter deep beam.

Figure 1.1.1-13 illustrates the loading system on the triangular cross-section beam when the running preload of 4.29 N/m is applied to the 667.5 m span. The maximum bending moment at the midspan is 3.35×10^{5} Nm. The curve shows the compression cap load as a function of beam depth. The cap load for the selected 7.5 m depth beam is 2.58×10^{4} N compression.

ALUMINUM STRUCTURE DESIGN

Beam Design

An aluminum beam design, which can be fabricated in space for the SPS solar array structure, is shown in Fig. 1.1.1-14. The aluminum triangular cross section beam design incorporates three roll formed closed section caps interconnected by battens spaced at 7.5 meters. Shear stiffness can be provided by either preloaded cross cables or compression/tension members. The cable concept is approximately 20% lighter and has been selected for the baseline aluminum structure. However, pretensioned cables for shear stiffening may induce potential problems such as: adjustment of all cable tensions to the proper preloads to prevent slack at any time, failure of cable attachments, potential for excessive material creep deformation under sustained load and temperature for 30 years increased by an appropriate scatter factor, effect of selected cable system on lattice column capability, etc.

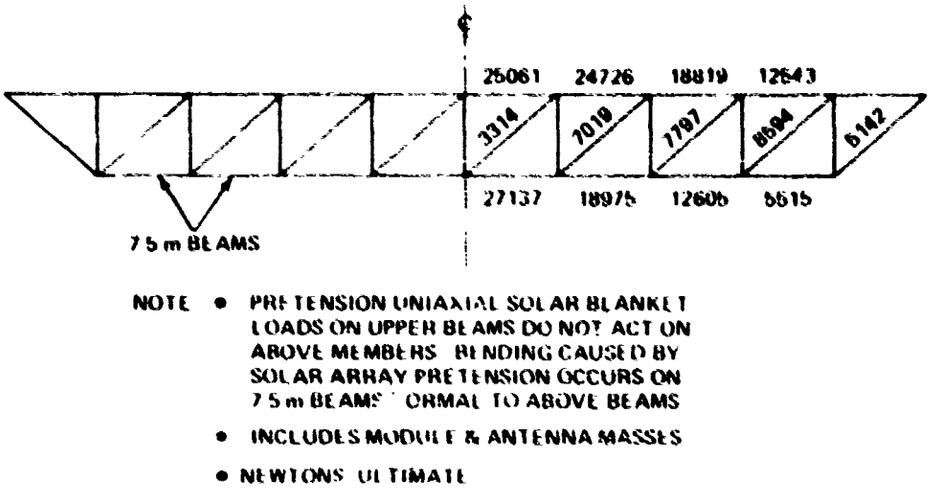

Figure 1.1.1 11 Summary Truss Loads Due to Orbit Transfer from LEO to GEO

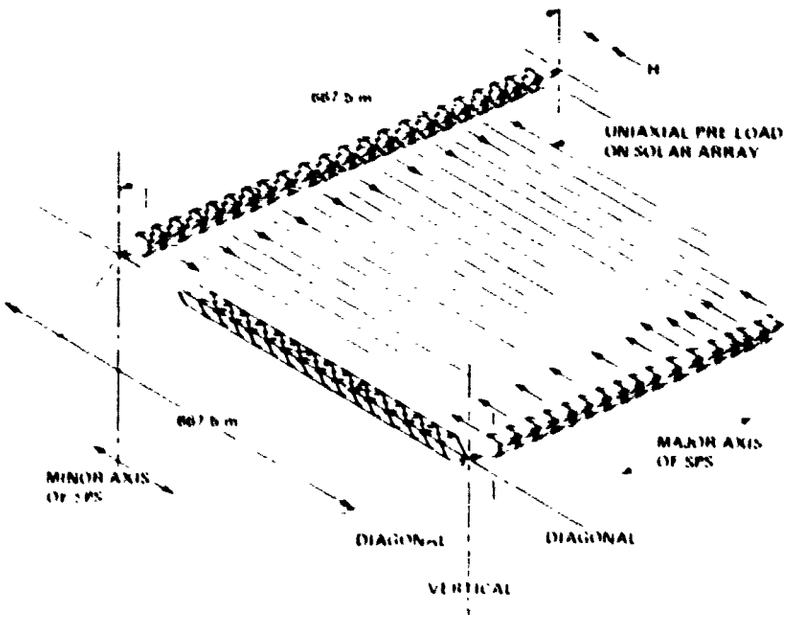

Figure 1.1.1-12 Solar Array Preload Design Condition

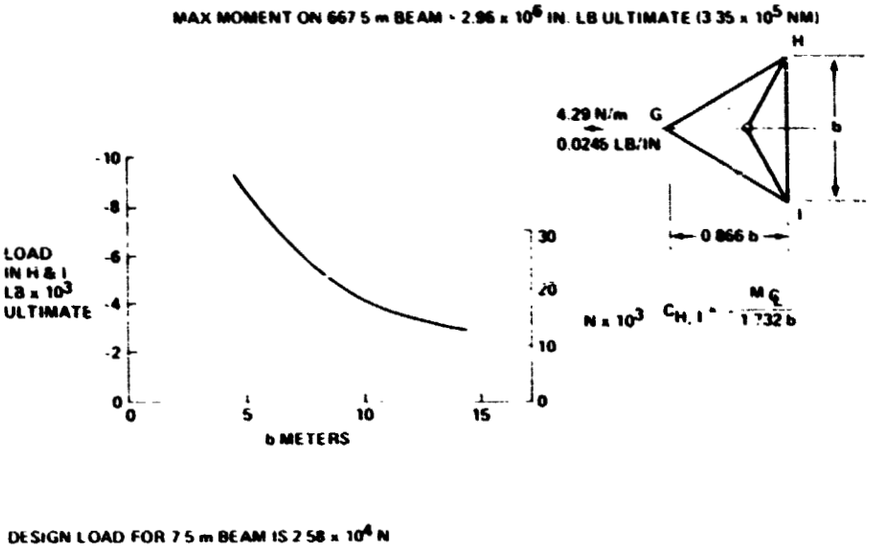

Figure 1.1.1-13 Variation of Critical Cap Compression Load vs Beam Depth

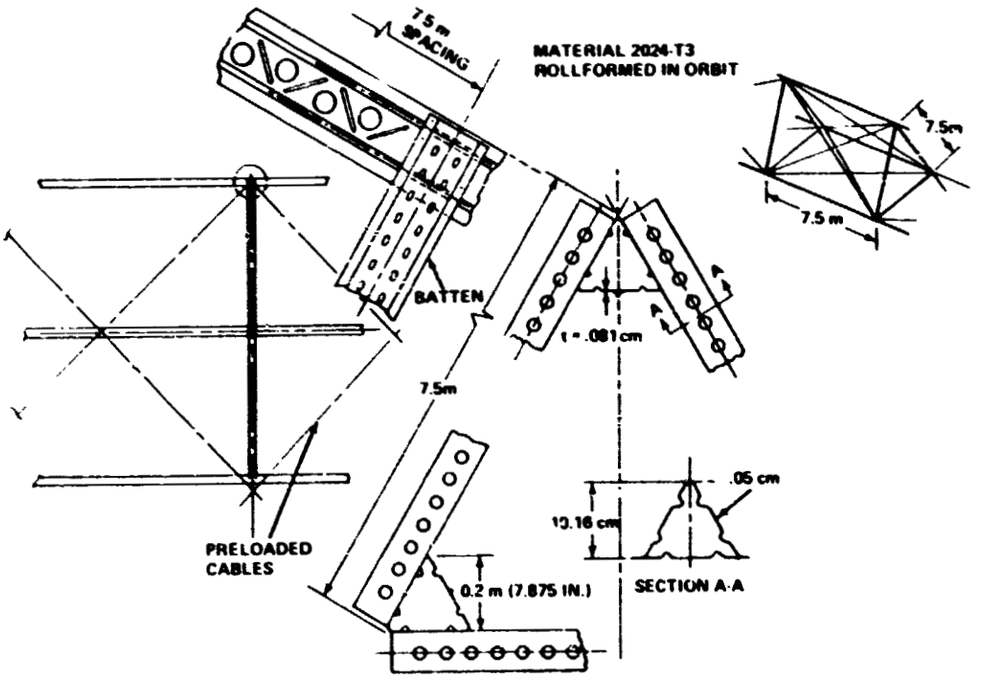

Figure 1.1.1-14 Aluminum Beam Design 7.5 Meters

The selected cap size for the design loads is .2 m deep and has a thickness of .081 cm. The batten is also a closed section with the bottom flanges extending outward for attachment to the cap. The depth is 10.16 cm and thickness of .05 cm.

In order to minimize thermal gradients in members and between members, flanged lightening holes have been spaced to reduce shadowing as much as possible. Several thermal coatings have also been evaluated to maintain temperatures and gradients within acceptable limits, although additional studies are required to obtain an optimum design.

The roll formed cap incorporates longitudinal stiffening beads near the corner sections in order to provide a high compression capability in the corners. Between the lightening holes, beads are rolled into the section for stiffening. The section is formed on a mandrel (Fig. 1.1.1-15) which is used for support during the attachment operation. The lower attachment on the centerline is not completed until after the battens are connected. The gap between flanges permits the mandrel support to extend inward to the beam machine; the mandrel support ends, and the two flanges are joined.

Aluminum Beam Closed Cap Design

Figure 1.1.1-16 shows the required thickness and depth of closed cap cross section for the 7.5 meter deep beam with a batten spacing, L, of 7.5 meters. The curves are based equating section crippling strength to column failure strength for various column fixity conditions. These data were developed as an initial design optimization procedure. However, the selected cap design represents an off optimum configuration because of the requirements to provide large lightening holes to reduce thermal gradients, to permit sufficient attachments between battens and cap and to provide stiffness for column stability. The selected section is .2 m deep and .081 cm thick.

Candidate Material Properties

Candidate aluminum materials are listed in Fig. 1.1.1-17 together with their more significant properties. These materials were selected because they can be roll formed in these tempers, are weldable and have relatively good compressive yield strengths. The spot weldability as the preferred method of attachment is of questionable value due to electrode wear; this characteristic may be overcome with sufficient future technology development.

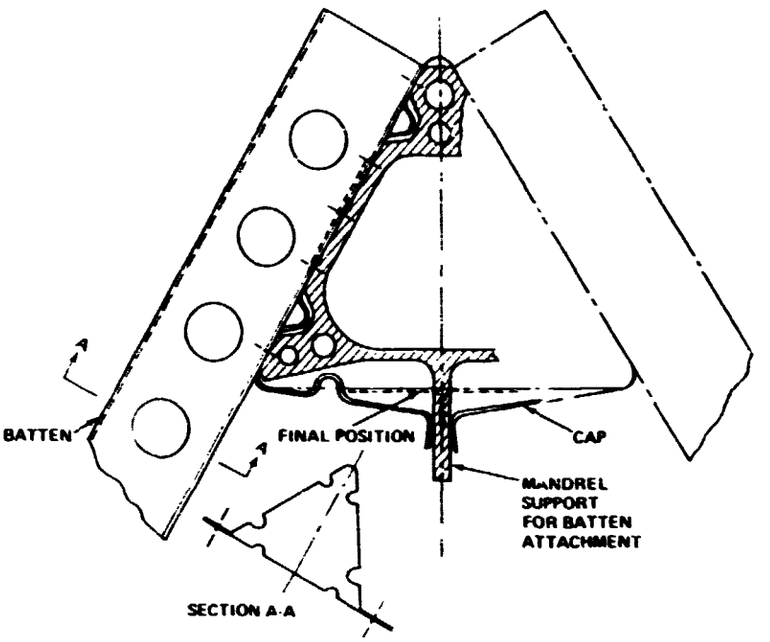

Figure 1.1.1-15 Roll Formed Aluminum Cap on 7.5 m Beam Closed Section

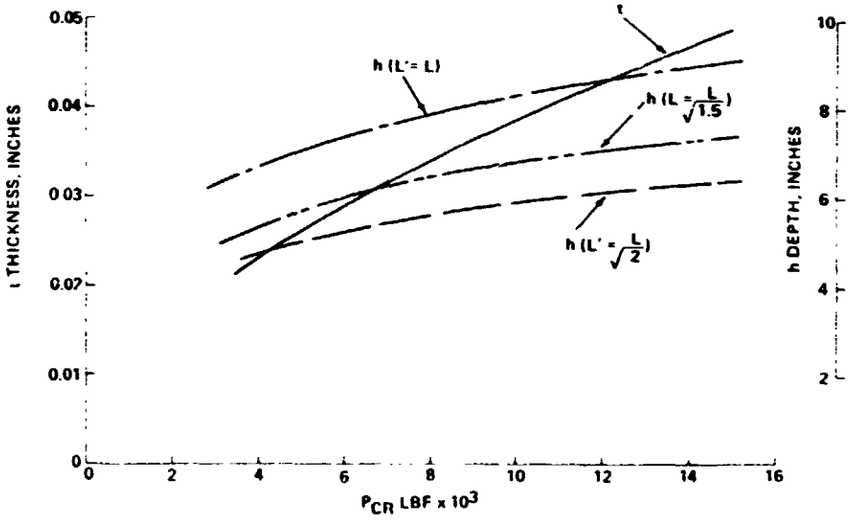

Figure 1.1.1-16 Aluminum Closed Section Beam Cap Thickness & Depth vs Critical Load; L = 7.5 m

	2024-T3	2219-T6	6061-T6
• F_{TU} ksi	64	54	42
• F_{TY} ksi	47	36	36
• F_{CY} ksi	39	38	35
• E_C ksi	10.7×10^3	10.8×10^3	10.1×10^3
• ρ LB/IN.^{3}	0.100	0.102	0.098
• α IN./IN./°F x 10^{-6} @ 200°F	12.9	12.4	13
• K BTU/(HR) (FT^2) (°F)/FT	80	74	96
• C BTU/(LB) (°F) @ 200 °F	0.22	0.23	0.23

Figure 1.1.1-17 Candidate Material Property Data

2955-012V

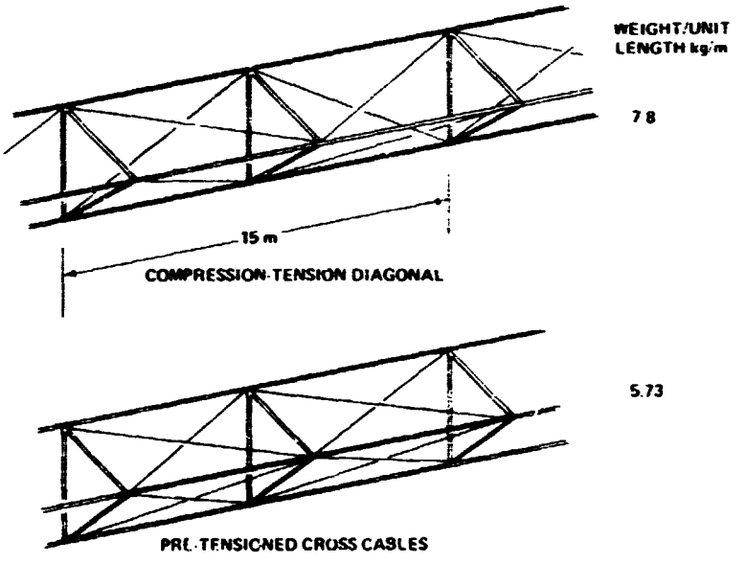

Figure 1.1.1-18 Candidate Truss Configurations

2955-013V

The area of joints and attachment techniques requires an in depth development program to evolve an optimum attachment method which requires minimal service, provides sound attachments, creates no debris, requires low power and has a high degree of reliability.

Candidate Truss Configurations

A weight comparison was made between several truss configurations considering various depths of truss and bay widths, as well as pretension cables versus compression capable diagonals. Figure 1.1.1-18 shows the comparison of the 7.5 meter beams with cables and compression diagonals. The cable system design is approximately 30% lighter and was chosen for the design baseline. The calculated weight for the selected sizes, which meet the strength requirements, shows the unit weight to be 5.73 kg/m (3.84 lbs/ft) for the cross cable design.

Aluminum Structure Weight

The weight of the 4 by 8 bay module was calculated for the aluminum structure and compared to the Boeing supplied weight for the composite design. The aluminum structure is approximately 23 percent heavier (282,000 Kg) than the composite module.

The weights shown in the Fig. 1.1.1-19 are for the basic structure only, not including thruster outriggers, plus a 5 percent increment for miscellaneous.

Aluminum Structure Natural Frequency

Based on the structural sizes and properties for the aluminum structure and the mass data for the SPS (9.75×10^7 Kg), the natural frequency was calculated for the baseline design point (aspect ratio AR = 4) with the two antennae lumped at the tips as shown in Fig. 1.1.1-20. The frequency calculated is $.75 \times 10^{-3}$ hz compared to a required 1.2×10^{-3} hz. The variation of natural frequency with aspect ratio was also calculated; the aspect ratio would have to be reduced to 2.3 to attain a frequency of 1.2×10^{-3} hz. A curve is also included which shows the effect of structural depth on frequency for an aspect ratio of 4.0. For the required 1.2×10^{-3} hz it is not feasible to increase frequency by this method. The frequency curve for the same mass, uniformly distributed shows a much higher frequency as might be expected; the very large

- WEIGHT OF 7.5 m BEAM = 5.73 kg/m (3.84 lbs/ft.)
- MEMBER LENGTHS IN 4 BAY BY 8 BAY MODULE
  - DIAGONALS = 1.26×10^5 m (4.134×10^5 ft.)
  - CHORDS & VERTICALS = 1.23×10^5 m (4.024×10^5 ft.)
- 4 X 8 BAY MODULE WEIGHT INCLUDING 5% ASSEMBLY PROVISIONS = 1.49×10^6 kg (3.29×10^6 lbs)
- WEIGHT OF COMPOSITE MODULE = 1.216×10^6 kg
- ALUMINUM STRUCTURE IS 23% HEAVIER THAN COMPOSITE STRUCTURE

Figure 1.1.1-19 Aluminum Structure Estimated Weight

2955-024V

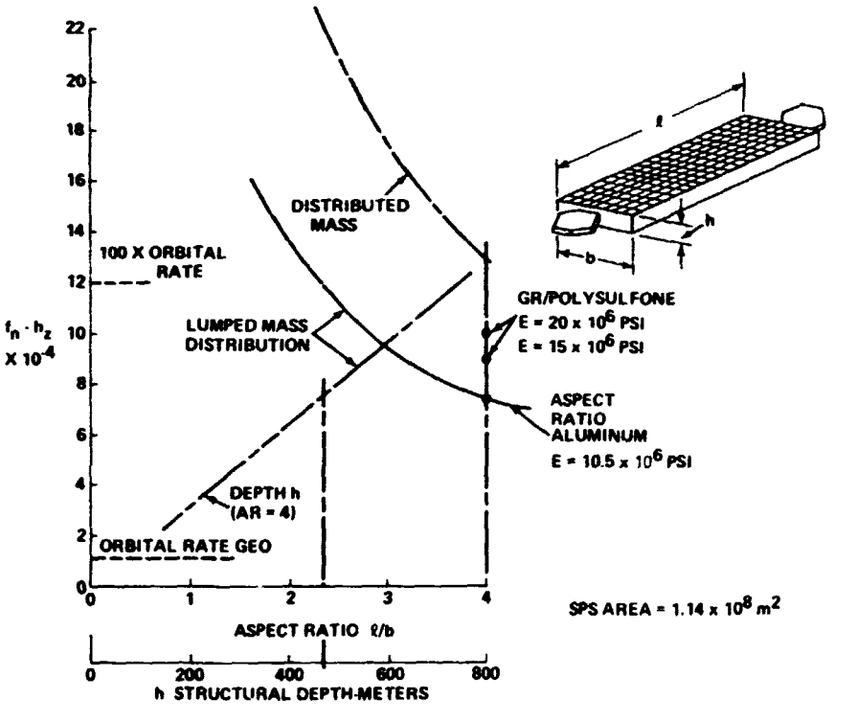

2955-014V

Figure 1.1.1-20 Aluminum Structure Natural Frequency

masses at the tips of the SPS cause an appreciable frequency reduction. The frequency change using a graphite thermoplastic material shows that additional cap area or depth is required to raise the frequency level to 1.2×10^{-3} hz.

The $.75 \times 10^{-3}$ hz is approximately 75 times the orbital frequency; the 1.2×10^{-3} hz is 100 times orbital frequency. An initial review indicates that the calculated frequency is adequate for control system stability although additional study must be carried out for verification.

THERMO/STRUCTURAL ANALYSES

This section incorporates the preliminary thermal and structural studies carried out to assess the feasibility of using an aluminum alloy for the solar array primary structure. Such a complex problem cannot be completely resolved in a short study program. In this study three conditions were investigated: (1) stresses and deflections in the .2 m deep cap of the 7.5 m beam (2) deflection of a 7.5 m by 667.5 m beam and (3) deflection of the 21420 m SPS. Thermal control for this initial study consisted of selection of proper coatings and by providing lightening holes to illuminate occluded surfaces. An area which was not examined in detail is the use of shielding and/or insulation to minimize both thermal differentials and thermal excursions in orbit. It is felt that this method of minimizing the thermal response of structures will provide a feasible solution to the problem.

The thermal analysis of the construction phase has been performed to yield the structural temperature distribution necessary to perform initial distortion/stress analyses. Both horizontal and vertical beam orientations were investigated for this preliminary study. To minimize thermal gradients, the horizontal beams were oriented so that the axes of the elements were aligned with the sun's rays so that the sun entering the holes in the two sun-facing surfaces impinged on the third (back) at 0° orbit angle as shown in Fig. 1.1.1-21. At the back side of the orbit (before entering the earth's shadow) solar energy enters the holes in the back surface to impinge on the other two.

The local temperature distributions in the beam cap using a very fine node grid were not part of this study. A finer grid might show larger temperature variations around the cap section than those shown resulting in significant thermal stresses and possible buckling. Further studies are required.

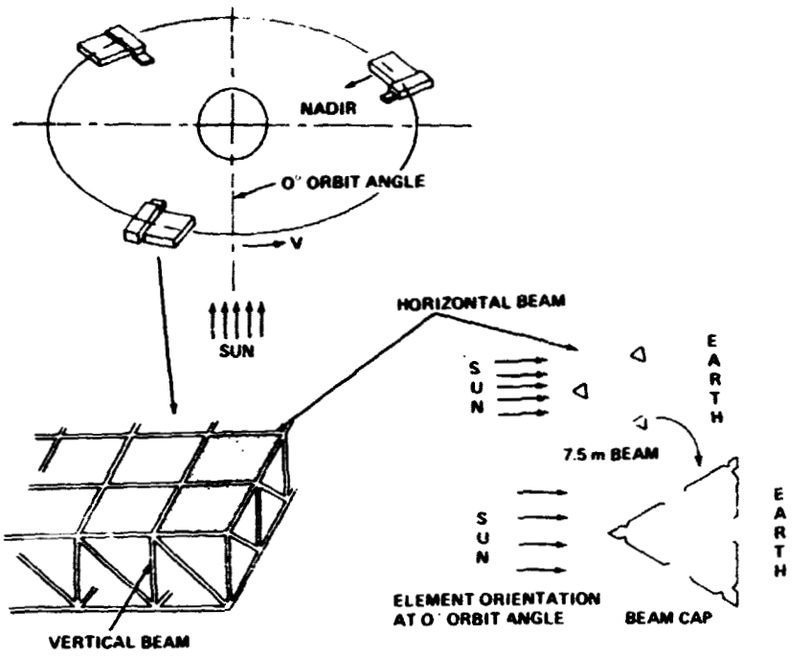

2995-015V

Figure 1.1.1-21 Orbital Attitude During Construction

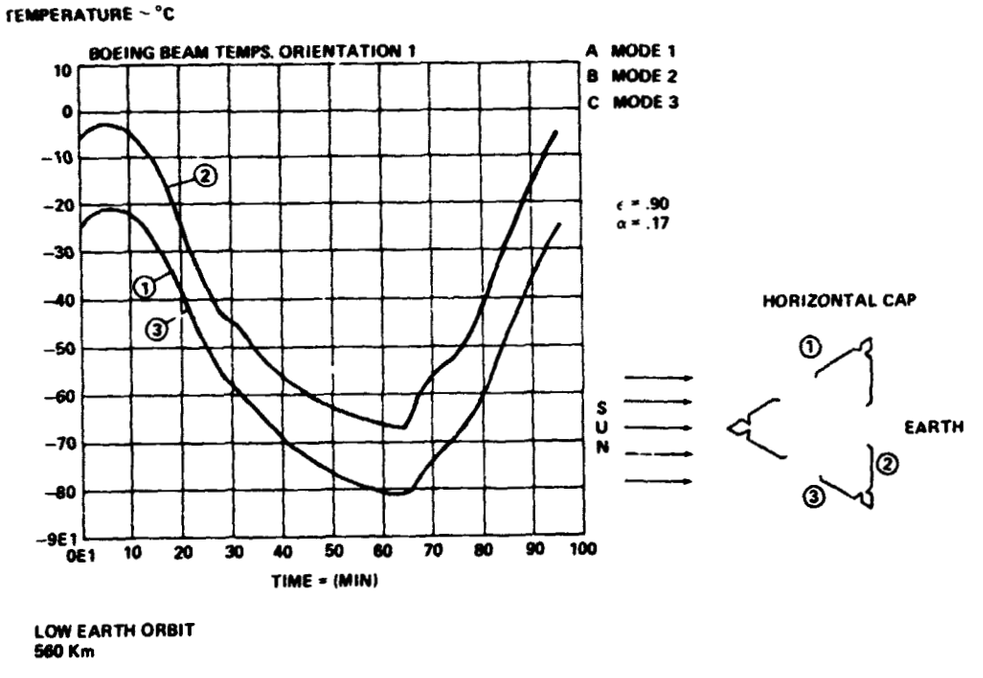

2995-018V

Figure 1.1.1-22 Aluminum Structure Cap Temperature vs Time

Other arrangements considered are the severe cases where the sun is normal to one of the surfaces at 0° orbit angle and where one element shadows another. The vertical beams, where intermittent shadowing takes place, were also investigated.

For the construction phase, a 560 Km altitude circular orbit is considered.

In GEO-synchronous orbit, the gradients between the sun-side horizontal beams, and those opposite have been calculated.

For this study, the inside of the elements are coated with black anodize (ϵ = .83, α = .86) and the outside surface with Z-93 white paint (ϵ = .90, α = .17).

The limited studies done in this segment were selected to surface some of the major thermo/structural problems; it by no means represents a total review of potential problem areas. Considerable additional study effort is necessary to point up problems and solutions.

Figure 1.1.1-22 shows time-temperature curves for selected locations around the 0.2 meter deep cap member of the 7.5 meter deep beam on low earth orbit for a coating of Z-93, a white paint (ϵ = .90, α = .17) selected for the outer surface and a black anodize (ϵ = .83, α = .86) for the inner. The peak gradient was 19°C (34°F) as shown for the selected sun orientation.

Stresses and Deflections in 7.5 m Beam

The thermal gradients were applied to the beam caps at segments A-B and C-D, as shown in Fig. 1.1.1-23. The cap from A to B was assumed simply supported at A and fixed at B. The curve of stress versus time shows the peak compression stress of approximately 16 x 10^6 N/M^2 (2200 psi) for the section. The maximum deflection is 0.48 cm (0.19 inches). The stress levels at C and D are lower than the values at B.

Beam Length Versus Temperature

Figure 1.1.1-24 shows the temperature for the 7.5 meter beam as a function of orbit time. The peak temperature excursion is 65°C (117°F). Depending on beam builder rate and the time of start and completion of the beam in the orbit, the lengthening or shortening of the beam is shown in the curve of beam length versus temperature change. The worst case shows a length change of .9 meter; a statistical evaluation is required to fully assess this potential

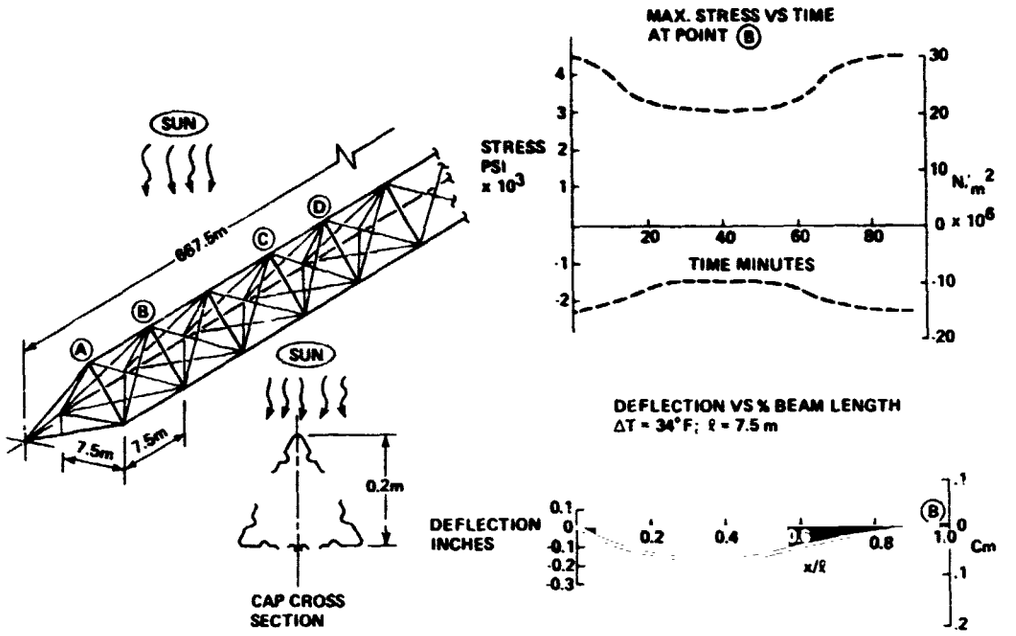

2955-017V *Figure 1.1.1-23 Aluminum Structure Stress & Deflections 7.5 m Beam*

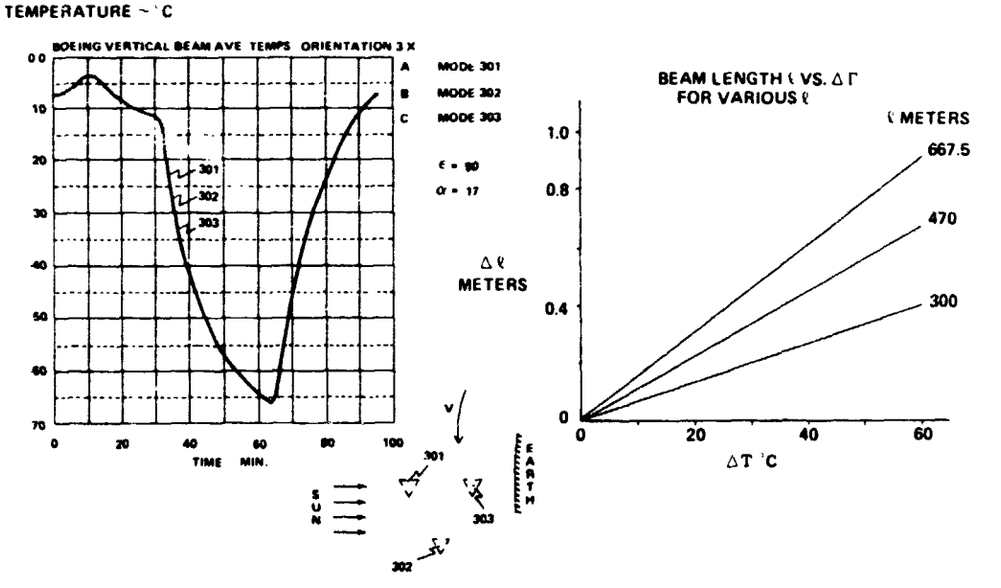

2955 018V *Figure 1.1.1-24 Aluminum Structure Beam Length vs Temperature in LEO*

problem. The installation of the dimensionally variable member into the structure requires an assessment of the dimension of next assembly. This problem may also exist although to a lesser extent on a composite structure. One possible solution requiring investigation is the use of insulation or shading to reduce thermal excursions.

Satellite Deflection due to Thermal Differential

The design condition given in Fig. 1.1.1-25 shows the SPS satellite in geosynchronous orbit with the sun orientation normal to the plane of the solar arrays, the temperature time curve gives the temperature differential between upper and lower members and includes occultation which occurs during the vernal and autumnal equinox. The temperature differential 55°C (99°F) was used to calculate the deflections for the 21 km satellite; the tip deflection is approximately 150 meters in 10.7 km, the angular deflection is approximately 2° which is not significant.

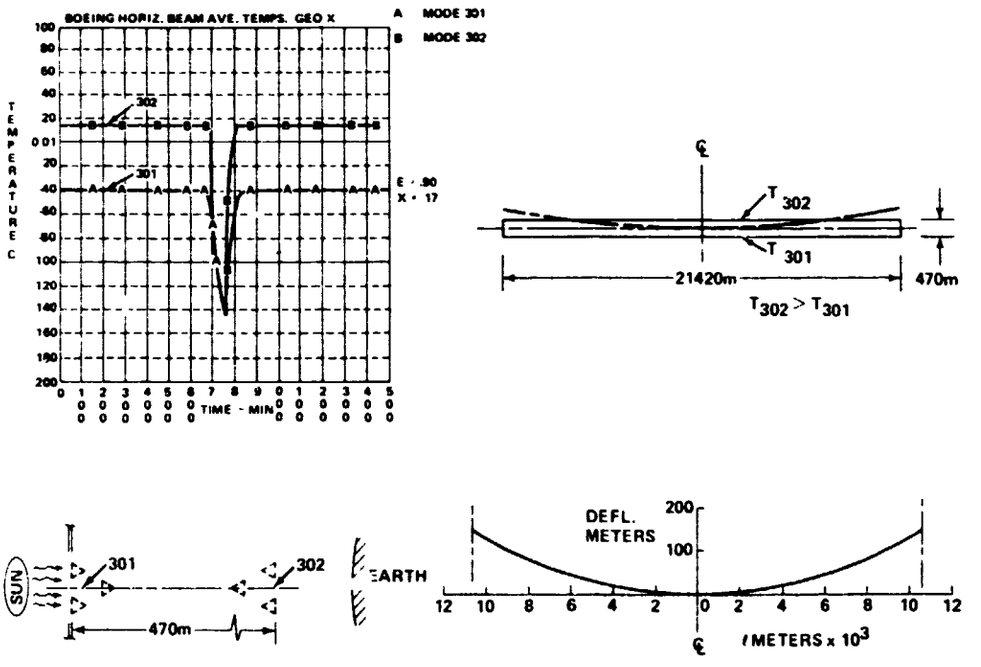

Figure 1.1.1-25 *Aluminum Structure Satellite Deflection Due to Thermal Differential (GEO)*

WBS Item 1.1.1.2 Satellite Energy Conversion Solar Blanket

Effects of array shadowing were investigated. If a segment or section of a long solar cell string is shadowed, it will not generate current. Current flow in the entire string is therefore interrupted. If other strings are connected to the load in parallel with the shadowed string, the difference between their loaded output voltage and the zero-current voltage of the shadowed string, appears as a reverse-bias voltage. The reverse bias voltage, if it is more than a few volts per shadowed solar cell, will destroy the shadowed cells if they are not protected. A small spacecraft flying across the face of an SPS could severely damage an unprotected solar array. Reverse-bias protection is therefore mandatory. The solar blanket panel design was modified to include shunting diodes.

WBS Item 1.1.1.3 Satellite Energy Conversion Maintenance

A summary of repair and replace requirements for the satellite was presented under WBS Item 1.1. This section addresses maintenance requirements peculiar to the energy conversion system.

The energy conversion system is designed to be as nearly maintenance-free as possible. Solar cells, blocking and shunting diodes, and attachment and tensioning devices all incorporate enough redundancy to provide a lifetime of more than 30 years. Exceptional maintenance requirements may rise, e.g., in the event of collisions of natural or manmade space objects with the SPS. These will be treated as unscheduled maintenance. Switchgear may require replacement of one or two units annually.

Occasional maintenance of the solar array by annealing to restore output due to damage of the solar cells by solar flare radiation is expected to be necessary. It would be possible to make the solar array maintenance-free with regard to expected radiation by oversizing or providing extra shielding (in the form of thicker coverglass). Annealing, however, has distinct cost advantages.

It is important to recognize that nearly all of the radiation damage to solar arrays at geosynchronous orbit comes from solar flares, which are a statistical phenomenon. Environment models are used to predict the amount of radiation for which arrays must be designed. The model used by Boeing was originated by the Goddard Space Flight Center. As is typical for such design models, it is roughly a 90% confidence model; an expected-value model would predict less radiation. Use of a conservative model is warranted by the fact that a severe solar flare event will affect all SPS's then in orbit.

Results of a statistical analysis of solar flare size are shown in Figure 1.1.1-26. The flare size probability distribution was assumed to follow a log-normal curve. The available statistical sample is too small to develop detailed conclusions as to flare size. It seems unlikely that a log-normal distribution would hold for very large flares since this distribution places no upper limit on flare size.

The two curves shown represent power-law and exponential-rigidity models for the proton spectrum. Available data fit either law about equally, yet these spectral distributions predict large differences in proton fluxes in the energy range from 2 MEV to 10 MEV. This energy range is of principal concern for thin solar cells with thin covers, but available data do not extend into this region.

Even this conservative model indicates that degradation more than 10% from a single large flare is highly unlikely. Much improvement in the confidence in this result can be expected due to continued accumulation of statistical data from the current solar cycle and with direct observation of proton fluxes in the 2 to 10 MEV range.

The estimated requirements for annealing are clearly sensitive to the model used and the statistical approach adopted. A comparative study of the available data for silicon and gallium arsenide SPS's and solar arrays was conducted. This analysis revealed a significant difference in the environment model used for the Boeing and Rockwell solar blanket degradation analyses. Most of the dfferences in degradation predicted by the studies is due to differences in environment models. The Rockwell model is less conservative; it would predict that neither a silicon nor a gallium arsenide SPS would be likely to need annealing in 30 years at geosynchronous orbit.

Boeing test data on silicon solar cells are compared in Figure 1.1.1-27 with the Rockwell projections for the gallium arsenide solar cell. It is clear that there is no significant degradation difference. Note the difference in proton/electron equivalences between silicon and gallium arsenide. This difference arises because of the difference in mass of the atoms of the two solar cell constituents. Our analysis would predict no significant difference in degradation between the two systems for the same fluence. Since the gallium arsenide solar blanket design has significantly less shielding, we would predict more degradation in the equivalent environment compared to the Boeing silicon blanket design.

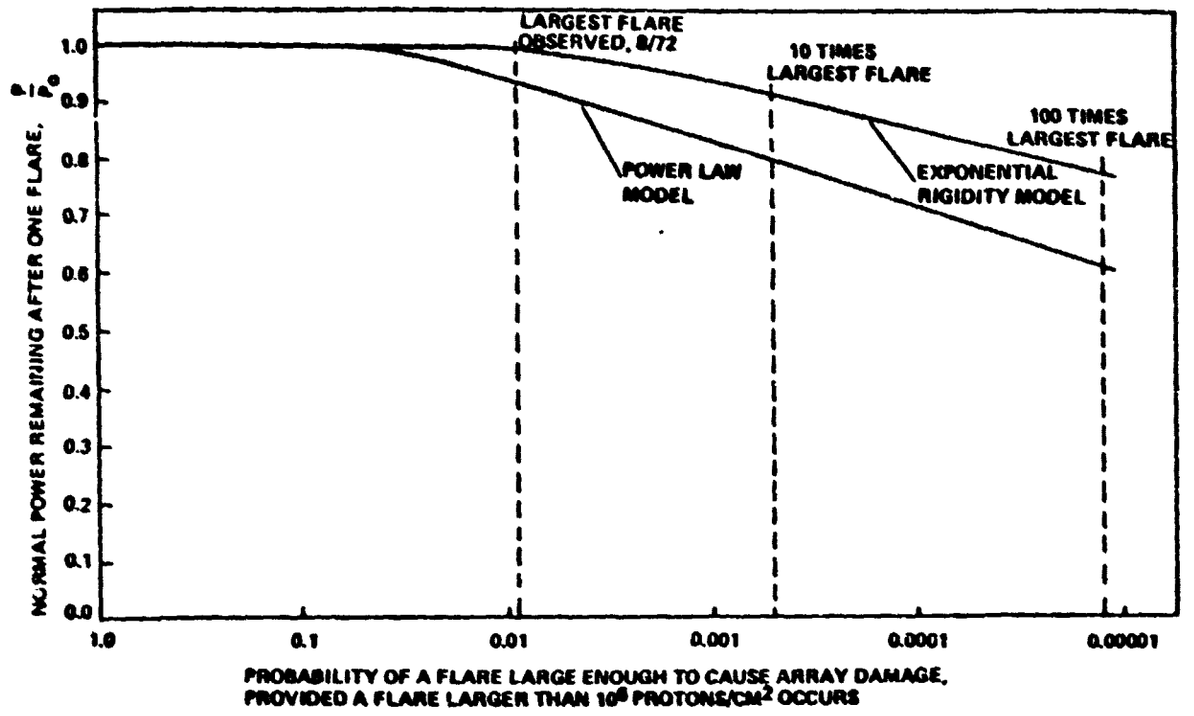

Figure 1.1.1-26 Large Flare Effect on Array Performance

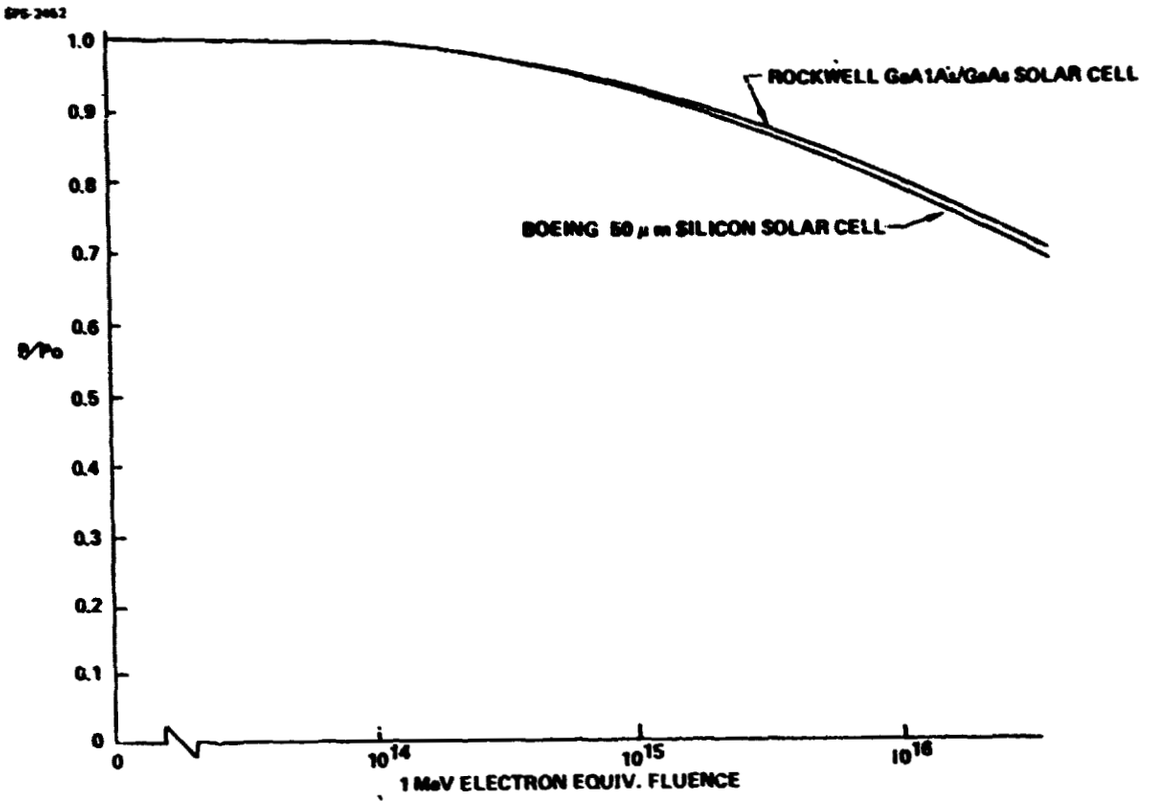

Figure 1.1.1-27 Degradation Comparison for Electron Irradiation

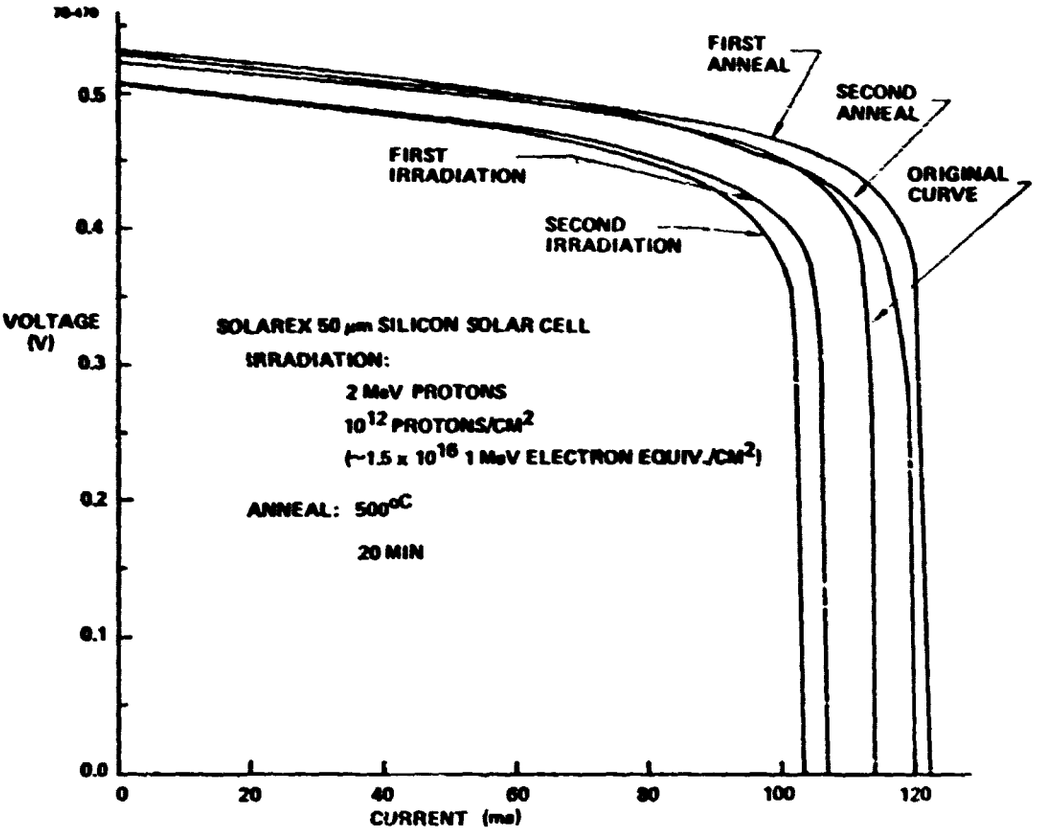

Figure 1.1.1-28 Thermal Annealing of Proton Damage in Silicon: Boeing Test Data

Recent results reported by Hughes show the radiation degradation of gallium arsenide to be a strong function of function depth. Additional radiation degradation testing is needed for both types of solar cells; gallium arsenide is reported to degrade less with shallow junctions. The possibility that gallium arsenide cells may anneal at relatively low temperatures also needs to be further explored by testing.

Annealing of radiation damage in silicon has been repeatedly demonstrated in the laboratory. Illustrated in Figure 1.1.1-28 are the results of oven annealing tests of bare 50 micron silicon solar cells. Several cells were tested with two irradiations and two anneals. Boeing tests of laser annealing of 50- micrometer solar cells are reported in Volume 4. All cells tested demonstrated some annealing recovery.

Annealing of the solar blanket on one SPS will require a technique tailored to that purpose, as well as a blanket design compatible with annealing temperatures. Attention has been given to laser directed energy annealing under this contract.

The concept of the actual annealing system is shown in Figure 1.1.1-29. Each laser gimbal would actually have 8-500 watt CO_2 lasers installed. The laser beams would be optically tailored to provide the desired illumination pattern and energy density. The gimbals would be mounted on an overhead gantry that would span the entire bay width; one bay of solar array would be annealed in fifteen meter increments. Solar array strings undergoing annealing will be taken out of service while they are annealed. Table 1.1.1-4 summarizes predicted performance parameters for the annealing systems.

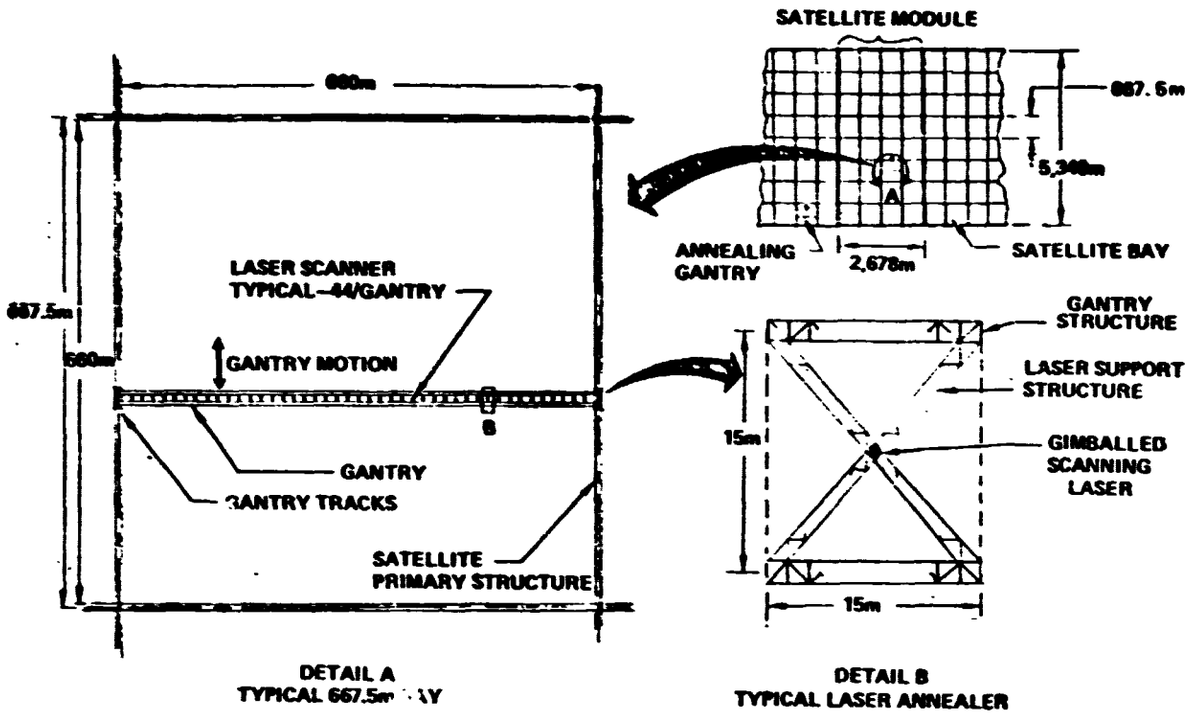

Figure 1.1.1-29 Laser Annealing Concept

Table 1.1.1-4 Gimbaled Scanning Laser Characteristics Update

• ANNEALING ENERGY DENSITY:	16 W-sec/cm^2
• POWER DENSITY:	8 W/cm^2
• T_{MAX} (ACTIVE REGION):	550^{0}C
• LASERS/GIMBAL:	8
• SCANNING SPOT SIZE:	500 cm^2 (44.0 x 11.4 cm)
• SPOT SWEEP RATE:	5.7 cm/s
• POWER REQUIRED/LASER GIMBAL:	28.7kW
• POWER REQUIRED/GANTRY:	1.17 MW
• NUMBER OF GANTRIES/SATELLITE:	8 (1/SATELLITE MODULE)
• TOTAL ANNEALING POWER REQUIREMENT:	9.4 MW
• TIME REQUIRED TO ANNEAL ARRAY:	147 DAYS

1.1.2 Microwave Power Transmission

1.1.2.1 Phase Control and Array Simulation

To assess phase control system performance extensive use jointly with JSC has been made of array simulation computer programs, particularly in the areas of grating lobe levels and subtilt effects. A qualitative summary of results is given on Table 1.1.2-1 prior to discussion of quantitative data derived during this contract period.

The main conclusion is that main beam wander is primarily due to correlated phase errors. This can be greatly minimized if the number of branches at the first level of phase distribution is increased so as to randomize the errors. In addition, a joint paper presented at the International Conference on Modeling of Electronic Systems, in Toronto in September, 1978, by Dr. D. Arndt of JSC and S. Rathjen of Boeing defined antenna tilt requirements more clearly and preliminary calculations made by Lincom became available.

The continuing modeling work on the phase control system proposed by JSC should provide the specific method by which to redistribute energy between sidelobes, error plateau in the array roll off and grating lobes. In phase 2, trade studies of phase error build up in cables (including fiber optics), "black boxes," the appropriate number of phase distribution tree levels and subarray size should provide detailed answers.

It is still our feeling that a back-up phase control system should be analysed and compared with the Lincom system in terms of phase error buildup and ease of implementation. This would, of course, have to be carried to the component demonstration level and would require additional resources.

1.1.2.1.1 BASELINE VERIFICATION

Phase Distribution Tree Layout

What the detailed layout of the phase distribution system should be depends on correlated and uncorrelated phase error buildup per node, redundancy, reliability and the level at which phase control is exercised.

Table 1.1.2-1 Effect of Phase Error and Tilt on Beam Shape

	EFFECT
PHASE ERROR BUILDUP	
• UNCORRELATED ERRORS	• NO EFFECTS ON MAIN BEAM SHAPE • FAR-OUT SIDELOBE LEVEL PLATEAU INCREASED
• CORRELATED PHASE ERRORS	
• FEW BRANCHES (4) AT FIRST/SECOND LEVEL	• SLIGHT RANDOM WANDER OF MAIN BEAM BEAM BROADENED BY 4%(95% CONFIDENCE)
• MANY BRANCHES	• PROBABLY NEGLIGIBLE
ANTENNA TILT	
• SYSTEMATIC TILT	• MAIN BEAM SHAPE UNAFFECTED BUT POWER REDUCED BY SCAN LOSS WHICH APPEARS AT GRATING LOBES
• RANDOM TILT	• MAIN BEAM SHAPE UNAFFECTED; RESULTING AMPLITUDE MODULATION CAN RAISE ERROR PLATEAU

Four different distribution trees are outlined on Figure 1.1.2-1, each indicative of different level of phase control and degree of power splitting. The baseline system of Lincom with 9 nodes (d) is based on a maximum of 4:1 power split whereas the 4 node system (a) elaborated by GE is based on a 20x19x19 distribution to the subarray level and a variable power splitting to the klystron level (4th node) using 4:1 power splitters at the edge and 36:1 power splitters at the array center.

The nine node system suffers from poor reliability, poor phase randomization (i.e., resulting correlated phase errors which produce beam pointing errors) and lowest allowable phase error per node. The four node system may be a viable candidate if 10 m x 10 m subarrays are retained and phase control is exercised down to the klystron level. A three node system may be possible if phase control is exercised at the subarray level only, and subarray size is reduced to 5 m x 5 m.

To reduce phase correlation effects, i.e., beam steering errors, the number of branches at the lower levels should be kept high. This also allows higher random phase error per level in the error budget. Even with 4 m x 4 m subarray, the 4-level system will require a total (1 GHz) phase accuracy of 2^{o} per level to achieve a 96% efficiency including tilt. This will require stringent design criteria. A possible 3 m x 3 m subarray could be accommodated by a 32 x 16 x 16 x 8 four node distribution system.

Phase error buildup affects only low level far sidelobes where power density is low and does not appear to constitute an environmental problem. Furthermore if the phase errors are correlated they are not expected to be of great importance in a system that has more than about ten branches per node.

In previous SPS studies phase distribution layouts were often selected on the basis of minimizing total cable length. This type of optimization may not be significant compared to other criteria such as minimizing phase error buildup and/or constant cable length since cable mass is only around 1% of the array waveguide mass, even in the case of redundant cables at lower levels. An array using fiber optics will have an even lower phase distribution mass fraction.

Table 1.1.2-2 lists calculated cable lengths for the GE 4 node system mentioned earlier for representative cable length at each node. Since the cable has about a tenth the mass per unit length of waveguide with a total length about a tenth that of the waveguide, the resulting cable mass is around 1% of the waveguide mass.

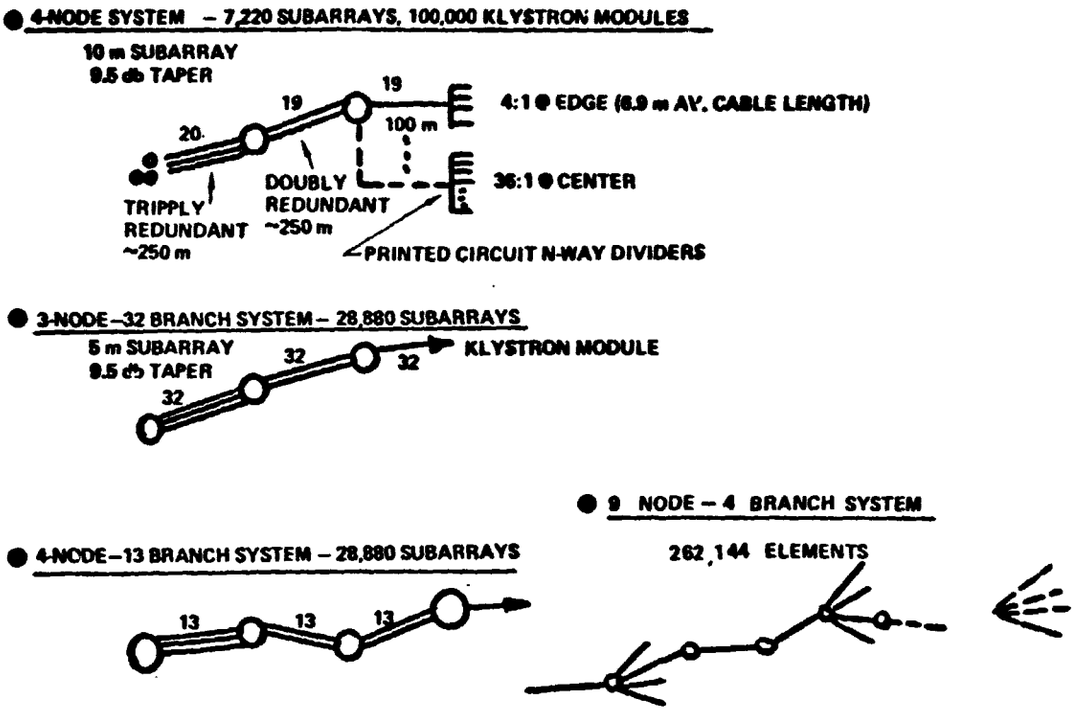

Figure 1.1.2-1 Potential Phase Distribution Tree Layouts

Table 1.1.2-2 Estimate of Required Cable Length for GE Phase Distribution System

• ALL CABLE LENGTHS EQUAL

1ST LAYER	20 CABLES ● 250 m	TRIPLY REDUNDANT	15 km (1/4" DIA)
2ND LAYER	380 CABLES ● 250 m	DOUBLY REDUNDANT	190 km (1/4" DIA)
3RD LAYER	7220 CABLES ● 100 m	NON-REDUNDANT	722 km (1/8" DIA)
4TH LAYER	100,784 CABLES @ 6.9 m	NON-REDUNDANT	702 km (1/8" DIA)
			1629 km

• NON-EQUAL CABLE LENGTHS

SAVING ~ FACTOR OF 2 — ~850 km

APPROX. CABLE WEIGHT ≅ 1% OF WAVEGUIDE WEIGHT
~ 9000 km OF W/G vs. 850 km OF CABLE

Line Attenuation Compensation

An input resulting from the Boeing critique of the baseline system was that implementation of the Lincom system will require compensation of cable loss between different nodes. (See Figure 1.1.2-2.) The limits of gain compensation due to diplexer leakage are indicated in the chart. For a signal to error ratio of 20 dB, with 40 dB of diplexer isolation,

$$0 - 2K + 40 = 20 - 40 \text{ dB, i.e., } K = 30 \text{ dB}$$

Thus, for example, the maximum cable length of RG8 cable which can be compensated at 500 MHz is 150 meters. By using LDF 4-50 cable one may do better, reaching 1 km at 500 MHz with an attenuation K = 30 dB.

Antenna Pattern Analysis

Continuing transmitting array analysis has concentrated on building an understanding of how arrays with imperfections as in real life will perform. More specifically, the effects of systematic and random subarray tilts on both beam efficiency and grating lobe level were investigated.

As a part of a small add-on contract by NASA JSC, a number of "Tiltmain" runs were made to check some available aspects of the Lincom "Solarsim" program, of which Figure 1.1.2-3 is typical. For the use of a 10 m x 10 m subarray, both one dimensional and two dimensional "Tiltmain" runs checked well with the Lincom results, provided that surface irregularity errors were accounted for in a similar manner. In these results, close coordination was made with related runs obtained directly on the JSC computer and the capability to access the JSC computer from the Boeing facility in Kent, Washington was implemented. Useful runs on start-up and shut-down procedures were initiated at JSC as a result of mutual discussions and additional work simulation of various types of failures in the MPTS system will be proposed. Although the initial check points in Figure 1.1.2-3 were obtained using a 1-D version of Tiltmain, these data points have since been confirmed using 2 dimensional tilts at each subarray.

Calculations by Lincom show that going to smaller subarray size desensitizes the transmitting antenna performance degradation due to systematic tilt. Selected results from recent Boeing computer runs are in good agreement with Lincom data and indicate that if greater tilts than presently allocated are experienced, a review of the baseline 10 meter subarray size is warranted.

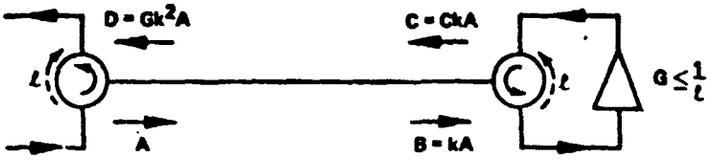

K = LINE ATTENUATION
= DEVICE ISOLATION

FOR -40 DB ISOLATION, S/E, K = -30 DB, I.E., MAX. LINE LENGTH OF RG8 CABLE IS 150 METERS @ 500 MHZ AND 60 METERS @ 2.5 GHZ.

Figure 1.1.2-2 Line Attentuation In Phase Distribution System

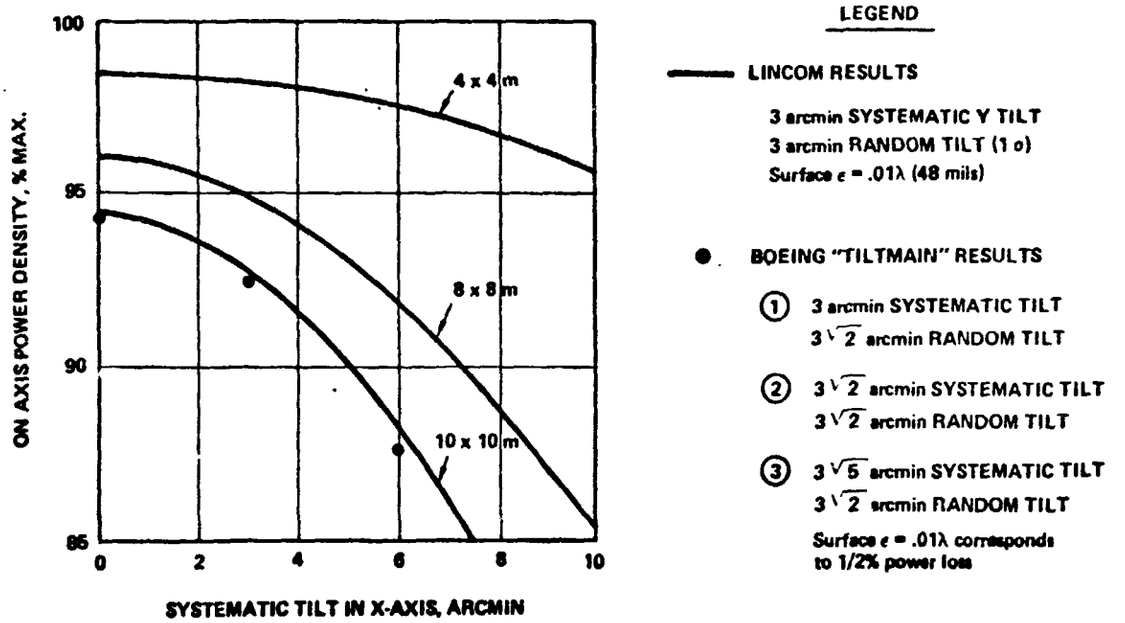

Figure 1.1.2-3 Comparison of Array Performance Degradation with Tilt

Further runs on the Tiltmain program, confirmed by graphical integration of superposed random tilts on various values of systematic tilt, indicate that random tilts can have greater effects than previously realized (see Figure 1.1.2-4). For instance, for 3 arc minutes of systematic tilt the efficiency is reduced from 98.5% for zero random tilt to 94.7% with $3\sqrt{2}$ arc min of random tilt. The choice of $3\sqrt{2}$ of random tilt (1 dimensional at 45° on the "Tiltmain" program) corresponds to a choice of 3 arc min of 2 dimensional tilt on the Lincom program.

Figure 1.1.2-5 illustrates typical grating lobe level amplitudes as a function of distance from the rectenna. The design requirement of 1 arc minute of systematic tilt is derived from these to meet the Soviet microwave level standard at the first grating lobe. The random tilts have only second order effect on grating lobe levels and primarily affect the array scanning loss.

Subarray Size Considerations

A critical review of the phase control baseline system needs to encompass a review of the viability of phase control to the klystron level in terms of trading complexity for performance improvement. One approach is to consider an increase in the number of subarrays by a factor of 4 with provision of phase control only to the subarray level. Since in the klystron level phase control concept passive elements will have to provide phase integrity within the allowable errors at the edge of the array (4 klystrons per 10 m x 10 m subarray, i.e., 5 m x 5 m size per klystron), the same cell size for retrodirective phase control could be used at the center, possibly using a thermally compensated waveguide for phase distribution to the 9 individual klystrons at this level. If compatible with overall array performance (to be checked when the "Medmain" program is running) this would result in 4:1 reduction in phase distribution complexity over phasing each klystron individually.

An added benefit of reduced subarray size would be reduction in the number and magnitude of grating lobes, as indicated in Figure 1.1.2-6. The grating lobe level would be reduced by 20 log D_2/D_1, which is 6 dB.

Due to the 70 kw per klystron power quantization only 9 possible subarray power levels exist. If a six-step power taper as shown on Figure 1.1.2-7 is synthesized with subarrays of 1, 2, 3, 4, 6 and 9 klystrons each the microwave beam pattern transmitted is effectively the same. The beam efficiency only degrades by half a percent and the first side lobe only rises by .4 dB.

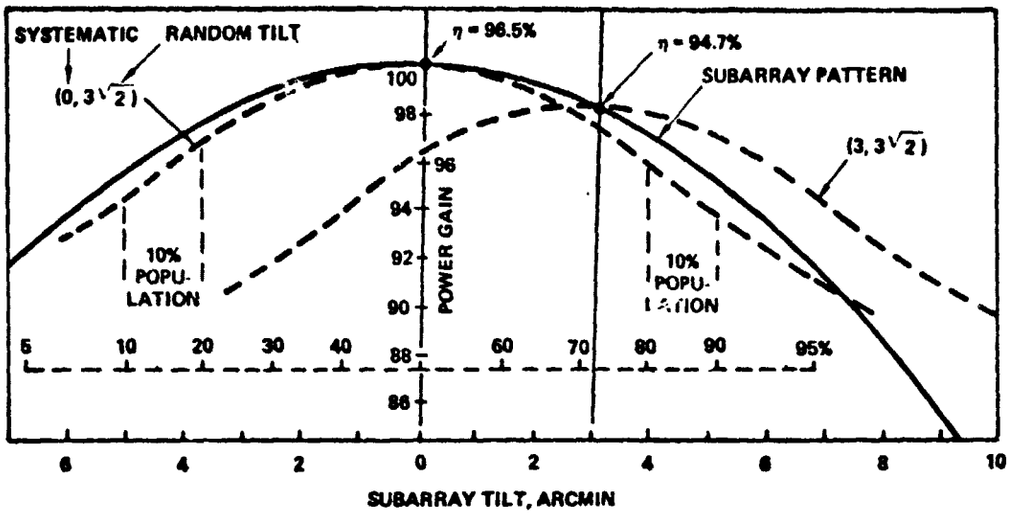

Figure 1.1.2-4 Effect of Systematic and Random Subarray Tilt

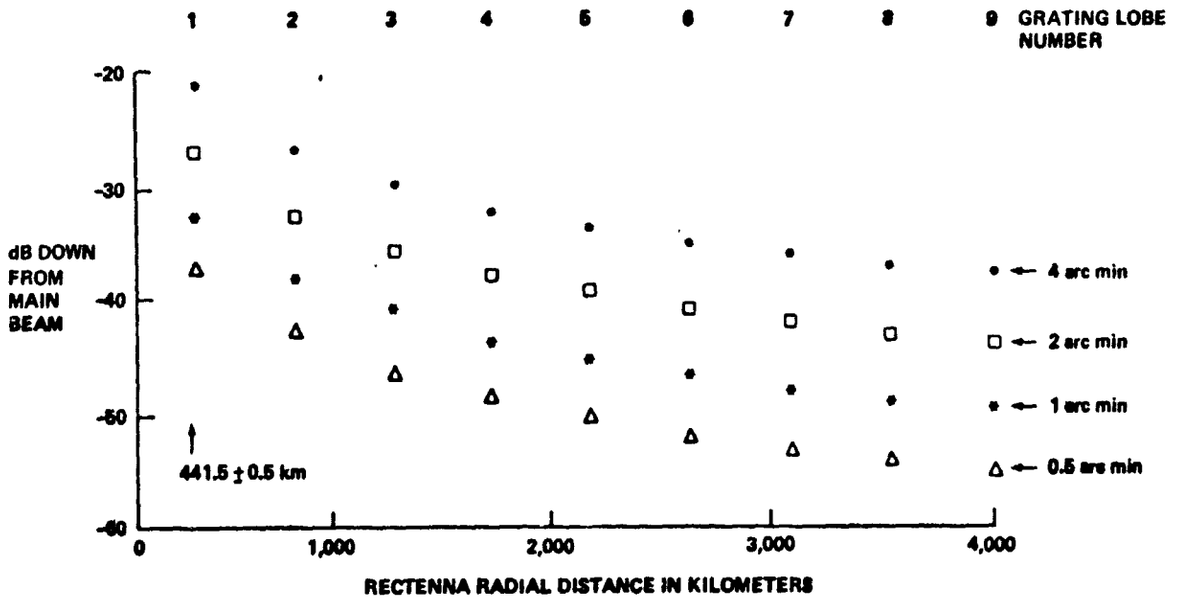

Figure 1.1.2-5 Grating Lobe Peaks Produced by Systematic Sacetenna Tilt

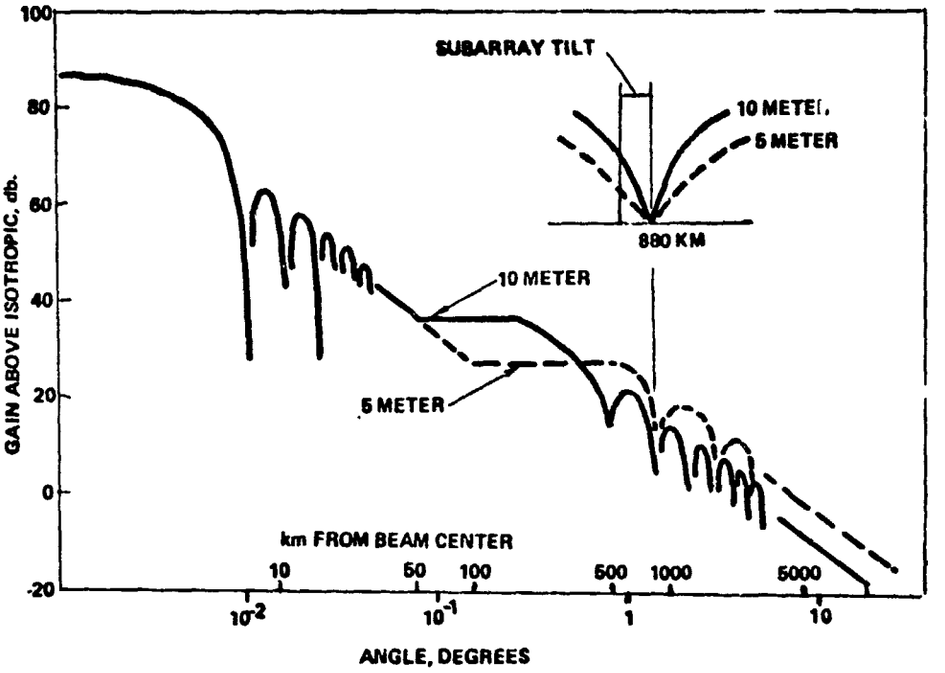

Figure 1.1.2-6 Effect of Subarray Size on Grating Lobes

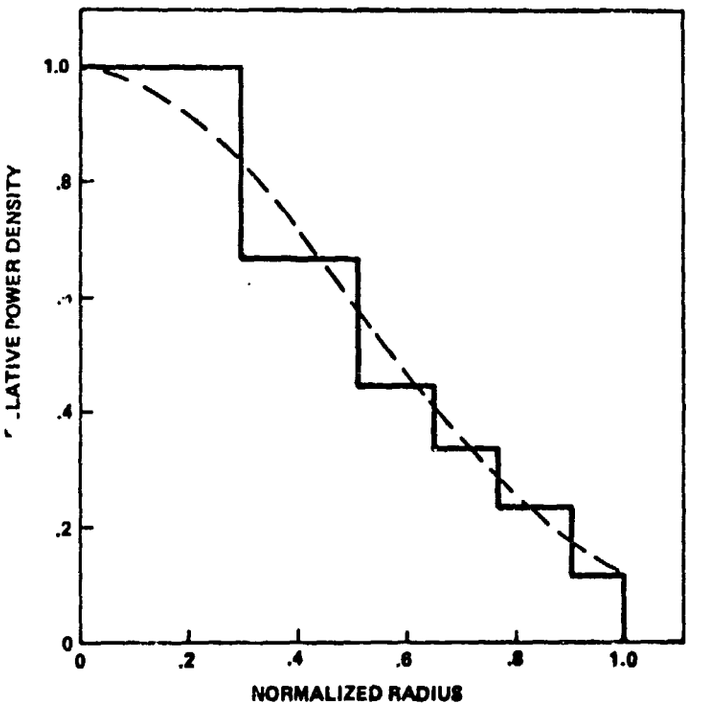

TAPER	SIX STEP	TEN STEP
η	96.2	96.7%
1ST SIDE LOBE	-24.5	-24.9 db

Figure 1.1.2-7 Six Step Taper Implementation for 5 Meter Subarrays

In view of the increased system simplicity with equivalent system performance, 5 m x 5 m subarrays are recommended for further study on their overall impact on SPS design.

1.1.2.1.2 SPS Array Computer Simulation

In the area of computerized array simulation routine use is now being made of the "Tiltmain" array program in checking grating lobe levels with systematic and random tilt. The "Modmain" program, which overcomes some of the storage limitations of Tiltmain is now 65% complete, and will ultimately enable modeling the SPS array to the klystron module level (100,000 elements). The program flow of each are indicated on Figure 1.1.2-8, and the status of each is indicated below.

- "TILTMAIN"
  - Phase Control Verification Studies are in Progress
  - Grating Lobe Levels and Tilt Effects are being Evaluated
- "MODMAIN"
  - Now has Capability to Access NASA-JSC Computer
  - Can Set up Files for Main Program and Subroutines

Modmain will have the following features:

- Capability to model the spacetenna down to the power module level without excessive storage requirements.
- Incorporation of variable spacing between modules.
- Capability to define level of phase control.
- More accurate modeling of grating lobe behavior.

So far "Modmain" has been matched to a no-error "Tiltmain" run for a 10 m x 10 m subarray. The first match between the two programs was the normalized electric field pattern near the rectenna. "Modmain" now prints out the power density as well as the decibel values. Efficiency calculations were next matched using 10.43 by 10.43 meter subarrays. As expected, the use of 5 m by 5 m subarrays in the basic program "Bigmain" created a storage overload problem but could be modeled in "Modmain."

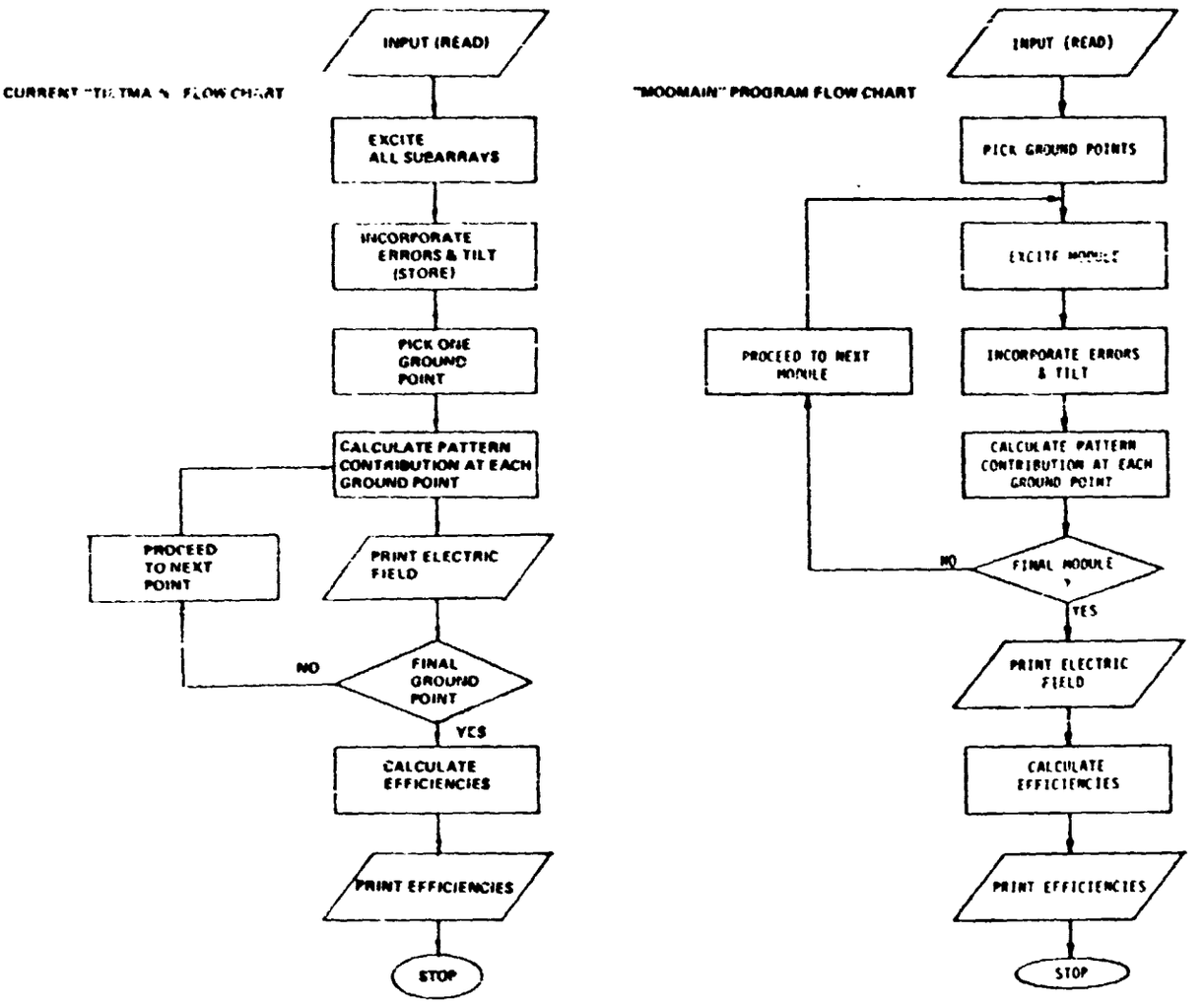

Figure 1.1.2-8 Array Simulation Computer Program Flow Comparison

Figure 1.1.2-9 shows the first grating lobe for the case of 5 m by 5 m subarrays. As predicted the 1st grating lobe is located at twice the distance of the 1st grating lobe for the 10 m by 10 m subarrays. The grating lobe is split because without tilt the center of the grating lobe falls in the null of the subarray pattern. Most importantly, the results indicate that the grating lobe amplitude is approximately six dB below the 10 m by 10 m subarray size case.

The plan for Phase 2 is to incorporate the "error" subroutine into "Modmain," match this to Tiltmain runs, and detail the model by changing the size and spacing of the modules. There will be ten different sizes of klystron modules corresponding to the ten step quantized illumination taper.

1.1.2.1.3 Fiber Optical Phase Distribution

Use of fiber optics in the phase distribution system has definite advantages, summarized on Table 1.1.2-3, over using coaxial cable as in the current baseline. Advanced multimode fibers may be able to accommodate signal frequencies approaching 1 GHz.

There is a factor of 10^2 cable mass reduction if optical fibers are used and also a somewhat lower cost per unit length. This has little impact on MPTS masses and costs, however, because the phase control system cabling mass and cost fractions of the MPTS are well under a tenth to begin with.

Comparison of temperature coefficient of signal phase delays in conventional coaxial cable and fiber optics indicates a twentyfold reduction with optical fibers. Low values for phase change suggest that the required compensation for cabling phase shifts may be simpler to implement because there will be no need to consider possible phase ambiguities.

Fiber optics have less signal loss per unit line length than coax, so less amplification will be needed in the system. More valuable than this, though, may be the fact the optical fibers have no short circuited failure modes, making fiber failures independent. They also allow the transmission of signal across high voltage differences without introducing possible metallic shorting paths as conventional cables do.

A candidate fiber optical single node reference phase distribution concept is illustrated in Figure 1.1.2-10 with design considerations outlined in Table 1.1.2-4. It features a twofold

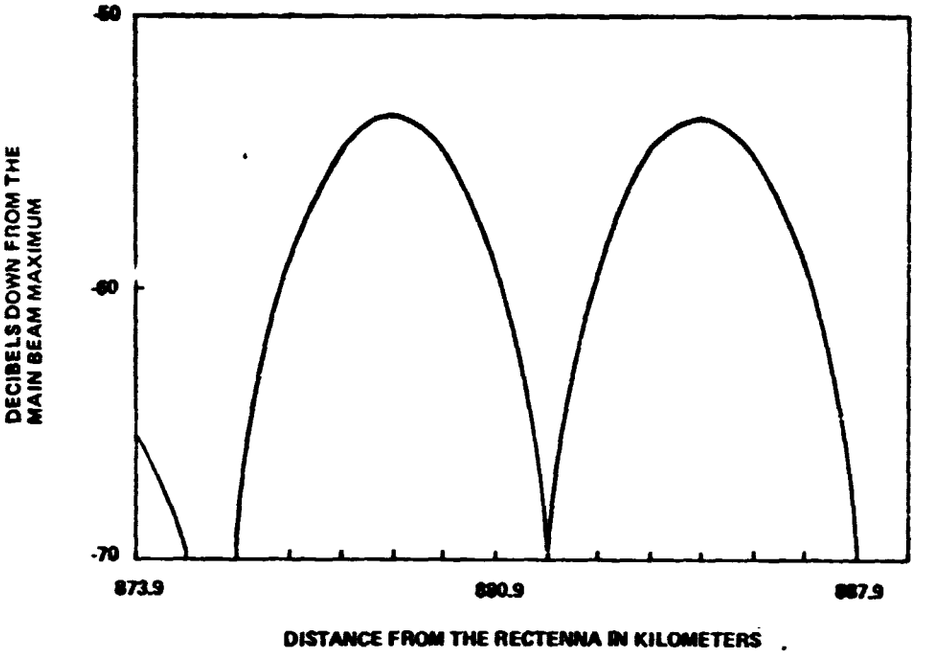

Figure 1.1.2-9 First Grating Lobe Power for 5m by 5m Subarray Size

Table 1.1.2-3 Comparison of Coaxial and Fiber Optic System

	COAXIAL CABLE		OPTICAL FIBER
	RG-58 SOLID DIEL.	LDF-50 FOAM DIEL. (1/2 DIA)	~5 MIL DIA (65 μm ACTIVE CORE)
ATTENUATION db/km (100 MHz)	180 db	35	5
MASS kg/km	43	160	.5
COST $/km	2,000	4,200	1500 (1978)
PHASE DELAY @ f_{IF} = 100 MHz	120°/METER (ϵ=1.0, λg=3m)		180°/METER (ϵ=1.5 λg=2m)
LINEAR EXPANSION	16.5×10^{-6}/k (COPPER)		5.5×10^{-7}/k (QUARTZ)
PHASE CHANGE FOR ΔT=150°K L=300m	89.1°		4.46°

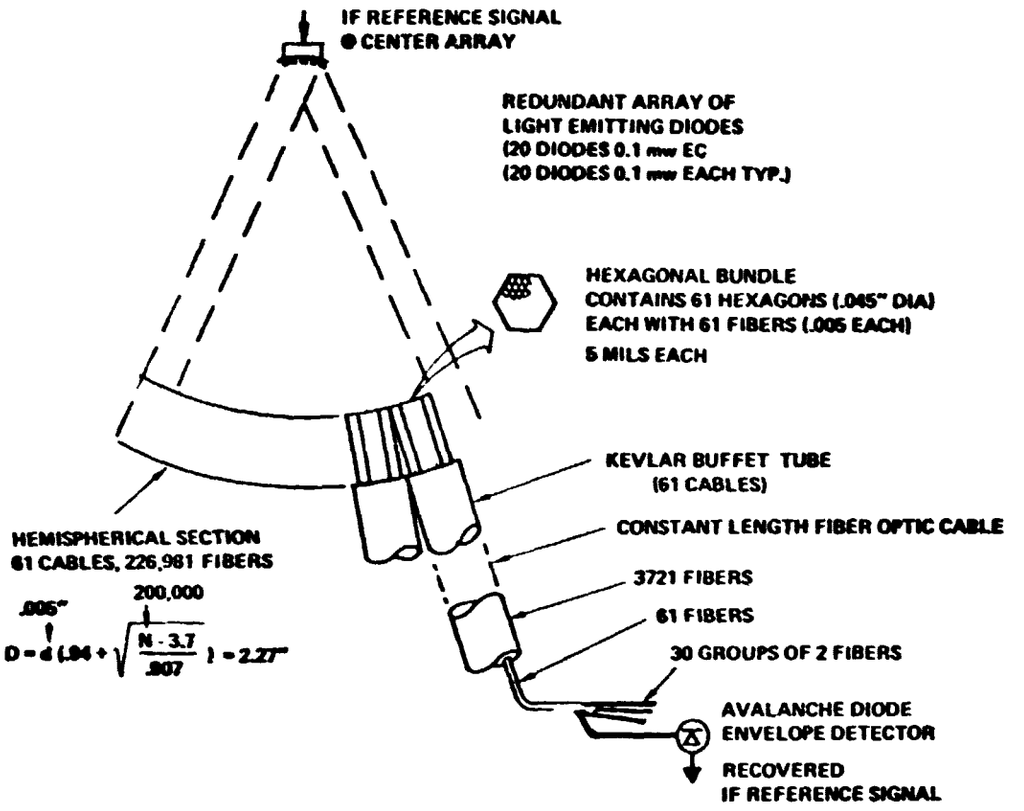

Figure 1.1.2-10 Fiber Optic Phase Distribution System Concept

Table 1.1.2-4 Fiber Optic Design Considerations for SPS Phase Control Distribution

- INCOHERENT LIGHT EMITTING DIODE
  - ONE EMITTER CAN ILLUMINATE BUNDLE OF >100,000 FIBERS
  - REDUNDANT LED EASY TO IMPLEMENT
- MULTIMODE GRADED INDEX FIBER
  - LOSS OF 10 DB/KM COMPATIBLE WITH SPS ($6 PER METER)
  - POTENTIALLY GOOD RADIATION RESISTANCE
  - CABLE BUNDLE ≈ 2.5" FOR DUAL FIBER REDUNDANCY (~200,000 FIBERS)
- SAMPLE LINK CALCULATION

  POWER DIVISION LOSS ≥ 55 db

  FIBER LOSS ≥ 5 db

  FOR 1 mw RADIATED POWER, RECEIVED POWER IS = -60 dbm = 1 nwatt

  AVALANCHE DIODE RECEIVER WILL HAVE S/N > 20 db @ THIS LEVEL FOR 5 MHz BANDWIDTH.

fiber redundancy for the case of a fiber per klystron and a twentyfold redundancy at the optical signal source, which is proposed to be light emitting diodes but could be lasers. If the source is coherent, single mode fibers may be used, but incoherent sources require multimode fibers

A number of candidate optical fibers in use today have been considered and are summarized on Table 1.1.2-5. The selection of the most suitable fiber will depend on the temperature requirements and the radiation environment on the array. The fiber optic cabling system looks sufficiently promising to recommend tests of a selected set of fibers to verify their temperature stability and link budget. Separately, a postulated radiation environment should be used to determine the possible effect on fiber life and required protection.

In summary, optical fiber technology appropriate for MPTS reference phase distribution systems is available today. It is recommended for use because of numerous advantages.

1.1.2.2 Failure Mode Analysis

1.1.2.2.1 Availability Assessment

MPTS availability assessment was done by GE using a representative klystron module and the GE reference phase distribution system with redundancy described in the previous section of this report.

The assumed layout of the klystron module is shown on Figure 1.1.2-11. Possible locations of the solid state phase control modules for good thermal distribution are shown. Selection of a pilot receiving antenna has not been finalized. What is shown is an example of an approach to be considered for achieving good uplink/downlink isolation when the power beam and pilot beam are at the same frequency. The radiator is indicative only and is not representative of an alternate lower mass active cooling system under consideration.

The MTBF values assigned to each component in the phase distribution path are shown in Figure 1.1.2-12 These values, together with the redundancy level selected, and the selected maintenance procedure assumed, lead to availability numbers detailed in the Part 4, Phase I, Final Report, Dec. 14, 1978, General Electric Space Division. The overall impact of the failure analysis on efficiency is summarized in Table 1.1.2-6.

Table 1.1.2-5 Candidate Fiber Optic Materials

- **FUSED SILICA CORE, SILICONE CLAD (VALTEC)**
  - LOW TEMPERATURE - - - ATTENUATION INCREASES FROM 3.5 DB/KM @ +85°C TO 14 DB/KM @ -40°C
  - HIGH TEMPERATURE - - - OK TO +150°C
  - RADIATION RESISTANCE - - - GOOD
- **FUSED SILICA CORE, POLYMER CLAD (DU PONT)**
  - LOW TEMPERATURE - - - OK TO 0°C, POSSIBLY TO -50°C
  - HIGH TEMPERATURE - - - CLADDING MELTS AT ~ +80°C
  - RADIATION RESISTANCE - - - REPORTED BEST
- **ALL GLASS, GRADED INDEX (CORNING)**
  - LOW TEMPERATURE - - - OK TO -50°C, LESS THAN 1DB/KM CHANGE -30° TO + 60°C
  - HIGH TEMPERATURE - - - BELIEVED OK TO +150°C
  - RADIATION RESISTANCE - - - POOR
- **ALL GLASS, STEP INDEX (GALILEO)**
  - LOW TEMPERATURE - - - 2 TO 3 DB INCREASED ATTENUATION AT -55°C SHRINKING BUFFER CAUSES MICROBENDS
  - HIGH TEMPERATURE - - - BELIEVED OK TO +150°C
  - RADIATION RESISTANCE - - - POOR, BUT IMPROVING

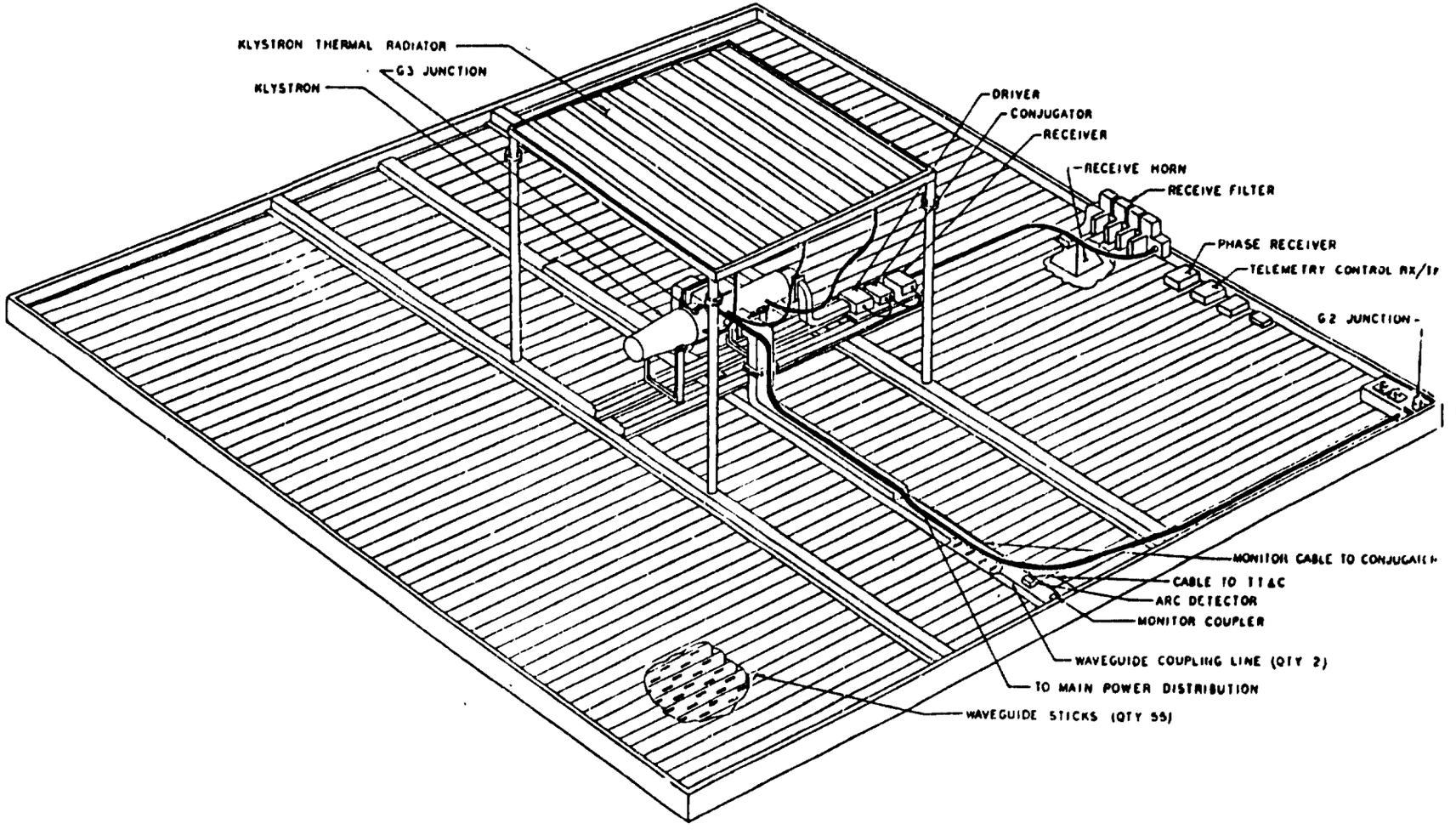

Figure 1.1.2-11 Typical Outer Ring Klystron Module Layout

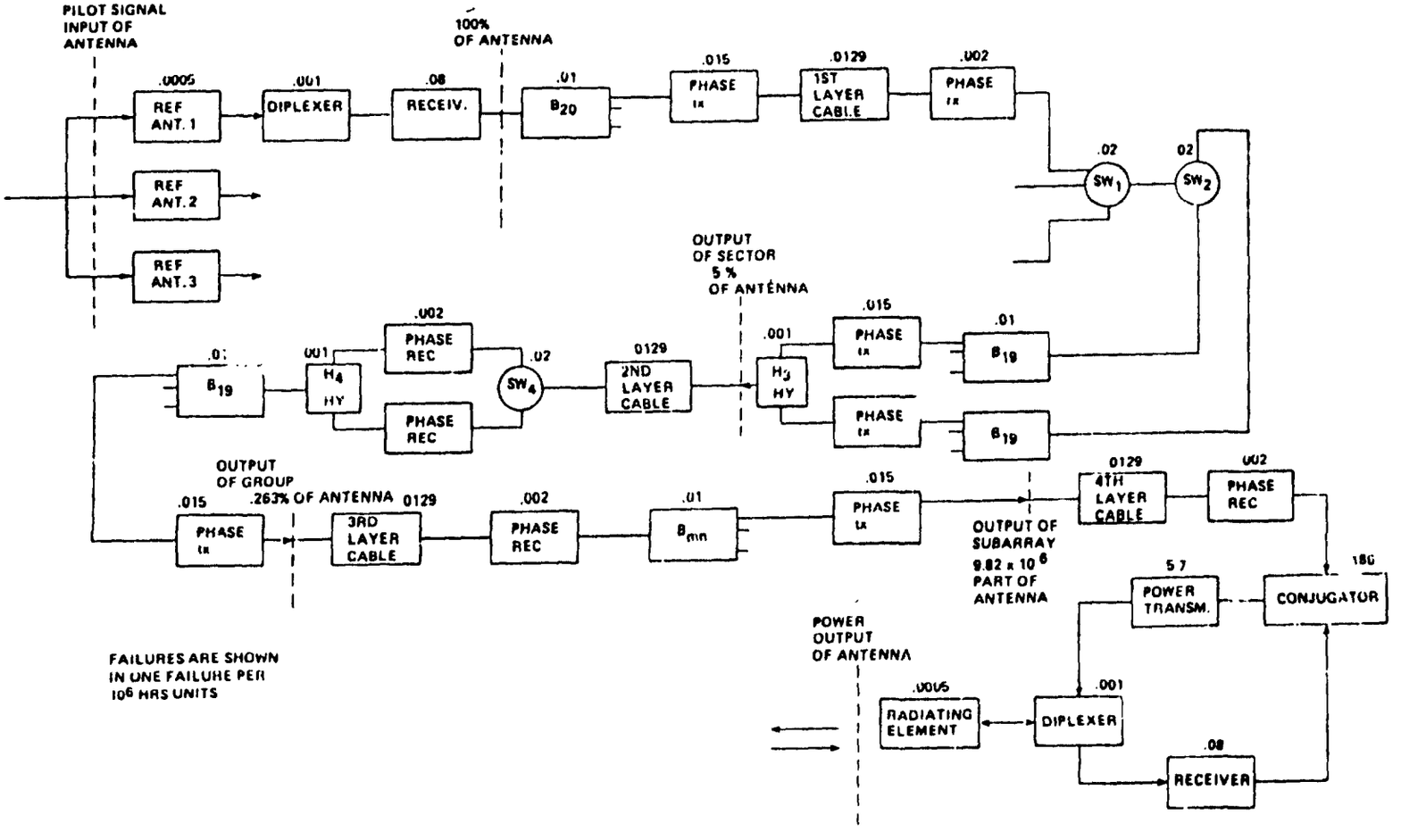

Figure 1.1.2-12 Block Diagram for Reliability Calculations

Table 1.1.2.6 Microwave Power Transmission Loss Factors

	Availability, %	Efficiency,	Comment
Phase Control	.989	.978	Power & Beam Loss Redundant 1st, 2nd Level Conjugator, Receiver 6 Months Maintenance
Klystron and Driver	.98	Previous Budget	No Redundancy 25 Year MTBF 6 Month Maintenance
Rectenna	.984	.984	Diodes Nonredundant No Maint[illegible]
			DC Panel Open/Short Circuit Continuous Maintenance
		3.8%	Microwave Related
		5.1%	Total MPTS

Note that there is a double penalty for phase control system component failure: loss of power, since the klystrons are not radiating in the main beam direction, and associated array thinning, which reduces beam efficiency. The 5.1% efficiency degradation figure includes losses due to bussbar failures on the space antenna and the rectenna.

1.1.2.2.2 MPTS Efficiency Chain Impacts

Table 1.1.2-7 summarizes overall impacts on baseline MPTS efficiency values for the cases of aluminum waveguide, the required baseline tilts, and transmitting antenna component failures for 10 m x 10 m and 5 m x 5 m subarray systems. Refinements in rectenna subsystem values are planned subjects for Phase 2 study.

The tilt requirements are 1 arc minute systematic tilt for realistic grating lobe levels and 1 arc minute random tilt from assembly and manufacturing tolerances. Note that the 5 m x 5 m subarray has fivefold lower tilt losses than 10 m x 10 m subarrays. The additional efficiency reduction due to metal waveguide (as opposed to composite) and failures is 4.94%.

1.1.2.3 Solid-State Microwave Power Transmission Summary

Solid state power amplifiers for microwave power transmission arrays seem well suited to SPS's with grid power outputs of around 2.5 gigawatts. With adequate development on efficient solid state microwave power amplifiers there is a relatively low risk associated with accomplishing a suitable solid state system design.

The key issues remaining are:

1) The feasibility of eliminating power processing,

2) Experimental verification of acceptable efficiencies of integrated assemblies of amplifier devices, coupling circuits and RF radiators, and

3) Microwave power amplification device cost. Gallium arsenide FET's today cost on the order of $100 per watt. This is obviously prohibitive. A production rate curve extrapolation to quantities appropriate to SPS leads to cost predictions in the acceptable range. These, however, will require further confirmation through experience in larger scale production.

Table 1.1.2-7 Nominal MPTS Efficiency Chain

- CURRENT BUDGET BASED ON COMPOSITE WAVEGUIDE
- SYSTEMATIC TILT 1.76 ARCMIN, NO RANDOM TILT

	EFFICIENCY DEGRADATION	
	10M X 10M	5M X 5M
ALUMINUM WAVEGUIDE	1.18%	1.18%
TILT { 1 ARC MIN SYSTEMATIC, 1 ARC MIN RANDOM }	2.7%	0.5%
RECTENNA	TBD	TBD
FAILURES	3.6%	3.6%
$\Delta\eta$	7.50%	5.41%

1.1.2.3.1 Solid State Amplifier Technology for SPS

Introduction

The approach taken for an SPS in the 1990 time frame is to assume that today's state of the art will be in mass production by 1990 with relatively minor improvements in performance parameters.

The primary requirements for solid state SPS MPTS are, in order, adequate DC-RF conversion efficiency, device lifetimes long enough to eliminate power amplifier replacement for 30 years and MPTS costs competitive with costs of other DC-microwave conversion options.

A wide variety of suitable solid state active devices currently exist. These include bipolar and field effect transistors, many types of two-terminal devices (Gunn, IMPATT, TRAPATT, and BARITT diodes) and hybrid devices such as electron bombarded semiconductors (EBS). EBS have been included as being solid state since the electron beam only supplies a small current, with the bulk of the supply current staying in the semiconductor.

Once device type is chosen, other technical alternatives remain to be considered. For active devices with more than two terminals there are several classes of amplifier circuit configuration that the devices may be used in. There is a growing number of commonly used solid state materials out of which components may be fabricated, with options in type of processes at each step in fabrication. Many of these options have been considered in this study and further improvements by industry will be included in periodically updated study results. In particular, close contact will be maintained with RCA Princeton Laboratories during their contracted work with Mr. L. Leopold of NASA-JSC.

State of the art power-added efficiency, gain and single device power as a function of frequency for various types of solid state devices are shown on Figures 1.1.2-13, 1.1.2-14 and 1.1.2-15.

Power-Added Efficiency

Power-added efficiencies for various devices are shown in Figure 1.1.2-13. GaAs FETs, silicon bipolar transistors and EBS have the best values. All the two terminal devices have efficiencies less than .36, which is so low as to make their use for SPS impractical and allows their elimination from further consideration.

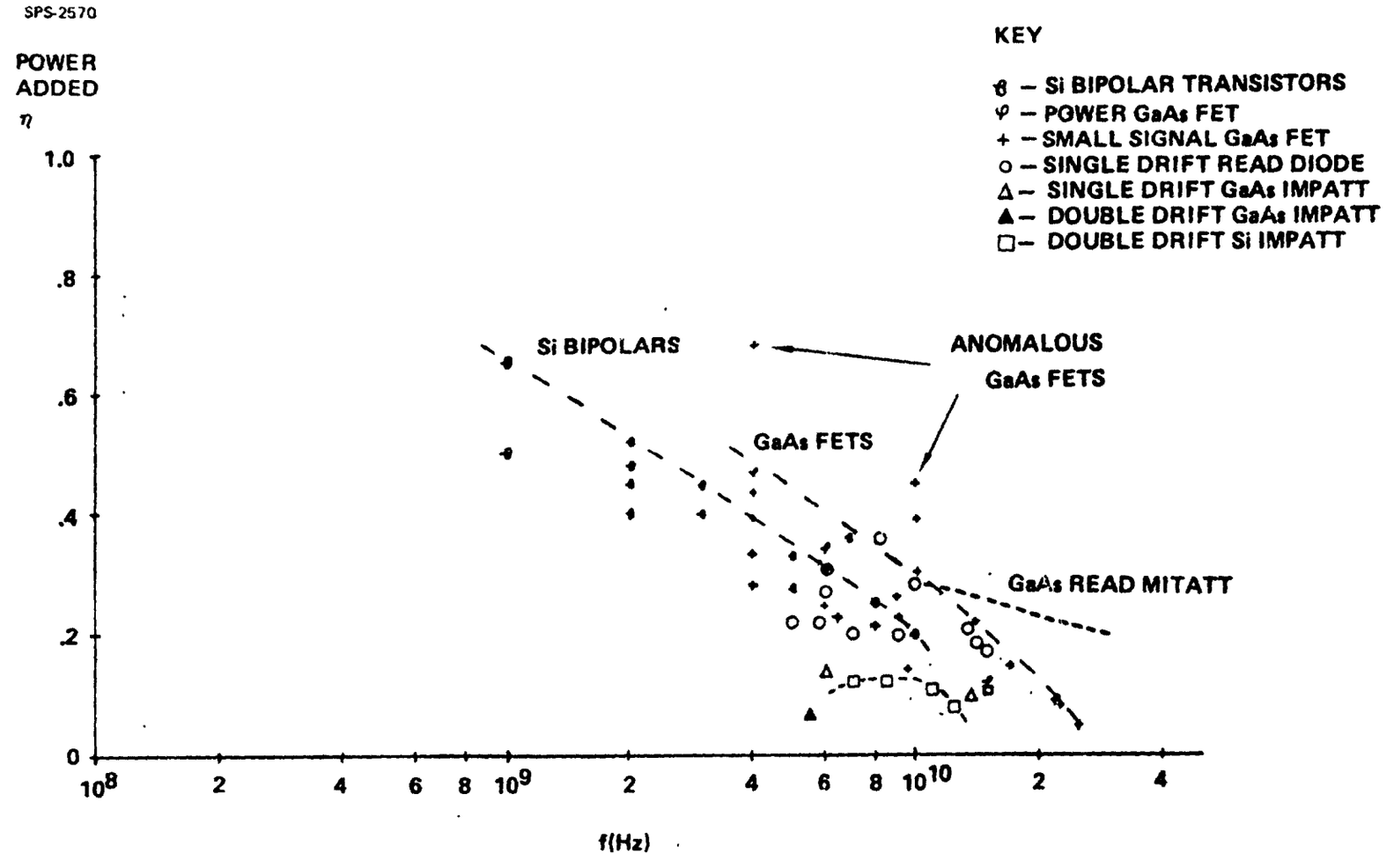

Figure 1.1.2-13 Solid State Device Efficiency v. Frequency

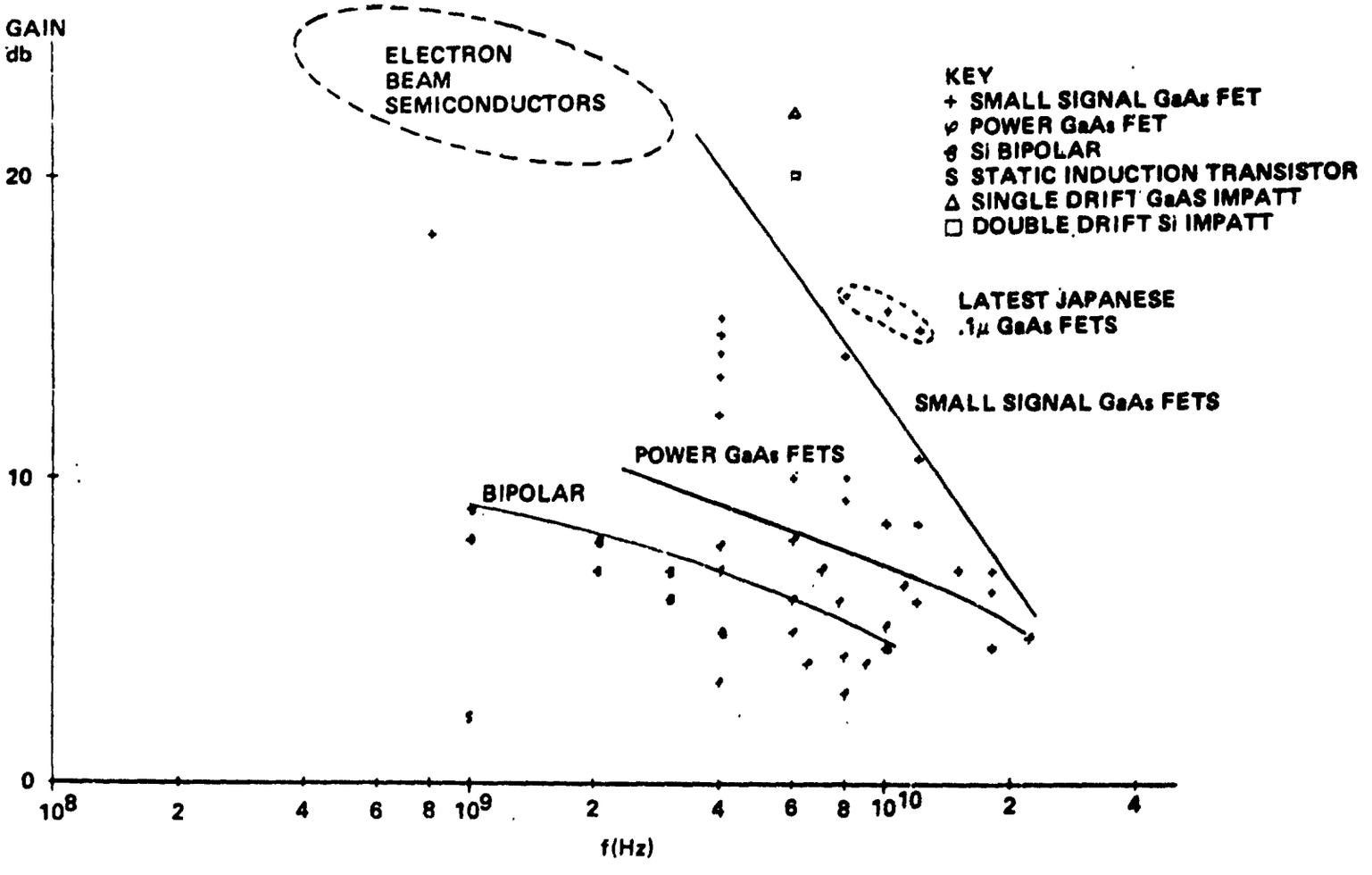

D180-25037-2

Figure 1.1.2-14 Solid State Device Gain vs Frequency

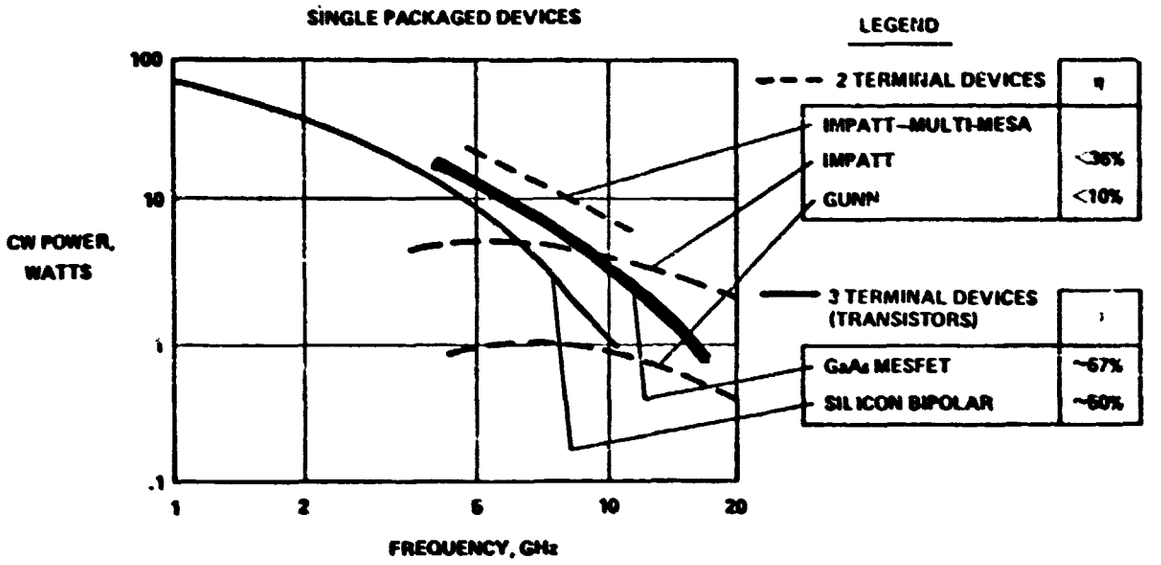

Figure 1.1.2-15 Solid State CW Power versus Frequency

It is worth noting that there are two GaAs FET data points substantially above the general GaAs FET trend. These represent occasional anomalously good lots from single wafers. Several manufacturers have observed this phenomenon which in the case of GaAs still remains somewhat unpredictable. Perhaps this unpredictability should be expected since GaAs is unstable in the sense that separation into separate Ga and As phases is energetically favorable at electronic device operating and storage temperatures.

In the case of three-terminal devices the results of Figure 1.1.2-13 correspond to class A and B amplifier configurations for GaAs FETs and to class C for bipolar transistors. This inherently limits their efficiency. Other classes of amplifier, summarized on Table 1.1.2-8, can have theoretical efficiencies approaching unity.

The classes of amplifiers grouped as "switched mode amplifiers" on Table 1.1.2-8 operate with the I-V product time integral over the operating cycle minimized as much as possible. This generally requires active device transition times about a factor of ten faster than the RF period. It also generally requires resonant reactive networks which make achieving bandwidths of a tenth or more of the operating frequency as desired by many communications users very difficult. In this sense, the narrow bandwidth required by SPS is a real advantage.

Present communications interests in microwave power amplifiers are increased linearity over wide bandwidth and RF output powers equivalent to present traveling wave tubes with longer life than the TWT's, whereas for SPS, efficiency, lifetime, low cost and narrow bandwidth are desired. It is anticipated that with adequate funding the development of high efficiency switched mode amplifiers for SPS presents a relatively low risk to the program's chances for success. However, SPS developers may have to take the initiative in this development because the communications industry can develop and prosper adequately with present DC-RF conversion efficiencies.

The present state of the art in switched mode amplifiers is common use in RF amplifiers at tens of megahertz. Experimental amplifiers at over 100 MHz have been successfully achieved and microwave amplifier experiments are pending. More discussion of efficient amplification techniques is given in References 1 and 2, with discussion of the particular type of switched mode amplifier known as the class E amplifier in References 4-6.

TABLE 1.1.2-8

	Amplifier Class	Maximum Power-added Efficiency for Sine Wave Output	Typical Efficiency Values Achieved	@ Frequency	Duty Cycle at Maximum Efficiency	Active Device Saturated ?	Active Device Cut Off ?
	A	.5	.3	@ 4 GHz	1.0	No	No
	B	.785	.5	@ 4 GHz	.5	No	Yes
	C (Unsaturated)	.896	.6	@ 2.5 GHz	.3	No	Yes
	D	1.0	.9	@ 10 MHz	.5	Yes	Yes
Switched Mode Amplifiers	E	1.0	.9	@100 MHz	.5	Yes	Yes
	F	1.0	.9	@ 10 MHz	.5	Yes	Yes
	S	1.0	.8	@ 100 KHz	Variable [1]	Yes	Yes
	Multivoltage	1.0	.8	@ 10 MHz	Variable	Yes	Yes
	G	.818	.7	@ 100 KHz	Variable	Yes	Yes

Device Gains

Achieved device gains vs frequency are shown on Figure 1.1.2-14. There is a striking difference between small-signal and power gain for FETs. At the SPS frequency of 2.5 GHz bipolars have about 8 db gain while GaAs FETs yield around 10 db. In general, GaAs FETs have several db more gain than bipolars throughout the spectrum. As for the other devices, IMPATTs can have gains of over 20 db and electron beam semiconductors are projected to yield about 20 db. The low gain of Static Induction Transistors (SITs) at 1 GHz eliminates them from consideration at present, although they appear to have great potential for further development due to their high power bandwidth product.

Device Power

The power per device is an important SPS parameter since the number of devices which can be efficiently combined in a module is limited by circuit losses and the power per module determines the RF power density per unit transmitting array area. The single device power chart (Figure 1.1.2-15) shows that silicon bipolar transistors, GaAs FETs and multi-mesa IMPATTs can all handle powers above 10 watts, which is an adequate power level for SPS application. Of the devices considered here, only E-beam semiconductor devices are capable of generating a power level of 100 watts per device which would be adequate for one device per radiating element. For the other devices, power combining will be necessary.

Device Lifetimes

The fundamental wearout failure modes in semiconductor devices tend to be concentrated at surfaces, both internal and exposed, and are generally electrochemical in origin. In the case of the internal surfaces, transport of species to and away from interfaces eventually degrades contacts. In the case of external surfaces, impurities can come in from outside to form compounds and oxides and high electric fields can cause breakdown.

EBS cathodes presently have an expected lifetime of 2×10^4 hours, over an order of magnitude less than that required for a 30-year satellite, so they appear unsuitable for SPS. The two remaining solid state amplifier candidates are GaAs FETs and Si bipolar transistors. Si bipolar lifetimes are limited by electromigration of emitter finger metallizations due to localized high current densities. This gives relatively sudden and complete hard (open or short circuit) failures, whereas GaAs FETs seem to suffer from contact degradation which decreases performance gradually.

Bipolar lifetimes have been improved recently by going to gold rather than aluminum metallizations, but at reasonable operating conditions and equal junction temperatures, GaAs FETs have a definite performance advantage. A current GaAs FET lifetime vs temperature curve is shown on Figure 1.1.2-16.

GaAs FETs were selected as the preferred DC-RF conversion devices because of their higher gain than silicon bipolars, equivalent expected power added efficiencies, roughly equal power capabilities at 2.5 GHz and much better expected contact metallization reliability due to current densities lower than Si bipolars. GaAs FETs for SPS application could be fabricated separately and mounted in hybrid fashion or combined with other components on larger GaAs chips in integrated circuits. The latter alternative is preferred because of its significantly lower costs in mass production, although it does entail somewhat more development.

1.1.2.3.2 Solid State Transmitting Antenna Configuration

Configuration Description

Synthesis of a solid state transmitting antenna configuration has been accomplished using design criteria for radiating module size developed in previous NASA studies and several concepts developed in prior proprietary Boeing IR&D work.

The basic elements of the solid state transmitting array are .59λ x .59 λ (λ = free space wavelength) radiating modules. These are fabricated on 20 mil thick alumina dielectric sheet which is metallized for signal, control and power circuitry. A candidate cavity radiator design has been subjected to initial test. Microstrip techniques are used for combining, filtering, and making antenna elements with 5 db gain over isotropic. Ways have been found to efficiently combine outputs from up to 6 amplifiers.

Proper phasing signals are to be distributed from a control unit at the center of the subarray to all other panels by a stripline phase feed network. Signal losses on the feed may be either made up for along the way with local amplifiers or handled through extra gain at the power amplifier chip.

Assuming a signal input power of 1 milliwatt, it appears that two stages of amplification are required prior to the power amplifier. These should only require a small

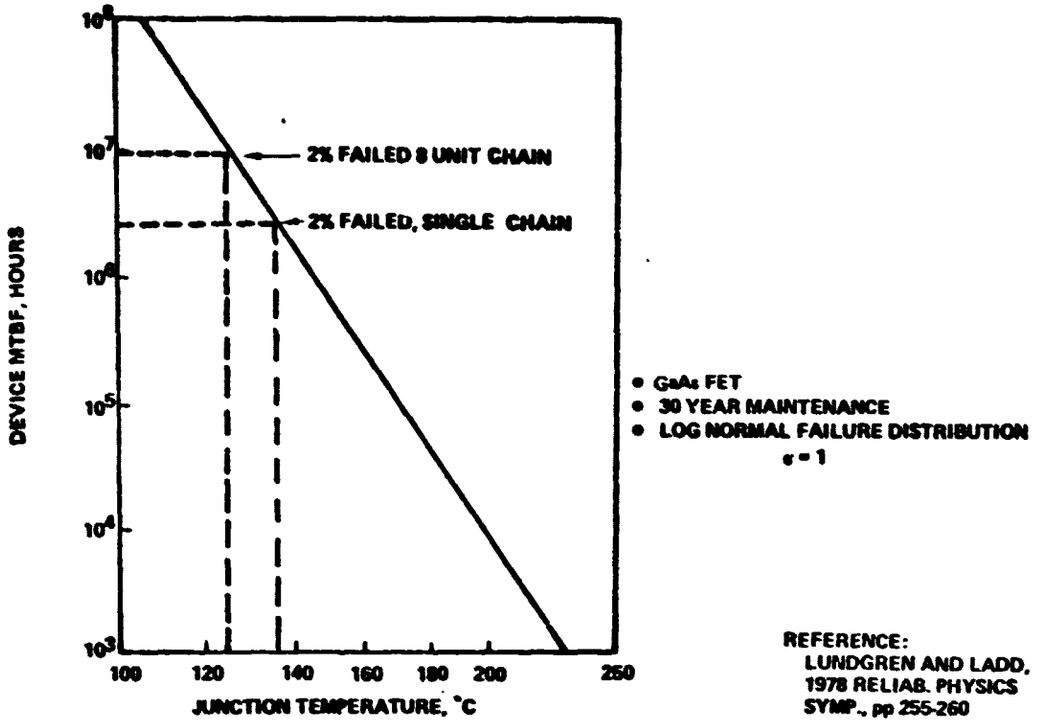

Figure 1.1.2-16 GaAs FET Lifetime vs Junction Temperature

fraction of the area on the chip, the power amplifier taking most of it. Feedback to allow phase correction between radiating element and amplifier may be necessary. The power amplification devices proposed for initial testing are GaAs metal-semiconductor field effect transistors (MESFETs) similar to those made by Fukuta et al, which were 15 watt 20 volt devices (Ref. 7). Thermal resistances from the active regions of the power FET will have to be reduced by use of plated-through pins, as described in Reference 8.

The aluminum ground plane on the radiating side of the modules provides a mounting surface for the power amplifier chips on raised pads, which fit into holes in the dielectric substrate. This minimizes thermal resistance between the chips and the metal surfaces used as thermal radiator. Further attention to the detailed thermal design will be required, but preliminary estimates ensure feasibility.

In the module proposed for test evaluation, the back plane of the alumina substrate is covered with a 10 mil aluminum cover which forms the RF cavities and provides environmental protection. This cover is electrically contiguous with the ground plane through tabs crimped around to the front in the last stage of the module manufacturing process. It is also thermally coupled to the ground plane metallization through the tabs and the substrate.

A surface of white thermal control coating with α/ε of .25 (Ref. 9) is presumed to coat the aluminum to increase thermal radiation capacity. This allows a thermal rejection capacity of approximately 1 kw/m^2 per side at 125°C. For a device efficiency of 75%, this implies an RF power density of $(\eta/1-\eta)(\dot{Q}/A) = 3$ kw/m^2.

For design purposes, a module combining six 5-watt amplifiers has been selected. These 30-watt, 15-volt power amplifier modules are to be connected in a series/parallel hierarchy illustrated in Figure 1.1.2-17. Modules are connected 4 in parallel to form units called rows. Twelve rows are connected in series to form strings. Three strings in parallel make up the panel, which is 0.75 m^2 in area and is considered to be the least replaceable unit. One hundred forty-four panels in a 12x12 series-parallel matrix form subarrays of the same size as the current baseline with a voltage of 2.16 kv.

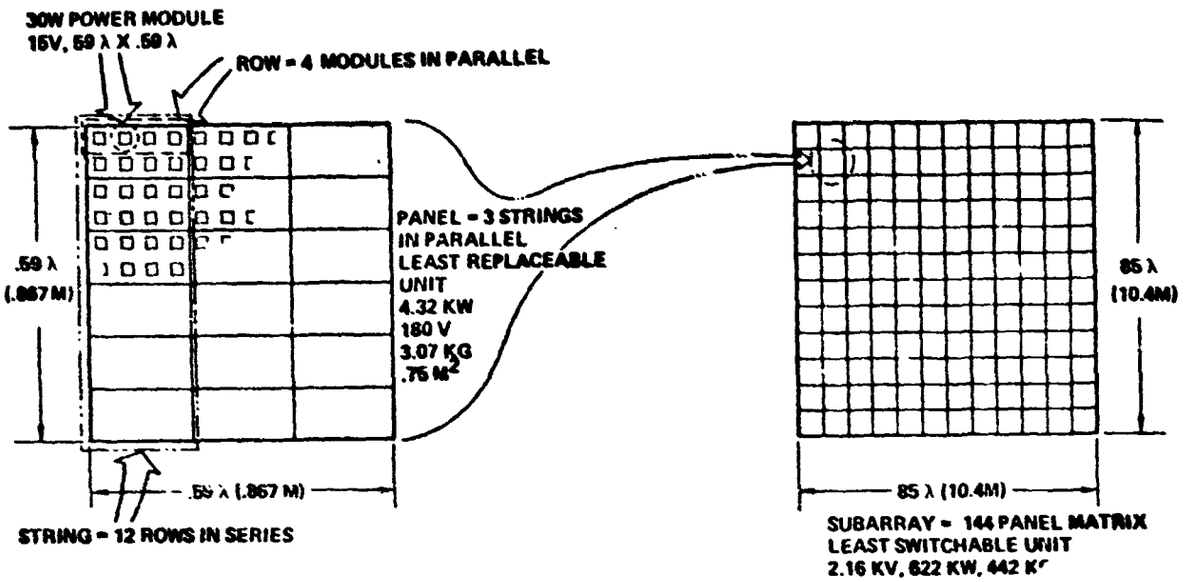

Figure 1.1.2-17 Solid State Subarray Layout

Going to series-parallel connections as proposed here makes system failure probability calculation somewhat more complex but still well within the state of the art. The result depends both on the failure modes of all the elements in the matrix and on system response to failed elements. A preliminary plan of overvoltage and short circuit protection by regulators, bypasses and fuses at various levels on the hierarchy is shown on Table 1.1.2-9.

An analysis of series/parallel connections for a case of modules consisting of two parallel amplifiers, in parallel rows of 4 modules and strings of 12 rows is shown on Figures 1.1.2-18 and 1.1.2-19. In the case illustrated, the row should be able to tolerate open failures in two out of the 8 amplifiers in order to not affect string reliability excessively. The results also show that, for the case where 2 amplifiers per row may fail, the string failure rate can be made much lower than the amplifier failure rate for cases where only one amplifier may fail. For example, probability of string failure is ten times lower than amplifier failure probability at $F_p = .04$. This will be even more dramatic for lower F_p's.

Table 1.1.2-10 presents a mass estimate for a representative solid state transmitting array design. The total mass per unit transmitting array area is approximately 5 kg/m^2, slightly more massive than the waveguide in the baseline design (4 kg/m^2). The r.f. power density for the configuration on Figure 1.1.2-17 is 5.5 kw/m^2, yielding a specific mass of about 1 kg/kw at the center of the transmitter.

This power density requires a DC-RF conversion efficiency of 82% or better in order to retain the 125°C surface temperature limit. Advanced technology power amplification devices which handle more power must be used in proportionately less lossy amplifiers if the same temperatures are to be retained. To match the 22 kw/m^2 aperture power density of the present baseline satellite design would require 96% efficient amplifiers which are unlikely. In the alternate approach of raising the temperature, 75 K more is required to double the radiated thermal power. This is not possible in terms of GaAs FET time to failure, which goes down a factor of 10 roughly every 25K.

Several things are apparent from the mass estimate. First of all, the mass of the dielectric dominates and can almost certainly be reduced by going to designs with less dielectric volume and/or less dense dielectric.

Table 1.1.2-9 Series–Parallel Unit Responses (Preliminary)

	MODULE	ROW	STRING	PANEL	SUBARRAY
UNDERVOLTAGE	NO RESPONSE	NO RESPONSE	NO RESPONSE	NO RESPONSE	NO RESPONSE
OVERVOLTAGE	NO RESPONSE	OPEN ON 1.2X LOAD ON 1.05X	NO RESPONSE	OPEN AND LOAD ON 1.2X	OPEN AND LOAD ON 1.15X
CURRENT LOW	NO RESPONSE	NO RESPONSE	NO RESPONSE	NO RESPONSE	NO RESPONSE
EXCESSIVE CURRENT	FUSE ON 3X	NO RESPONSE	FUSE ON 2X OPEN ON 1.5X LOAD ON 1.4X	OPEN ON 1.5X	OPEN ON 1.5X

ALL FAILURES SHOULD BECOME OPEN OR SOFT

Figure 1.1.2-18 String Reliability Analysis Configuration

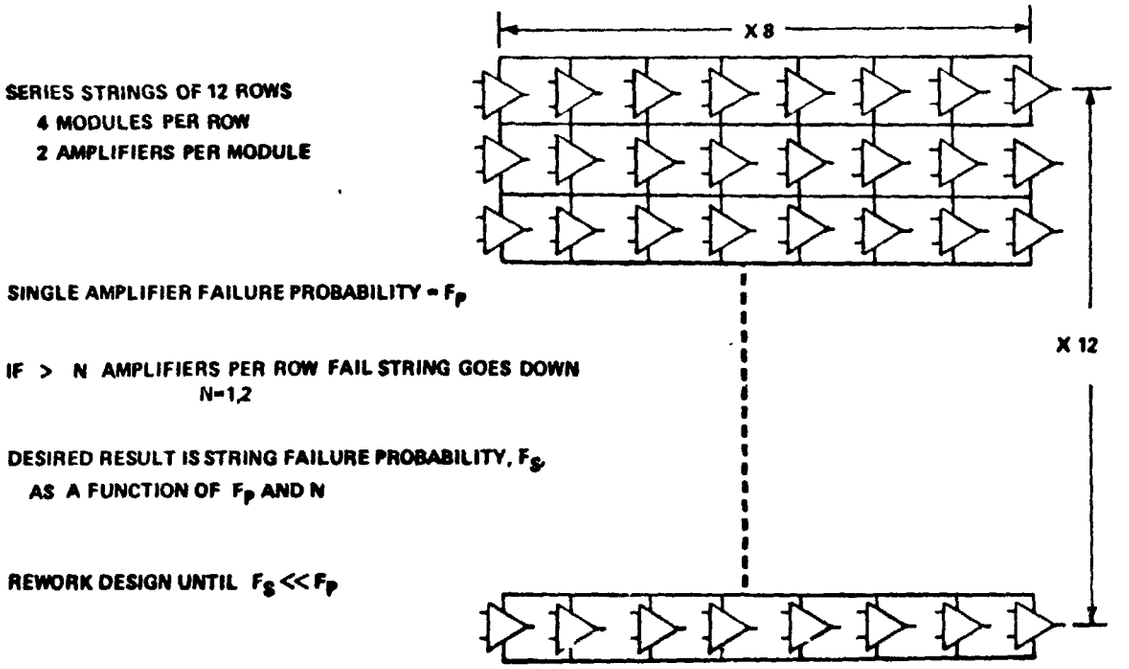

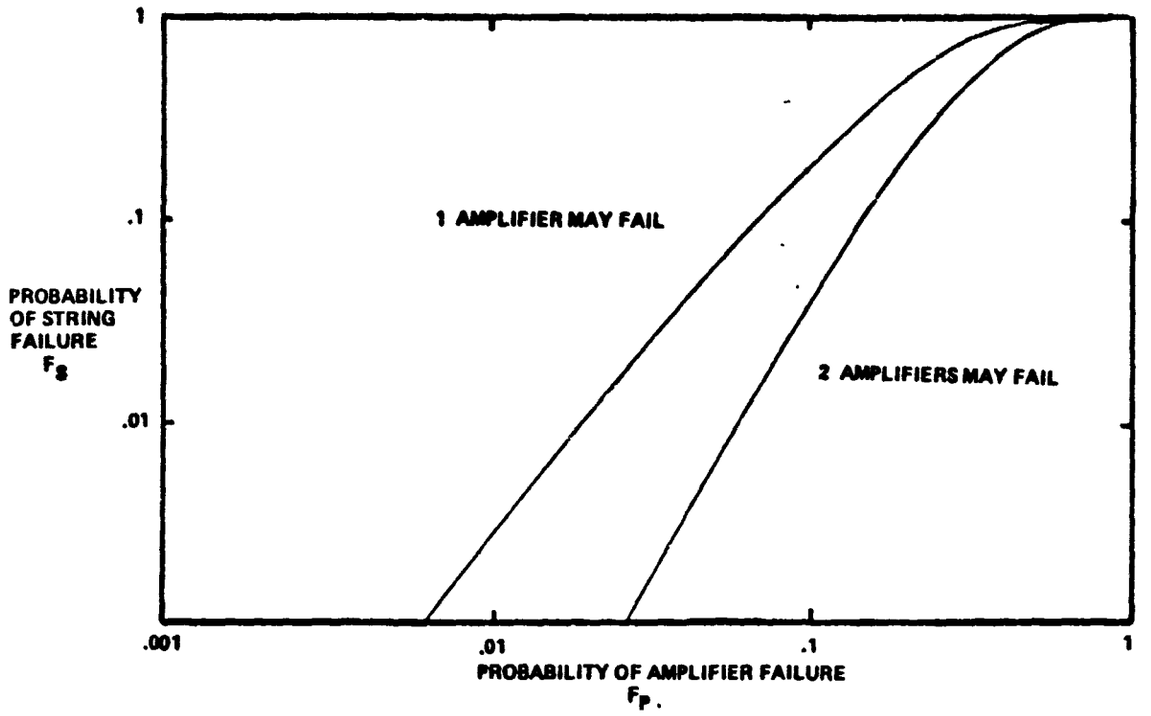

Figure 1.1.2-19 Series–Parallel String Failure Overhead

Table 1.1.2-10 Solid State Transmitting Array Mass Estimate

Component	Mass Per Unit Area (kg m^{-2})
MPTS Primary Structure	.07
MPTS Secondary Structure	.72
7.5 mils Aluminum (Front Side Average)	.52
20 mils Alumina	1.99
7.5 mils Aluminum (Back Side Average)	.52
5 mils Al equivalent for radiation shielding	.35
5 mils Al equivalent for phase feed	.35
5 mils Al equivalent for intersubarray structure	.35
Total	4.87

Secondly, the housekeeping masses of support structure and phase feed add up to about a third of the total.

Lastly, the power processing system should be designed and included in order to fairly compare the baseline and solid state transmitting options. This will be done in Phase II after design refinement and detailing.

Power Supply Options

In the present SPS concept of a separate transmitting antenna connected through a rotary joint to distant solar cell panels, the method of providing power to individual modules appears to be the largest identifiable system design uncertainty. Three basically different options have been identified (see Figure 1.1.2-20), with a choice to be made after further study in Phase II. These are: (1) Direct High Voltage DC (DHV DC), (2) DC-DC conversion at the transmitting antenna; and (3) AC power distribution.

For the initial design, direct high voltage DC is assumed since the solid state amplifiers, unlike klystrons and magnetrons, do not require voltage regulation. Fast overvoltage protection will have to be provided, however. The main problem with DHV DC is the proper connection topology if buss voltages of tens of kilowatts are to be reached. (High electric field values between adjacent subarrays restrict how the subarrays may be connected together.)

DC/DC conversion offers the lowest risk option but AC distribution may minimize distribution losses and allow lower solar array voltages. For both DC/DC and AC, a mass penalty on the order of 1 kg/kw is incurred. However, some series connections to raise voltages and reduce conductor mass are still expected to be necessary in an economically viable system.

1.1.2.3.3 Solid State Satellite System Analysis

This section deals with preliminary values of solid state SPS microwave power transmission system masses and costs and their overall impact on SPS.

Mass Estimates

A simple mass model of the SPS microwave transmitting antenna has only two terms: one depending linearly on antenna area, which has a coefficient of approximately

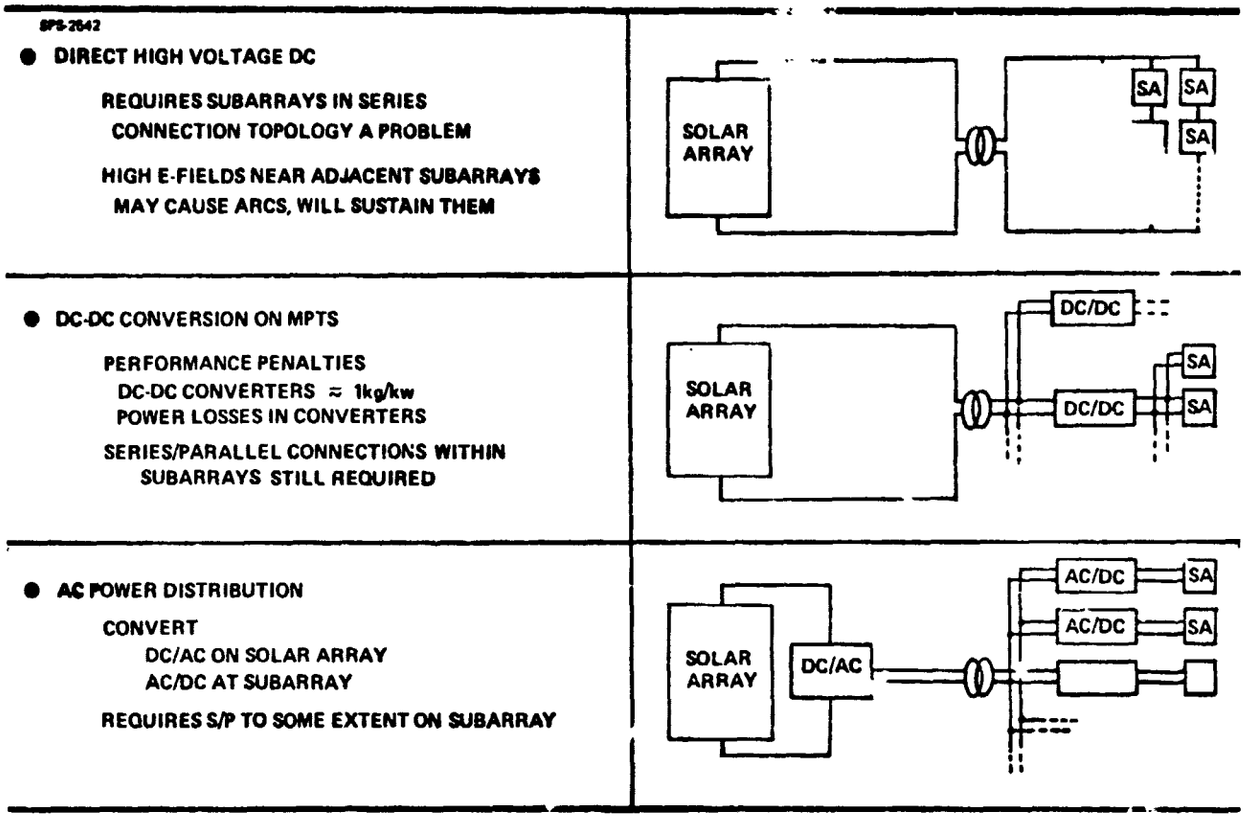

Figure 1.1.2-20 Solid State Power Supply Options

4 kg/m^2 for waveguide; and another depending linearly on the power transmitted, which has a coefficient of about 1.4 kg/kw for klystrons. The effect of going to a solid state antenna, assuming it does not require power processing, is to eliminate the power-dependent term in the mass. If power processing is required, a power-dependent term of around 1 kg/kw will be added.

Cost Estimates

As in the case of mass estimates, cost components can be split into area dependent and power dependent terms. The entire phase control system is included in the area term and is probably significantly more costly per unit area than in the baselined (klystron) system because phase must be distributed to power amplifiers a factor of 10^4 smaller. Because of the lack of definition of the phase control system at this point, a meaningful prediction of its cost for an alternative solid state satellite is not possible but is anticipated to make a difference.

For the power-dependent cost component of the transmitting array, rough predictions may be made by taking costs and production rates for present microwave semiconductor devices and running them down a production rate improvement curve for an SPS buy. Figure 1.1.2-21 shows costs of microwave power for present-day devices and Figure 1.1.2-22 illustrates SPS production rate cost reductions. Surprisingly, klystron costs are nearly matched.

If the phase control system cost is a fifth that of the power amplifier cost, single 1.4 km diameter antenna satellites of approximately 2.5 Gw Earth output are near cost optimal (see Figure 1.1.2-23). With a 70% production rate improvement curve (i.e., units produced at the rate of 2n per year cost 70% as much as units produced at the rate of n per year), cost per unit power for GaAs FETs is about the same as the projected cost per unit power for klystrons.

Sizing Aids

A nomograph was developed to assist in power beam sizing estimates for these systems (Figure 1.1.2-24). The assumptions in this design tool are based on the assumed nominal SPS efficiency chain and are described in Reference 10.

Figure 1.1.2-25 plots RF power density and module power of a .7λ x .7 λ module for uniform and Gaussian transmitting apertures versus DC grid power output.

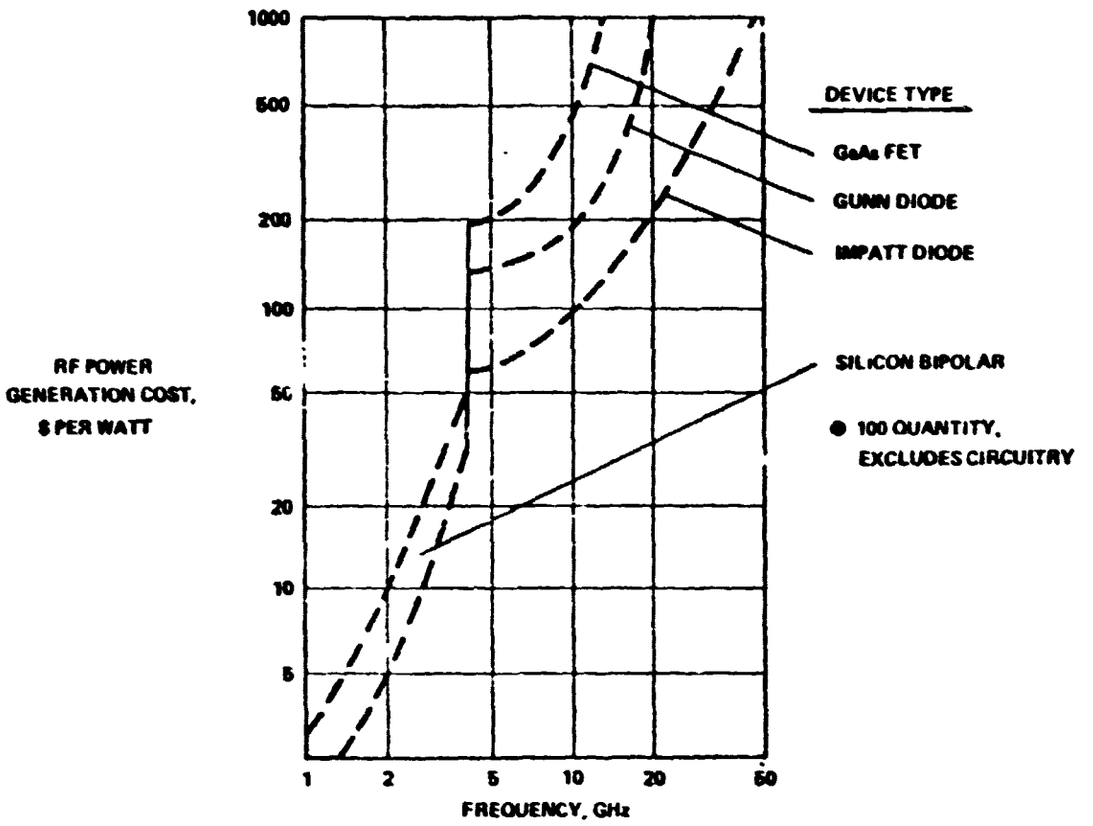

Figure 1.1.2-21 Device Cost Trends—1978

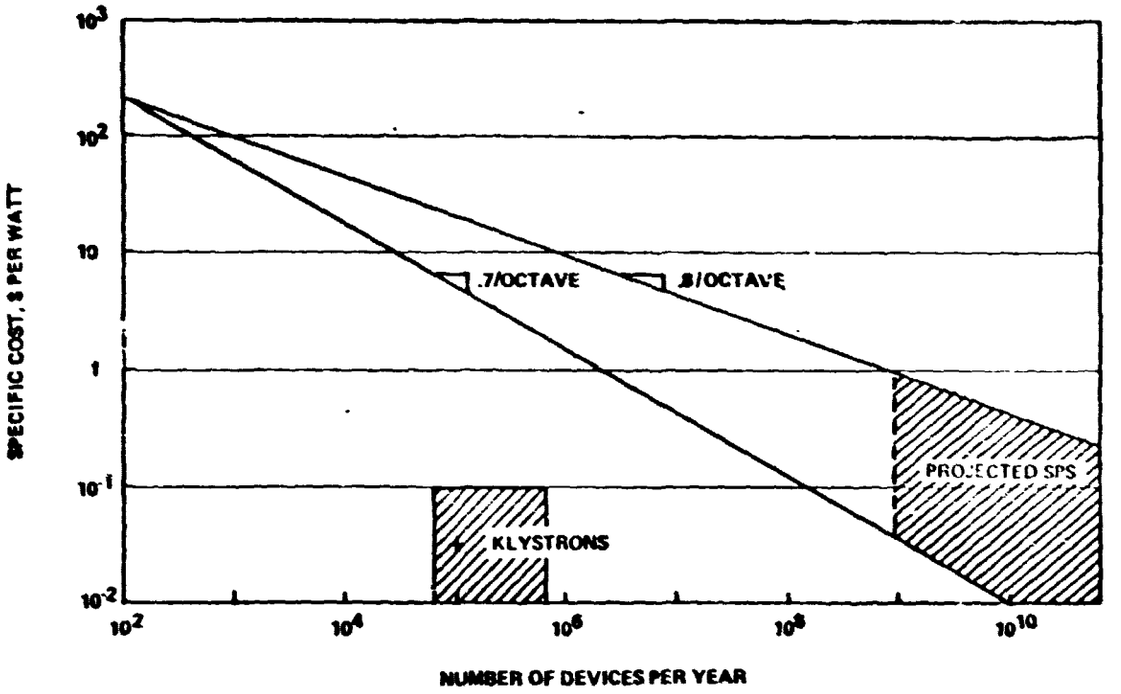

Figure 1.1.2-22 Solid State Device Mature Industry Costing

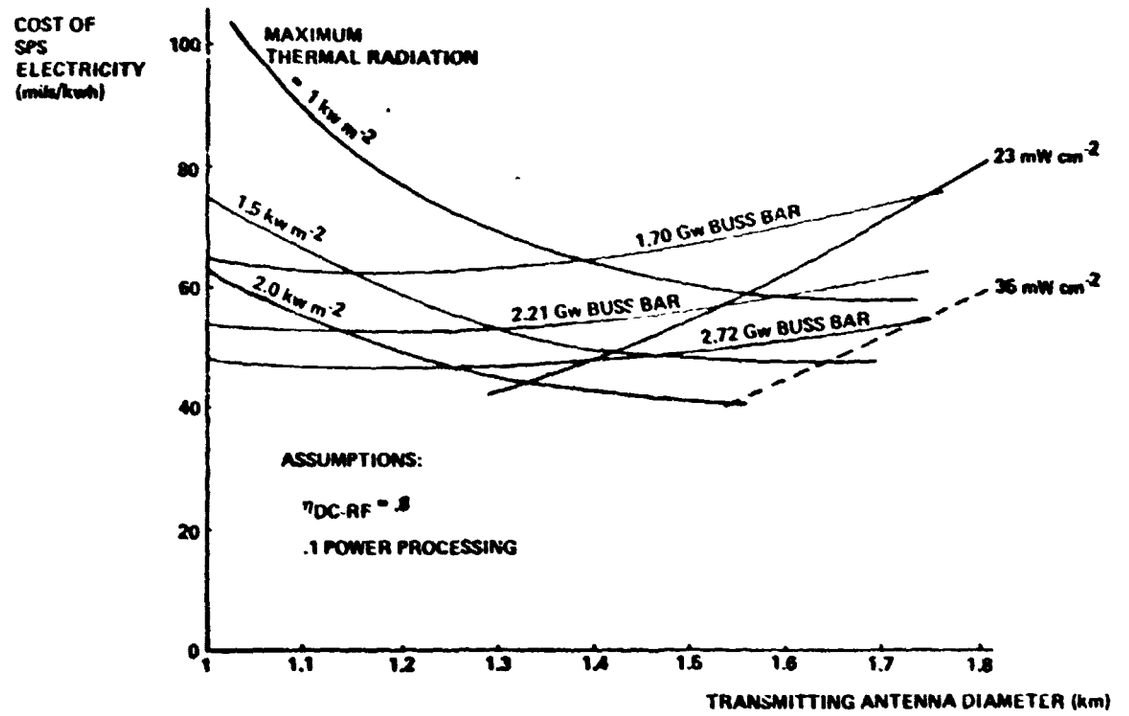

Figure 1.1.2-23 Representative Solid State SPS Costs and Sizing

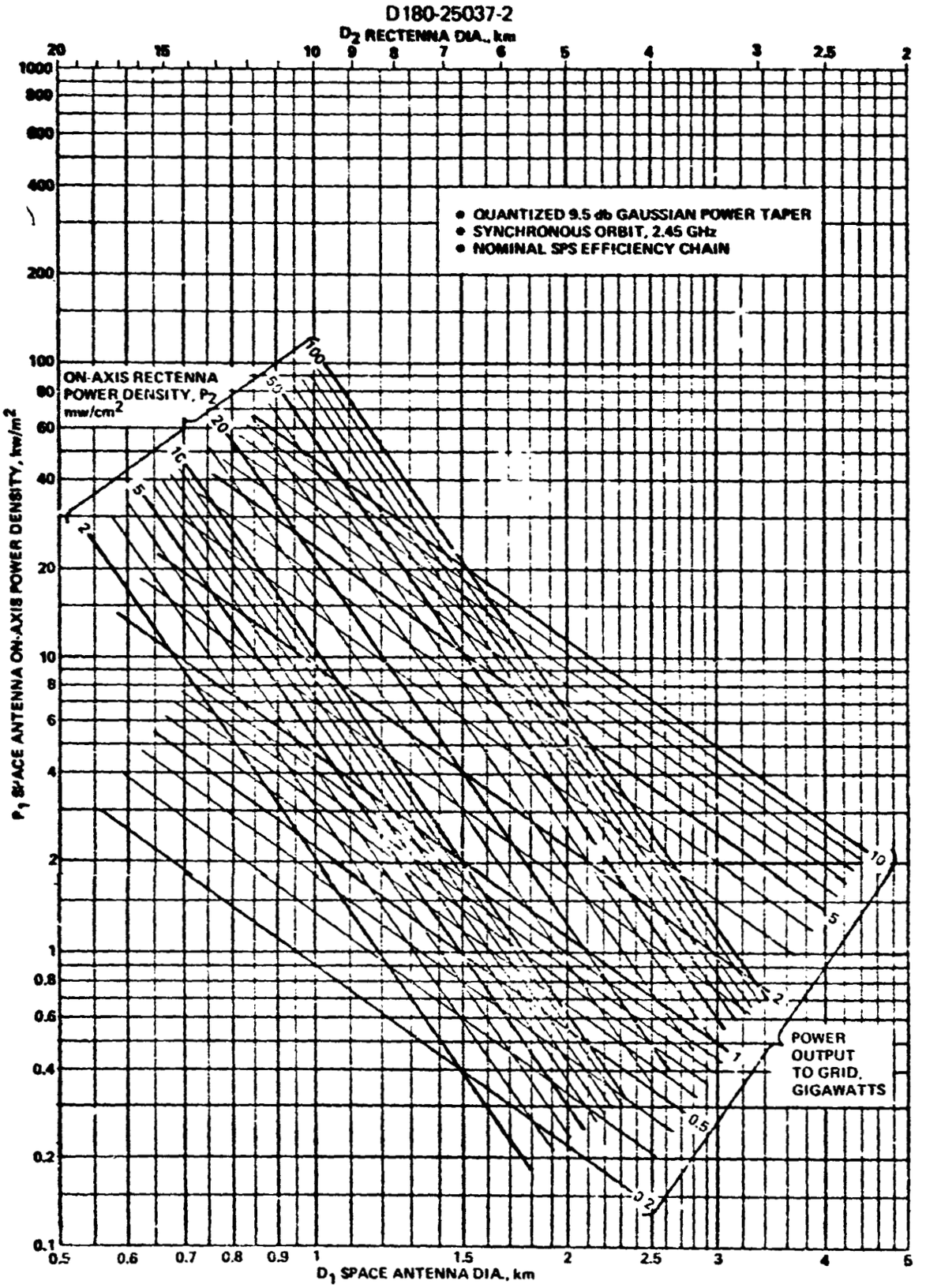

Figure 1.1.2-24 Solar Power Satellite Beaming Nomograph

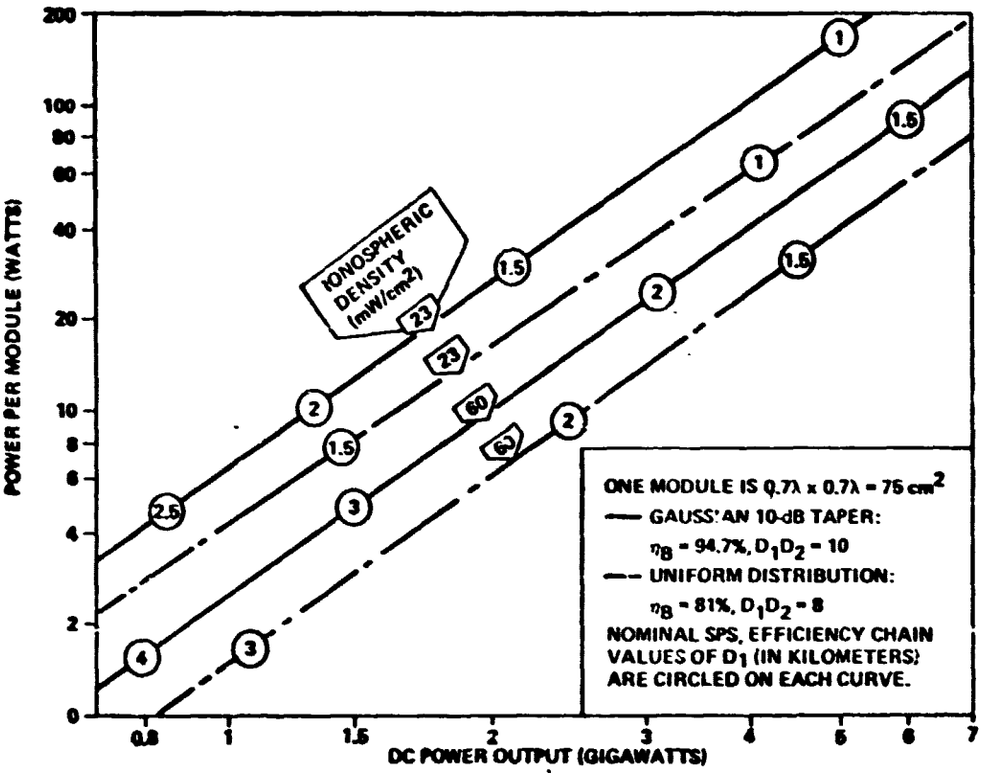

Figure 1.1.2-25 Comparison of Uniform and Gaussian Illumination Function

1.1.2.3.4 Preliminary Noise Analysis

Calculations of incoherent noise spectral density near the operating frequency indicate that the solid state MPTS should have significantly less ground noise than the baseline MPTS with 70 kw klystrons. This is not due to the fact that klystrons are noisier but rather that the solid state power is radiated over a larger solid angle. Further refinements of these calculations, both close to the carrier and out of band, will be needed once all of the components in the MPTS are better defined, but for now these estimates suffice and indicate feasibility.

Phase locking may be used to combine the best spectral characteristics of several devices in a system. If this is done for the SPS MPTS by locking local Gunn oscillators to a crystal controlled reference oscillator a noise spectrum with a floor near -160 dbc/Hz similar to Figure 1.1.2-26 can be expected.

The noise at the power amplifier outputs of the klystron and solid state MPTS options are essentially the same because in a series of amplifiers noise figures of prior stages overwhelm contributions from the following stages. Thus even though a klystron may have a noise figure of 30 db as opposed to approximately 5 db for a solid state amplifier it makes no noticable difference in the system noise figure, if they both have similar front ends.

Since the solid state panels have substantially less area than klystron modules, the panels will spread their noise over a wider solid angle than the klystron modules will, thereby reducing the ground noise power per unit area. (See Figure 1.1.2-27.) Table 1.1.2-11 shows calculations of the type made by Dr. D. Arndt of NASA-JSC for the klystron and indicates a level 14 db lower for the solid state satellite with the parameters chosen.

The coherent contributions close to the carrier are expected to result in negligible offset from nominal beam center. For a frequency deviation of 5 MHz (phase lock loop bandwidth, say), $df/f = d\lambda/\lambda = d\theta/\theta = 5/2500 = 1/500$. With a 10 km rectenna diameter the expected offset would be

$$Rd = \frac{(10{,}000)}{500} = 20 \text{ meters.}$$

(X-BAND, SINGLE SIDEBAND)

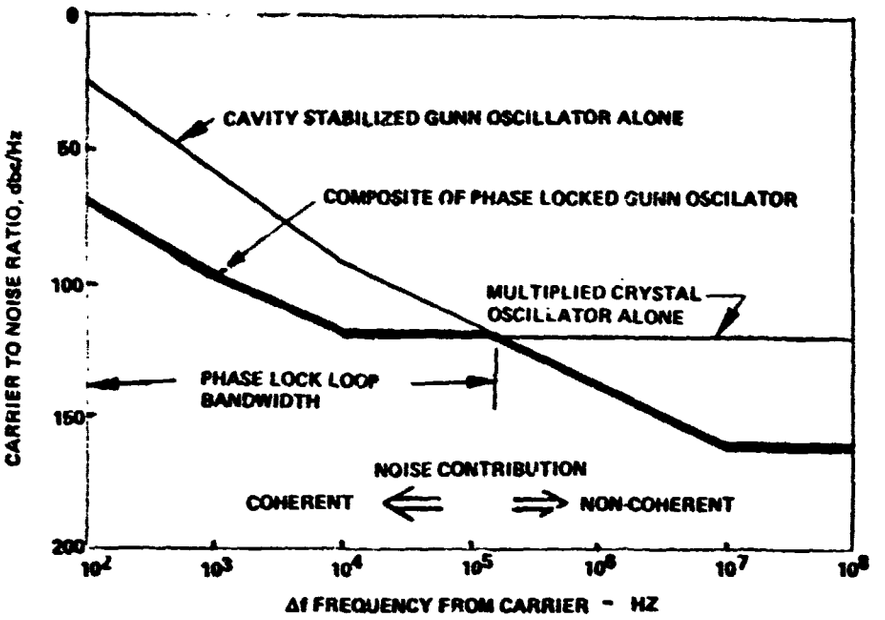

REF: HAMILTON, S. MICROWAVE JOURNAL, JUNE '78 P. 105-109

Figure 1.1.2-26 Impact of Phase Locking on Phase Noise

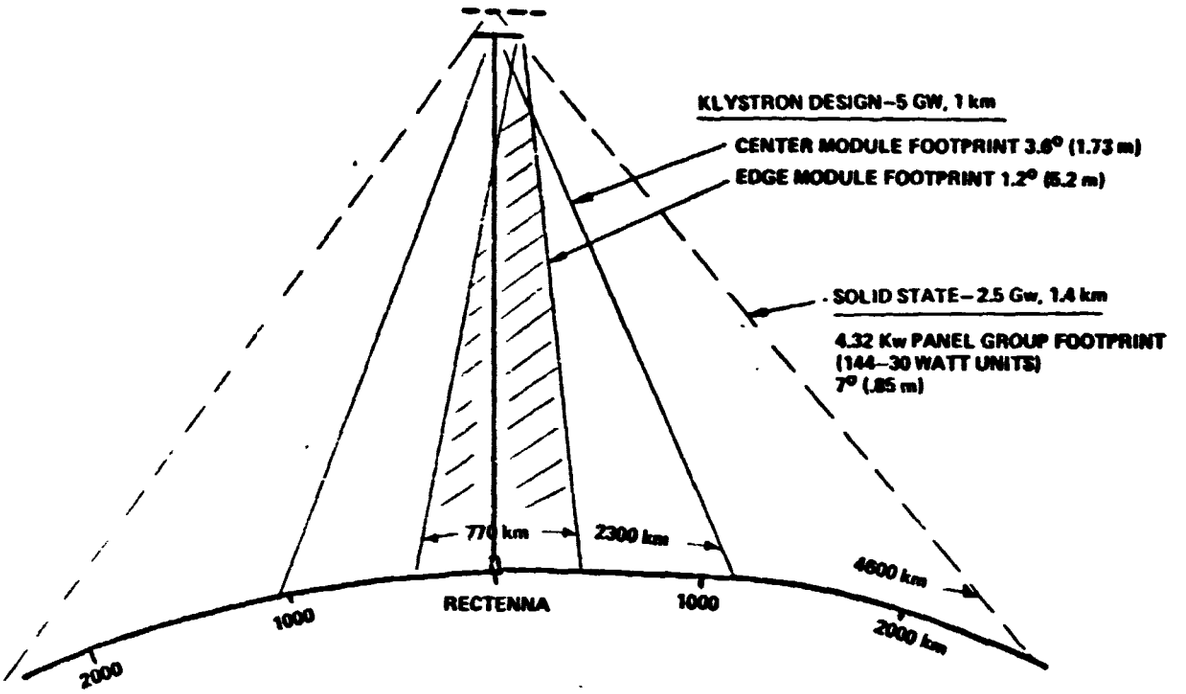

Figure 1.1.2-27 Incoherent Noise Power Distribution

Table 1.1.2-11 Comparative Calculation of Ground Noise

SOLID STATE	KLYSTRON
$P_N = 3.5 \times 10^9 \times 10^{-16} = 3.5 \times 10^{-7}$ W/Hz	$P_N = 7 \times 10^9 \times 10^{-16} = 7 \times 10^{-7}$ W/Hz
$G_N = 4\pi A_{eff}/\lambda^2 = 308$	$G_N = 3650$ FOR AV. AREA PER KLYSTRON OF 8.7 m^2
N = .5 COHERENCY FACTOR AREA = $(7\lambda)^2$	
NOISE SPECTRAL DENSITY = $P_N G_N / 4\pi R_o^2$	
P' = 7×10^{-21} WATTS/m^2/Hz = -201.5 dbw/m^2/Hz	P' = 1.54×10^{-19} WATTS/m^2/Mf = -187.4 dbw/m^2/Hz
EXTERNAL FILTER CAN PROVIDE ADDITIONAL ATTENUATION	MULTIPLE CAVITY DESIGN PROVIDES 24db/OCTAVE ATTENUATION

1.1.2.3.5 References

1. Raab, F. H., IEEE Circuits and Systems, V. 7, No. 10, pp. 3-11 (Dec. 1975)

2. Oxner, E., Electronic Design News, Oct. 20, 1978, p. 119

3. Sokal, N. O. and Sokal, A. D., "High Efficiency Tuned Switching Power Amplifier," U.S. Patent 3,919,656 (Nov. 11, 1975)

4. Sokal, N. O. and Sokal, A. D., IEEE J. Solid State Circuits, SC-10, No. 3, pp. 168-176 (June 1975)

5. Sokal, N. O. and Raab, F. H., IEEE J. Solid State Circuits SC-12, No. 1, pp. 86-88, (Feb. 1977)

6. Sokal, N. O., Electronic Design, V. 20, Sept. 27, 1977, pp. 96-102.

7. Fukuta et al., IEEE ED-25, No.6 p.559-563, (June 1978)

8. D'Asaro et al., IEEE ED-25, No. 10, p. 1218, (Oct. 1978)

9. Kendrick, J. B., Editor, TRW Space Data, TRW Systems Group, Redondo Beach, Ca., 1967, p. 86.

10. Nalos, E. J., Microwave Systems News, Dec. 1978

1.1.2.4.1 Klystron Module Thermal Control

Failure analyses performed as part of the critique also indicated a problem with the heat pipe cooled klystron. The difficulty was that the 500°C segments would utilize liquid metal heat pipes. In the event of a meteroid puncture or other leak, the liquid metal would be released into the high voltage environment of the transmitter system, and leading to arcing and damage. Possible permanent damage due to plating of liquid metals on insulators would require repair and/or replacement.

A Vought Corporation circulating fluid cooling option shows that a possible mass reduction exists with fluids that can be selected to minimize risk of arcing. Vought's analysis indicates that a circulating fluid system can be made as reliable as the heat pipe system and certainly more reliable than the expected lifetime of the klystrons

themselves. Table 1.1.2-12 shows principal features of the circulating fluid system for the klystron cooling circuit and Figures 1.1.2-28, 1.1.2-29 and 1.1.2-30 illustrate the Vought thermal control concept.

1.1.2.4.2 Antenna Waveguide Material

Using waveguides made of plated composites is probably a high risk approach based on today's knowledge because of potential breaks or delamination of the plating under thermal cycling or high RF power conditions. However, the cost advantages of a material with a low coefficient of thermal expansion are sufficient that development of a suitable approach for waveguides should be identified as a priority development item for SPS. Table 1.1.2-13 summarizes the current status of this topic.

Included in the analysis of aluminum structural options was analysis of use of aluminum for the waveguides in the transmitting antenna. Due to expected temperature changes, and aluminum's high coefficient of thermal expansion compared to the graphite used in the earlier baseline, the aluminum waveguides will significantly detune. This results in power losses as tabulated on Table 1.1.2-14.

Table 1.1.2-12 Klystron Module Thermal Control System Characteristics

VOUGHT CORPORATION

	500°C	300°C
MATERIAL	COPPER	COPPER
FLUID	AIR @ 60 ATM	DOWTHERM–A
INLET TEMP	477°C	277°C
OUTLET TEMP	413°C	260°C
LENGTH X WIDTH	0.57m x 1.61m	1.04m x 1.61m
TUBE SPACING	3.7 cm	2.84 cm
TUBE DIAMETER	5.6 mm	1.27 mm
TUBE THICKNESS	0.886 mm	0.71 mm
FIN THICKNESS	0.163 mm	0.066 mm
EMISSIVITY	0.8	0.8
ABSORTIVITY	0.3	0.3
TSINK	36.3°C	36.6°C
PUMP EFFY	0.3	0.3
FIN EFFECTIVENESS	0.894	0.920
AREA	0.91 m^2	1.67 m^2
MASS/MODULE	7.95 kg	5.13 kg
CURRENT MASS/MODULE – 13.18 kg PART III MASS/MODULE – 18.88 kg		

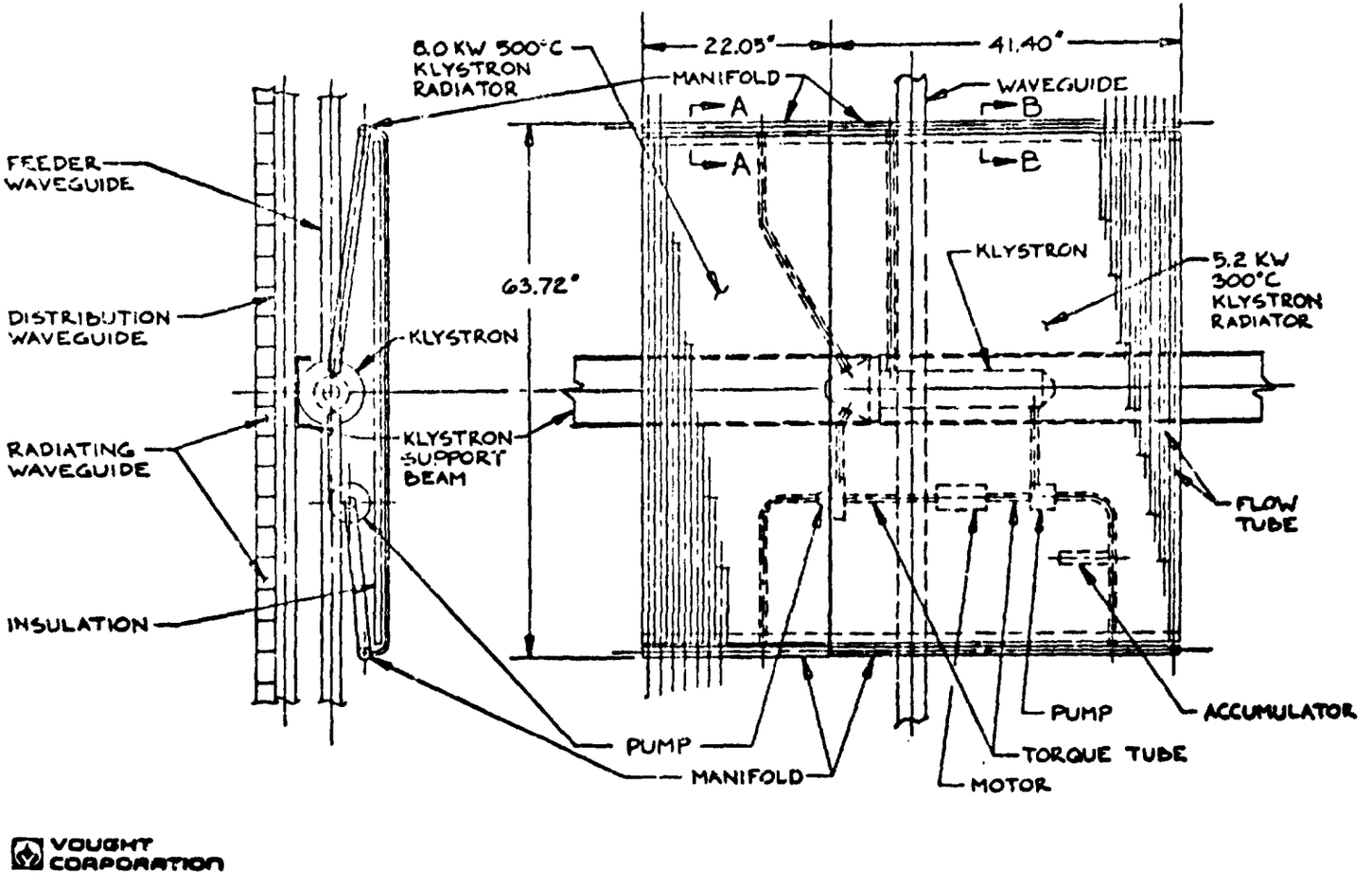

Figure 1.1.2-28 Klystron Pumped Fluid Thermal Control System

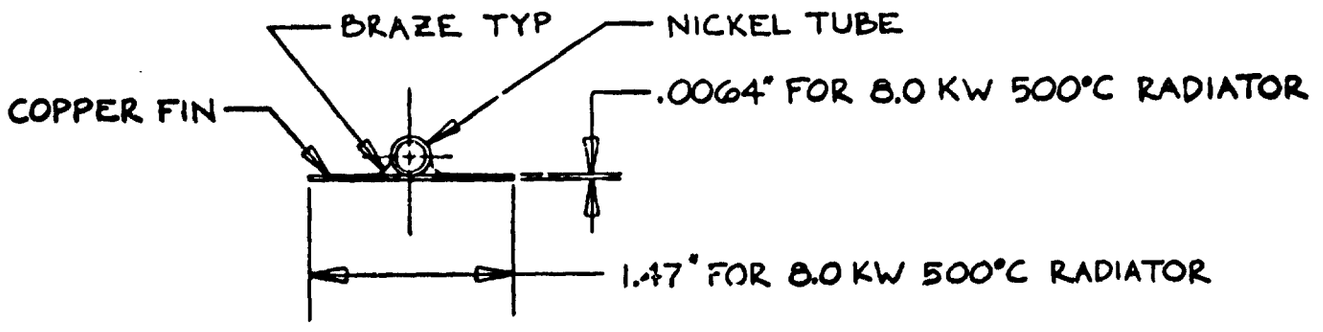

TYP RADIATOR FIN AND TUBE

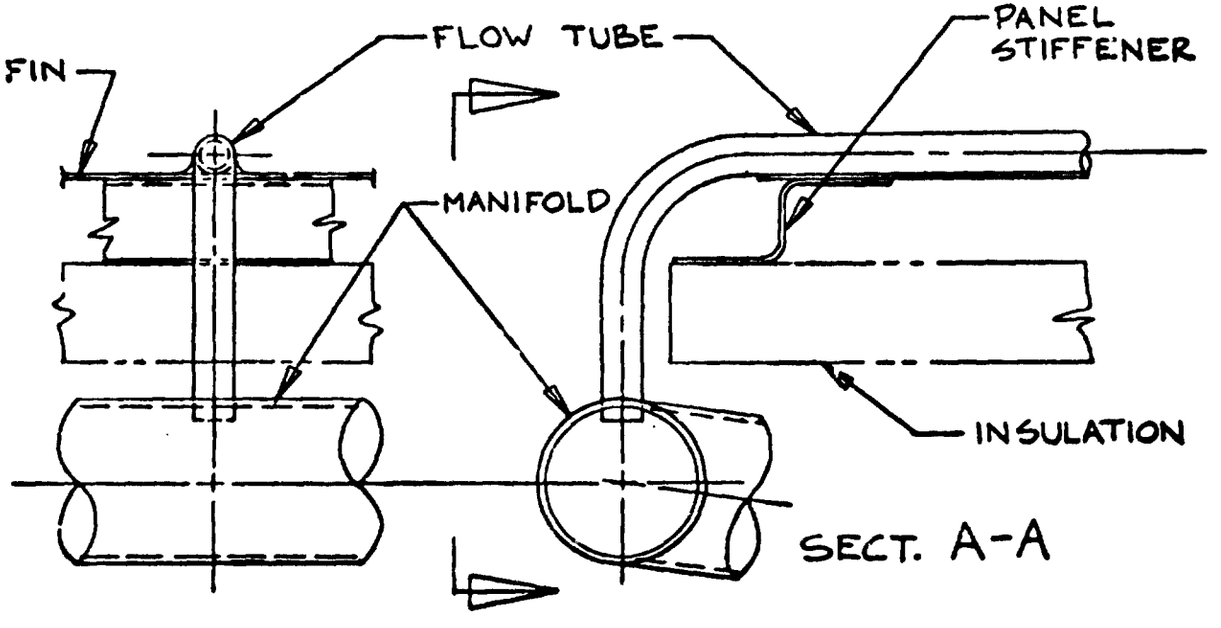

Figure 1.1.2-29 500°C Pumped Air Radiator Details

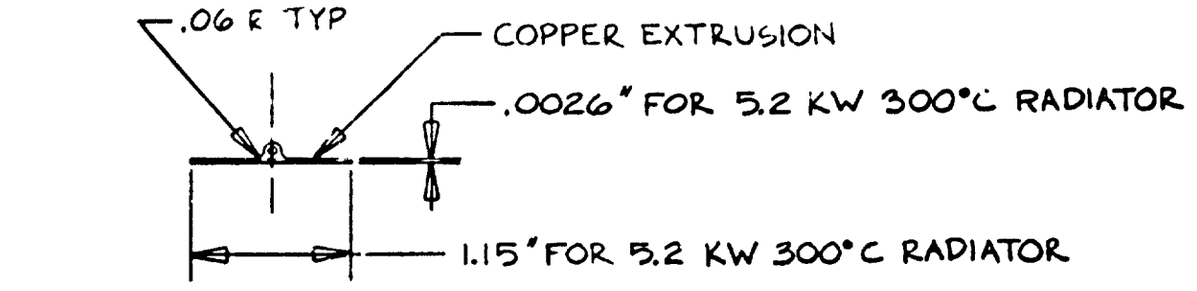

TYP RADIATOR FIN AND TUBE

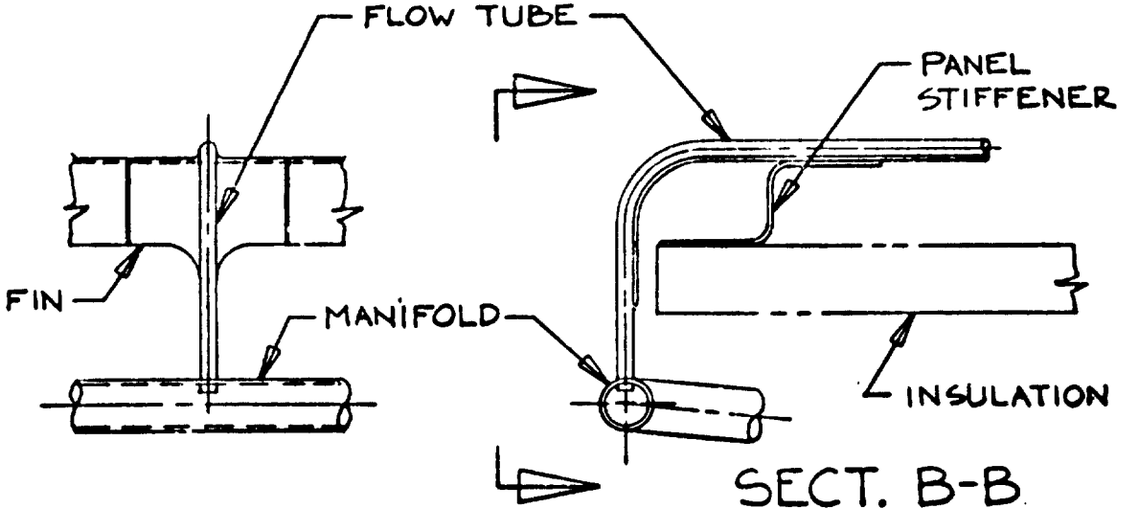

Figure 1.1.2-30 300°C Pumped Fluid Radiator Details

Table 1.1.2-13 Antenna Waveguide Material

- **Low CTE-plated composite detuning loss is 0.2% compared to 1.3% for aluminum.**
- **Cost of 1% efficiency loss is $75 million per 5-GW SPS.**
- **Plated composite as high-risk, based on today's knowledge.**
- **Recommend using low-CTE characteristics for waveguide performance and mass; flag development of suitable material as high-priority research item.**

Table 1.1.2-14 Comparison of Losses for Metal & Composite Waveguide

- AVERAGE STICK = 2.76 METERS
- $\Delta T = 55^{\circ}C$

	PERCENT POWER LOSS	
	ALUMINUM	COMPOSITE
STICK LENGTH	.67	.02
STICK WIDTH	.42	.12
CROSS GUIDE LENGTH	.17	.02
CROSS GUIDE WIDTH	.11	.03
	1.37%	.19%

1.1.2.5 Analysis of Antenna Structure Options

Summary of Options and Features

Early investigations of the SPS microwave power transmission systems antenna structure developed the tetrahedral truss primary and secondary structure concept. This system represents a maximum of structural efficiency for such an antenna. However, it constrains the subarrays to a non-square system and presented certain difficulties with respect to maintenance access. This configuration is compared to other options in Figure 1.1.2-31.

The center illustration in the figure represents the antenna structure as visualized by the maintenance engineer. It provides easy access to subarray repair or replacement and allows square subarrays but structurally is not very efficient and employs tension members. The use of tension members results in dubious dynamic qualities for the structure. Further, the secondary structure is required to provide stability of the primary structure. Analysis of this combination indicated a relatively poor stiffness efficiency.

The pentahedral truss shown at the left appears to offer a way out. It maintains good access with good efficiency, eliminates tension members and allows square subarrays. A potential interference problem has been identified with respect to the operation of the maintenance gantry and the existence of cross beam members for the primary pentahedral truss structure. This is better illustrated in the next figure 1.1.2-32.

The pentahedral structure is shown in more detail in Figure 1.1.2-32. Simplification of the secondary structure appears in order. The upper cross-braces in the primary structure create an interference with operation of the maintenance gantry. Further investigation during phase 2 of the study is expected to find a way to eliminate this interference.

STRUCTURAL ANALYSIS OF THE A-FRAME MPTS ANTENNA

The purpose of this study was to develop as much design information as time permitted to aid in evaluating the A-frame antenna's viability from a structural standpoint. Two types of results were developed:

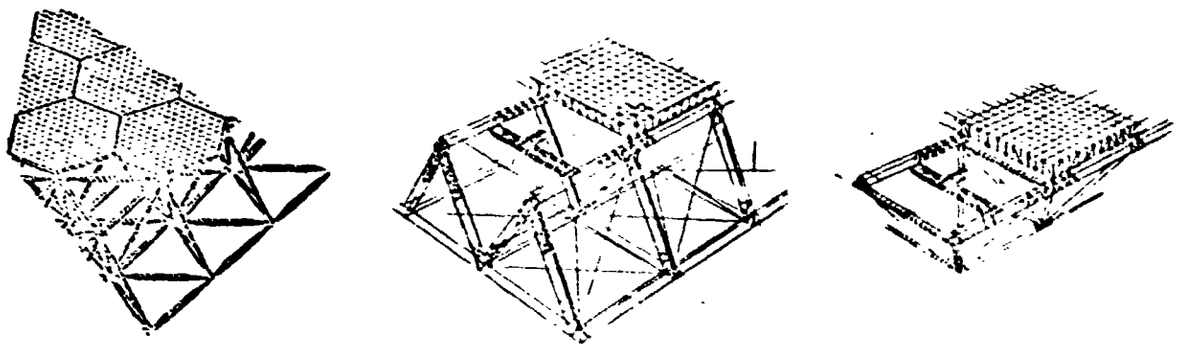

TETRAHEDRAL TRUSS

- MAXIMUM EFFICIENCY
- NO TENSION MEMBERS
- NON-SQUARE SUBARRAYS
- MAINTENANCE ACCESS DIFFICULT

A-FRAME

- GOOD ACCESS
- SQUARE SUBARRAYS
- POOR EFFICIENCY
- USES TENSION MEMBERS
- SECONDARY STRUCTURE IS PART OF PRIMARY STRUCTURE

PENTAHEDRAL TRUSS

- GOOD ACCESS
- GOOD EFFICIENCY
- NO TENSION MEMBERS
- SQUARE SUBARRAYS

Figure 1.1.2-31 Antenna Structure Options

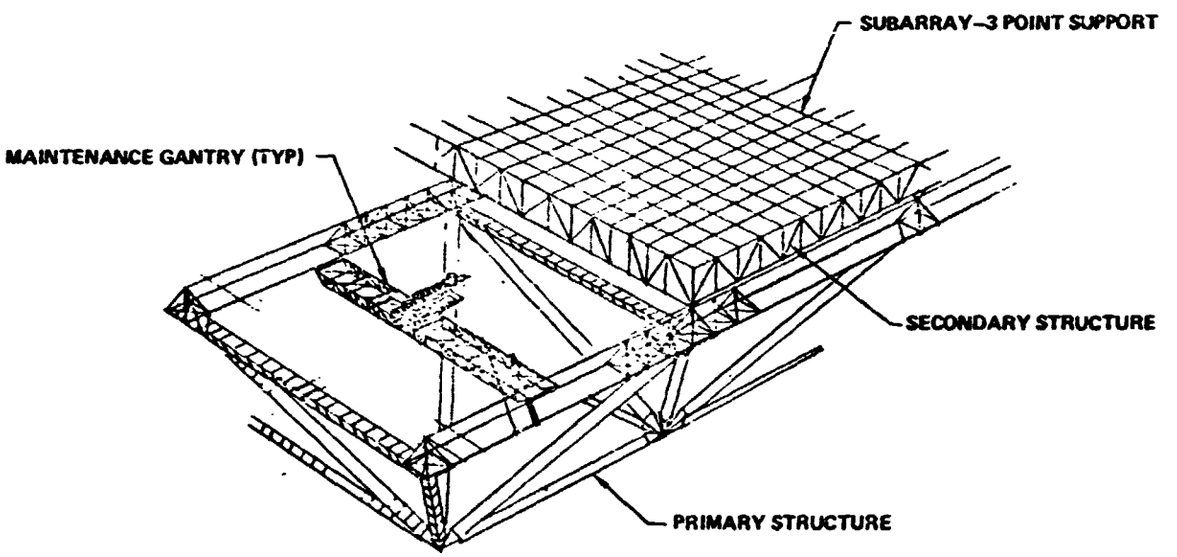

CROSSBEAMS ON FACE OF PENTAHEDRAL STRUCTURE ELIMINATE USE OF SECONDARY STRUCTURE AS PRIMARY LOAD PATH.

Figure 1.1.2-32 Pentahedral MPTS Structure

1. The stiffness characteristics of the structure, in terms of its natural vibration modes and frequencies, were determined by means of a NASTRAN finite element model.

2. An estimate of thermal deformations and associated deviations from flatness for an aluminum structure was made, also via NASTRAN.

RESULTS

1. Secondary Structure Model

The first step in the study was to ascertain the vibratory characteristics of the secondary structure, which consists of a series of truss modules as sketched below in Figure 1.1.2-33. Its relation to the primary structure is shown in Figure 1.1.2-34.

To size the plate a pin-jointed NASTRAN model of the truss was analyzed first. Members were made of Gr/Ep and were sized assuming an annular cross-section with a wall thickness of 0.030 in and an outside diameter chosen to give an r/t 200. The sizes appear in Table 1.1.2-15.

The above sizes correspond to a total antenna secondary structure mass of 565 MT, which is 2.9 times the mass given in (1).

Mode shapes and frequencies for the truss simply supported at its four corners are shown in Figures 1.1.2-35 through 1.1.2-39. The frequency range, 0.39 Hz to 1.24 Hz, is well above that the full antenna fundamental. Hence adverse resonant coupling is not a concern.

In constructing the overall antenna model each truss was replaced by a single plate element having the same fundamental frequency as the truss. To determine plate thickness a quarter model with free-free boundary conditions was analyzed. The latter boundary conditions were chosen, since analytical expressions for natural frequencies of plates pinned at their corners are not readily available. Furthermore, in a model where mass is lumped at the four corners of the plate, pinning the corners would completely prevent any vibratory motion. A first estimate of plate thickness was made using a method described below.

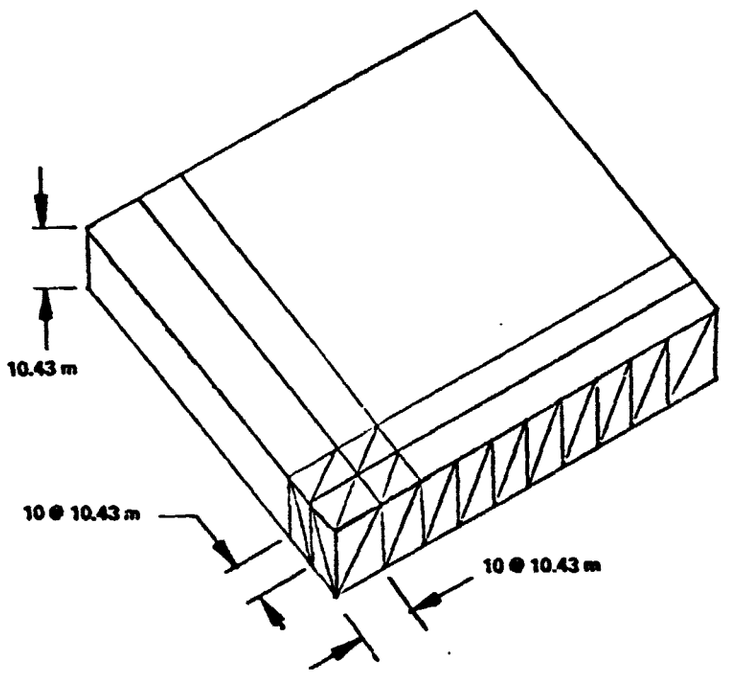

Figure 1.1.2-33 Secondary Structure Module Truss

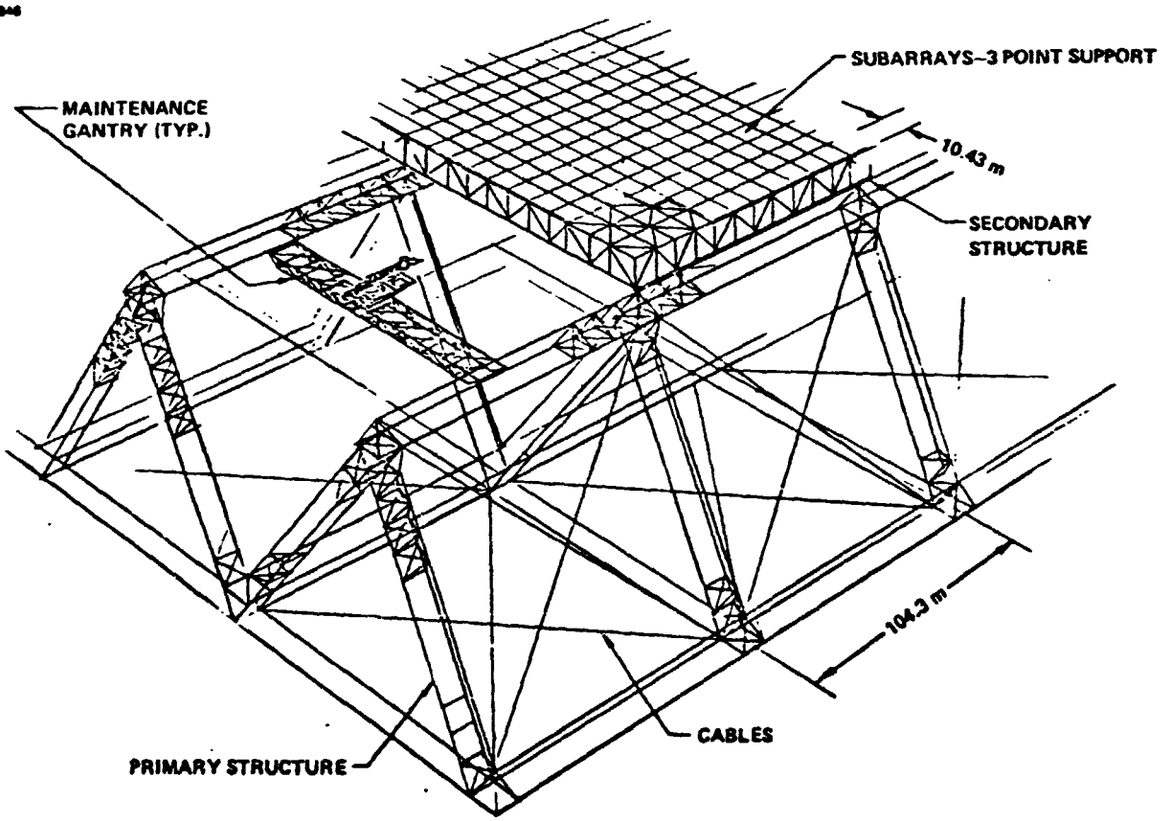

Figure 1.1.2-34 Reference MPTS Structure Interfaces

Table 1.1.2-15 Secondary Structure Member Sizes

	d_o, in	A, in^2	L/
Horizontals & Verticles	2.5	0.4684	234
Diagonals	3.5	0.6569	236

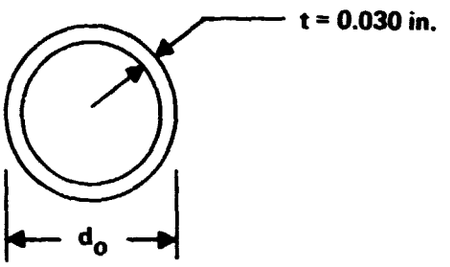

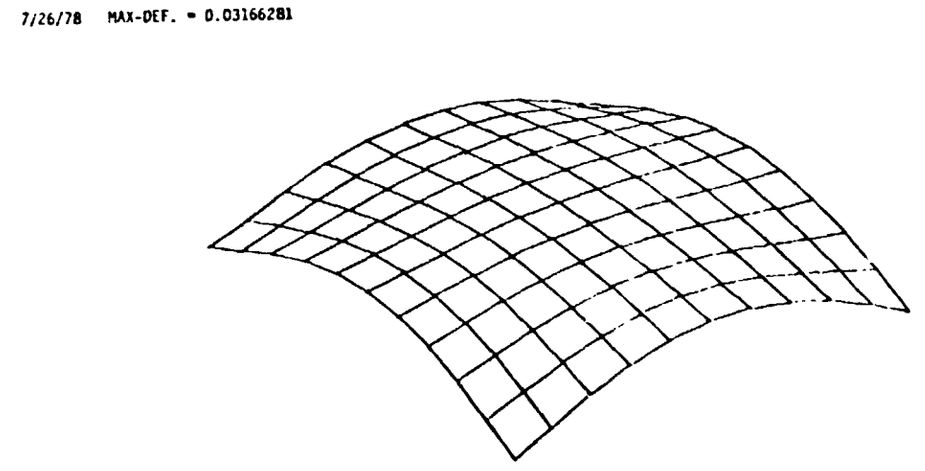

Figure 1.1.2-35 SPS Secondary Structure Module Mode Shapes, Mode 1

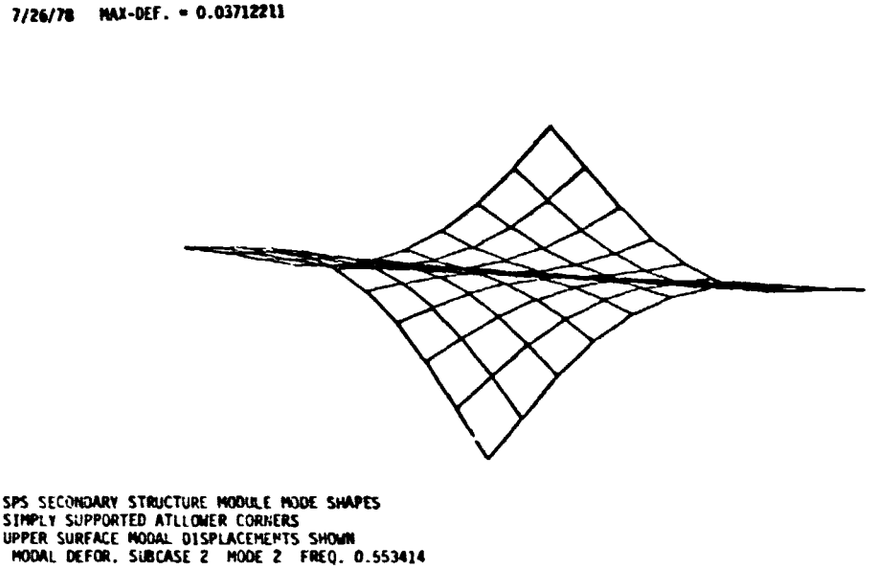

Figure 1.1.2-36 SPS Secondary Structure Module Mode Shapes, Mode 2

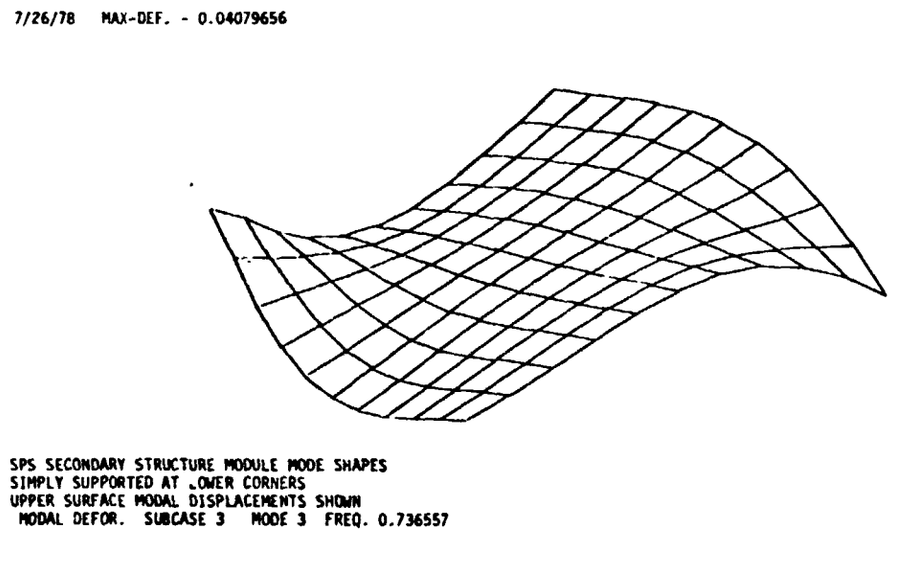

Figure 1.1.2-37 SPS Secondary Structure Module Mode Shapes, Mode 3

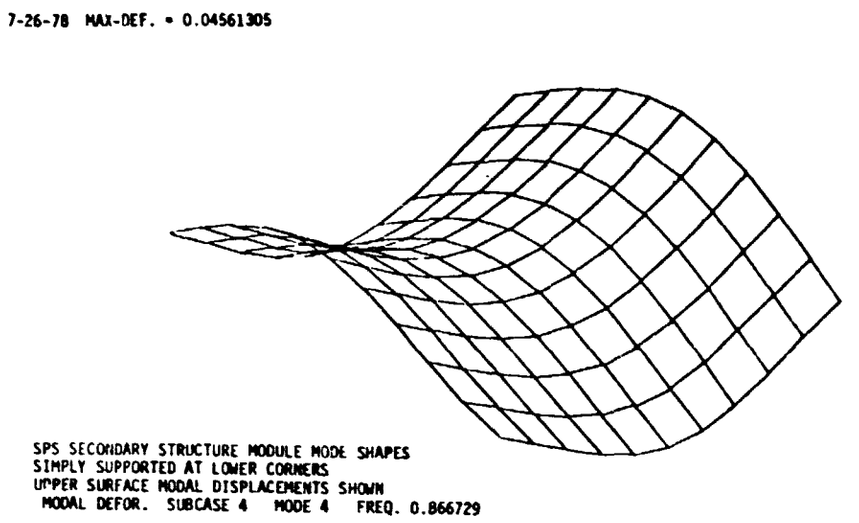

Figure 1.1.2-38 SPS Secondary Structure Module Mode Shapes, Mode 4

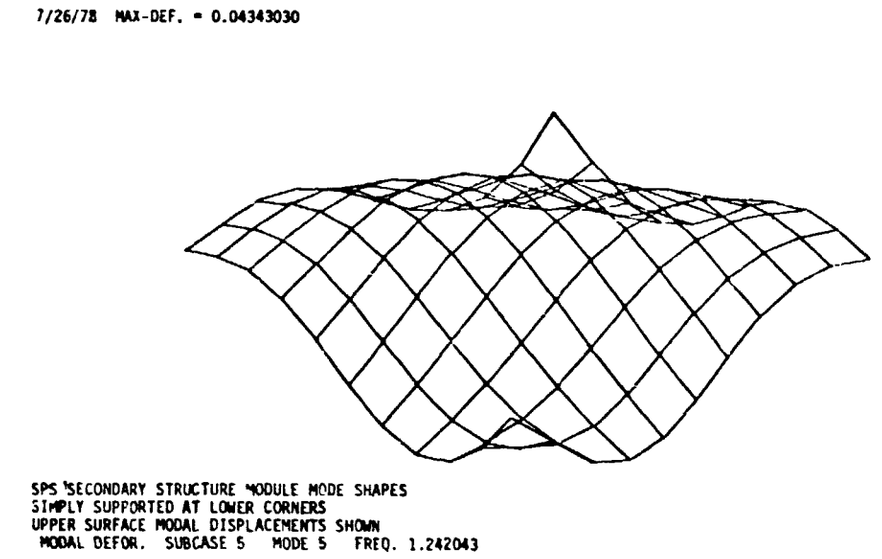

Figure 1.1.2-39 SPS Secondary Structure Module Mode Shapes, Mode 5

The plate frequencies were obtained by analyzing a NASTRAN model consisting of a single plate element. The non-structural mass corresponds to that of the heaviest modules located near the center of the antenna. Non-uniformity of the mass distribution over the surface of the module was considered to be a small effect and was neglected.

2. Antenna Model

One of the main structural features of the A-frame antenna is the utilization of the secondary structure as a primary load-carrying agent. Each module is independently fixed to the A-frame ridges of the primary structure. Thus there is no direct load path from one module to another. This reduces the overall in-plane stiffness of the antenna. Incorporating this feature in the finite element model was considered of prime importance. Figure 1.1.2-40 shows schematically the idealized attachment of a typical module to the primary structure. As an example, standoff beam 1-5 is fixed to the plate at node 1 and pinned to the primary structure at node 5. Torsional stiffness is also included. There is no direct connection between adjoining plates, as in the actual structure. Although the plates are shown slightly separated in Figure 1.1.2-40 for clarity, the corners of adjoining plates occupy the same point in space in the NASTRAN model. This contact exists in a geometric sense, but not in a structural sense.

Primary structural members were sized in a way similar to that described earlier for the secondary truss, using an $l/t = 200$. Table 1.1.2-16 summarizes this data.

The primary structure was pin-jointed. To reduce the order of the problem a half-model was used with the axis of symmetry lying perpendicular to the antenna's axis of rotation and passing through the center of the antenna. The structure was simply supported at the connection to the yoke as shown in Figure 1.1.2-41.

The antenna mass was distributed over the surface in accordance with the klystron layout shown in Figure 1.1.2-42. In the overall antenna model, structural mass, which represents about 6% of the total, was neglected.

The undeformed finite element model appears in Figure 1.1.2-43. Figures 1.1.2-44 through 1.1.2-48 show the first five vibration modes. Of these the first three are symmetric and the last two are anti-symmetric. In order to compare the baseline

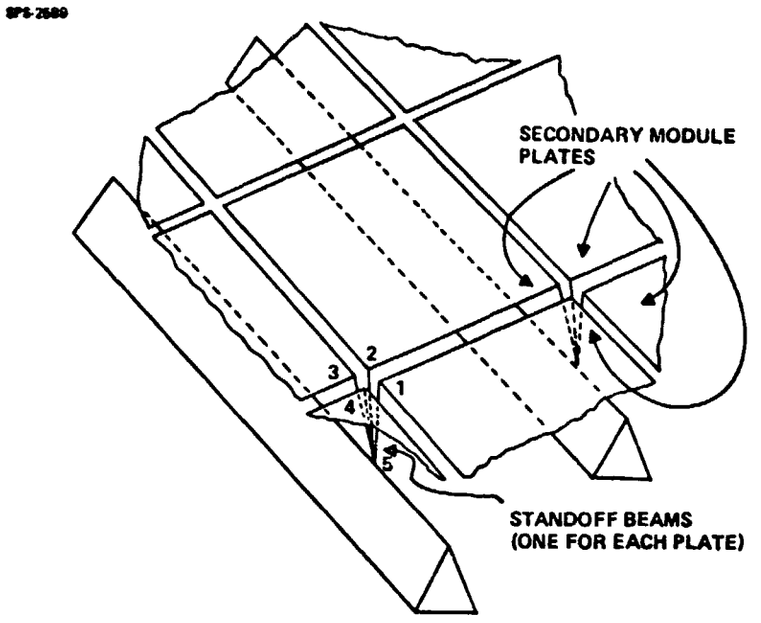

Figure 1.1.2-40 Attachment of Secondary Module to Primary Structure

Table 1.1.2-16. Primary Structural Member Sizes

	d_o, in	A, in^2	L/
All Members Except Diagonals	58.17	5.480	= 200
Diagonals	82.15	7.739	= 200

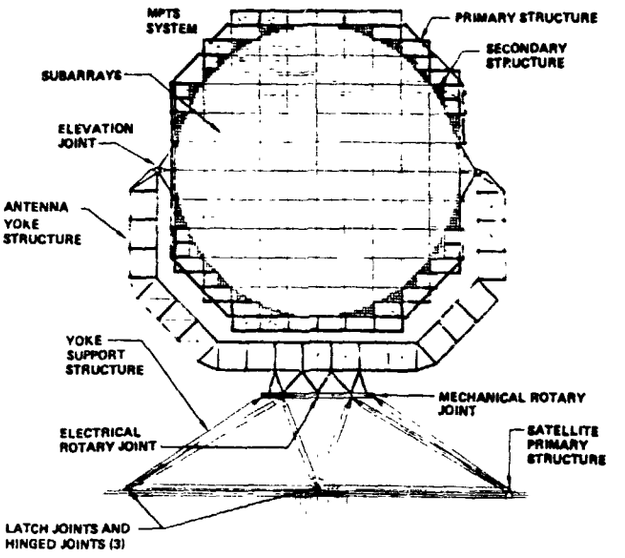

Figure 1.1.2-41 Reference MPTS Structural Approach

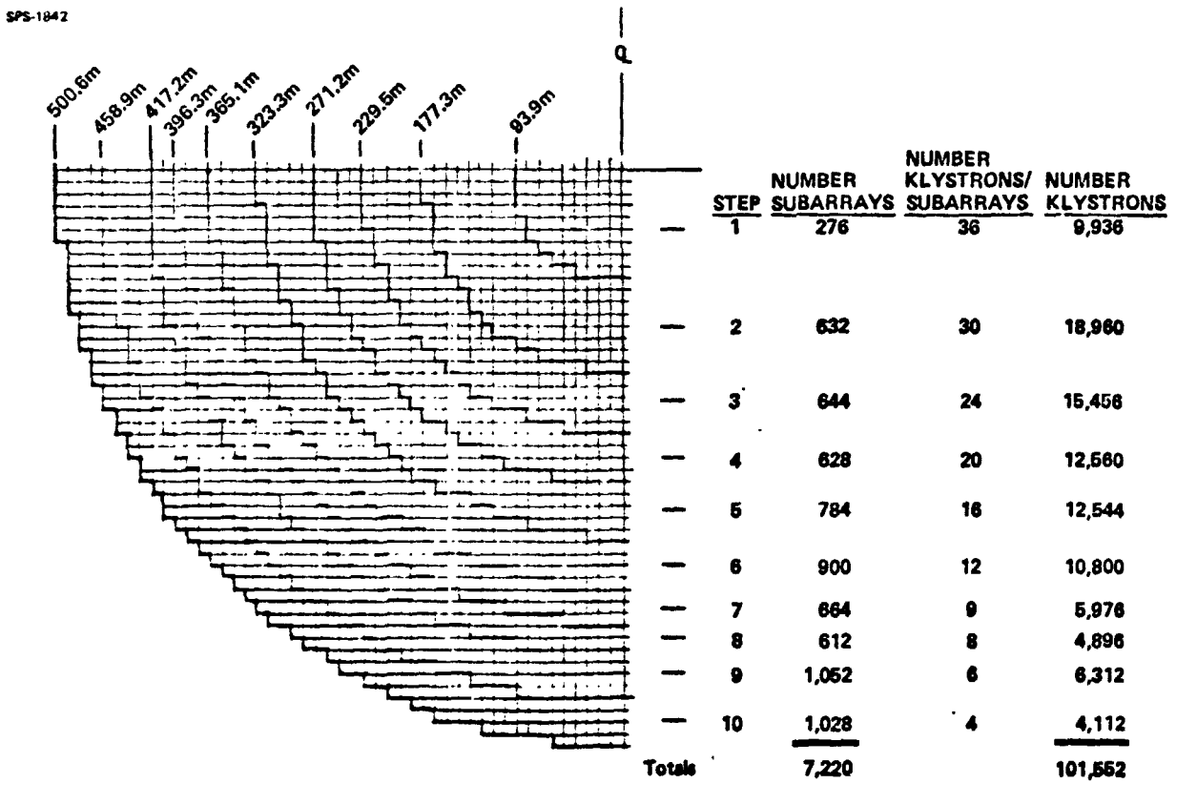

STEP	NUMBER SUBARRAYS	NUMBER KLYSTRONS/ SUBARRAYS	NUMBER KLYSTRONS
1	276	36	9,936
2	632	30	18,960
3	644	24	15,456
4	628	20	12,560
5	784	16	12,544
6	900	12	10,800
7	664	9	5,976
8	612	8	4,896
9	1,052	6	6,312
10	1,028	4	4,112
Totals	7,220		101,552

Figure 1.1.2-42 MPTS Reference Power Taper Integration

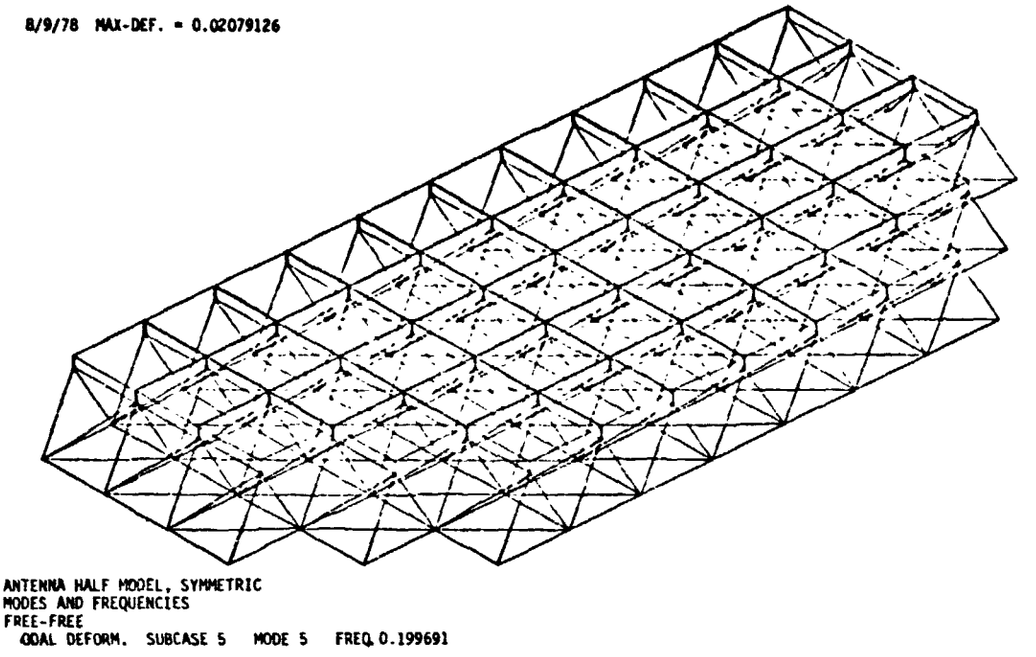

Figure 1.1.2-43 Antenna Half Model

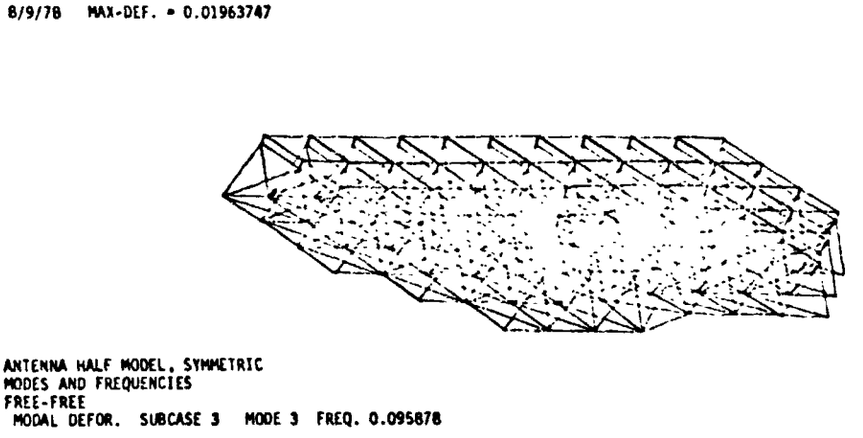

Figure 1.1.2-44 Antenna Half Model Displacements Mode 1

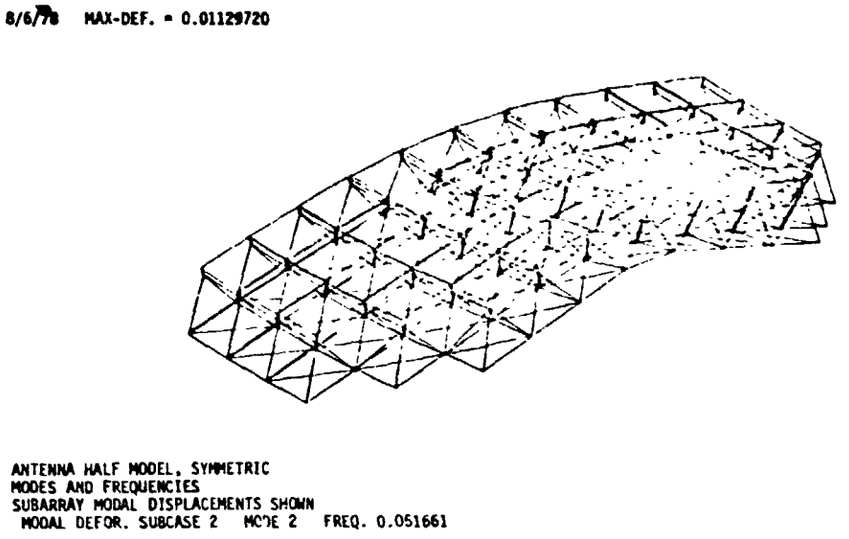

Figure 1.1.2-45 Antenna Half Model Displacements Mode 2

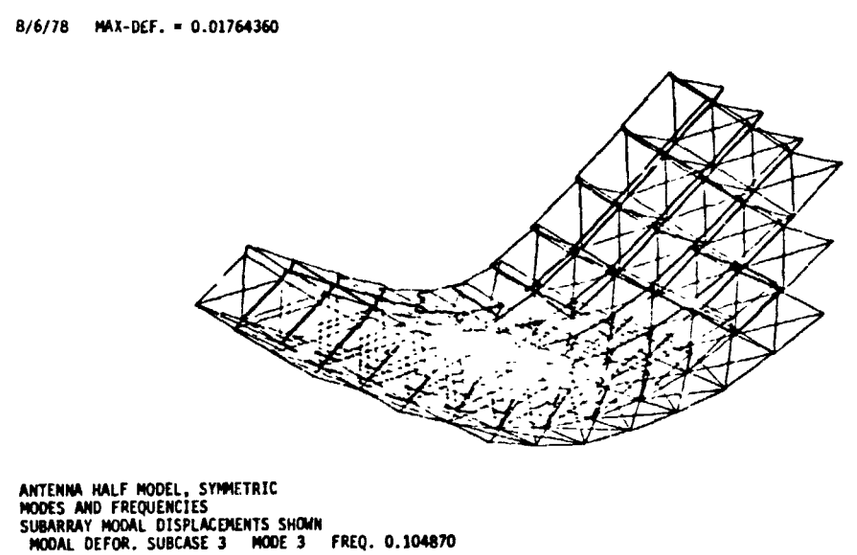

Figure 1.1.2-46 Antenna Half Model Displacements Mode 3

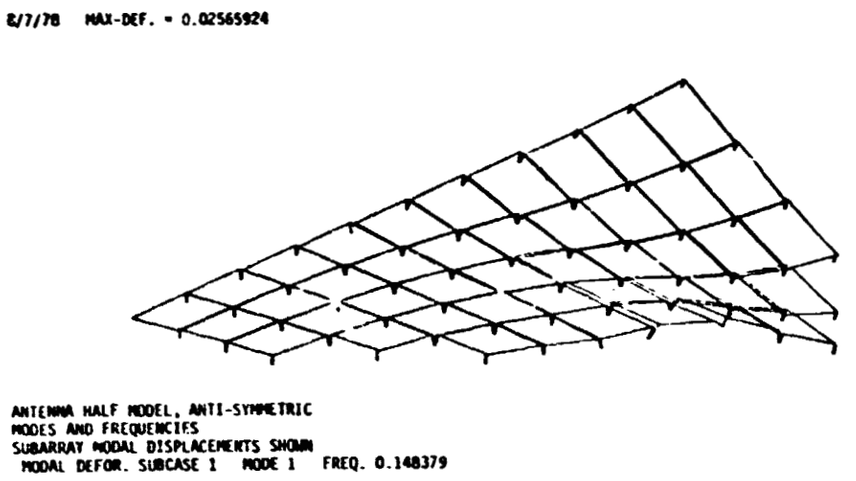

Figure 1.1.2-47 Antenna Half Model, Free-Free Mode 1

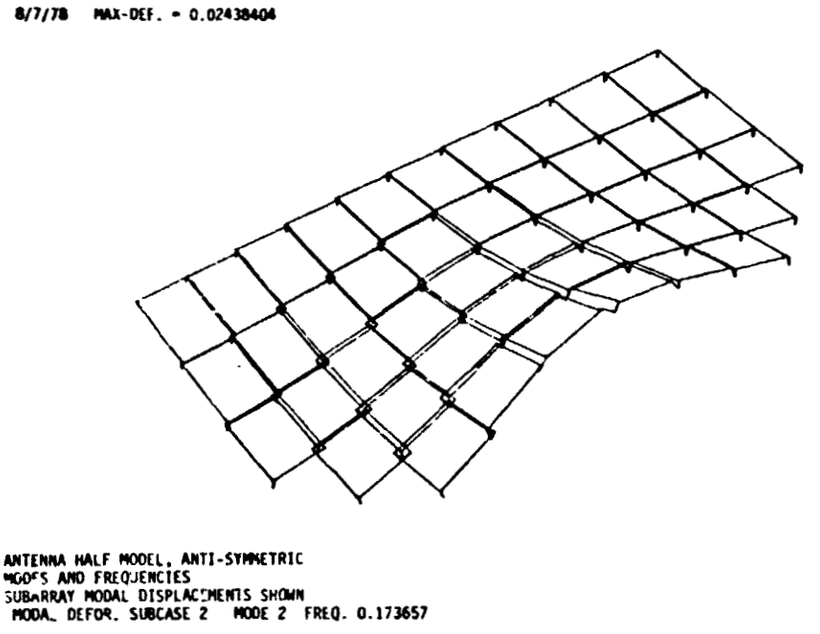

Figure 1.1.2-48 Antenna Half Model, Free-Free Mode 2

stiffness to that of the tetratruss as reported by General Dynamics in (3), the unconstrained modes and frequencies of the former were obtained. The first three symmetric free-free modes are shown in Figures 1.1.2-49 to 1.1.2-51. For comparison purposes the first four tetratruss modes are reproduced from (3), pg. 79 and appear in Figure 1.1.2-52.

The final result to be presented is an estimate of the thermal deformations resulting from the temperature distribution of Figure 1.1.2-53, reproduced from (3), acting on an aluminum antenna structure. The deformations are shown in Figure 1.1.2-54.

Two conclusions resulted from this analysis:

1. Thermal deformation of an aluminum antenna far exceed those allowable within the requirements for MPTS beam-forming performance. An aluminum antenna therefore would require active deformation control.

2. The A-frame structure is not very efficient because of the relative softness of the secondary structure in providing stability of the primary structure. A pentahedral truss antenna structure appears to provide a good design compromise between structural efficiency and maintenance access.

1.1.2.6 DC to DC Converter Analysis

The critique of the reference concept raised the issue of DC to DC converter life based on corona induced failures within transformers and inductors used in filters. The reference DC to DC converter concept was derived by selecting a converter chopping frequency of 20 kilohertz in order that the overall satellite mass was minimized. However, the reliability analysis was performed using failure rate data based on 400 hertz. Corona-induced failures within transformers are dependent upon the total number of AC cycles to which the transformer is subjected. The main-time-to-failure at 20 kilohertz is 50 times shorter than at 400 hertz.

As a result of the critique an analysis was accomplished to investigate the following three approaches to increasing the predicted life of the converter.

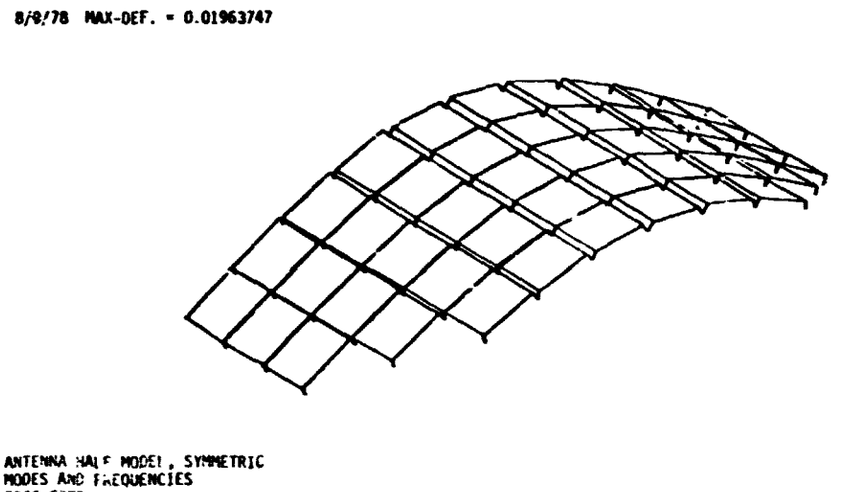

Figure 1.1.2-49 Antenna Half Model, Free-Free Mode 3

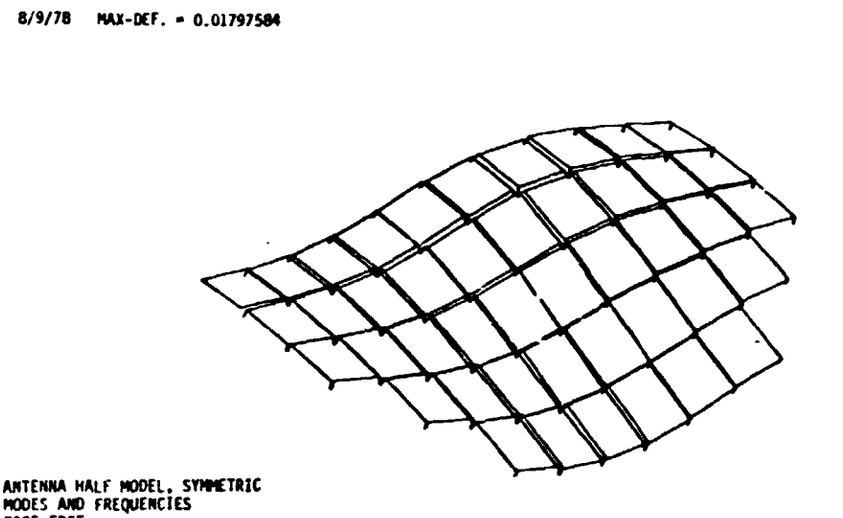

Figure 1.1.2-50 Antenna Half Model, Free-Free Mode 4

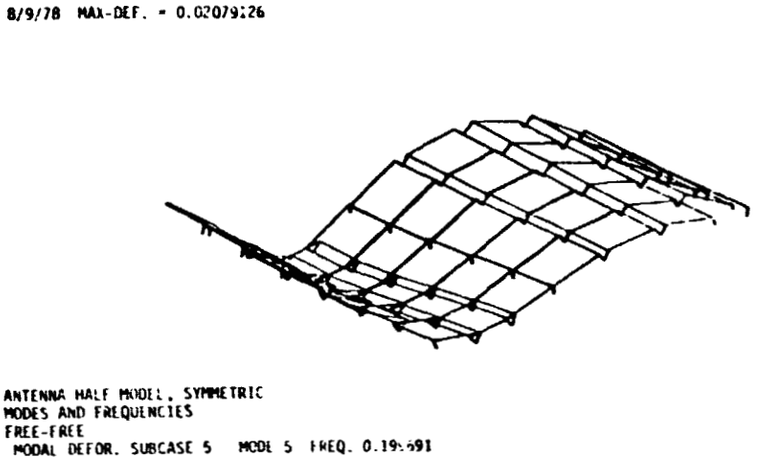

Figure 1.1.2-51 Antenna Half Model, Free-Free Mode 5

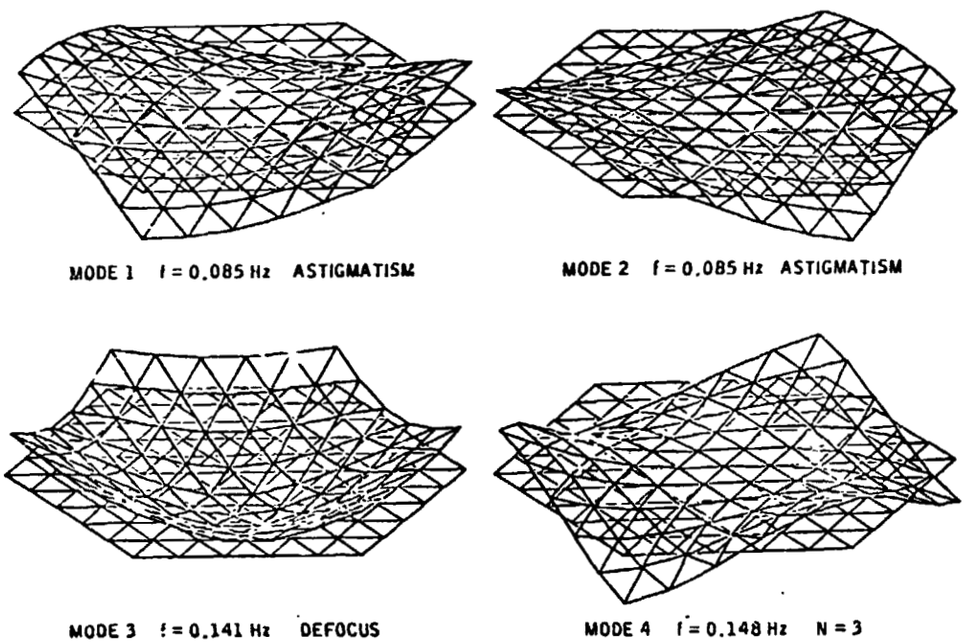

Figure 1.1.2-52 Preliminary Modal Analysis

- SUBARRAY RADIATOR SURFACE TEMPERATURE BOUNDARY CONDITIONS FOR SUPPORT STRUCTURE THERMAL ANALYSIS

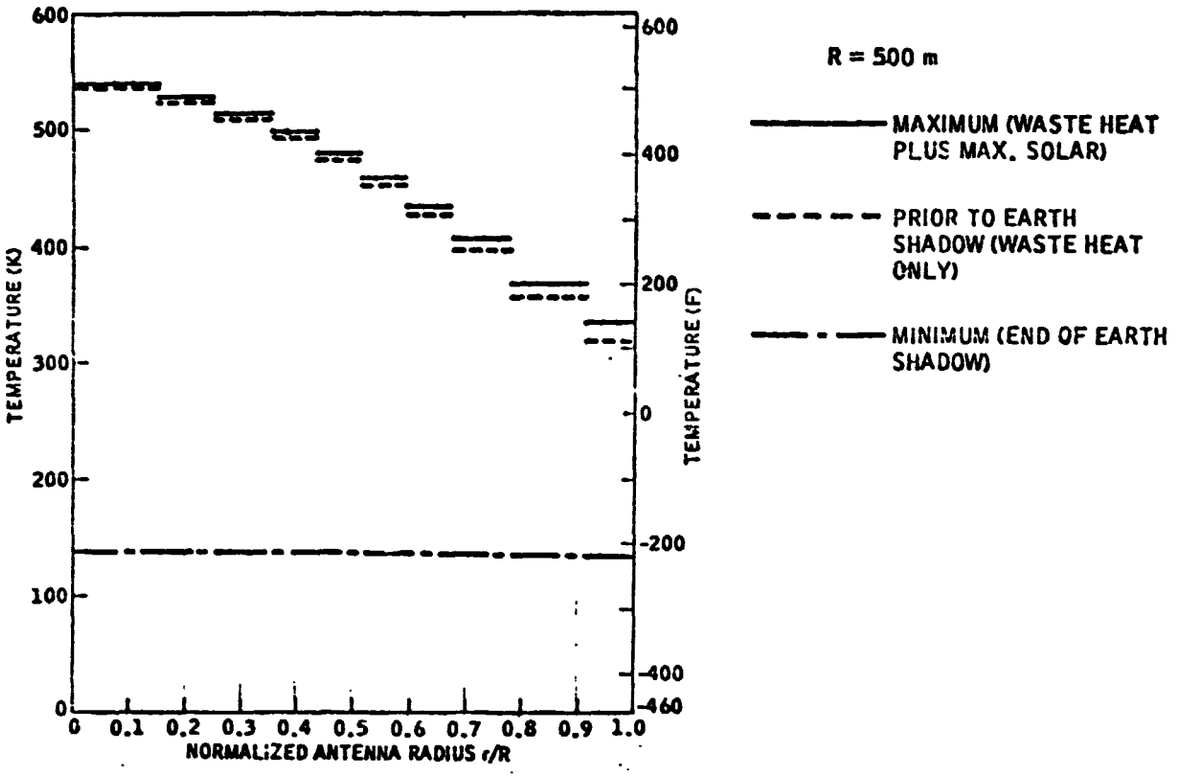

Figure 1.1.2-53 Antenna RF Thermal Loads

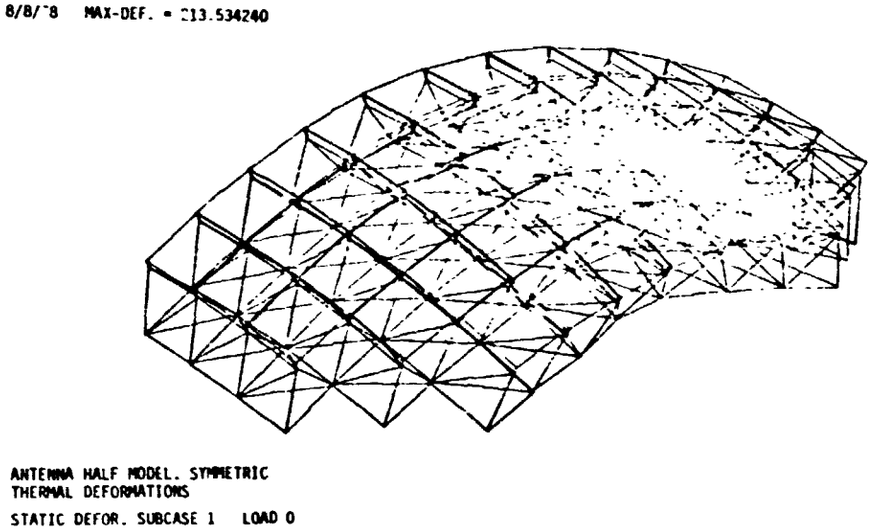

Figure 1.1.2-54 Antenna Half Model, Thermal Deformations

a) Reduce the converter system chopping frequency
b) Increase the transformer life by derating the dielectric material (i.e., operate at a lower voltage stress)
c) Redesign the transformer to increase its operating life.

Reducing the converter system chopping frequency incurs a significant mass penalty. The converter specific mass including thermal control at 1 kilohertz is approximately 2.9 kg/kw and is approximately 1.7 kg/kw at 20 kilohertz. Derating the dielectrics in the converter results in a converter specific mass (including thermal control) of 2.0 kg/kw.

An effort is underway by Thermal Technology Labs (funded by the USAF Aero Propulsion Laboratory) to develop lightweight transformers for airborne power supplies. A computer program has been developed, and a 50 KVA prototype fabricated to verify the computer optimized design, to enable the design of lightweight liquid cooled transformers. The computer optimization was used to develop a design for a 6,000 kw liquid cooled transformer.

The analysis was used to develop design parameters for the transformer as a function of frequency. The pertinent parameters for the transformer are shown in Table 1.1.2-17. In order to increase the overall converter lifetime dielectrics were derated for all filters in the converter. The losses for the revised converter are tabulated as a function of frequency in Table 1.1.2-18.

In order to select the chopping frequency for the long life processor, the curves shown in Figure 1.1.2-55 were developed for the baseline converter design, the baseline converter with derated dielectrics in all filters and a liquid cooled transformer as a replacement for the baseline transformer. It is apparent from the curves of Figure 1.1.2-55 that the minimum mass system occurs when the liquid cooled transformer is used (with derated dielectrics in all filters) at a chopping frequency in the 15 to 20 kilohertz range. This converter concept was selected to replace the baseline converter concept.

Table 1.1.2-17 Liquid Cooled Transformer

SPS-2505

POWER IN	5610 KW
POWER OUT	5540 KW
EFFICIENCY	98.73%
WEIGHT	170 KG
INTERNAL SIZE	$(14\ IN)^3$
OPERATING FREQUENCY	20 KHZ

Table 1.1.2-18 Itemized DC/DC Converter Losses--New Design

SPS-2479

CONVERTER SECTION	LOSSES IN KW AT CHOPPING FREQUENCY			
	1 KHZ	10 KHZ	20 KHZ	30 KHZ
INPUT FILTER	30	42	48	54
SWITCHING COND	12	12	12	12
SWITCHING SW	2.4	12	24	36
DRIVE AND SUPPRESSION	2.2	5.5	11	16.5
TRANSFORMER	70	70	70	70
RECTIFIERS	2.2	2.2	2.2	2.2
OUTPUT FILTERS	60	120	138	149.5
TOTAL LOSSES	178.8	263.7	305.2	340.2
EFFICIENCY (%)	96.8	95.3	94.7	94.1

● MASS = CONVERTER MASS + THERMAL CONTROL MASS + ARRAY MASS (REQUIRED TO MAKE UP FOR CONVERTER LOSSES)

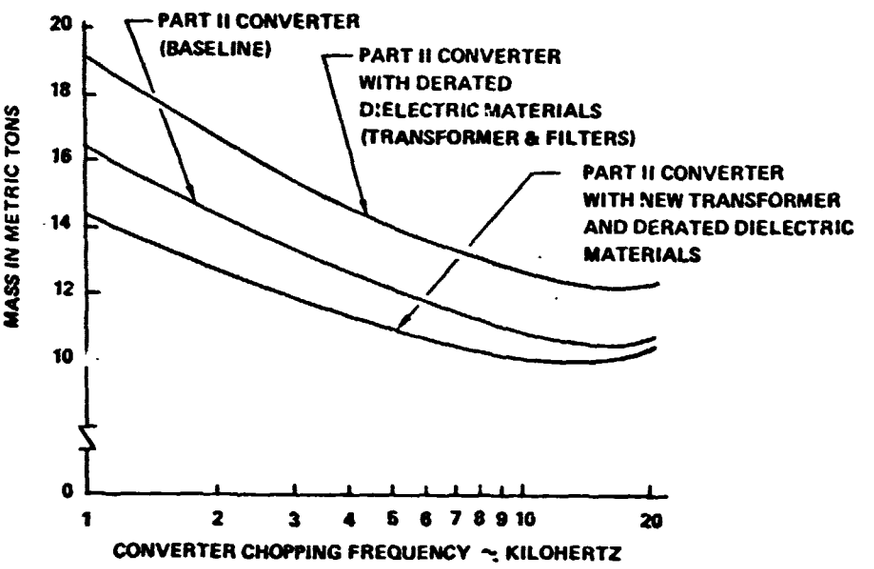

Figure 1.1.2-55 DC/DC Converter Switching Frequency Selection

PASSAGE OF LOWER SATELLITES THROUGH THE SPS POWER BEAM

Introduction

If one or more Solar Power Satellites are deployed in geosynchronous orbit (GEO), the possibility will arise of encounters with the (microwave) power beams by other satellites, in orbits below geosynchronous altitude. The power beams may usefully be visualized as spokes of a wheel, rotating with the Earth as hub and with GEO as the rim, although the beams will of course not be evenly spaced, being concentrated near longitudes where high power demand exists. The problem considered here is that of determining the frequency and duration of encounters with lower satellites, both in circular orbits and in low-thrust transfer from LEO to GEO.

Problems arising from the existence of SPS power beams may include the following:

i) Radiofrequency interference (RFI) with the operation of some lower satellites.

ii) Damage to sensors or other components of satellites, for which the owners of the SPS involved would presumably be liable.

iii) Design constraints and additional costs imposed on all satellites, to avoid damage or maintain operation in the event of encounters with power beams. These costs should clearly be borne by the SPS system, but

there are inherent difficulties both in levying independent, international SPS operators and in allocating compensation to owners of satellites.

iv) Brief outages in the power from a given SPS, due to intentional shutdown to avoid damage to a sensitive satellite or because of occultation of the beam by large vehicles (such as an SPS module in self-transfer from LEO to GEO).

v) Legal disputes arising from the fact that each SPS preempts, not only a location in GEO, but a large region of space (of order one million cubic kilometers), fixed relative to the Earth, for its power beam.

vi) Legal, administrative and perhaps security problems involved in the maintenance of an up-to-date ephemeris for all satellites which might be affected, so that encounters may be predicted, and in coordination between multinational governmental and private operators of power and other satellites.

Fortunately, as will be shown, these problems are not as serious as they may at first seem, because these encounters are generally rare and brief, even when a large number of power satellites are in operation.

Orbital Geometry

It is clear that, if the inclinations of the orbits of both the SPS and a lower satellite are exactly zero, and if the SPS is feeding a rectenna which is exactly on the equator, then the satellite will encounter the power beam in every revolution. In the general case, in which the rectenna is at latitude L and the lower satellite is in an orbit of inclination i, the frequency of encounters is much less.

For present purposes, it is sufficient to assume that both the SPS and the rectenna are at longitude zero. The line defined by the power beam then intersects the polar axis of the Earth at a point A, as shown in Fig. 1.1.2-56, whose distance from the equatorial plane is

$$z_0 = r_s \tan \phi = r_s \sin L/(r_s - \cos L) \qquad [2.1]$$

where the unit of distance is the radius of the Earth, $r_s = 6.63$ is the radius of GEO, and ϕ is the angle which the power beam makes with the equatorial plane. As the SPS moves around its orbit each day, the beam thus generates a conical surface about the polar axis. The intersection of the inclined orbital plane with this surface is, of course, a conic section: an ellipse, parabola or hyperbola according to whether i is less than, equal to, or greater than ϕ. Since $\phi < 7.4°$ for $L < 50°$, the intersection will be a hyperbola except for essentially equatorial satellite orbits. The locus of the power beam in the lower satellite orbital plane starts at geosynchronous altitude when the SPS passes through the right ascension of the ascending node (assuming the orbit is posigrade); it sweeps down, during a period of six hours, to a minimum altitude (from Fig. 1.1.2-56

$$r_m = r_s \frac{\sin \phi}{\sin(\phi + i)} \qquad [2.2]$$

and then sweeps up again to meet GEO at the right ascension of the descending node. There is no intersection with the satellite orbital plane during the next 12 hours, until the SPS reaches the ascending node again.

Note that in the elliptic case ($i < \phi$), [2.2] implies $r_m > \frac{1}{2} r_s$. The elliptic locus is significant only for high, not quite equatorial orbits, and is not considered further here.

It is also noteworthy that the shape and orientation of the locus are fixed when the latitude of the rectenna and the inclination and orientation of the lower satellite orbital plane are given. The beams from several SPS's, feeding rectennas at the same latitude, will thus follow identical paths in a given orbital plane, the longitude of the rectenna and SPS fixing only the time of day when the beam intersection starts its sweep.

In a geocentric equatorial inertial coordinate system with the x-axis towards the ascending node and the z-axis along the north polar axis, the radius vector to a point in the line defined by the power beam, a distance b from the intersection with the polar axis, is

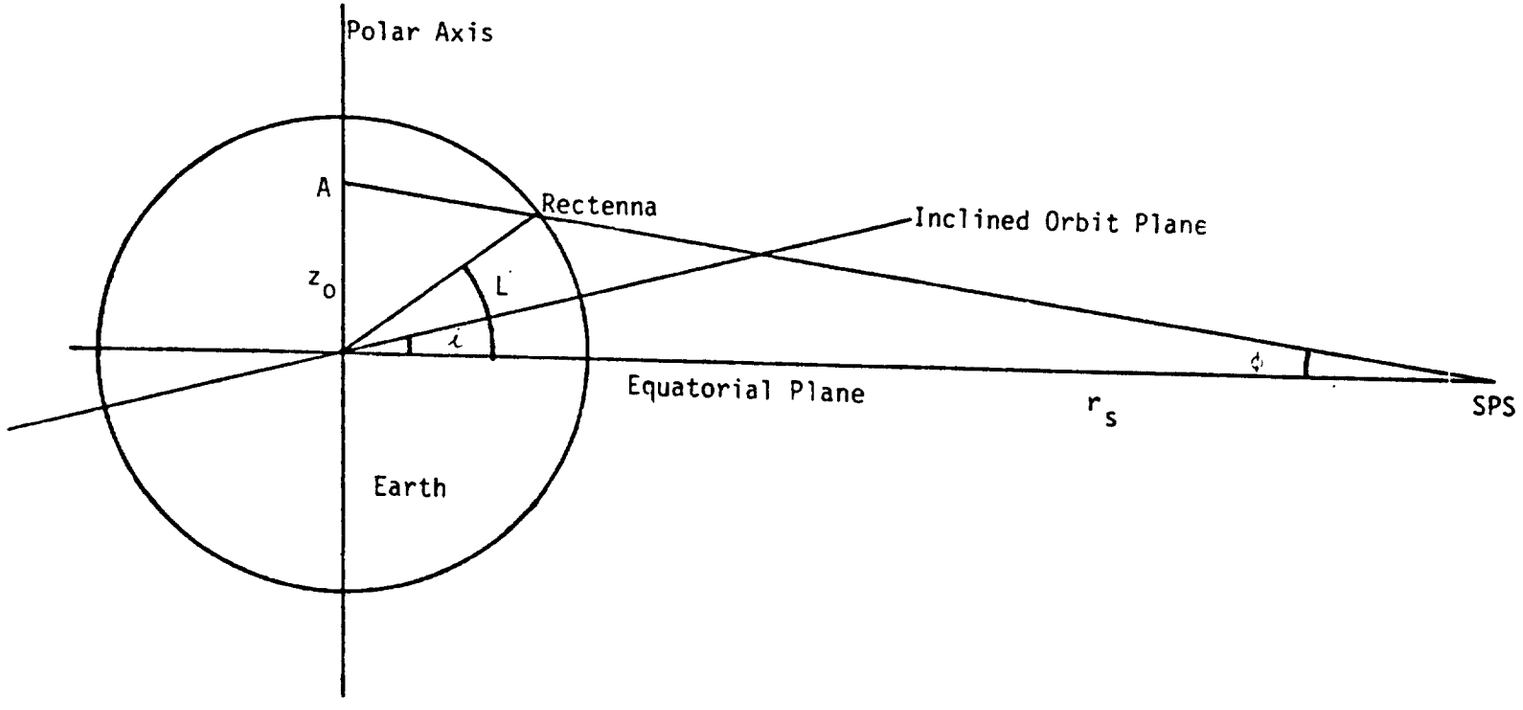

Figure 1.1.2-56: Orbital Geometry

$$\underline{\rho} = \begin{vmatrix} x \\ y \\ z \end{vmatrix} = \begin{vmatrix} - b \cos \phi \sin \Omega t \\ b \cos \phi \cos \Omega t \\ z_0 - b \sin \phi \end{vmatrix} \qquad [2.3]$$

and the unit vector up the power beam, towards the SPS, is

$$\underline{i}_\rho = \begin{vmatrix} - \cos \phi \sin \Omega t \\ \cos \phi \cos \Omega t \\ - \sin \phi \end{vmatrix} \qquad [2.4]$$

In these expressions, Ω = 72.7 microradians/second is the GEO angular velocity and time is measured from an instant when the locus of the beam in the inclined orbital plane is at its lowest altitude, given by [2.2].

The unit vector along the inclined orbit normal is

$$\underline{i}_{z'} = \begin{vmatrix} 0 \\ - \sin i \\ \cos i \end{vmatrix} \qquad [2.5]$$

Now transform [2.3] to a coordinate system with the same x-axis but with the z-axis along the inclined orbit normal. The transformation matrix is

$$\begin{vmatrix} 1 & 0 & 0 \\ 0 & \cos i & \sin i \\ 0 & - \sin i & \cos i \end{vmatrix}$$

so that the transformed vector is

$$\underline{\rho}' = \begin{vmatrix} x' \\ y' \\ z' \end{vmatrix} = \begin{vmatrix} - b \cos\phi \sin\Omega t \\ b \cos\phi \cos i \cos\Omega t + (z_0 - b \sin\phi)\sin i \\ - b \cos\phi \sin i \cos\Omega t + (z_0 - b \sin\phi)\cos i \end{vmatrix} \qquad [2.6]$$

The locus of the intersection of the beam with the inclined orbital plane is given by $z' = 0$, or

$$b^* = b/z_0 = \cos i/[\sin\phi \cos i + \cos\phi \sin i \cos\Omega t] \qquad [2.7]$$

so that, dropping the primes on the coordinates,

$$x = \frac{- r_s \cos i \sin\phi \sin\Omega t}{[\sin\phi \cos i + \cos\phi \sin i \cos\Omega t]} \qquad [2.8a]$$

$$y = \frac{r_s \sin\phi \cos\Omega t}{[\sin\phi \cos i + \cos\phi \sin i \cos\Omega t]} \qquad [2.8b]$$

where [2.1] has been used to eliminate z_0. The polar freedom equations of the hyperbolic locus are then readily obtained as

$$r = \frac{r_s \sin\phi [1 - \sin^2 i \sin^2\Omega t]^{1/2}}{[\sin\phi \cos i + \cos\phi \sin i \cos\Omega t]} \qquad [2.9a]$$

$$\tan\theta = - \cos i \tan\Omega t \qquad [2.9b]$$

The path followed in an orbital plane of inclination $i = 28.5°$ by the intersection with the power beam to a rectenna at latitude $L = +35°$ is shown in Fig. 2.2.

The time when the beam crosses an orbit of radius r may readily be found by solving [2.9a], which is quadratic in $\cos\Omega t$.

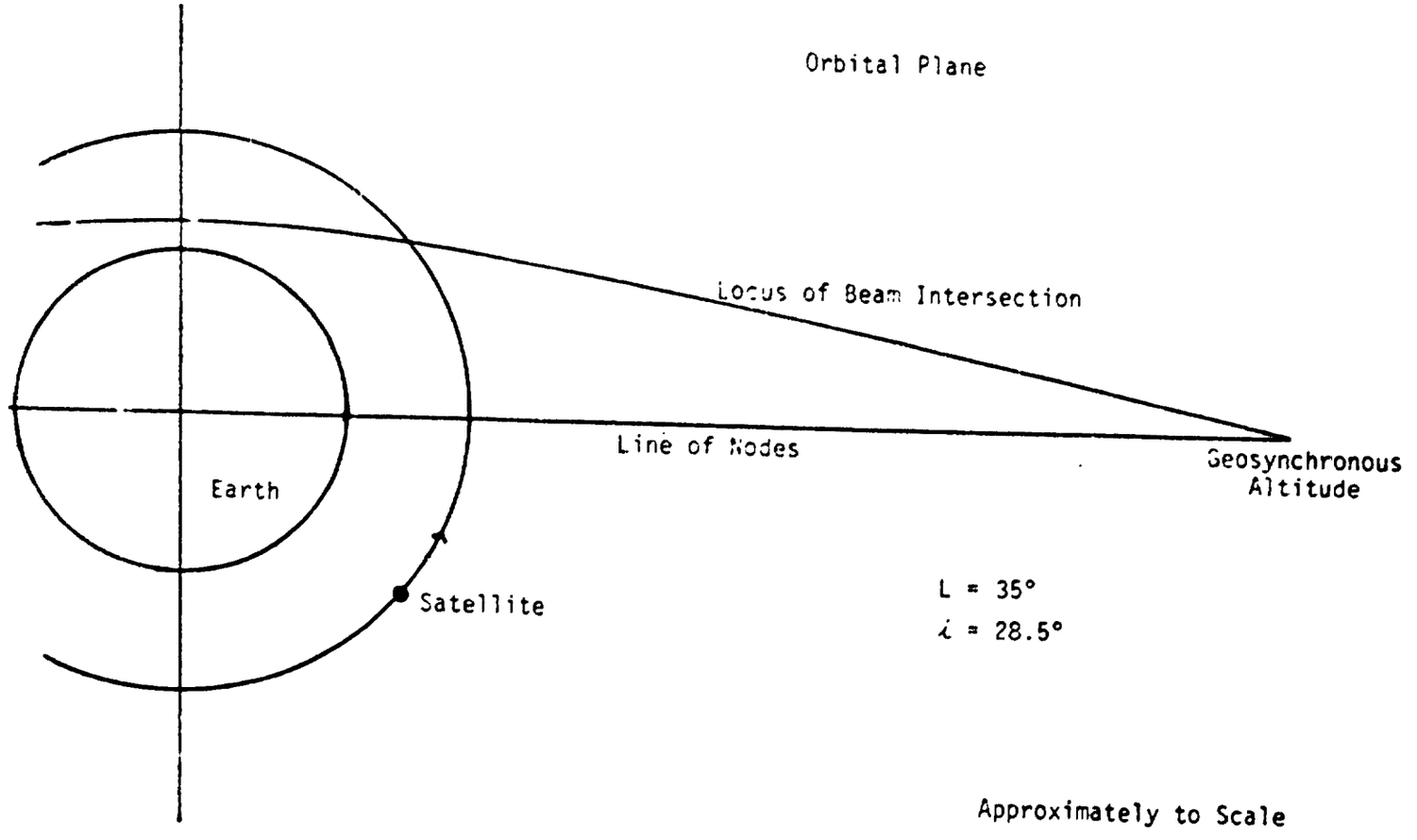

Figure 1.1.2-57 Locus of Beam Intersection with Orbital Plane of Lower Satellite

Duration of Beam/Satellite Encounters

In order to estimate the maximum time that a satellite in an orbit of radius r can spend in the power beam from a given SPS, it is sufficient to assume that the region of significant flux density expands linearly from the diameter D_s of the antenna at the SPS to the (east-west) diameter D_r of the rectenna at the surface of the Earth. At a distance d from the SPS, the effective diameter of the beam is then

$$D = D_s + \frac{d}{d_r}(D_r - D_s) \qquad [2.10]$$

where

$$d_r = \sin L / \sin \phi \qquad [2.11]$$

is the distance from the SPS to the rectenna (in Earth radii). Writing

$$d = \frac{r_s}{\cos \phi} - b \qquad [2.12]$$

and substituting from [2.7], the diameter of the beam, at the intersection with inclined orbit plane is found to be

$$D = D_s + \frac{(D_r - D_s) r_s \sin \phi \sin i \cos \Omega t}{\sin L \left[\sin \phi \cos i + \cos \phi \sin i \cos \Omega t\right]} \qquad [2.13]$$

The rate at which the beam intersection moves in the orbital plane is found by differentiation of [2.8] as

$$\dot{x} = -\Omega r_s \cos i \sin \phi \frac{\left[\sin \phi \cos i \cos \Omega t + \sin i \cos \phi\right]}{\left[\sin \phi \cos i + \sin i \cos \phi \cos \Omega t\right]^2} \qquad [2.14a]$$

$$\dot{y} = \frac{-\Omega r_s \sin^2 \phi \cos i \sin \Omega t}{\left[\sin \phi \cos i + \cos \phi \sin i \cos \Omega t\right]^2} \qquad [2.14b]$$

In order to use these expressions, [2.9a] is solved to give the time when the beam crosses the given satellite orbit. For an encounter to occur, the satellite must then be at the angular position given by [2.9b], and its components of velocity will be

$$\begin{aligned} v_x &= -v_c \cos\theta \\ v_y &= v_c \sin\theta \end{aligned} \qquad [2.15]$$

where v_c is the circular orbit velocity, related to the zero-altitude value $v_{co} = 7.91$ km/sec $= 1.24 \times 10^{-3}$ Earth radii/sec by

$$v_c = v_{co} r^{-1/2} \qquad [2.16]$$

The relative velocity of the satellite and beam intersection, in the orbital plane, is then

$$\Delta \underline{v} = \begin{vmatrix} \dot{x} - v_x \\ \dot{y} - v_y \\ 0 \end{vmatrix} \qquad [2.17]$$

The unit vector up the beam was given in [2.4], in equatorial coordinates. Transforming it to orbital-plane coordinates gives

$$\underline{i}_p = \begin{vmatrix} -\cos\phi \sin\Omega t \\ \cos i \cos\psi \cos\Omega t - \sin i \sin\psi \\ -\sin i \cos\psi \cos\Omega t - \cos i \sin\psi \end{vmatrix} \qquad [2.18]$$

The relative velocity vector of the satellite makes an angle α with the beam axis, given by

$$\cos\alpha = (\Delta \underline{v} \cdot \underline{i}_p)/\Delta v \qquad [2.19]$$

The distance through the beam, at this angle, is

$$D' = D/\sin\alpha \qquad [2.20]$$

and the duration of the encounter is

$$\tau_e = \frac{1}{\Delta v}\left(\frac{D}{\sin} + X\right) \qquad [2.21]$$

where X is the diameter of the satellite, measured in the direction of the relative velocity vector.

Fig. 1.1.2-58 shows the encounter duration as a function of the satellite orbit radius, for a small satellite and for a large one for which X = 5 km. As before, L =35° and i = 28.5° in this figure.

It is clear from the figure that, if a shutdown of the power beam is necessary to avoid a satellite encounter, or if the beam is occulted by a large satellite, the outage will be brief, not more than several seconds.

2.4 Frequency of Beam/Satellite Encounters

2.4.1 Satellites in Circular Orbits

The minimum radius in the orbital plane reached by the power beam intersection is given by [2.2]. It is easy to show that $r_m > 1$ if $L > i$. There are no encounters with the beam by satellites orbiting below this radius. The maximum safe orbital altitude (in km) is shown in Fig. 2.4 as a function of the orbit inclination, for several rectenna latitudes. The cross-hatched region shows the range of latitudes from 30° to 45°, where the majority of rectennas may be expected.

One strategy for reducing the frequency of beam encounters is to use a low-inclination orbit for satellites wherever feasible. Because of the steepness of the curves in Fig. 1.1.2-59, and because of the expected geographic distribution of rectennas, small reductions in inclination could produce significant effects. For example, a satellite in an orbit of inclination 28.5° and altitude 500 km will never encounter beams to rectennas at higher latitudes than about 31°; a plane change of 2°, to

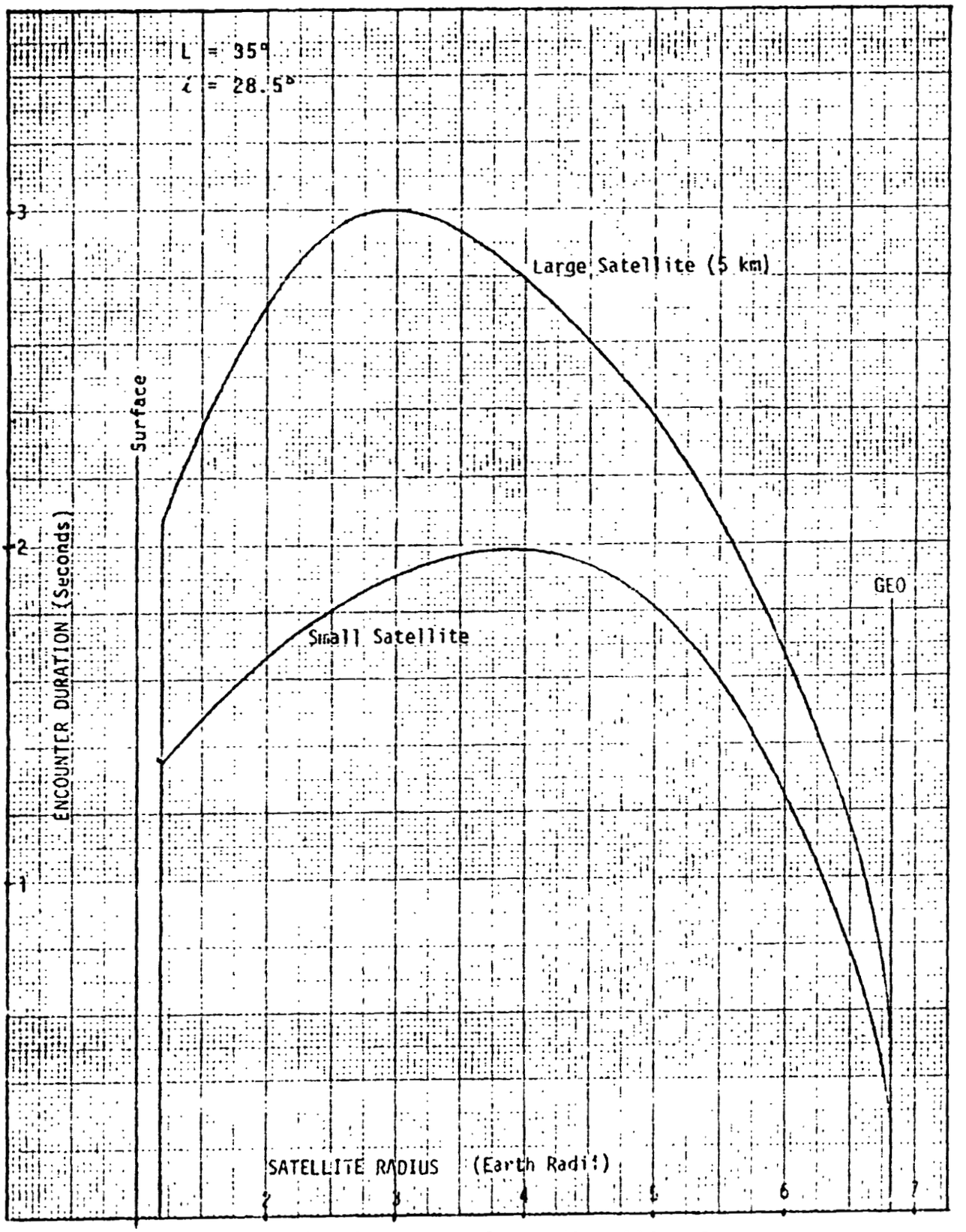

Figure 1.1.2-58: Duration of Beam/Satellite Encounters

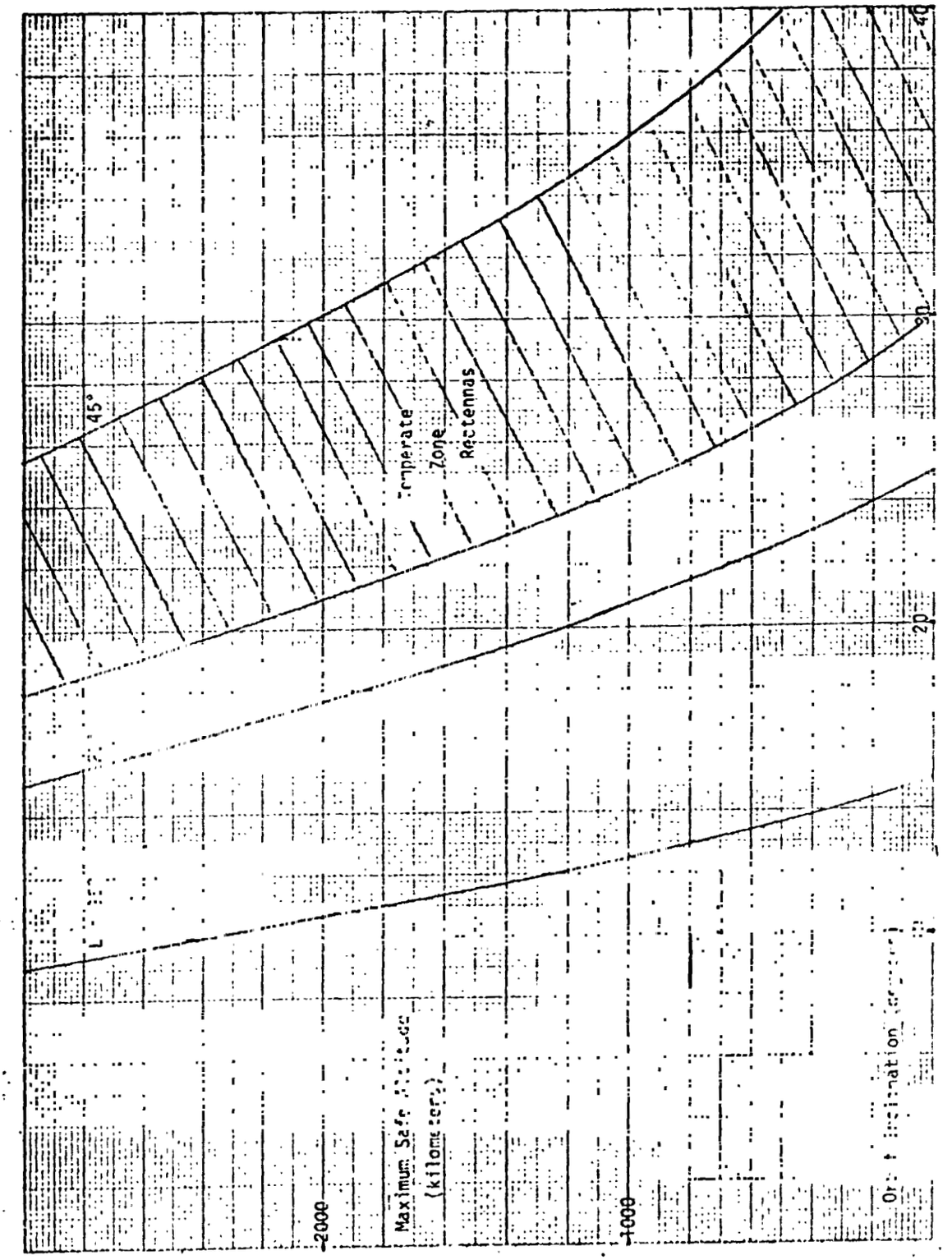

Figure 1.1.2-59: Altitudes Below Which There Are No Beam Encounters

26.5°, could eliminate encounters with beams feeding New Orleans, Houston, San Antonio and other major cities near 31° latitude.

In general, however, there will be satellites in orbits above the maximum safe altitude for a given rectenna. In such a case, an estimate of the probability of a beam encounter may be obtained by considering the width of the intersection between the beam and the orbital path. The unit vector tangent to a circular orbit at the beam intersection is

$$\underline{i}_t = \begin{vmatrix} -\cos\theta \\ \sin\theta \\ 0 \end{vmatrix} \qquad [2.22]$$

in orbital-plane coordinates. The angle which the tangent to the orbit makes with the beam axis is then given by

$$\cos\lambda = \underline{i}_t \cdot \underline{i}_p \qquad [2.23]$$

where $\underline{i}_p$ is given by [2.18]. The width of the intersection is then

$$D'' = D/\sin\lambda \qquad [2.24]$$

If the *a priori* probability of the satellite being anywhere in its orbit at a given instant is uniform (e.g., if there is no coordination between the satellite and SPS), then the encounter probability on a given day (i.e., during a single pass of the beam) will be simply

$$P_e = \frac{D''}{\pi r} \qquad [2.25]$$

where a factor of two has been included to account for the two beam-intersection regions in the orbit.*

This function is plotted in Fig. 1.1.2-60, for $i = 28.5^0$ and several

*Note that there are some special orbits for which encounters at the two intersections during a single beam pass are not mutually exclusive events.

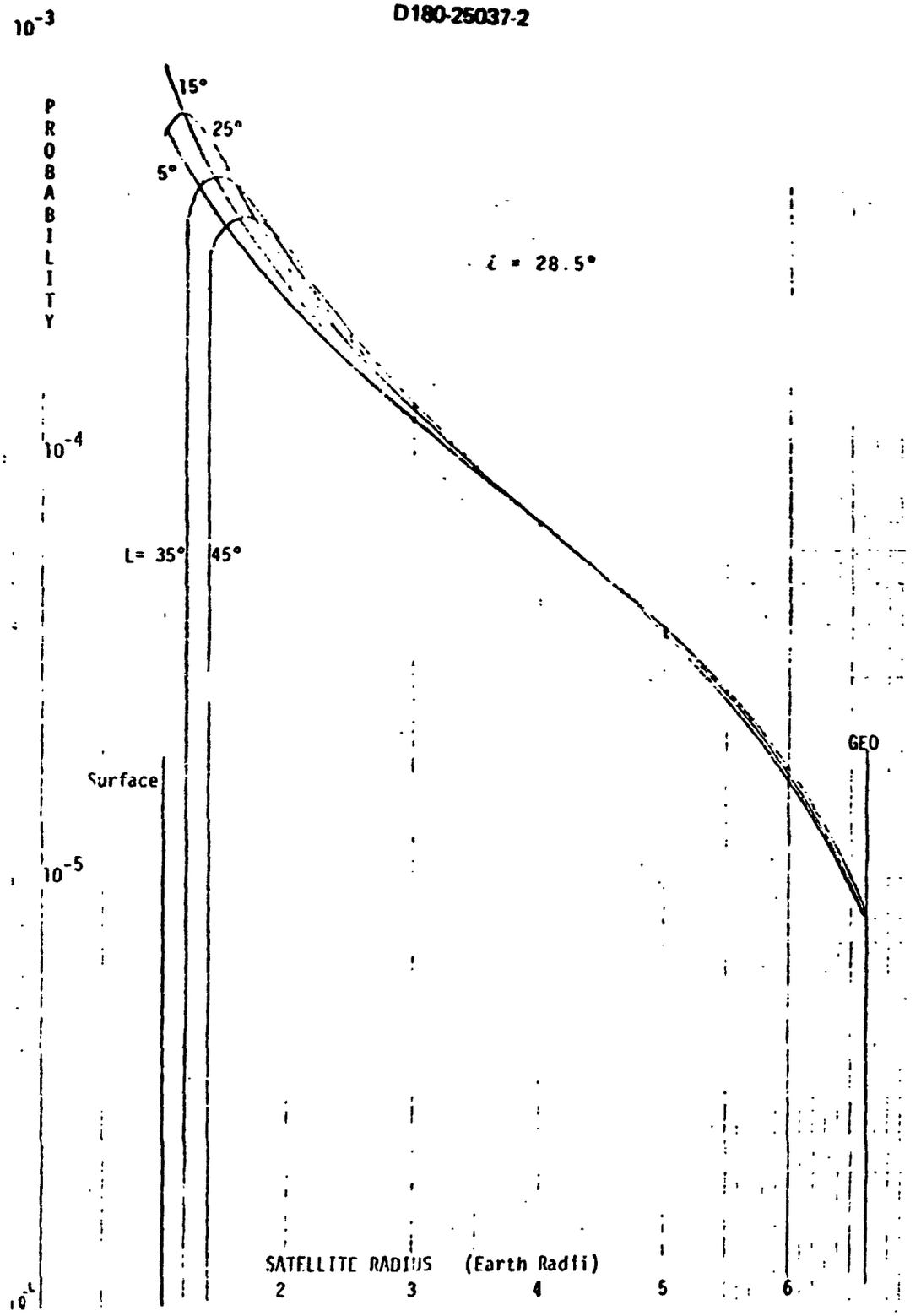

Figure 1.1.2-60: Probability of Beam Encounter

rectenna latitudes L. The maximum probability of encounters occurs for satellites at relatively low altitudes -- for example, a satellite launched at a random time into an orbit of altitude 2000 km has, during its first day of operation, about one chance in 2000 of encountering the beam to a given temperate-zone rectenna.

While this probability seems fairly low, encounters of course become much more likely if multiple satellites and/or multiple SPS's are considered. For example, if there are 20 satellites in randomly-phased low orbits (but above the maximum safe altitude), the beam from a newly commissioned SPS to a temperate zone rectenna has about 1% probability of encountering one of them during the first day. Conversely, if one hundred SPS's are in operation, a satellite at this altitude has about a 5% chance of an encounter during a given day.

It should be noted that, once a beam encounter has occurred, or once the orbital position of a satellite has been otherwise determined, prediction of future beam encounters is a deterministic problem (apart from stochastic orbit perturbations). In the ideal case, in which the satellite moves without perturbations in an inverse-square field, and there is no beam wander due to SPS station-keeping errors, the beam intersects the orbit at exactly the same time each day. If the satellite period is an exact sub-multiple of a day, encounters will occur every day, or not at all. More generally, encounters will repeat every n days (if at all) if the radius of the (circular) satellite orbit is

$$r = r_s(n/j)^{2/3} \qquad [2.26]$$

where j is any integer which is not a divisor of n. In order for the orbit to lie between the surface and GEO,

$$n < j < n\, r_s^{3/2} \qquad [2.27]$$

There are thus about 16n orbital radii, in a given orbital plane, for which the period between encounters with a given power beam will recur every n days. In each of these orbits, it is ideally possible to choose

the orbital phase so as to avoid all encounters with a given beam. In practice, because of periodic perturbations, the choice of n for encounter avoidance will be limited to fairly small values and there will therefore be a finite set of orbits with this property. If the satellite has no station-keeping ability, secular perturbations will eventually lead to a beam encounter in any of these orbits; the interesting question of how long encounter avoidance may be maintained, and of what happens thereafter, needs further study.

The problem is more complex when there are multiple beams to be avoided. For a given orbit, there will be a set of small, discrete beam-interaction regions (two for each rectenna), symmetrically distributed about the perpendicular to the line of nodes. The angular separation of each pair depends only on the latitude of the corresponding rectenna, and the times when the beams are in each interaction region depend on the longitudes of the rectennas. Even if mission considerations do not restrict the choice of orbital parameters, it is not in general possible to avoid all the interaction regions at all the appropriate times, but the frequency of encounters can presumably be minimized by choosing the best possible orbit. Moreover, it may be possible to develop guidelines for rectenna locations such that some special orbits are available, for use by particularly sensitive satellites, in which encounters are greatly reduced or eliminated.

A satellite equipped with thrusters can of course always maneuver so as to avoid beam encounters, but the thrust level and fuel requirements for this have not yet been investigated.

Beam Encounters by Vehicles in Transit to GEO

The number of encounters with power beams from operational SPS's which may be expected during low-thrust transfer from LEO to GEO (e.g., by an SPS module in self-powered transit, or by an electric orbit transfer vehicle (EOTV)) can be calculated only in the context of a full trajectory analysis. Orbital perturbations, especially in low orbit, can produce accelerations an order of magnitude larger than the thrust acceleration, and hence cannot be ignored in calculating the times when the EOTV will cross the beam trajectories in its instantaneous orbital plane. It is also obviously necessary to specify the thrust program and guidance algorithm, as these control the shape and orientation of the ascent spiral.

It would be quite premature to carry out such an analysis for the purpose of investigating beam encounters, if only because there is still controversy over various scenarios for transporting SPS modules or components to GEO. In the present study, in order to obtain some estimate of the magnitude of the encounter problem, the simplest possible ascent trajectory model was used to calculate the number of encounters with a single SPS power beam during a typical transit to GEO. The results presented here should be regarded, not as a prediction as to what might occur during an actual transit, but as a simple numerical experiment providing a first data point for this subject.

In the model assumed here, the thrust vector is assumed always to lie in the orbital plane, in the direction of the local horizontal, and the thrust acceleration is assumed constant in magnitude. Circumferential thrust is not the most efficient thrust steering law, and the restriction to the coplanar case means that the model cannot include the necessary plane change to GEO. It may be possible to control engine parameters (power, mass flow, or specific impulse) so as to maintain constant thrust acceleration as the vehicle mass decreases, but it is not necessarily desirable to do so. Moreover, a solar-powered EOTV clearly cannot thrust on the night side of the planet unless energy storage or auxiliary power is provided. The model assumes an ideal inverse-square force field, so

that perturbations are also neglected.

Despite these limitations, the simplest model provides a useful starting point for further work on beam encounters during ascent. For example, with minor modifications it could be used in an investigation of on-off thrust programs intended to minimize such encounters, when several SPS's are in operation.

In any case, with the above assumptions the equations of radial and circumferential motion of the vehicle are

$$\ddot{r} = r\dot{\theta}^2 - \mu/r^2 \qquad [2.22]$$

and

$$\frac{d}{dt}(r^2\dot{\theta}) = ra_o \qquad [2.23]$$

where μ is the gravitational constant of the Earth and a_o is the constant thrust acceleration. For low values of a_o, the orbits will be nearly circular and the radial acceleration may be neglected, so that [2.22] gives the circular-orbit result

$$\dot{\theta} = \mu^{1/2}/r^{3/2} \qquad [2.24]$$

Substituting this in [2.23] gives an equation which is easy to integrate, yielding

$$r = r_i/(1 - t/\tau)^2 \qquad [2.25]$$

where r_i is the initial orbit radius and

$$\tau = (\frac{\mu}{r_i})^{1/2}/a_o = v_{ci}/a_o \qquad [2.26]$$

where v_{ci} is the circular velocity in the initial orbit.

If the vehicle is to reach synchronous altitude at time t_2, then, from [2.25],

$$\tau = t_2/(1 - (r_i/r_s)^{1/2}) \qquad [2.27]$$

If the transfer starts from low altitude ($r_i \approx 1.1$ Earth radii) and takes 180 days, then $\tau \approx 304$ days. From [2.26], the required thrust acceleration is only about 30 microgees.

With [2.25], [2.24] reads

$$\dot{\theta} = \omega_i(1 - t/\tau)^3 \qquad [2.28]$$

where $\omega_1 = \mu^{1/2}/r_i^{3/2}$ is the initial orbital angular velocity. Integration yields

$$\theta = \tfrac{1}{4}\,\omega_i\tau[1 - (1 - t/\tau)^4] \qquad [2.29]$$

This equation shows that about 638 revolutions take place during a transfer lasting 180 days.

For a numerical experiment using this model, the EOTV was assumed to be in an orbital plane of inclination 28.5°, starting at an altitude of 750 km. The rectenna latitude was taken as 30°. Thrusting started at t = 0, when the beam locus in the orbital plane was at its lowest point, with the EOTV also on the y-axis of the orbital-plane coordinates. The EOTV radius was first calculated at intervals of exactly 24 hours, using [2.25], and this value was used in the solution of [2.9a] to give the times in that day when the beam crossed that radius. These times were added and subtracted to the integer days and new values of r calculated. Several iterations of this procedure always produced convergent values of the EOTV radius at the times on that day when the beam passed by. These beam passage times were then used in [2.9b] to give the angular position of the beam intersections with circles of these radii, and in [2.29] to give the angular position of the EOTV. The differences in angular position of the EOTV and the beam-intersection regions,

multiplied by the orbit radius at these times, gave a measure of the miss distances between the beam and the OTV.

In a transfer lasting 180 days, there are of course 360 opportunities for an encounter with the beam from a single SPS. In the above calculation, it was however found that there were no occasions when the beam passed within 100 km of the EOTV, and there were only ten occasions when the miss distance was less than 1000 km -- seven of these occurred on the descending half of the beam intersection locus in the orbital plane, and three on the ascending half.

While the conditions for this calculation may have been fortuitously well chosen, it does appear that it should be possible to find ascent trajectories from LEO to GEO in which beam encounters are quite unlikely. In future work, this issue can be explored by taking other combinations of orbit inclination and rectenna latitude, as well as different initial orbital positions for the EOTV.

Conclusions and Recommendations

As noted in Section 2.1, the consequences of encounters between SPS microwave beams and lower satellites may be serious, in terms of engineering, economic, political and legal costs. A first and most important conclusion from the present analysis is that such encounters will not be as frequent as intuition might suggest. Moreover, for rectennas in the temperate zone and relatively low-inclination orbits, there are satellite altitudes for which encounters will not occur. The duration of encounters is not more than several seconds: at the flux levels expected of SPS microwave beams, this rules out direct heating as a significant satellite damage mechanism.

In general, it appears that, if large numbers of satellites (>100) are in orbits of moderate altitude (<5000 km) and inclination, one of them will pass through the beam of a given SPS (to a temperate zone rectenna) about once or twice a month. Conversely, if there are large numbers of SPS (>100), feeding randomly scattered rectennas, a typical low satellite might expect to encounter one of the beams once or twice a month.

There does not at present appear to be any significant encounter problem for vehicles in low-thrust transfer from LEO to GEO, although further study of the question is needed.

It is of course possible to design most satellites to withstand passage through the power beams, where the flux may reach hundreds of milliwatts per square centimeter (at higher altitudes). Radar-type grounding switches can be used to protect the inputs to sensitive RF receivers (especially those designed for use at S-band) and sensitive components may be shielded -- in some cases, it may be possible to enclose the entire satellite in a Faraday cage. In order to evaluate realistically the costs of such protective measures, it would be useful to undertake a survey of a range of existing (civilian and military) satellites, to see what penalties would have been incurred if it had been necessary to design them for SPS beam encounters.

SPS system recommendations arising from the present analysis include:

i) No rectennas should be allowed on or close (e.g., less than one degree latitude) to the equator, in order to avoid frequent beam encounters by equatorial satellites.

ii) Where options exist, rectennas should be built at as high latitudes as is economically and geographically feasible, in order to minimize interference with low satellites in orbits of moderate inclination.

iii) Where mission objectives permit and launch penalties are not excessive, the use of the lowest possible orbit inclination for all sensitive satellites should be encouraged, to minimize beam encounter frequency.

iv) The SPS power beam should be designed for rapid on-off switching (in times of a second or two), in order to minimize outages if it becomes necessary to interrupt the beam to avoid an unacceptable encounter with a sensitive satellite. Continuous power to the utility grid could be provided by a very small energy storage capacity at the rectenna (it is probable that adequate storage will be available in order to compensate for other, considerably longer outages).

It should be noted that the conclusions reached in this study were based on the use of microwave power transfer from a geosynchronous SPS.

A similar study should be undertaken of encounters between satellites and laser power transmission beams, as an input to evaluation of this option. The flux densities are of course higher in the laser case, but no general statement is possible concerning the relative hazards of infrared and microwave radiation to the operation or integrity of satellites. Here again, a survey of existing satellites could be useful. Additional encounter problems may arise in the laser case, even if the SPS is in GEO, if the laser beams are switched rapidly from one receiver to another, in response to terrestrial weather. In many laser-transmission proposals, the SPS is assumed to be in sun-synchronous orbit, either irradiating receivers of opportunity as it passes over them, or else relaying via mirrors in GEO. In the latter case, there are twice as many power beams as in the geosynchronous SPS, and half of them move as the solar collectors orbit the Earth, greatly increasing encounter probabilities. In the purely low-altitude system, the sun-synchronous orbit is at high inclination and above most LEO satellites, so that the laser beams will cross the orbits of nearly all satellites on every revolution: it would be interesting to compute encounter probabilities for this system.

1.2 SPACE CONSTRUCTION AND SUPPORT

1.2.1 Space-Based Construction Systems Analysis

The primary focus of this task was to investigate alternative construction concepts and to refine the baseline construction concept. Table 1.2.1-1 lists the phase 1 subtasks that were performed under task 4.2.1 of the study and lists subsections of this report that display the study results. Grumman was a major contributor to this analysis under subcontract. Grumman and Boeing results are integrated in this report section.

1.2.1.1 Series Construction Analysis

1.2.1.1.1 Introduction

The baseline construction concept was designed so that the antenna and the modules were constructed in parallel. The motivations for this approach were that 1) the maximum amount of time would be available for constructing each of these major end items, and 2) the antenna and module components have to be mixed in the HLLV cargo pallets to achieve mass limited launch conditions so it made sense to utilize the components as they were delivered.

One of the construction sensitivities that was not explored earlier was to determine the ramifications of a construction approach wherein the antenna and the modules would be constructed in series instead of in parallel. The motivation for exploring this approach was that potentially the crew size could be reduced thereby reducing the number of crew modules (the most expensive items at the base).

The objectives of this analysis were to determine the cost effectiveness and practicality of a series construction concept as compared to the baseline parallel construction concept.

1.2.1.1.2 Summary

This analysis compares two series construction concepts to the baseline construction concept. The series construction approach will require the modules, yokes, and antennas to be constructed in about half the time as would be required for the baseline approach. In order to construct at this faster rate, it will be necessary to operate the construction equipment at faster rates (Option 1) or to use more equipment (Option 2), or by some combination of these two strategies.

Table 1.2.1-1 Spaced-Based Construction Systems Analysis

Spaced-Based Construction Systems Analysis

Section	Task 4.2.1 Subtasks	①	Title of Sub-Section
4.2.1.1	42101		Series Construction Analysis
4.2.1.2	42102		Equipment Characteristics Analysis
4.2.1.3	42103		Identification of Alternative Construction Concepts
4.2.1.4	42106 42107 42108 42109 42111 42112		End Builder Construction Concept Characterization
4.2.1.5	42110		Single Deck Construction Concept Characterization
4.2.1.6	42117 42118		Antenna Construction Concept Refinement
4.2.1.7	42114 42115 42116		Preferred Construction Concept Selection

① NOTE: Task 42113 Update Baseline Final Assembly Base was not performed as this was a task that was applicable to the LEO construction approach which was not selected as the reference concept.

Table 1.2.1-2 summarizes the equipment rates and quantities and the crew sizes required for the two options and these are compared to the baseline requirements. Figure 1.2.1-1 shows the net effect of these two options. Figure 1.2.1-2 shows that the resulting cost deltas will range from an additional 10% for Option 2 to as much as -20% for Option 1.

Table 1.2.1-3 summarizes the preliminary conclusions of this analysis.

1.2.1.2 Equipment Characteristics Analysis

This task incorporates three subtasks: beam builder production rate analysis, module indexing rate analysis, and equipment manning requirements analysis.

1.2.1.2.1 Beam-Builder Production Rates

Discussion:

The attempt to establish a preliminary determination of realistic beam builder production rates started with a review of current technology. Sources utilized were GDC/JSC (NAS9-15310) SCAFEDS Report #CASD-ASP77-017 and results from GAC/MSFC (NAS8-32472) SFDS in-house test program. An overview of the two technological approaches to beam making is shown in Figure 1.2.1-3. Both designs are based on cyclic (run/stop) operation where the caps are formed in the "aft" bay and the bracing fastened in the "forward" bay. A notable difference lies in the heating/cooling operations required for the composite beam builder.

Both the composite and aluminum beam builders presently in technology development are sized in geometry, power, etc., to operate from the payload bay of the STS in a time frame anticipated to be in the 1980's. Figure 1.2.1-4 and -5 show the major subsystems for the two units.

The subject investigation concerned itself with a beam builder fabricating a much larger structure (6.5-m deep x 7.5-m bay length) and operating in a later time frame where production rates are considerably more critical. Therefore, the study concentrated in identifying potential growth options in the current machine rates of 1.08 meters/min (composite) and .682 meters/min (aluminum). The study was aimed primarily at the composite beam builder since that is the baseline structure in the present contract effort, however, comparable data was also derived for the aluminum beam builder to establish additional credibility.

Table 1.2.1-2 Series Construction LEO Base Rates and Quantities

	BASELINE	SERIES	
		OPTION 1 FASTER RATES	OPTION 2 MORE EQUIPMENT
EQUIPMENT RATES			
BEAM MACHINE	5.08 m/min	10 m/min	5 m/min
SOLAR ARRAY DEPLOYERS	12.6 m/min	23.7 m/min	10.2 m/min
SUBARRAY DEPLOYERS	20 min/SUBARRAY	12.9 min/SUBARRAY	25.7 min/SUBARRAY
POWER BUS DEPLOYERS	0.7 m/min	1.2 m/min	0.6 m/min
EQUIPMENT QUANTITY			
BEAM MACHINES	2	2	4
SOLAR ARRAY DEPLOYERS	4	4	8
SUBARRAY DEPLOYERS	1	1	2
CRANE/MANIPULATORS	31	23	46
POWER BUS DEPLOYERS	3	2	4
CREW SIZE			
MANAGEMENT	10	10	10
CONSTRUCTION	362	219	314
BASE OPERATIONS	39	39	39
BASE SUPPORT	77	57	77
	488	325	440

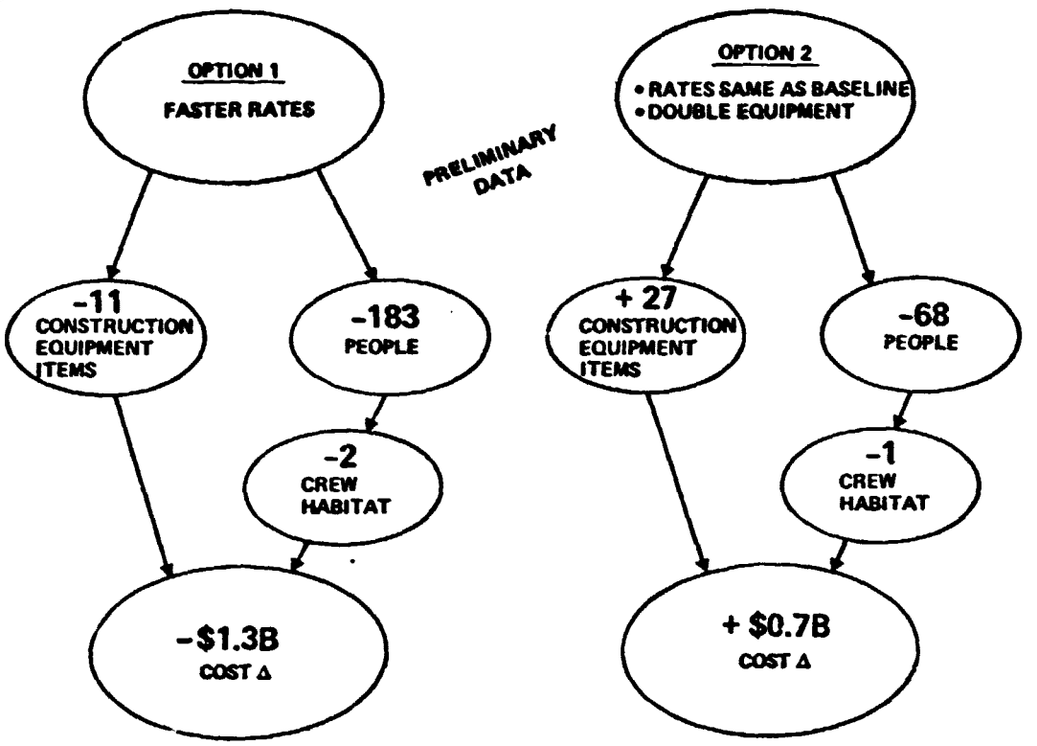

Figure 1.2.1-1 Series Construction Options

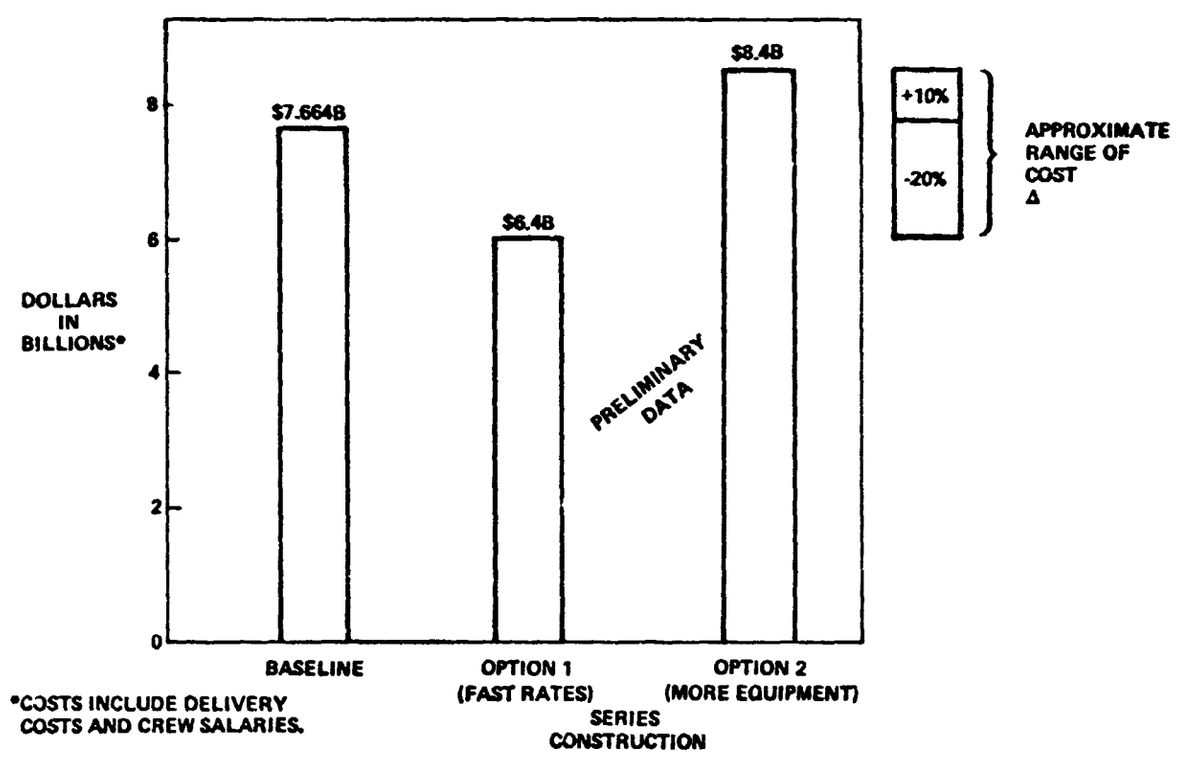

Figure 1.2.1-2 Series Construction Cost Deltas

Table 1.2.1-3 Series Construction Preliminary Conclusions

- SERIES CONSTRUCTION MAY RESULT IN +10% TO -20% COST Δ
  - EXACT Δ WILL DEPEND UPON–
    - GENERIC CONSTRUCTION FACILITY CONCEPT SELECTION
    - CONSTRUCTION EQUIPMENT RATE, COST, AND MASS DEFINITION
    - CREW MODULE COST AND MASS DEFINITION
- ADVANTAGES:
  - POTENTIAL COST SAVINGS
- DISADVANTAGES:
  - IDLE EQUIPMENT
  - DISRUPTION IN PRODUCTION CONTINUITY
  - WAREHOUSING AND INVENTORY CONTROL COMPLICATIONS

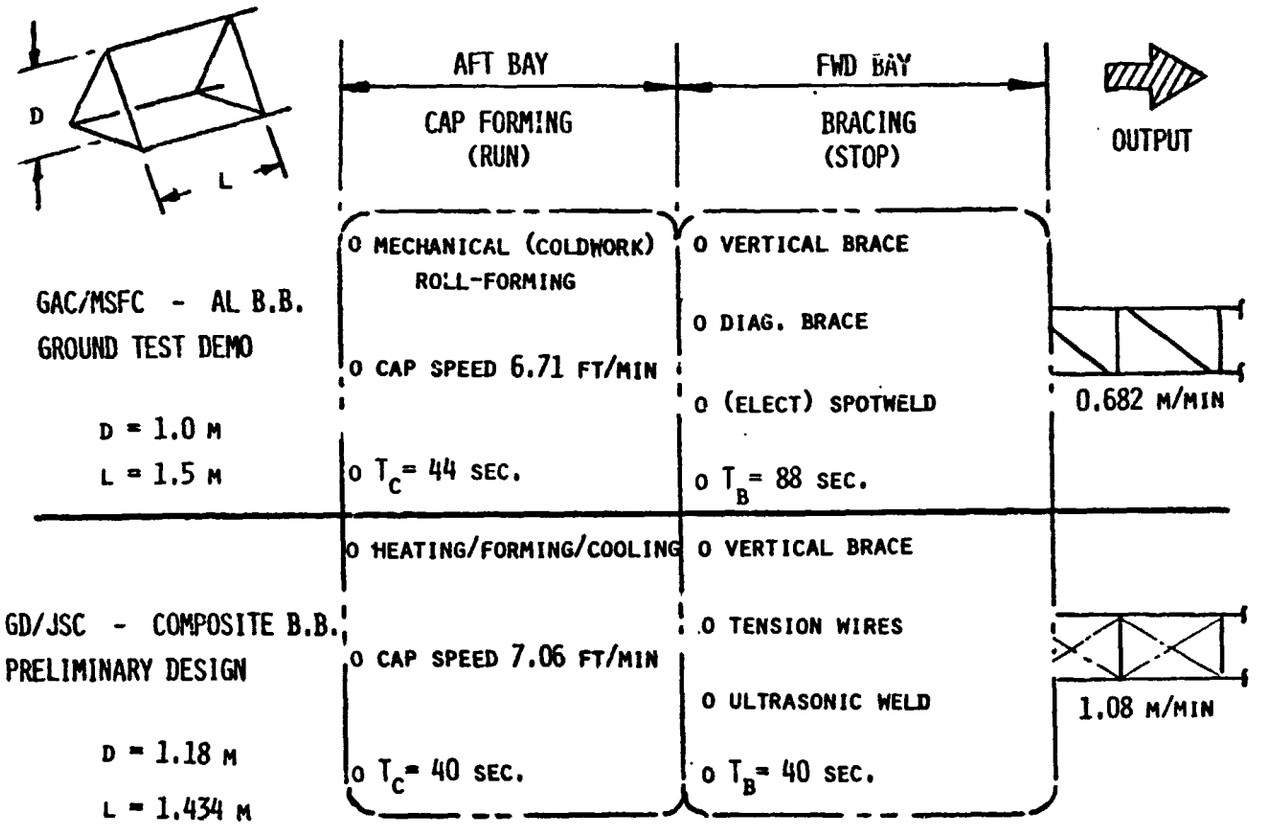

Figure 1.2.1-3 Beam Builder –Current Technology Overview

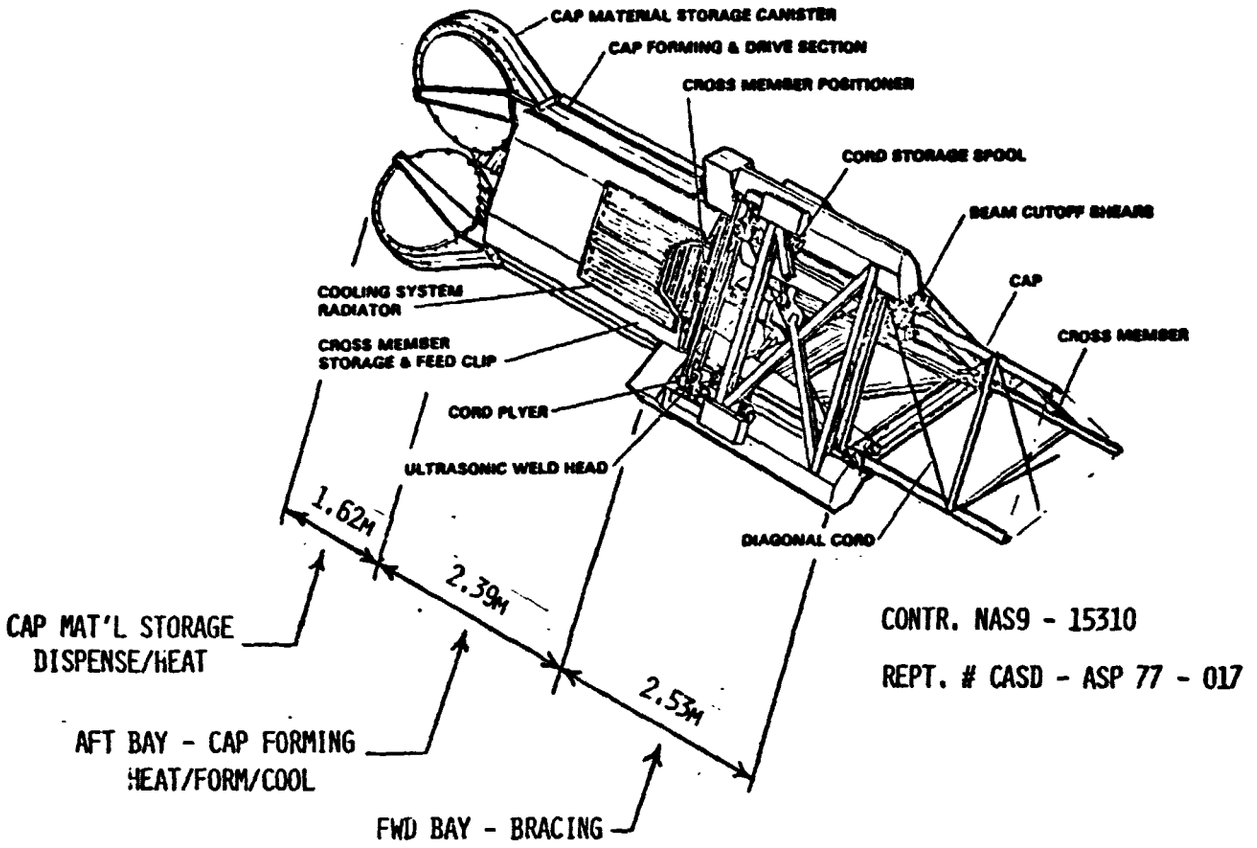

Figure 1.2.1-4 Composite Beam Builder–Preliminary Design

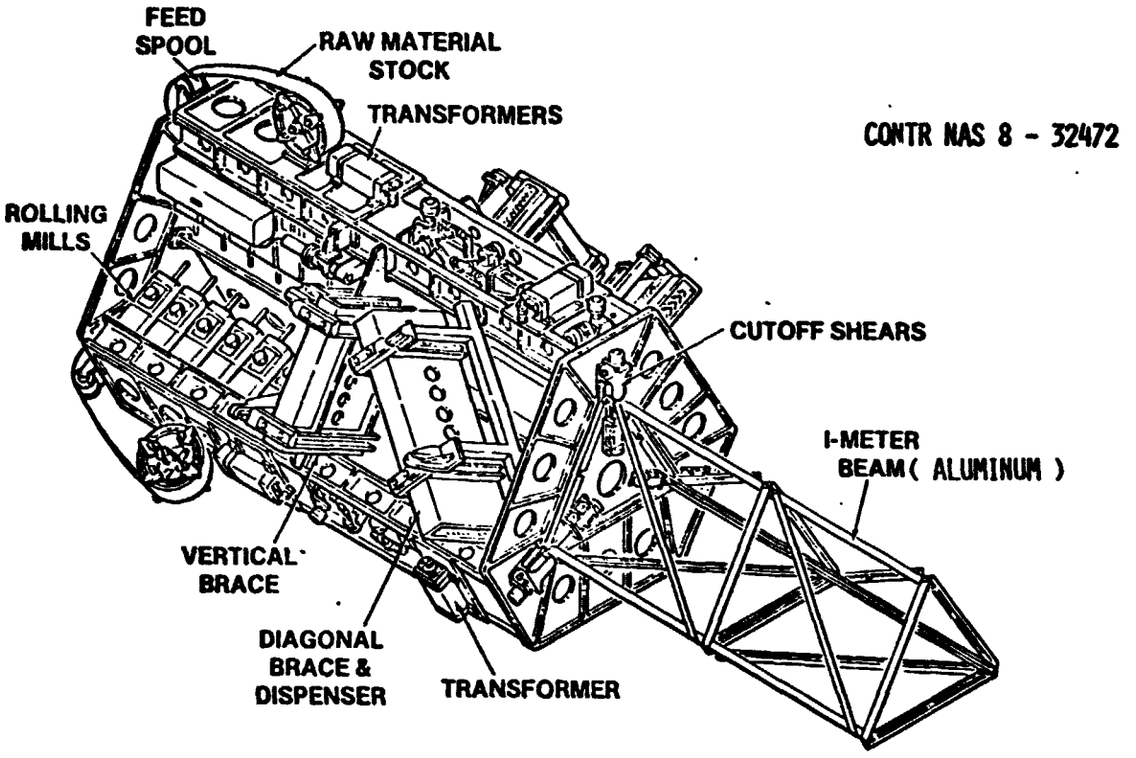

Figure 1.2.1-5 Automated Beam Builder

A discussion of the effects of increasing cap forming rate and of various scale effects follows:

Option A–Higher Cap Forming Rates

In the composite beam builder, two means are available for increasing the cap forming rates. The first is to provide higher heating and cooling rates to compensate for the desired higher cap speed. The second is to increase the dimensional length of the heating and cooling subsystems proportionally with the increase in cap speed so that total time exposure to both heating and cooling is constant. The latter maintains existing heater and coolant temperatures and, with the resources available, is therefore simpler to deal with. Figure 1.2.1-6 shows the potential gained from increasing cap speeds of the 1.18-m composite beam builder together with the anticipated increase in the length of the "aft" bay.

Option B–Batten Spacing (Scale Effect)

This option concerns a "windfall" which is attributable more to beam geometry than to beam builder operation. When scaling up from a 1.434-m batten spacing to the present 7.5-m baseline, a proportionally greater amount of time is spent in the "run" mode of the run/stop cycle for the same unit bay construction. The assumption is made that while the battens are longer, the time required to dispense them is essentially constant (t_B = 40 sec). The diagonal cords are dispensed during the "run" mode, and cord fastening time is regarded as the same. Figure 1.2.1-7 shows the effect of batten spacing on production rates while maintaining the current machinery rates.

Option C–Beam Dept (Scale Effect)

This option relates ultimately to the selection of a reasonable cap forming rate and is another scale effect attributed to beam geometry.

In beam builder operation, dissimilar cap speeds will produce warping (bow) of the beam with an attendant objectionable eccentricity in beam-column load applications. Figure 1.2.1-8 shows the relationship between a beam's eccentricity and the difference in cap exit rate expressed as a cap error. It is assumed that the top cap had a higher rate than the bottom two, whose rates were identical. Note that a deeper beam may be permitted to have a greater cap error for the same eccentricity ratio (h/l) and that the increased permissable cap error is in direct proportion to beam depth.

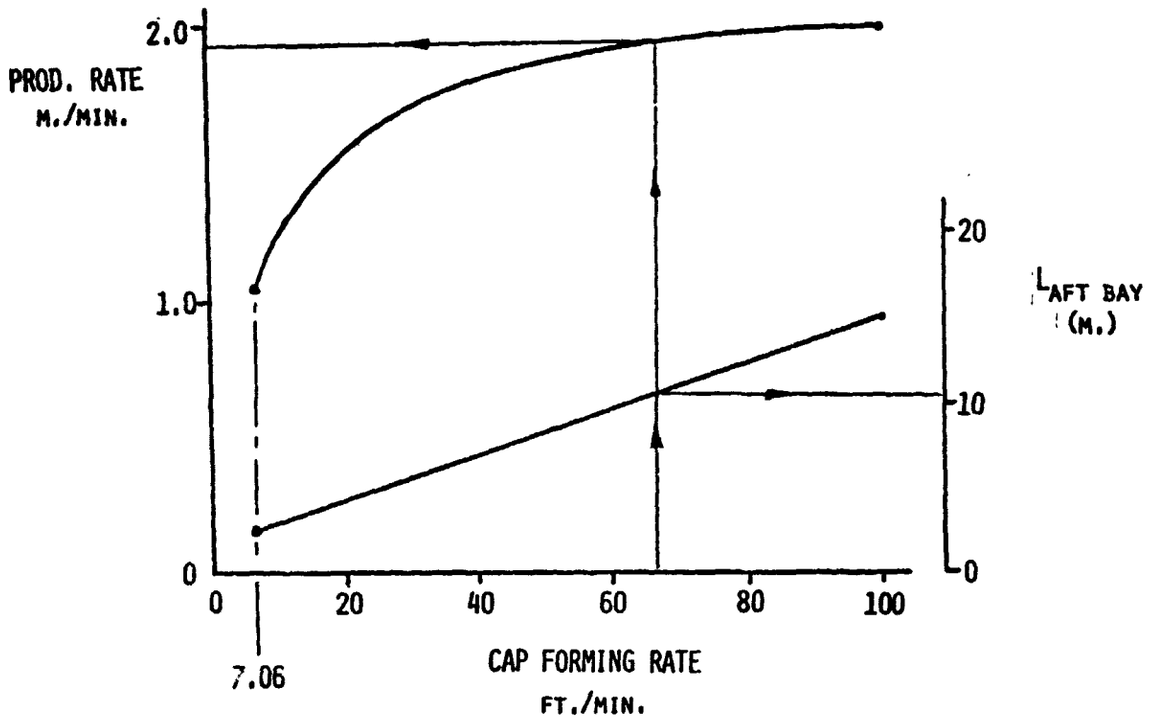

Figure 1.2.1-6 Composite Beam Builder—Option A—Cap Forming Rate

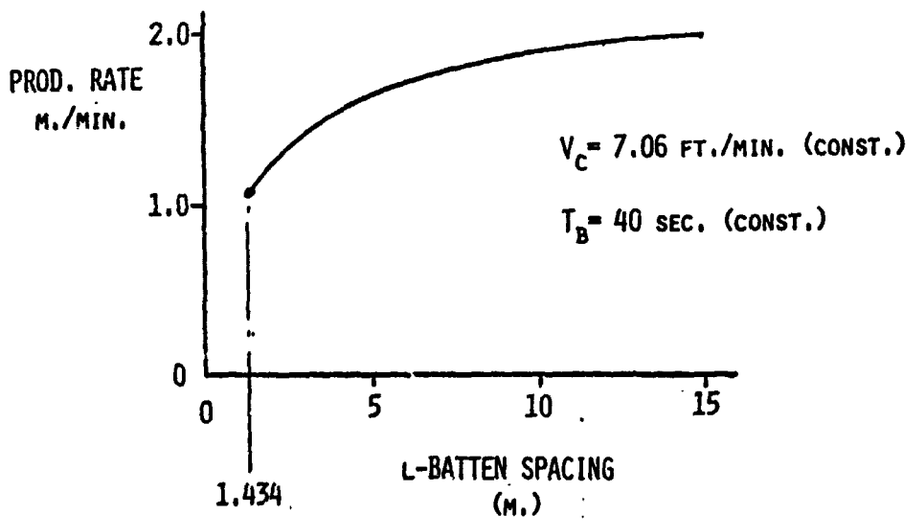

Figure 1.2.1-7 Composite Beam Builder—Option B—Batten Spacing

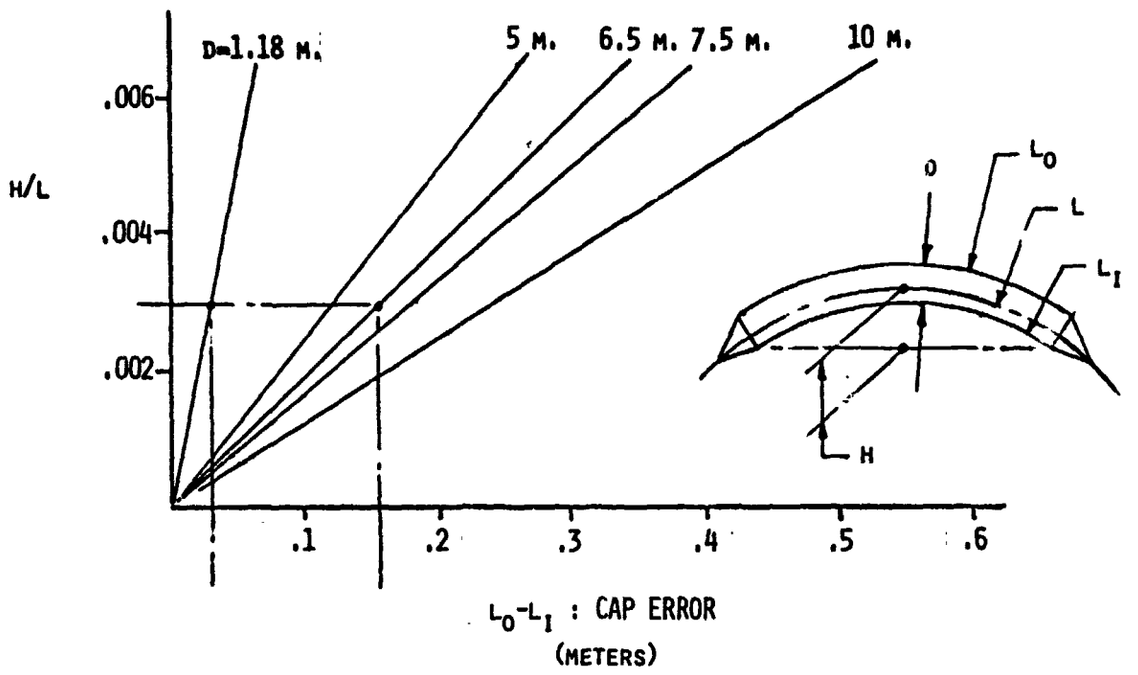

Figure 1.2.1-8 Composite Beam Builder—Option C—Cap Speed/Error

In terms of beam builder machinery, the same control system required for synchronizing cap speeds therefore, appears to perform better, in effect, when the beam builder is scaled-up for the greater depth. However, rather than accept the better performance, it may be preferable in this instance to trade the better performance for a greater cap speed.

It would be conservative to assume that the control system can be designed to limit the increase in cap error to a value in direct proportion to an increase in cap speed. Given this approach, a direct relationship (Fig. 1.2.1-9) can be established between beam depth and permissable cap forming rate. For example, the permissable cap forming rate of a 6.5-m deep beam will be 6.5/1.18 = 5.51 times the cap rate of a 1.18-m deep beam. Its cap error would also be 5.51 times greater, but spread-out over a greater depth will produce the same h/l value.

Conclusions:

A. The combined options (A, B, and C) are shown in Figure 1.2.1-10. Note that a production rate of 5.7-m/min for the baseline beam configuration can be readily achieved with higher values permissible for greater beam depths and longer batten spacings. Further increases can be realized when the 40 sec "stop" mode is reduced. However, the latter requires further study of the cooling radiator subsystem to establish a rationale for reducing the 40 sec time lapse.

   Figure 1.2.1-11 shows the increase in beam builder length expected when heating and cooling temperatures are held constant.

B. Figure 1.2.1-12 shows the combined options A, B, and C as they apply to the aluminum beam builder, with a fourth option included to operate on the stop mode (t_B). The current aluminum beam builder fastens its braces, during the stop-mode, by spot-welding in an in-series sequence mostly to maintain low power requirements. However, given a "high-power" environment, spot-welding can be performed in an in-parallel sequence with a t_B of 14 sec minimum and 30 sec maximum. Corresponding production rates would be 10-m/min and 7.3-m/min respectively.

C. A further option beyond those discussed exists for increasing production rate. The "stop" mode in both current designs can be eliminated by performing all bracing

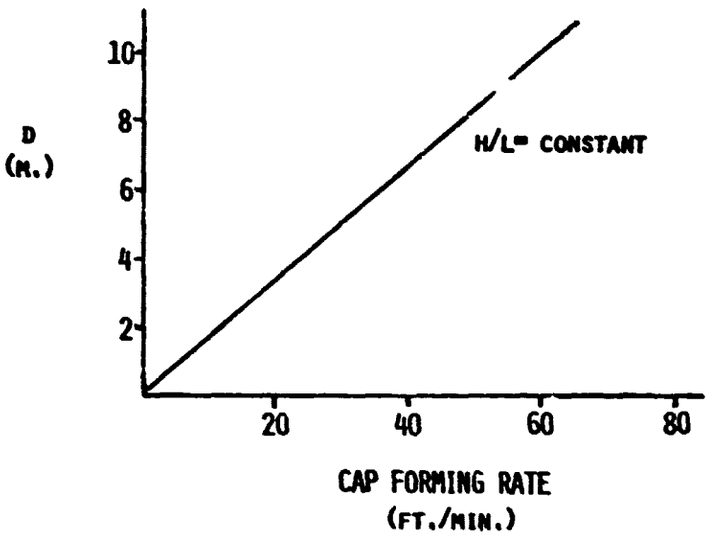

Figure 1.2.1-9 Composite Beam Builder—Option C (continued)—Cap Speed/Error

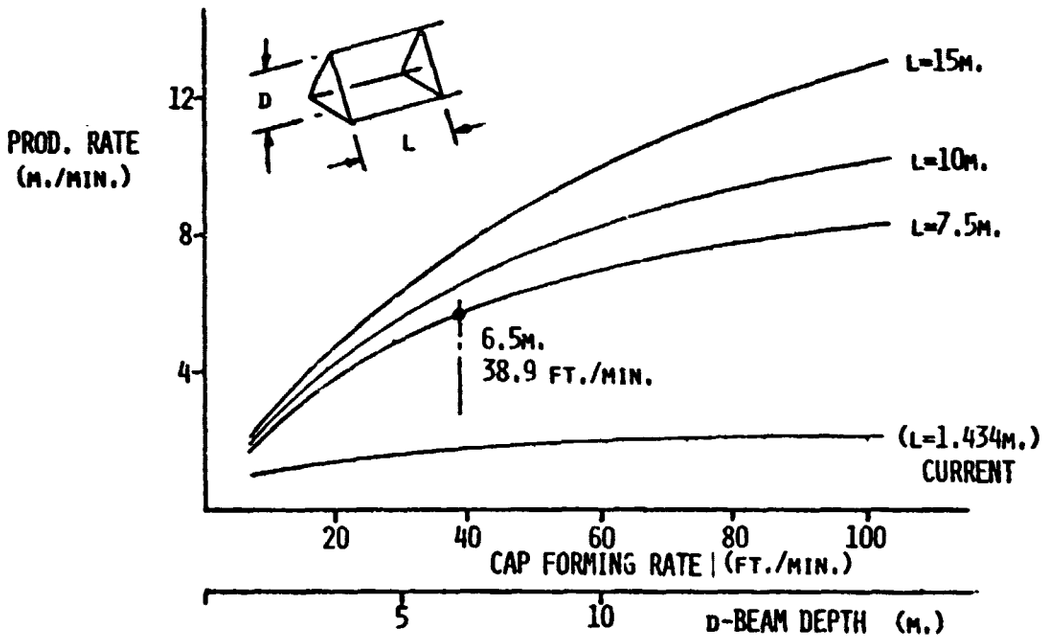

Figure 1.2.1-10 Composite Beam Builder—Options A, B and C—T_B = 40 sec. (Const.)

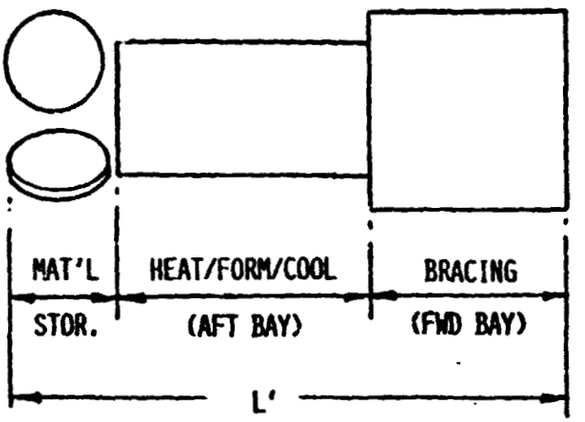

D	L	MAT'L. STOR.	AFT BAY	FWD BAY	L'
1.18	1.434	1.62	2.39	2.53	6.54
6.5	7.5	-	12.5	8.6	21.1 + MAT'L. STOR.
7.5	10	-	16.7	11.1	• 27.8 + MAT'L. STOR.
10	15	-	25	16.1	41.1 + MAT'L. STOR.

Figure 1.2.1-11 Composite Beam Builder—Increase in Machine Length

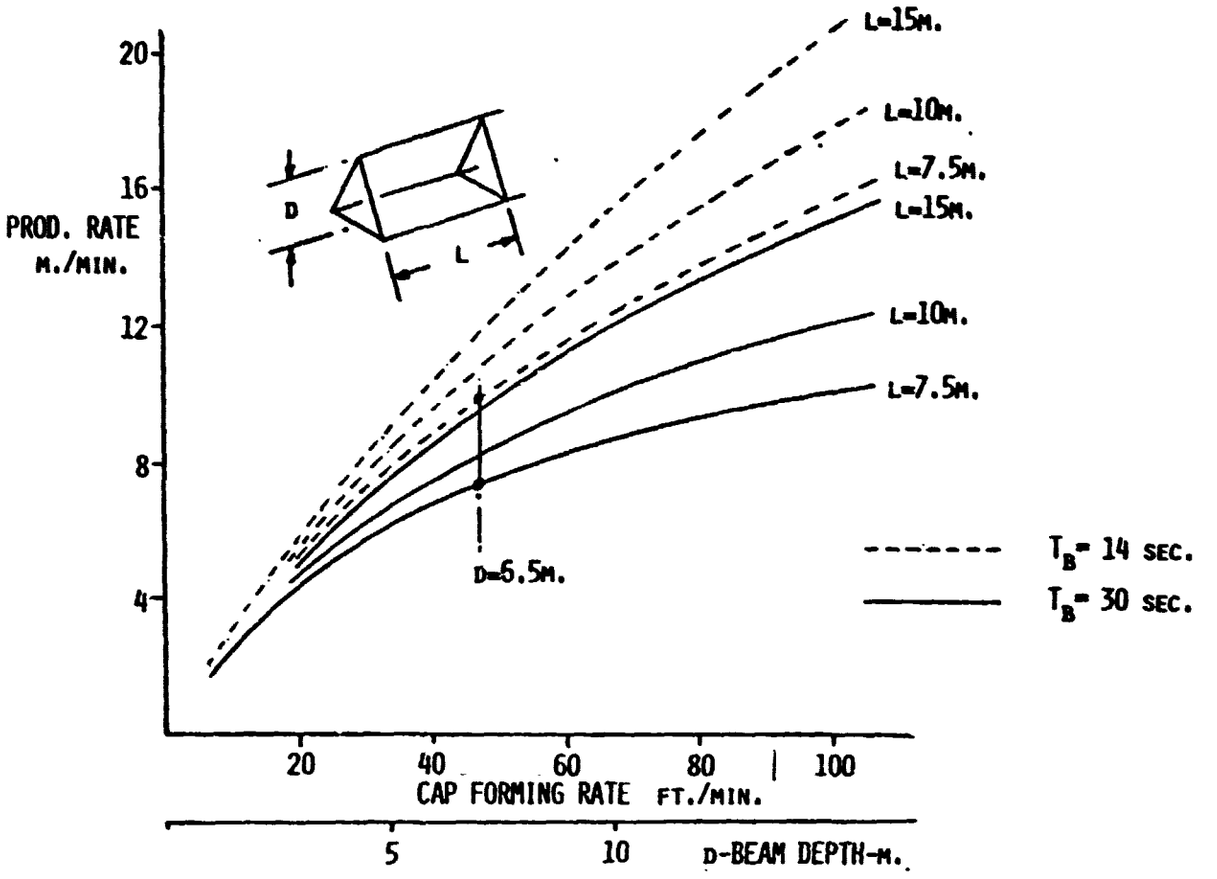

Figure 1.2.1-12 Aluminum Beam Builder

operations "on-the-fly." This option, beyond being merely identified here, has not been studied in detail.

1.2.1.2.2 Module Indexing Rate Analysis

There are two subtasks: (1) Single deck construction base module indexing rate analysis and (2) End builder construction base module indexing rate analysis.

1.2.1.2.2.1 Single Deck Construction Base Module Indexing Analysis

A "quick-look" analysis was performed to determine whether or not a module indexing rate of 10 meters/min was feasible.

Two cases were considered:

1) LEO assembly–all translations normal to long axis of construction base
2) GEO assembly–translations both parallel to and normal to construction base long axis.

Assumptions:

- Loads are transmitted between modules by "indexers" which roll on tracks on the construction base surface.
- Ground rule: module translation speed will be held to the lowest value which is consistent with the construction rate. This value has been tentatively set at 10 meters/min.
- GEO construction base mass = 5×10^6 kg.

Analysis:

t = 33.37 min
x = 337.5 m

Let $S = \frac{1}{2} a t^2$

For acceleration profile as shown.

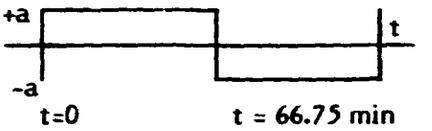

$$a = \frac{2S}{t^2} = \frac{2(337.5)}{(33.75)60^2} = 1.65 \times 10^{-4} \text{ m/s}^2.$$

$V_{max} = at = 1.65 \times 10^{-4}$ m/s (2025 S) = 0.334 m/s = 20 m/min

Thrust Req = $m\bar{a} = (1.65 \times 10^{-4} \text{ m/sec}^2)(5 \times 10^6 \text{ kg}) = 825$ N.

Maximum power required = 825 N (0.334) m/s = 275 W. (100% efficiency).

Conclusions:
10-m/min indexing rate is sustainable with essentially no impact on the module structural design. Considerable margin is available to allow shaping of acceleration and jerk profiles. BAC studies have shown that proper control of these profiles is an - effec tive method of limiting structural excitation, and that such limitation will be required for structures characteristic of SPS. As the force required to accelerate the module sufficiently to meet the 10 m/m average translation rate (825 N) can be readily applied by a single indexer, these results can be considered to apply to both LEO and GEO construction scenarios.

1.2.1.2.2.2 End Builder Construction Base Module Indexing Rate Analysis

Preliminary estimates were made of the loads acting on the end builder construction base during construction and are presented in Figures 1.2.1-13 and -14. The satellite array/antenna configuration are shown in the first figure. Since the satellite mass is very much greater than the construction base, it can be assumed that the relative motion of the satellite is zero.

A force-time curve is shown in the second figure for an index rate of 20 m/minute. Additional study is required to evaluate the effect of the impulse on the construction base.

1.2.1.2.3 Equipment Manning Requirements

Automatic Beam Machine Manning
The baseline approach initially assigned two operators to each beam machine. Although a work load analysis had not been performed, a two-man crew is a conservative ground rule considering previous mission safety constraints and the fact that only two independent mobile machines were included in the baseline concept. Direct use of this ground rule, however, was not applicable to the end builder construction concept since it relies upon synchronized operation of several beam machines. Each beam machine is fully automatic and does not have to be controlled on site. In fact all fixed beam machines, which fabricate continuous longitudinal beams on the end builder, must be centrally controlled. The remaining structural members can either be fabricated with separate gimballed beam machines located next to each longitudinal member or with mobile gimballed beam machines as in the baseline. The gimballed beam machines operate independently and have a few more functions than the fixed beam machines (i.e., aiming, fab different length beams, etc.).

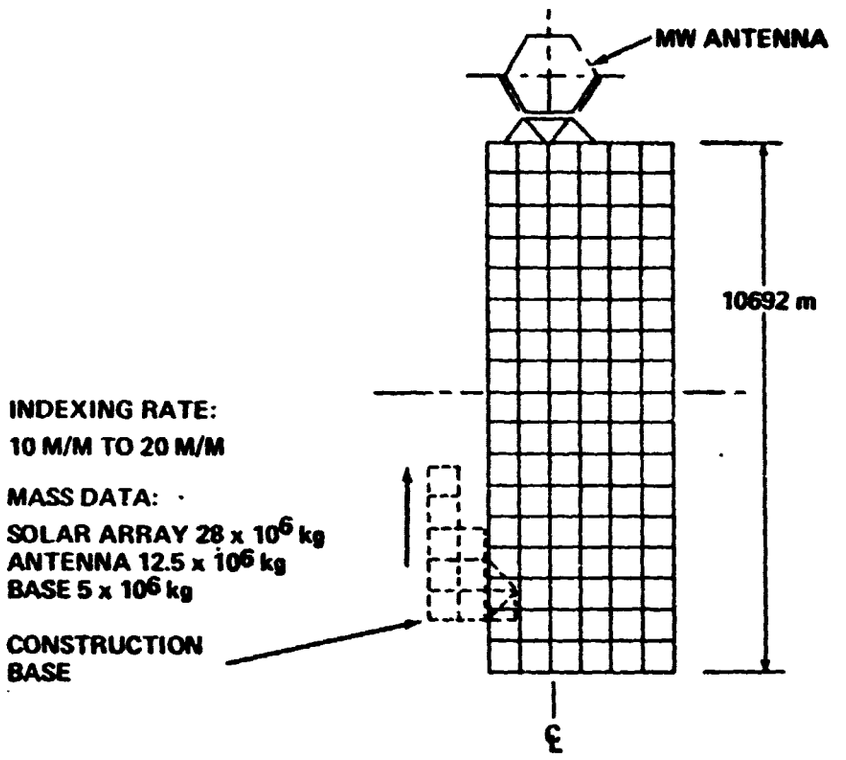

Figure 1.2.1-13 5GW SPS End Builder Construction Base Indexing Condition

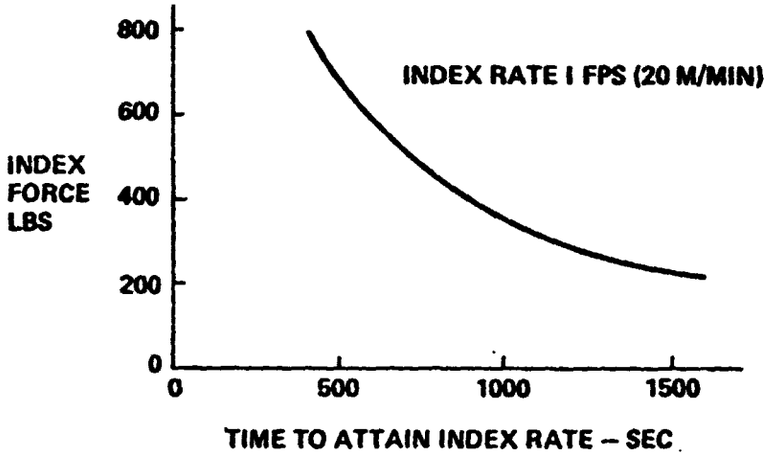

ASSUMPTIONS:

CONSTRUCTION BASE MASS IS A SMALL PERCENT OF TOTAL MASS; RELATIVE MOTION OF SATELLITE IS NEGLECTED

Figure 1.2.1-14 End Builder Construction Base Indexing Force

These machines can also be preprogrammed for remote centralized control to minimize crew operators. Increased use of automated equipments, however, also implies added requirements for maintenance and repair.

Therefore to facilitate the comparison of the single deck and end builder concepts, the groundrules for manning automatic beam machines were revised to accommodate different construction applications as shown in Figure 1.2.1-15.

Based on previous studies, one operator was assigned to control 8 synchronized fixed beam machines. This appears to be a rather conservative estimate when compared with present automated procedures in the lumber industry.

It was assumed that fewer gimballed machines could be controlled by each man due to the added functions as listed in Figure 1.2.1-15.

One man was assigned to operate 4 fixed gimballed beam machines. Generally 94 to 212 minutes are required to fabricate the various length beams at 5.0 meters per minute. Allowing 10 minutes for hand-off and aiming implies that 90 to 95% of the time is spent monitoring operations. Even if the four beams are all the same length and fabrication ends simultaneously the handoff and aim functions can be performed in series.

Finally one man was assigned to each mobile beam machine. This follows the original groundrule similar to a crane/truck on Earth or an SPS crane/manipulator, where the operations are performed in series: (1) moving from location to location, (2) positioning, and (3) performing required operations. The reduction in crew staffing from two men to one man was consistent with the revised crew staffing logic developed for cherry picker operations.

Cherry Picker Usage and Manning

The original ground rule required the use of two cherry pickers at both ends of each segmented beam during beam handling and structural joining operations. This requirement was carried over from Boeing's previous SPS study which examined the assembly

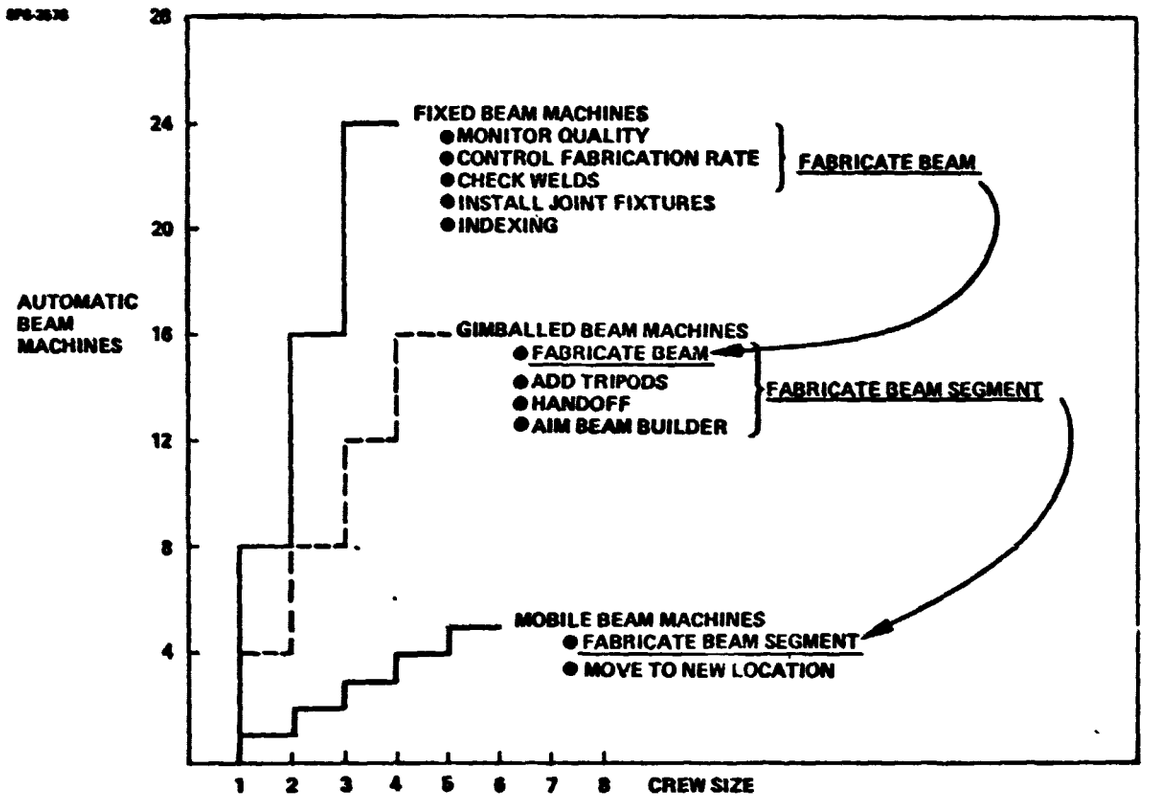

Figure 1.2.1-15 Automatic Beam Machine Applications and Manning

of 20 meter pentahedral segmented beams built with preformed struts. These structural members were made to size with squared off ends for attaching special end fittings at the structural joining site. Hence one cherry picker was required to hold the beam in position while a second cherry picker/crane installed the required connecting struts. The present baseline, however, uses a space fabricated continuous chord beam which can be made with the appropriate end fitting (i.e., nodal, butt, lap, etc.) at the time of manufacture. The preferred end fitting design and how it might be integrated into the beam machine operation remains as an area for future study. Nevertheless, if it is assumed that the beam is made with nodal end fittings then one cherry picker at each end is sufficient for handling and joining, provided it is equipped with separate grapplers and dexterous manipulators.

As previously noted the staffing of remote work station for cherry pickers and beam machines was originally baselined as a two-man-crew for reasons of safety and not necessarily due to operator work load. In the SPS era, it is believed that a manned remote work station (MRWS) can be designed with sufficient redundancy to meet crew safety requirements. Therefore crew staffing should only be based on specific work load requirements. Based on recent MRWS studies, it is believed that SPS construction tasks (e.g., assembling the joints) can be readily performed by one operator. Therefore, until further analysis or simulation shows otherwise, only one operator can be justified for each cherry picker or mobile beam machine.

1.2.1.3 Identification of Alternative Construction Concepts

The method of construction selected for building the full size Solar Power Satellite (5 to 10 GW) will directly impact the size of the construction work zone and the minimum equipments needed for space fabrication and assembly. The method of construction can also impose constraints on the design of SPS subsystems. Two alternate methods for construction, segmented build-up and continuous build-up, are depicted in Figure 1.2.1-16 for a typical SPS solar array module.

The baseline LEO construction approach, for example, follows a two-step segmented build-up method. This method allows minimal equipment to be used for structural assembly while other time consuming subsystem functions, such as installing solar array blankets, are performed on fully assembled structural bays. The solar array structural bays are constructed with space fabricated tri-beam elements joined at the corners. Accordingly, the construction work zone needs a two bay facility depth to

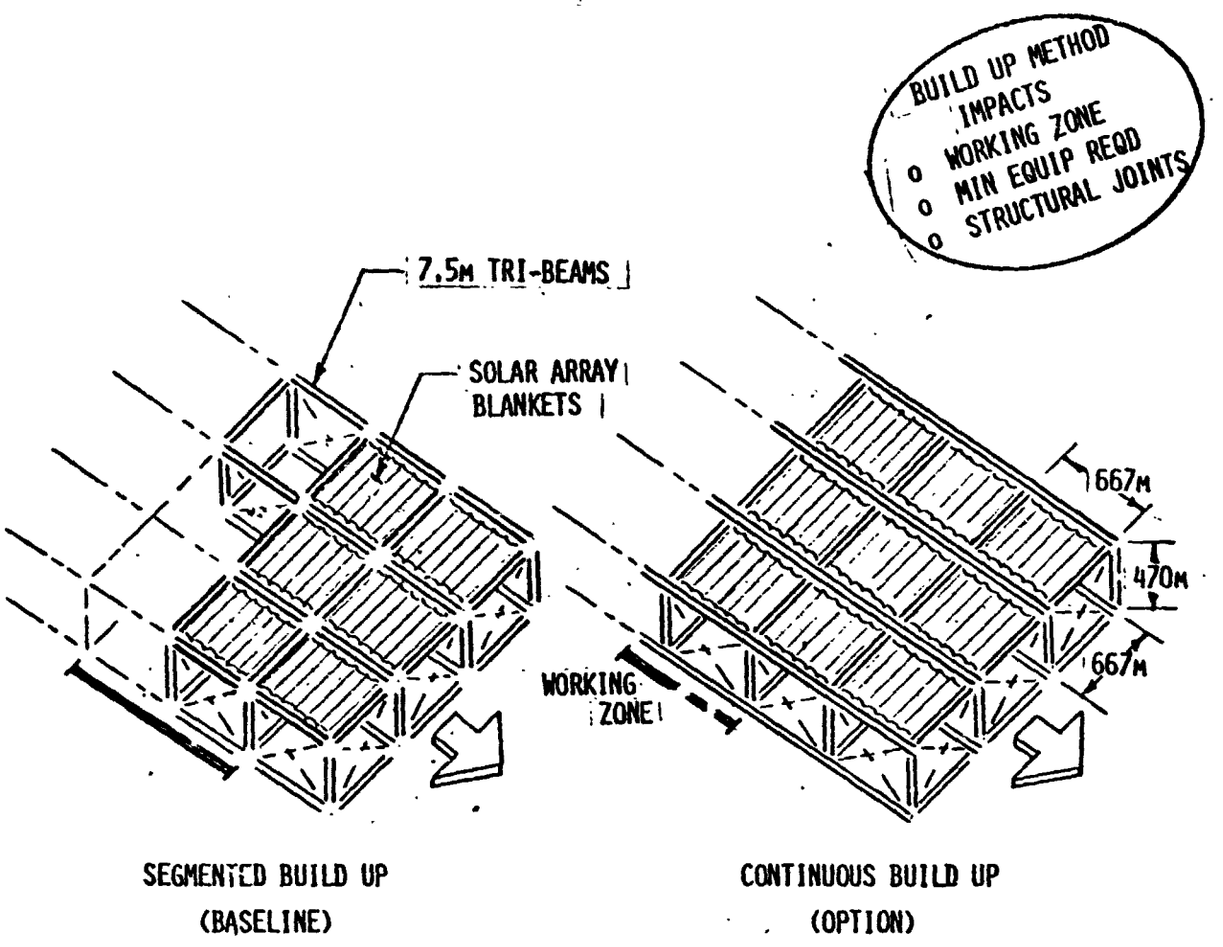

Figure 1.2.1-16 Alternate SPS Construction Methods

accommodate both structural and nonstructural construction operations, whether double deck or single deck base arrangements are used.

The continuous build-up option, however, is keyed to the continuous fabrication of longitudinal structural elements which allows the build-up of other subsystems to be more closely coupled. While this method of construction requires more construction equipment than the segmented build-up concept, it also needs a shorter construction work zone, hence, a smaller base to implement. The use of continuous longitudinal elements of course requires a different joint design for assembling the structural framework.

The segmented and continuous construction methods discussed above lead toward generic families of external construction bases shown in Figure 1.2.1-17. That is, segmented construction can be implemented by the baseline double deck and its derivatives encompassing single deck options and smaller size base arrangements. Derivatives of the continuous end builder can also vary in size or include added features if needed to facilitate SPS construction.

Other construction approaches are derived by considering hybrid concepts which may have an economic advantage over the external system concepts discussed above. For example, the internal construction system shown in the figure constrains the base to a small volume by building the SPS structure around itself. This hybrid system can be adapted to either the segmented or continuous construction concept. On the other hand, an even smaller base can be envisaged if the SPS is self-constructed by portable beam machines or multi-purpose subsystem installation/maintenance equipment which in effect implement "bootstrap" construction.

The alternative construction concepts that were examined in this study are shown in Figure 1.2.1-18.

The major areas emphasized during Phase I include:

- Comparison of segmented versus continuous SPS GEO construction.
- Development of alternate base arrangements and required construction elements to encompass:
  -Satellite structural build-up (beam machines and construction aids).
  -Antenna yoke build-up and assembly to satellite.

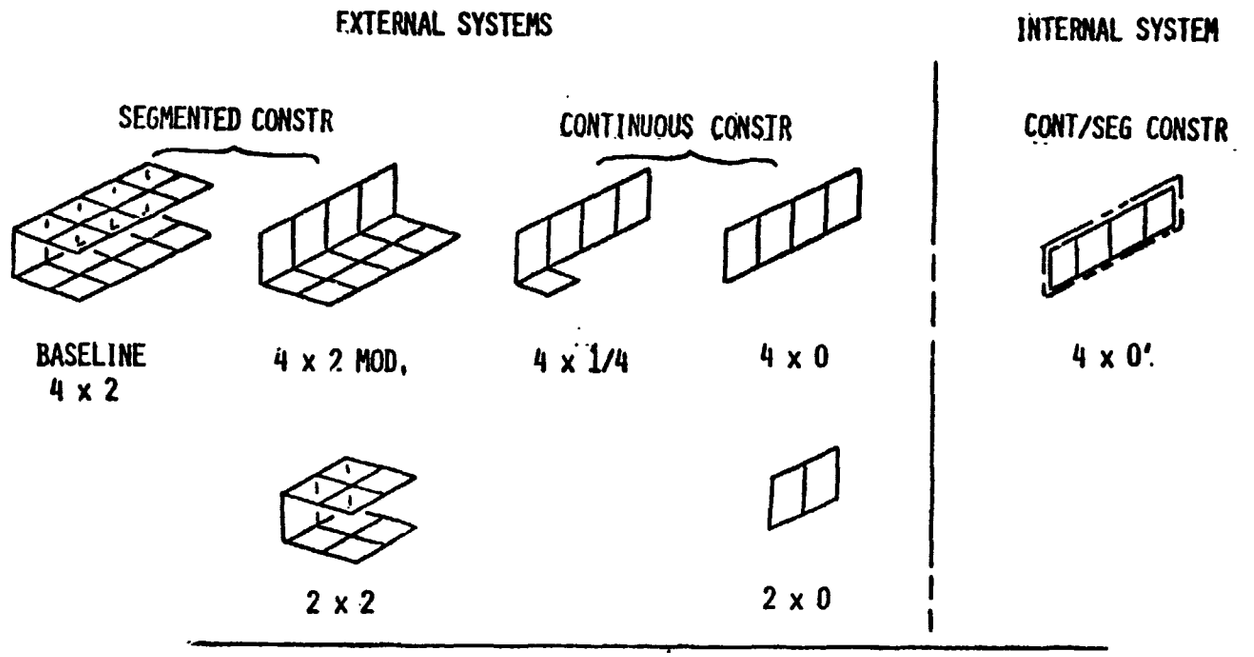

Figure 1.2.1-17 Alternate Construction Bases

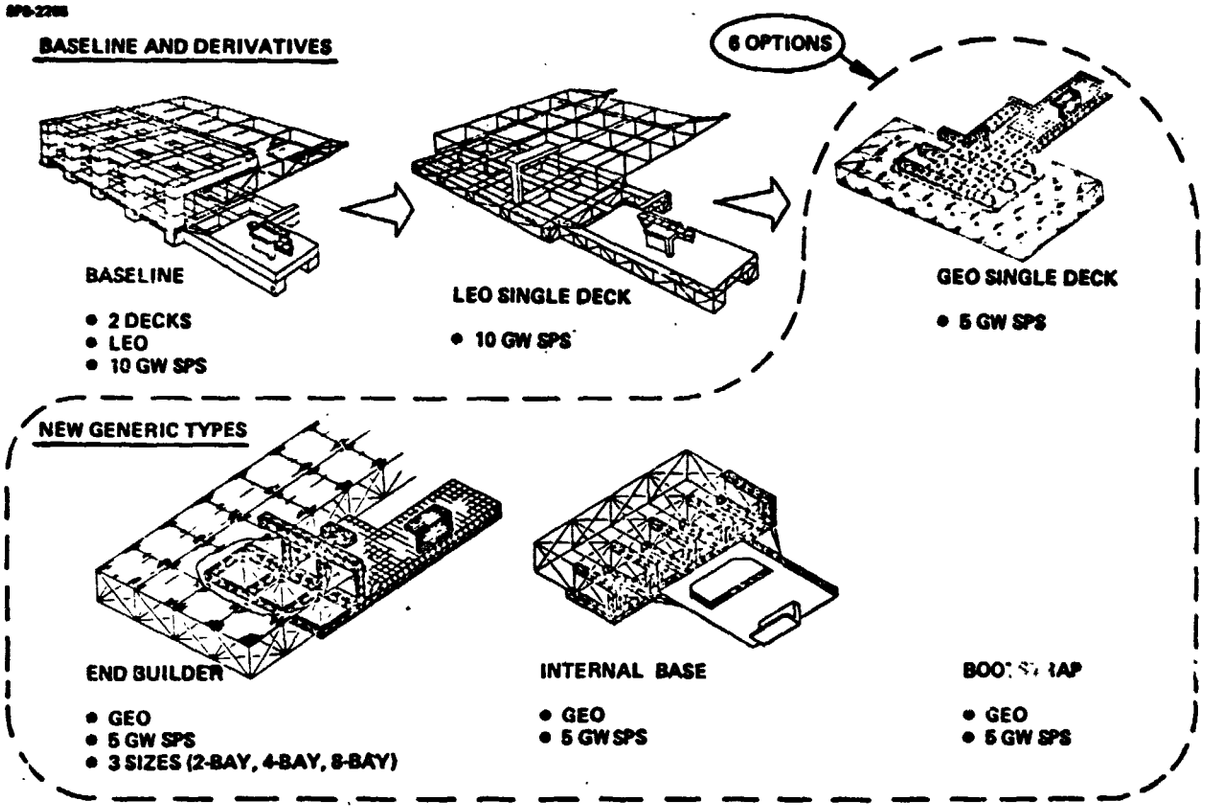

Figure 1.2.1-18 Alternative Construction Concepts

–Subsystem installation operations (solar array deployers, microwave subarray deployers, etc.).

–Crew support.

o Base/module interface loading during satellite build-up.

1.2.1.4 End Builder Construction Concept Characterization

1.2.1.4.1 End Builder Construction Requirements and Issues

1.2.1.4.1.1 End Builder Satellite Construction Options

Several options for building the SPS with continuous structural beams are shown in Figure 1.2.1-19. The end builder construction base has been allowed to vary in size from 8 bays wide (maximum) to 2 bays wide (minimum) to permit identification of critical aspects in the production buildup of the baseline SPS. In addition, [illegible] configurations were examined (i.e., alternate SPS aspect ratio = 8 and the small LEO constructed module) in order to assess the interaction of base-size and SPS configuration.

The baseline 8 X 16 bay SPS can be constructed by using either 8 bay wide, 4 bay wide, or 2 bay wide construction bases. The large 8 bay wide end builder constructs the satellite on a single pass. It can install the antenna at the beginning or the end of power collection module construction. The other bases require 2 or more passes to complete the satellite and can phase the antenna installation to coincide with either the mid point or completion of power collection module construction. The 8 bay wide and 2 bay wide options encompass the lowest and highest levels of production activity to meet the 6 month build cycle.

The two remaining options address alternate SPS designs which favor single pass production buildup for the 4 bay wide option. The LEO constructed modules also require that the antenna be installed normal to the direction of construction.

1.2.1.4.1.2 Typical End Builder Structural Assembly Sequence

The end builder construction system is tailored to the structural cross section of the satellite and uses dedicated beam machines to automatically fabricate continuous longitudinal members. Additional beam machines are needed to fabricate the other required lateral and diagonal members used in the structural assembly. A typical

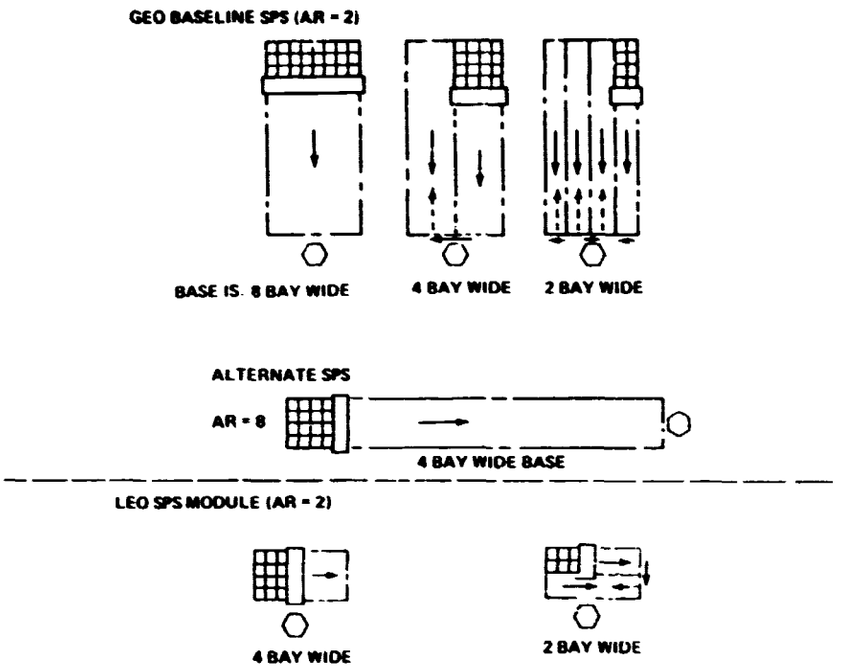

Figure 1.2.1-19 End Builder Satellite Construction Options

assembly sequence is shown in Figure 1.2.1-20 for the first construction pass of a 2 bay end builder. It is also typical for a 4 bay and 8 bay end builder.

As shown, the assembly process begins with step 1, when the first frame is built up on the longitudinal members. The structural members of the frame can be fabricated by separate beam machines; located next to each longitudinal member or with mobile beam machines that travel from one position to the next. The upper and lower horizontal beams are fabricated in parallel and then positioned for assembly. As these members are being joined, the beam machines are pivoted and the other members of the frame are fabricated as needed to complete the assembly. Step 2 indexes the frame for one bay length by fabricating the continuous longitudinal beams from dedicated beam machines. In Step 3, the next frame is built as in Step 1. During these three steps, power busses and solar array blankets can be installed in parallel. If solar array blankets are to be deployed in the direction of build, they are fed out as the structure indexes. If they are laterally strung, then the structure is indexed incrementally and blankets strung across the structure, from the base, at each increment. Longitudinal busses are installed "on the fly" as the structure is indexed; lateral busses are installed before a bay is indexed.

Step 4 fills in the bay structure with diagonal beams to complete that structure. This bay is then indexed, as in Step 2, and the whole process repeated until the solar array structure is built.

1.2.1.4.1.3 Structural Joints During End Building Construction

Several types of structural joints can be adapted to the end builder construction process. Figure 1.2.1-21 illustrates three types of joints which could be used at the intersection of structural beams. The preferred joint is termed a 'nodal fitting.' Here, the continuous beam caps are uninterrupted and the pitch of the lateral posts maintained. In the appropriate bay of the beam, diagonals are replaced by a fitting which provides an anchor point for the pin jointed ends of the other intersecting beams. This anchor point is at the centroid of the continuous beam, and the tubular end of each other beam is aligned with the centroid of that beam. The lengths of tube ends will be dictated by access to the fitting past the continuous beam members. Ground fabrication of the fitting, with folding of its legs for launch, seems feasible.

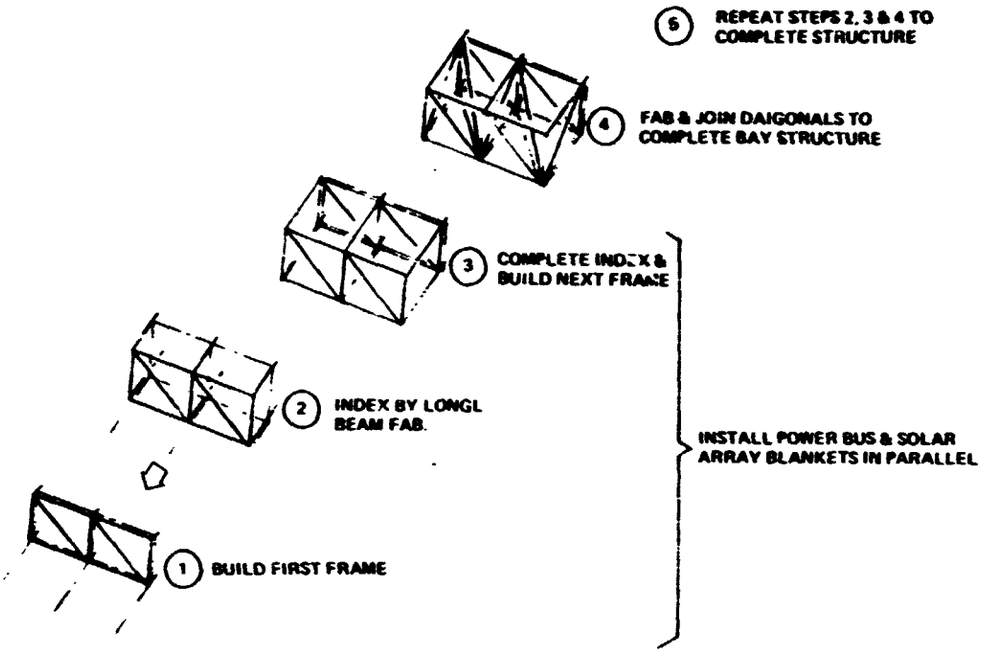

Figure 1.2.1-20 Typical End Builder Structural Assembly Sequence

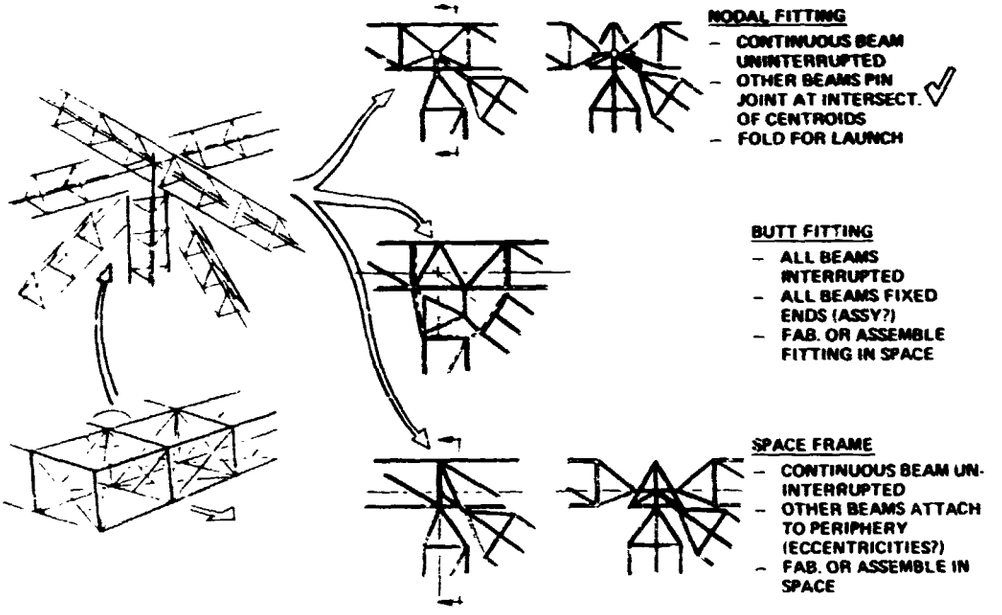

Figure 1.2.1-21 Structural Joints During End Building Construction

A second joint option provides for butt joining the beams ends. All beams are interrupted to accommodate a comprehensive fitting which presents a face to each intersecting beam for it to butt and attach to. Such a joint would demand adjustment of each butting face to accommodate eccentricities, etc., in each beam. The fitting itself would be either space fabricated, or ground fabricated in pieces and space assembled. It would be volumetrically inefficient to launch the completed fittings from the ground.

The third option shown is a space frame that does not interrupt the continuous beam caps. It replaces one set of lateral posts. Lateral and diagonal beams attach to points on the periphery of the frame. These attachments may be either pinned or fixed joints. The joints are located so that the end load in each beam is aligned with the centroid of the continuous beam. Eccentricities or misalignments of the beams will result in torsion in the continuous beams. This frame would also be space fabricated, or ground fabricated in pieces and space assembled.

1.2.1.4.1.4 Automatic Beam Fabrication Requirements

The end builder construction performance is keyed to the expected output rates of future automatic beam machines and the synchronized operation of multiple longitudinal beam machines. The following paragraphs discuss longitudinal beam fabrication and synchronized indexing.

Longitudinal Beam Fabrication Requirements. Beam fabrication and satellite indexing are closely related in the end-builder construction operations. The longitudinal beam builders provide the driving force to index the satellite structure, while performing their basic function of beam-element fabrication. This end builder characteristic leads to the necessity for certain requirements shown in Figure 1.2.1-22 regarding beam builder performance. Those requirements identified to date are:

- Limit startup and shutdown accelerations to insure that beam builder subsystem machinery will safely sustain forces induced during indexing. Include the affect of mass differences in the 2, 4, and 8-bay end-builder configurations as well as the progressive mass increase in the satellite under construction.
- Provide for synchronized indexing. Tolerances in the simultaneously operating beam builders produce variations in beam builder forces during indexing. These variations shall be limited to safe levels as determined by allowable forces not only on subsystem machinery but on the base structure and satellite structure as well.

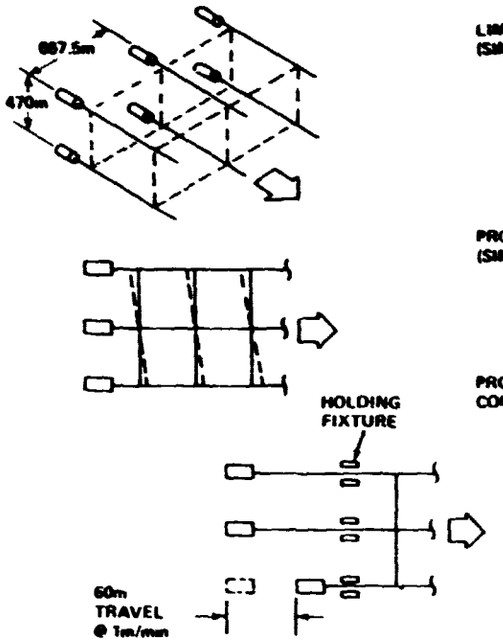

LIMIT STARTUP & SHUTDOWN ACCELERATIONS (SIMILAR TO SINGLE-DECK SATELLITE INDEXING)

ISSUES FOR STUDY:

- LOADING COND'S. (C.G. OFFSET, S/A TENSION, ETC)
- IMPACT OF LOADS ON:
  - BASE & SATELLITE STRUCTURE
  - BEAM-BUILDER S/S OPERATION
- CENTRALIZED CONTROL

PROVIDE FOR SYNCHRONIZED INDEXING (SIMILAR TO SINGLE-DECK SATELLITE INDEXING)

- CONTROL TOLERANCES GENERATE BASE/SATELLITE INTERFACE LOADS
- CENTRALIZED CONTROL

PROVIDE FOR CONTINUITY OF CONSTRUCTION OPS

- RELIABILITY/REDUNDANCY
- 60 MIN REPAIR TIME
- ON LINE/OFF LINE MAINTENANCE & REPAIR

Figure 1.2.1-22 Longitudinal Beam Fabrication Requirements

- Design for construction continuity in the event of a beam builder failure. Emphasis shall be placed on reliability of subsystem machinery including redundant operating modes, where possible, to avoid beam builder shutdown. In addition, consideration should be given to subsystem designs that limit repair time to approximately 60 minutes, while the shutdown beam builder tracks along at the same rate as the indexing structure. Holding fixtures to facilitate on-line/off-line maintenance and repair shall also be considered.

It should be noted that the above requirements for limitation of accelerations and for synchronization apply to any base assembly function where simultaneity of operation is critical, including the use of multi-indexers driving simultaneously to propel either the base (in the end-builder construction approach) or to propel the satellite (in the single-deck construction approach). For all such functions, centralized control is necessary to limit locomotion forces to acceptable values.

Synchronized Indexing. Control tolerances in the simultaneously operating longitudinal beam machines generate interface loads between the base and satellite as a function of the satellite's structural stiffness. If it is assumed that one of the beam machines has a slightly higher output rate than the rest, this rate difference can be seen as a difference in beam length and can be treated as a deflection induced on the satellite structure.

A preliminary study of beam synchronization requirements suggests that the control technique presently used within the beam machine itself to synchronize the 3 cap rates can also be used to control multiple machines by increasing the number of feedback control loops to include all caps in those machines operating simultaneously. Assuming tolerance levels achieved to date in the GAC/MSFC (NAS 8-32472) beam builder, estimates of beam length differences between machines are derived and shown in Figure 1.2.1-23. The induced loads shown are based on deflections imposed on an elastic structure idealized in the curve also included in the figure. (Beam properties used were E = 20,000,000 PSI and A = 3.75 in^2). Preliminary load values computed are given parametrically based on the frequency (7.5m, 5.0m, and 2.5m) with which recalibration checks in the control system are performed. For example, a slotted hole spacing of 7.5 m along the caps limits the accumulation of error in the encoder device to .533 cm max. This deflection produces a maximum load of 2670 newtons which, for the present, is well under the 13000 N allowable.

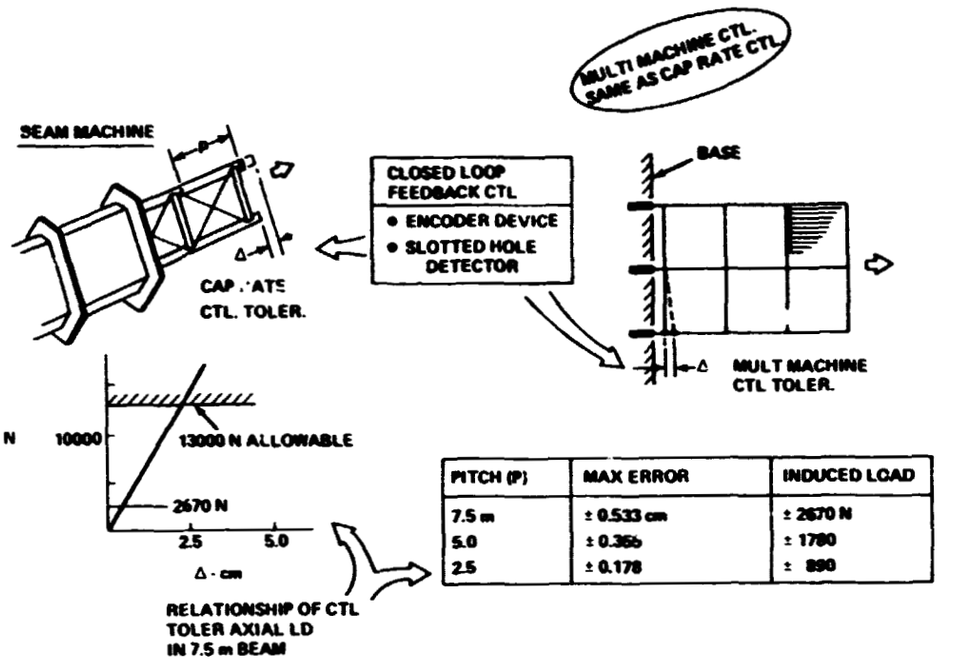

2955-020V

Figure 1.2.1-23 Synchronized Indexing

It should be noted that the effects of thermal gradients in the construction base, which are a necessary consideration in this kind of analyses, have not been included.

1.2.1.4.1.5 Satellite Support During End Builder Construction

As presently conceived the L shaped facility for building the solar array carries beam machines on one leg of the L and supports for emerging structure on the other leg. As illustrated in Figure 1.2.1-24, disturbance of the structure already built will result in moments reacted by end loads in the beams and beam machines and by shears reacted by the supports on the other leg. The beam machines also provide the forces for indexing the structure, as it is built, by fabricating the longitudinal beams. The capability of the beam machines to provide the forces necessary to react disturbance torques and to index the assembled satellite structure requires further study.

Three options are presented in this figure for relieving the beam machines of this function. Option 1 adds on-line indexing mechanisms to the process of fabricating the longitudinal beams. These synchronized mechanisms are dedicated to indexing the beams and to reacting disturbance end loads similar to the indexers used on the single deck baseline. Shears are still reacted by the leg supports. Option 2 adds a leg to the top of the L to make a C section base. Thus, the structure has supports on two opposite faces which react all disturbance loads and index the structure. The third option extends that leg of the base which mounts the supports. Additional supports are provided on the extension at one bay distant from the originals. These two sets of supports react all disturbance loads and index the structure.

1.2.1.4.1.6 Solar Array/Structure Assembly Methods

Four methods are shown in Figure 1.2.1-25 for coupling the installation and deployment of solar array blankets with the end builder structural assembly sequence. The baseline solar array segments are oriented normal to the continuous longitudinal beams. Hence, the arrays may be either installed during progressive stop-and-go beam fabrication operations (i.e., built 15m length-deploy array-built 15m, etc.), installed in series with the completed structural bay (as in the segmented build-up approach), or installed during synchronized operations with continued beam fabrication. A unidirectional method is also shown which aligns the solar array segments with the direction of construction. In this method, all the solar arrays in the bay can be automatically deployed, as the beam fabrication process continues from one frame to the next frame. Reorienting the arrays in this manner, however, requires the satellite to be

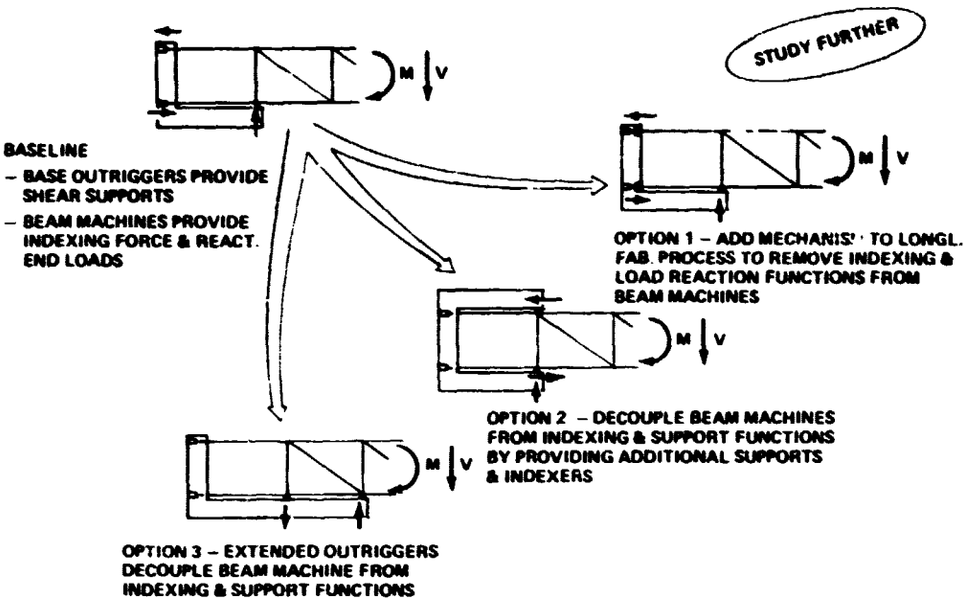

2955 055V

Figure 1.2.1-24 Satellite Support During End Builder Construction

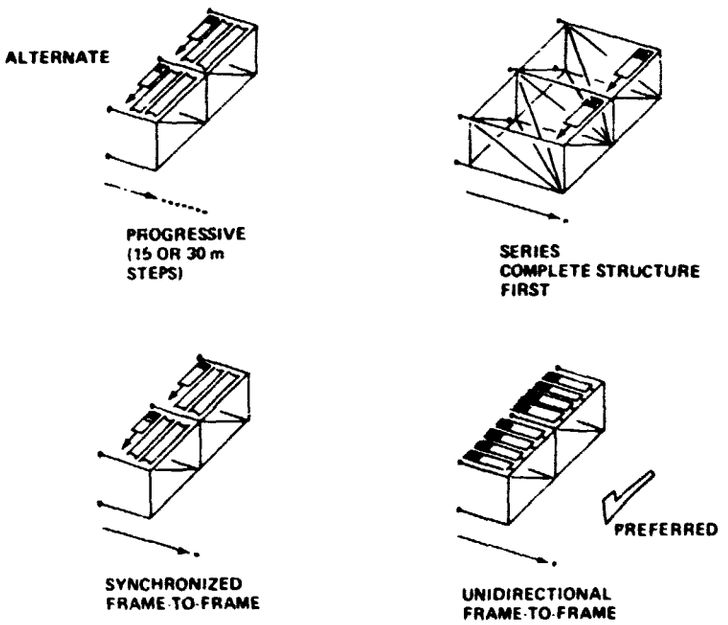

2955 056V

Figure 1.2.1-25 Solar Array Structure Assembly Methods

designed with a different power bus routing. Boeing analysis indicates that the power bus can be rerouted with no weight penalty.

The unidirectional solar array/structure assembly method is preferred because it allows shorter construction times to be achieved while also permitting significantly slower rates for thin film solar array blanket deployment. This method requires the least equipment to implement. The progressive method of assembly is the alternate approach since it can also be implemented with little impact on construction base design. Both methods are illustrated in Figure 1.2.1-26.

Further discussion of solar array blanket installation requirements and the comparative assembly methods are provided below.

Solar Array Blanket Installation Consideration. The solar array installation method must deal with the mechanical and electrical requirements for hooking up the opposite ends of each blanket and the required rate of deployment. The baseline solar array installation cycle, shown in Figure 1.2.1-27, takes 82 minutes, which includes 55 minutes for attaching and connecting the trailing edge (TE) and the leading edge (LE). The trailing edge connections are made in parallel as the leading edge deploys. With the blanket oriented normal to the direction of construction it must be deployed at a faster rate than if it were aligned with the emerging longitudinal beams. High rates of deployment are generally undesirable since they impose increased braking requirements during extended blanket deceleration. The baseline deployment rate of 12.5 mpm can be reduced significantly by aligning the solar array segments with the direction of build-up. Reorienting the arrays also requires the power distribution system to be designed with multi-busses in lieu of the baseline centerline bus.

Solar Array/Structure Assembly Comparison (128 Bays). The four assembly methods (progressive, series, synchronized, and unidirectional) are compared in Figure 1.2.1-28 in terms of their structural fabrication methods, blanket installation direction, required deployment rates, solar array installation equipments, construction base impact and related satellite impact.

Approximately 148 days are available for constructing the power collection module, within the specified six months, when yoke assembly, antenna/yoke mating and final test and check out are considered. The required rates for fabricating the longitudinal

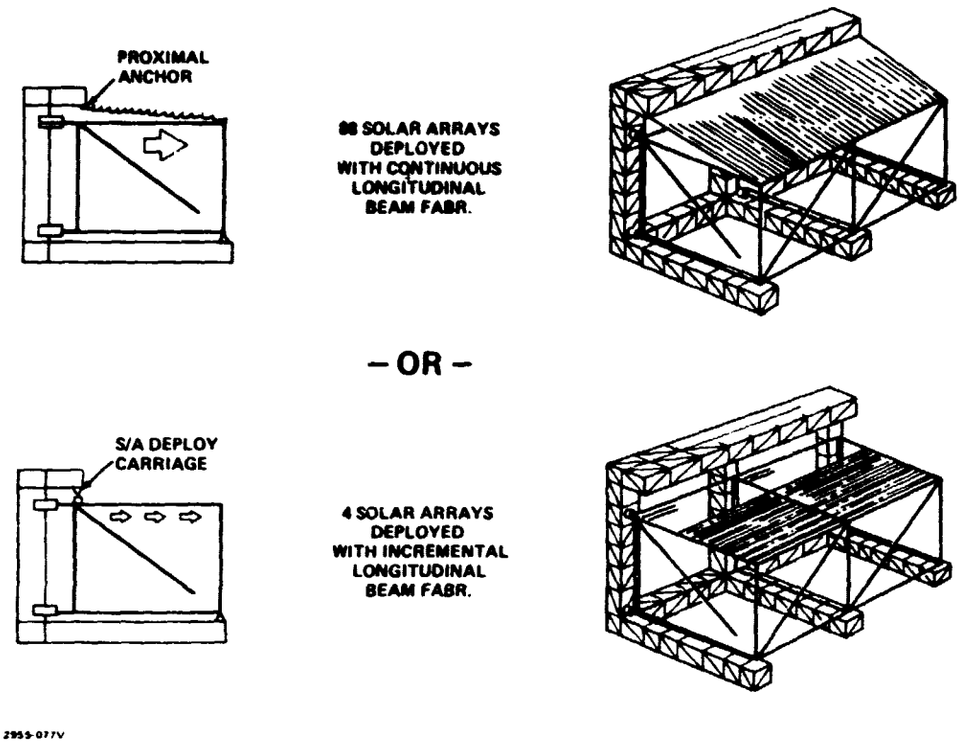

Figure 1.2.1-26 End Builder Frame Assembly/Solar Array Deployment (Coupled Operations)

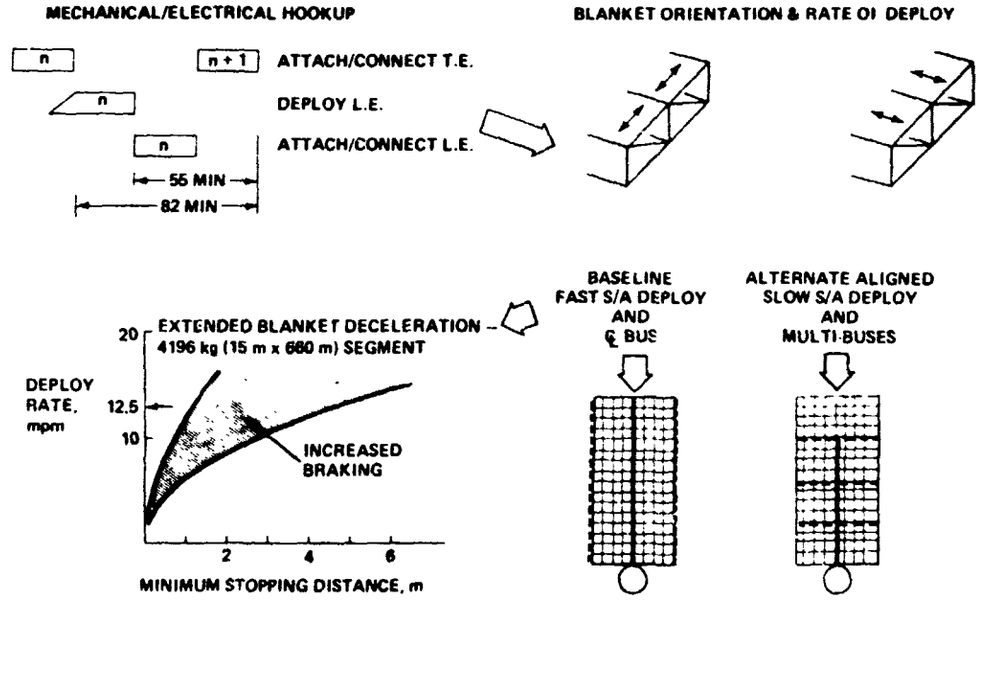

Figure 1.2.1-27 Solar Array Blanket Installation Considerations

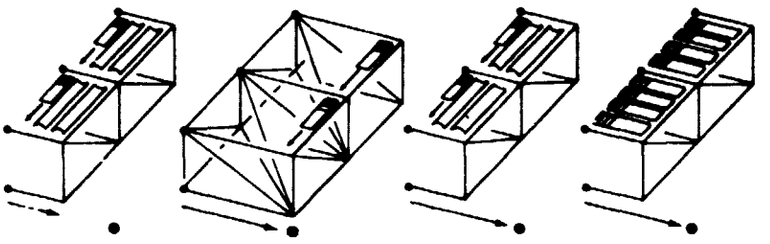

ASSY METHOD	PROGRESSIVE	SERIES	SYNCHRONIZED	UNDIRECTIONAL
STRUCTURAL FAB	15 m STEPS	COMPLETE BAY	FRAME-TO-FRAME	FRAME-TO-FRAME
BLANKET INSTALLN	BASELINE-LAT.	LATERAL	LATERAL	ALIGNED
148 DAY INDEX/DEPLOY 8-BAY WIDE RATES (mpm) 4-BAY WIDE RATES 2-BAY WIDE RATES	(L. BEAM & S/A) 0.17 & 12.5 0.36 & 12.5* –	(L. BEAM & S/A) 0.17 & 12.5 0.36 & 12.5* –	(L. BEAM & S/A) 0.09 & 5.8 0.18 & 12.3 0.42 & 28.4	(L. BEAM & S/A) 0.12 & 0.12 0.54 & 0.54 1.47 & 1.47
S.A. INSTALL. EQUIP.	INSTALLERS & DEPLOYER	INSTALLERS, DEPLOYER & CROSS BAY GANTRY	INSTALLERS & DELOYERS	INSTALLERS
CONSTR BASE IMPACT	STRAIGHT TRACK LEDGE	667 m SUPPORT ARMS	CURVED RETURN TRACK OVERHANG	STRAIGHT TRACK LEDGE
SATELLITE IMPACT	STRUCT. – TBD	STRUCT. – TBD	STRUCT. – TBD	STRUCT. – TBD PWR BUS – NONE

*DEPLOY 2 BLANKETS/BAY

ALTERNATE

PREFERRED

2955-058V

Figure 1.2.1-28 Solar Array/Structure Assembly Comparison (128 Bays)

beams and deploying the solar array blankets in 128 bays are shown for the 8 bay, 4 bay, and 2 bay wide construction bases. The analysis includes the time for fabricating and assembling satellite frames and diagonal supports and performing solar array mechanical and electrical hook-ups. It should be noted that the longitudinal beams are fabricated at much lower rates than the 5 mpm rate used to fabricate laterals and diagonals. For the cases examined, it was not possible to apply either the progressive or series methods for the 2 bay wide base since it took too long to accomplish. Both the synchronized and unidirectional methods, however, were able to work within the available time. The unidirectional method exhibits the same low rates, of course, for beam fabrication and blanket deployment. Therefore it was selected for the 2 bay base design. The alternate progressive method of assembly was also analyzed for the 8 bay and 4 bay base designs to demonstrate that it could be made to work in 6 months.

The unidirectional method is also attractive for the 4 bay and 8 bay designs because it requires the least equipment and has little impact on the construction base. Recent Boeing analysis has indicated that the satellite power bus can be reconfigured with no weight penalty. An assessment of structural impact due to end builder construction methods and realigned solar blanket preloading remains to be performed.

1.2.1.4.1.7 End Builder Antenna Installation Concepts

Several options were investigated for locating the antenna construction site. These options included top deck (horizontal and canted), back side, and rear deck (forward and lateral pass) as shown in Figure 1.2.1-29. The top-deck horizontal, originally selected as the baseline approach because of base size and weight consideration, was later discarded because of undesireable off-site antenna assembly procedures necessitated by this approach. The top-deck canted concept exhibits the same problems. The back side approach required excessive antenna handling and was also discarded. The rear deck - forward pass has the desireable feature of in-line antenna handling, however the slide-through feature imposes critical requirements for satellite support and satellite clearance and further the construction base to be greater than 2-bays wide. The preferred approach is the rear deck lateral pass because of its in-line characteristic and its much simpler mating procedure. After mating the antenna, the base is indexed clear of the antenna in a simple, straight forward manner.

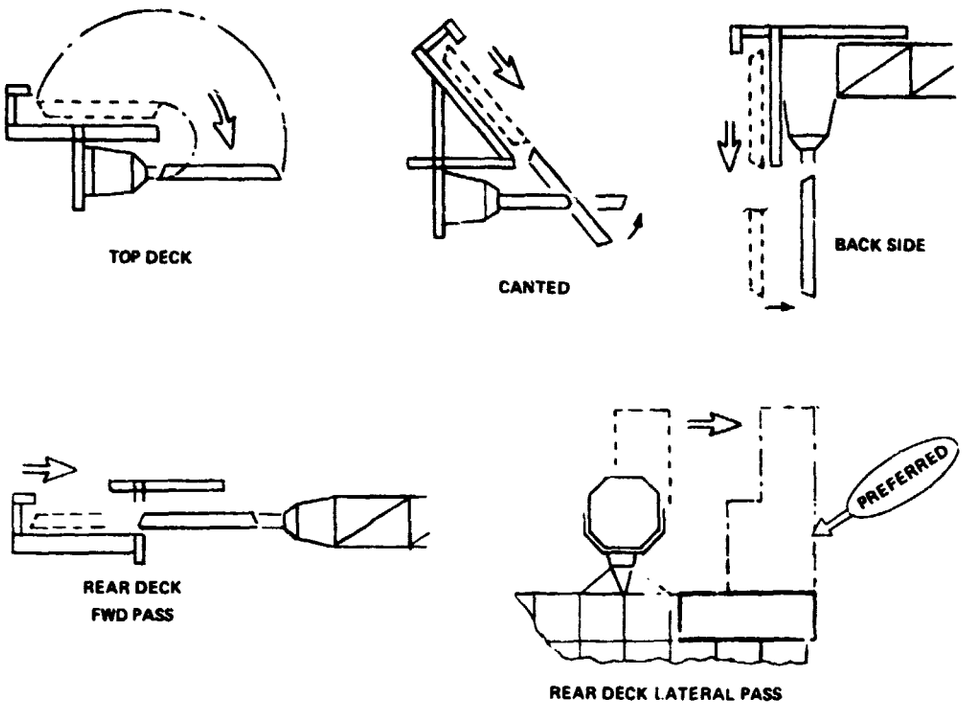

Figure 1.2.1-29 End-Builder–Antenna Installation Concepts

1.2.1.4.2 End Builder Concepts and Capabilities

End builder concepts were defined for the construction of the baseline, 8 x 16 bay, SPS. The configurations derived were classified as 2-bay, 4-bay, and 8-bay construction bases (shown in Figure 1.2.1-30) and their operational capabilities were investigated. Production buildup methods for the satellite's primary structure and onboard systems were established for purposes of deriving timeline, crew size, equipment count, cost, etc., data.

The basic differences in overall operations of the three bases shown lie in the number of "passes" required to construct the satellite. The 2-bay base builds the satellite in four passes; the 4-bay base in two; and the 8-bay base in one. Described below are the major system characteristics for each of the three bases.

1.2.1.4.2.1 2 Bay End Builder

The main feature of this base are listed in Figure 1.2.1-31. The baseline SPS is constructed by multiple passes of this end builder, which builds a 2-bay wide strip, 16 bays long, then indexes over to build successively, three more strips. Construction system characteristics include the cost, mass and crew information presented at the Phase I Final Briefing. Major construction equipment for the solar array module are also itemized and the impact on satellite design are identified.

The following paragraphs discuss the 2-bay base satellite construction sequence, base arragnement, construction system, satellite construction approach and antenna/yoke mating. Most of these characteristics apply as well to the 4-bay and 8-bay end builders.

2 Bay - Construction Sequence. The 2-bay base uses longitudinal and lateral indexing rails to construct the 8 x 16 bay satellite in 4 successive passes. After completing the first 2-bay wide strip, the base is indexed laterally (2-bays) as shown in Figure 1.2.1-32 and then longitudinally (16 bays) to begin, at that point, the second pass. Note that the antenna is constructed in parallel. This procedure is repeated until the power generation and distribution system structure and subsystems are completed.

At the end of the 4th pass, the antenna, yoke, etc., are also completed. The base is then indexed laterally to a position with the antenna on satellite centerline. Mating operations are then begun to transfer the antenna mass from the construction base to

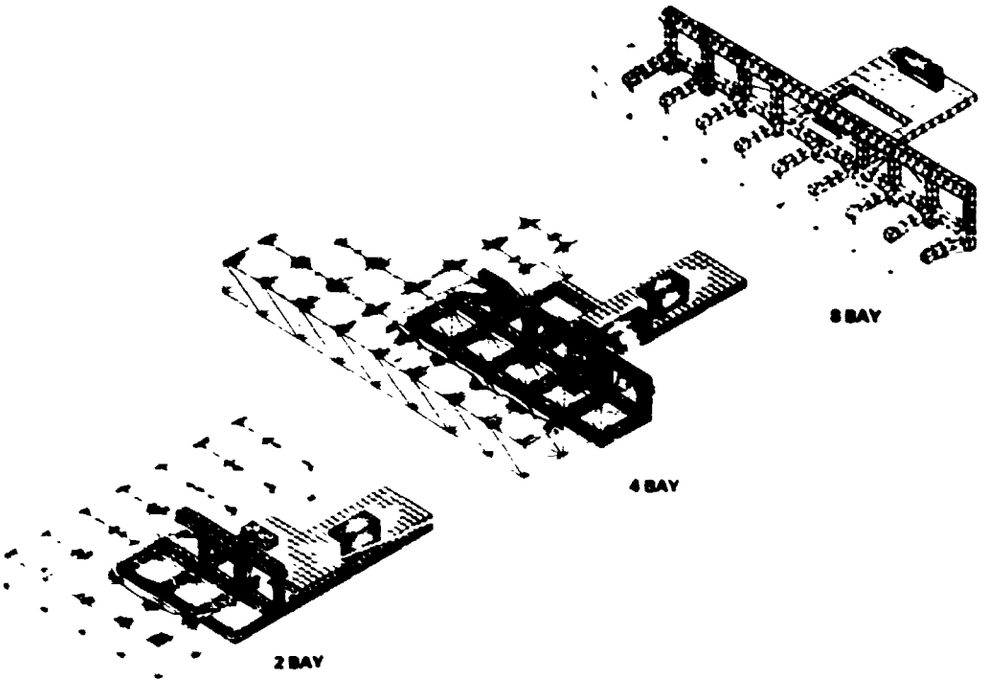

Figure 1.2.1-30 End Builder Construction Bases

- MULTI-PASS CONSTR. OF 8 x 16 BAY SPS
- CONSTR. SYS
  - UNIT COST (1977 $) = $8.63B
  - SIZE L x W x H = 3.37 x 2.05 x .76 km
  - MASS
    - STRUCTURE = 2.40 x 10^6 kg
    - TOTAL BASE = 5.74 x 10^6 kg
  - CREW TOTAL = 383
- ARRAY MODULE CONSTR. EQUIP.
  - BEAM MACHINES = 9
  - CRANE/C.P. = 11
  - INDEXERS = 5
  - BUS DEPLOYERS = 1
  - SOLAR BLANKET DEPLOYERS = 0
- SATELLITE DESIGN
  - SOLAR ARRAY ORIENTATION = LONGITUDINAL
  - LONGITUDINAL BEAMS = CONTINUOUS

Figure 1.2.1-31 2-Bay End Builder Base Features

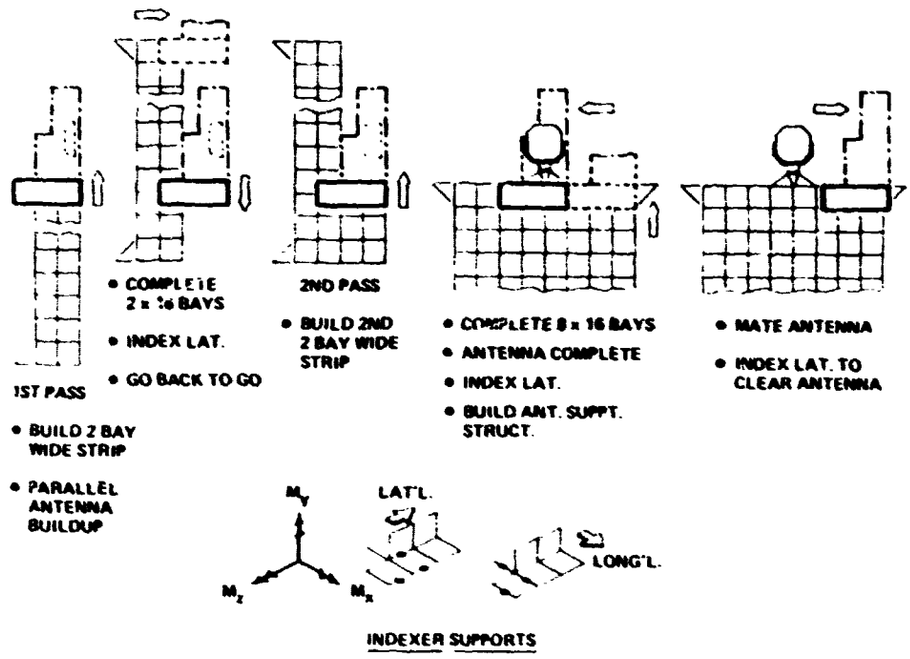

Figure 1.2.1-32 2-Bay End-Builder—Construction Sequence (Update)

the satellite. When the antenna is completely mated the base is then indexed away from, and clear of, the antenna.

2 Bay-Construction Base. The 2-bay end builder construction base shown in Figure 1.2.1-33 builds an 8-bay wide SPS, 16 bays long in four passes. The only difference from the SPS baseline configuration is the continuous, rather than segmented, fabrication of all longitudinal beams. Solar arrays are deployed parallel to the longitudinal beams and the antenna facility conforms to all aspects of the baseline antenna construction scenario, except that it includes a yoke fabrication and assembly area.

While defined as a 2-bay base, its width (2050m) encompasses a 3-bay segment of the power collector structure to provide a one bay overlap for lateral and longitudinal indexing operations. The 760m high base, built in the form of an open truss "L" - shaped framework, is sufficient to house necessary equipment and machinery to construct the power collector module. The antenna construction site is located at the rear of the base, making the total base length 3370m although only approximately 800m is required for power collection module construction. A short platform extends into the antenna work area to facilitate rotary-joint assembly which is described further below.

2 Bay-Construction System. Major equipment functions and their specific locations in the base are identified in Figure 1.2.1-34. A 60 m travel distance is provided for the longitudinal beam builders to permit on line maintenance and repair in a 60-min period (assuming a fabrication rate of 1m/min).

The two views shown represent what is probably the most active location in the base. The 12.7 m beam machines gimbals 180 degrees to provide the required S/A support beams, while nearby a mobile (track mounted) 7.5 m beam machine is shown at its mid point of travel between one end of the base and the other. In addition, the 7.5 m longitudinal beam machine, bus installer and solar array implacement equipments are shown.

2 Bay-Construction Approach (Primary Structure). The production buildup of the power collection module starts with assembly of 7.5 m and 12.7 m structural tri-beams. Figure 1.2.1-35 depicts major beam installation activity at each frame-station

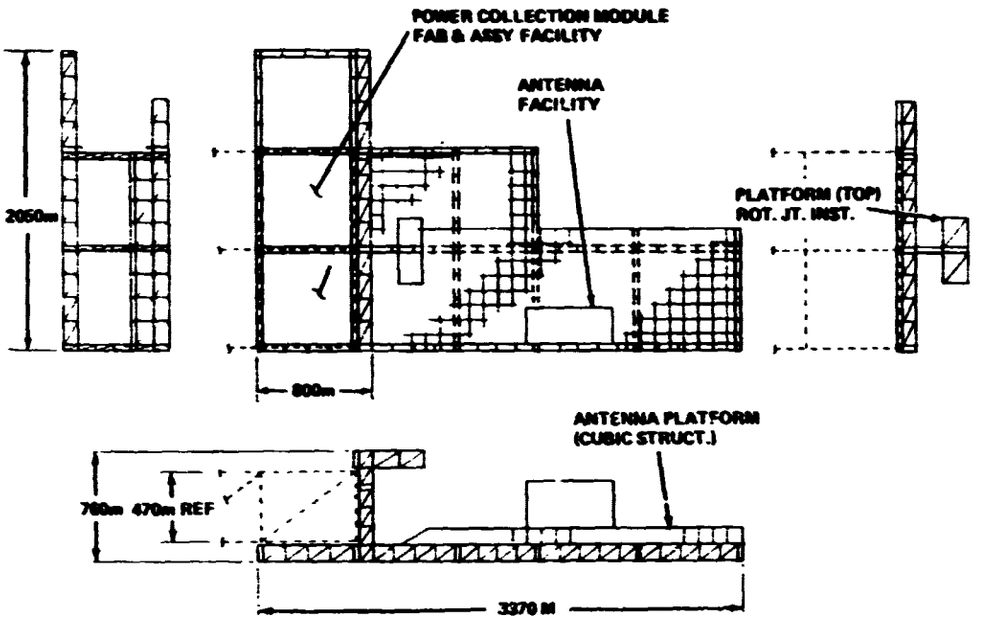

Figure 1.2.1-33 2-Bay End-Builder—Construction Base (Revised)

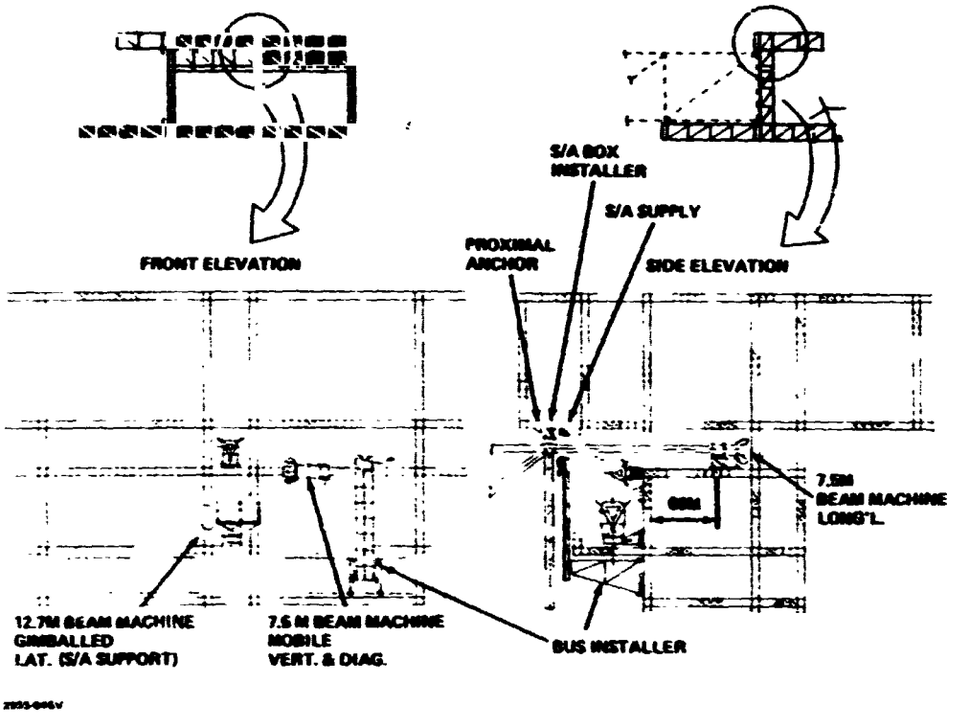

Figure 1.2.1-34 2-Bay End-Builder—Construction System

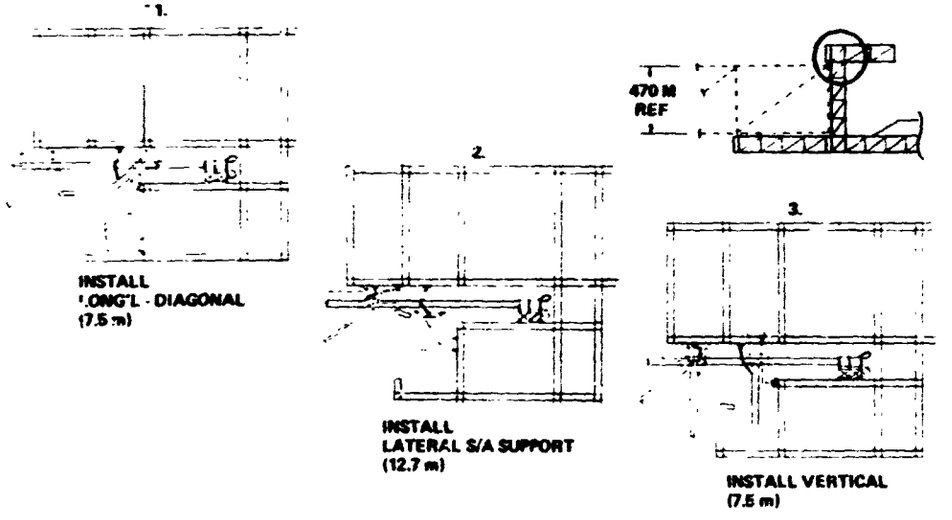

Figure 1.2.1-35 2-Bay End-Builder Construction Approach (Pri Struct)

with the forward longitudinal-diagonal (7.5 m) being installed before the lateral S/A support beam (12.7 m) to facilitate cherrypicker accessibility and mobility in the end-attachment process. The 12.7 m beam machine shuttles up and down on a short length of track to preclude interference with the beam machine producing the vertical beam elements. The beam elements in the plane of each frame (verticals, lateral diagonals, and lower-transverse elements) are installed last and complete the structural buildup of each bay.

2 Bay-Construction Approach (Solar Array). The installation of solar arrays shown in Figure 1.2.1-36 occurs at the same work station in the base as the assembly of in-plane structural frame elements, described above, to obtain maximum time-line benefits from parallel activities.

Subsequent to the installation of a 12.7 m solar array support beam, the cherrypicker removes a S/A box from the supply crib shown and fastens it to the proximal anchor. The distal-end of the blanket is then connected to the beam. When the frame has been indexed one bay away, the blankets are fully deployed and the box is removed from its anchor support fittings and fastened to the next 12.7 m support beam to complete the cycle.

2 Bay-Antenna/Yoke Mating. With the antenna facility in its revised location in the construction base shown in Figure 1.2.1-37, antenna mating operations are performed after the completion of the 8 x 16 power collection module. The antenna is constructed in parallel with the S/A so that after the 4th pass, it is ready for installation. At the end of the 4th pass, the base is indexed to the left 3-bays to put the antenna in the S/A centerline. The interface structure between rotary joint and solar array is attached in incremental steps to permit the base to gradually transfer the antenna mass while indexing itself away from, and clear of, the antenna.

1.2.1.4.2.2 4 Bay End Builder

The main features of this base are shown in Figure 1.2.1-38. The baseline 8 x 16 bay SPS is constructed in two successive passes by the 4-bay end builder. The construction system characteristics, major equipments and the impact on satellite design are also identified in the figure.

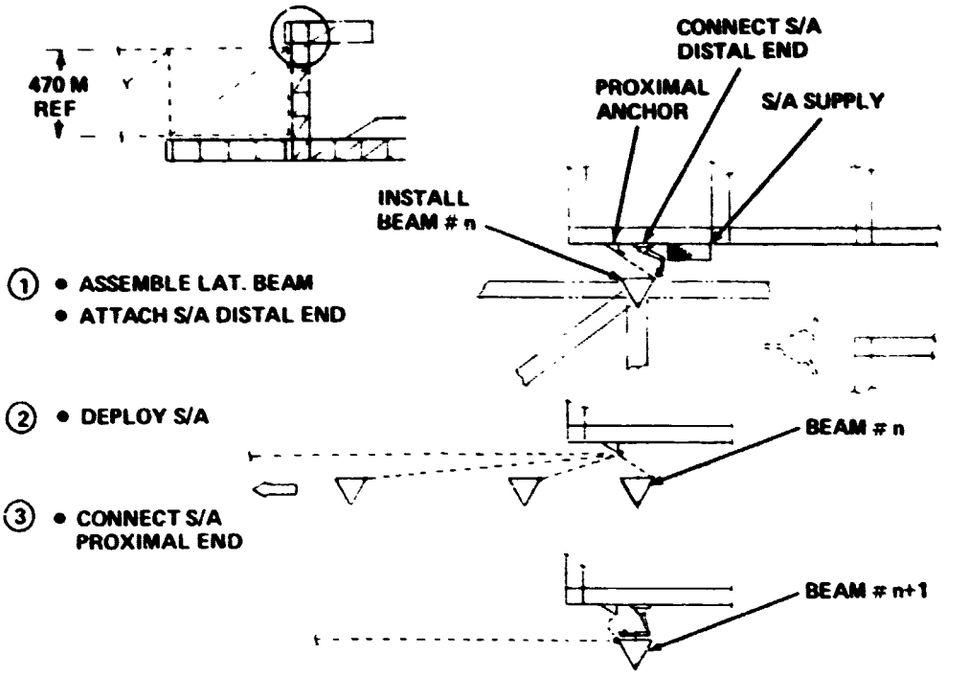

2955 064V

Figure 1.2.1-36 2-Bay End-Builder Construction Approach (Solar Array)

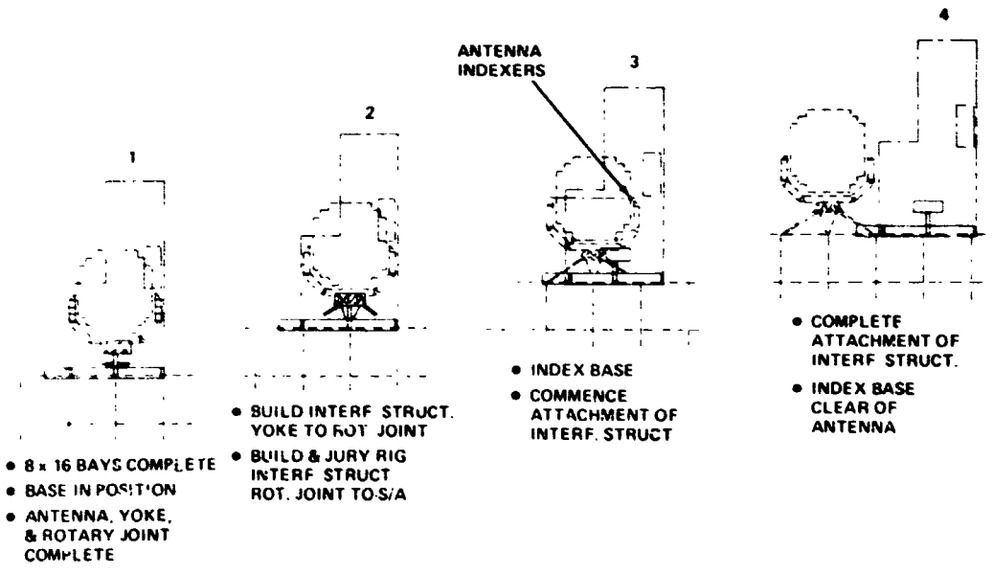

Figure 1.2.1-37 2-Bay End-Builder Yoke Con. · ction/Antenna Mating (Revised)

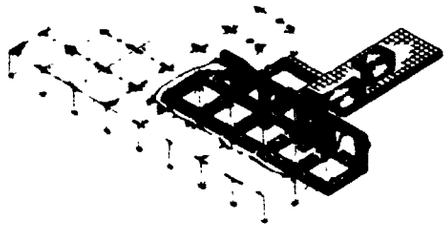

- MULTI-PASS CONSTR. OF 8 x 16 BAY SPS
- CONSTR. SYS
  - UNIT COST (1977$) = $9.07B
  - SIZE L x W x H = 3.88 . 2.96 x .70 km
  - MASS
    - STRUCTURE = 2.93×10^6 kg
    - TOTAL BASE = 6.37×10^6 kg
  - CREW TOTAL = 386
- ARRAY MODULE CONSTR. EQUIP.
  - BEAM MACHINES = 13
  - CRANE/C.P. = 11
  - INDEXERS = 4
  - BUS DEPLOYERS = 1
  - SOLAR BLANKET DEPLOYERS = 0
- SATELLITE DESIGN
  - SOLAR ARRAY ORIENTATION = LONGITUDINAL
  - LONGITUDINAL BEAMS = CONTINUOUS

Figure 1.2.1-38 4-Bay End-Builder Base Features (Update)

2055-071V

This 4-bay base operates very similarly to the smaller 2-bay wide end builder. Solar arrays are deployed in the direction of build. The antenna construction platform conforms to the baseline in area but includes a yoke construction facility. This base mates the antenna to the solar array in the preferred location with the antenna aligned with the longitudinal centerline of the solar array.

Construction of the solar array takes place in an L-shaped facility, shown in Figure 1.2.1-39 (2.96 Km long with 700 m and 360 m wide legs). This facility is constructed from the joining of square section open truss beams, provisionally sized at 100 m per side. Mounted on the 700 m deep leg are such construction equipments as beam machines and handling devices, solar blanket installation facilities, and bus installation mechanisms, as well as habitation, docking, storage, etc. Beam machine and solar blanket installations are similar to the 2-bay end builder. The other leg of the facility guides and supports the longitudinal beams of the SPS until the bay structure is completed and self supporting.

The antenna and yoke construction platform is mounted at a distance from the solar array facility to provide an area in which the rotary joint and mating structure can be built. It is also located so that during second pass construction, the first pass solar array structure does not foul the antenna under construction. When the antenna and yoke have been built, they are assembled to the rotary joint. The mating structure to the solar array is then built, but not completed at its solar array end. This entire assembly is then indexed along the backface of the solar array facility until one set of legs of the mating structure is at the mating overhang for structural completion of those legs and mating to the solar array. The base is now indexed outboard so that the center mating legs can be completed and attached in the mating overhang. This sequence of indexing and mating is repeated to complete the mating of the solar array and antenna assemblies. Indexing of the base, laterally across the solar array, is continued until the base is separated from the satellite.

1.2.1.4.2.3 8 Bay End Builder

This base builds the baseline SPS in a single pass and is shown in Figure 1.2.1-40 and 1.2.1-41. The 8-bay base as shown includes a pre-midterm antenna construction facility. Satellite antenna mating operations are performed with a "forward-pass" hand off, rather than the "lateral-pass" hand off technique used by the 2-bay and 4-bay bases. The "forward-pass" hand off is conducted through the large opening in the "L" shaped

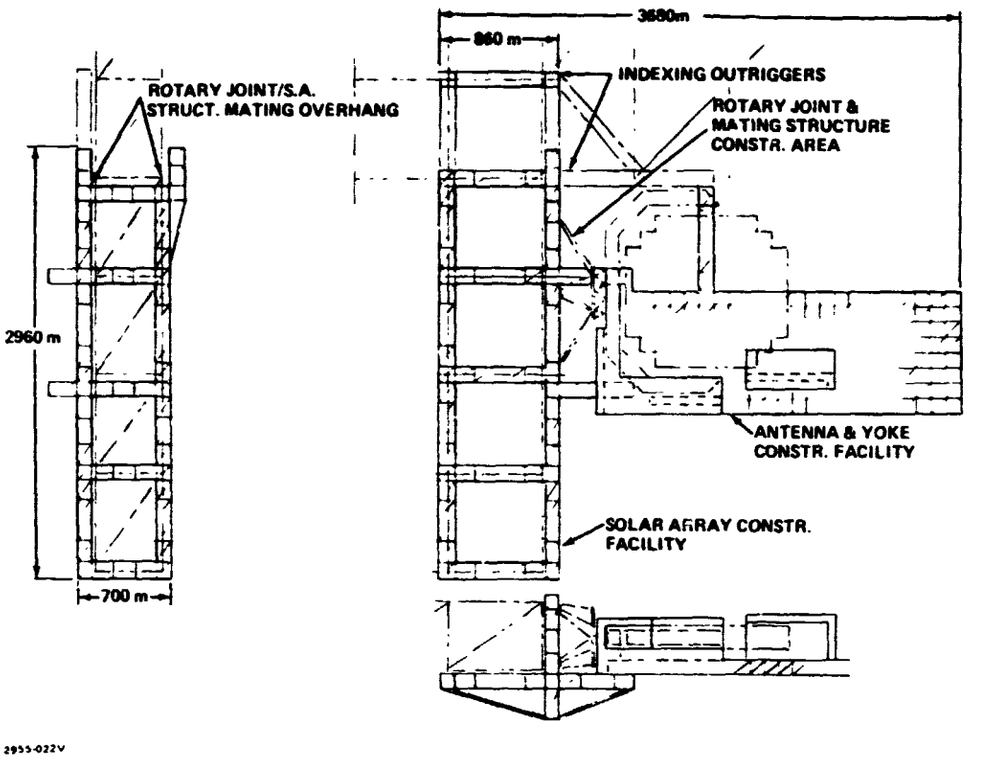

Figure 1.2.1-39 4-Bay End-Builder Construction Base (Revised)

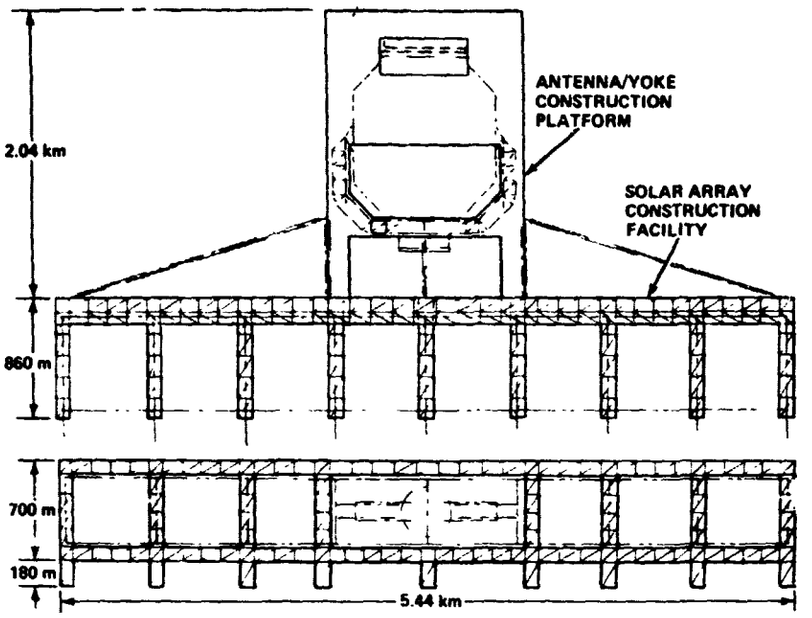

Figure 1.2.1-40 8-Bay End-Builder Construction Base

2636-031W

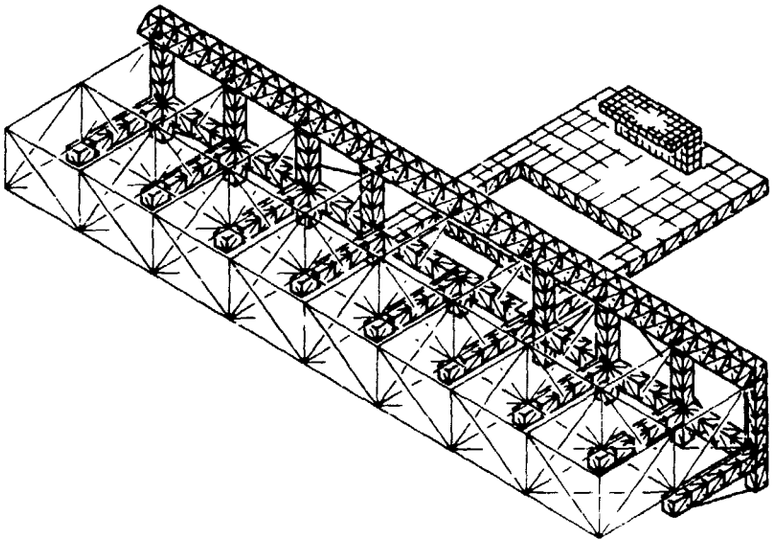

Figure 1.2.1-41 8-Bay End-Builder

2955 067V

structure. Other differences include the necessity for 18 dedicated longitudinal beam builders, and added cherry pickers to fully operate this wider facility.

1.2.1.4.2.4 Base Configuration Structural Analysis

Preliminary studies were made to assess the structural design of the end builder construction base during operations in geosynchronous orbit. Gravity gradient and indexing design conditions were examined for the 2-bay end builder during the construction of the baseline SPS satellite.

- Gravity Gradient Condition, Natural Frequency/Mode - Figure 1.2.1-42 shows the configuration evaluated for gravity gradient induced loads; the solar array is 4 by 16 bays, the construction base is in position at the antenna end and the microwave antenna fully constructed is located in the aft position of the base. Mass data and orbital orientation are as shown in the figure. A worst case gravity gradient torque was assumed with $\theta_2 = 45^\circ$ and $\theta_1 = 0$ was assumed.

  Figure 1.2.1-43 shows the free-body diagram of the solar array/construction base/antenna configuration. The control thrusters were assumed located as shown at each end of the construction base. The moment at the section A-A does not exceed the strength of a composite material beam.

  The frequency for the selected configuration shown in the previous figure was calculated using the given mass data. The stiffness data shown in Figure 1.2.1-44 was calculated for the Boeing selected composite cap member with an area of $8.065 \times 10^{-4} m^2$ and a modulus of elasticity of $1.378 \times 10^{11} N/m^2$. The array was assumed attached to the base at the indicated locations; the total antenna mass was located at its center of gravity.

  The results show the frequency of 0.0031 Hz is well above the required 0.00124Hz.

- Construction Base Indexing - Preliminary estimates were made of the loads acting on the end builder construction base during construction. The satellite array/antenna configuration is shown in Figure 1.2.1-45. Since the satellite mass is very much greater than the construction base, it can be assumed that the relative motion of the satellite is zero.

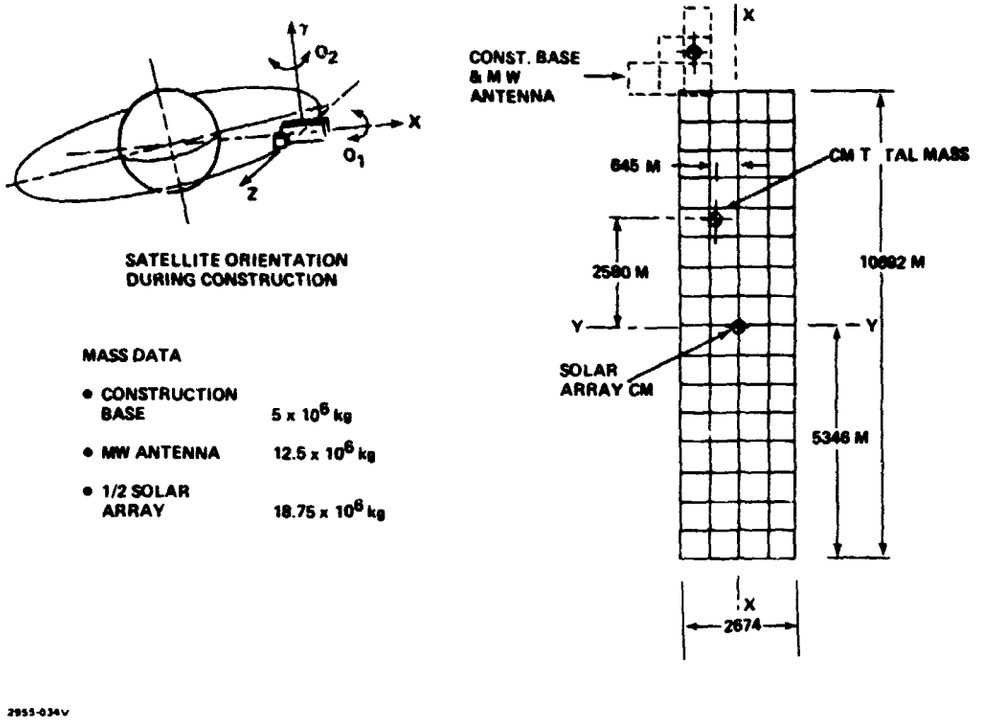

2955-034V

Figure 1.2.1-42 5GW SPS GEO Construction—End-Builder Gravity Gradient Condition

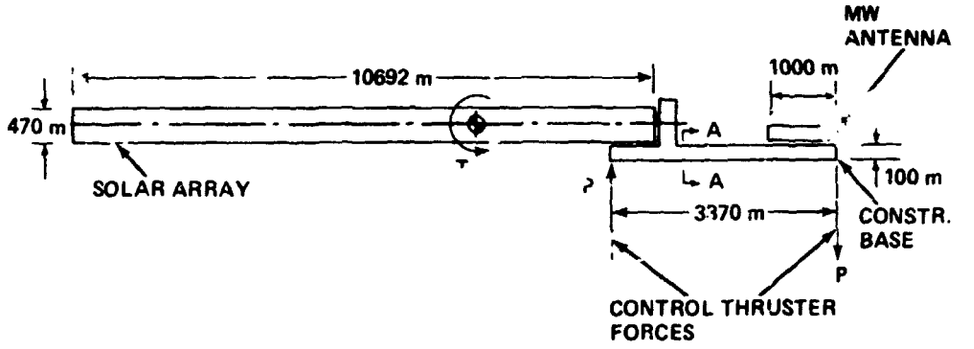

- ESTIMATED BENDING MOMENT AT SECTION A-A M = 1.46 x 10^6 Nm
- ULTIMATE LOAD PER BEAM CHORD MEMBER P = ± 4857 N
- LOAD NOT CRITICAL FOR CLOSED CHORD COMPOSITE MEMBER

Figure 1.2.1-43 5GW SPS End-Builder Construction Base Gravity Gradient Condition

2955-036V

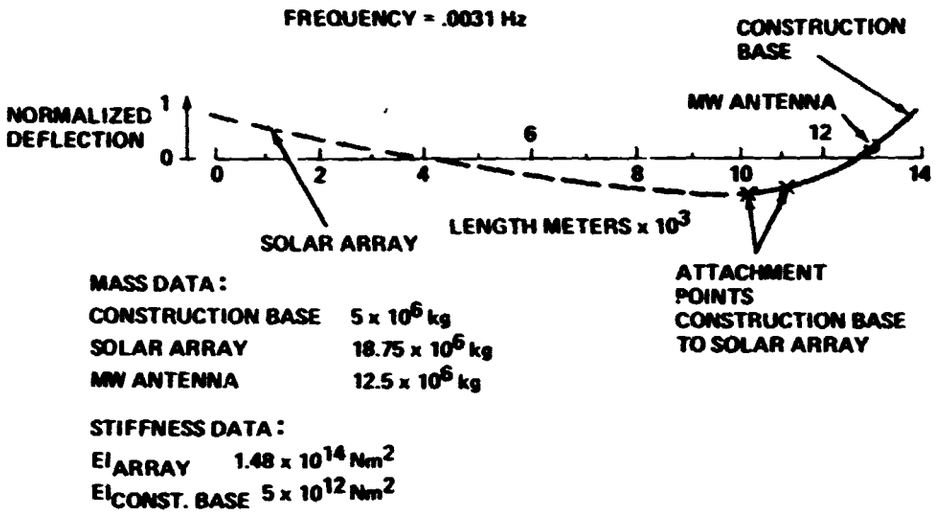

Figure 1.2.1-44 5GW SPS GEO Construction End-Builder Natural Frequency and Mode Shape

2955-037V

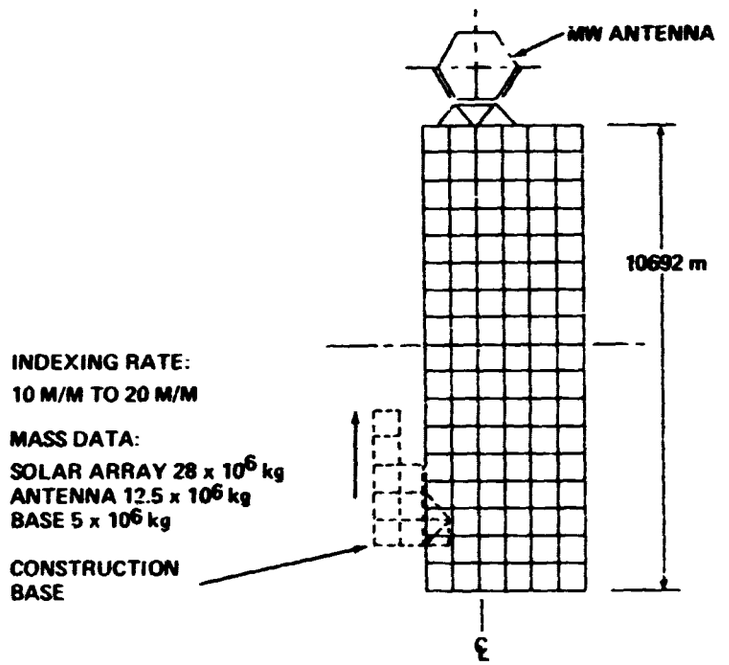

2955-039V

Figure 1.2.1-45 5GW SPS End-Builder Construction Base Indexing Condition

A force-time curve is shown in Figure 1.2.1-46 for an index rate of 20 m/minute. Additional study is required to evaluate the effect of the impulse on the construction base.

1.2.1.4.2.5 Timelines and Performance Potential

Throughout the Phase I study effort, emphasis has been placed on one over-riding ground rule; to complete 5GW satellite construction within 180 days ±5%. In meeting this requirement, the end builder timelines underwent several interactions in defining minimum crews and equipments to maximize base construction productivity. The major timeline parameters were revised during the course of the study only if needed to compare alternate construction methods and supporting rationale were available. The following paragraphs describe the evolution of timeline parameters, define the end builder timelines, and describe techniques for accelerating SPS construction operations with the end builder base.

- Evolution of Timeline Parameters - Figure 1.2.1-47 identifies the major timeline parameters and ground rules which have been updated since the Mid Term Briefing. The impact of these changes on the overall requirements for usage of crews and equipment are also provided. Some of the changes shown are interrelated. For example, as a result of a revised ground rule, whereby the reindex rate was increased from 1 mpm to 10 mpm, there was a significant saving in time. That time was applied to the solar array attachment phase, which could then be accomplished with less cherry pickers and crew.

  As a result of re-evaluating the manning requirements for the cherry pickers and the beam machines, there was a significant saving in manpower. The original ground rules specified that each cherry picker and each beam machine would be operated by a two-man crew, for reasons of safety and not necessarily due to operator workload.

  By orienting the solar array deployment longitudinaliy for the 4-bay end builder (similar to the orientation of the 2-bay end builder), it was possible to (1) delete the solary array deployer, (2) lower the solar array deployment rate from 12.5 mpm to 1 mpm, and (3) shorten the overall construction time.

- 2 Bay and 4 Bay End Builder Timelines - The end builder timelines are provided in Figure 1.2.1-48. As shown therein, the SPS assembly operations commence with

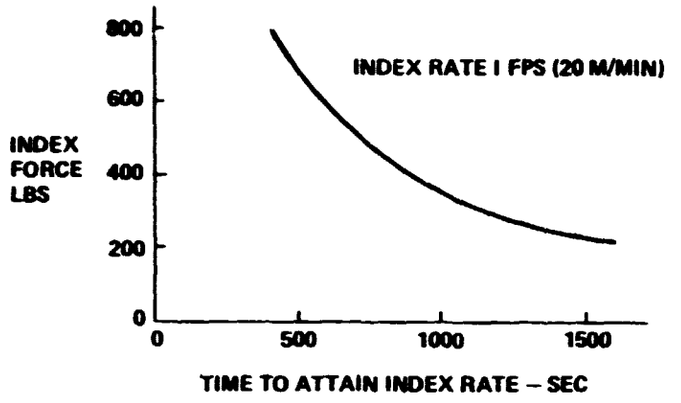

ASSUMPTIONS:

CONSTRUCTION BASE MASS IS A SMALL PERCENT OF TOTAL MASS; RELATIVE MOTION OF SATELLITE IS NEGLECTED

Figure 1.2.1-46 5GW SPS End-Builder Construction Base Indexing Force

2955-038V

	FACTOR	MIDTERM	FINAL	IMPACT
OPERATIONS	I.O.C.	180 DAYS	180 DAYS	
	ON-LINE MACH. FAB. RATE	AS REQD. (<5 mpm)	AS REQD. (<5 mpm)	NO CHANGE
	SEG-BEAM MACH. FAB. RATE	5 mpm	5 mpm	
	MATE ANTENNA	MIDPOINT OPS	FINAL OPS	AVOIDS EARLY START UP
	REINDEX RATE	1 mpm	10 mpm	REV. GRND. RULE – REDUCE TIME
	STRUCT. ASSY.	DEDICATED CPs (4BAY)	MOBILE CPs	REDUCE C & E
	SUB SYS. ASSY	UNDEFINED	4 DEDICATED CPs	ADDS CPs & CREW
	S/A ORIENTATION	LONG(2BAY)LAT(4BAY)	LONG (2 & 4 BAY)	REDUCE EQUIP., LOWER S/A DEPLOY. RATE, SHORT CONST. TIME
CREW	REMOTE WORK STATIONS	2 MEN/CAB	1 MAN & CHANGE-OVER	MIN. STAFFING REQT.
	AUTO. BEAM MACHINES	2 MEN/MACHINE	8 FIXED OR 4 GIMBLED OR 1 MOBILE/MAN	
EQUIPMENT	ON LINE MACH.	7.5 m FIXED	7.5 m FIXED	NO CHANGE
	SEG. - BEAM MACH.	DEDICATED	MOBILE	REDUCE EQUIP.
	INDEXERS	8 (2BAY)	5	CONFIG. UPDATE
	BEAM ASSY. CPs	6 CPs (2BAY)	4 CPs	MIN. SUPT. REQT.
	S/A ATTACH. CPs	6 CPs (2BAY)	4 CPs	USES TIME FROM 10 mpm INDEX

Figure 1.2.1-47 Evolution of Timeline Parameters

2955-079V

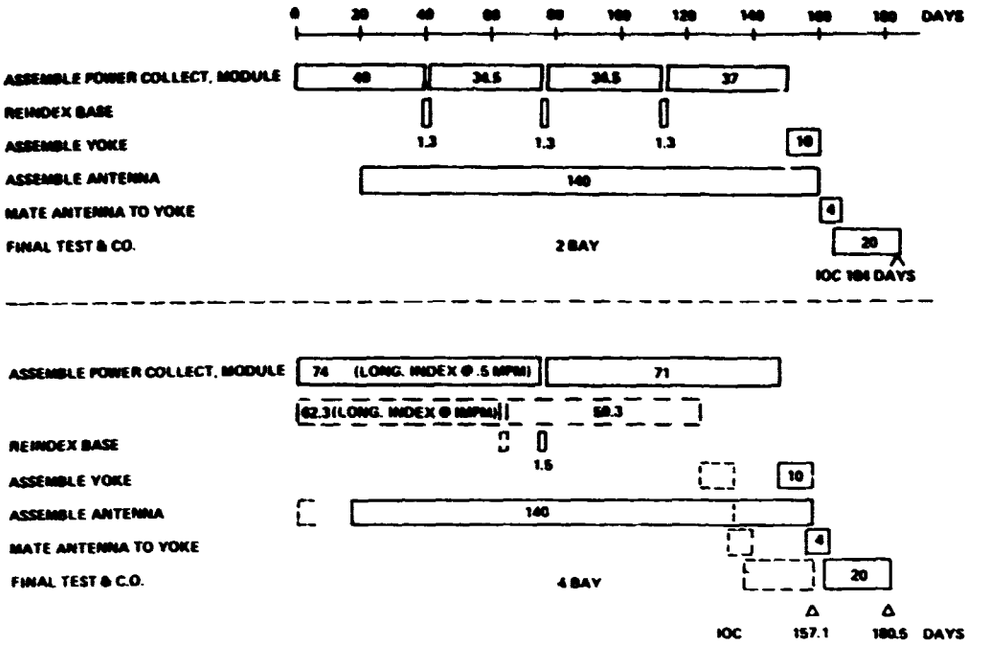

2955-040V *Figure 1.2.1-48 2-Bay and 4-Bay End-Builder Timelines*

the construction of the power collection module. For the 2-bay end builder, it is constructed in four passes through the construction base. Each pass provides a 2-bay by 16-bay submodule and reindexing occurs between passes. The first and fourth construction passes include the installation of thrusters. The centerline main bus is installed during the second pass, but that does not effect the timeline since it is installed in parallel with the fabrication of the longitudinal beams. The second, third and fourth construction pass are shorter than the first pass, because one side of the modules are common with the structure previously assembled and therefore two fewer beams are required. The fourth pass would require the same construction time as the second and third, except for the addition of the thrusters. After completion of the fourth pass, the yoke is assembled and then mated to the antenna, which was begun during the assembly of the first 2 x 16 power collection submodule. Allowing additional time for checkout, the total 2-bay end builder construction time is 184 days.

The 4-bay end builder operates identically to the 2-bay end builder, as shown in Figure 1.2.1-48. There are, of course, only two passes through the construction base, each pass providing a 4-bay by 16-bay submodule with only one reindexing pass. When the longitudinal beam fabrication occurs at 0.5 mpm, the total 4 bay end builder construction time is 180.5 days. However, if the longitudinal beam fabrication process is accelerated to one mpm, then the total construction time can be reduced to 157.1 days.

- 2 Bay End Builder Satellite Module Assembly Operations - Figure 1.2.1-49 illustrates the satellite module assembly operations for the 2-bay end builder. The assembly operations commence with the fabrication of short lengths of the longitudinal beams for implacement of the joints to which the lateral and diagonal beam segments of the end frame will be connected. Then, the 12.7 meter upper lateral beams for the end frame are fabricated and joined to the longitudinal beams. Next, the mobile beam machines begin fabricating the beam segments, which comprise the remainder of the end frame and simultaneously solar array canisters are anchored on the construction base and the distal end of the solar arrays are attached to the upper laterals.

  Upon completion of the end frame assembly and solar array attachment, the structure is indexed longitudinally. Meanwhile, the fixed beam machines fabricate the 667 meter longitudinal beams, the main bus is deployed (on the second pass) and the solar array panels are also being deployed.

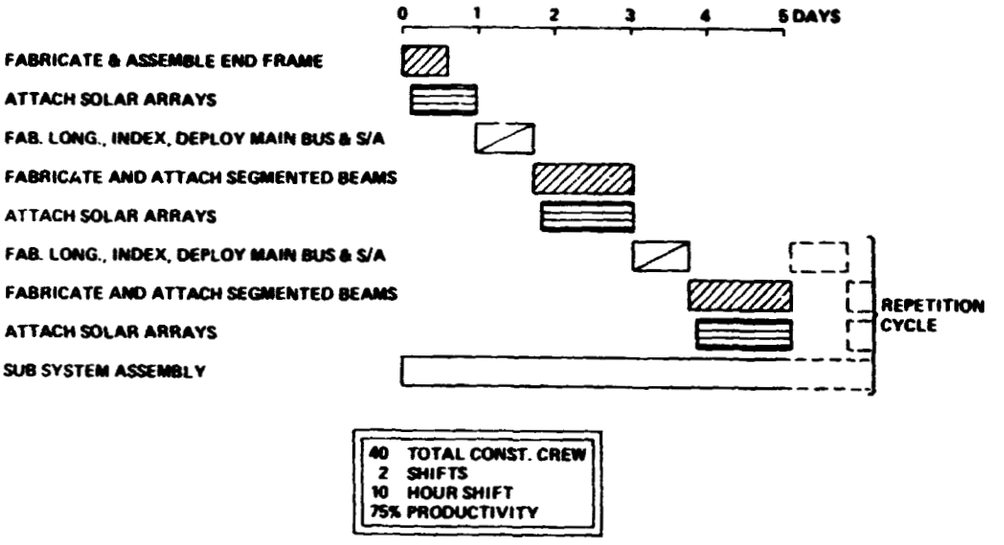

2955-074V *Figure 1.2.1-49 2-Bay End-Builder Satellite Module Assembly Operations*

After completion of the indexing phase, the upper lateral beam segments of the next frame are fabricated and installed. Then, collector busses and switches are attached. Next the solar array canisters are detached from the construction base, mounted on the upper laterals and the proximal ends are connected to collector busses. Simultaneously, new solar array canisters are anchored on the construction base and the distal ends are attached to the upper laterals and connected to collector busses. Finally, pigtails are installed across the upper laterals to provide electrical connection between busses. These assembly operations are repeated until the entire 2-bay by 16-bay module is completed.

- Techniques for Accelerating Space Construction Operations - The baseline configuration was a four-step, decoupled assembly approach. For that configuration, accelerating space construction operations can be accomplished by adding equipment to shorten the time required for any step (except the index phase) or by coupling operations, as shown in Figure 1.2.1-50.

  The end builder configuration uses a two-phase, coupled assembly approach. Those operations that can be accomplished, while the structure is being indexed, are grouped together in the first phase and the indexing rate controls the operation. Accelerating space construction operations in this phase cannot be accomplished by adding more equipment. It can only be done by increasing the indexing rate and yet it is limited by the maximum rate for fabrication of the longitudinal beams and deployment of the solar arrays and the main bus. During the second phase of the end builder construction approach, the controlling operation is the fabrication and attachment of the segmented beams. The amount of crew and equipment required for the solar arrays is adjusted to finish that installation concurrent with the segmented beam operation. Accelerating space construction operations during this phase requires a coordinated increase of equipment for both operations. For example, adding cherry pickers for solar array attachment will help to shorten the construction process until some other function becomes more critical. At that point, other types of equipment (e.g., beam machines) must also be provided.

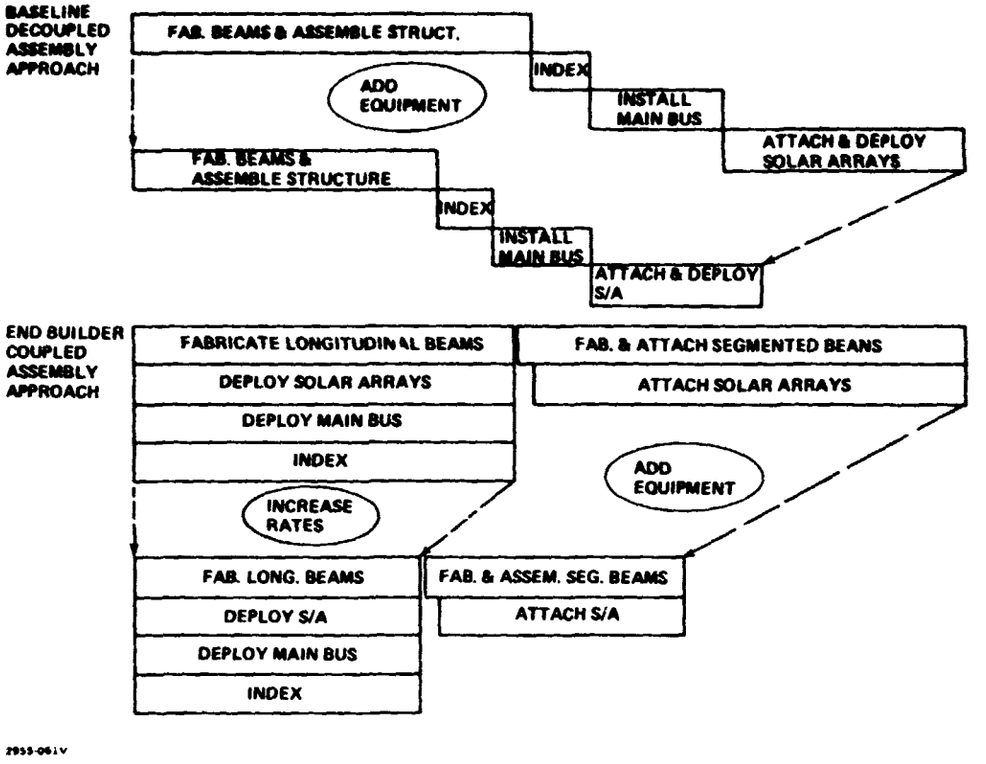

Figure 1.2.1-50 Techniques for Accelerating Space Construction Operations (Typical Cycle)

- End Builder Longitudinal Beam Production Capability and Benefits Fixed Crews and Equipments - In order to satisfy the ground rule which limits GEO assembly of the 5GW satellite to 6 months, it was necessary to operate with skeleton crews, use minimal equipments and slow the operating rates of on-line beam machines. The impact on total satellite construction time is shown in Figure 1.2.1-51 for various longitudinal beam fabrication rates with the 2-bay, 4-bay, and 8-bay end builder concepts. A significant reduction in overall construction time can be realized by simply operating these on-line machines a little faster, such as at 3.5 meters per minute rather than the .25 to 1.5 meters per minute shown at 180 days. It is not efficient to operate these machines at much higher rates since other construction operations are constrained by limited crews and equipments (e.g., for solar array hook up).

  The benefit of being able to shorten the construction time without adding additional crews and equipments can be reflected in reduced payments for construction interest. Using a daily interest rate of $2.7 M, the 4-bay end builder can complete construction 40d as early (at 3.5 m/min) at a saving of about $107M per satellite. Equivalent savings in construction interest are also shown for other fabrication rates for the three end builder concepts.

- End Builder Production Scale Up Potential - Added Crews and 30 Meter Cherry Pickers - The performance improvement that can be achieved by adding crews and equipments to the end builder concept is shown in Figure 1.2.1-52. Increasing cherry picker crews can speed up the solar array hook-up times. Both the 2-bay and 4-bay end builders are currently defined with 7 cherry pickers for solar array hook-up and structural assembly. The 4-bay end builder, however, could have been defined with 5 cherry pickers by relying upon a greater shared usage between these various solar array and structural assembly operations. Available resources, however, did not allow this option to be adequately explored to develop this multi-usage timeline further. Nevertheless, significant improvements in overall construction time can be achieved by increasing the crews and equipments in selective construction activities.

  The cost penalty for adding tnese crews and equipments is also shown in Figure 1.2.1-52. This cost penalty reflects the added costs for cherry pickers, crew modules, crew operations, and related transportation costs. The interest saved by

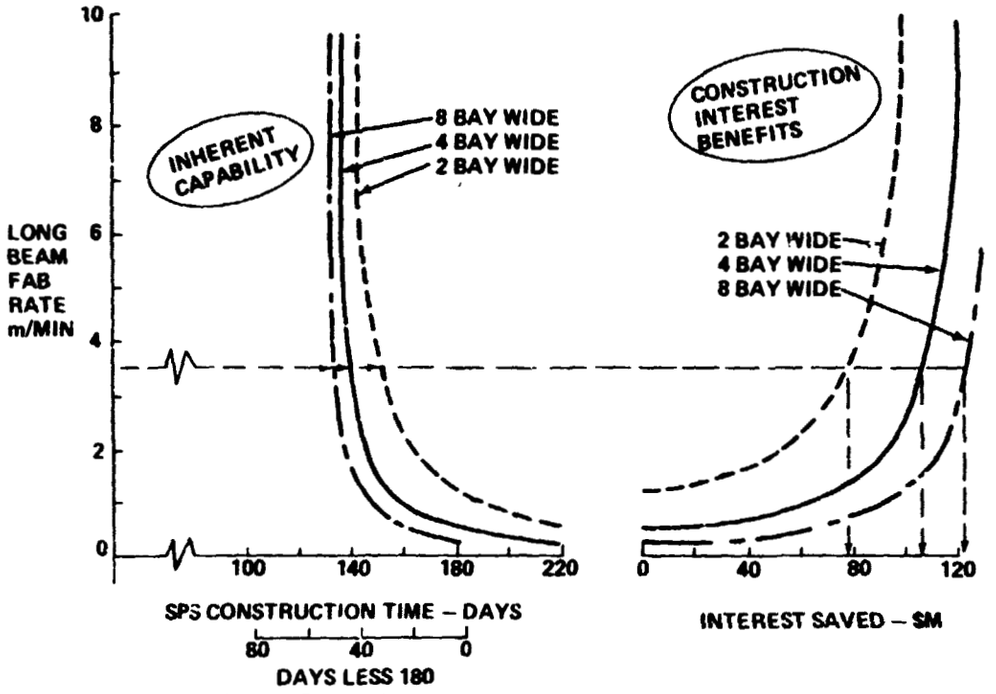

Figure 1.2.1-51 End-Builder Long Beam Production Capability and Benefits Fixed Crews and Equipment

2955-025V

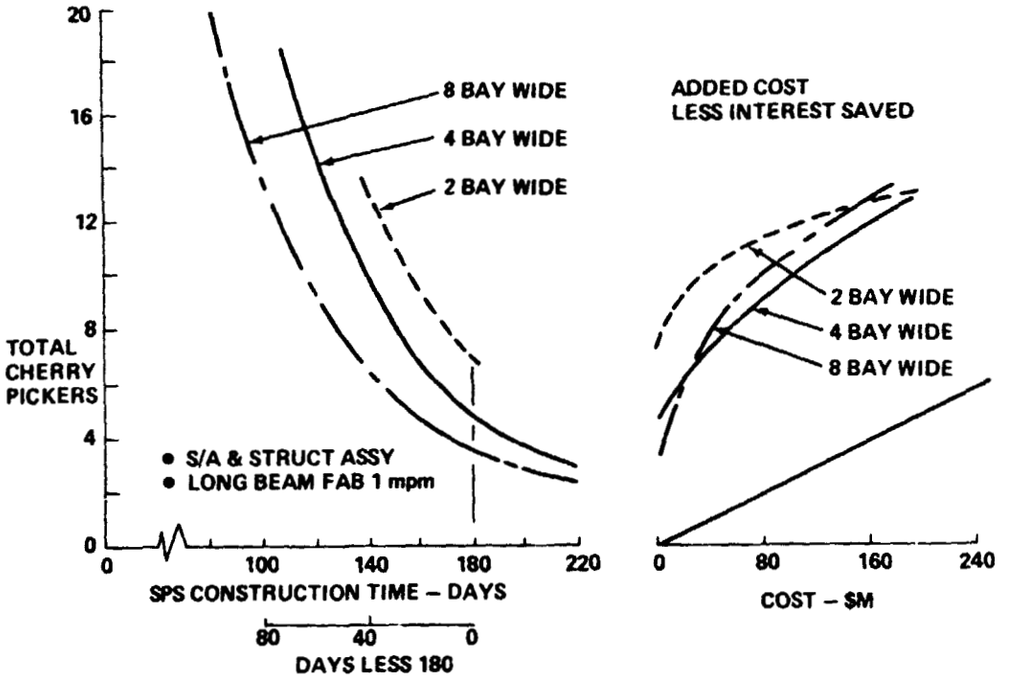

2955-027V

Figure 1.2.1-52 End-Builder Production Scale Up Potential Added Crews and 30 M Cherry Pickers

adding these additional equipments is also shown for each end builder in terms of the added cost, less the interest saved.

- End Builder Satellite Construction Potential - The cumulative effect of faster end builder production capabilities are illustrated in Figure 1.2.1-53. Assuming that the SPS program requires 10 GW to be added each year, then 30 years are needed to achieve 300 GW by constructing one 5GW satellite every 6 months. By operating the 4-bay end builder at 3.5 meters per minute, the same number of satellites could be completed at least 6-1/2 years sooner. This performance advantage can either be used to complete production sooner, build more satellites or be applied as a production schedule reserve to cope with unscheduled delays (i.e., weather, strikes, etc.)

1.2.1.5 Single Deck Construction Concept Characterization

At the end of the previous contractual SPS concept definition study, the baseline construction concept entailed construction of 8 SPS modules and the 2 antennas at a low Earth orbit (LEO) construction base. The LEO construction base was a C-shaped facility that had both upper and lower decks that provided surfaces from which construction equipment could operate. Going into the current study, it was recognized that the upper deck and back wall of the facility could be eliminated by using a mobile construction gantry that could be used to mount the construction equipment required at the upper surface.

This section presents the details of two versions of a single deck construction base concept: 1) a LEO single deck construction base, where 8 modules are constructed, and 2) a GEO single deck construction base, where a 5 GW monolithic SPS would be constructed. As these concepts utilize the construction techniques (frame assembly, solar array deployment, bus deployment) developed for the 2-deck construction base, the description of the single deck concepts does not describe these operations. It is expected that the reader can refer to previous contract documentation for details.

1.2.1.5.1 LEO Single Deck Construction Base Characterization

The reference satellite configuration to be constructed is shown in Figure 1.2.1-54. The LEO construction concept is illustrated in Figure 1.2.1-55. This concept entails constructing 8 modules and 2 antennas at the LEO base. The configuration of the

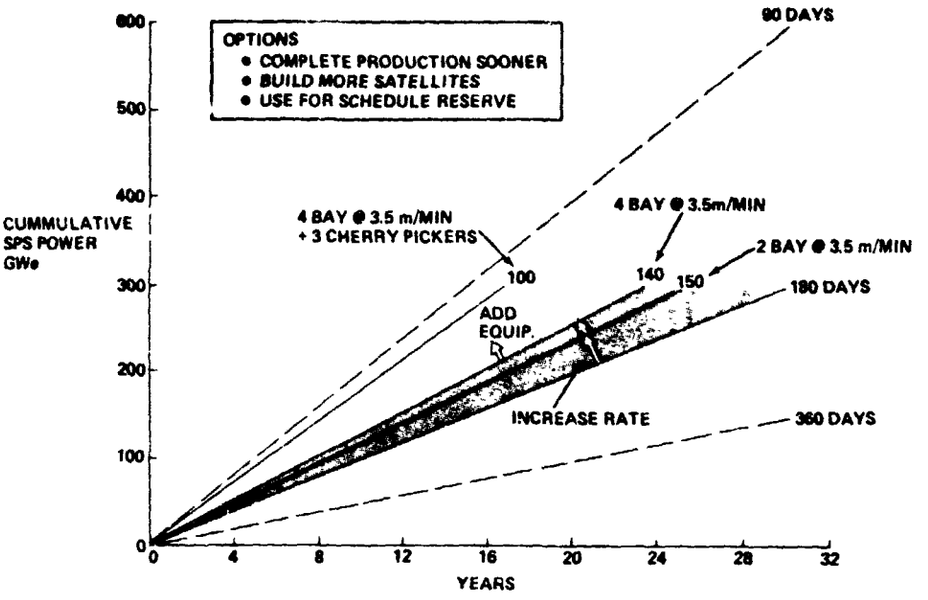

2955-026V

Figure 1.2.1-53 End-Builder Satellite Construction Potential

SPS-2201

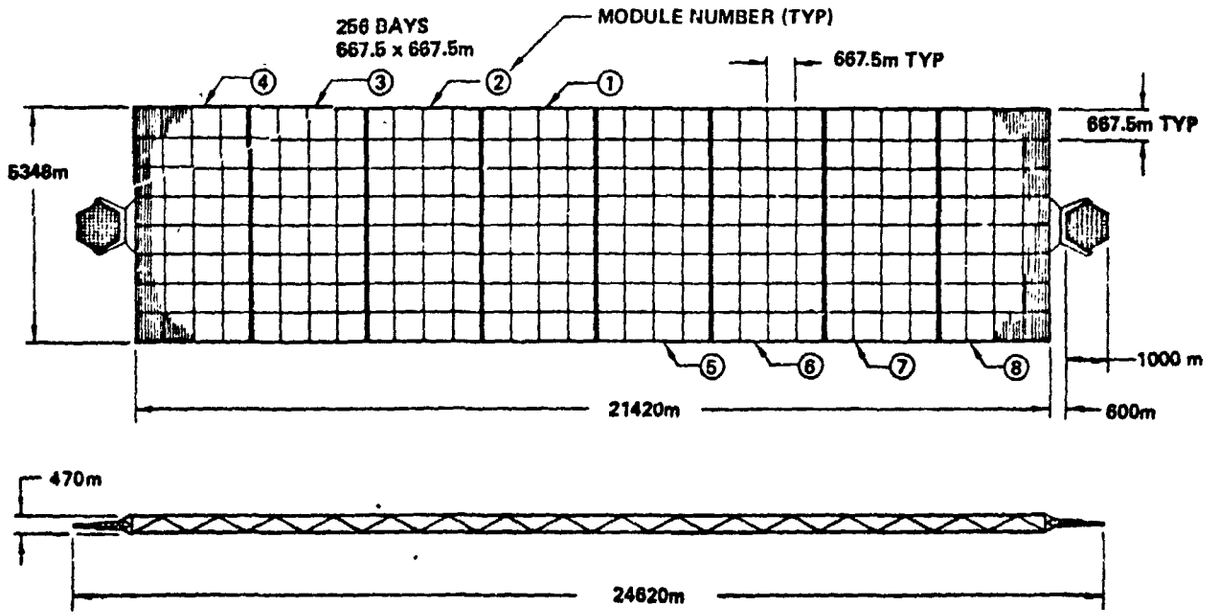

TOTAL SOLAR CELL AREA:	101.8 km^2
TOTAL ARRAY AREA:	110.2 km^2
TOTAL SATELLITE AREA:	114.5 km^2
OUTPUT:	16.93 GW MINIMUM TO SLIPRINGS

Figure 1.2.1-54 Photovoltaic Reference Configuration (5,000 MW Output Each Transmitter)

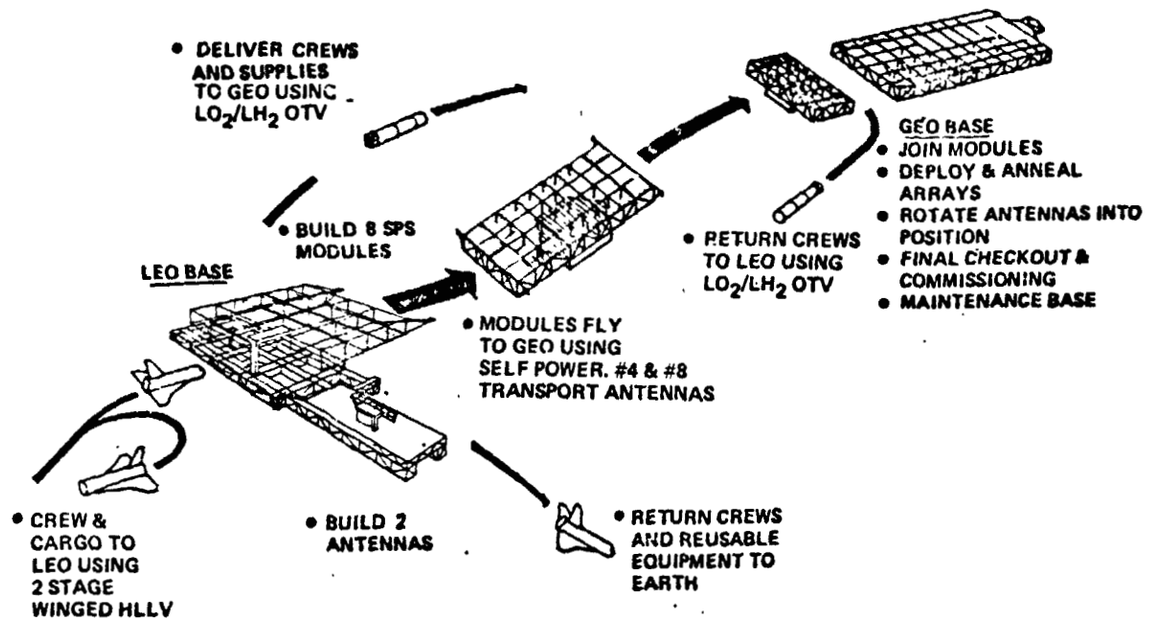

Figure 1.2.1-55 LEO Construction Concept—Self Power Modules

modules to be constructed is shown in Figure 1.2.1-56. The top-level construction timeline is shown in Figure 1.2.1-57.

1.2.1.5.1.1 LEO Construction Operations

The modules and antennas are constructed at LEO using the single-deck construction base shown in Figure 1.2.1-58. This facility concept is shown in more detail in Figure 1.2.1-59. The track network on this base is shown in Figure 1.2.1-60.

This facility concept is identical in plan form to the baseline C-clamp facility. The "roof" and "back wall" have been eliminated. The indexers have been moved to a lower deck. The construction gantry, shown in more detail in Figure 1.2.1-61 and -62, provides the capability of placing beam machines and cranes where they can be used to assemble the upper surface of the modules and yokes.

The gantry is mounted on a carriage that operates from a dedicated track system. The gantry can rotate 360° about the vertical axis of the carriage. The cantilevered arm of the gantry spans one SPS bay. The gantry location provides enough clearance at the base so that the facility-mounted beam machines and cranes have working room.

Figure 1.2.1-63 shows snapshots of the gantry locations and orientations during different phases of the construction operations.

The detailed module construction operations (frame assembly, solar array deployment, power bus installation, thruster installation) and timeline (40 days per module) are identical to those described for the baseline. The frame assembly and solar array deployment operations are shown in Figure 1.2.1-64.

The detailed yoke construction operations (frame assembly, power bus installation, rotary joint installation, elevation joint installation) are identical to those described for the baseline.

The detailed antenna construction operations (primary frame assembly, secondary frame deployment, power distribution system installation, and subarray installation) are identical to that described for the baseline.

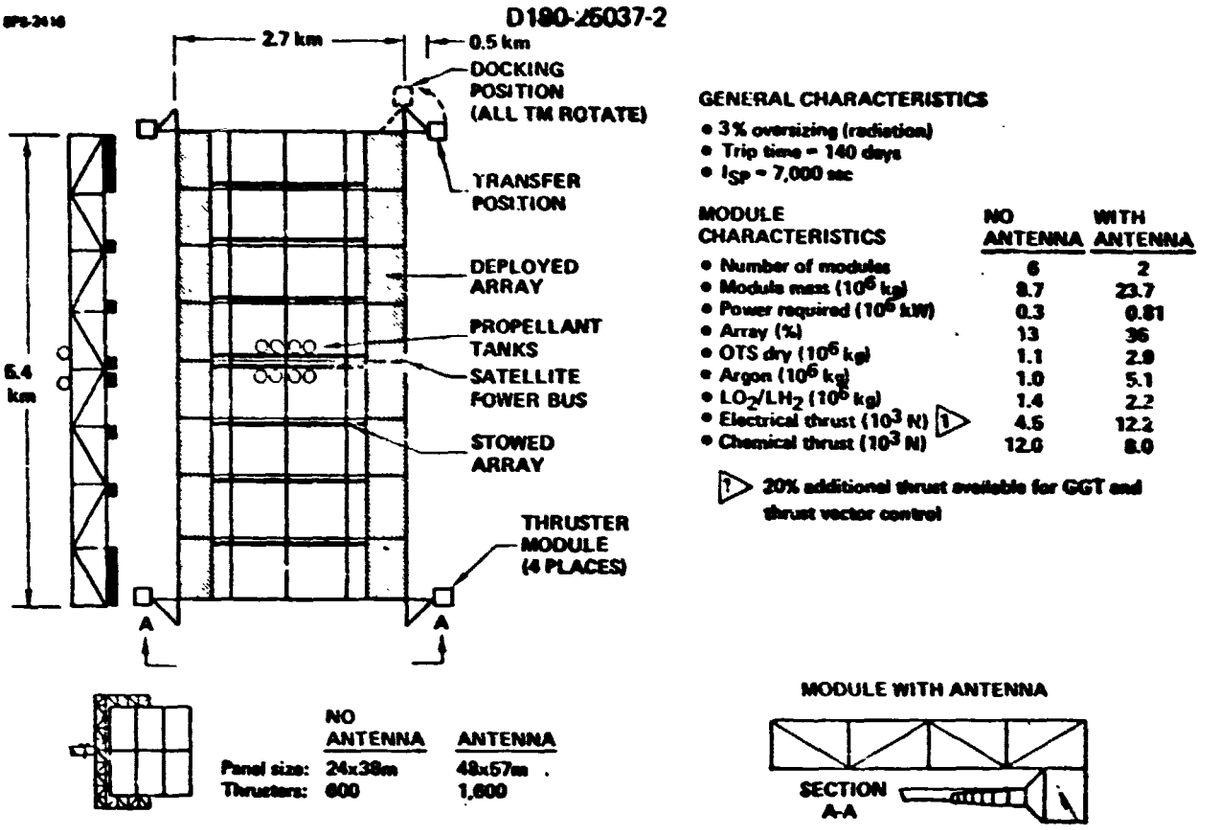

Figure 1.2.1-56 Self-Power Configuration—Photovoltaic Satellite

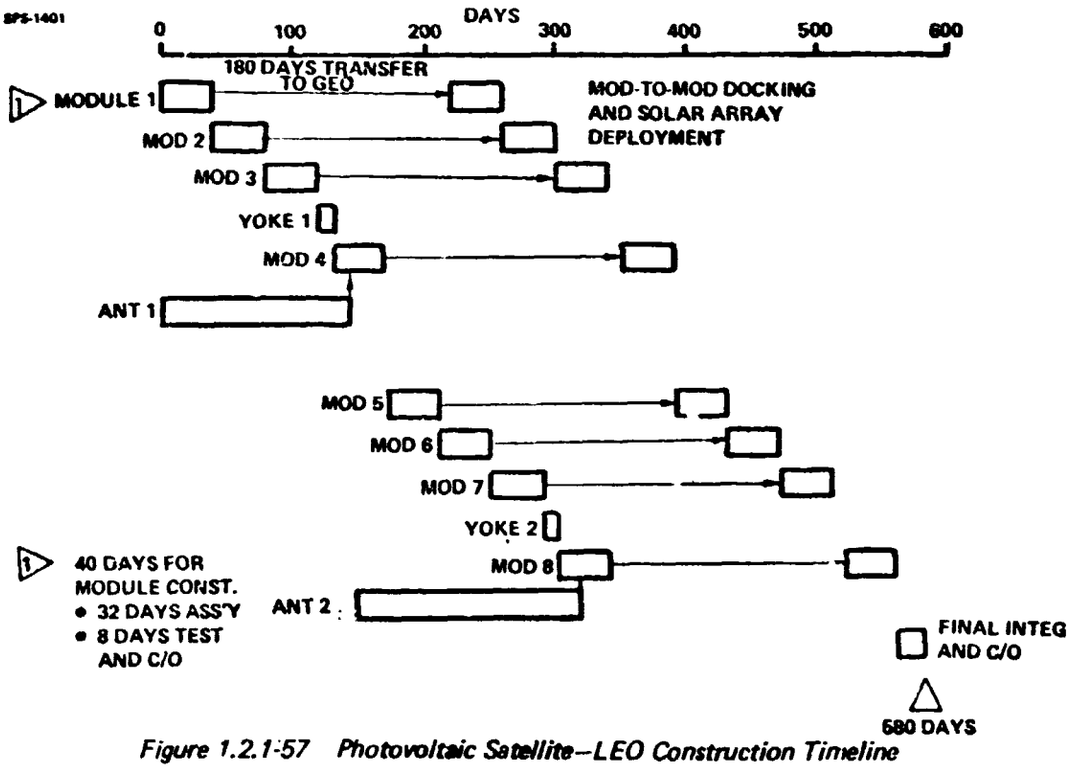

Figure 1.2.1-57 Photovoltaic Satellite—LEO Construction Timeline

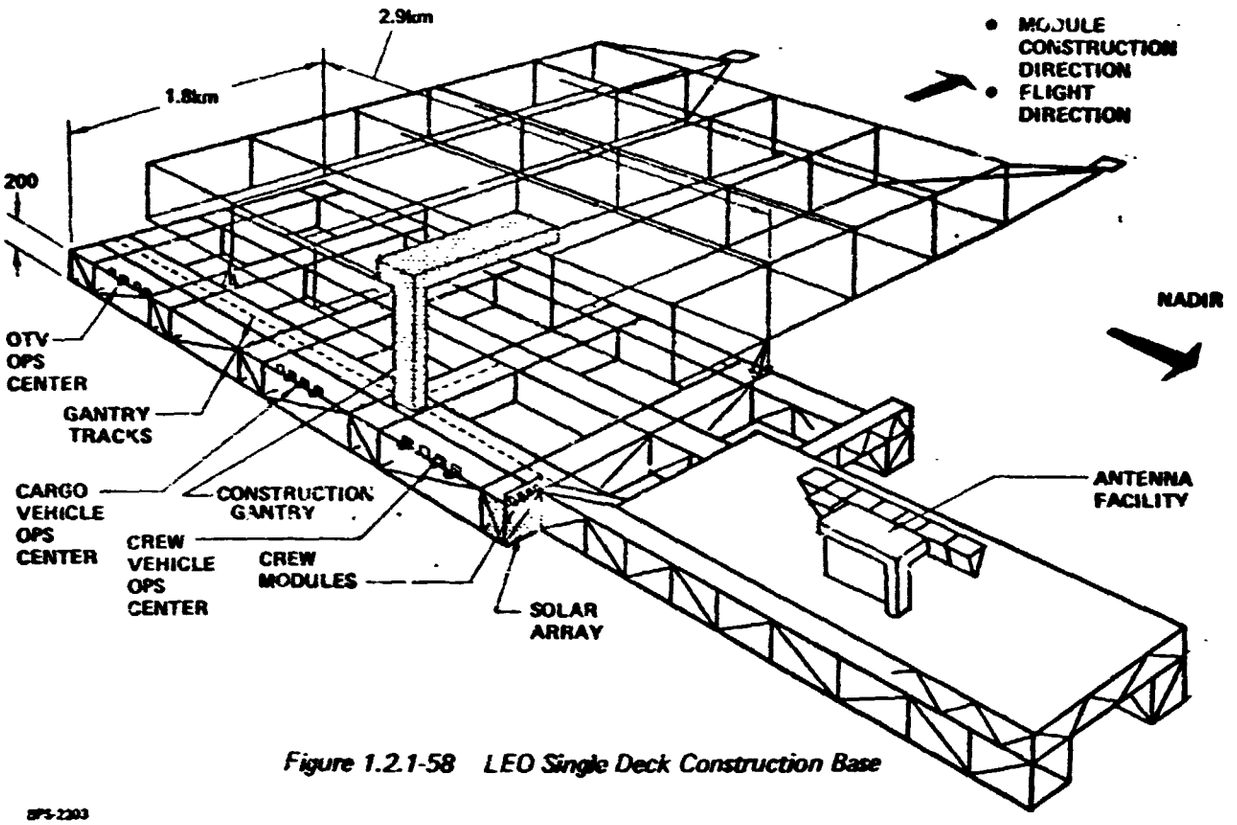

Figure 1.2.1-58 LEO Single Deck Construction Base

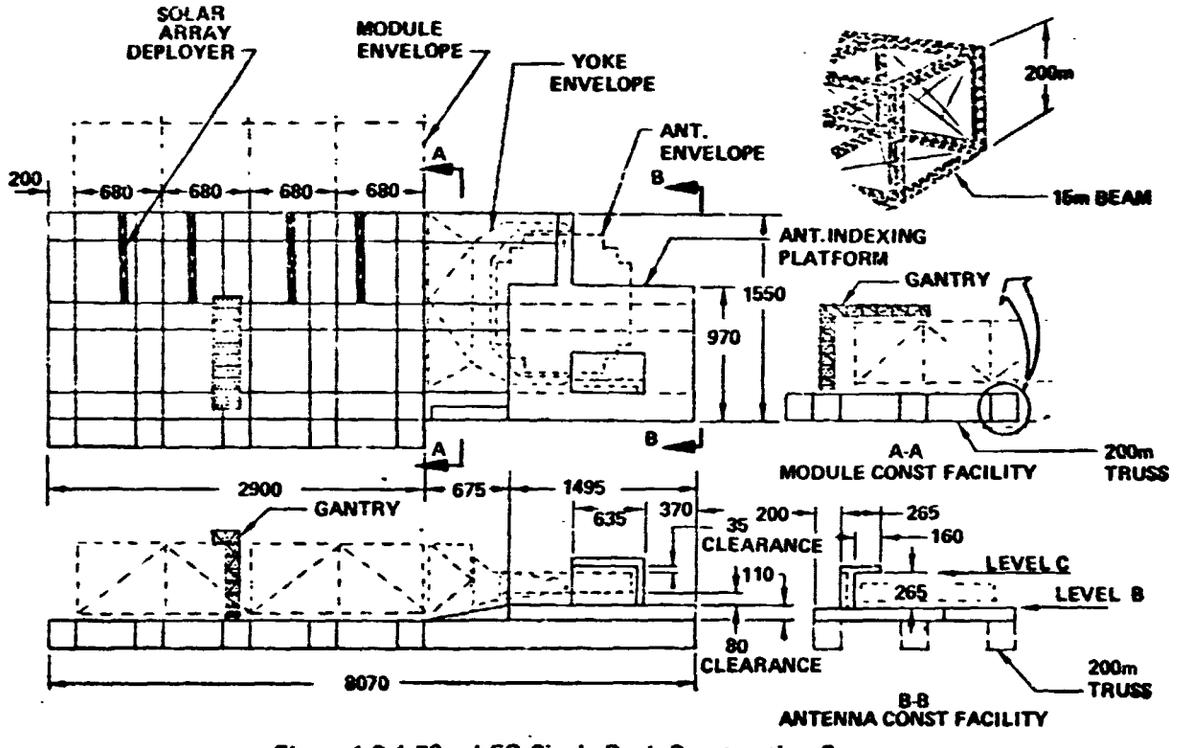

Figure 1.2.1-59 LEO Single Deck Construction Base

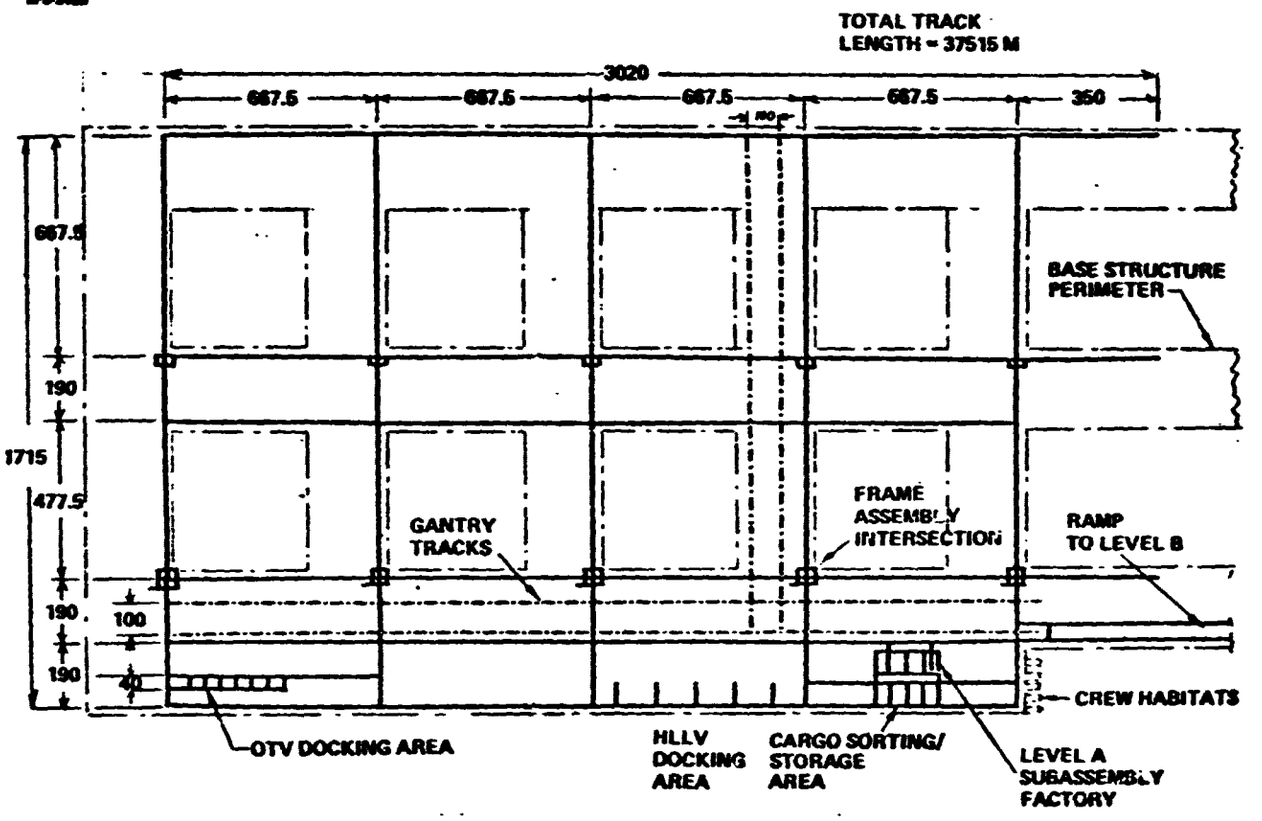

Figure 1.2.1-60 Level A Track Network

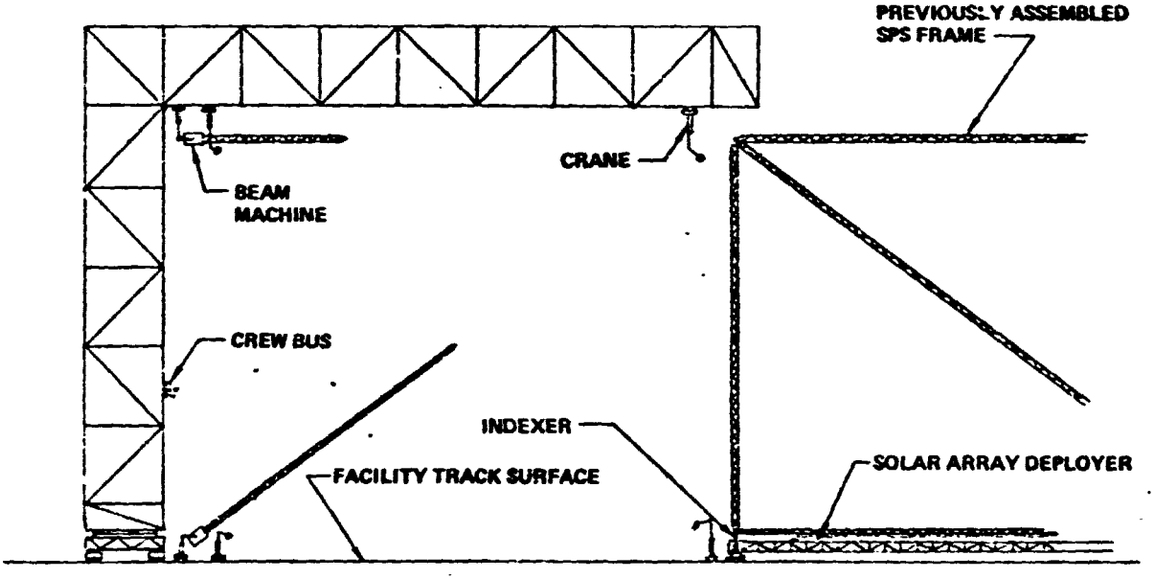

Figure 1.2.1-61 Construction Gantry

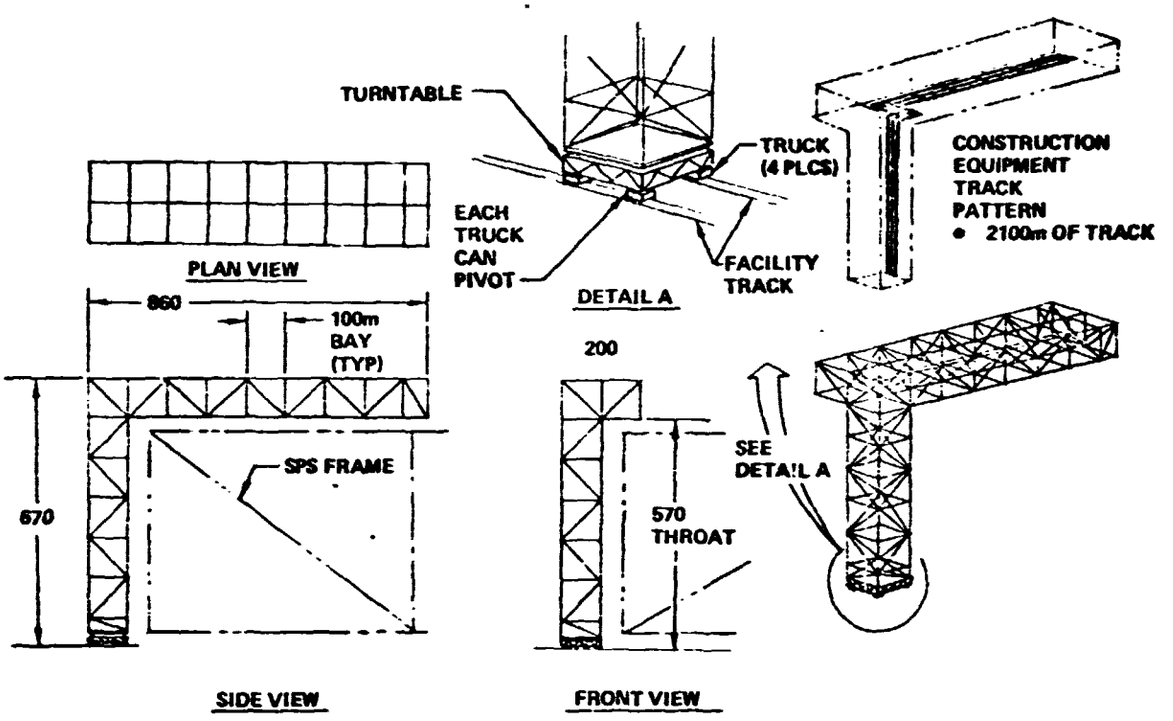

Figure 1.2.1-62 Construction Gantry Configuration

SPS-2208

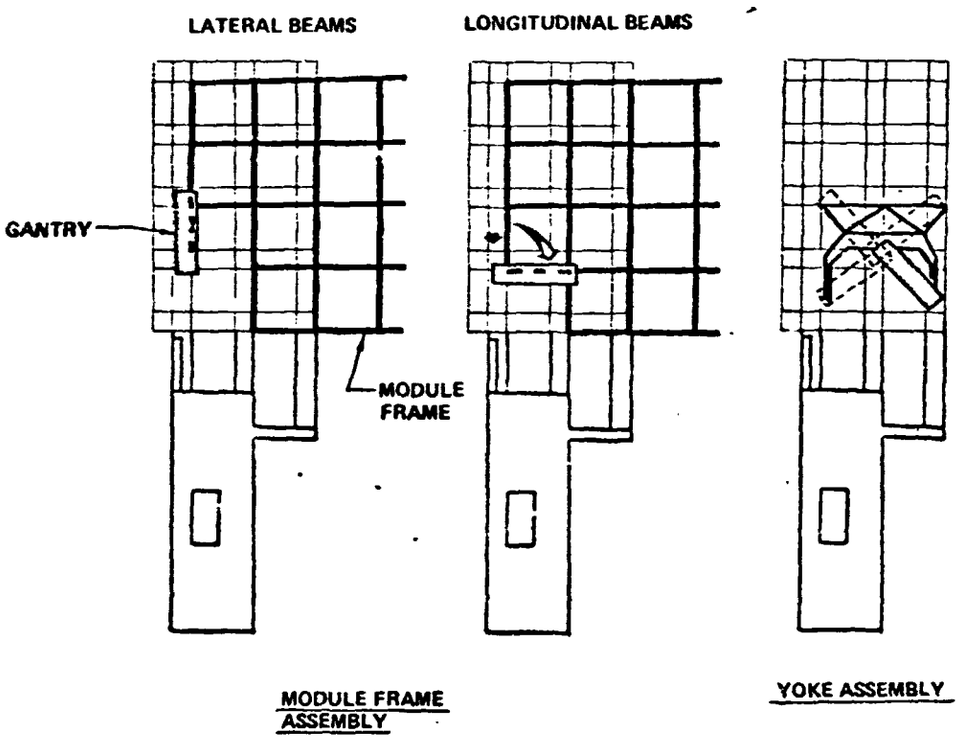

Figure 1.2.1-63 LEO Single Deck Construction Base–Gantry Orientations

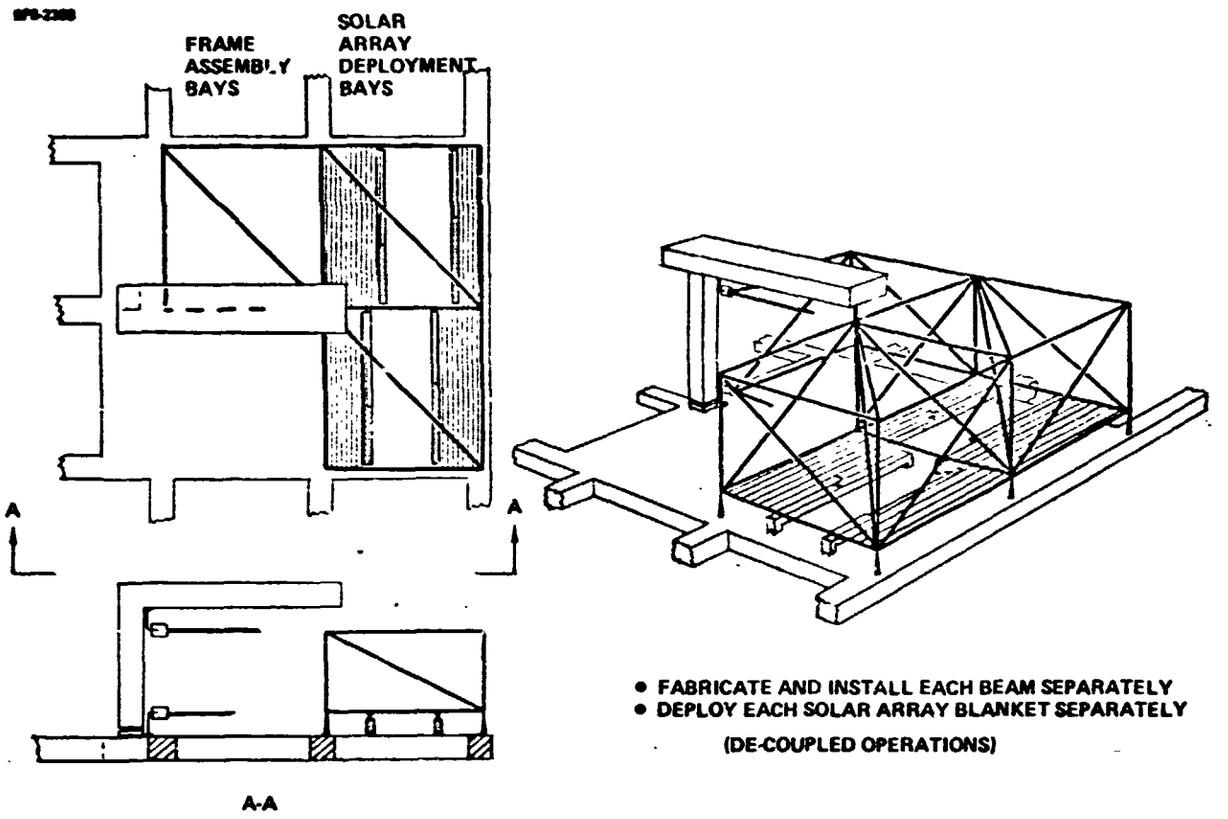

Figure 1.2.1-64 Single Deck Frame Assembly/Solar Array Deployment

The antenna-to-yoke and yoke/antenna-to-module mating operations are identical to those described for the baseline.

1.2.1.5.1.2 Construction Equipment

The construction gantry is the only new piece of construction equipment. All other equipment item configurations and quantities are identical to those described for the baseline.

- –Add one construction gantry.
- –Delete 2 250-m crane manipulators

1.2.1.5.1.3 Facility

Framework. The facility framework differs from that described for the baseline in the following respect:

- –Use 10-m beams instead of 20-m
- –Delete top deck
- –Delete back wall
- –Add framework for dedicated gantry tracks.

Base Subsystems. Identical to baseline except that the thruster system has been relocated.

Crew Modules. Identical to baseline.

Work Modules. Identical to baseline.

Cargo Handling/Distribution. This system differs from that described for the baseline in the following respects:

- –Delete all tracks associated with top deck and back wall
- –Add dedicated gantry tracks
- –Add one crew bus (dedicated to the gantry)

1.2.1.5.1.4 Crew Size

Crew size identical to that given for the baseline LEO base.

1.2.1.5.2 GEO Single Deck Construction Base Characterization

The reference satellite configuration to be constructed is shown in Figure 1.2.1-65. The GEO construction concept is illustrated in Figure 1.2.1-66. This concept entails constructing a monolithic satellite. The top-level construction timeline is shown in Figure 1.2.1-67.

1.2.1.5.3 Geo Construction Operations

The monolithic satellite is constructed at GEO using the single-deck construction base shown in Figure 1.2.1-68. This facility concept is shown in more detail in Figure 1.2.1-69.

The single-deck is similar to that shown for the LEO single-deck facility described in the previous section. The most notable differences are the orientation of the solar array deployers and the location of the antenna facility. The construction gantry is identical to that described previously.

To construct a monolithic satellite it is necessary to employ lateral and longitudinal indexing. The module construction operations are conducted in a 2 x 2 bay area. The 2 facility bays on either side of this 2 x 2 construction area are utilized to provide support points for the indexers when the module is laterally indexed.

The solar array deployers have been reoriented so that the solar array is deployed in the lateral direction. It is necessary to put 2 deployers in each of the two solar array deployment facility bays in order to keep the deployment rates comparable to the baseline rates.

To alleviate competition for track by the four solar array deployers and the indexers, it was necessary to create dedicated tracks for the deployers. Figure 1.2.1-70 shows the location of these dedicated tracks. Figure 1.2.1-71 shows how the deployers, indexers, and facility tracks are interfaced.

The detailed module construction operations (frame assembly, solar array deployment, power bus installation, thruster installation) are identical to those described for the baseline, see Figure 1.2.1-72. The module construction timeline is shown in Figure 1.2.1-73.

SPS-2200

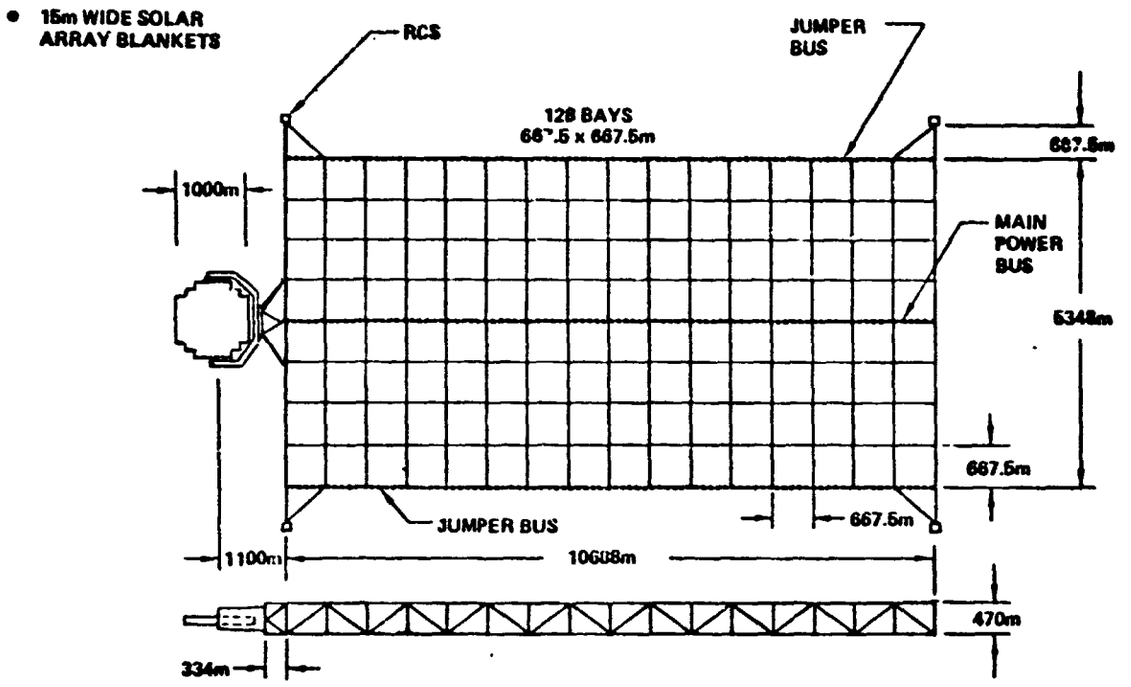

Figure 1.2.1-65 5GW SPS Reference Configuration (Silicon Cells)

SPS-2497

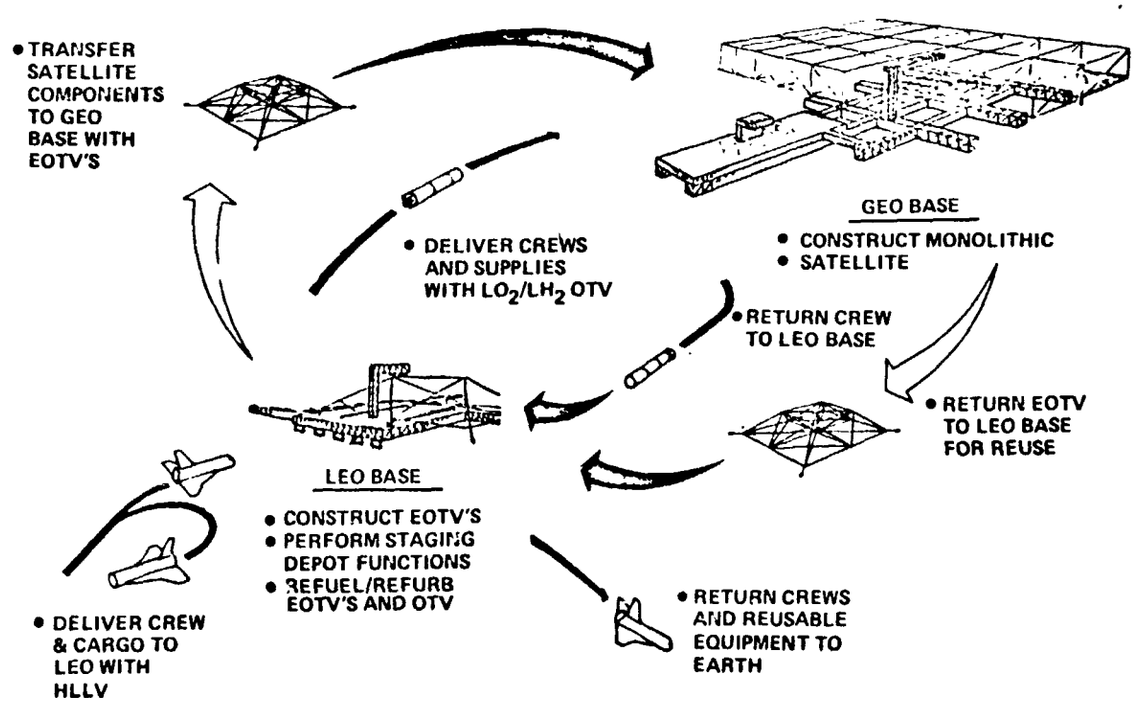

Figure 1.2.1-66 GEO Construction/Electric OTV Concept

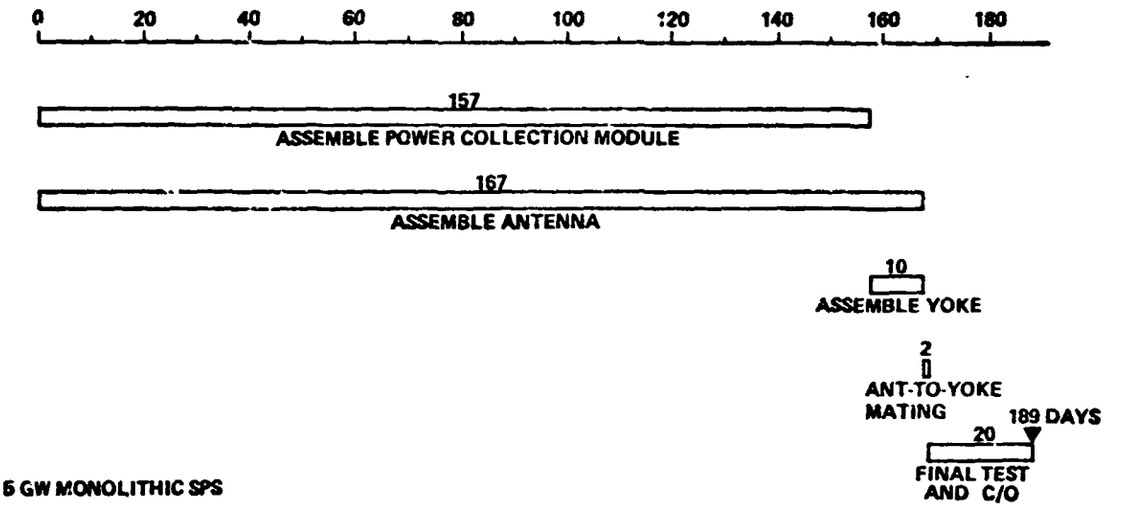

Figure 1.2.1-67 GEO Single Deck Base—Top-Level Construction Timeline

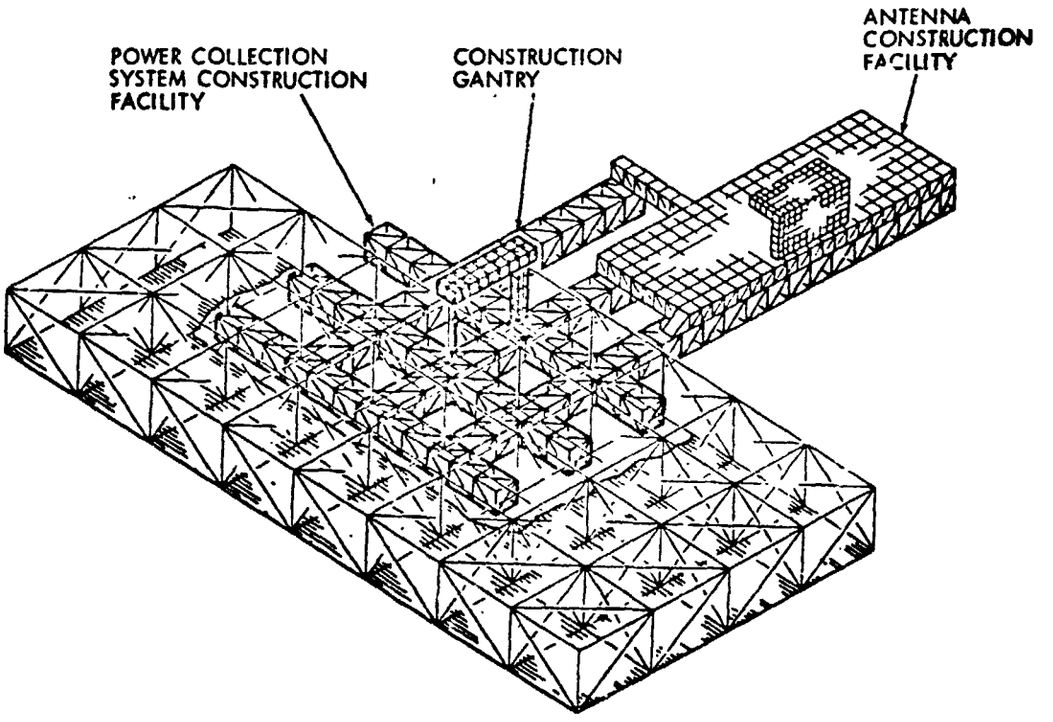

Figure 1.2.1-68 GEO Single Deck Construction Base

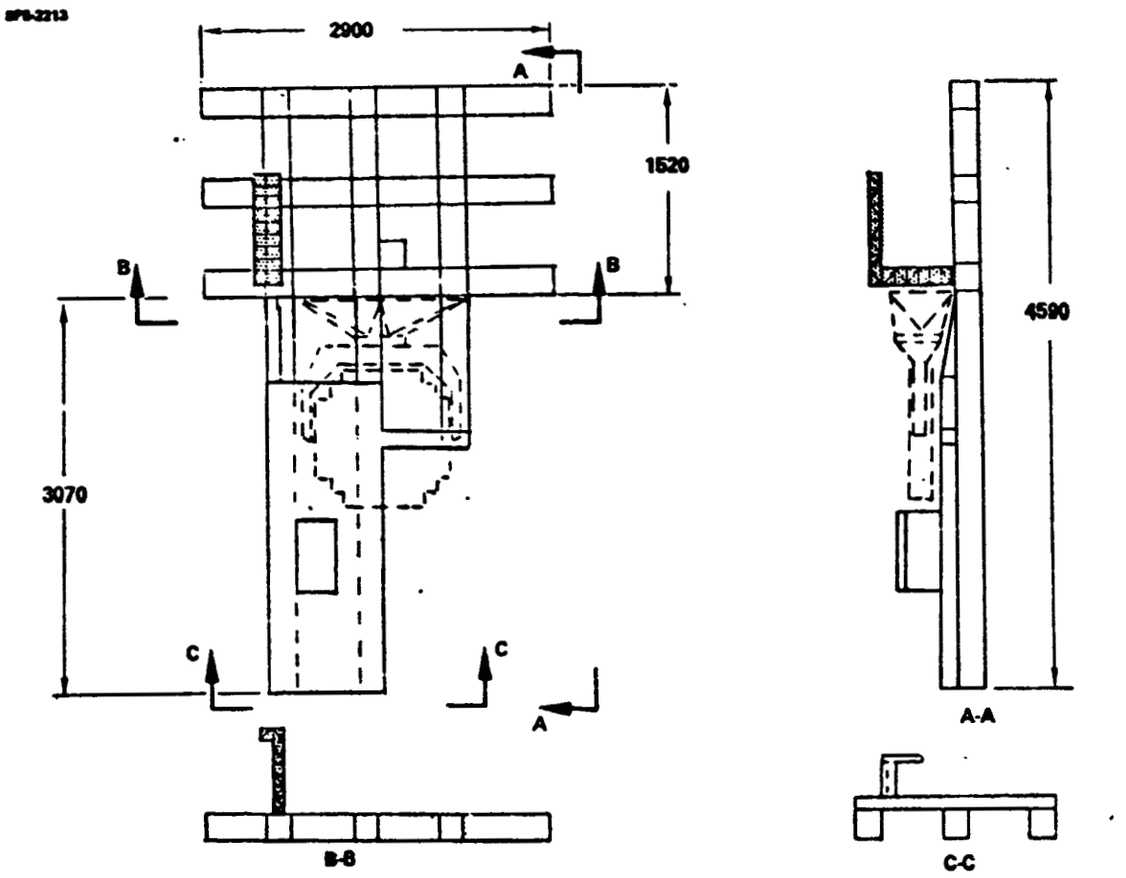

Figure 1.2.1-69 GEO Single Deck Construction Base

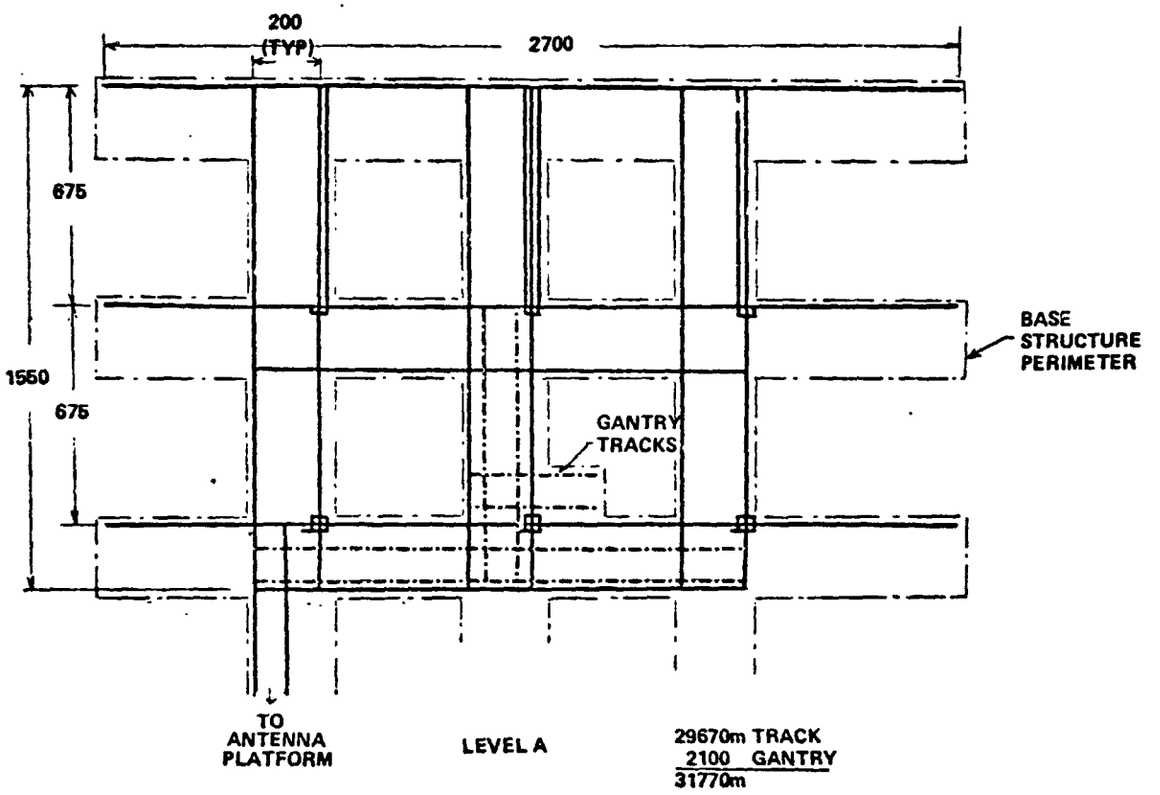

Figure 1.2.1-70 GEO Single Deck Track System

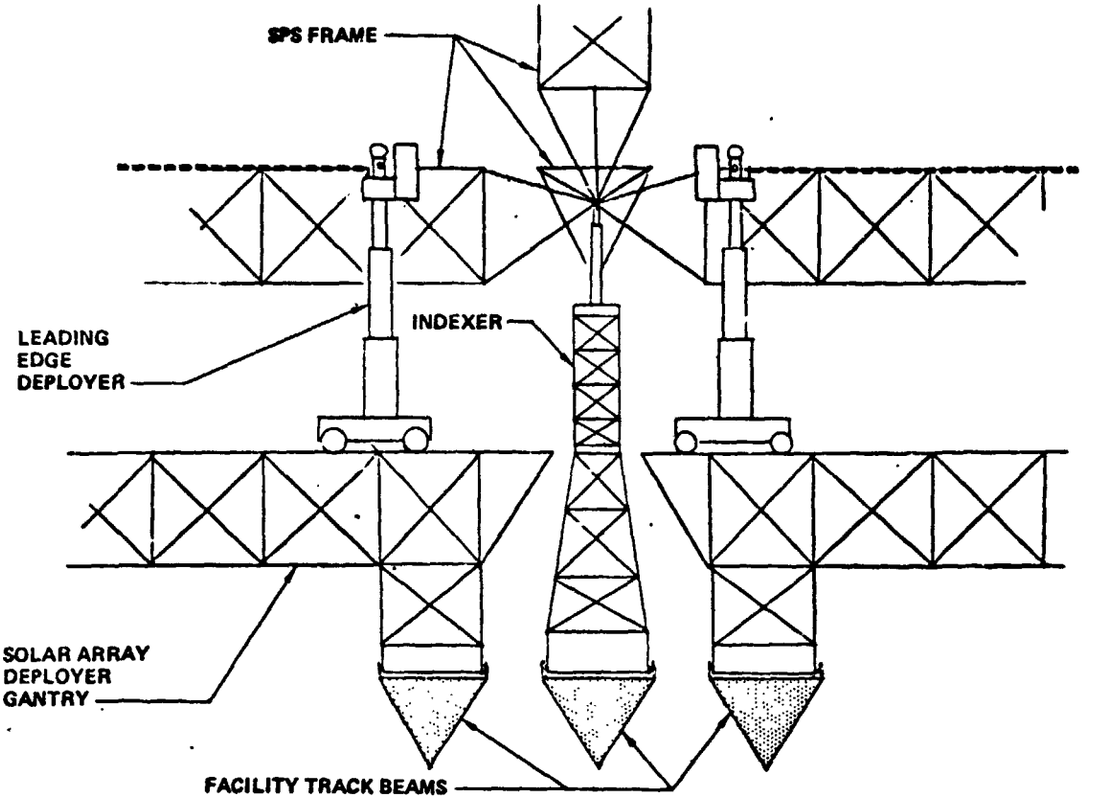

Figure 1.2.1-71 GEO Single Deck Construction Base Indexer/Solar Array Deployer Interface

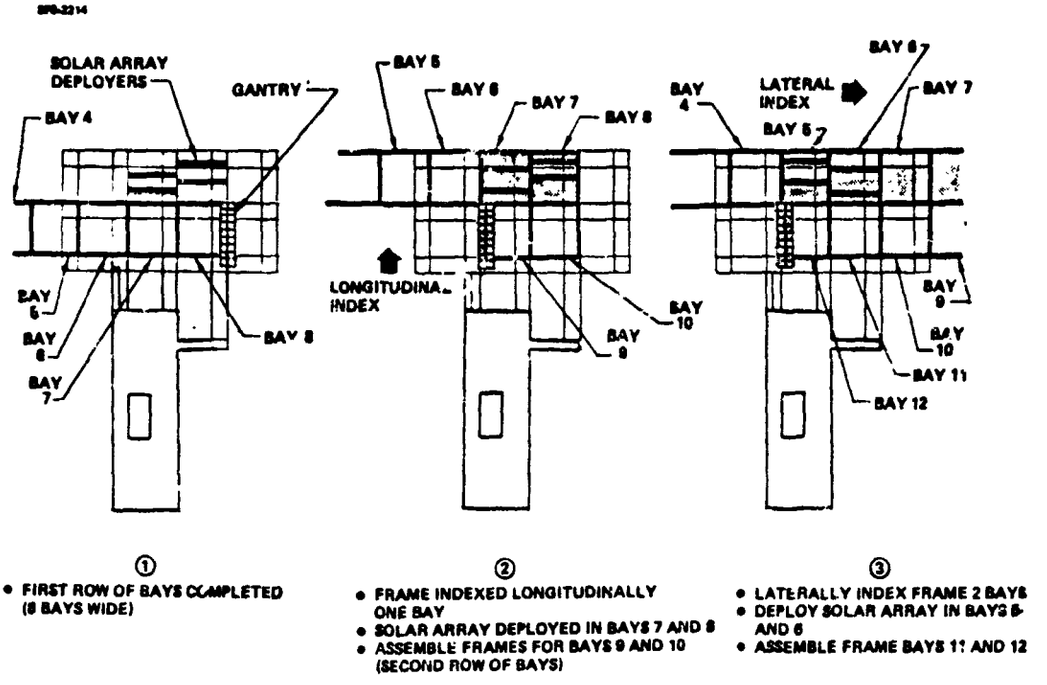

Figure 1.2.1-72 Power Collection System Construction Sequence (GEO Construction)

SPS-2218

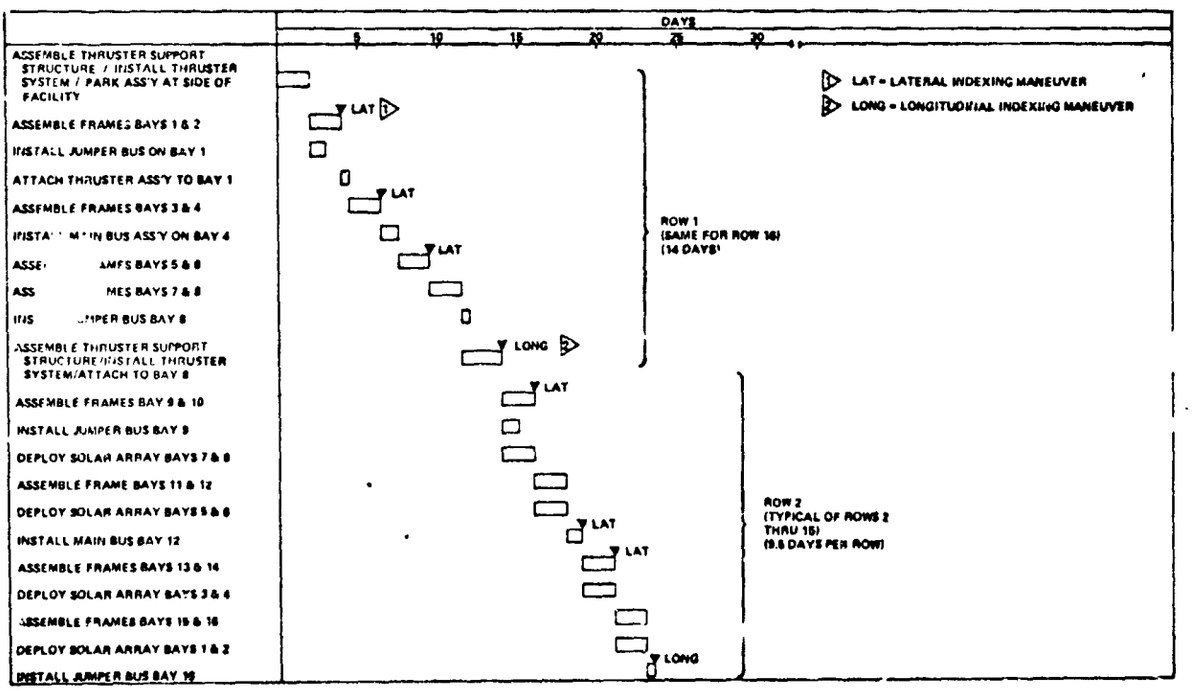

Figure 1.2.1-73 Power Collection Module Construction Timeline (5GW Monolithic SPS)

The antenna construction operations are identical to the baseline. There are 167 days available to construct the antenna (compared to 120 days for the baseline) so the equipment rates could be 40% slower.

The yoke construction and mating operations are described in Figure 1.2.1-74.

1.2.1.5.4 Construction Equipment

No change from that described for the LEO single deck.

1.2.1.5.5 Facility

Framework—The framework for the facility differs from that described for the baseline in the following respects:

- –Use 10 m beams
- –Delete top deck
- –Delete back wall
- –Delete 200 m truss along back edge
- –Add framework for dedicated gantry and solar array deployer tracks.

Base Subsystems—The base subsystems are identical to the baseline except that the thruster system has been relocated.

Crew Modules—Identical to baseline.

Work Modules—Identical to baseline.

Cargo Handling and Distribution—This system differs from the baseline in the following respects:

- –Delete all tracks associated with top deck and back wall.
- –Add dedicated gantry and solar array deployment machine tracks.
- –Move the cargo receiving, sorting, and warehousing track system to the antenna platform (no net change).
- –Add one crew bus (dedicated to the gantry).

SPS-2717

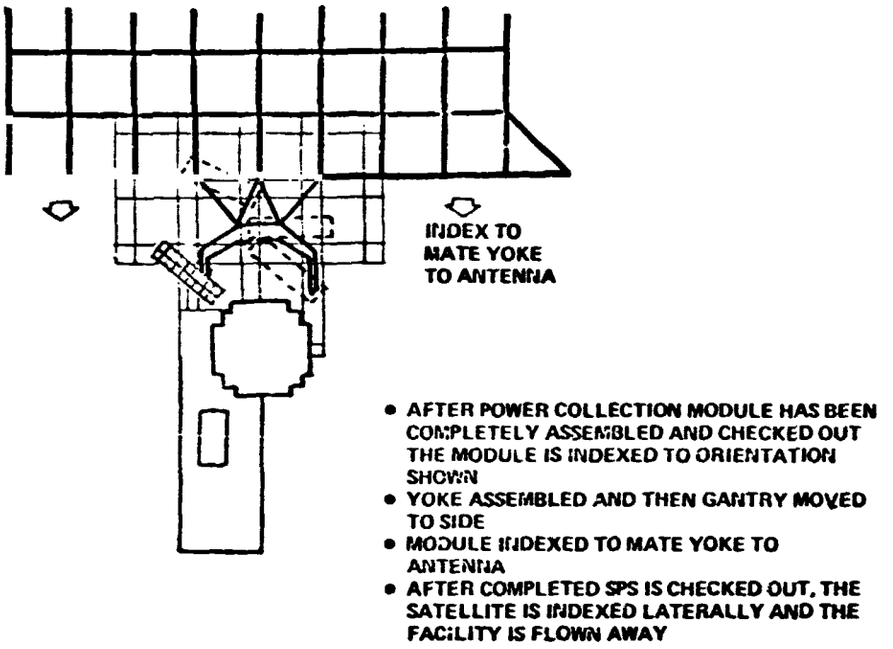

Figure 1.2.1-74 Yoke Assembly and Mating Operations

1.2.1.5.6 Crew Size

The crew size is listed in table 4.2.1-4.

1.2.1.6 Antenna Construction Concept Refinement

This section contains the analysis pertaining to antenna construction refinement. There are two subsections: 1) Review of the antenna design for construction impact, and 2) refinement of the antenna construction operations concept.

1.2.1.6.1 Review of the Antenna Design for Construction Impact

The antenna construction concept described in the Part III Preferred Concept Description document had two significant inconsistencies that were never resolved due to the press of time. These inconsistencies, their construction impact and resolution are described below.

1.2.1.6.1.1 Primary Frame Configuration Update and Construction Approach

Figure 1.2.1-75 shows the antenna primary frame configuration defined at the end of Part III. This structure was composed of 10 m beams and incorporated tension cables. In the first part of the current study, a structural analysis of the antenna framework (MPR #2, Attachment 2) recommended that the tension cables be replaced by beams. The resulting configuration of the primary structure is shown in Figure 1.2.1-76. The analysis did not specify the dimensions of the beams, e.g., 5 m or 10 m beam, but it did specify the attributes of the beam (see Table II in MPR #2, Attachment 2). For the construction analysis, it is not necessary to know the specific cross-sectional size of the beams; beam length is the important dimension.

The construction issues that were to be defined for the new primary frame configuration are the following: (1) How many beam machines are required? (2) How many cherrypickers are required? (3) What is the assembly sequence? (4) How long does it take?

Construction issues (1) through (4) are resolved in Figure 1.2.1-77. This figure shows how two beam machines and four cherrypickers can assemble a primary frame bay in about 4 hours per bay.

Table 1.2.1-4 GEO Single Deck Facility—Crew Size

Base Management	(10)
Construction	(297)
Management	22
Module Construction	62
Antenna Construction	40
Subassembly	46
Maintenance	37
Logistics	42
Test/QC	40
Base Operations	(41)
Base Support	(67)
Total	407

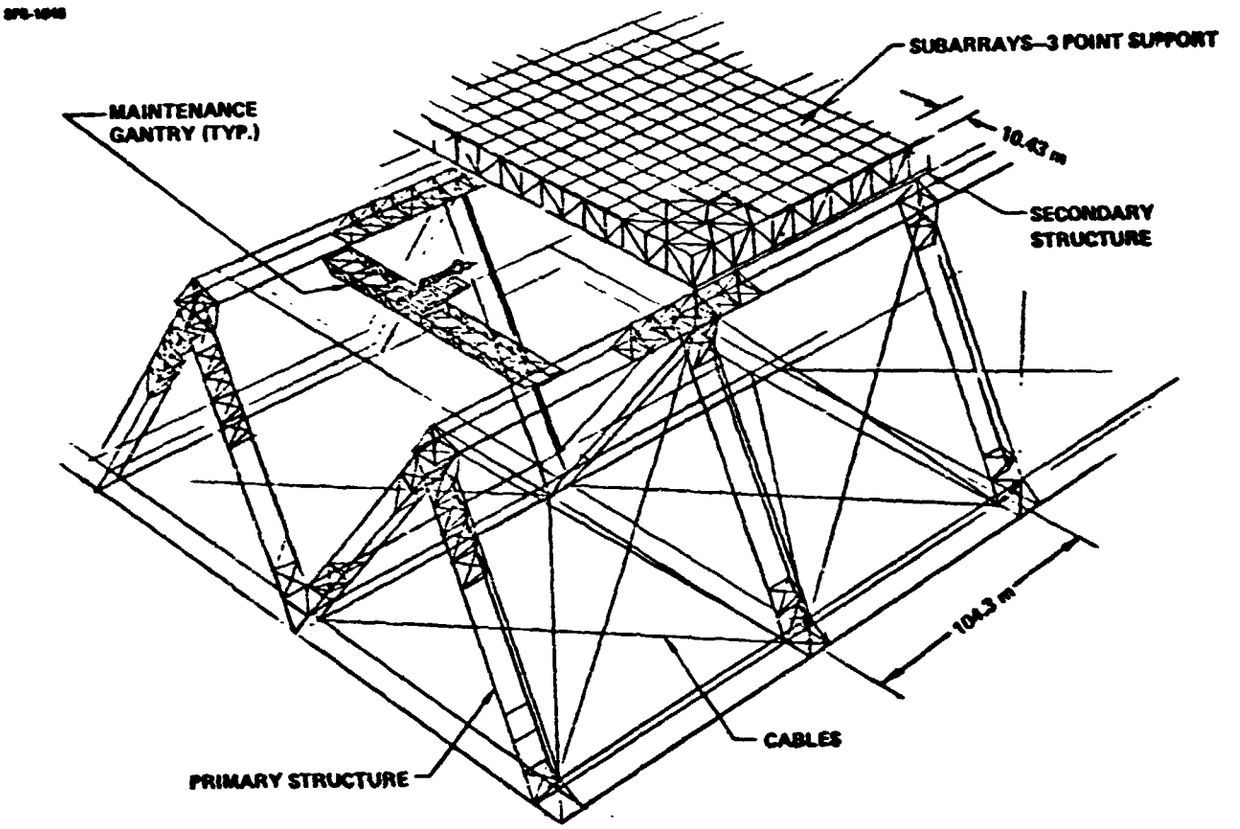

Figure 1.2.1-75 Reference MPTS Structure Interfaces

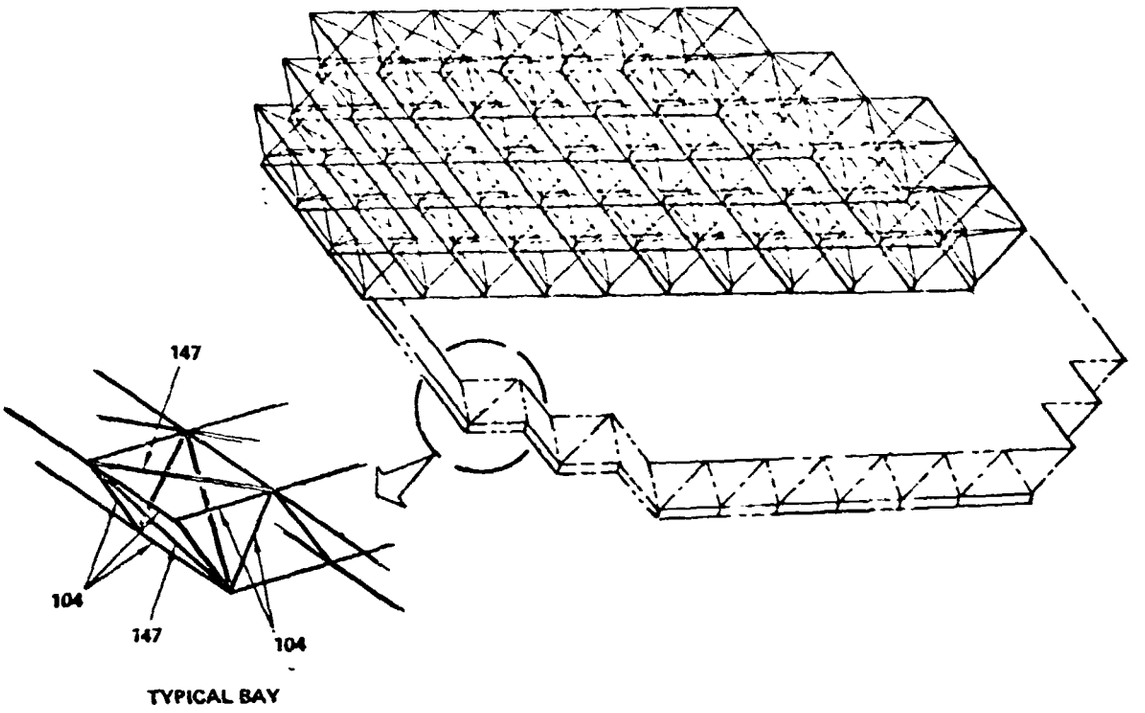

Figure 1.2.1-76 Revised MPTS Primary Structure

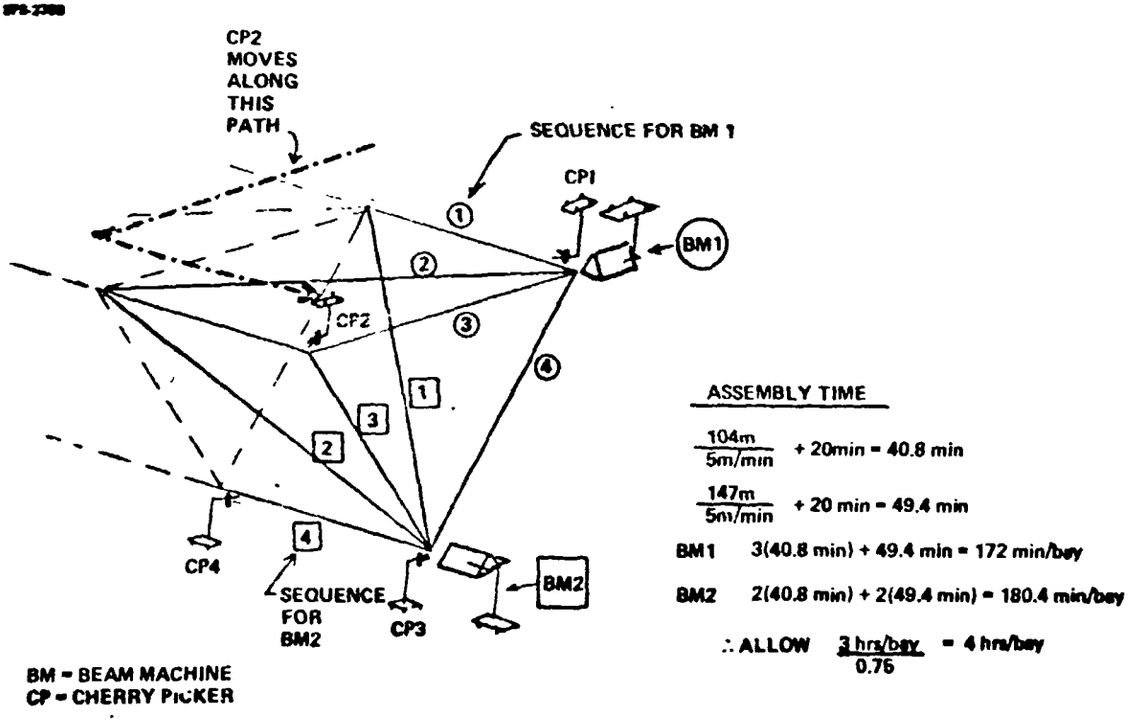

Figure 1.2.1-77 MPTS Primary Frame Assembly Equipment, Sequence, and Timeline

1.2.1.6.1.2 Elevation Joint Location

One of the most significant inconsistencies between the Part III antenna configuration concept and the antenna construction concept is the orientation of the A-frame primary structure with respect to the yoke, see Figure 1.2.1-78. In the antenna configuration concept, the A-frame structure is oriented so that the elevation joints tie into the ends of the center A-frames. However, in the construction concept it is necessary for the A-frames to be oriented orthogonally to that just described. This is necessary so that toward the end of the antenna construction timeline the antenna can be indexed while it is being constructed within the confines of the yoke, see Figure 1.2.1-79.

In order to implement the construction-required A-frame orientation, there are two issues that need to be resolved: (1) Can the elevation joint be mated into the side of the A-frames? (2) Is there any impact on the antenna maintenance system concept?

The first issue is illustrated in Figure 1.2.1-80. The structures analysts indicate that the elevation joint could be made into the side of the A-frames if some provision could be made to take out the axial loads on the upper surface without relying on the secondary structure. This would require beams to bridge between the peaks of the A-frames as shown in the figure. These beams would complicate the maintenance gantry clearance and would create a problem for the cherrypickers on the maintenance gantries to gain access to the subarrays located directly above the beams. Time does not permit these problems to be resolved. In view of the fact that the antenna primary structure may be changed to a pentrahedral design during Phase II, it does not seem to be critical to resolve the issues defined above.

1.2.1.6.2 Refinement of the Antenna Construction Operations Concept

The antenna construction operations have been explored in detail in the previous studies. However, there are several construction issues that needed to be refined in order to incorporate MPTS configuration updates and to pin down some loose ends. The antenna construction concepts that were re-explored are the following:

1. Re-examine the configuration of the antenna construction platform.
2. Determine construction operations, equipment, and manpower required to install the phase control system.

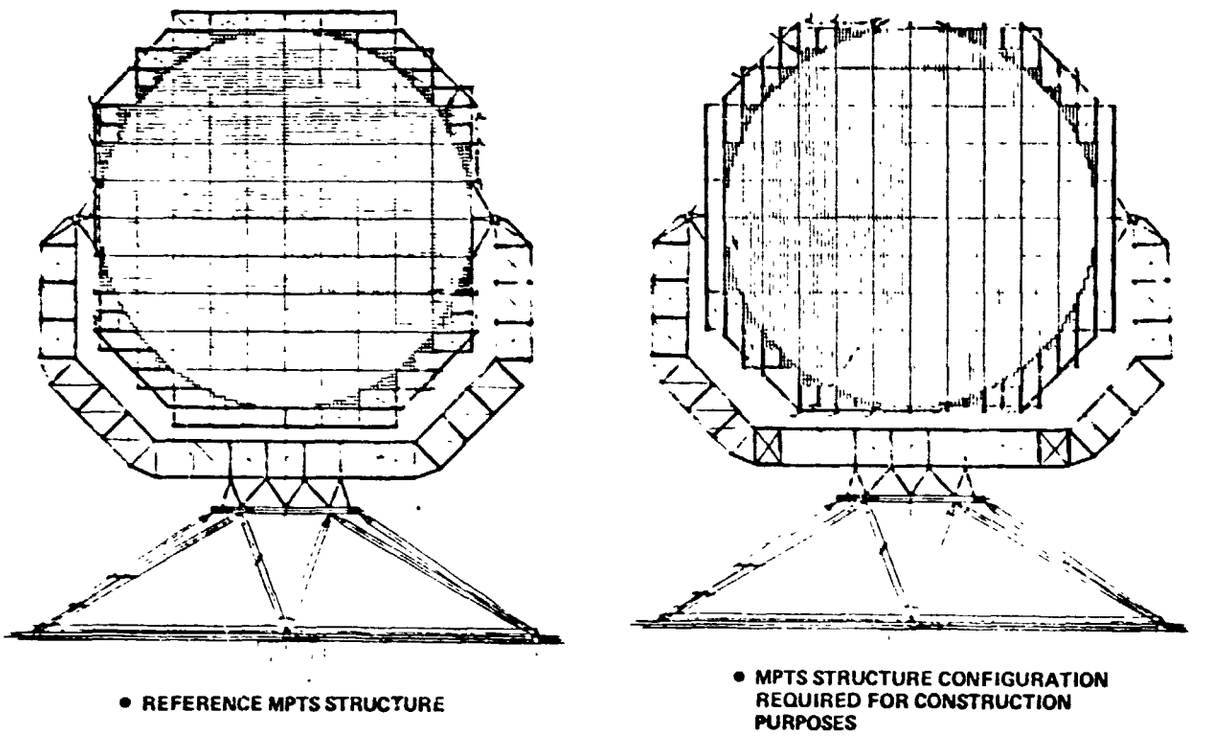

Figure 1.2.1-78 Conflicting Antenna Primary Structure A-Frame Orientation

SPS-2376

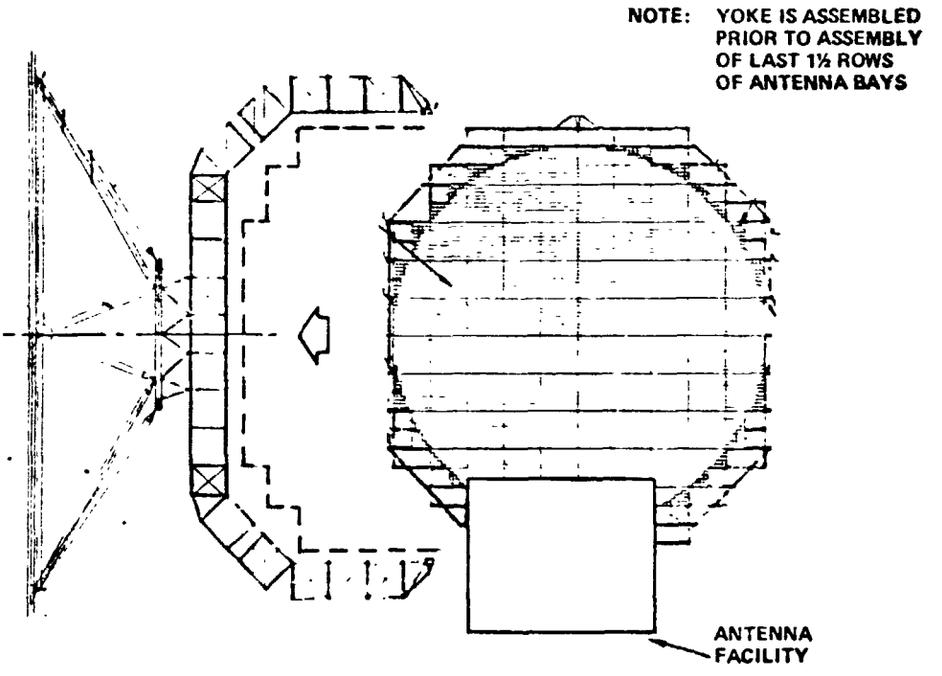

Figure 1.2.1-79 Provide Capability to index Antenna within Confines of the Yoke

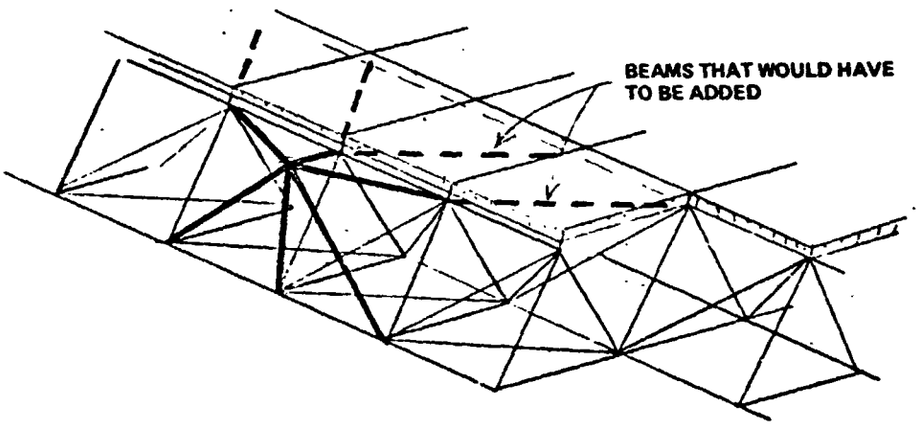

Figure 1.2.1-80 Antenna Elevation Joint Structural Interface

3. Determine the construction operations, equipment and manpower required for assembly and installation of the maintenance system.
4. Develop an integrated timeline for the MPTS construction.
5. Develop updated construction equipment and manpower count.

1.2.1.6.2.1 Antenna Construction Platform

Figure 1.2.1-81 shows the reference antenna construction platform. This platform provides the following purposes: (1) Supports the antenna facility, (2) Provides support structures for the track network, and (3) Provides space for a subassembly factory. The only one of these that will be addressed here is Item 2.

The majority of the antenna construction platform surface area is devoted to support of the indexing track. A closer look at the indexing requirements show that it is necessary to provide tracks for both "tall" and "short" indexers, see Figure 1.2.1-82. The "tall" indexers are required only during the construction of the first row of bays. It was not deemed feasible to support the assembled structure from the peaks of the A-frames alone. After the second row of bays is partially completed, it is possible to support the structure using "short" indexers only. It is necessary to add dedicated tracks for the "tall" indexers for this early phase of frame assembly.

Another factor that became apparent (which was not recognized before) was that it is necessary to support the antenna at the perimeter only. After the second row of A-frames are partially completed, the secondary structures are added. These structures prohibit attaching indexers to the face of the antenna. The only place left to grab the structure is out at the extreme edges of the primary structure. Subsequently, the antenna platform needs to be extended on either side of the antenna facility so that the indexers attached to the perimeter have track to run on. The resulting configuration of the platform is shown in Figure 1.2.1-83. This configuration is a significant change from the reference configuration. The integrated track network on this platform is shown in Figure 1.2.1-84. All of the single deck and end-builder construction base concepts were updated to incorporate this new configuration.

1.2.1.6.2.2 Phase Control System Installation

The phase control system configuration is still in the process of being defined. The installation of this system has never been considered in the antenna construction

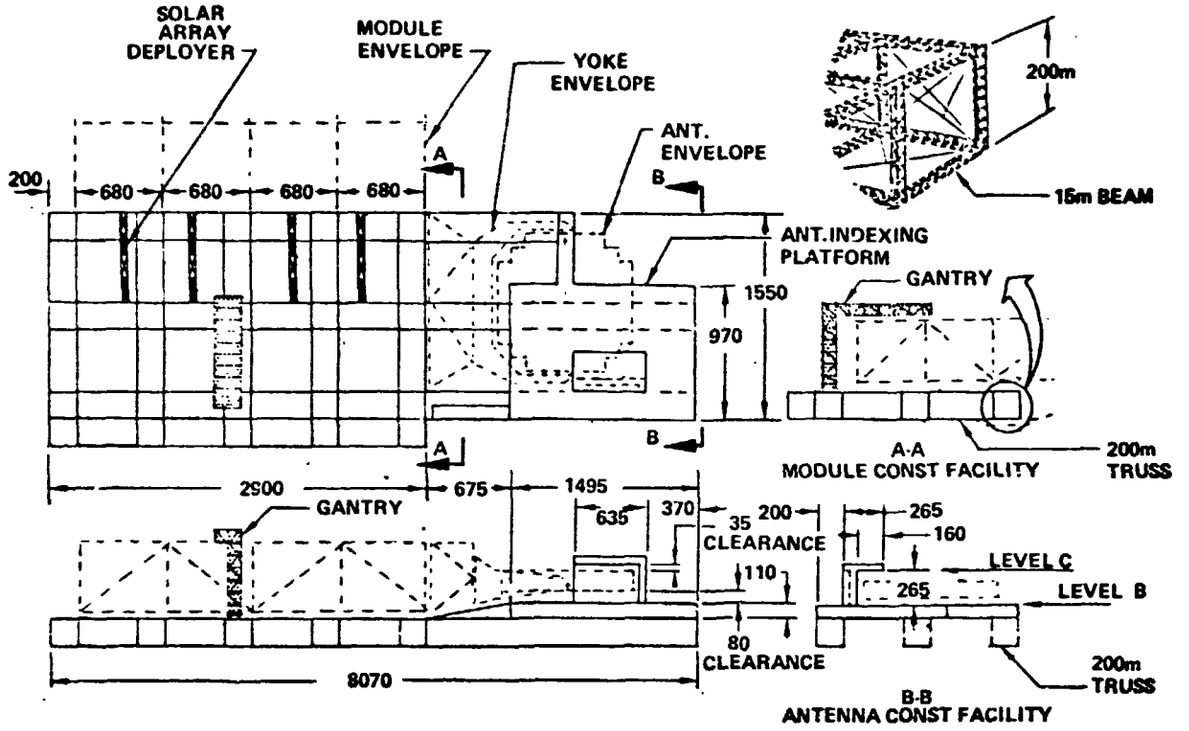

Figure 1.2.1-81 LEO Single Deck Construction Base

SPS-2388

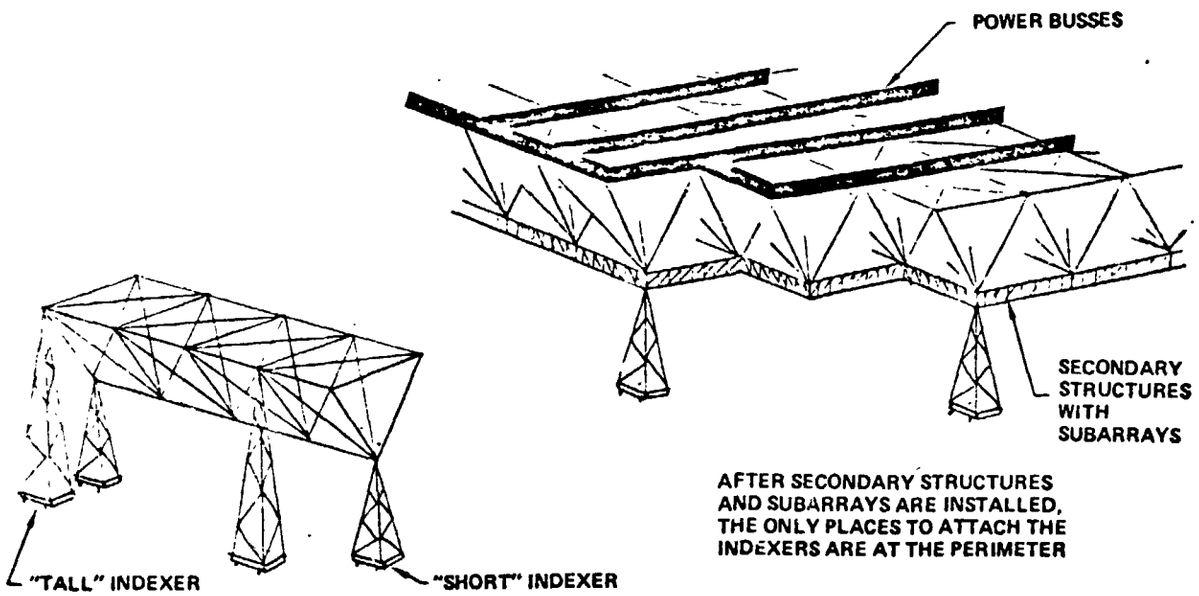

Figure 1.2.1-82 Indexers

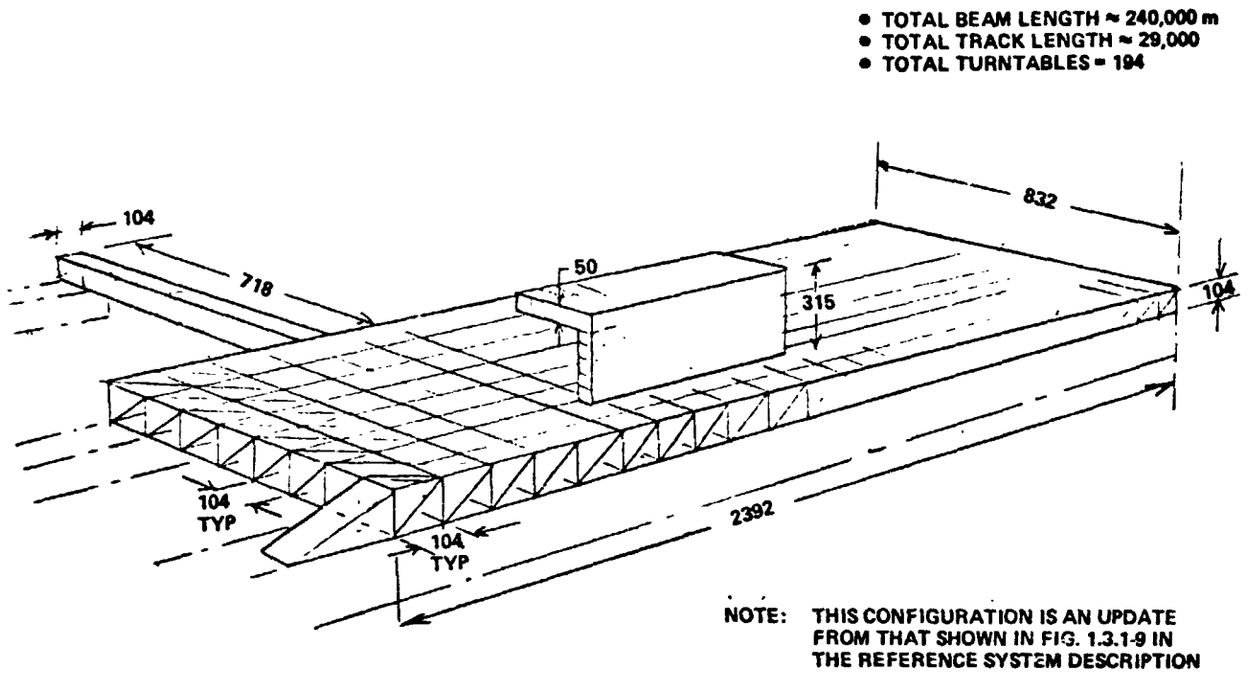

Figure 1.2.1-83 Antenna Construction Platform

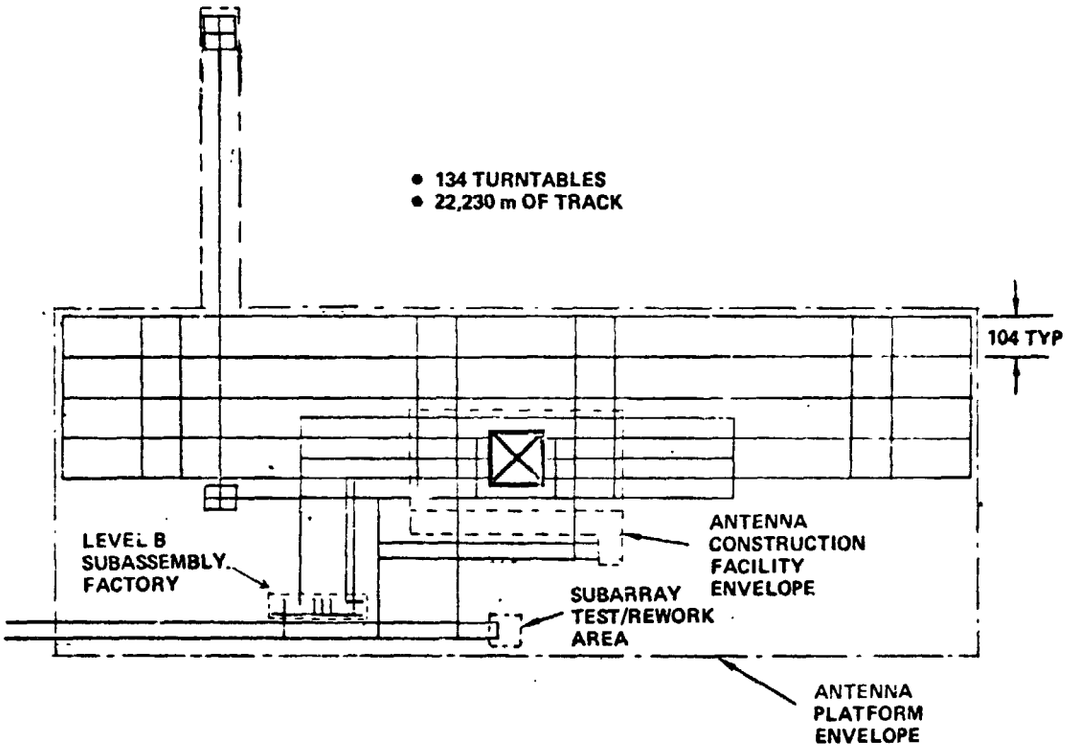

Figure 1.2.1-84 Antenna Platform (Level B) Track Pattern

concept to date. Preliminary discussions with the MPTS experts has exposed a requirement to add some equipment and people for performing this installation.

It will be necessary to add a gantry and cherrypicker to the Deployment Platform so that a phase control wiring or fiber optics distribution harness can be installed on the secondary structure on the side adjacent to the subarrays. The revised Deployment Platform concept is shown in Figure 1.2.1-85. This will force a requirement for the "short" and "tall" indexers to be 230 m and 110 m in length.

Maintenance Systems Installation

Figure 1.2.1-86 shows the maintenance systems that need to be installed on the antenna as it is fabricated. The issues to be resolved are the following:

a. What beam machines are required to make the track beams and the gantry beams?

   The timeline analysis that is discussed later will show that the beam machine used on the lower level (Beam Machine 2 in Figure 1.2.1-77) is only used intermittently for primary frame assembly. It seems reasonsable to assume that this machine could be used to fabricate both the gantry and the track beams.

b. What cherrypickers could be used for maintenance system installation?

   The two cherrypickers associated with Beam Machine 2 (CP3 and CP4) are also used intermittently, only 4 hours every other day. It is reasonable to assume that these machines could be used to install the gantries, the cherrypickers on the gantries, the track beams, the cargo transporters, and the crew busses. Remember that these systems are installed only on the outboard ends of the primary frame, so there would be plenty of time available to use CP3 and CP4 to do the necessary preassembly operations on the maintenance systems prior to installation.

Antenna Construction Timeline

Each of the construction operations have now been examined in detail to define the times required. The integrated timeline is shown in Figure 1.2.1-87. The locations of some of the construction equipment is shown in Figure 1.2.1-88.

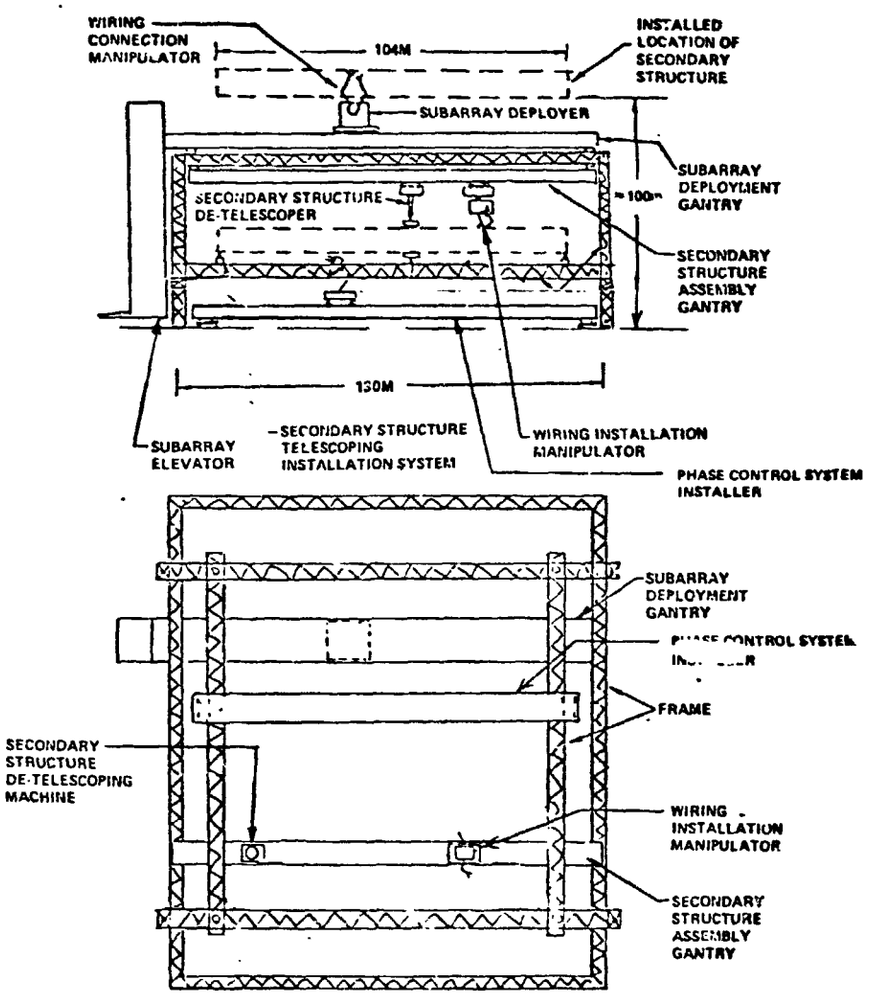

Figure 1.2.1-85 Antenna Construction Platform

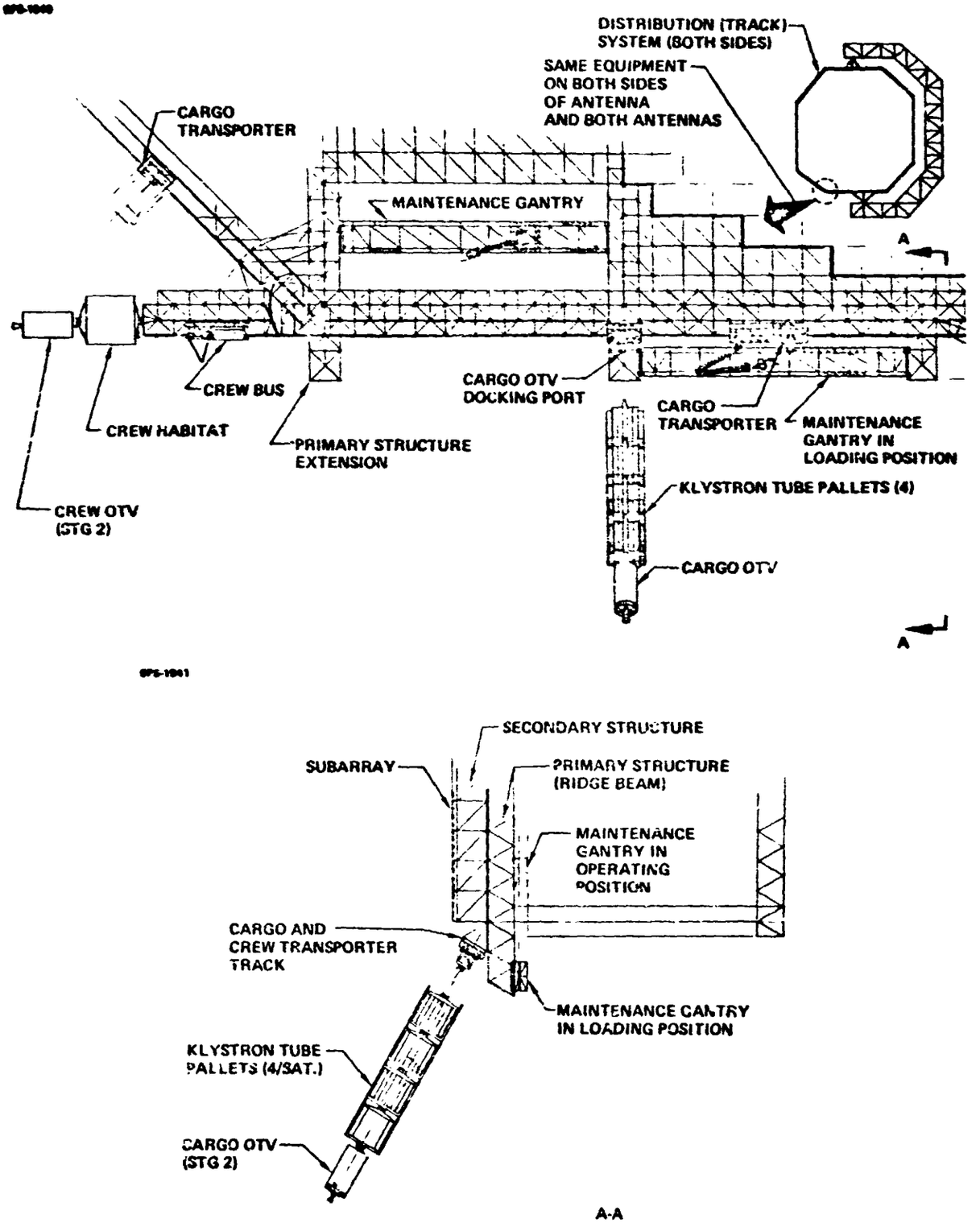

Figure 1.2.1-86 MPTS Maintenance Systems

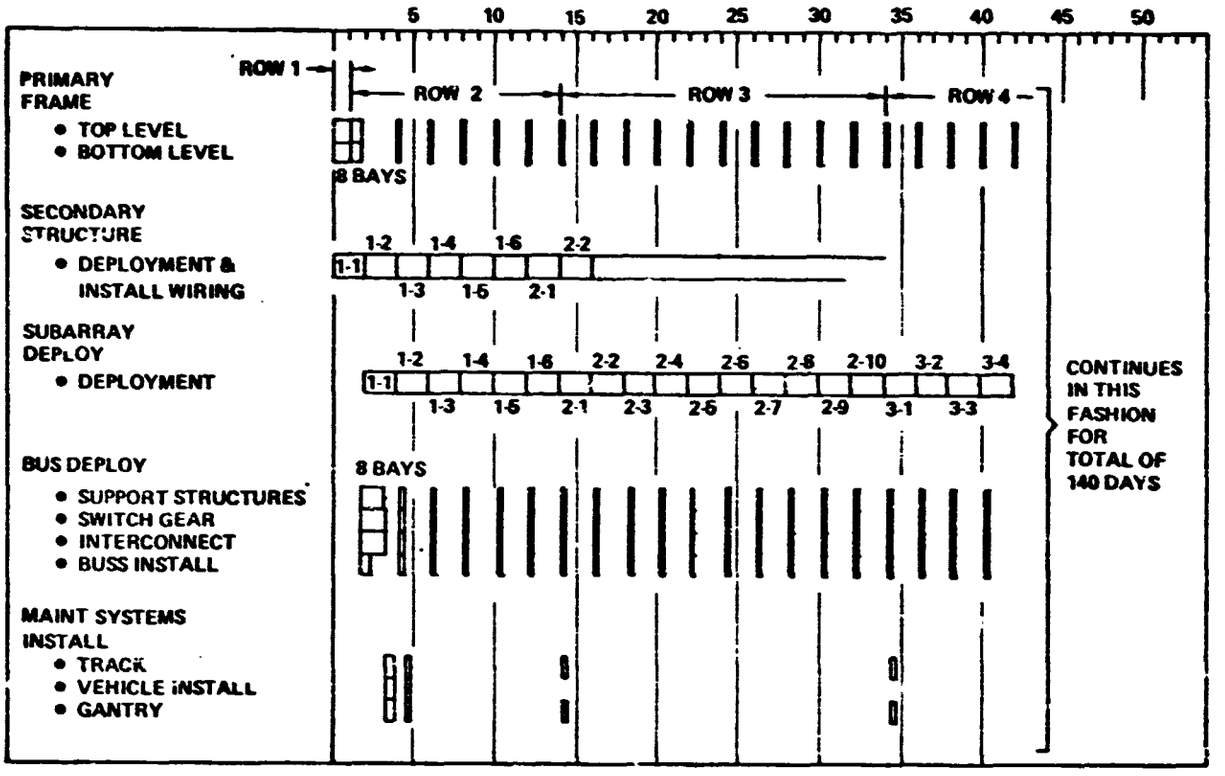

Figure 1.2.1-87 Antenna Construction Timeline

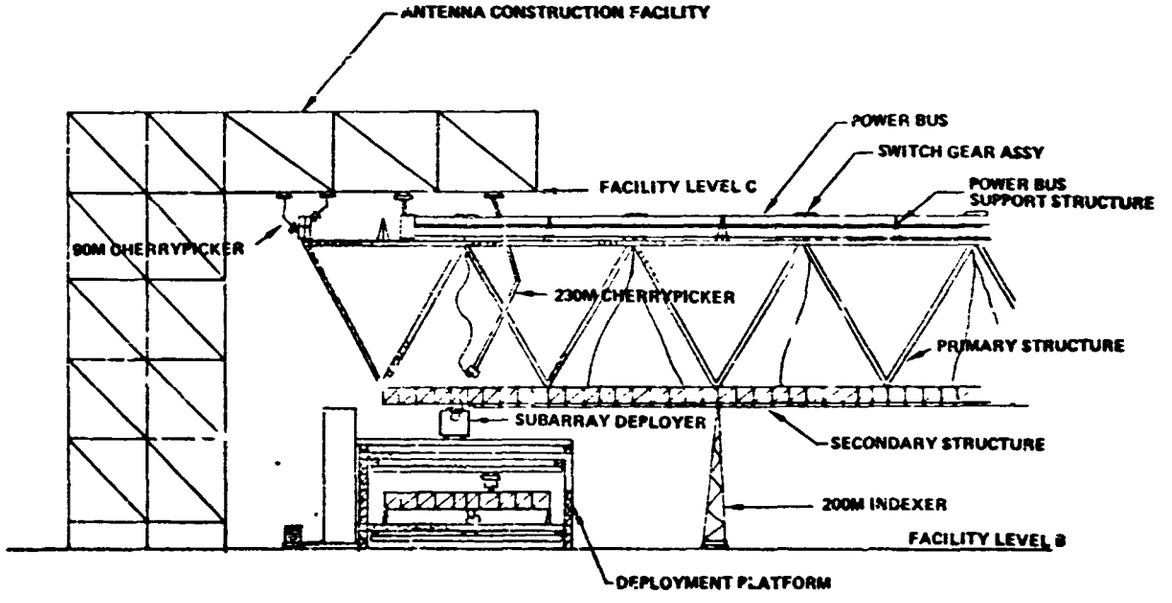

Figure 1.2.1-88 Antenna Construction Equipment Locations

Antenna Construction Equipment and Manning Requirements

The construction equipment revised requirements are summarized in Table 4.2.1-5. The revised manning requirements are shown in Figure 1.2.1-89.

1.2.1.7 Preferred Construction Concept Selection

The single deck and 2 bay/4 bay end builder concepts were all defined to meet the requirements for constructing a 5 GW satellite in GEO every six months. Figure 1.2.1-90 shows the single deck with the 2 bay end builder to approximately the same scale. These concepts were to be evaluated in terms of cost, performance complexity, system complexity, operations complexity, development risk and growth potential. This set of criteria encompasses broad categories which include other factors related to specific programmatic issues and system design considerations.

1.2.1.7.1 Construction Base Cost Comparison

Comparative costs are shown in Figure 1.2.1-91 for the alternate satellite construction approaches. The nominal construction time and maximum construction capabilities are also shown for the alternate bases. Total base costs and the related annual amortization costs are shown. Potential construction interest that can be saved each year by operating at faster rates are also shown and the net annual cost with this interest benefit is provided.

Although the total cost difference is not great, the 2 bay end builder features the least total base cost and a low annual amortization cost with interest benefit.

Further discussion on the cost estimate details and a projected 8 bay base comparison are provided below.

- GEO Construction Base Cost Estimates - The same methodology was used to develop comparable cost data for Boeing's single deck baseline and Grumman's alternate end builder concepts. Cost estimates shown in Figure 1.2.1-92 were developed to the level of base framework, crew modules, construction equipment and logistic equipment (i.e., tracks, turntables and vehicles). Common subsystem and maintenance costs were included in all concepts, as were costs related to antenna construction, yoke construction and subassembly construction activities. A 47% wraparound factor is also included to account for management, system engineering and integration, system test, and the other cost elements noted in the figure. The added costs for transporting base hardware to GEO and conducting recurring crew operations (i.e. for 1 year) are also included.

Table 1.2.1-5 Antenna Construction Equipment Summary

ITEM	QTY	USED FOR
• 7.5m BEAM MACHINE (1)	2	• PRIMARY FRAME BEAMS, MAINT. GANTRY BEAMS, MAINT. TRACK BEAMS
• 120m CHERRY PICKER	2	• (LEVEL B) FRAME ASSY, MAINT. SYS. INSTALLATION
• 80m CHERRY PICKER	2	• (LEVEL C) FRAME ASSY, BUS SYS. INSTALLATION
• 230m CHERRY PICKER	1	• (LEVEL C) POWER DIST. INSTALLATION
• 130m INDEXER	6	• (LEVEL C)
• 230m INDEXER	2	• (LEVEL B)
• 80m BUS DEPLOYER	1	• (LEVEL C)
• DEPLOYMENT PLATFORM		
• SUBARRAY DEPLOYER • GANTRY • ELEVATOR • DEPLOYMENT MACHINE	1	• SUBARRAY INSTALLATION
• WIRING INSTALLER • GANTRY • CHERRY PICKER	1	• POWER DISTRIBUTION WIRING HARNESS INSTALLATION
• PHASE CONTROL SYS. INSTALLER • GANTRY • CHERRY PICKER	1	• PHASE CONTROL DISTRIBUTION WIRING HARNESS INSTALLATION
• DE-TELESCOPES	1	• SECONDARY STRUCTURE DEPLOYMENT
• STRUCTURE INSTALLATION ELEVATORS	4	• SECONDARY STRUCTURE INSTALLATION

(1) EXACT SIZE OF ANTENNA PRIMARY FRAME BEAMS TBD.
FOR BOOKKEEPING PURPOSES A 7.5m BEAM HAS BEEN ASSUMED.

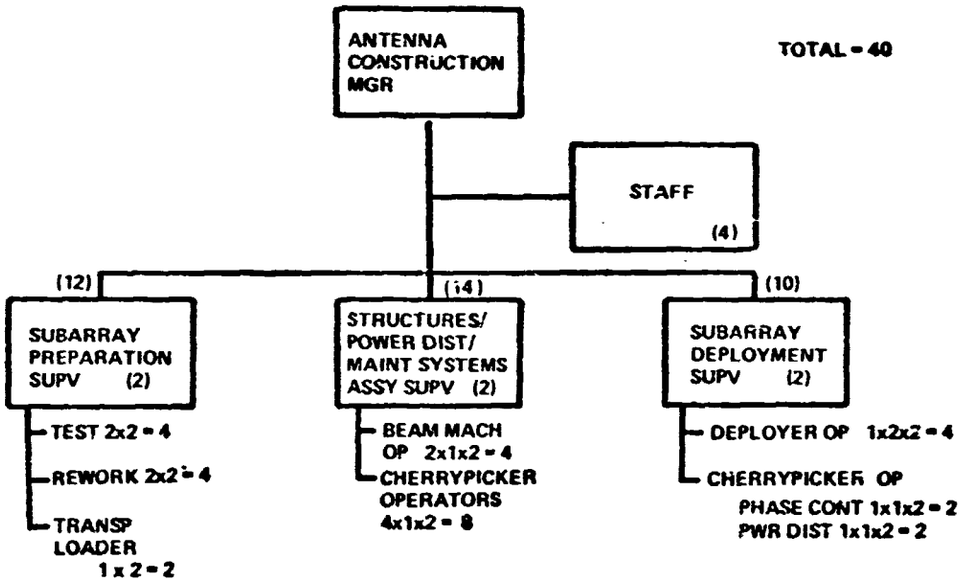

Figure 1.2.1-89 Antenna Construction Crew Size

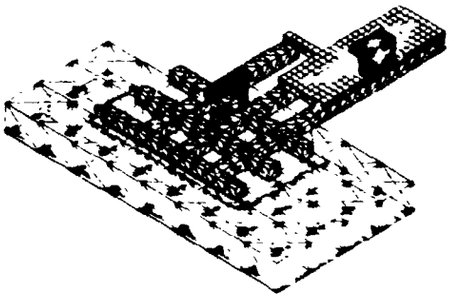

SINGLE DECK
(WITH CONSTRUCTION GANTRY)

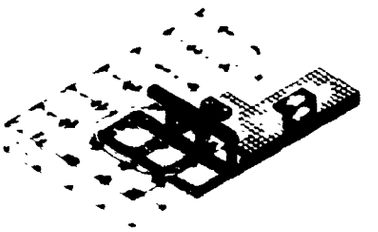

END BUILDER
2 BAY S

- GEO CONSTRUCTION
- 5GW MONOLOTHIC SPS
- 180 DAY CONSTRUCTION TIME
- SAME ANTENNA CONSTRUCTION FACILITY

2955-060V

Figure 1.2.1-90 Alternate Construction Base Concepts

	SINGLE DECK BASELINE	4 BAY END BUILDER	2 BAY END BUILDER
LONG. BEAM DESIGN	SEGMENTED	CONTINUOUS	CONTINUOUS
5GW SPS CONSTR TIME	185 DAYS	181 DAYS	184 DAYS
MAX CONSTR CAPABILITY	185 DAYS	141 DAYS	154 DAYS
TOTAL BASE COST	$9278 M	$9067 M	$8634 M
ANNUAL AMORTIZATION	$ 845 M	$ 830 M	$ 785 M
ANNUAL INTEREST SAVED (@ 3.5m/MIN LONG FAB)	———	$ 215 M	$ 155 M
ANNUAL COST WITH INTEREST BENEFIT	$ 845 M	$ 615 M	$ 630 M

2955-060V

Figure 1.2.1-91 SPS GEO Construction Base Cost Comparison (1977 $)

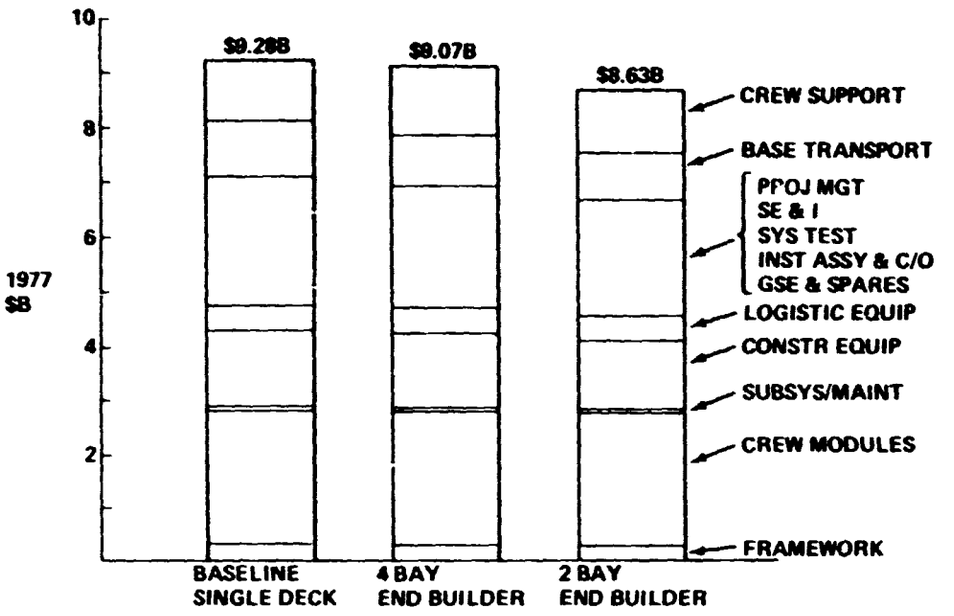

Figure 1.2.1-92 GEO Construction Base Costs

2955-042V

The estimates shown in Figure 4.2.1-93 were jointly reviewed and adjusted, if needed, to assure that comparable design definitions were used across the board. Base framework costs, for example, assume that each configuration employs 100 meter deep structural sections in lieu of the range of "as-drawn" dimensions, which await further loads and stress analysis.

The 2 bay end builder exhibits the lowest cost primarily because it features less costly construction equipment and related crew modules. The 4 bay end builder has more equipment but is slightly less costly than the single deck baseline because of its smaller crew size.

- 8 Bay Base Cost Comparison - Figure 1.2.1-93 provides a graphic comparison of the major cost differences between the alternate construction bases. Total base cost, annual amortization and related interest benefits due to faster construction are shown for the single deck and end builder concepts. Total base costs for the 8 bay end builder were derived from earlier 8 bay versus 2 bay end builder cost comparisons. Accordingly, the 8 bay end builder is projected to cost almost 10% more than single deck baseline and have an equivalent increase in annual amortization costs. It is interesting to note, however, when annual interest benefits are considered, the net annual costs for the 8 bay end builder are no higher than the single deck. Nevertheless, the 4 bay and 2 bay end builder still show the lowest net annual cost with the interest benefit.

1.2.1.7.2 Construction Base Performance Comparison

Comparative performance data are provided in Figure 1.2.1-94 for the alternate construction bases. The base characteristics related to longitudinal beam design, satellite construction approach and nominal construction times are shown together with their comparative masses and maximum construction capabilities. The online beam machines, which are used for continuous fabrication of end builder longitudinal beams, provide an inherent capability for increasing the overall rate of construction. By operating the longitudinal beam machines at 3.5 meters per minute it is possible to save up to 40 days of satellite construction time. The baseline single deck segmented beam method of construction is not able to shorten the rate of construction without

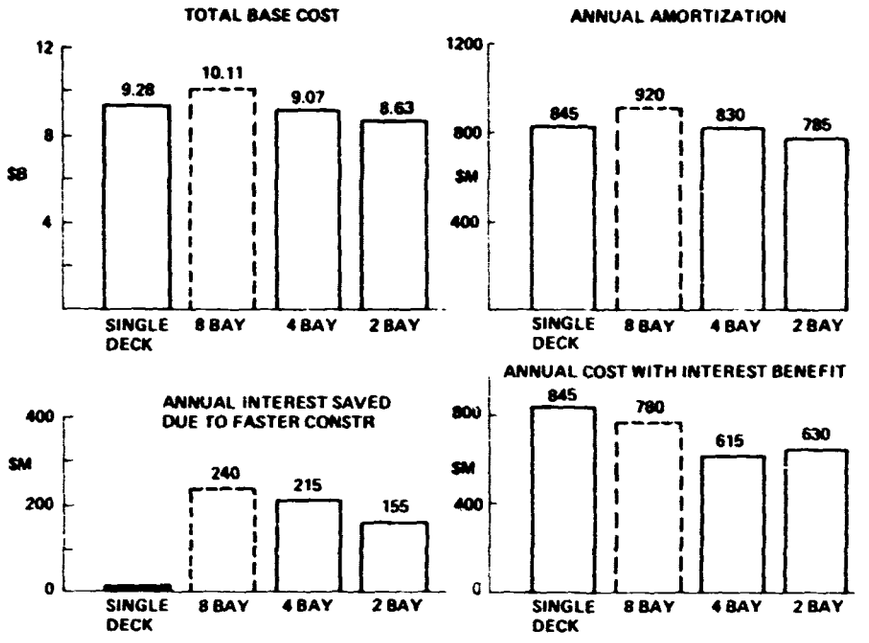

2955-064V

Figure 1.2.1-93 GEO Base Cost Comparison

	SINGLE DECK BASELINE	4 BAY END BUILDER	2 BAY END BUILDER
SATELLITE CONSTR APPROACH	MULTI INDEX	MULTI PASS	MULTI PASS
LONG BEAM DESIGN	SEGMENTED	CONTINUOUS	CONTINUOUS
5GW SPS CONSTR TIME	185 DAYS	181 DAYS	184 DAYS
MASS – TOTAL BASE	6247 x 10^3 Kg	6371 x 10^3 Kg	5740 x 10^3 Kg
– BASE FRAMEWORK	2792 x 10^3 Kg	2927 x 10^3 Kg	2399 x 10^3 Kg
– CONSTR EQUIP	340 x 10^3 Kg	387 x 10^3 Kg	337 x 10^3 Kg
MAX CONSTR CAPABILITY	185 DAYS	141 DAYS*	154 DAYS
SPS CONSTR TIME SAVED		40 DAYS	30 DAYS
ANNUAL CONSTR ADVANTAGE		80 DAYS	60 DAYS
*3.5m/MIN LONG BEAM FAB			

2955-059V

Figure 1.2.1-94 SPS GEO Construction Base Performance Comparison

adding additional crews and equipments. By building two 5 GW satellites a year, the 4 bay end builder therefore can offer an 80 day advantage in faster performance over the single deck.

Comparison of the total base relative masses (see Figure 1.2.1-95) shows that most of the weight difference is attributed to the difference in base configuration framework. As previously noted, the weight of base framework listed herein is normalized to the extent each base was assumed to employ 100 meter deep structural sections, rather than the various deeper and shallower "as drawn" sections which have not been analyzed and sized.

1.2.1.7.3 Construction Base System Complexity Comparison

The major system differences between the alternate construction bases are compared in Figure 1.2.1-96. The single deck builds the segmented beam design and constructs the satellite by performing multiple lateral and longitudinal indexing operations. The end builder concepts, in turn, build the continuous longitudinal beam design and construct the satellite by fabricating in one direction and then re-indexing for a subsequent pass. Other system differences are characterized in terms of the overall base size (with and without the antenna construction facility), module construction work station, major module construction equipment, total crew size, and logistic track. The end builder concepts are generally smaller in size and can be operated with fewer people than the single deck. However, the single deck requires fewer automatic beam machines and cherrypickers than the two end builder concepts. It should be noted, however, that the end builder uses some of its cherrypickers to perform solar array installation functions, using simple proximal anchors from its built in logistic track, in lieu of the large cross bay gantries and related installation/deployment equipment used by the single deck.

1.2.1.7.4 Construction Base Operations Complexity Comparison

The major difference in alternate GEO base construction operations are summarized in Figure 1.2.1-97. All of the alternate bases build the satellite by indexing the base either laterally or longitudinally as permitted by the longitudinal beam design. The single deck segmented longitudinal beam assembly method allows either decoupled or coupled construction techniques to be employed. The baseline single deck approach uses decoupled solar array structure assembly operations. On the other hand, coupled solar array/structure assembly operations are facilitated by the end builder continuous

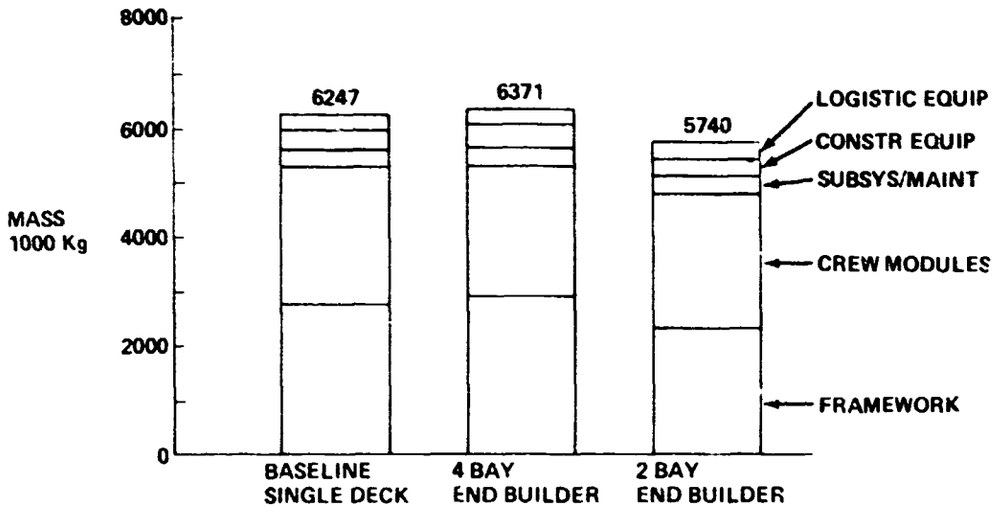

Figure 1.2.1-95 GEO Construction Base Mass Comparison

2955-043V

	SINGLE DECK BASELINE	4 BAY END BUILDER	2 BAY END BUILDER
SATELLITE CONSTR APPROACH	MULTI INDEX	MULTI PASS	MULTI PASS
LONG BEAM DESIGN	SEGMENTED	CONTINUOUS	CONTINUOUS
BASE SIZE – TOTAL	4.59 x 2.9 x .87 Km	3.68 x 2.96 x .70 Km	3.37 x 2.5 x .76 Km
– W/O ANT PLATFORM	2.9 x 1.52 x .87 Km	.86 x 2.96 x .70 Km	.80 x 2.05 x .76 Km
MODULE CONST FACILITY	FLAT DECK W UPPER LEVEL GANTRY STA	FIXED UPPER/ LOWER LEVEL WORK STA	FIXED UPPER/ LOWER LEVEL WORK STA
MODULE CONST EQUIP DELTA			
AUTO BEAM MACHINES	3 MOBILE	3 PLUS 10 SYNC	3 PLUS 6 SYNC
CHERRY PICKERS (30 & 80m)	8	11*	11*
INDEXERS	6	8	8
S/A INSTALL EQUIP	4 INSTALLER, DEPLOYER & CROSS BAY GANTRIES	PROXIMAL ANCHORS & SHARED C.P.S*	PROXIMAL ANCHORS & SHARED C.P.S*
CREW SIZE	407	385	383
LOGISTIC TRACK	60800 Km	77700 Km	60800 Km

Figure 1.2.1-96 SPS GEO Construction Base System Complexity Comparison

2955-073V

	SINGLE DECK BASELINE	4 BAY END BUILDER	2 BAY END BUILDER
LONG BEAM DESIGN	SEGMENTED	CONTINUOUS	CONTINUOUS
SATELLITE ASSY MODE	16 ROW LATERAL BUILDUP	2 PASS LONG BUILDUP	4 PASS LONG BUILDUP
SOLAR ARRAY/STRUCTURE ASSY	DECOUPLED	COUPLED	COUPLED
LONG BEAM FAB	AS REQD	SYNCHRO-NIZED	SYNCHRO-NIZED
BEAM MACHINE MAINTENANCE	OFF LINE	ON/OFF LINE	ON/OFF LINE
S/A BLANKET DEPLOY	SINGLE STRIP @ A TIME	176 STRIPS OR SINGLE STRIP	88 STRIPS OR SINGLE STRIP
ANTENNA MATING MODE	TRANS LONG	TRANS LATERAL	TRANS LATERAL

Figure 1.2.1-97 SPS GEO Construction Base Operations Complexity Comparison

2955-029V

longitudinal beam approach. This end builder approach necessitates that all automatic longitudinal beam machines be synchronized and be capable of being maintained and repaired both on and off line. The end builder solar blankets can either be deployed longitudinally (88 or 176 strips) or laterally (single strip) as the baseline. Each alternate base uses a similar method for translating and mating the satellite antenna.

1.2.1.7.5 Construction Base Development Risks

The major construction elements that must be developed for either the single deck or the end builder concepts are listed in Figure 1.2.1-98. Some of the differences in system development requirements include single deck upper level gantry control, end builder automatic longitudinal beam machine synchronization, and other differences in single deck/end builder solar array installation and deployment equipments. None of the above differences are judged to be significant, hence all concepts are cited to have a moderate development risk.

1.2.1.7.6 Construction Base Growth Capability

The ability of the alternate construction bases to be adapted to other requirements than those studied for GEO construction are summarized in Figure 1.2.1-99.

Growth in SPS production rate requirements implies added crews and equipments for the single deck. For the end builders these added costs can be deferred until the longitudinal beam fabrication rate capability is reached (i.e., about 3.5 meters/min).

All alternate bases can be expanded if needed to build the 8 x 16 bay satellite in one pass. Each concept can also build pentahedral structures or be adapted for use in LEO construction. In addition they can readily build smaller or larger satellites which require fewer or more bays of the same size. Should smaller or larger satellites be required with different size bays after the base has been built, then the single deck approach is probably easiest to adapt.

1.2.1.7.7 Alternate Construction Concept Summary Comparison

The major differences identified in the evaluation of alternate GEO construction bases are summarized in Figure 1.2.1-100. Each concept is compared in terms of its major costs (total base cost and annual amortization with interest benefits) system characteristics (base mass and crew size), operations complexity, performance capability, development risk and growth capability related to SPS size. Both the 2 bay and 4 bay

	BASELINE SINGLE DECK	4 BAY END BUILDER	2 BAY END BUILDER
MAJOR CONSTR ELEMENTS	• FLAT DECK SYS • UPPER LEVEL GANTRY CTL • MOBILE BEAM MACH • CHERRY PICKERS • INDEXERS • SOLAR ARRAY INSTALLER • S/A DEPLOYER • S/A CROSS BAY GANTRY • BUS DEPLOYERS • LOGISTIC EQUIP	• 4 BAY SYS • MOBILE BEAM MACH • BEAM MACH SYNC • CHERRY PICKERS • INDEXERS • PROXIMAL ANCHOR • BUS DEPLOYERS • LOGISTIC EQUIP	• 2 BAY SYS • MOBILE BEAM MACH • BEAM MACH SYNC • CHERRY PICKERS • INDEXERS • PROXIMAL ANCHOR • BUS DEPLOYERS • LOGISTIC EQUIP
DEVELOPMENT RISK	• MEDIUM	• MEDIUM	• MEDIUM

Figure 1.2.1-98 SPS GEO Construction Base Development Requirements

2955-030V

	SINGLE DECK BASELINE	4 BAY END BUILDER	2 BAY END BUILDER
PRODUCTION RATE SCALE UP (FASTER PRODUCTION)	• ADD EQUIP & CREWS	• INCREASE L BEAM FAB RATES (0.5 TO 3.5 m/MIN) • ADD EQUIP & CREWS	• INCREASE L BEAM FAB RATES (1.0 TO 3.5 m/MIN) • ADD EQUIP & CREWS
SINGLE PASS 8 x 16 BAY SATELLITE CONSTR	EXPAND BASE TO SUIT	EXPAND AS REQ	EXPAND AS REQ
SUITABLE FOR PENTAHEDRAL CONSTR	OK	OK	OK
ADAPTABLE TO LEO CONSTR	OK – MOVE ANT PLATFORM TO END	OK – EITHER TURN ANT PLATFORM SIDEWARD OR LOCATE ON TOP	
SMALLER SATELLITE – FEWER BAYS	OK	OK	OK
– SMALLER BAYS	RESIZE UPPER LEVEL GANTRY	RESIZE BASE	RESIZE BASE
LARGER SATELLITE – MORE BAYS	OK	OK	OK
– LARGER BAYS	RESIZE DECK & GANTRY	RESIZE BASE	RESIZE BASE

Figure 1.2.1-99 SPS GEO Construction Base Growth Capability

2955-028V

CRITERIA	SINGLE DECK	4 BAY END BUILDER	2 BAY END BUILDER
BASE COST	$9.28B	$9.07B	$8.63B
ANNUAL AMORT W INTEREST BENEFIT	$845M	$615M	$630M
BASE MASS	6247 x 10^3Kg	6371 x 10^3Kg	5740 x 10^3Kg
CREW SIZE	407	385	383
OPERATIONS COMPLEXITY	DECOUPLED S/A-STRUCT ASSY	COUPLED S/A STRUCT ASSY	COUPLED S/A STRUCT ASSY
PERFORMANCE CAPABILITY	ADD EQUIP FOR FASTER PRODUCTION	40 DAY FASTER INHERENT	30 DAY FASTER INHERENT
DEVELOPMENT RISK	MEDIUM	MEDIUM	MEDIUM
GROWTH (SPS SIZE)	EASIEST TO ADAPT	MODIFY AS REQ	MODIFY AS REQ
RECOMMENDATION			
SIMPLE OPS IMPORTANT	✓		
FASTER PROD IMPORTANT		✓	✓

7955-041V

Figure 1.2.1-100 Alternate Construction Concept Summary Comparison

end builders provide higher performance capability (40 days faster at 3.5 m/min). Hence if faster production capability is important then the 4 bay end builder is preferred.

However, the single deck appears simpler to operate due to having less construction equipment. The single deck is probably also easier to adapt to major changes in satellite design. Therefore, if simple operations are more important than faster production capability, then the single deck is preferred.

1.3 SPACE TRANSPORTATION

Three study activities were conduced under this WBS item:

1) HLLV trajectory analyses investigating ways of ameliorating potential environmental effects of HLLV operations with high launch rates;

2) Evaluation of dedicated electric orbit transfer vehicles for delivery of SPS cargo to geosynchronous orbit, including evaluation of space construction and SPS design factors related to the relative cost of electric OTV's as compared to the earlier self-power baseline.

3) An exploratory investigation of possible effects of electric propulsion operations on the geomagnetosphere.

1.3.1 HEAVY LIFT LAUNCH VEHICLES

1.3.1.1 Launch Trajectories

Problem Statement

A preliminary study by the Los Alamos Scientific Laboratory raised concerns over depletion of the ionosphere F-layer by exhaust products from HLLV's. This study assumed that the HLLV ascent trajectory will reach the F-layer. The reference trajectory is shown in Figure 1.3.1-1; it never gets closer than 75 km from the bottom of the F-layer. Boeing conducted a preliminary analysis under IR&D to examine the possibility of deleterious effects from this trajectory. It was concluded that:

(1) The effects on the ionsophere will be about a factor of five less than projected by the LASL study. Even though the trajectory stays well below the ionsophere, the hydrogen from the rocket engines will diffuse rapidly up to the F-layer and cause some depletion.

(2) There does not appear to be any concern regarding the ozone layer. It is even possible that water diffusing downward could reduce ozone depletion by other reactants such as aerosol propellants.

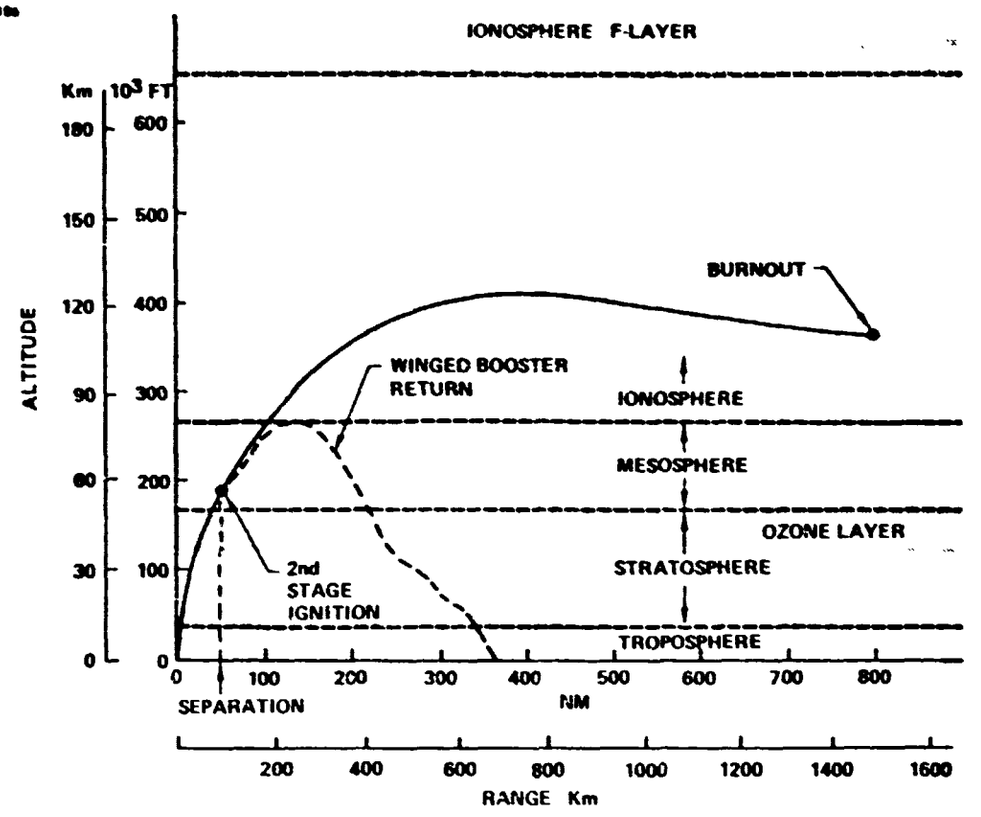

Figure 1.3.1-1 Reference HLLV Launch Trajectory

(3) If the trajectory peak altitude could be suppressed to about 100 km, the ionosphere concerns would be much reduced.

Trajectory Analyses

It was concluded that the trajectory modification task should investigate the feasibility of reducing the ascent trajectory maximum altitude to about 100 km. (The earlier reference trajectory has a maximum altitude of about 125 km for injection to a 100 km x 477 km transfer orbit.) Three trajectory shaping methods were studied: (1) changing injection altitude; (2) using a commanded rather than optimized upper stage angle of attack profile; (3) using a commanded rather than optimized booster initial tilt. (All booster trajectories were zero-angle-of-attack gravity turns.) Figure 1.3.1-1 presents a summary of results. Table 1.3.1-1 summarizes key trajectory parameters. The trajectory plots from which these points were taken are shown in Figures 1.3.1-3 through 1.3.1-16.

The scatter in Figure 1.3.1-2 results from non-optimality of the path depression strategies. Best vehicle performance occurred with a peak altitude of 110 km (360,000 feet). The performance penalty for suppression to 100 km is about 2-1/2%.

1.3.1.2 Return Trajectories

Overpressures (sonic booms) result from supersonic flight of vehicles departing for, or returning from, space. In the case of a launch site on the Eastern Seacoast, such as KSC, the departure overpressures occur some distance at sea and are of little environmental concern. The same is true for booster reentries. (Booster flyback to the launch site will be subsonic). The orbiter, however, returns to the launch site. The level of expected overpressure is greater with larger vehicle size and higher wing loading and varies considerably with the local weather conditions. The baseline SPS HLLV orbiter is much larger than the shuttle orbiter but lower in wingloading--its predicted overpressure is about twice that for the Shuttle. The overpressure level, roughly 145 pa (3 psf) is in the nuisance (not damaging) range, but the potential frequency of occurrence, on the order of once a day, motivates a search for trajectory strategies than can ameliorate this problem.

The highest overpressures come from that part of the trajectory near Mach 1.5. The hypersonic part of the trajectory produces relatively little overpressure. Accordingly, a potentially beneficial strategy is the supersonic turn: Cross the coastline at a

SPS-2625

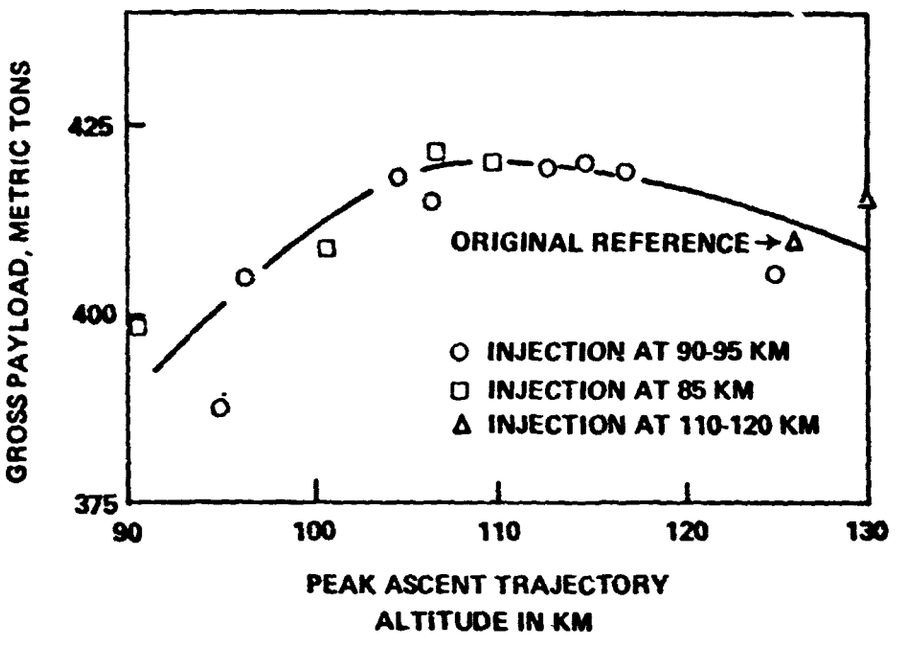

Figure 1.3.1-2 Launch Trajectory Suppression Results

Table 1.3.1-1 Trajectory Summary (by perigee)

SPS-2624

RUN #	PERIGEE (km)	ΔV_C (FPS)	WMECO	ΔW_{CIRC}	$\Delta W_{CIRC\ TRIM}$	RCS TRIM	$W_{P/L}$
006	93	364.1	1,918,250	44,553	4397	11,807	924,134
007	93	364.1	1,886,240	43,805	4323	11,609	893,518
001	93†	364.1	1,916,800	44,515	4393	11,797	922,581
004	93†	364.1	1,909,520	44,348	4377	11,753	915,761
002	93†	364.1	1,845,750	42,855	4229	11,357	854,608
014	93†	364.1	1,883,790	43,793	4322	11,606	893,003
008	93	364.1	1,918,190	44,552	4397	11,806	924,077
005	90	366.0	1,920,100	44,926	4224	11,817	925,658
003	86†	371.0	1,922,360	45,485	4488	11,326	927,186
012	86†	371.0	1,875,310	44,367	4777	11,535	882,221
013	86	371.0	1,894,870	44,829	4423	11,656	900,813
010	120	336.7	1,003,620	40,920	4042	11,739	913,691
011	110	348.5	1,905,000	42,129	4160	11,740	910,168
009	80†	376.9	1,924,260	46,125	4550	11,834	928,339

* INDICATES ENTIRE TRAJECTORY <100km
† INDICATES TRAJECTORY NEAR 100 km <105km

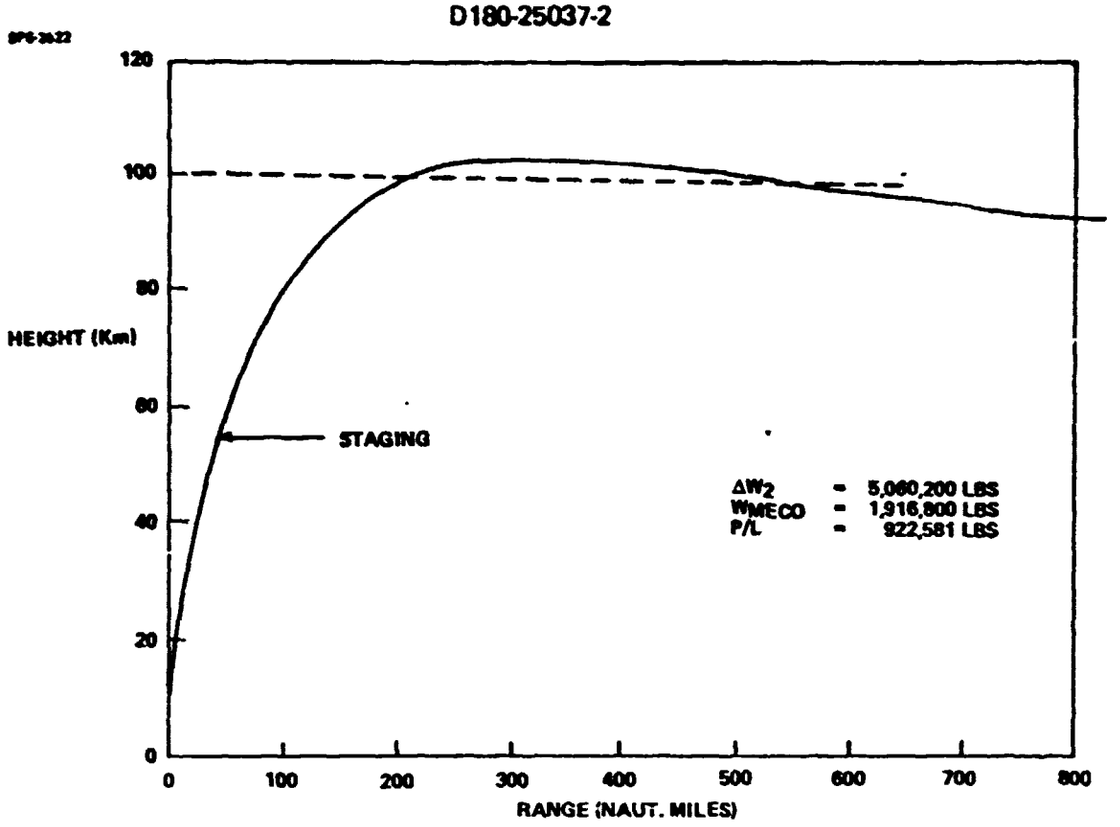

Figure 1.3.1-3 93x477 km orbit "Manual Alpha"

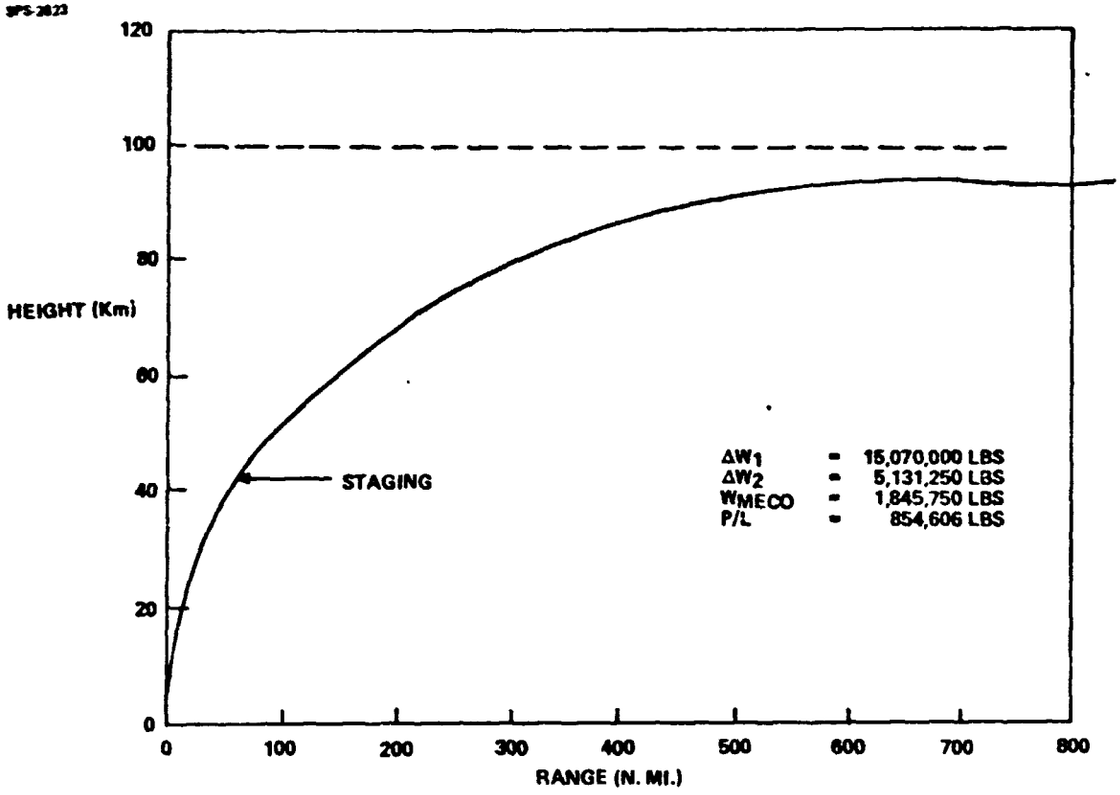

Figure 1.3.1-4 93x477 km explicit trajectory Tilt = 82.0

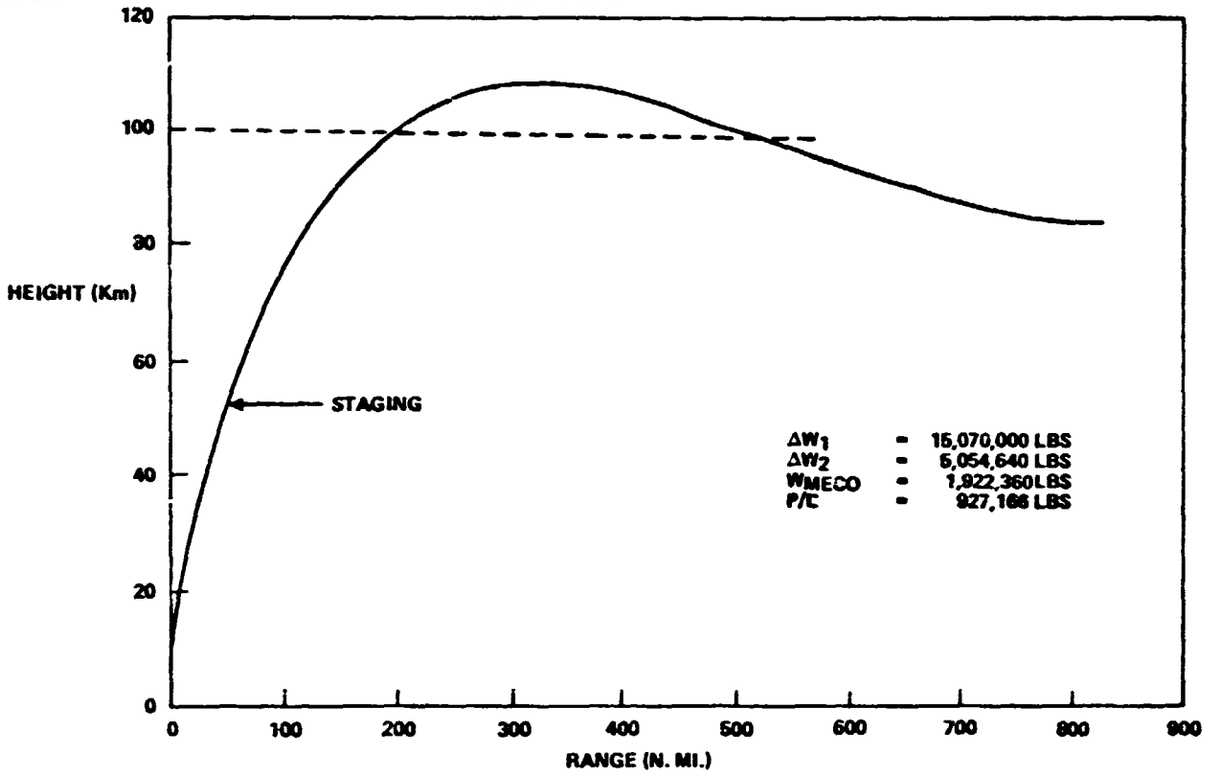

Figure 1.3.1-5 85x477 km Reference Case Explicit Trajectory

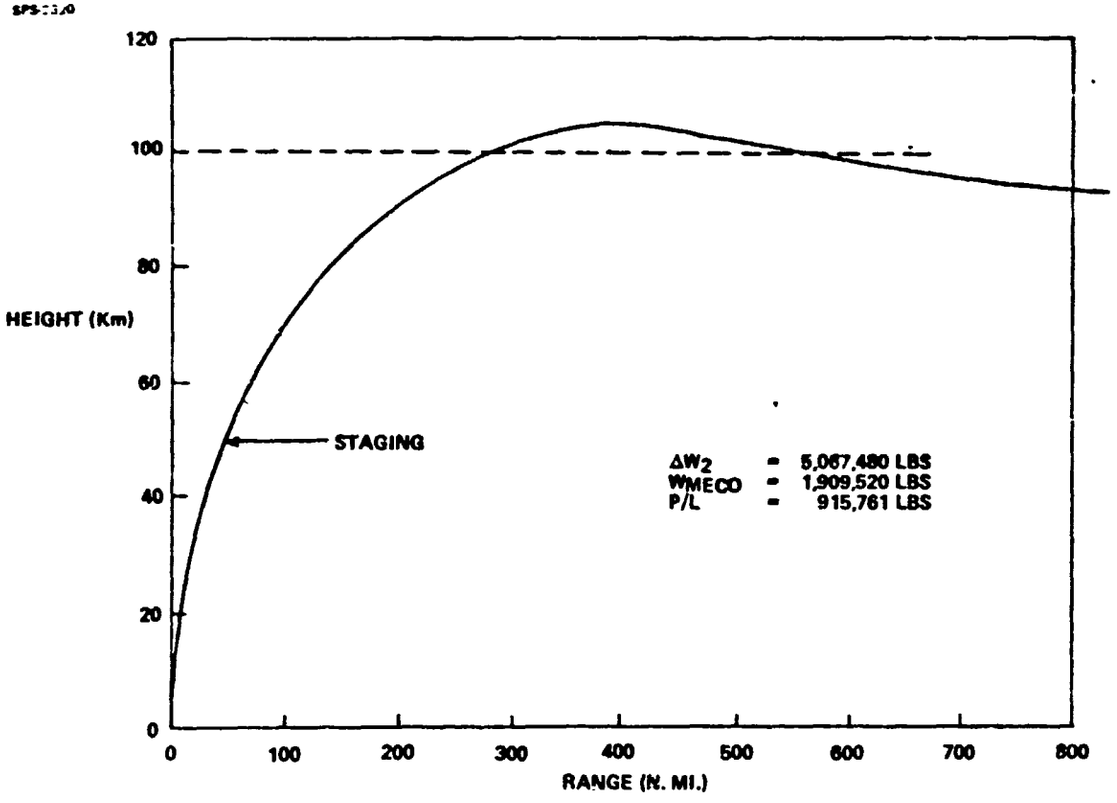

Figure 1.3.1-6 Insertion to 93x477 km Orbit (Fixed Tilt = 83°)

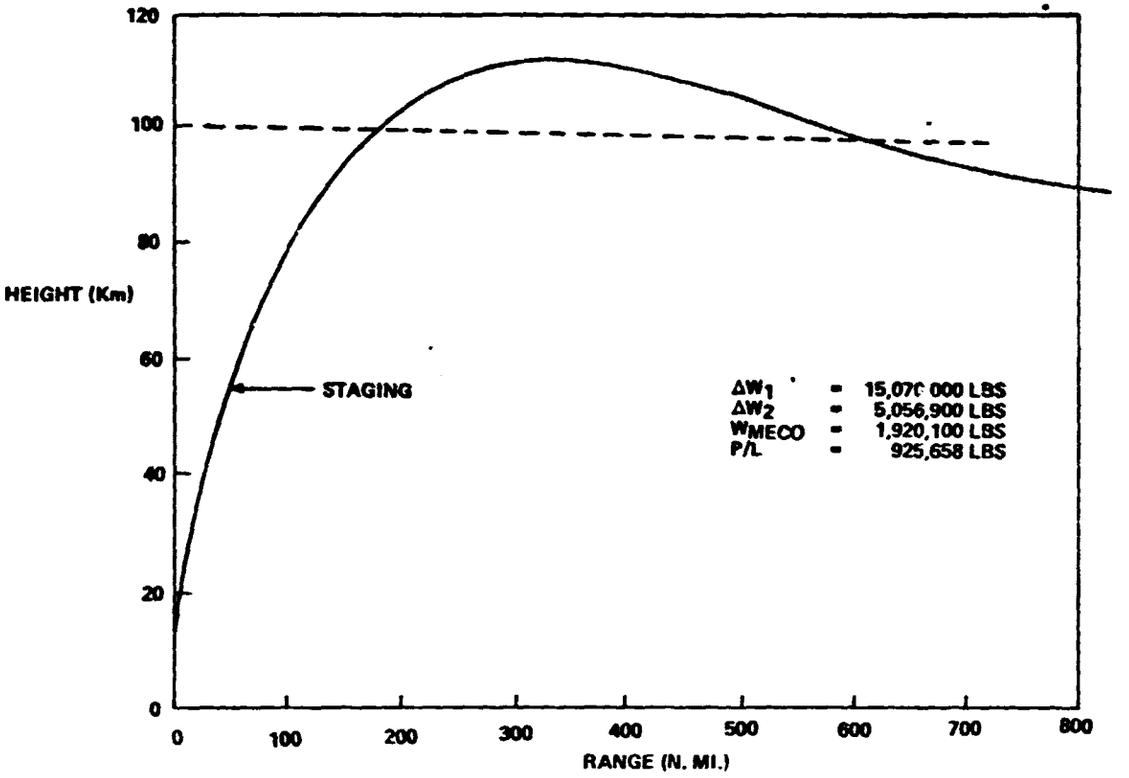

Figure 1.3.1-7 90x477 km Orbit (Reference Case)

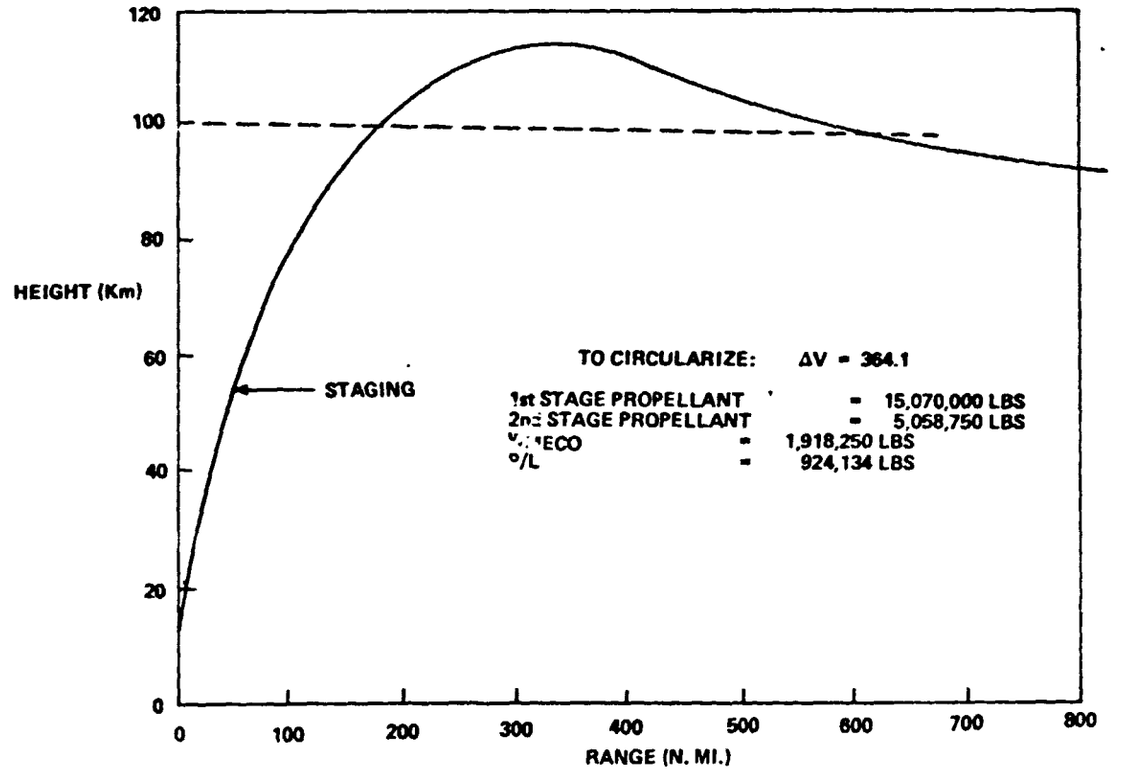

Figure 1.3.1-8 Insertion to 93x477 km Orbit (Reference Case)

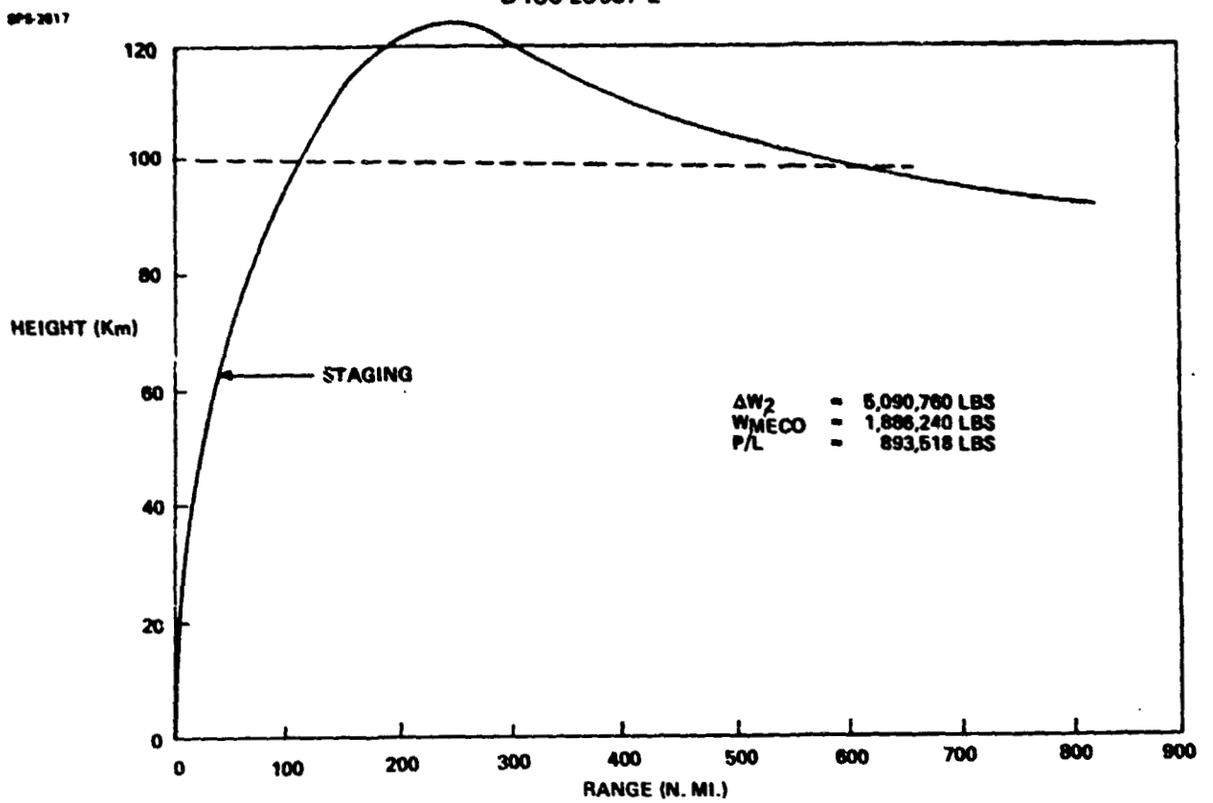

Figure 1.3.1-9 Insertion to 93x477 km Orbit (Manual Angle of Attack)

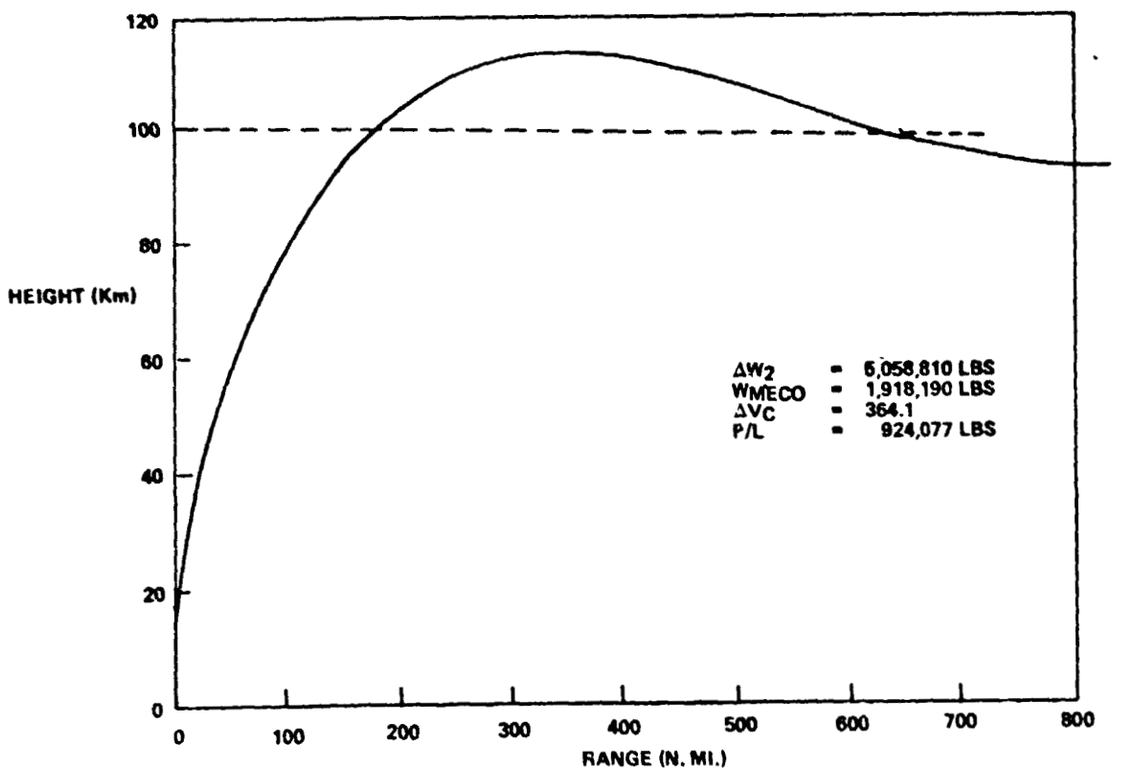

Figure 1.3.1-10 93x477 km Orbit (Tilt = 83.5°)

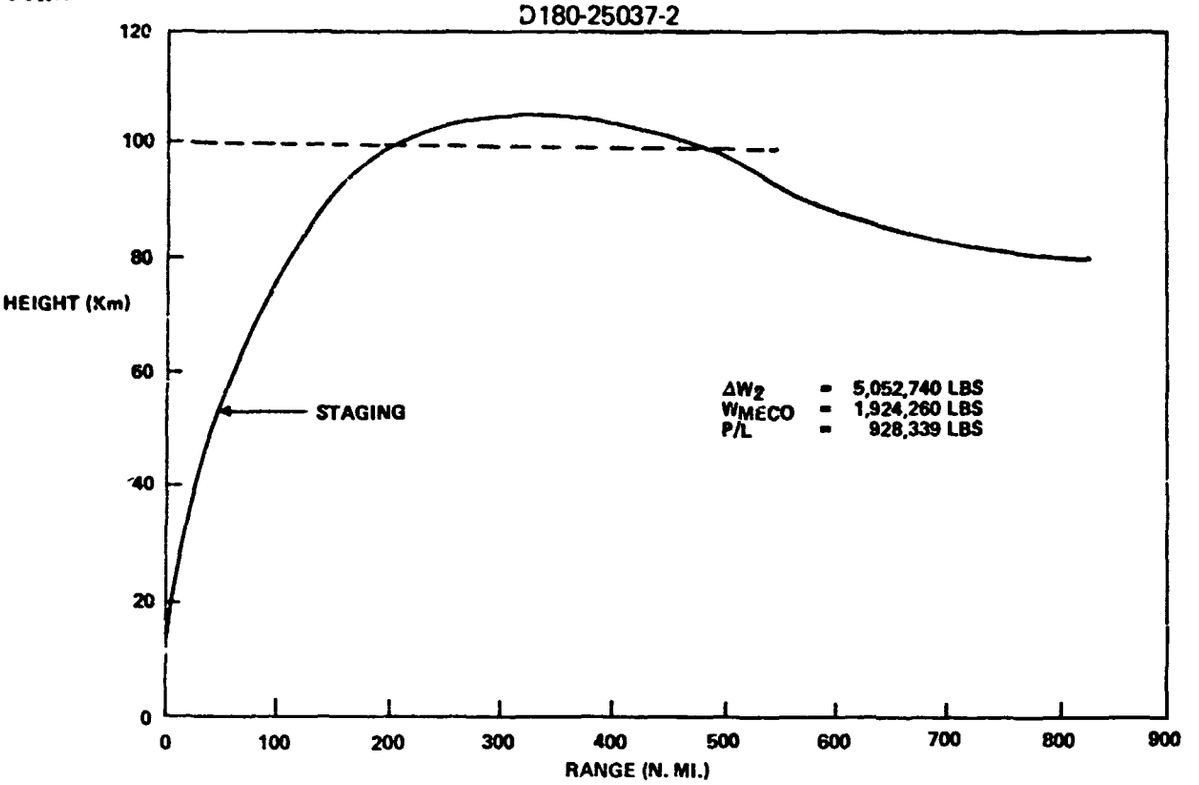

Figure 1.3.1-11 80x477 km (Reference)

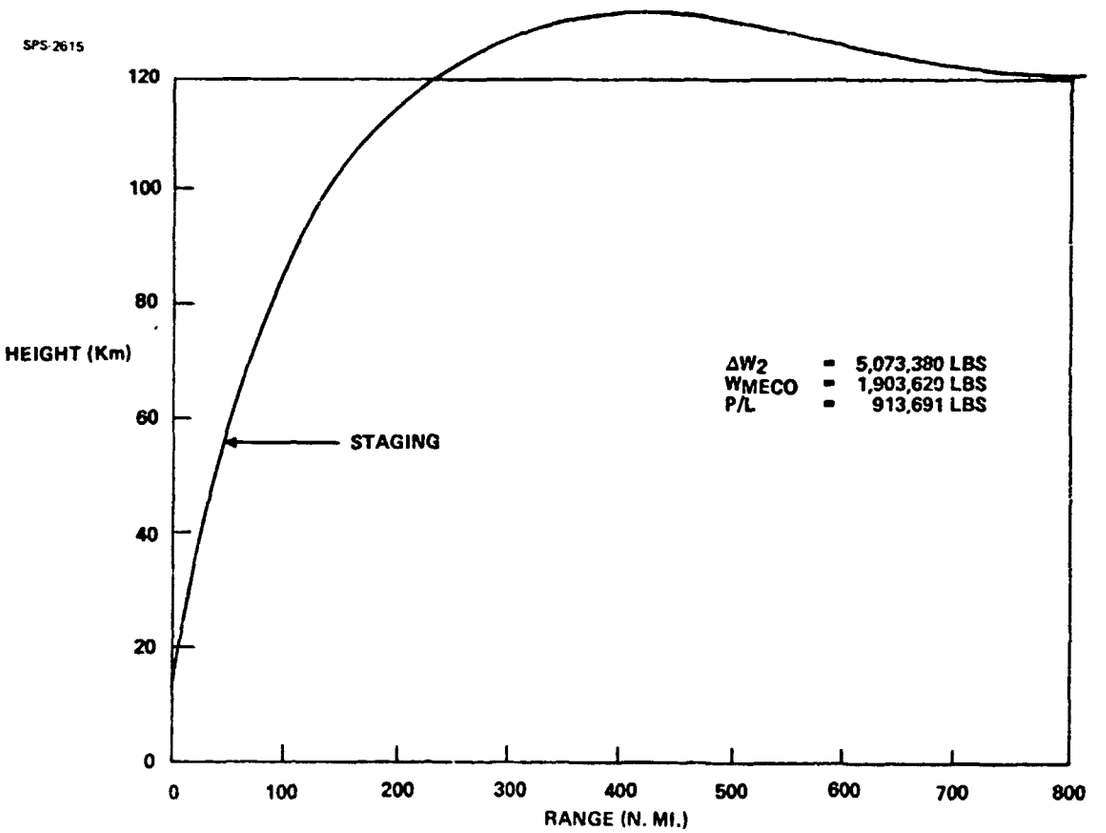

Figure 1.3.1-12 120x477 km (Reference)

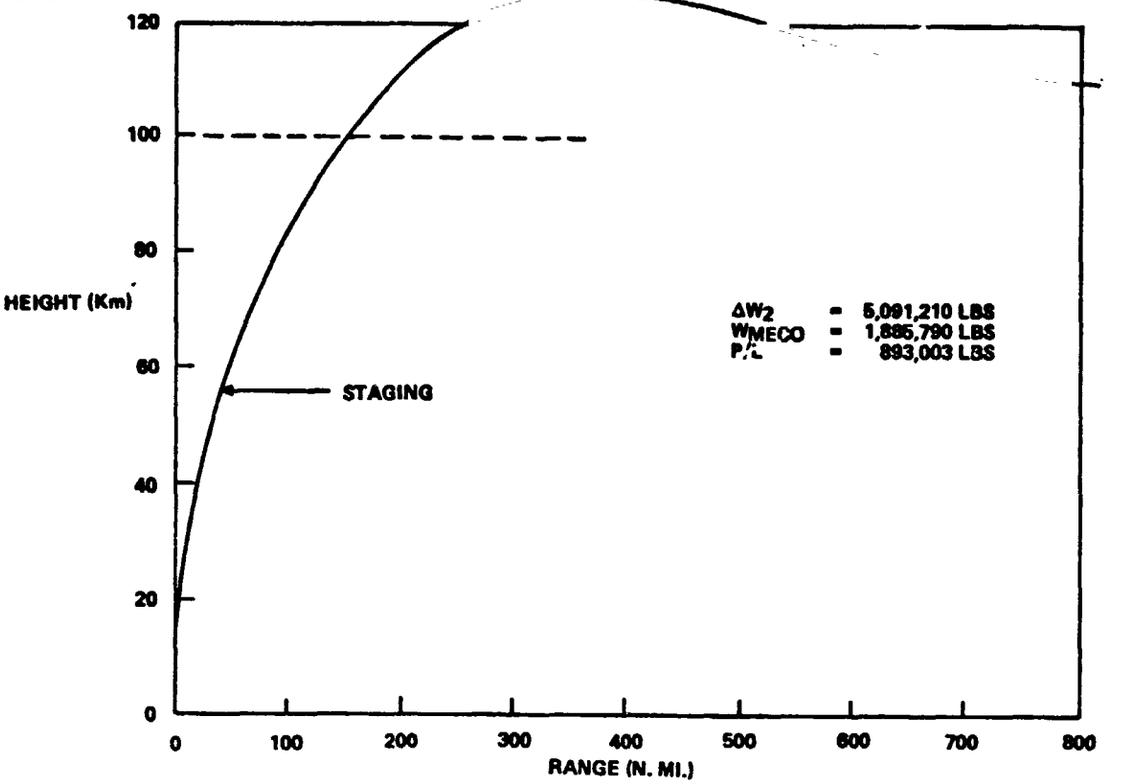

Figure 1.3.1-13 110x477 km (Reference)

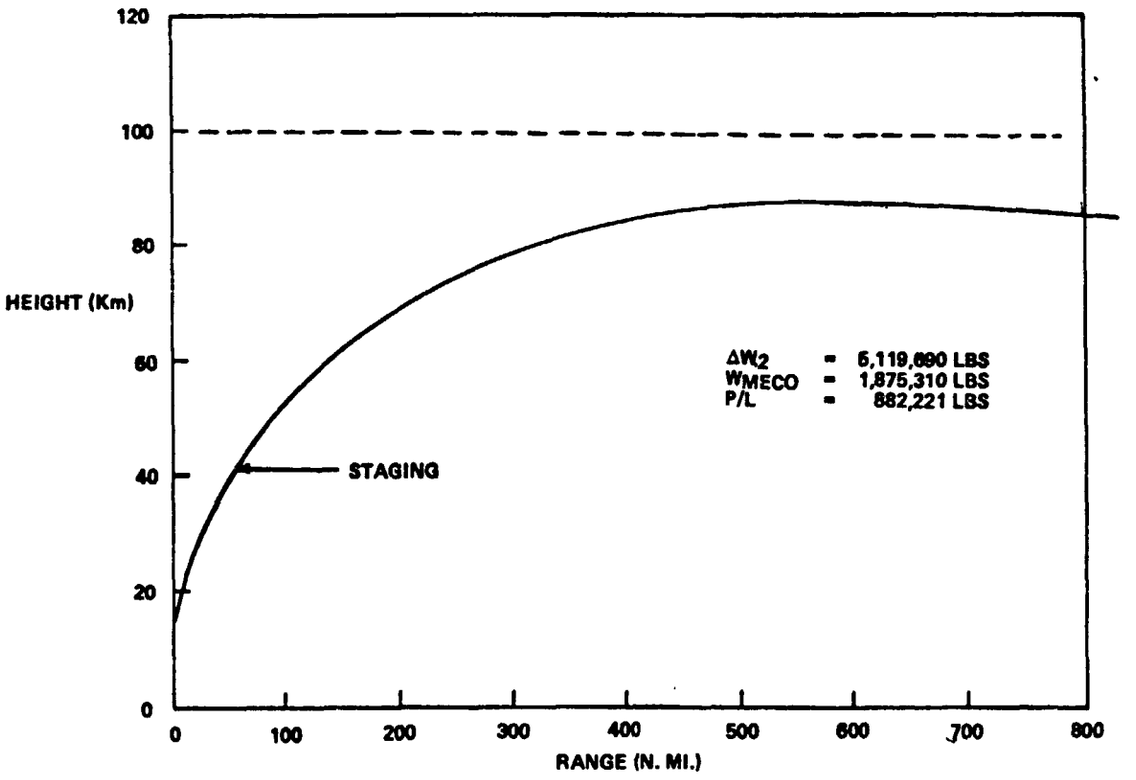

Figure 1.3.1-14 85x477 km (Tilt - 82.0)

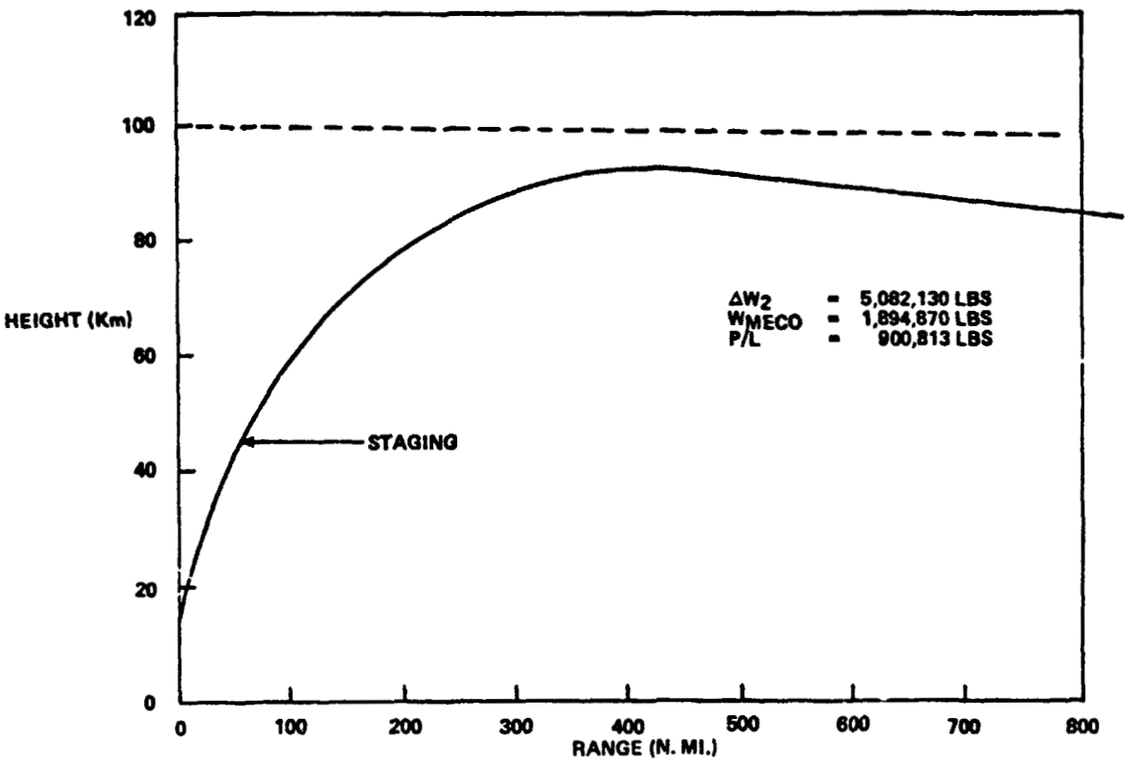

Figure 1.3.1-15 85x477 km (Tilt - 82.5°)

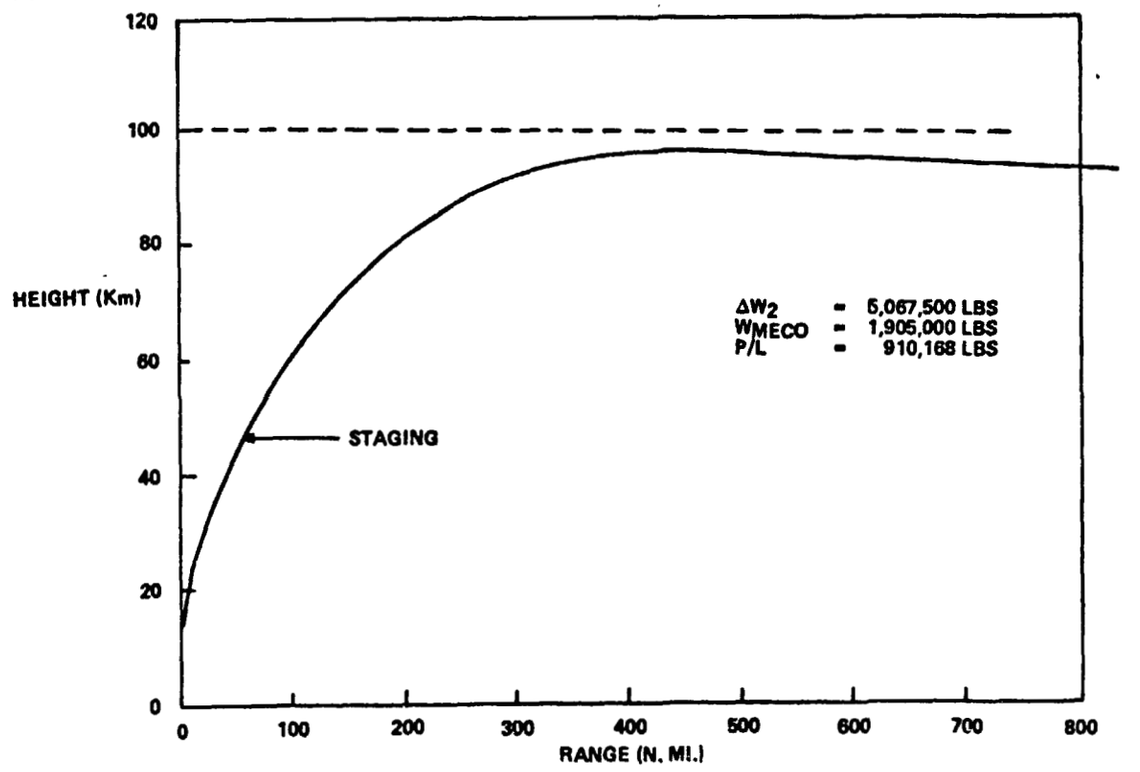

Figure 1.3.1-16 93x477 km (Tilt = 82.5°)

high supersonic or hypersonic speed; initiate a turn to reverse direction; complete the turn at sufficiently high altitude and speed to allow a return to the launch site with sufficient altitude left at arrival to permit a safe approach and landing; try to accomplish subsonic transition far enough at sea to avoid strong overpressures reaching land.

The trajectory design entails several considerations. (1) The hypersonic flight portion should occur at maximum lift coefficient (angle of attack about 55 degrees) to maximize flight altitude and thereby minimize heating rates and overpressures; (2) the turn should be flown at maximum L/D to enable turn completion at maximum speed* and altitude. Maximum L/D occurs at an angle of attack between 20 and 25 degrees; (3) if a sudden transition is made from 55° angle of attack to 25° angle of attack and 45° bank, the lift will decrease markedly below weight and a dive will result. Accordingly, a transition is needed. Smooth transitions were found possible by gradually reducing angle of attack from 55 degrees at M=10 to 20 degrees at M=5; (4) attempts to control the turn by maintaining a normal load factor of $\sqrt{2}$ (the "ideal" turn at 45° bank) generally resulted in a progressively increasing angle of attack until C_L max was exceeded and the normal load factor could not be maintained. Holding a constant angle of attack at 20° to 25° resulted in good turn control; (5) glideback should be performed at L/D max to maximize range. Subsonic L/D max occurs at an angle of attack of about 10 degrees.

Several trajectory strategies were investigated. There did not appear to be much advantage to turn initiation at speeds greater than about Mach 5.

Figure 1.3.1-17 shows the command sequence (angles of attack and bank) found most effective. Figure 1.3.1-18 shows the resulting altitude and dynamic pressure as a function of Mach number. Figure 1.3.1-19 shows a map of the 180° turn superimposed on Florida. Figure 1.3.1-20 shows altitude as a function of great circle range.

The vehicle response in terms of altitude, and particularly dynamic pressure, to the command angle-of-attach changes is clear. The vehicle crosses the coastline at

* Note that the ratio of change of momentum vector direction to loss of momentum due to drag (at constant altitude) is $dm_{\perp}/dm_{\parallel} = (L/D \sin \phi)$ where ϕ is bank angle. One can readily show that $V_2/V_1 = \exp. (\theta/L/D \sin \phi)$ if altitude and L/D are constant.

Mach 4 and 120,000 feet. At this point the predicted sonic overpressure is under 2 psf. Further slight improvements in this trajectory could be made by maintaining the angle of attach at 20° until speed drops to about 0.8 Mach number. It may also be noted that if the vehicle approaches Florida on a southerly azimuth, a turn of only slightly over 90° is required.

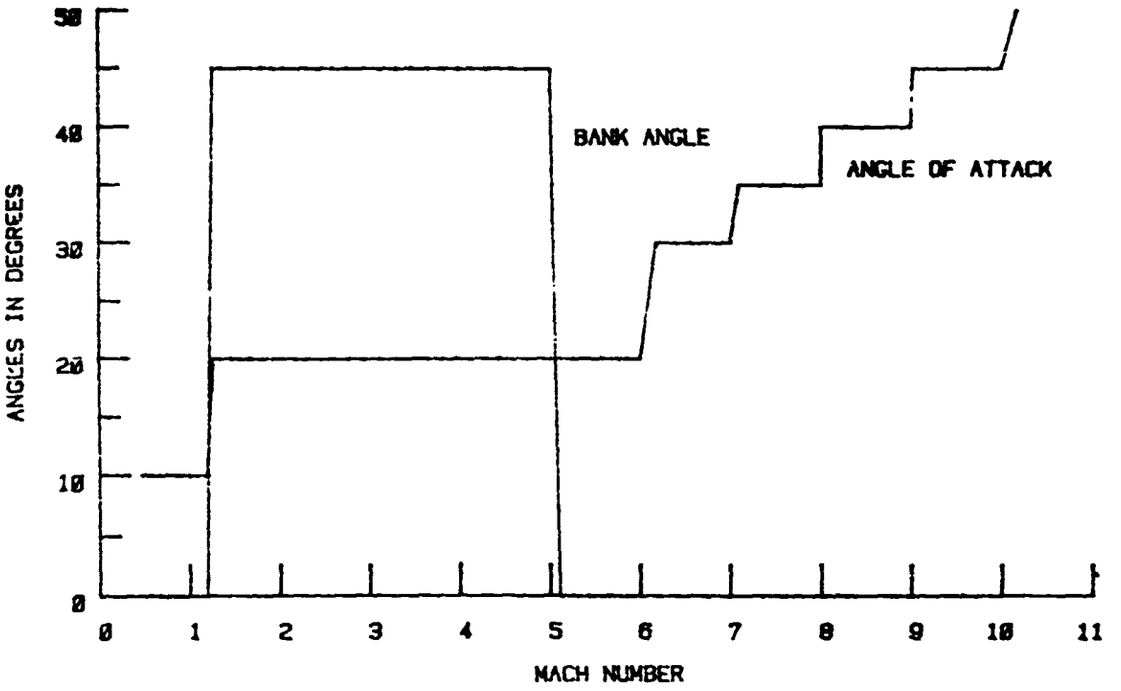

Figure 1.3.1-17 Trajectory Command Sequence

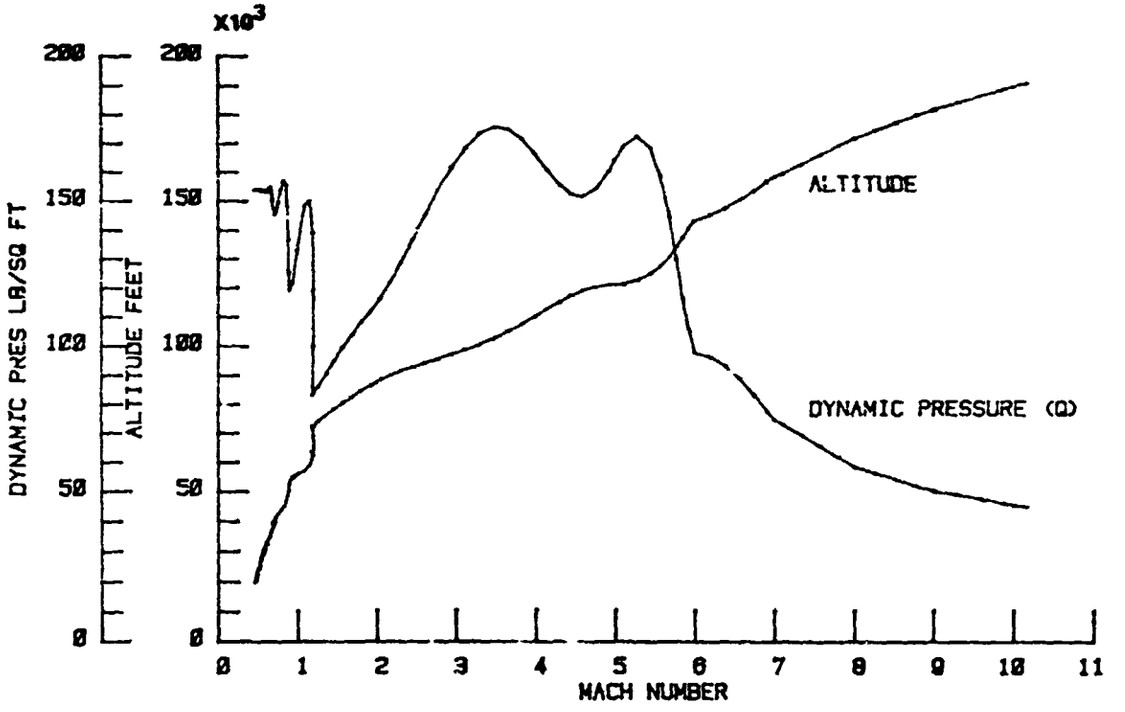

Figure 1.3.1-18 Trajectory Results

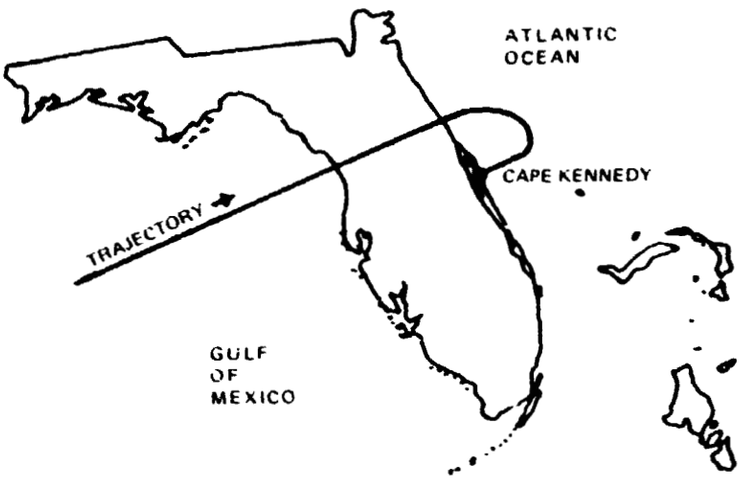

Figure 1.3.1-19 Ground Track

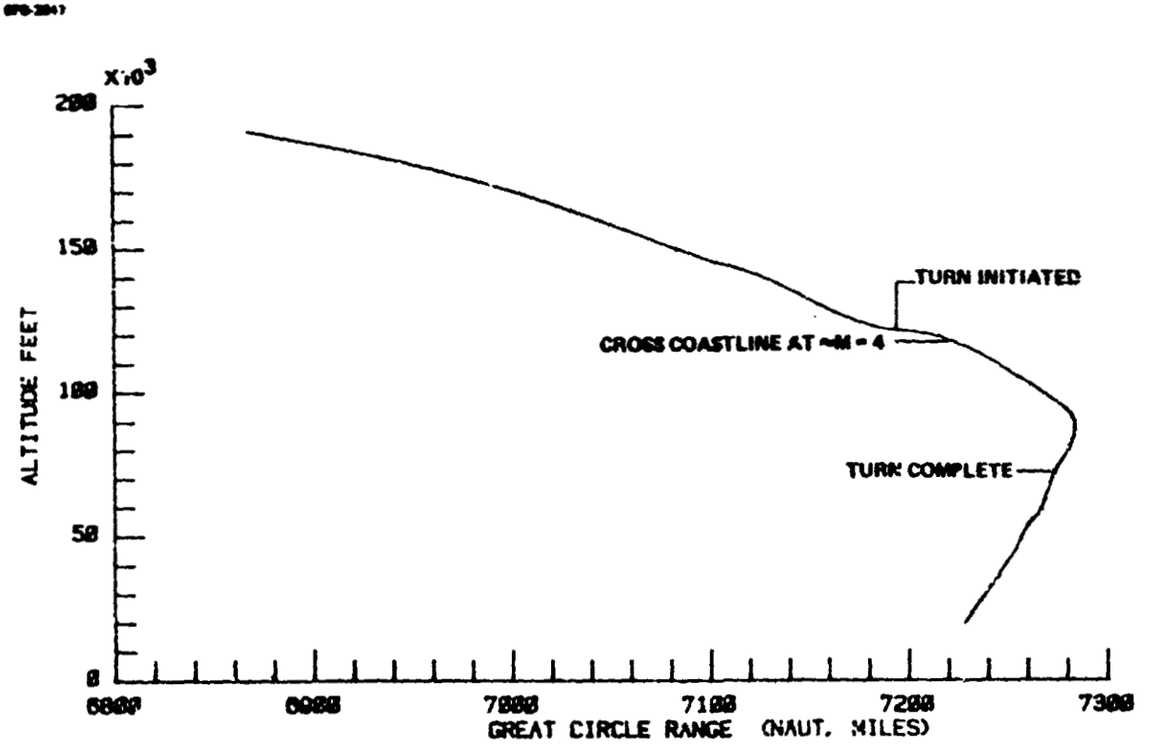

Figure 1.3.1-20 Altitude–Range Track

1.3.2 CARGO OTV: CONSTRUCTION LOCATION/ORBIT TRANSFER OPTIONS

1.3.2.1 INTRODUCTION AND SUMMARY

As part of a previous NASA JSC contract NAS9-15196, Boeing analyzed solar power satellite (SPS) concepts where the satellite would be constructed in either low earth orbit (LEO) or geosynchronous earth orbit (GEO). The LEO construction concept consists of building portions of the satellite (called modules) in LEO and using electric power generated by the module to drive electric propulsion systems that propel the modules up to GEO where they are docked together to form the complete satellite. The original GEO construction concept utilized large LO_2/LH_2 OTV's to transport SPS components from LEO to GEO where a monolithic type satellite could be constructed. The comparison of these two concepts indicated approximately a $2 billion savings per 10 GWe satellite when using the LEO construction/self-power concept. This significant advantage was primarily attributed to the use of electric propulsion rather than LO_2/LH_2 propulsion for orbit transfer.

Another orbit transfer option using high performance electric propulsion has been analyzed in performance of the current contract NAS9-15636. This concept also has the satellite constructed in GEO but uses independent electric propulsion orbit transfer vehicles (EOTV) to move the SPS components from LEO to GEO. The EOTV's are designed to be reusable so they are returned to LEO and deliver many loads of SPS components over their lifetime.

The Phase I effort concerning the construction location/orbit transfer options is illustrated in Figure 1.3.2-1 and consisted of 1) defining the GEO construction concept using EOTV's to a comparable level as that previously done for other options, 2) analyzing potential improvements to the LEO construction/self-power option, and 3) conducting a comparison of these two options, considering all aspects of transportation, construction and impact on satellite design.

The results of the comparison indicate that the LEO construction concept using self-power transfer of the modules and no recovery should be utilized for the initial stages

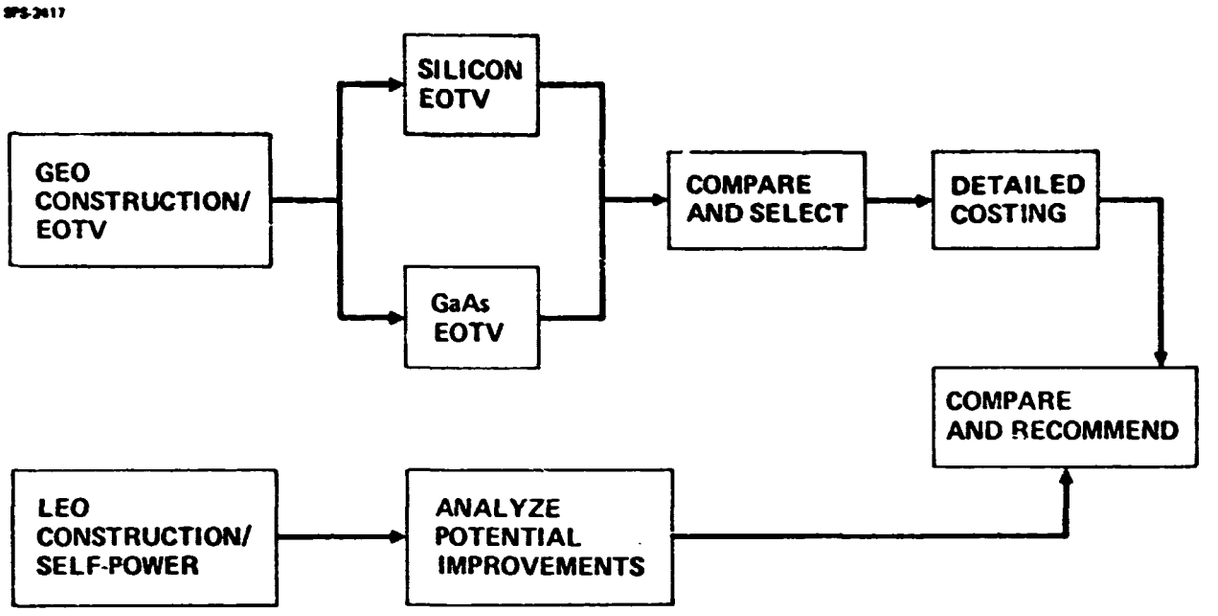

Figure 1.3.2-1 Construction Location Analysis

of the operational SPS program. The main reason for this recommendation is that it has significantly lower front end cost with recurring cost being competitive out to at least 150 gigawatts of installed power. In addition, this concept does not require reuse of the power generation system which may be quite sensitive to the environment between LEO and GEO. Finally, this concept allows natural evolution to the recovery of the electric propulsion system, which would result in the lowest recurring costs of any of the concepts evaluated.

1.3.2.2 GEO CONSTRUCTION WITH EOTV's

The major system elements and operations associated with the GEO construction concept using electric orbit transfer vehicles are illustrated in Figure 1.3.2-2. In summary, the LEO base serves as a staging depot and construction base for the EOTV's. SPS cargo and personnel are delivered to the LEO base using two stage winged HLLV's. A fleet of EOTV's transfer cargo from the LEO base to the GEO construction base where the satellite is constructed. Personnel are transferred between LEO and GEO using LO_2/LH_2 OTV's.

The following material will concentrate on the EOTV definition in terms of performance, design, operations, construction and costing.

1.3.2.2.1 EOTV Performance and Cost Optimization

The size, performance and cost characteristics of an electric propulsion vehicle are sensitive to the selected specific impulse and trip time. Accordingly, these two parameters are the chief variables to be investigated for given type of EOTV.

1.3.2.2.1.1 Guidelines

The key guidelines used in conducting the performance and cost optimization of the EOTV's are shown in Table 1.3.2-1. The annual mass to be delivered relates to satellite(s) capable of producing 10 GWe ground output. Delivery of all cargo associated with the satellite in 330 days allows sufficient time for final installation and checkout so that a satellite can come on line at the end of one year. Satellite mass includes a growth factor of 21%. The total cargo delivery mass includes not only components but the containers for the components and the rack to support the containers. Five percent of the component mass has been allocated to both the containers and the payload rack. The majority of the containers such as those associated with the solar arrays will be used in the actual installation process. Other

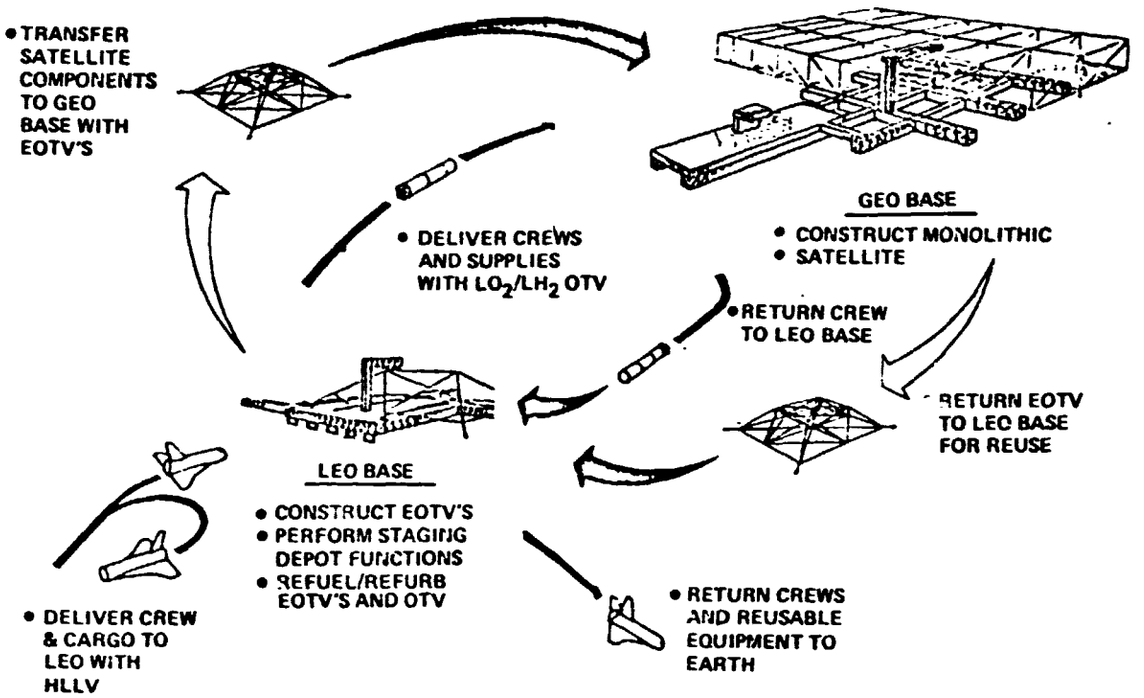

Figure 1.3.2-2 GEO Construction Concept Electric Orbit Transfer Vehicles

Table 1.3.2-1 Performance and Cost Optimization Guidelines

- Silicon CR=1 Solar Power Satellites at the Rate of 10 GW_e Ground Output Per Year
- Cargo Delivery Completed Within 330 Days of First Delivery to GEO
- Satellite(s) Mass of 99000 MT
- Total Cargo Delivery Mass
  - Up = 110000 MT (Components + Containers + Rack)
  - Down = 5500 MT (Rack)
- EOTV Delivery Capability
  - Up = 4000 MT (Components + Containers + Rack)
  - Down = 200 MT (Rack)
- 120 cm Argon Ion Thrusters

containers are judged not to be worth the value of recovery so consequently the down requirement is only the 5% associated with the payload rack.

Payload delivery capability for each EOTV was somewhat arbitrarily established at 4,000 metric tons after considering such factors as the size of the vehicle and the number of vehicles in flight for different payload capabilities. Payload return requirements again reflect the 5% associated with the payload rack itself. The 120 cm argon ion thrusters are the same as used in the self-power LEO construction concept.

1.3.2.2.1.2 Analyses Models and Methodology

Performance and cost optimization is done through the use of an "integrated sensitivity and interrelationship analysis" (ISAIA) model that includes 90 dependent variables and 28 independent variables organized into three submodels.

A performance submodel shown in simplified form in Figure 1.3.2-3 has as its principal output the propellant and electric power requirements for the EOTV. Another model called "TRANSIM" is used to provide an Isp adjustment factor. The "TRANSIM" model provides an orbit by orbit simulation of the transfer from LEO to GEO taking into consideration occulations and expenditure of LO_2/LH_2 propellant for supplemental attitude control. The net result is an effective Isp which allows propellant estimates to be made.

A mass estimating submodel is shown in Figure 1.3.2-4. This model takes the propellant quantities and power requirements and through the use of various specific masses and mass fractions calculates the mass for all major system elements.

The final submodel is that associated with cost. A simplified version of this submodel is shown in Figure 1.3.2-5. Key inputs to this model come from the performance and mass models as well as the independent variables. Three major elements make up the EOTV cost per flight. The capital cost factors are one-time expenditures amortized over the life or number of flights flown by the vehicle. Direct cost deals with the fueling and refurbishment of the vehicle for each flight. Trip delay cost relates to the time required to make the last EOTV flight which is effectively delaying the construction. Added to these three factors is that of the launching of the payload itself which in combination gives the total transportation cost for each EOTV flight. It should be noted that capital costs and trip delay costs are included in these models

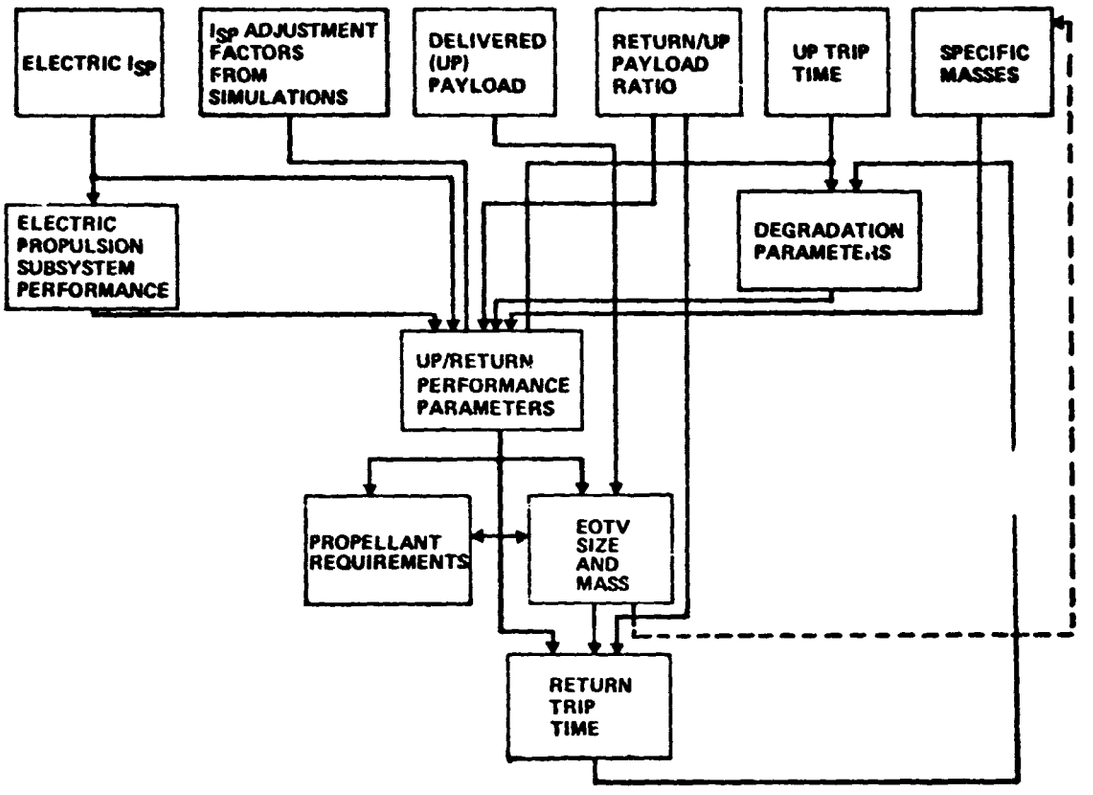

Figure 1.3.2-3 EOTV Performance Submodel Simplified Flow

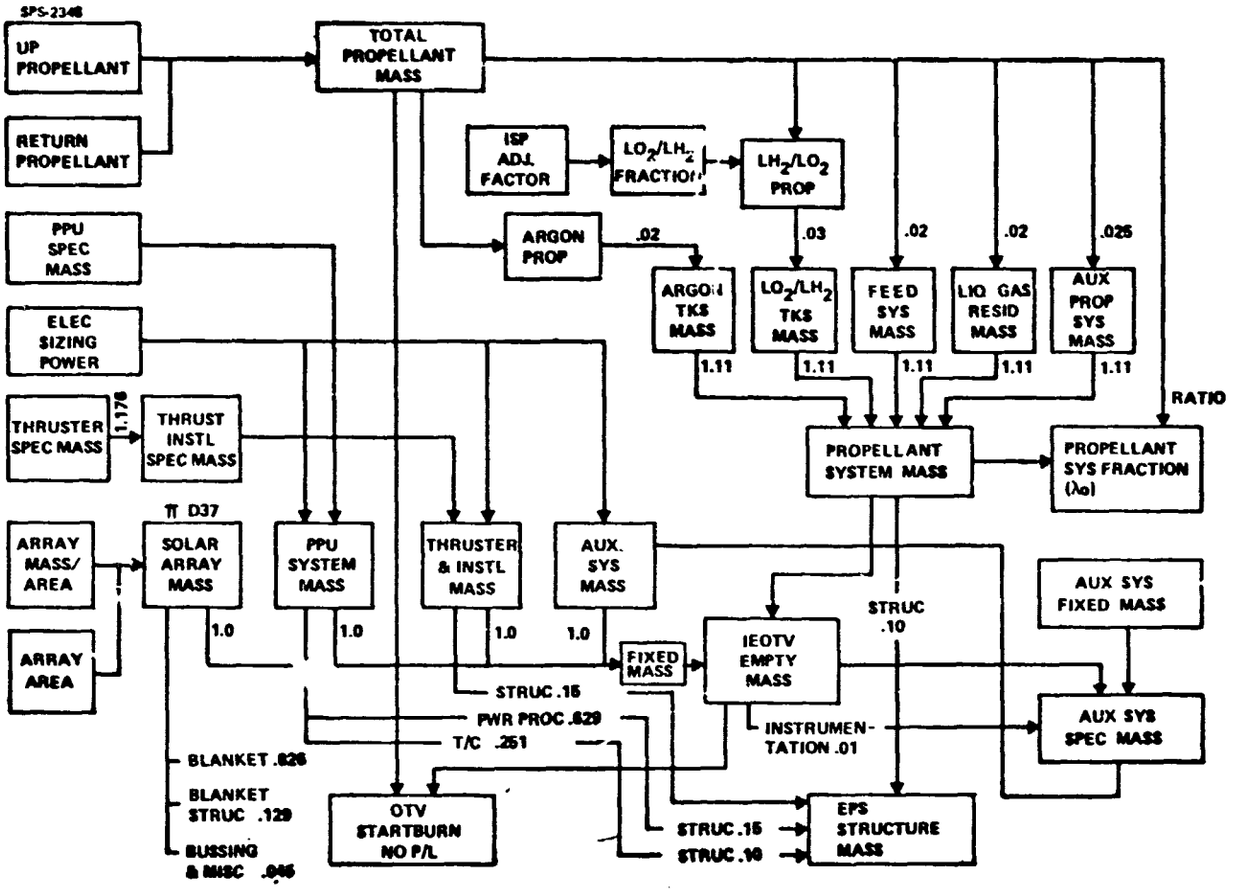

Figure 1.3.2-4 Mass Estimating Submodel

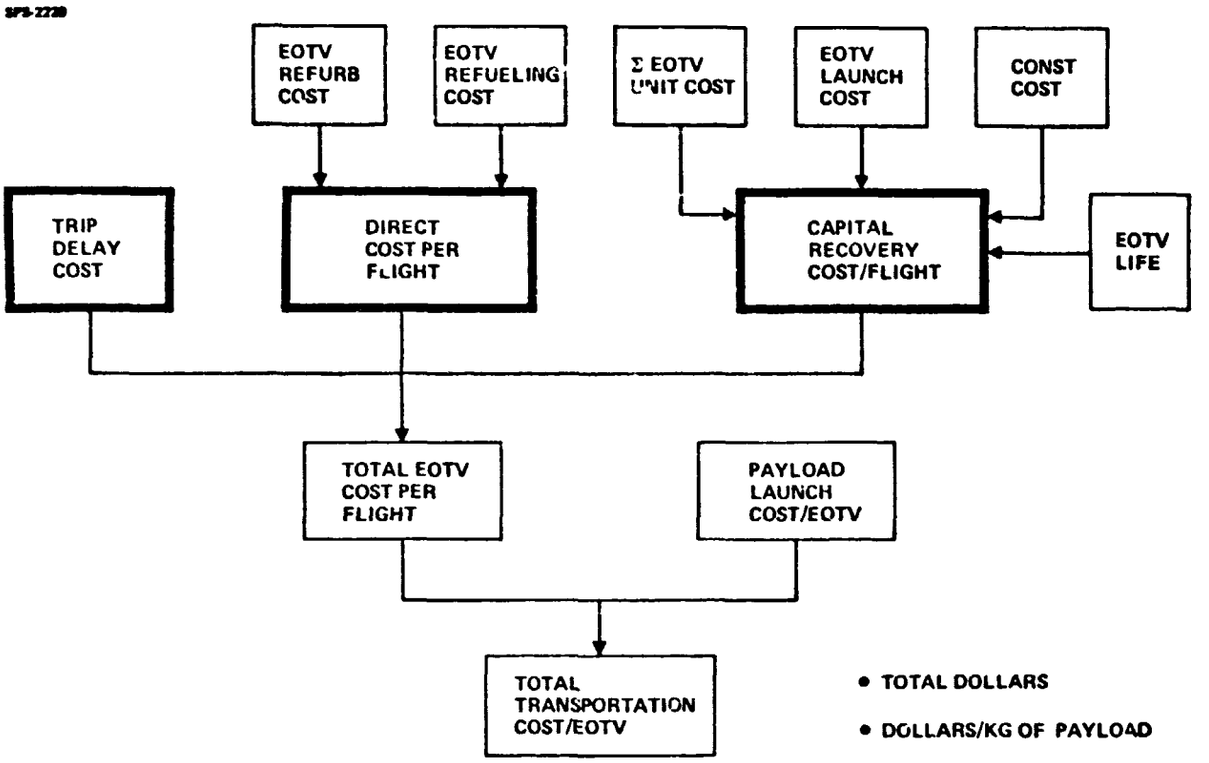

Figure 1.3.2-5 EOTV Flight Cost Factors

in order to obtain global optima for speciic impulse and trip time. In the system descriptions, capital and interest csts are accounted separately from transportation costs.

A typical result of the performance and cost model is shown in Table 1.3.2-2 for the case of an up trip time of 180 days and specific impulse of 8,000 sec. The independent variables associated with the indicated results are presented in Table 1.3.2-3. Cost sensitivity to any of the independent variables can also be obtained. Cost sensitivities are also obtained through use of various combinations of trip time and specific impulses. The results of the various combinations are presented in the next section.

1.3.2.2.1.3 Silicon EOTV's

The key factors influencing the EOTV performance and cost optimization are (1) the performance of the solar array particularly when subjected to the radiation environment between LEO and GEO and (2) argon ion thruster performance.

Solar Array Performance

The solar array blanket initially considered for the EOTV was the same as that used in the satellite which had a 3 mil coverglass, 2 mil textured surface cell and 2 mil substrate. The power output of this blanket as a function of radiation fluence is shown in Figure 1.3.2-6. It should be noted that 30 years of satellite operation at GEO with this blanket results in a cumulative fluence of approximately 2.5×10^{16} of 1 MeV electron equivalent while the EOTV experiences in one LEO-GEO roundtrip, a total of 1.06×10^{17} of 1 MeV equivalent. The roundtrip transfer value is based on the trapped proton and electron spectra shown respectively in Figure 1.3.2-7 and 1.3.2-8.

Solar array performance for EOTV application is also sensitive to the duration of the transfer between LEO and GEO as shown in Figure 1.3.2-9. Longer trip times mean more time in the Van Allen belts resulting in a degree of degradation and less power output.

Another important aspect of solar array performance is the use of annealing to improve power output after radiation damage. Prior to discussing the value of annealing solar arrays to remove radiation damage, it is necessary to consider what happens as a result of the annealing operation in terms of the method used to establish the resulting array output. The approach is illustrated in Figure 1.3.2-10 using a 60

Table 1.3.2-2 Performance and Cost Model Results Trip Time 180 Days Specific Impulse 8000 sec

SOLUTION RESULTS

1	ONE-WAY MASS RATIO	=	1.088E+00	
2	GROSS PAYLOAD RATIO	=	2.824E+00	
3	PAYLOAD EQUATION BRACKET	=	3.988E+06	
4	PAYLOAD EQUATION BRACKET	=	9.956E-01	
5	ZETA*UP, PERFORMANCE PAR	=	1.320E-02	KG/WATT
6	PHI-2, DOWN DEGRADATION	=	7.092E-01	
7	PHI-3, UP DEGRADATION	=	8.271E-01	
8	RETURN TRIP FLUENCE	=	2.812E+16	E/CM2
9	UP TRIP FLUENCE	=	1.069E+17	E/CM2
10	RETURN TRIP LOG FLUENCE	=	1.645E+01	
11	UP TRIP LOG FLUENCE	=	1.713E+01	
12	FLUENCE FOR 180-DAY TRIP	=	1.070E+17	E/CM2
13	ARRAY MASS/AREA	=	6.284E-01	KG/M2
14	TOTAL UP+RETURN DEGRADAT	=	5.865E-01	
15	THRUSTER-PPU EFFICIENCY	=	7.179E-01	
16	ZETA*-UP BRACKET TERM	=	6.199E-03	KG/WATT
17	THRUSTER SPECIFIC MASS	=	4.344E-01	KG/KWE
18	ZETA* DOWN	=	1.079E-02	KG/WATT
19	ZETA*-DOWN BRACKET TERM	=	7.749E-03	KG/WATT
20	POWER PROC SPECIFIC MASS	=	1.908E+00	KG/KWE
21	AUX SYS SPEC MASS	=	1.171E-01	KG/KWE
22	ARRAY SPEC MASS	=	3.663E+00	KG/KWE
23	D21/PHI-2	=	1.649E-01	KG/KWE
24	D22/PHI-2	=	5.165E+00	KG/KWE
25	IEOTV FIXED MASS	=	1.416E+03	METRIC T
26	RETURN PAYLOAD	=	2.000E+02	METRIC T
27	JET POWER DOWN	=	1.312E+02	MEGAWATT
28	AVG JET POWER UP	=	1.423E+02	MEGAWATT
29	ELEC SIZING POWER	=	1.828E+02	MEGAWATT
30	ARRAY DESIGN POWER	=	2.964E+02	MEGAWATT
31	RETURN TRIP TIME	=	4.734E+01	DAYS
32	IEOTV MASS AT GEO	=	1.621E+03	METRIC T
33	RETURN TRIP TIME TERM	=	4.192E-06	
34	UP PROPELLANT	=	4.928E+02	METRIC T
35	RETURN PROPELLANT	=	2.230E+01	METRIC T
36	PROPELLANT SYSTEM MASS	=	4.916E+01	METRIC T
37	PWR GEN & DISTR MASS	=	9.440E+02	METRIC T
38	PPU SYSTEM MASS	=	3.487E+02	METRIC T
39	THRUSTER & INSTL MASS	=	9.340E+01	METRIC T
40	AUX SYSTEM MASS	=	2.137E+01	METRIC T
41	IEOTV EMPTY MASS	=	1.457E+03	METRIC T
42	TOTAL PROPELLANT MASS	=	5.151E+02	METRIC T
43	OTV STARTBURN MASS NO PL	=	1.972E+03	METRIC T
44	BLANKET MASS	=	7.798E+02	METRIC T
45	BLANKET STRUC	=	1.218E+02	METRIC T
46	BUSSING & MISC	=	4.248E+01	METRIC T
47	POWER PROCESSORS MASS	=	2.194E+02	METRIC T
48	PPU THERMAL CONTROL MASS	=	8.753E+01	METRIC T
49	INSTRUMENTATION MASS	=	1.457E+01	METRIC T
50	THRUSTERS MASS	=	7.939E+01	METRIC T

Table 1.3.2-2 Performance and Cost Modu[illegible]ts (Cont)

51	PROPELLANT SYS FRACTION	=	9.543E-02	
52	ARGON TANKS MASS	=	9.375E+00	METRIC T
53	LO2/LH2 TANKS MASS	=	1.391E+0[illegible]	[illegible]TRIC T
54	FEED SYS MASS	=	1.030E+0[illegible]	TRIC [illegible]
55	LIQ & GAS RESID MASS	=	[illegible].030E+01	METRIC T
56	AUX PROP SYS MASS	=	1.288E+01	METRIC T
57	EPS STRUCTURE MASS	=	6.058E+01	METRIC T
58	LO2/LH2 FRACTION	=	9.000E-02	
59	LO2/LH2 PROP MASS	=	4.636E+01	METRIC T
60	ARGON PROP MASS	=	4.688E+02	METRIC T
61	ARRAY AREA	=	1.502E+06	M2
62	THRUST PER THRUSTER	=	2.854E+00	N
63	THRUSTER BEAM CURRENT	=	7.777E+01	AMPS
64	TOTAL THRUST	=	3.345E+03	N
65	THRUST PER CORNER	=	8.363E+02	N
66	TOTAL NO OF THRUSTERS	=	1.172E+03	
67	NO. OF THRUSTERS/CORNER	=	2.930E+02	
68	SUPPLY VOLTAGE	=	1.619E+03	VOLTS
69	ZETA*-UP TERM	=	9.222E-01	
70	THRUST INSTL SPEC MASS	=	5.110E-01	KG/KWE
71	HLLV FLTS TO LIFT OTV	=	3.831E+0[illegible]	
72	HLLV FLTS TO REFUEL	=	1.355E+0[illegible]	
73	EPS TOTAL MASS	=	5.127E+02	METRIC T
74	P GEN & D SYS COST	=	9.410E+01	MILLION
75	EPS COST	=	5.998E+01	MILLION
76	TRIP TIME COST	=	1.769E+01	MILLION
77	HLLV COST TO LIFT OTV	=	5.402E+0[illegible]	MILLION
78	HLLV COST TO REFUEL	=	1.910E+01	MILLION
79	HLLV COST TO LIFT PL	=	1.483E+02	MILLION
80	EOTV CAP RECOV COST/FLT	=	3.152E+01	MILLION
81	AMORTIZATION TIME PERIOD	=	7.046E+00	YEARS
82	TOTAL ROUND TRIP TIME	=	2.574E+02	DAYS
83	EOTV TOTAL CAP COST	=	2.381E+02	MILLION
84	PAYLOAD COST	=	3.200E+0[illegible]	MILLION
85	DIRECT COST/FLT	=	2.910E+0[illegible]	MILLION
86	EOTV TOTAL COST/FLT	=	7.830E+01	MILLION
87	TOTAL TRANSP COST	=	2.26[illegible]E+02	MILLION
88	TOTAL TRANSP COST/KG	=	6.295E+01	$/KG
89	AVERAGE/1ST TRIP TIME RA	=	1.150E+00	
90	ARRAY COST/AREA	=	6.264E+01	DOLLARS

Table 1.3.2-3 Independent Model Variables

	NOMINAL VALUES, INDEPENDENT VARIABLES			
1	ISP ADJUSTMENT FACTOR	=	9.100E-01	
2	1-WAY DELTA V INCL GG LO	=	6.000E+03	M/S
3	ELECTRIC SPECIFIC IMPULS	=	5.000E+03	SEC
4	OCCULTATION ADJUST FACTO	=	1.100E+00	
5	PROPELLANT SYSTEM FRACTI	=	1.000E-01	
6	UP TRIP TIME	=	1.200E+02	DAYS
7	RETURN/UP PAYLOAD RATIO	=	5.000E-02	
8	UP PAYLOAD	=	4.000E+03	METRIC T
9	DEGRAD. TIME FACTOR TAU	=	5.500E-01	
10	ARRAY OVERSIZE FACTOR	=	1.000E+00	
11	COVERGLASS THICKNESS	=	7.500E+01	MICRONS
12	THRUSTER REDUND FACTOR	=	1.200E+00	
13	PPU SYSTEM SPEC MASS	=	1.908E+00	KG/KWE
14	AUX SYS FIXED MASS	=	5.000E+00	METRIC T
15	ARRAY AREA EFF'Y	=	9.000E-01	
16	NUMBER OF THR INSTL	=	4.000E+00	
17	THRUSTER DIA	=	1.200E+02	CM
18	ACCUMULATED DEGRADATION	=	1.000E+00	
19	SOLAR CELL OPERATING EFF	=	1.620E-01	
20	INTEREST RATE	=	7.500E-02	
21	EOTV NO. OF FLTS	=	1.000E+01	
22	PAYLOAD COST	=	8.000E+01	$/KG
23	EOTV SERVICE TIME	=	3.000E+01	DAYS
24	DUMMY	=	1.000E+00	
25	EOTV CONSTR COST	=	3.000E+01	MILLION
26	EOTV SERVICE & SPARES CO	=	1.000E+01	MILLION
27	HLLV COST/FLT	=	1.410E+01	MILLION
28	I-SQ-R & STORAGE PENALTY	=	1.500E-01	

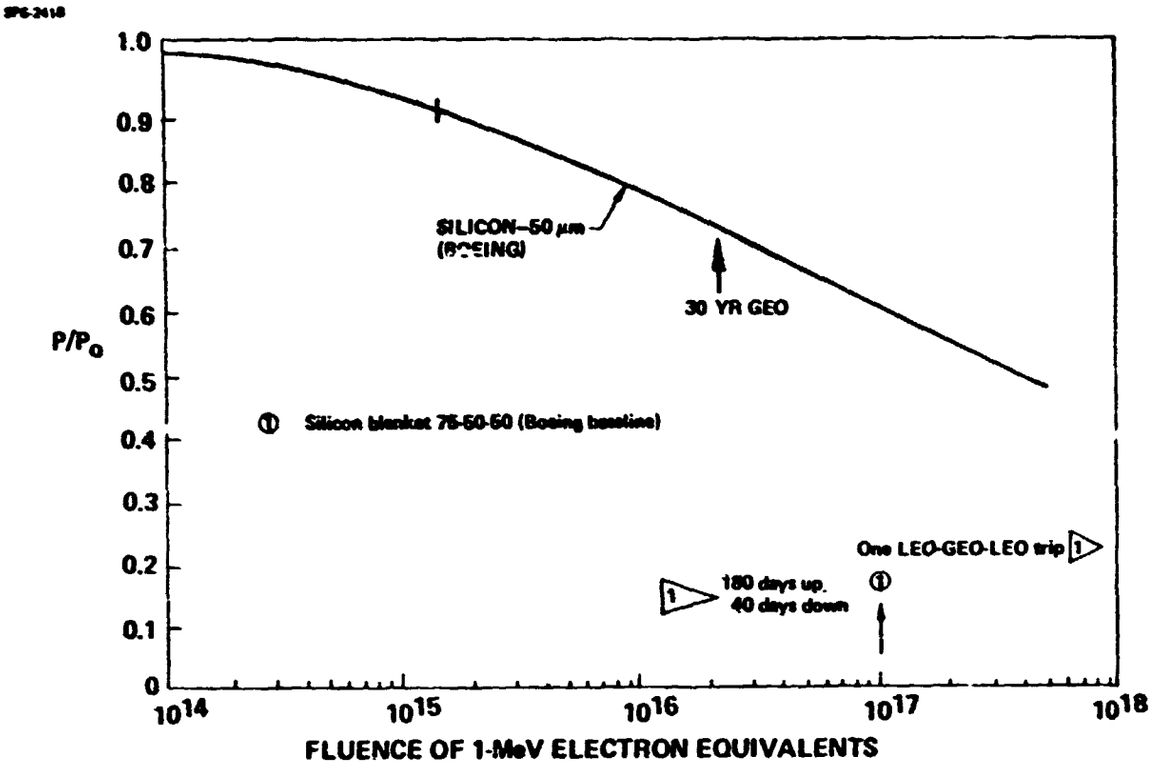

Figure 1.3.2-6 Solar Cell Radiation Sensitivity

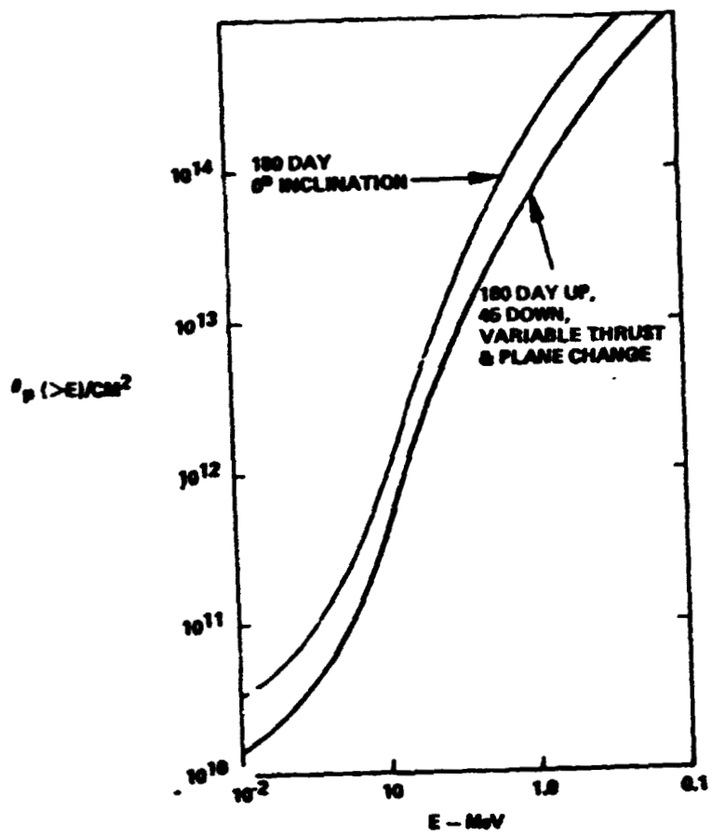

Figure 1.3.2-7 Trapped Proton Transfer Spectrum

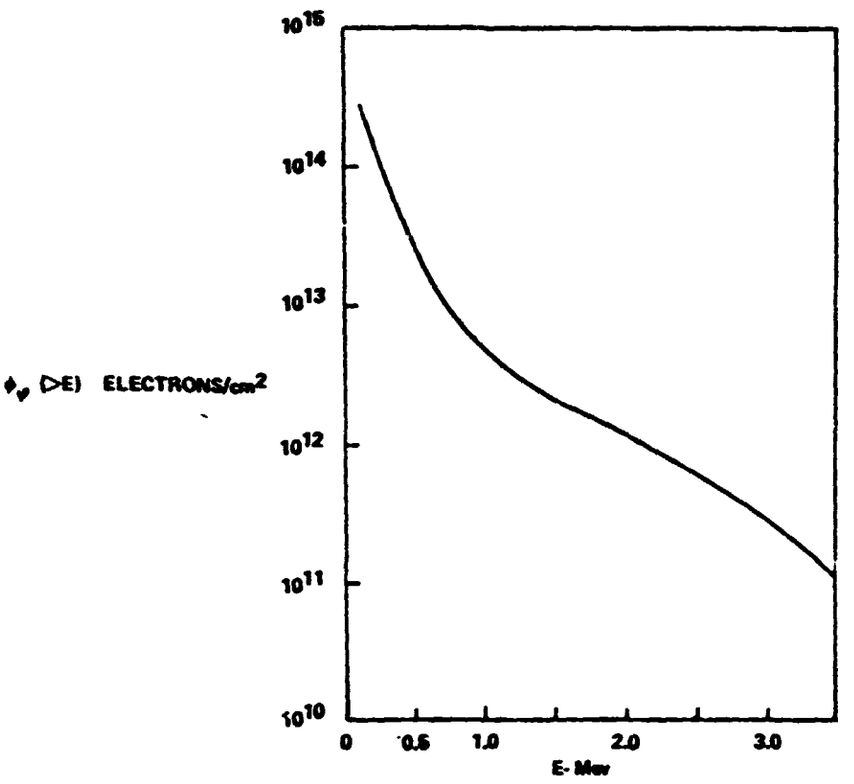

Figure 1.3.2-8 Trapped Electron Transfer Spectrum

● TRIP TIME SENSITIVITY

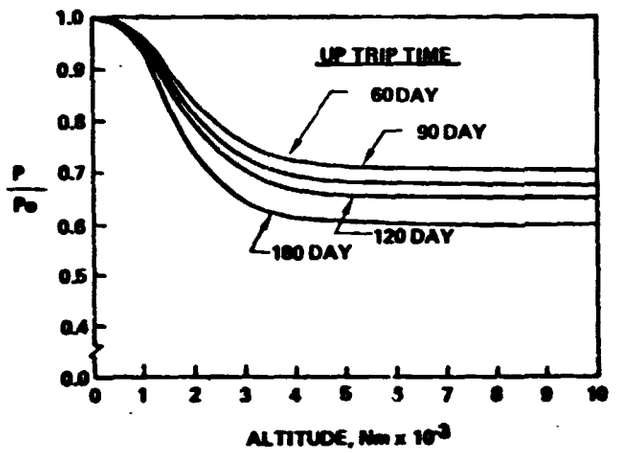

Figure 1.3.2-9 Power Output Sensitivity to Trip Time

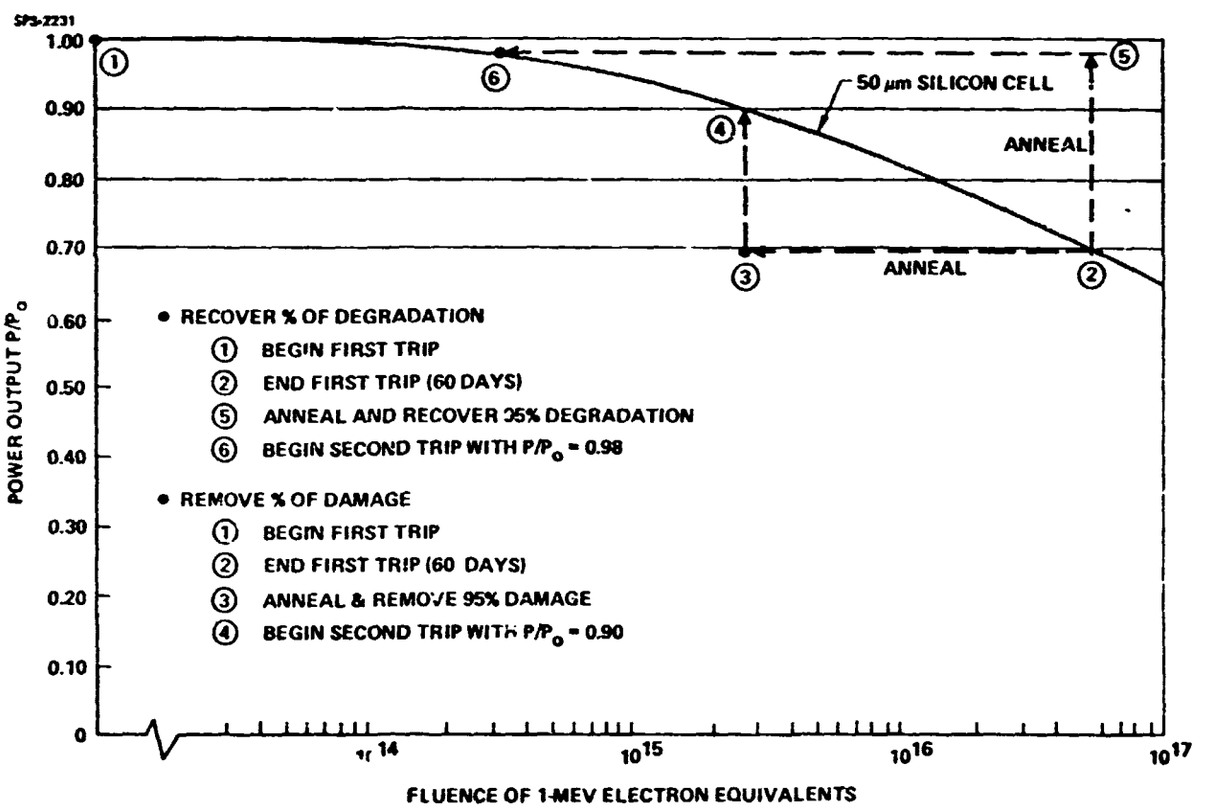

Figure 1.3.2-10 Power Recovery After Annealing

day up transfer time. During the transfer from LEO to GEO, the power output will degrade to approximately 70% of the initial output as indicated by point 2 on the chart. Previous analysis has assumed recovery after annealing to be 95% of the degradation based on annealing tests performed by SPIRE. It should be noted, however, that the recovery value has a degree of uncertainty since the test cells had 1/15 as much fluence as a cell exposed during an orbit transfer and, in addition, a 6 mil cell was used rather than a 2 mil cell. Using this approach, the power output would be approximately 97% as indicated by point 6. The current belief, however, is that the annealing operation actually removes damage (effects of a quantity of fluence) with the resulting power output being a function of the remaining damage. The SPIRE test removed 98% of the damage, but since the EOTV damage is much more severe, a damage removal value of 95% is used which results in the use of points 2, 3, 4 and an output of 90%. In the case of the self-power transfer, the difference betwen these two approaches is not significant since the solar array is only used one time. However, in the case of the EOTV operation where multiple trips will be made, considerable differences will result when the vehicle is flown, 5, 10 or 15 times. Consequently, the approach used in this study was to assume removal of a percent of the damage from the array rather than recovering a percent degradation. The percent of damage removal, however, remains uncertain due to the large disparity between test experience and predicted fluence expected during transfer. This uncertainty can only be reduced by performing additional radiation and annealing tests specifically designed for EOTV operations.

The power range before annealing and after annealing as a function of the number of trips is shown in Figure 1.3.2-11 along with the average power expected during the trip. It should also be noted that as the average power decreases within a given trip as well as each subsequent trip, the voltage will also be decreasing at about half the rate as the power output (should power go down 30%, voltage will go down 15%). The benefit of annealing can be illustrated by using the case of 10 roundtrips. With annealing, the average power output during the tenth trip will be approximately 58% of the initial power output. Should annealing not be used, power output for the tenth trip would be approximately 45% of the initial output.

Another parameter that can be varied in the silicon solar array EOTV is the amount of shielding placed around the cell and its influence regarding radiation damage. An option to the basic 3-2-2 mil blanket that has been investigated is a 6 mil cover, 2 mil

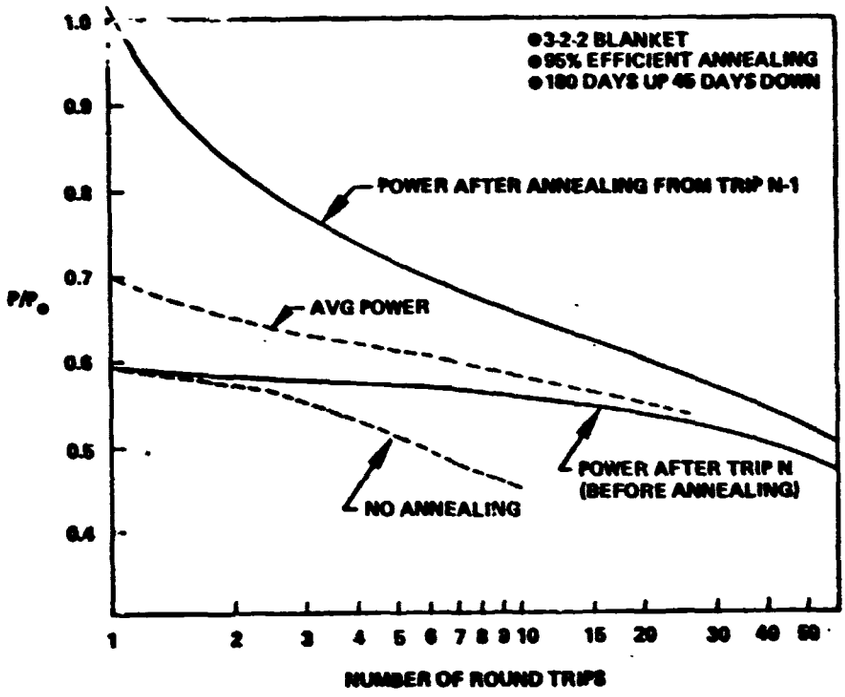

Figure 1.3.2-11 Benefits of Solar Array Annealing

cell and 4 mil substrate. The power output of the 6-2-4 blanket is 8-10% greater than for the basic blanket when exposed to the LEO-GEO environment. The 6 mil coverglass blanket, however, has greater blanket mass per square meter and the cost per square meter. Mass per square meter for the 6-2-4 blanket is 1.06 Kg/m^2 vs 0.628 Kg/m^2 for the 3-2-2 blanket.* These figures include the support structure and a 21% mass growth/contingency allowance. The cost of the 6-2-4 blanket is estimated at $\$68/m^2$ and the 3-2-2 blanket $\$62.6/m^2$. The mass shows a much greater percent increase since the cost is expected to be mainly dependent on area.

120 Centimeter Argon Ion Thruster Performance

The principal ion thruster performance characteristics as a function of specific impulse are presented in Figure 1.3.2-12. The influence of each of these parameters are as follows: Beam voltage will have an impact on the I^2R losses and the amount of plasma losses involved in the power distribution system; efficiency influences the amount of propellant required for the operation; thrust level will establish the number of engines required; and finally, the input power will determine the amount of solar array which must be deployed for the transfer operation. These characteristics along with trip time options and solar array performance were incorporated into the optimization performance/cost model.

Vehicle Optimization

The first trip flown by the vehicle is used to obtain the optimum vehicle in terms of performance and cost as influenced by trip time and specific impulse. These characteristics are shown in Figure 1.3.2-13. Total vehicle start-burn mass is shown as a function of specific impulse and up trip time, and indicates the minimum mass has not been reached at 240 days, however, the optimum specific impulse appears to be 8,000 seconds. Cost data reflect the amortized hardware cost, the cost of refueling and refurb and trip time interest cost. The cost is minimum with a combination of a specific impulse of 3,000 seconds and trip time of 240 days.

Similar optimization curves have been developed for the 6 mil coverglass blanket with an Isp of 8,000 sec also providing the least cost. The cost curves for the 6-2-4 blanket are shown in Figure 1.3.2-14 and indicates the 3-2-2 blanket to provide a savings of approximately $2 per kg of SPS at the optimum Isp and trip time. Further detail concerning the comparison of the two silicon blanket options is presented in Figure 1.3.2-15 using a specific impulse of 8,000 sec and an up trip time of 210 days.

* These figures include the support structure and a 21% mass growth/contingency allowance.

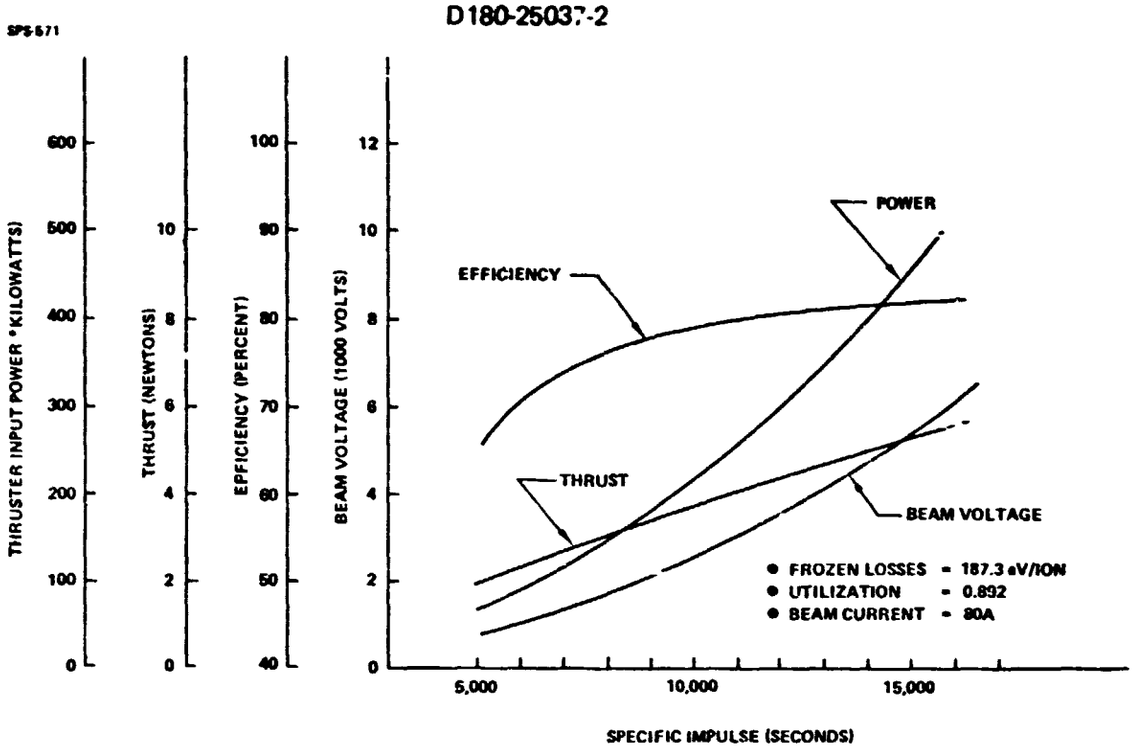

Figure 1.3.2-12 120-CM Argon Ion Thruster Performance

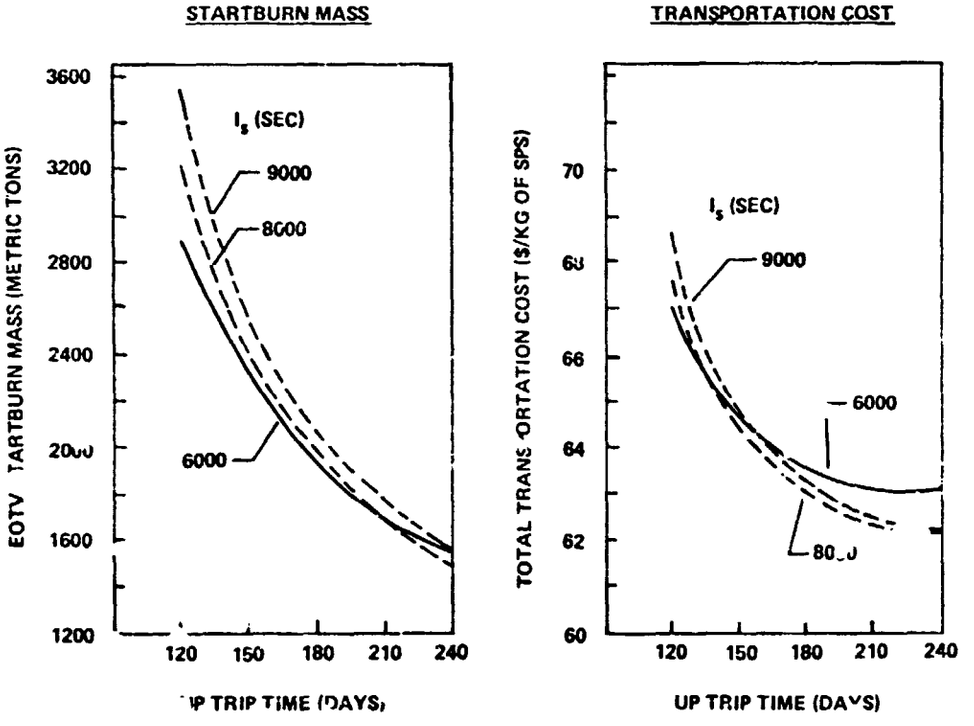

Figure 1.3.2-13 Vehicle Optimization

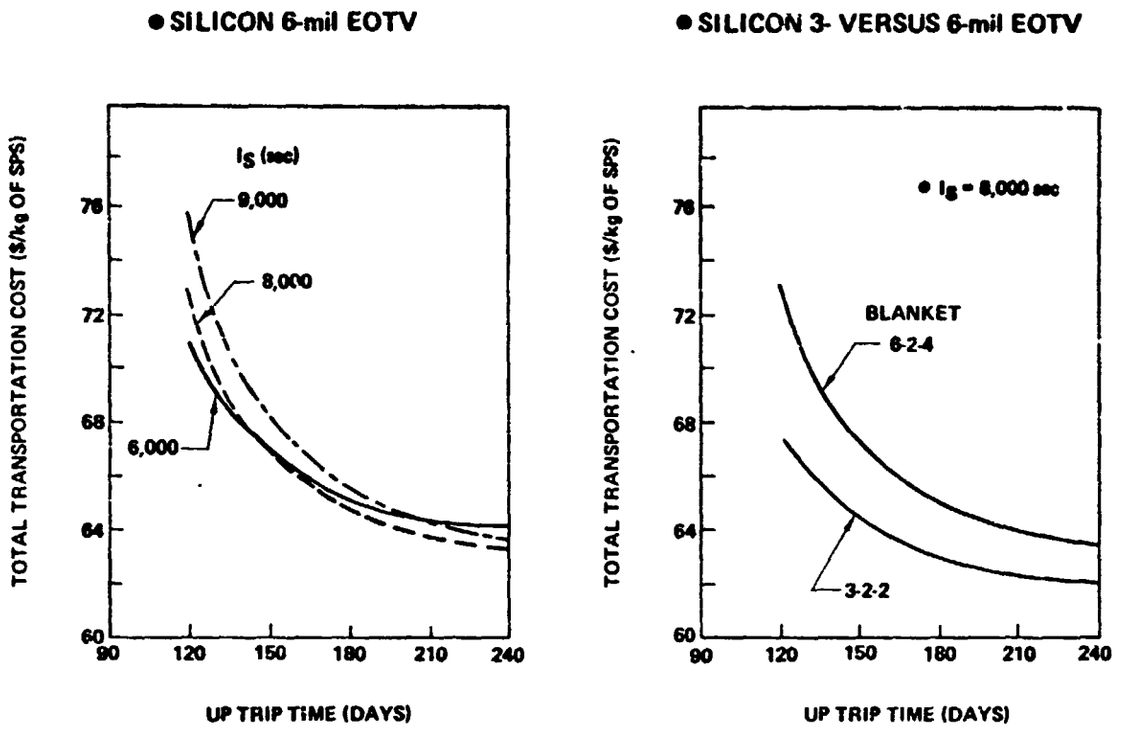

Figure 1.3.2-14 Silicon EOTV Cost Optimization

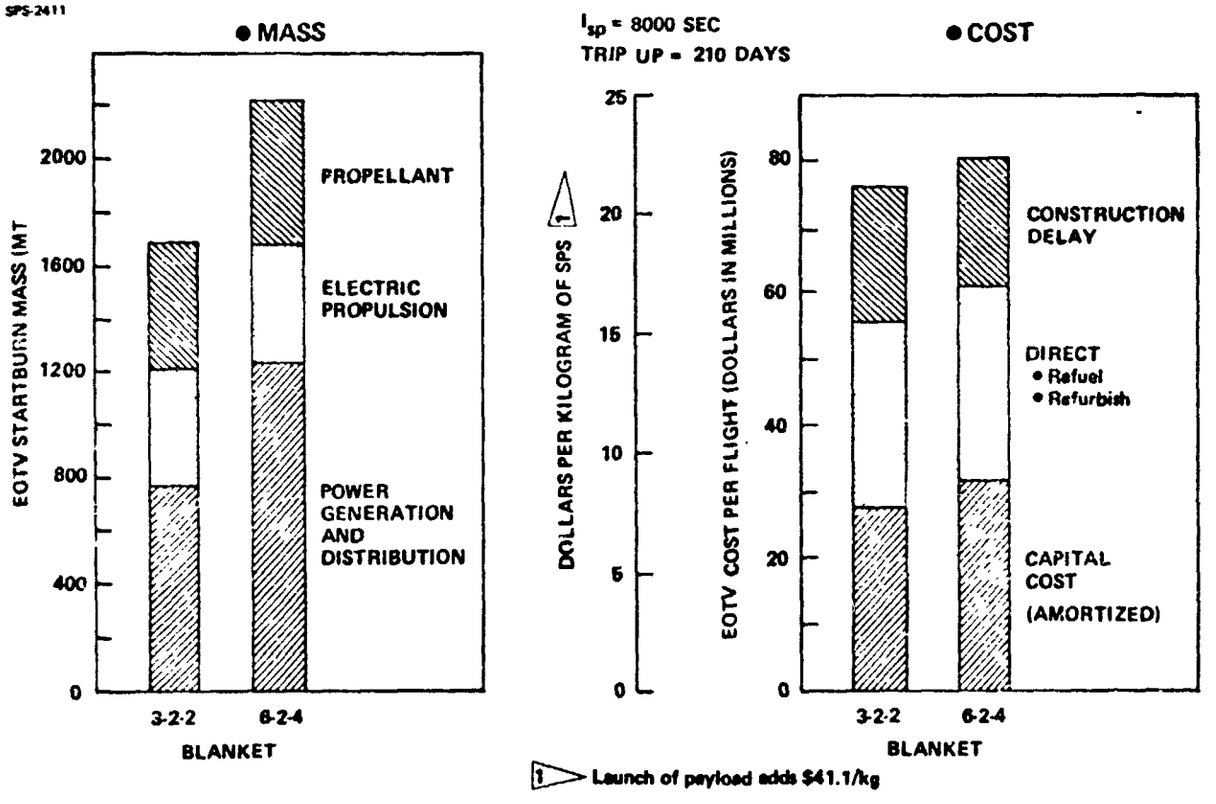

Figure 1.3.2-15 Silicon EOTV Comparison

The mass comparison shows a significant penalty for the power generation and distribution system of the 6-2-4 blanket configuration primarily because of the heavier solar array. The propulsion and propellant requirements are approximately equal, although the 6-2-4 case has slightly greater requirements because of the heavier PGDS. The cost comparison reflects amortized capital cost and is expressed in terms of EOTV dollars per kilogram of SPS. Although the unit cost of the 6-2-4 blanket EOTV would be considerably greater than that for the 3-2-2 EOTV, when amortized over the life of the system, little difference occurs between the two concepts. Again, the propellant requirements were approximately equal so the direct costs in terms of refueling the EOTV's are approximately the same. Since both concepts use the same trip time, the construction delay cost is also the same. The net result is that the 3-2-2 blanket EOTV provides a $2 per kilogram of SPS benefit over that of the 6-2-4 case and will be used in the comparison with a GaAs blanket EOTV.

1.3.2.2.1.4 Gallium Arsenide EOTV

An alternative to the silicon EOTV is the use of gallium arsenide (GaAs) solar cell blankets. Several factors indicated in Table 1.3.2-4 are pertinent to the consideration of the GaAs EOTV. The reasons indicated for its consideration are discussed in the following paragraphs. The key factor in establishing the benefit of a GaAs blanket is the cost per square meter that will occur. (The analysis assumes a program that uses silicon solar cells for the satellite thereby resulting in a relative small production rate for the gallium arsenide blanket.) Emphasis was given to an EOTV with a configuration concentration ratio of 1 rather than some higher concentration ratio. This eliminates the problems associated with uneven illumination resulting from higher concentration ratios.

Performance and Cost Characteristics

Blanket characteristics. The makeup of the silicon blanket and gallium arsenide blankets are indicated in Figure 1.3.2-16 with the gallium arsenide blanket being that as defined by Rockwell International for Marshall Space Flight Center. The gallium arsenide blanket provides an improvement in terms of the efficiency and power output (before radiation is applied to the blanket) and for the basic blanket as defined by Rockwell, a considerable mass per square meter improvement over the silicon blanket. A second mass value is indicated for the gallium arsenide blanket that uses a 40 micron coverglass rather than a 20 micron coverglass. This option has been included in an attempt to reduce radiation degradation for the gallium arsenide blanket.

SPS-2414

Table 1.3.2-4 GaAs EOTV

- **Reasons for consideration**
  - **Higher cell performance**
  - **Lower mass/m^2**
  - **Better resistance to radiation**
- **Key factor in evaluation**
  - **Cost/m^2**
- **Key assumptions**
  - **Payload**
    - **Up = 4,000 MT**
    - **Down = 200 MT**
  - **Configuration concentration ratio = 1**

SPS-2419

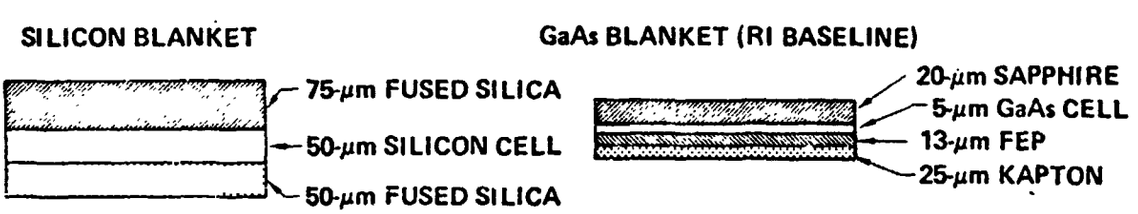

• Efficiency: 17.3%	19% TO 20%
• Power output: 197 W/m^2	237 W/m^2
• Mass (without growth: 0.427 kg/m^2)	0.252 kg/m^2 (20 - 5 - 13 - 25) 0.412 kg/m^2 (40 - 5 - 13 - 25)

Figure 1.3.2-16 Blanket Design Characteristics

Radiation sensitivity. The power output of the GaAs as well as silicon blankets is shown as a function of radiation fluence in Figure 1.3.2-17. The gallium arsenide prediction is taken directly from the Rockwell/MSFC study whereas the silicon cell predictions are from Boeing test data. As would be expected, the gallium arsenide cell for a given amount of fluence provides a power output benefit over the silicon cell. However, what is important is how the complete blanket performs when exposed to the orbit transfer environment. In the lower righthand portion of this chart are indicated the fluence levels expected to be experienced by the two blankets for 180 days uptrip and a 40 day downtrip. In the case of the silicon blanket, one round trip will provide about 10^{17} equivalents of 1 MeV electrons, which results in a power output of approximately 60%. Should the basic gallium arsenide blanket (20 micron coverglass) be used, a fluence level of approximately 4.4×10^{17} will be experienced resulting in a 52% power output value. This explains the rationale for investigating a thicker coverglass. The blanket considered was one using a 40 micron coverglass (Option 2) which experiences 2.2×10^{17} of fluence, resulting in a 58% power output, but still lower than the 60% provided by the silicon blanket. This suggests that additional shielding around the gallium arsenide cell may be beneficial for the orbit transfer operations.

Blanket cost. As suggested earlier, a key factor in assessing the benefits of the gallium arsenide EOTV as compared to silicon is the cost that must be paid per square meter. The method used to achieve this value is illustrated in Figure 1.3.2-18. The silicon cell blanket curve is the same as used in the past analysis of the Boeing silicon satellite. This curve was established by beginning with 50 kilowatts of solar array produced in 1977, following a 70% production rate curve down to the point where the cost is approximately two times the material cost of the solar array at which point no further improvement is expected. Thereafter the cost per square meter will be the same regardless of the production rate. In the case of the 10 gigawatt silicon satellite indicated by Point 2, the basic cost is about $44 per square meter. The data point (43) used to establish the gallium arsenide blanket cost was that predicted by Rockwell in their study for MSFC where approximately 52 million square meters of gallium arsenide solar array was produced per year at a cost of $71 per square meter. It was assumed that this production rate is in the "mature industry cost" region as for the silicon blanket. The array production required for the gallium arsenide EOTV was established by taking the total fleet requirements and dividing equally over the seven years of operating life and adding a 20% margin per year. As a result, approximately

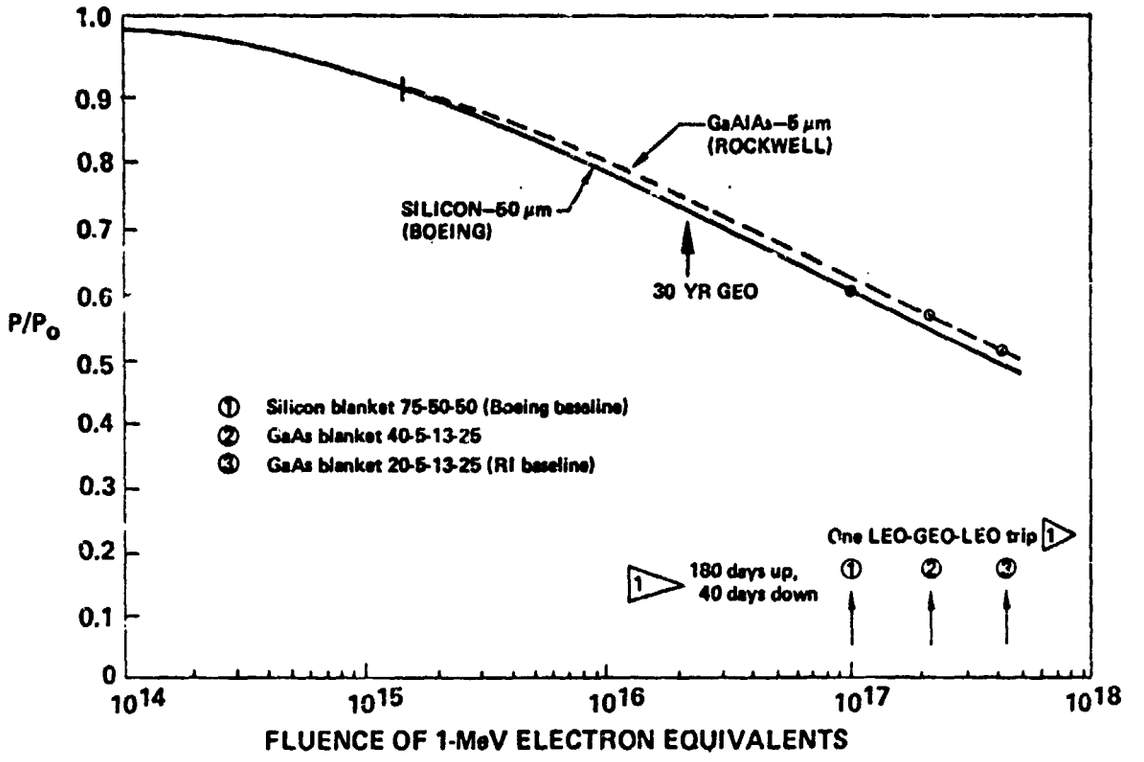

Figure 1.3.2-17 Solar Cell Radiation Sensitivity

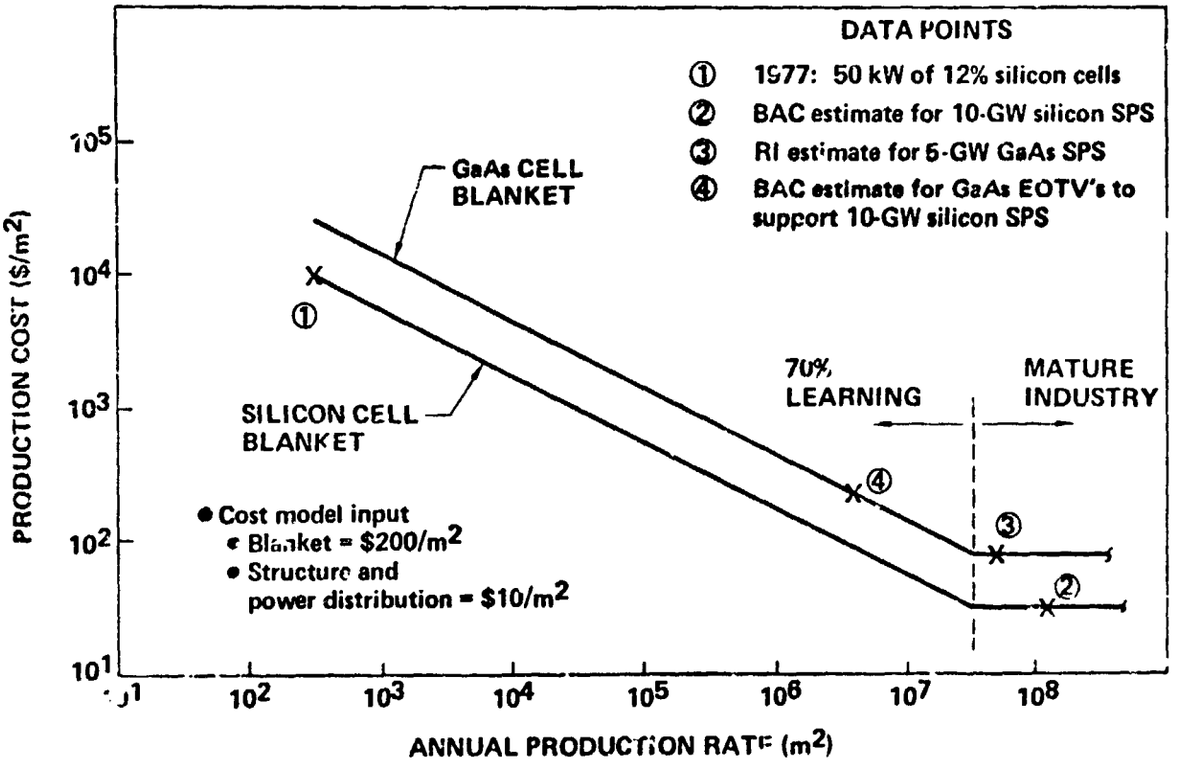

Figure 1.3.2-18 GaAs Blanket Cost

3.8 million square meters of the gallium arsenide blanket were produced per year, resulting in a cost of approximately $200 per square meter. That combined with the $10 per square meter associated with the structure and power distribution of the gallium arsenide EOTV resulted in a total of $210 per square meter versus approximately $60 per square meter for a silicon blanket EOTV that used a 5 x 10 centimeter cell.

It should be recognized that the results of this analysis are strongly influenced by these cost projections.

Cost Optimization

The transportation cost optimization of the two gallium arsenide blanket EOTV designs is indicated in Figure 1.3.2-19. In both cases, an ISP of 7,000 seconds and uptrip time of 240 days is optimum with the 40 micron coverglass blanket providing an advantage of approximately $2 per kilogram of SPS.

1.3.2.2.1.5 EOTV Comparison and Selection

The key performance and design characteristics of the silicon and GaAs EOTV's are shown in Table 1.3.2-5. In terms of optimization, the key features are that of the specific impulse and trip time. The baseline silicon EOTV uses a higher specific impulse and shorter trip time which will influence both electric power requirements, the degradation and eventually the propellant requirements for the EOTV. Also included in order to provide a direct comparison in terms of these parameters is an EOTV (reference case) with the same trip times and specific impulses as the GaAs EOTV. In terms of design characteristics, the baseline EOTV has electric sizing power requirements considerably greater primarily because of its higher I_{SP} and faster trip time. Power remaining after one round trip, however, is the highest for the silicon baseline for the reasons indicated on a preceding chart discussing radiation sensitivity. The design power required for the concepts reflect the basic electric power requirements to drive the electric thrusters, I^2R losses and also oversizing to cover the initial degradation. Array area requirements reflect the design power required as well as the power output of each square meter of the array. Empty mass characteristics includes the power generation distribution system and the electric propulsion system elements but excludes propellant.

SPS-2426

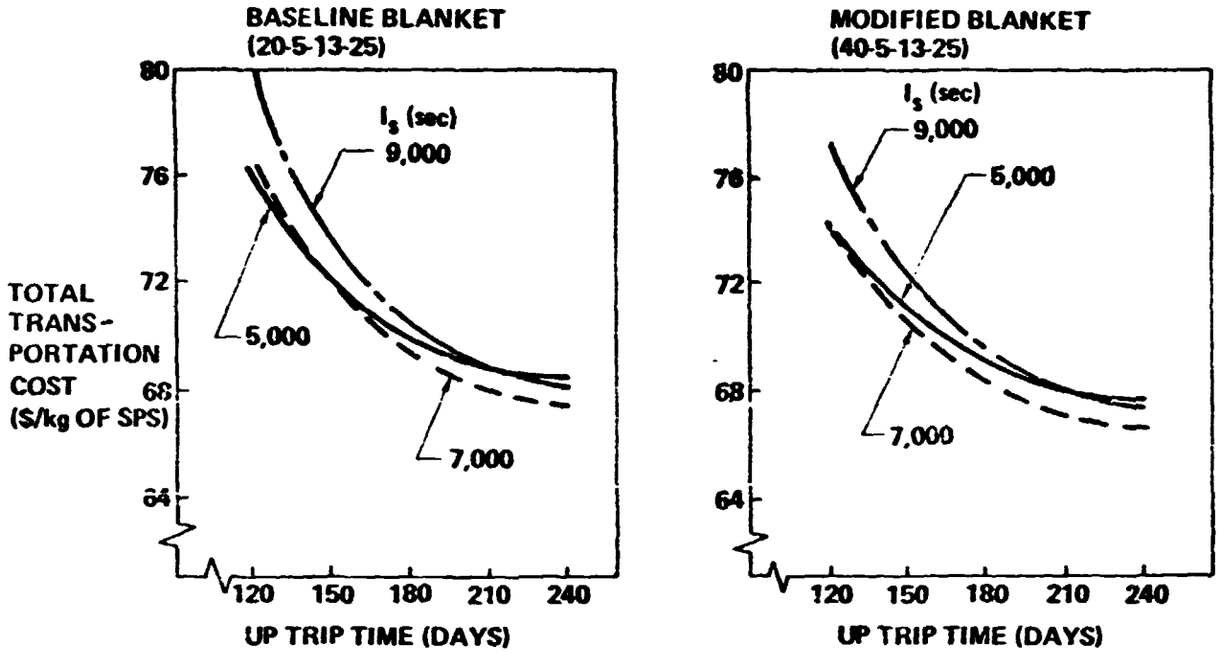

Figure 1.3.2-19 Cost Optimization GaAs EOTV

SPS-2427

Table 1.3.2-5 EOTV Design Characteristics

	GaAs EOTV		Silicon EOTV	
	Basic blanket	Modified blanket	75-50-50 blanket	
	20-5-13-25	40-5-13-25	Baseline	Direct Comparison
•Optimization				
• I_s (sec)	7,000	7,000	8,000	7,000
• Trip time up (days)	240	240	180	240
• Trip time down (days)	37	37	47	49
•Design characteristics				
• Electric sizing power (MW)	125	118	182	115
• P/P_0 after one round trip (%)	48	52	58	56
• Design power (MW)	230	203	296	187
• Array area (km^2)	0.97	0.85	1.5	0.95
• Empty mass (MT)	767	718	1,457	957

Further comparison of the EOTV's is provided in Figure 1.3.2-20 through use of mass, unit cost and total transportation cost. In the case of mass, the baseline silicon EOTV has a solar array which is heavier per square meter and there is less power per square meter resulting in a much heavier vehicle. Propellant requirements are also larger due to the greater empty mass of the vehicle. Unit cost of the three candidates, however, show a benefit to the silicon EOTV primarily as a result of the cost per square meter of the array being approximately 25% that of the gallium arsenide blanket. The electric propulsion system on the silicon system is greater because of the heavier start burn mass of the system which also explains the higher launch cost. The total transportation cost amortizes the capital investment (unit cost plus launch of the EOTV's), and results in the silicon EOTV providing a savings of approximately $7 per kilogram of SPS over the baseline gallium arsenide and about a $6 per kilogram improvement over gallium arsenide with a thicker coverglass.

It may be seen from this cost comparison that the result is driven by the assumption that a GaAs EOTV was used with a silicon SPS. It is clear that the EOTV and SPS should share a common solar array technology.

With the level of definition conducted to date, the silicon cell blanket with 3 mil coverglass is recommended as the preferred solar array for the EOTV. Should future analysis indicate less optimism regarding solar array performance and its recovery with the annealing, the 6 mil coverglass may require reassessment. The gallium arsenide cell with minimum coverglass does not appear to be worthwhile for orbit transfer operations. Again future analysis concerning radiation effects on the blanket may provide the rationale for investigating GaAs blankets with thicker coverglasses. The EOTV defined and updated for comparison with the LEO construction option employed a silicon (3 mil coverglass) blanket.

1.3.2.2.2 EOTV Design Life

In addition to establishing the first trip optimum performance characteristics associated with an EOTV, it is also necessary to decide the design life or establish how many trips should be made by a given EOTV. This decision should be based on cost data, as well as considerations related to uncertainty in performance characteristics and hardware limitations. Data pertaining to these topics is presented in Figure 1.3.2-21. The left hand portion of this chart shows the total transportation cost per EOTV trip as a function of the number of round trips that a EOTV may make. Several cost items

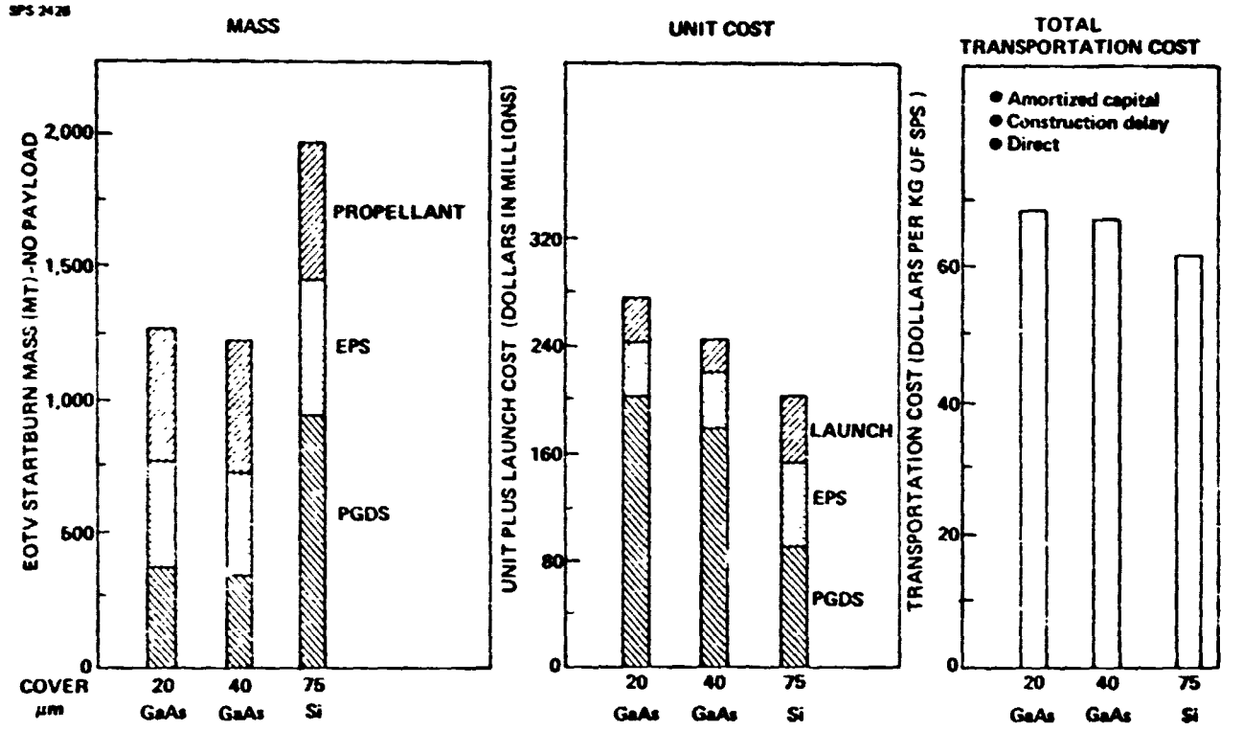

Figure 1.3.2-20 EOTV Comparison Silicon Versus GaAs

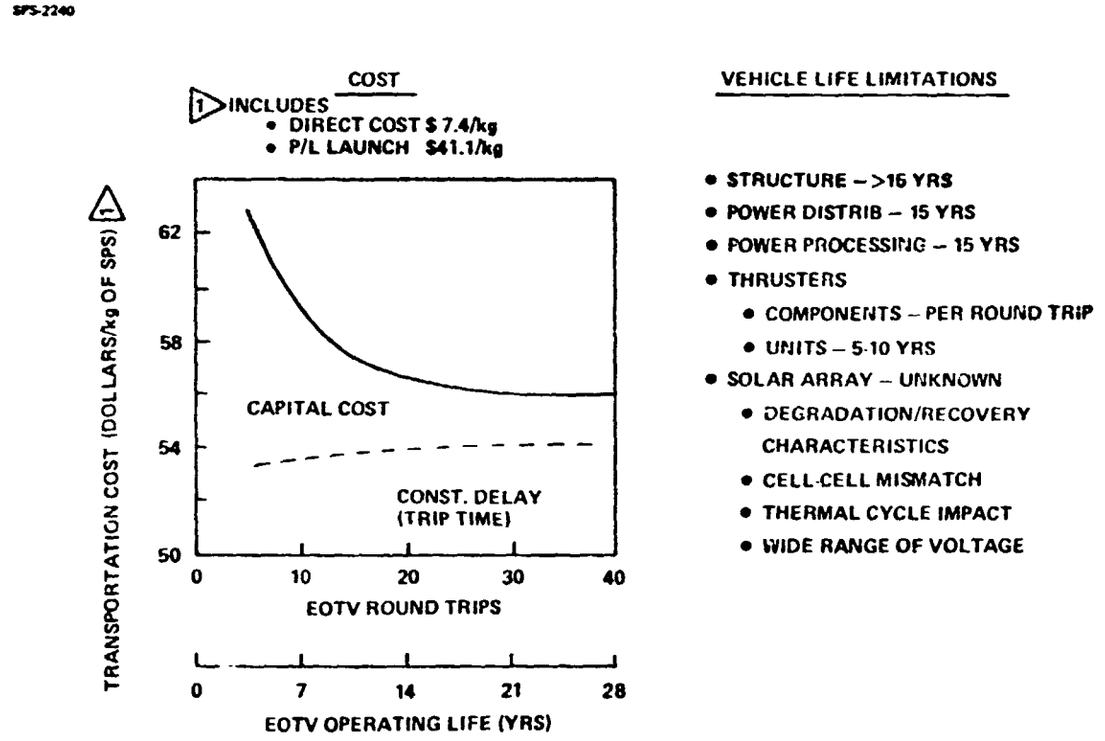

Figure 1.3.2-21 EOTV Round Trip Comparison

such as the launching of the payload as well as the direct cost are for the most part constant. Construction delay (trip time) cost increases with additional number of round trips since the average power is less with each subsequent trip, thus increasing the total round trip time. Capital cost is decreasing since the initial cost is amortized out over more flights. One cost increment not included in this data is that associated with a larger refurbishment cost with each ten trips because the complete thruster is replaced rather than just the grids and cathodes. A cost of $56 per kg of SPS component is indicated when assuming 20-25 round trips per EOTV which would correspond to approximately 17 or 18 years of operating life.

Before making the selection of the number of round trips for each EOTV, one must also consider the limitation that may occur in terms of component lifetime. No significant problem appears to exist for the structure, power distribution and power processing components although each of these items must be examined to verify this opinion. Thrusters can be refurbished after each trip and as previously indicated complete units are replaced at the end of ten trips. There is great uncertainty, however, relative to the life of the solar array and its performance. Several points should be considered. In the case of degradation/recovery characteristics, there is the fact that each leg of an EOTV trip will experience a fluence level ten times greater than that to be experienced by the satellite in 30 years of GEO operation. There is no test experience relative to the recovery capabilities from this amount of radiation or the number of times that recovery can be performed. Cell-to-cell mismatch arises because each cell would not be affected exactly alike in terms of its radiation characteristics, thereby resulting in additional contribution to overall power output loss. The thermal cycle impact must consider both the case of occultations that occur during the orbit transfers as well as the annealing of the solar array. In the case of the occultations, one round trip transfer has as many occultations as fifteen years of operational life of the SPS system. Another factor to be considered is the 10-15% variation in voltage that occurs throughout a trip.

The selection of the number of trips that should be flown by an EOTV is a difficult issue. On one hand, cost optimization would suggest 20 to 30 round trips per vehicle. However, in terms of expected component limitations, a system providing ten flights (7 years of operating life) appears to have significantly less risk. Consequently this more conservative EOTV design approach was used in the comparison with the LEO construction concept.

1.3.2.2.3 EOTV Fleet Size

The analysis thus far discussed addressed the performance and cost optimizations associated with a single EOTV. A number of EOTV's will be required however, to deliver all the components necessary for a complete 10 GW SPS in the required time interval. The factors establishing the required number of EOTV's (fleet size) include the total round trip time (transfer, refurb, cargo handling) and payload capability of the EOTV. The fleet sizing results are shown in Figure 1.3.2-22. The initial estimate of the fleet size considers only first trip performance of the EOTV and is called "basic fleet size" as illustrated on the left hand portion of the chart. The satellite cargo must be delivered in 330 days to satisfy the one year construction time and with 3600 MT net cargo per EOTV a total of 28 flights are required.

The selected first trip performance characteristics include an uptrip time of 180 days rather than 240 days because the cost of fewer EOTV's would offset the cost penalty for a given EOTV. The resulting basic fleet size is 20 vehicles based on first trip performance. Since each successive trip to be flown by an EOTV will take longer (due to array degradation), the 20 vehicles which initially fly 28 flights per year, will only fly 24 flights on their tenth trip as shown on the right hand portion of the chart. Consequently, to maintain an average of 28 deliveries per year a total of 22 vehicles will be required in the fleet. One additional vehicle is added to the fleet for a spare giving a total of 23 vehicles.

1.3.2.2.4 EOTV Design Characteristics

The EOTV design characteristics discuss the selection of the preferred configuration, general characteristics of the power generation system, the method employed to collect and distribute the power, and the electric propulsion systems.

1.3.2.2.4.1 Configuration

Options

With the performance optimization data available at the midterm (power and voltage requirements) a nearly square solar array resulted. This configuration is shown in Figure 1.3.2-23 as Option 1. The key characteristics of this configuration are that there are four thruster module locations and the EOTV is approximately square (provides the most desirable moment of inertia characteristics). Several variables exist however, that could present different configuration options also shown in Figure 1.3.2-23. These variables include the cell size to be used in the blanket and also the

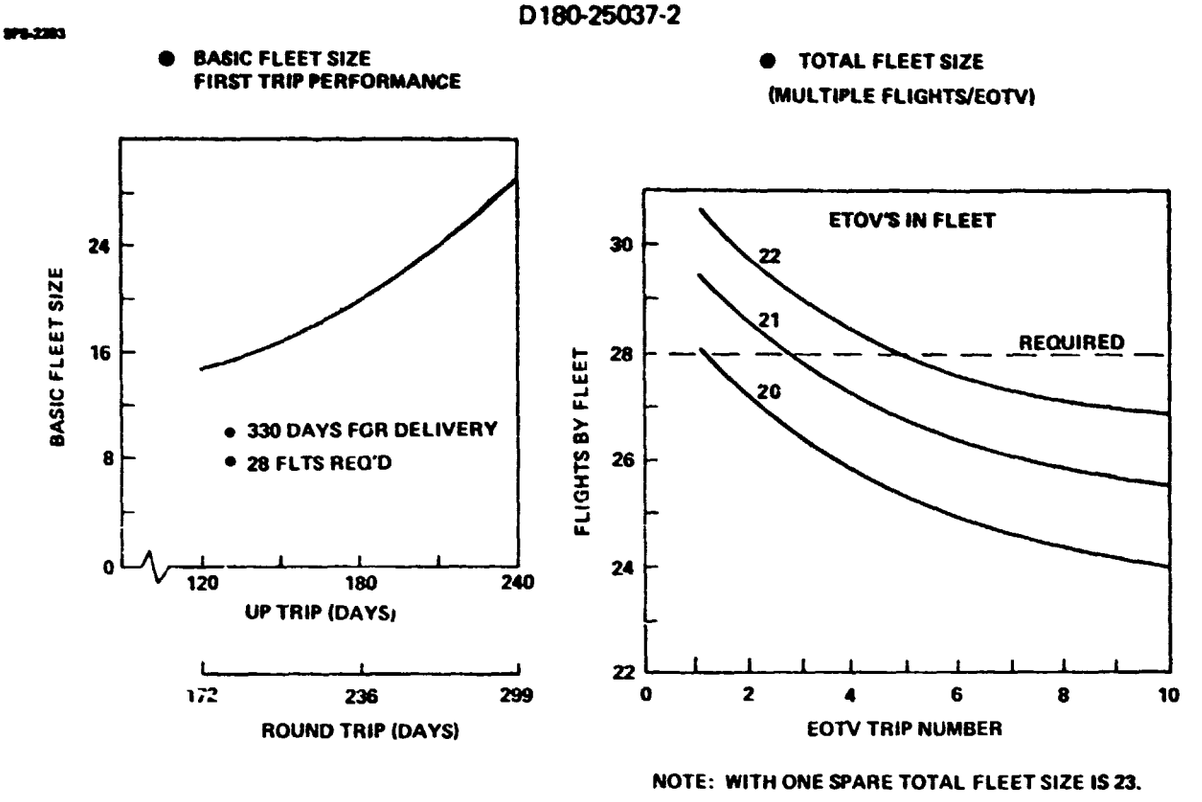

Figure 1.3.2-22 Fleet Sizing

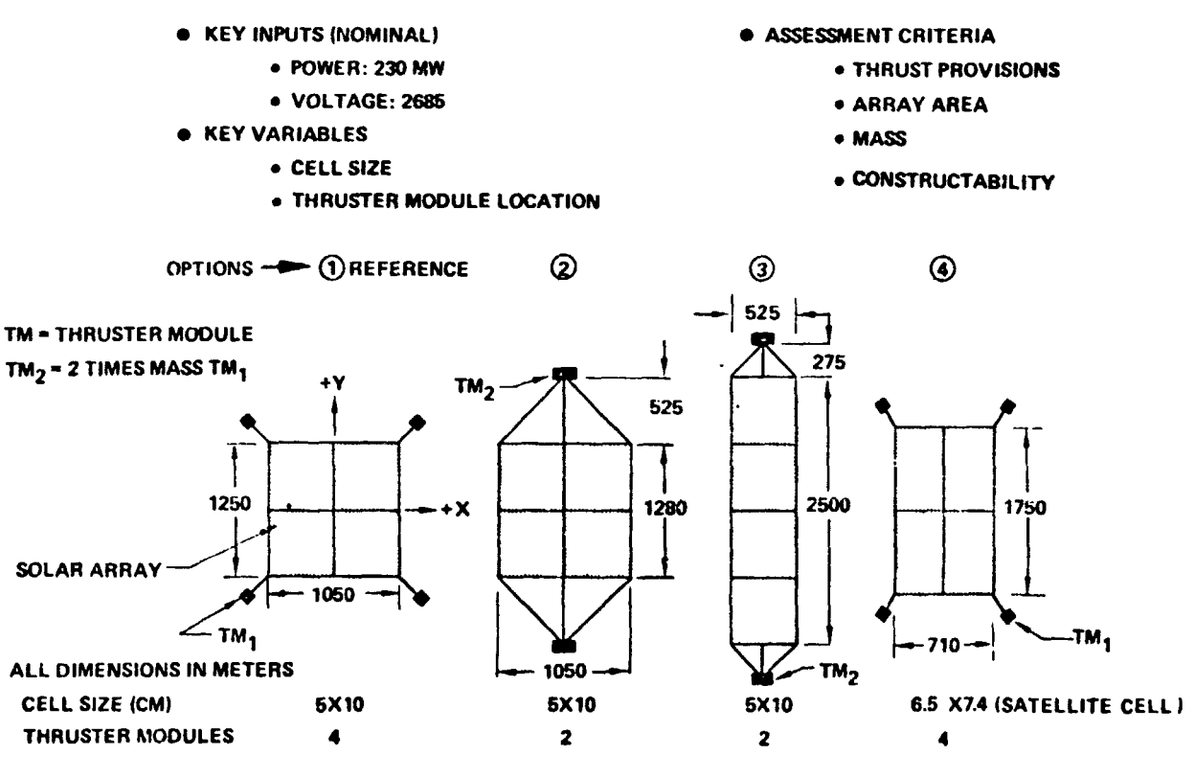

Figure 1.3.2-23 EOTV Configuration Options

thruster module location. The first three options indicated all used a 5 x 10 centimeter cell which differs from the basic satellite cell dimension of 6.5 by 7.4 centimeters. The reason for deviating from the satellite cell shape was the desire to have a solar array as nearly square as possible to provide the most favorable moment of inertia and with the required voltage and power requirements this could best be obtained by changing the cell dimension. Option 4 shows the configuration that results if the basic satellite cell is used. In either case, a small penalty in cost per m^2 would occur due to provisions necessary to operate in the more severe operating environment. Option 3 uses two thruster module locations but changes the aspect ratio of the satellite to approximately 5 to 1 in an attempt to decrease the control requirements for the Y axis. The options were assessed for the total amount of thrust required to perform the mission, difference in solar array area as brought about by different thrust requirements and I^2R losses, variation in vehicle mass and finally any differences in constructability.

The comparison of these configuration options is presented in Figure 1.3.2-24. The first item under thrust provisions is associated with thrust vector pointing efficiency: the percent of available time that the thruster modules can be used at their full thrust. Orbit geometry and the need to continue to point the array at the Sun while the Earth is being orbited, causes configurations having 4 thruster modules to encounter periods when one or two of the modules must be vectored away from their desired direction. Otherwise the high velocity plume would hit the vehicle and cause considerable damage. Options 2 and 3 with only two thruster module locations, do not have this constraint and can operate at full power whenever the vehicle is in sunlight. In terms of gravity gradient torque control requirement, the second option requires a thrust level of approximately twice that required to control the torque around the X axis for the reference configuration. Control around the Y axis is about one-third, while control around the Z axis requires a torque level six times greater than the reference. This same approach is used in comparing Option number 3. Option 4 was not analyzed in detail, but due to its elongated configuration it will be worse than the reference case. Another factor to be considered however, is the fact that although Options 2 and 3 require far less torque control for the Y axis, some control is required and consequently thrusters in addition to those of the two main modules must be provided. The net effect of comparing the amount of thrust required in terms of the thrust vector pointing efficiency compared to that of gravity gradient torque and full

SPS-2494

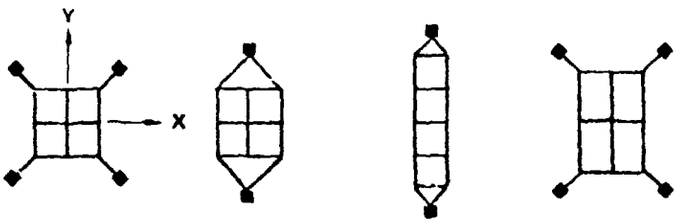

• OPTION	(1)	(2)	(3)	(4)
• *THRUST PROVISIONS*				
• T.V. POINTING EFF.	REF.	+6%	+6%	SAME AS REF
• GGT CONT REQ'T				
X AXIS	REF	> 2X	> 5X	WORSE THAN (1)
Y AXIS	REF	< 3X	< 100X	WORSE
Z AXIS	REF	> 6X	>16X	WORSE
• OTHER FACTORS	–	SUPPLEMENTAL THRUSTERS REQ'D FOR Y AXIS CONT OPT 2 & 3		–
• NET EFFECT:	THRUST VECTOR POINTING AND GRAVITY GRADIENT CONTROL REQ'TS TEND TO OFFSET ONE ANOTHER			
• I^2R LOSSES (MW)	REF	+6.1	+7.2	NOT EVAL
• ARRAY AREA (KM^2)	REF	+0.035	+0.057	NOT EVAL
• MASS (MT)	REF	+51	+73	NOT EVAL
• CONSTRUCTABILITY	REF	TM INSTALLATION MORE DIFFICULT	SMALLER BASE	LARGER BASE

Figure 1.3.2-24 EOTV Configuration Comparison

3 axis control is such that little difference is evident at this time between two and four thruster module configurations. In terms of I^2R losses, the extra length of the power buses required to reach the two thruster module locations results in a small penalty for Options 2 and 3 over the reference case. The I^2R losses are reflected in terms of additional solar array area requirement and the associated mass plus the additional bus bar lengths results in a small mass penalty for Options 2 and 3. In terms of constructability, the only significant difference would be that associated with the size of the construction base as influenced by the size of the bays making up the EOTV or the location of the thruster modules. In summary, there is not too much difference between the options investigated. A firm resolution as to which is better will require an additional level of detail regarding the amount of thrust necessary to satisfy all requirements. Consequently, the configuration using 5 x 10 cells and four thruster modules will be used for the remainder of the analysis.

Selected Configuration

The selected EOTV configuration is shown in Figures 1.3.2-25 and 1.3.2-26 and consists of four solar array bays, with each bay formed by a pentahedron. The apices of the pentahedrons are tied together to serve as a mounting location for the payload and propellant tanks. This location provides a good moment of inertia balance to minimize gravity gradient torque control requirements and simplifies the docking of the payloads as well as propellant tankers. Thruster modules are attached to beams protruding from the four corners of the configuration. Power for the thrusters is drawn from solar arrays in the bay adjacent to the thruster module. The vehicle is sized to deliver 4,000 metric tons and return 200 metric tons with an uptrip time of 180 days and down time of 40 days, with a specific impulse of 8,000 seconds. The total dry mass of the vehicle is 1462 metric tons while the total propellant loading is approximately 500 metric tons. The 1510 m dimension of the configuration reflects the change in power requirements that occurred after the Phase I midterm. The 1044 m dimension is the same as that used at the midterm and is a function cell size and voltage requirements.

1.3.2.2.4.2 Power Generation System

In terms of power generation and distribution systems, the EOTV is divided into four separate bays with each bay providing power to a thruster module as shown in Figure 1.3.2-27. Each bay is divided into fifty-four 14.5 meter segments and produces approximately 74 megawatts. The optimum voltage was found to be 2685 volts as

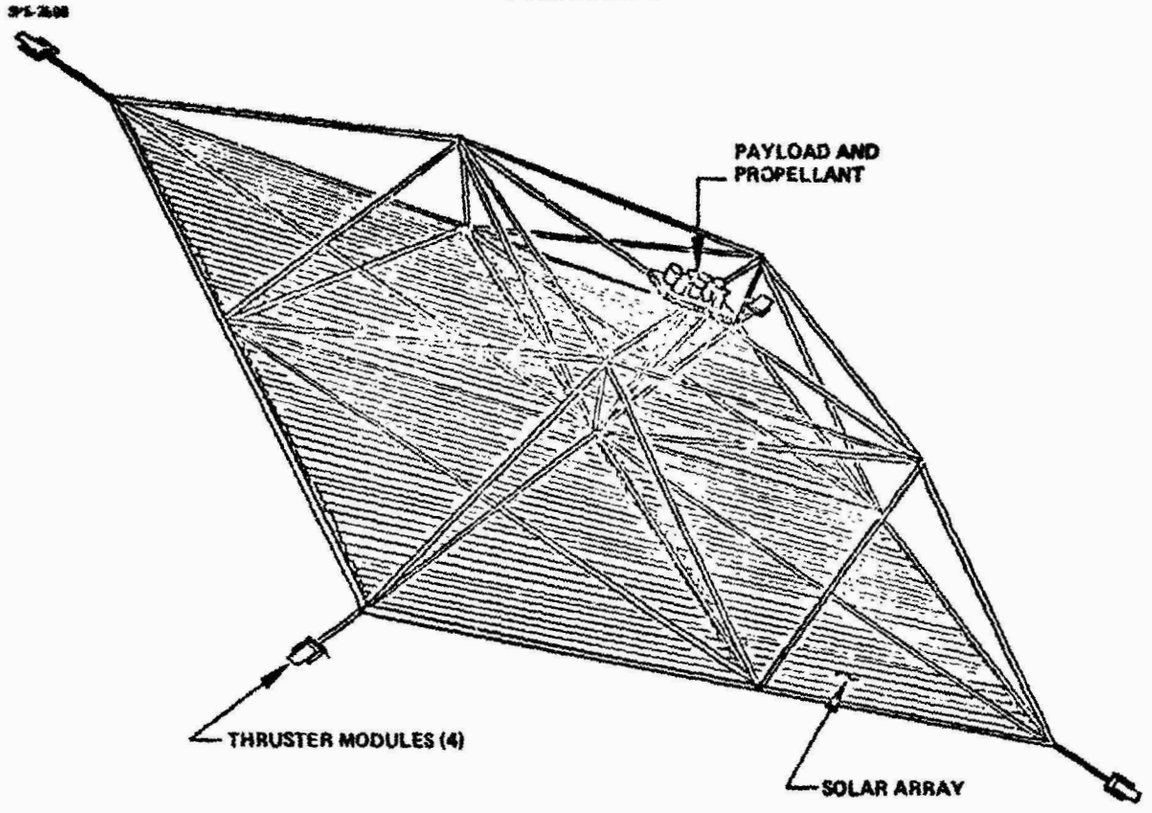

Figure 1.3.2-25 EOTV Configuration Concept

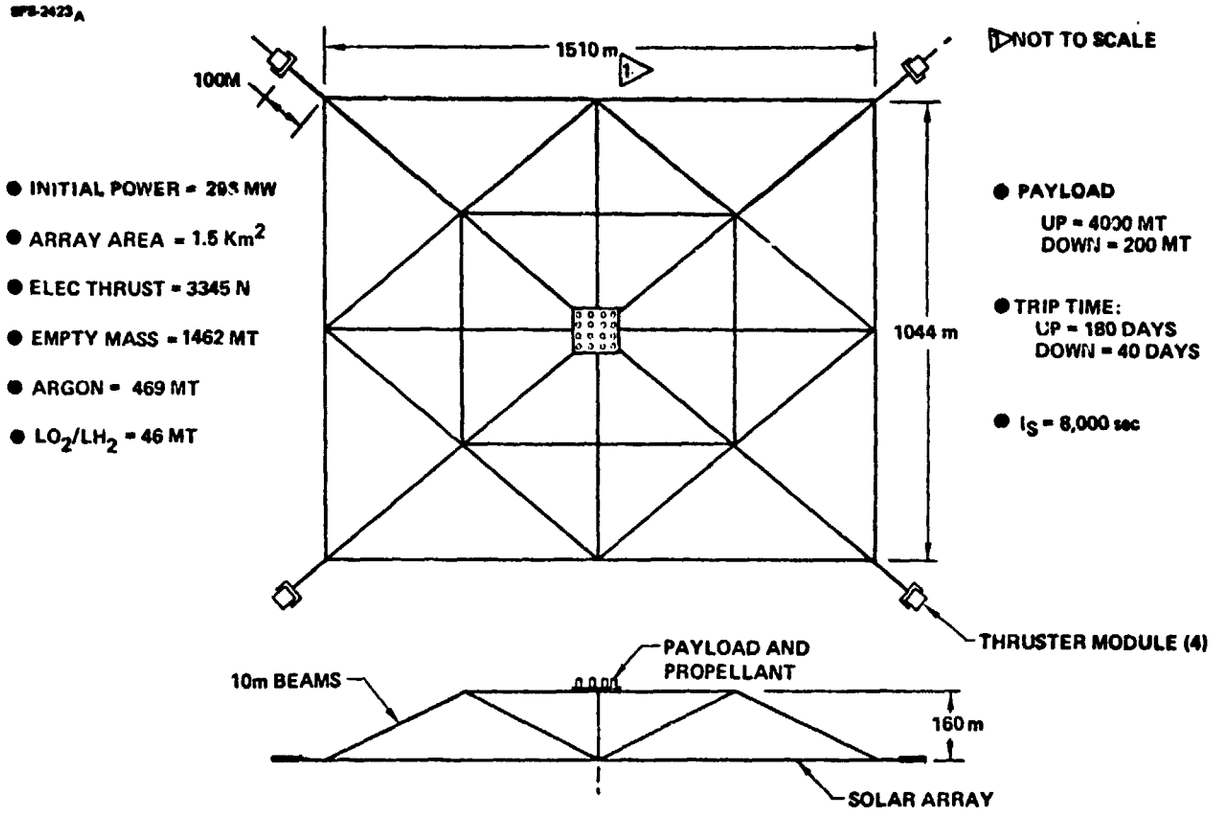

Figure 1.3.2-26 Electric OTV Configuration

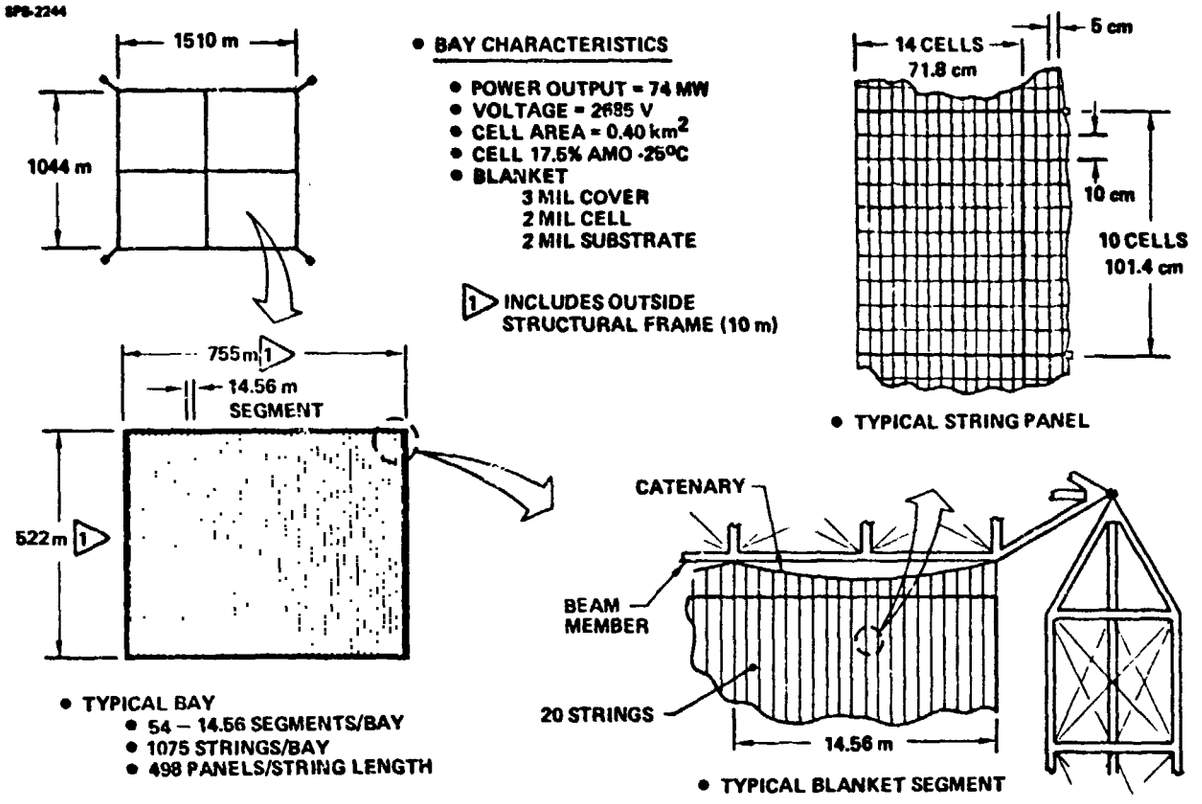

Figure 1.3.2-27 EOTV Power Generation System

shown in Figure 1.3.2-28. Each segment consists of 20 strings, with each string in turn consisting of 498 panels. Each of the panels include (140) 5 x 10 centimeter cells. The cell shape change is the result of compromise between a desired square satellite shape and the power and voltage requirements dictated by the propulsion system.

1.3.2.2.4.3 Power Collection and Distribution

Power busses are located on three sides of each bay of the EOTV as illustrated in Figure 1.3.2-29. Each bay is divided into 7 sectors in order to minimize the impact on the switch gear complexity should a fault occur. Five sectors each collect power from 8 segments while two sectors collect power from 7 segments. A bus from each sector runs to the associated thruster module where the power is processed. Each of the busses is one milimeter thick by 80 centimeters deep. The optimum bus temperature was found to be 50°C as shown in Figure 1.3.2-30.

1.3.2.2.4.4 Electric Propulsion System

Electric propulsion modules are located at four corners of the EOTV. The key characteristics of each module are shown in Figure 1.3.2-31. Each module consists of a gimbal, yoke, thruster panel containing thrusters and power processing units and a thermal control system. For the reference design, 289 thrusters are used at each of the four corners. The principal components of the 1..2m diameter ion thruster and performance characteristics associated with a specific impulse of 8000 sec are shown respectively in Figure 1.3.2-32 and Table 1.3.2-6.

Several methods were considered for supplying power to the thrusters. One of these options involves obtaining power directly from the arrays with no processing or no regulation. The chief disadvantage in this option is that the voltage is decreasing at the same time the power is degrading. As the flight proceeds, the lower voltage will result in a loss of approximately 1,000 seconds of specific impulse. A second option regulates and sectionalizes the array so that as additional power is required, additional sectors can be switched into operation. The main disadvantage of this concept is the extremely complicated switch gear system. The final power supply method considered involves processing all the power. The array voltage generated in this concept is the optimum voltage from the standpoint of I^2R and plasma losses. The resulting voltage is 268 V as compared to 1700V required by the thrusters. A complete comparison was not done on these concepts, however, the all-processing method appears to be the most straightforward and since some of the power needs to be processed anyhow this

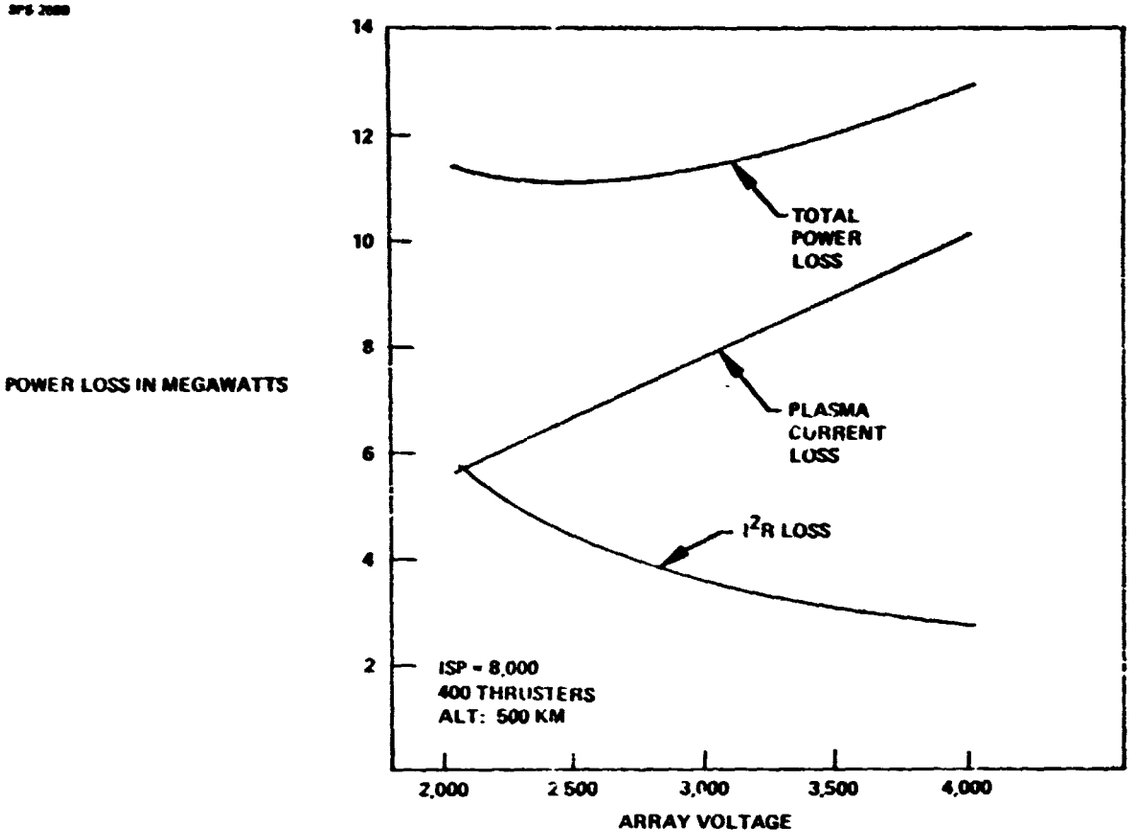

Figure 1.3.2-28 Optimum Array Voltage

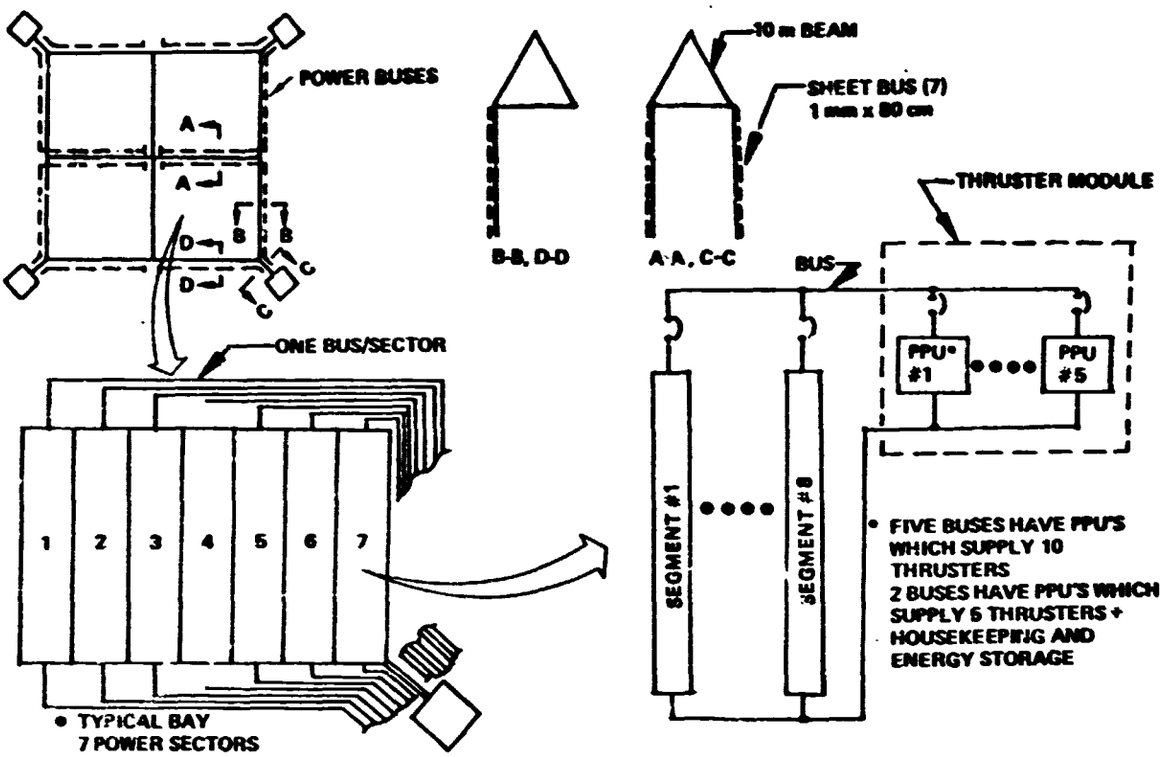

Figure 1.3.2-29 Power Collection and Distribution

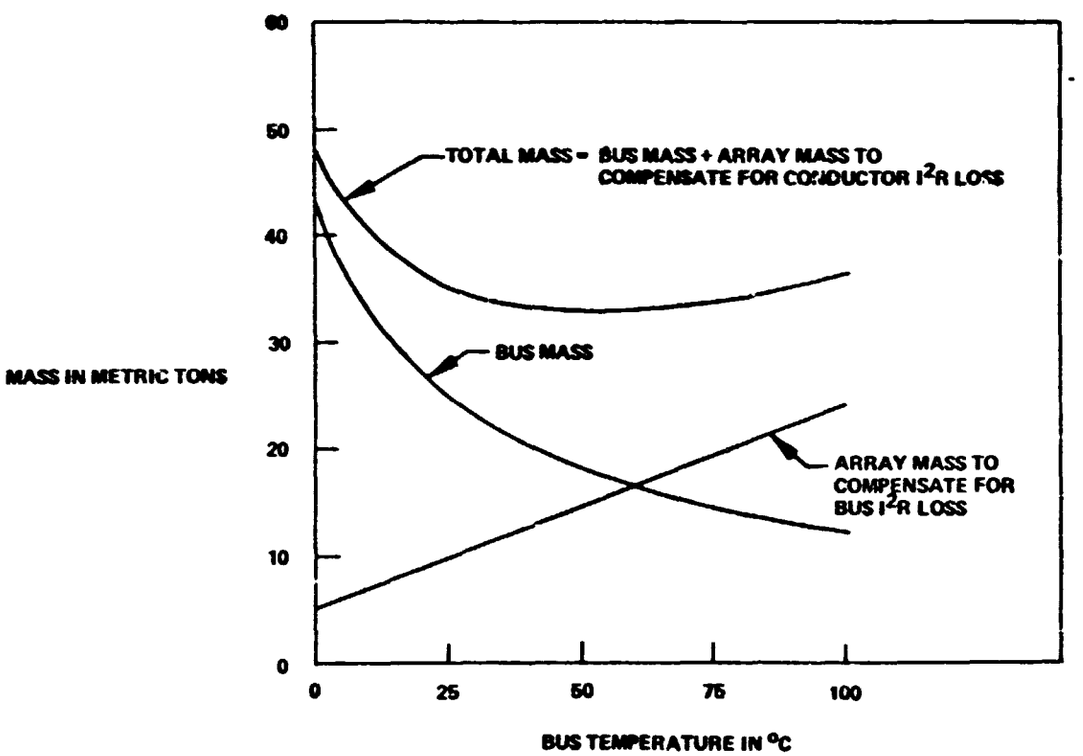

Figure 1.3.2-30 Optimum Power Bus Temperature

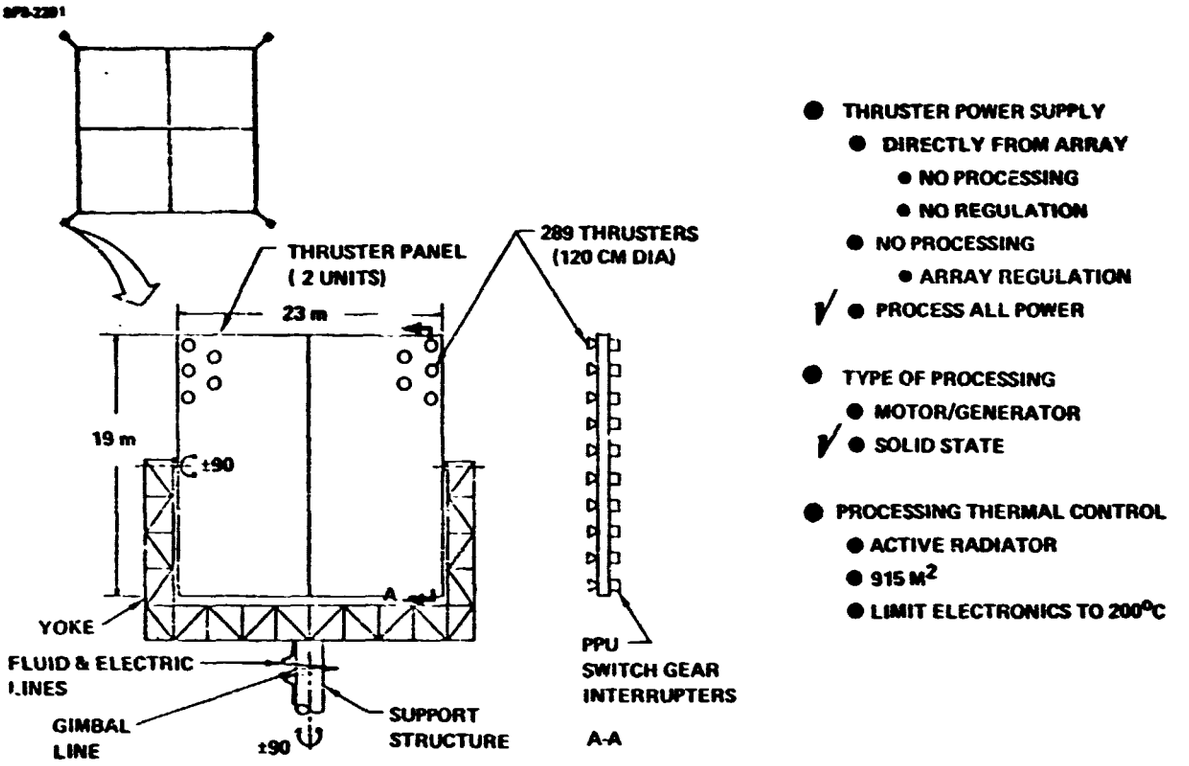

Figure 1.3.2-31 Electric Propulsion System

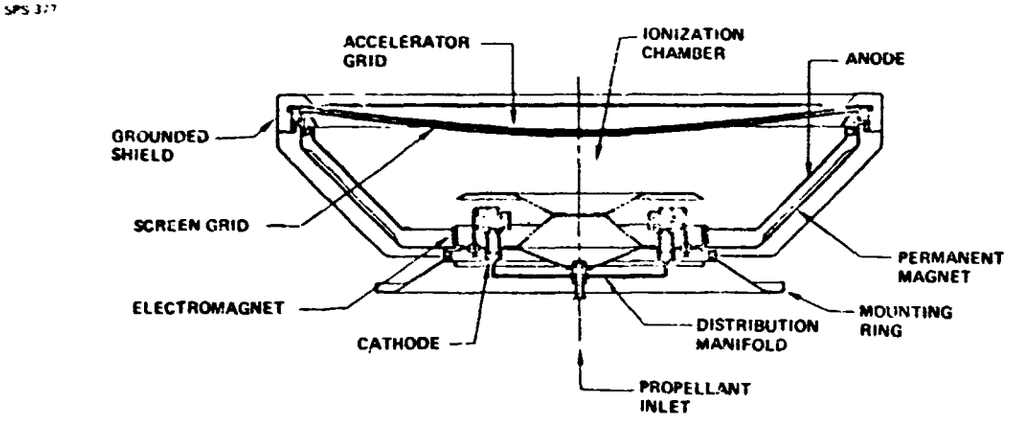

Figure 1.3.2-32 120 CM Argon Ion Thruster

Table 1.3.2-6 Selected 1.2 M Argon Ion Thruster Characteristics

SPS-2000

FIXED CHARACTERISTICS		
BEAM CURRENT:	80.0	AMPS.
ACCEL. VOLTAGE:	500.0	V.
DISCHARGE VOLTAGE:	30.0	V. (FLOATING)
COUPLING VOLTAGE:	11.0	V.
DBL. ION RATES:	0.16	(J2/J1)
NEUTRAL EFFLUX:	4.8384	AMP. EQUIV.
DIVERGENCE:	0.98	
DISCHARGE LOSS:	187.3	EV/ION
OTHER LOSS:	1758.0	W.
UTILIZATION:	0.892	W.
LIFE:	8000	HR.
*WEIGHT:	50.	KG.
SELECTED CHARACTERISTICS		
SCREEN (BEAM) VOLTAGE:	1700	V.
INPUT POWER:	130	KW
THRUST.	2.9	N
EFFICIENCY:	78	

*WEIGHT PREDICTION COURTESY OF T. MASEK OF HRL.

method was selected for the reference. The type of processing equipment selected was solid state due to its longer MTBF. Thermal control of the processing equipment is required and is accomplished using an active radiator.

1.3.2.2.5 Mass Summary

The mass characteristics of the EOTV are summarized in Figure 1.3.2-33. The empty mass for the configuration is shown for both mid-term and final values. The most significant change was that associated with the solar array mass, which increased as a result of using a more accurate model reflecting the power requirements for I^2R losses, storage provisions, changing power conditioning efficiencies as a result of using solid state equipment rather than motor generator equipment and also a revision in the radiation degradation analysis. These changes to the solar array, in turn, have reflected or resulted in changes in all other elements of the vehicle resulting in approximately a 300 metric ton increase over the mid-term values. Accordingly, the startburn mass also reflects a 300 metric ton increase over the mid-term value.

1.3.2.2.6 EOTV Cost

A preliminary cost for the EOTV was established at the mid-term of Phase I. It was indicated at that time that the estimate was probably optimistic. The guidelines used to establish more accurate EOTV costs than that shown at the mid-term are indicated in Table 1.3.2-7. The fleet size and amortization period are the same as was used for mid-term. The chief difference in costing, however, deals with the method in which the costing was done. At the mid-term, a scaling relationship was used where the power generation and distribution system cost was scaled to similar systems of the satellite and the electric propulsion system cost for the EOTV was scaled to costs associated with the selfpower orbit transfer systems. As such, this scaling method presented an optimistic cost primarily because of using a component production rate much higher than that possible when amortizing the hardware over a number of years. The final costing of the EOTV, included establishing detailed first unit costs using component mass and quantities directly associated with a single EOTV. These TFU costs were then used in conjunction with the annual production rate of the components for the entire EOTV fleet to establish the average cost of an EOTV.

As indicated earlier, amortizing or spreading out the total hardware requirements over the operating life of the system greatly influences the unit cost of the EOTV and subsequently the cost per flight. A comparison of the annual production rate for some

SPS 2496

ITEM	• EMPTY MASS (M.T.) MIDTERM	FINAL
POWER GEN & DISTRIB	(736)	(951)
SOLAR ARRAY	608	780 [1]
STRUCTURE	95	122
DISTRIBUTION	33	42
ENERGY STORAGE	–	7
ELECTRIC PROPULSION	(447)	(496)
THRUSTERS	71	79
POWER CONDITIONING	195	219
THERMAL CONT	55	88
STRUCT/MECH	80	61
PROPELLANT FEED SYS	46	49
AUXILIARY SYSTEMS	(12)	(15)
TOTAL	1195	1462

• STARTBURN MASS (M.T.)

PAYLOAD	4300
EMPTY	1462
PROPELLANT	
ARGON	469
LO_2LH_2	46
	5977

[1] MORE ACCURATE MODEL
- POWER REQ'T ADDITIONS
  - I^2R & STORAGE
  - PPU EFF
  - REVISED RADIATION DATA
- ARRAY AREA
  - BASED ON DESIGN POWER NOT ELEC
- OTHER CHANGES ARE RESULT OF [1]

Figure 1.3.2-33 EOTV Mass Summary

Table 1.3.2-7 EOTV Costing Guidelines

SPS-2482

	MIDTERM	FINAL
• FLEET SIZE	23	23
• AMORTIZATION PERIOD (YR)	7	7
• FLIGHT UNIT COST	SCALING	DETAILED MODELING • DETAIL TFU MASS & QUANTITY • AVG. TO REFLECT COMPONENT ANNUAL PRODUCTION RATE
• POWER GEN & DISTRIB	SCALE TO SATELLITE ($95/KG)	
ARRAY CONTRIB	$44/M^2	$53/M^2 DUE TO 5 X10 CM CELL
• ELECTRIC PROPULSION	SCALE TO SELF POWER OTS ($117/KG)	
• PROGRAMMATIC	NOT CONSIDERED	CONSIDER

of the EOTV and self-power components is presented in Table 1.3.2-8. In the case of the GEO construction concept, the total components for the 23 vehicles has been spread out equally over 7 years of its operating life with an additional 20% added to the annual requirement to cover manufacturing problems, etc. As indicated, nearly all components for the GEO/EOTV case reflect a significant decrease in the annual production rate, which will eventually reflect in the average unit cost of the EOTV's.

The final Phase I EOTV hardware and cost per flight numbers are presented in Table 1.3.2-9. In the case of the hardware costs, both mid-term and final costs are presented. The final flight unit costs have almost doubled from that of the mid-term, reflecting the influence of the more detailed cost analysis. The power generation and distribution system has not increased as much as electric propulsion system primarily because the solar array, which is the largest contributor, was and still is being costed on mature industry basis with the increase over preceding mid-term values primarily the result of the 20% penalty paid for using the 5 x 10 centimeter cell and also the 21% cost growth factor. Electric propulsion costs, are greater by almost a factor of 3 and reflect a significant difference in the cost for individual elements as a result of lower production rate. As indicated earlier, programmatic costs were not indicated in the mid-term. On a cost per flight basis, including amortization of the capital, the change from the mid-term has been approximately $30 million per flight.

Cost for the complete GEO construction concept is presented in Section 1.3.2.4 which compares this concept with a LEO construction concept.

1.3.2.2.7 Mission Operations

1.3.2.2.7.1 Key Mission Events

Mission events that occur whle using an EOTV for GEO construction are indicated in Table 1.3.2-10. A total of 16 days of on-orbit time has been indicated for the turnaround of the vehicle, in addition to the 219 days of time required for the up and down transfers.

Once the vehicle reaches GEO, it will be placed in a standby condition approximately 1 kilometer from the base. At that time small LO_2/LH_2 tug(s) will be used to move the cargo from the EOTV to the GEO construction base. Annealing of the solar arrays will occur at GEO and will be discussed in more detail in a subsequent chart. Once the

Table 1.3.2-8 Component Annual Production Rate

SPS-2481

KEY COMPONENT	ANNUAL PRODUCTION RATE (UNITS)		
	LEO/SPM	GEO/EOTV	LEO/SPM/EOTV
THRUSTERS	26800	5340	
PPU'S	384 (1 PER 80 THRUSTERS)	534 (1 PER 10 THRUSTERS)	
SWITCHGEAR	1920	534	
INTERRUPTERS	26800	16500	
CABLING	192	30	
TANKS–ARGON	32	8	
GIMBALL ASSY	32	15	
AVIONICS			
COMMUN	32	15	
COMPUTER	32	15	
THERMAL CONT	384	15	
POWER DIST	160	105	
STANDOFF STRUCT	32	15	

Table 1.3.2-9 Silicon EOTV Cost

SPS-2483

• COST IN MILLIONS

	EOTV HARDWARE		COST PER FLIGHT		
	PART 1 MIDTERM	PART 1 FINAL		BASIC	AMORT.
• FLIGHT UNIT	(124)	(247)	• CAPITAL	(347)	(52)
• POWER GEN & DISTRIB	(69.9)	(99.7)	• EOTV HRDW	284	
SOLAR ARRAY		79.6	• EOTV LAUNCH	54	
STRUCTURE		12.1	• CONST BASE	13	
DISTRIBUTION		1.6	• DIRECT		(29)
ENERGY STORAGE		6.4	• REFUEL		19
• ELECTRIC PROPULSION	(52.7)	(141)	• REFURB		10
THRUSTERS		15.4	• CONST TIME DELAY		(18)
POWER COND.		87.2	• PAYLOAD LAUNCH		(148)
THERMAL CONTROL		22.1	TOTAL		247
STRUCT/MECH		11.3			
PROPELLANT SYS		5.0			
• AVIONICS	(1.0)	(6.5)			
• PROGRAMMATIC		(36.6)			

Table 1.3.2-10 Mission Events

SPS-2232

EVENT	DESCRIPTION	Δ TIME (DAYS)	
		ON-ORBIT	TRANSFER
• TRANSFER TO GEO	COST OPTIMIZED FIRST FLIGHT		180
• TERMINAL MANEUVERS	RENDEZVOUS AND PLACE ON STANDBY CONDITION	1	
• UNLOAD CARGO	(10) 400 MT UNITS	1	
• ANNEAL SOLAR ARRAY	1.2 MILLION SQ METERS	4	
• PREPARE FOR RETURN	ACTIVATE, CHECKOUT AND LOAD CARGO	1	
• TRANSFER TO LEO	DICTATED BY POWER AVAILABLE		39
• TERMINAL MANEUVERS	RENDEZVOUS AND PLACE ON STANDBY CONDITION	1	
• REFURB ELEC THRUSTERS	1600 UNITS	4	
• CARGO HANDLING	UNLOAD CARGO AND LOAD (10) 400 MT UNITS	1	
• UNSCHEDULED MAINT	– – –	1	
• PROPELLANT RESUPPLY	ARGON, LO_2, LH_2	1	
• PREPARE FOR TRANSFER	ACTIVATION AND CHECKOUT	1	
	TOTAL	16	219

vehicle has returned to low earth orbit, it will again be placed in a stationkeeping standby condition approximately 1 kilometer from the LEO base. Again, small tugs will fly out from the LEO base to the EOTV to perform refurbishment operations on the thrusters, unload and load cargo propellant and deliver propellant. The propellant resupply will be done by tankers rather than removal of the propellant tanks.

1.3.2.2.7.2 EOTV Annealing Operations

The method of annealing the EOTV solar array is essentially the same as that employed by the operational satellite. The major operations associated with the EOTV annealing operations are shown in Figure 1.3.2-34. In general, the method consists of CO_2 laser systems attached to a gantry that can move across each bay. Each gantry system anneals a 15m strip the entire width of the bay. For EOTV application, 2.5 hours is required per strip (segment) with a continuous power requirement of 8.7 MW. The total time required to do the annealing is of course a function of total area involved and the number of gantries employed. The phase I midterm EOTV had a total of 1.2 million square meters of solar array. Use of only one gantry would result in approximately 20 days of annealing time which is judged to be too excessive. Although no optimization has been done at this point, the reference system will use four annealing gantries, thus resulting in an annealing time of approximately four days. When using four gantries, however, two are placed in each of two bays so that power can be drawn from the other two bays to operate the annealing systems. When a given bay has been completely annealed, the gantries will move to a bay that has not been annealed and repeat the annealing operation. Annealing can be performed at either LEO or GEO, however, such factors as continuous sunlight to generate power and minimum orbit keeping propellant suggest annealing at GEO will be slightly better than if the operation was performed at LEO.

1.3.2.2.7.3 Thruster Refurbishment

The other key mission event to be discussed is that of refurbishment of the EOTV thrusters. The first point to establish is the frequency of the refurbishment. In this case, the life of the grids of the thruster are the major concern, although there is some indication that the cathodes will also have a life problem. Figure 1.3.2-35 presents a plot of the thruster grid life as a function of beam current. This data is a result of combining the results of a model that predicts the double ion production rate (which is the major factor in erosion) as a function of beam current with another model that predicts erosion. Using this data to check the erosion rates of a 30 cm

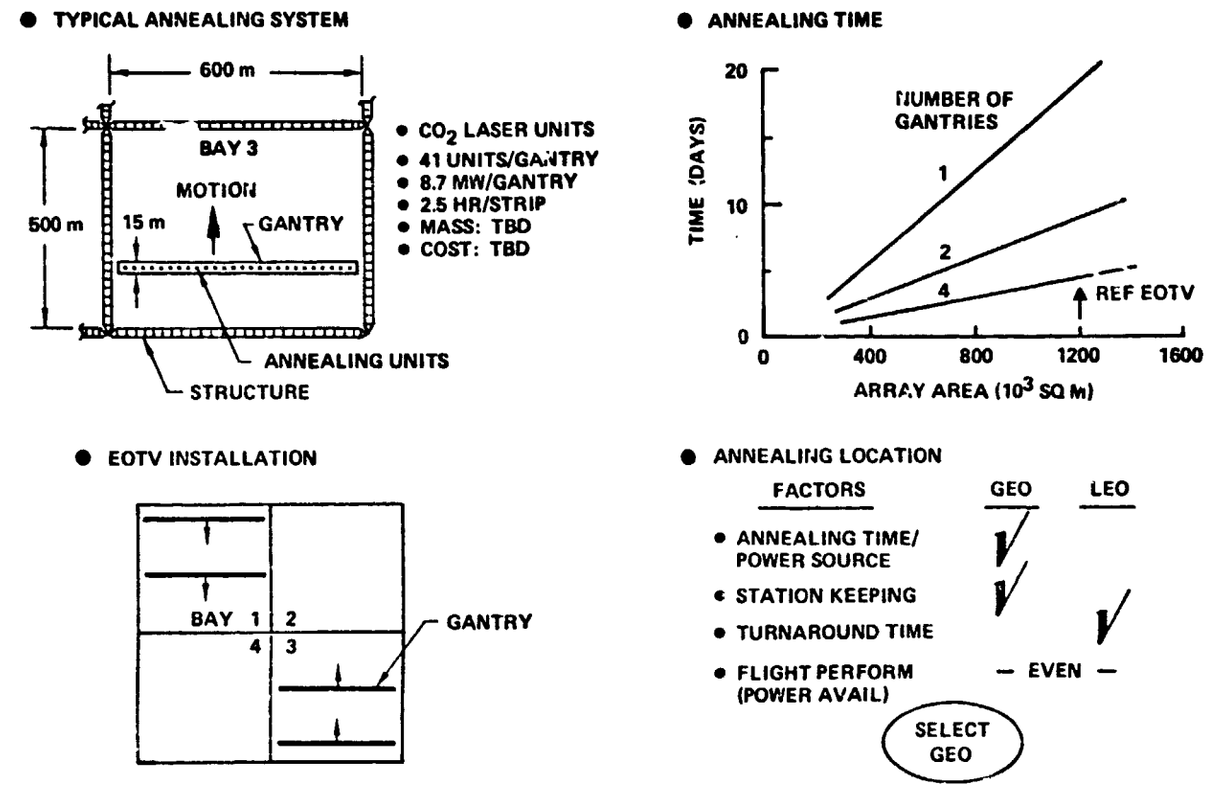

SPS-2318 *Figure 1.3.2-34 EOTV Annealing Operations*

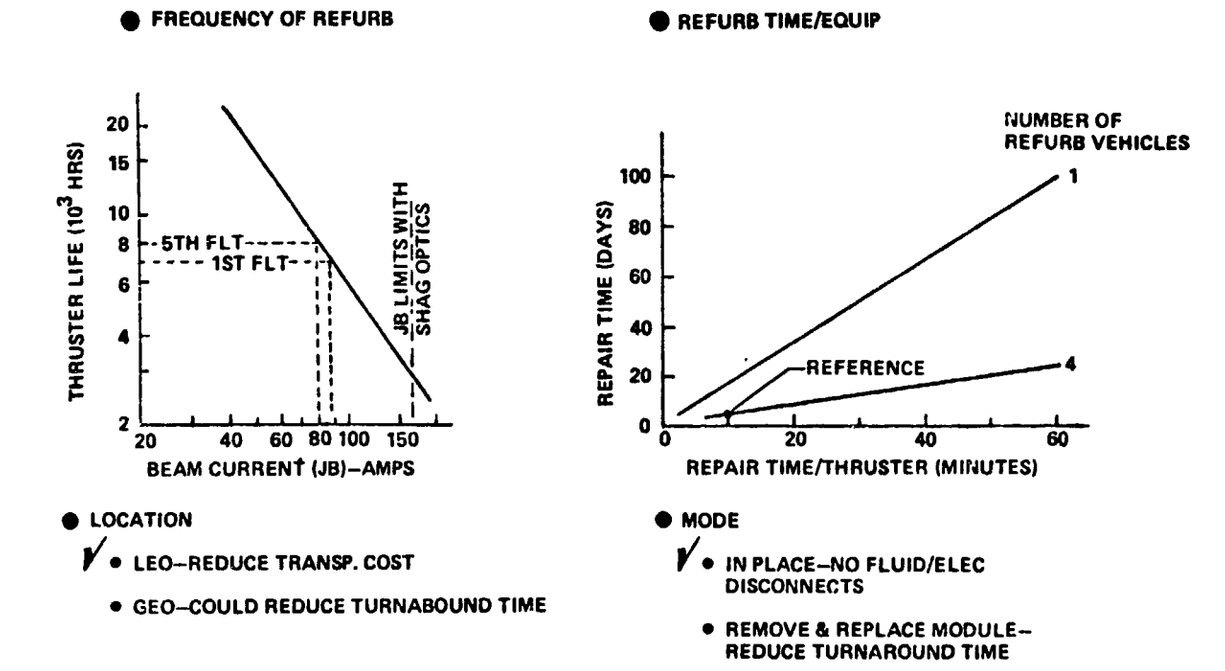

Figure 1.3.2-35 Thruster Refurb

mercury thruster whose erosion characteristics are known has resulted in a very good correlation, providing confidence in the methodology. Thruster life requirements are indicated for the first and fifth trips of an EOTV and reflect the actual burn time plus a 50% margin. These burn times indicate that 80 amps is about the most that can be expected and corresponds to the thruster design and performance characteristics that have been used in the Boeing SPS studies to date. The second point to establish is the amount of time required for the refurbishment and the amount of equipment required. Figure 1.3.2-35 also indicates that four refurb vehicles would be required in order to result in a reasonable refurb time. The reference system assumes that each thruster is repaired in ten minutes resulting in a repair time of four days and four refurb vehicles. Refurb could be done at either LEO or GEO, with LEO providing the lower transportation cost while the chief advantage of the GEO being a reduction in the turnaround time since it can be done in parallel with annealing of the solar array. At this point in time it is judged that the reduced transportation cost would be more beneficial, consequently, the refurb of the thrusters are done at LEO. As indicated earlier, the vehicle would be placed approximately 1 kilometer away from the base. Refurb on the thrusters can be done in place at the EOTV which eliminates fluid and electrical disconnections or the complete thruster panel could be removed and flown back to the base where it would be refurbed with another panel immediately installed to allow the next trip. The latter approach would reduce the turnaround time but would present the problem of disconnecting fluid lines and electrical wiring. Consequently, the in-place concept is selected for the reference case.

1.3.2.2.8 LEO Support Base Design and Operations

This section will discuss the overall configuration and operations of the LEO support base used in the GEO construction concept.

1.3.2.2.8.1 Configuration

The primary functions of the base are to support construction operations associated with the EOTV's and to perform depot type operations during the ongoing satellite construction operations. The overall base concept and key characteristics are shown in Figure 1.3.2-36 and its dimensions in Figure 1.3.2-37. The base is sized to construct one bay of an EOTV at a time. Outriggers are used to support the bays as they are being constructed. Opposite of the construction platform is the location used for the docking of the OTV's and HLLV's. Crew modules are located at one corner of the facility and consist of two crew modules for the primay crew, one module for

SPS-2517

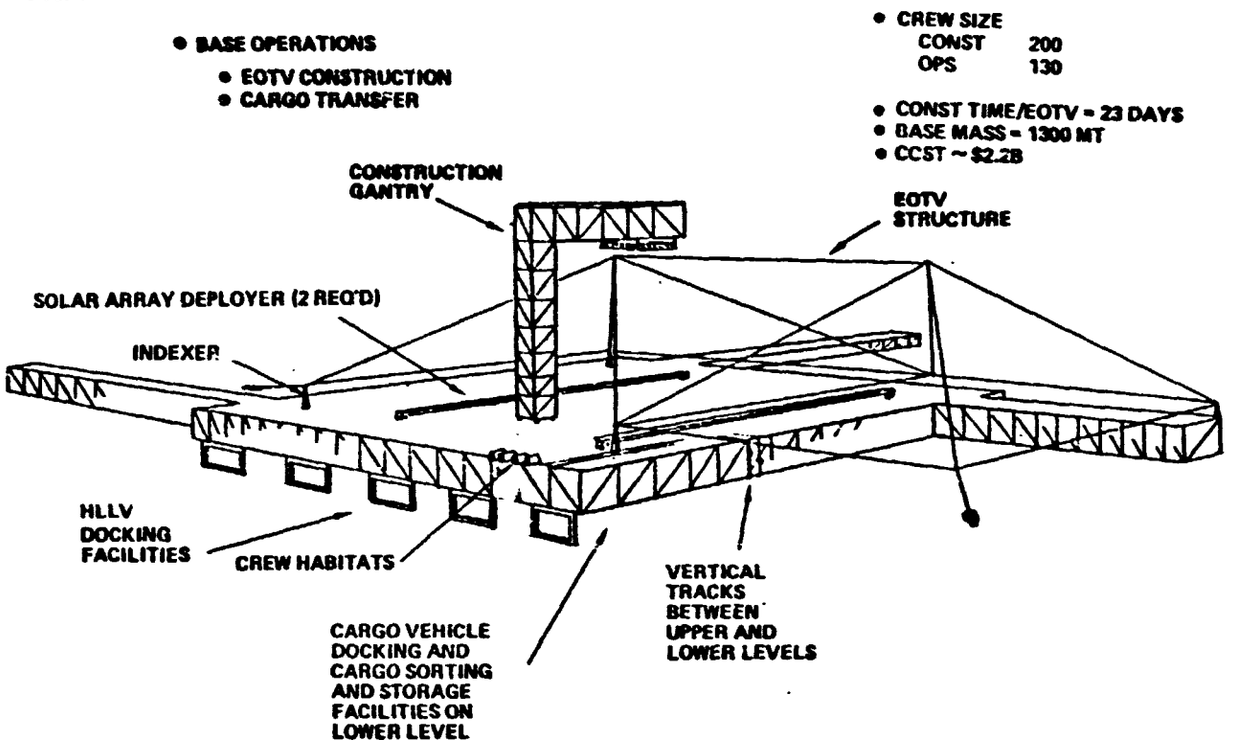

SPS-2441

Figure 1.3.2-36 LEO Support Base for GEO Construction

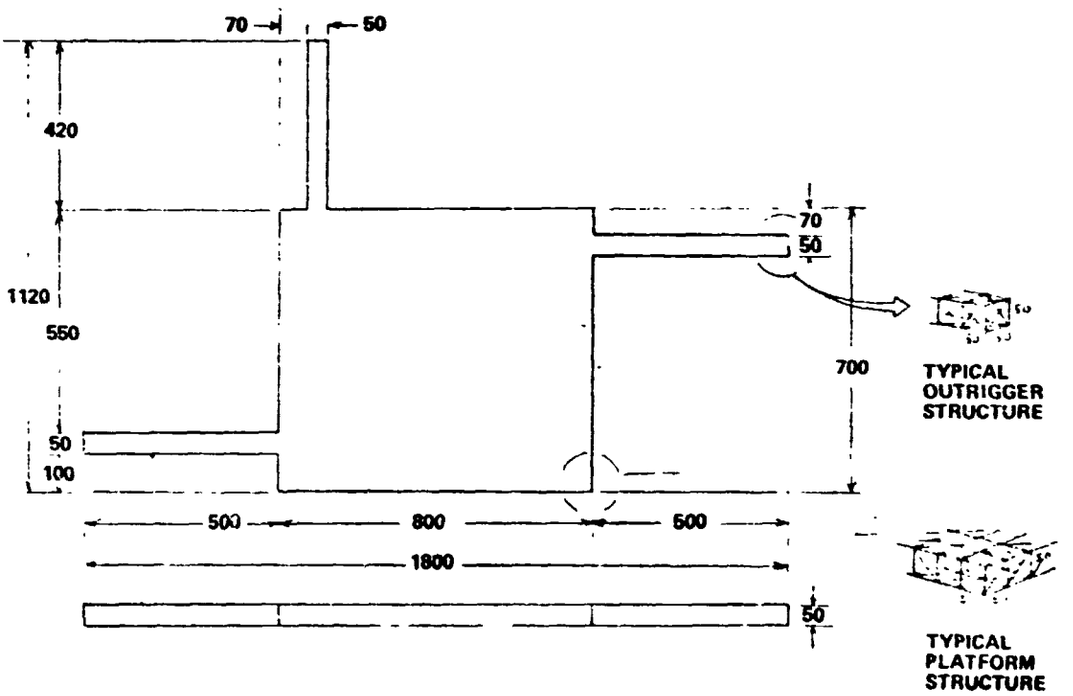

Figure 1.3.2-37 LEO Base Configuration

personnel involved in rotation operations and a maintenance and operations module. Total mass of base is estimated at 1.3 million kilograms and cost estimated at $2.2 billion. The average crew size is 200 during the construction operations.

1.3.2.2.8.2 EOTV Construction

The overall construction sequence associated with an EOTV is shown in Figure 1.3.2-38. In the overall sequence, a simple diagram is used to illustrate each bay. Five days are required to construct each bay of the EOTV. Indexing occurs following the construction of each bay. Construction of the EOTV is completed at the end of 20 days. The final operations involve installation of propellant tanks, payload and the final vehicle checkout so that the vehicle is ready for flight at the end of 23 days. With 23 vehicles required in the fleet approximately 1-1/2 years is required to construct the entire EOTV fleet.

Details of the construction operation associated with each bay of the EOTV are illustrated in Figure 1.3.2-39. Again it should be emphasized that the base has been sized to construct one bay at a time, rather than a complete EOTV. The construction operation requires a construction platform, beam machines, cherry pickers, solar array deployers, indexers and a construction gantry which is used to support several beam machines and cherry pickers. The sequence which is used to form the structure of each bay is illustrated in the lower left hand portion of the chart. Both the gantry beam machine and the platform beam machine work in parallel forming the beams. In this particular operation, the platform beam machine is relocated one time in order to complete the formation of its designated beams and the gantry must be moved to the side to allow the last beam of the pentahedral base to be installed. Total construction time to complete a single bay of the EOTV including checkout and its indexing so the next bay can be made is 5 days with the provision that two solar array machines are used. Should only one solar array machine be used, then the construction time per bay will be increased to seven days.

1.3.2.2.8.3 Depot Operations

Another function to be performed by the base is to provide support to the transportation operations or flights which interface with the base. The flight schedule is presented in Figure 1.3.2-40. In summary, crew rotation/resupply flights occur at four week intervals. Further discussion concerning crew rotation/resupply is presented in Section 1.3.2.2.9. EOTV flights will occur at approximately 11 day intervals. HLLV's

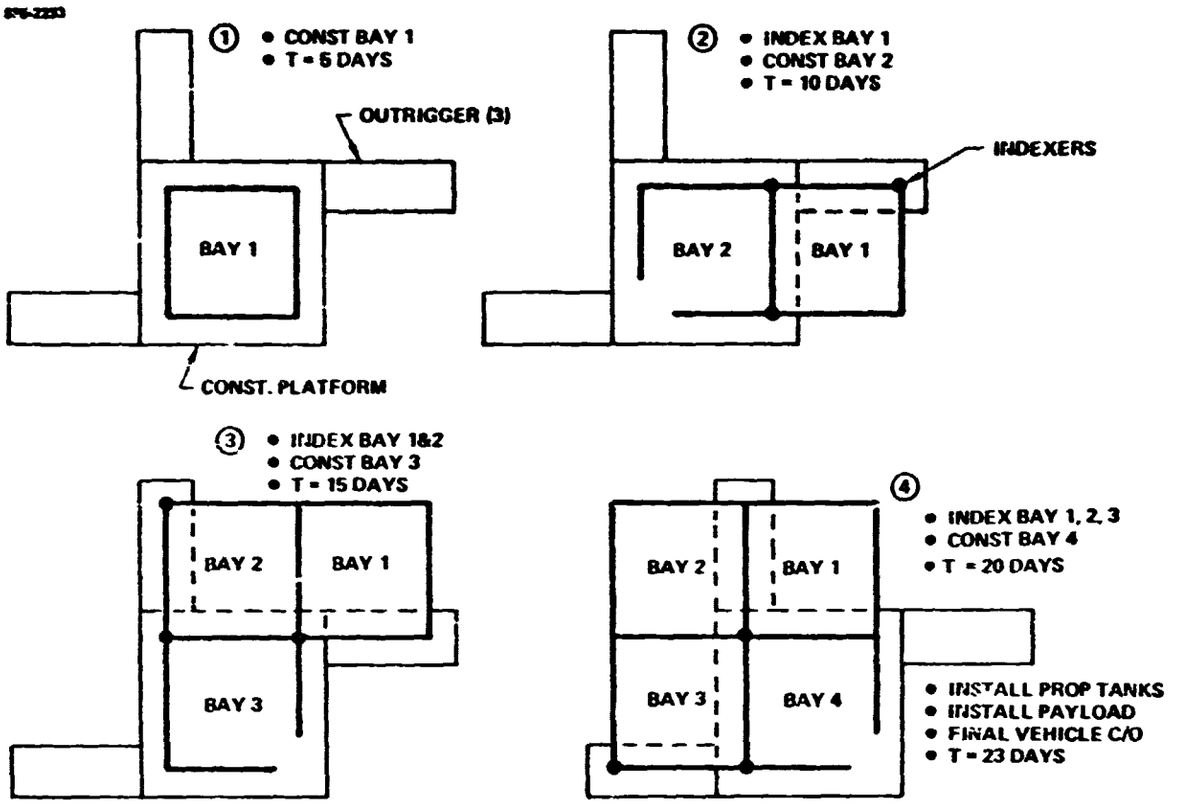

Figure 1.3.2-38 EOTV Construction Sequence

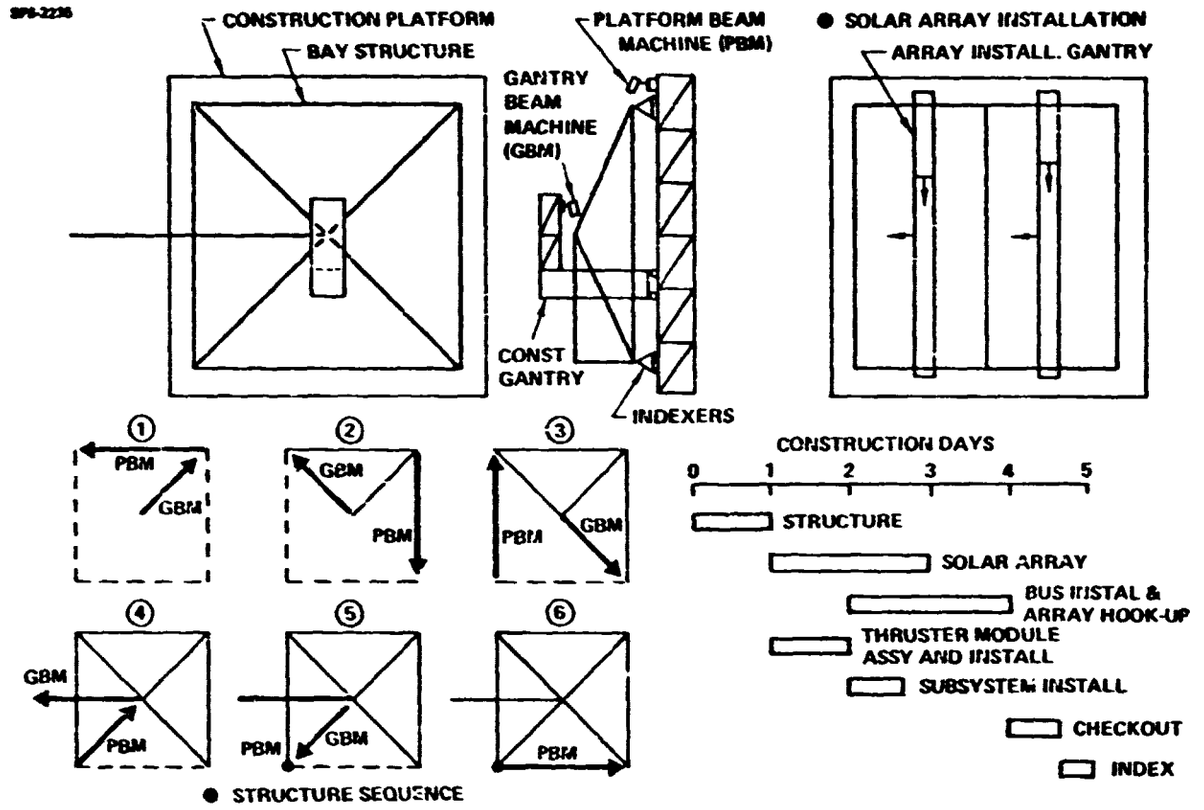

Figure 1.3 2-39 EOTV Bay Construction Operations

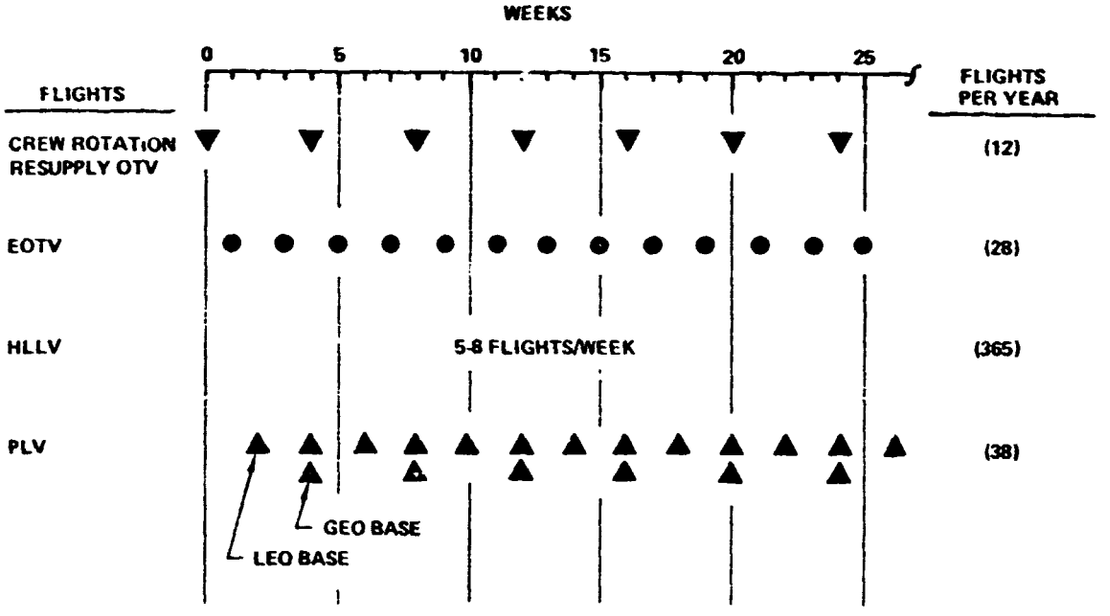

Figure 1.3.2-40 LEO Base Depot Operations

will deliver payloads to the LEO base on an average of 7 times per week. Personnel launch vehicles deliver new crewmen to orbit approximately every two weeks. Double flights are indicated for the GEO base PLV flights because each crew OTV transports 160 people while the PLV transports only 80 per flight.

1.3.2.2.8.4 LEO Base Crew Size

The crew size to maintain the base is presented in Table 1.3.2-11 for three different time periods. The EOTV construction period requires approximately 200 people, the on-going operation period when EOTV flights are delivering SPS components to GEO requires 134 people and the time period which has on-going operations as well as the construction of the second set of EOTV's requires a total of 220. To accommodate this crew size, a total of two large crew modules will be provided. The characteristics of these modules are the same as described for the crew modules used with the LEO base of the LEO construction concept described in Part III of Contract NAS9-15196,

1.3.2.2.8.5 LEO Base Mass and Cost

Mass and cost are presented in Table 1.3.2-12 and indicate that both characteristics are dominated by the crew/work modules. Again, there are two modules that serve as full time crew quarters, one module for transient crews (and as back-up primary module) and a fourth module which serves as a combination maintenance/operation center. Base subsystems include a solar array for primary power, nickel hydrogen battery for secondary power and a LO_2/LH_2 flight control subsystem. Vehicle and cargo handling elements include or-base transportation systems for moving cargo and personnel, as well as the docking ports required in support of the various transportation systems. Since the base will also be serving as an OTV support base, a propellant storage and distribution system is provided. The construction equipment includes the capability of building each EOTV in approximately 23 days and the total fleet of 23 vehicles in 1.5 years. This concludes the basic definition of the silicon EOTV, its operations and suppot systems for GEO construction concept.

1.3.2.2.9 GEO Construction Crew Rotation/Resupply

Prior Boeing SPS GEO construction analysis had been done using LO_2/LH_2 OTV's to deliver SPS cargo. This same vehicle was also used for LEO/GEO crew rotation and resupply. The concept employing electric OTV's for SPS cargo delivery to GEO therefore necessitated a review of the size of the two stage LO_2/LH_2 OTV that should be used for crew rotation/resupply. Several sizing options exist Basically these

Table 1.3.2-11 LEO Base Crew Size

SPS-2227

	EOTV CONSTRUCTION	ON-GOING OPERATIONS	EOTV CONST + OPERATIONS
BASE MGMT	(7)	(7)	(7)
CONSTRUCTION	(77)	(0)	(77)
MGMT	6		6
EOTV CONST	46		46
SUBASSY	10		10
TEST & QC	15		15
BASE OPS & SUPPORT	(93)	(34)	(93)
MGMT	6	6	6
MAINTENANCE	14	10	14
VEH/CARGO HANDLING	16	13	16
FLIGHT CONTROL	6	6	6
COMMUNICATION	8	8	8
DATA PROCESSING	6	6	6
UTILITIES	12	12	12
HOTEL OPS	16	16	16
MED/DENTAL	9	7	9
TRANSPORTATION OPS	(21)	(43)	(43)
MGMT	4	4	4
PROP HANDLING	8	8	8
FLIGHT READINESS	7	7	7
EOTV MAINT	0	22	22
VEHICLE COORD	2	2	2
TOTAL	198	134	220

Table 1.3.2-12 LEO Base Mass and Cost

SPS-2220

WBS	MASS (10^3 Kg)		COST ($10^6)	
STRUCTURE	200		20	
CREW/WORK MODULES	810		1150	
BASE SUBSYSTEMS	50		5	
VEHICLE/CARGO HANDLING	50		40	
PROP. STORAGE/DELIV.	35		15	
CONSTRUCTION EQUIP.	115		260	
	DRY	1260	BASIC	1490
	CONSUMABLES (90 DAY)	60	WRAPAROUND 47% BASIC	700
		1320		2190

options are 1) to combine the two functions in one flight and 2) have separate flights for each function. Transportation requirements for these two options along with the propellant requirements per flight and annual propellant requirements are shown in Figure 1.3.2-41. On a per flight basis, the option consisting of the combined crew rotation/resupply requires approximately 800,000 kilograms per flight, while the propellant loading for the option having separate crew and supply delivery has an average of approximately 500,000 kilograms which is approximately the OTV size for the LEO construction concept. On an annual basis, the combined crew rotation/ resupply flight reduces the total propellant requirement by 2 million kilograms resulting in approximately 100 million dollars savings per year. Consequently, the combined crew rotation/resupply option has been selected for the GEO construction/ EOTV option.

This concludes the basic definition of the GEO construction concept using EOTV's. The comparison of the concept with LEO construction is done in Section 1.3.2.4.

1.3.2.3 LEO CONSTRUCTION WITH SELF POWER TRANSFER

This concept has been discussed extensively in documentation associated with NASA JSC/Boeing contract NAS9-15196. Figure 1.3.2-42 illustrates the overall construction and operation scenario associated with the LEO construction concept. In terms of transporting the satellite, eight separate modules are constructed in low Earth orbit with portions of the solar array deployed to provide power necessary to drive the electric thrusters that propel the vehicle to GEO where the modules are joined together to form the total satellite.

Several improvements have been considered for this concept. The first deals with improving the overall module configuration for the transfer operation. The second considers the cost benefits that might occur through recovery of the electric propulsion components and their subsequent reuse. Both of these improvements will be discussed in subsequent paragraphs.

1.3.2.3.1 Configuration

The self power module orbit transfer configuration including key characteristics associated with transferring with and without an antenna are shown in Figure 1.3.2-43. The optimum trip time is 140 days and I_{SP} = 7000 sec although the time averaged I_{SP} including occultations and LO_2/LH_2 contribution for gravity gradient torque (GGT) is

- REQUIREMENTS
  - 480 PEOPLE
  - 3 MONTH STAYTIME
  - 230 Kg/MAN MONTH

• DELIVERY OPTIONS	(1) COMBINED CREW + SUPPLY	(2) SEPARATE CREW	SUPPLY
• FLT/MO	1	1	1
• CREW	160	160	–
• MAN MO. SUPPLIES	480	–	480
• P/L UP (10^3 Kg)	150	52	96
• P/L DN (10^3 Kg)	90	62	48

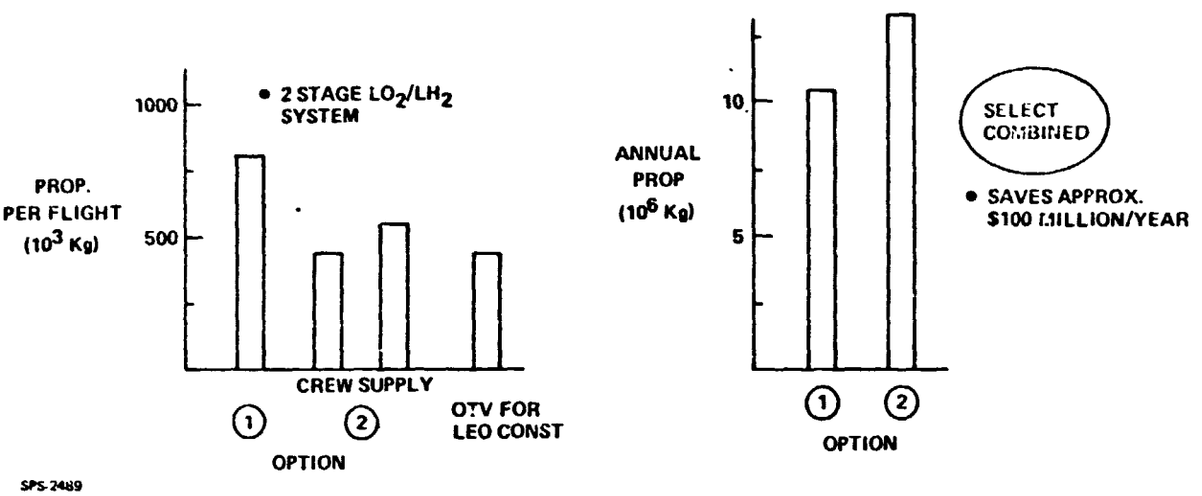

SPS-2489

Figure 1.3.2-41 GEO Construction Crew Rotation/Resupply

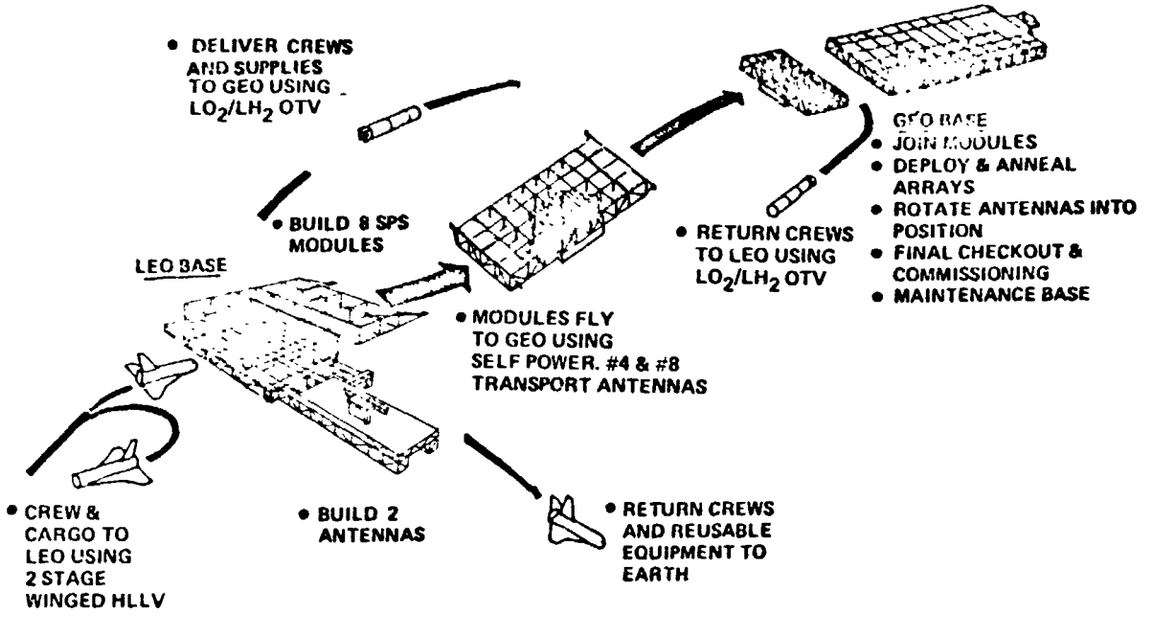

Figure 1.3.2-42 LEO Construction Concept Self Power Modules

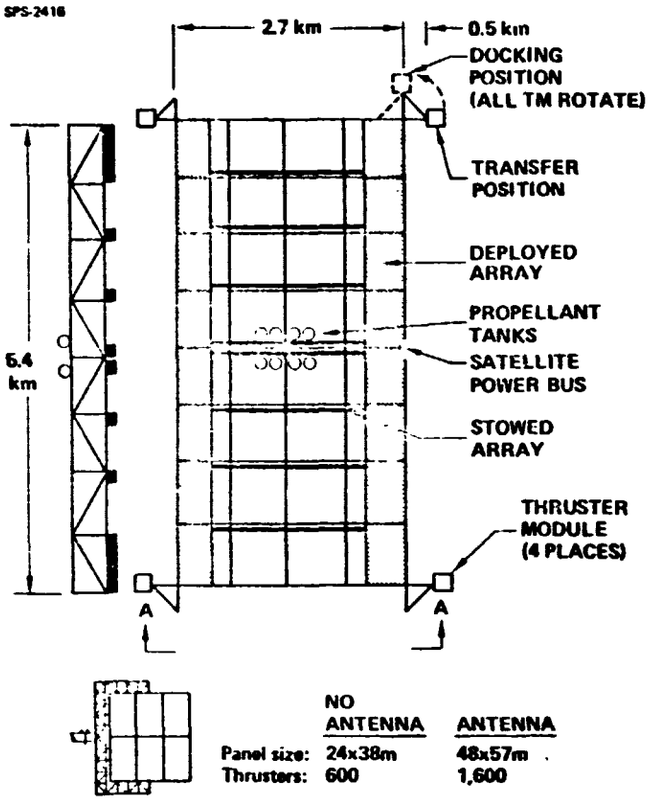

GENERAL CHARACTERISTICS

- 3% oversizing (radiation)
- Trip time = 140 days
- I_{SP} = 7,000 sec

MODULE CHARACTERISTICS	NO ANTENNA	WITH ANTENNA
• Number of modules	6	2
• Module mass (10^6 kg)	8.7	23.7
• Power required (10^6 kW)	0.3	0.81
• Array (%)	13	36
• OTS dry (10^6 kg)	1.1	2.9
• Argon (10^6 kg)	1.0	5.1
• LO_2/LH_2 (10^6 kg)	1.4	2.2
• Electrical thrust (10^3 N) [1]	4.5	12.2
• Chemical thrust (10^3 N)	12.0	8.0

[1] 20% additional thrust available for GGT and thrust vector control

- Moment of Inertia (10^{13} Kgm^2)

I_{xx}	2.4	3.6
I_{yy}	1.3	1.8
I_{zz}	2.75	5.2

MODULE WITH ANTENNA

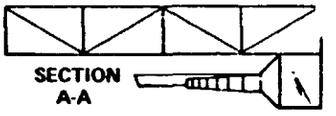

Figure 1.3.2-43 Self-Power Configuration Photovoltaic Satellite

only 2500 sec. In an attempt to reduce the gravity gradient torque requirements and thereby reduce the propellant requirements, several configuration changes have been incorporated. The first of these deals with the location of the deployed solar array. Prior self-power module configurations had the solar array deployed at both ends of the module and parallel with the X-axis. The new configuration however has the arrays deployed along the Y-axis of the configuration and along both sides. This not only improves the moment of inertia characteristics of the configuration, but also eliminates the mismatch between cells that occurred with the previous deployment since some cells in the string had been exposed to radiation and othes were not. The other change resulting in better moment of inertia characteristics and eventually lower gravity gradient torque penalty was that of positioning the thruster modules out along the X axis rather than the Y axis for the orbit transfer. Once GEO is reached, the thruster modules are rotated into a position where they are along the Y axis so no interference occurs during docking of one module to the other. The overall impact of the improved moment of inertia characteristics is that the propellant requirements decreased from about 34 million kilograms per satellite down to 29 kilograms per satellite.

1.3.2.3.2 Self Power Orbit Transfer System Reusability

The chief reason for considering recovery and subsequent reuse of the electric orbit transfer system (OTS) components is the fact that there are approximately 1.3 billion dollars of components for each 10 GWe satellite. Consequently, each component has been investigated for its cost in terms of dollar per kilogram of value and for the ease in which it could be removed. The results are presented in Table 1.3.2-13. Those components judged to be good candidates include the thrusters, processing units, gimbals, avionics and propellant tanks. Recovery of these components would result in 87% of the unit cost and 56% of the mass of the electric transfer system.

1.3.2.3.2.1 Recovery System Options and Sizing

The methods considered for the recovery of electric orbit transfer systems are shown in Figure 1.3.2-44. Use of LO_2/LH_2 orbit transfer vehicles for the return of the components includes the delivery of the OTV's piggyback on the self-power modules. Once GEO is reached, the electric propulsion elements would be attached to the chemical OTV's which would return the systems back to the LEO base where they would be refurbished and used on a subsequent self-power module. Chief disadvantage in this concept has been the long storage requirements for the LO_2/LH_2 and the large

SPS-2422

Table 1.3.2-13 OTS Recovery Motivation

OTS components	One satellite per year			
	Cost($M)	Mass (10^6 kg)	$/kg	Recovery
Thruster panel thrusters, PPU, switchgear, yoke, interrupters	815	6.14	132	Yes
Gimbal	133	0.09	1,477	Yes
Avionics	46	0.003	15,300	Yes
Tanks	149	0.4	370	Yes
Standoff structure	35	0.6	58	No, low value
Propellant feed system	16	0.58	28	No, integral
Thermal control	98	1.0	98	No, attach to standoff
Power distribution	22	3.0	7	No, integral
Total	1,314	11.8		
Recovery %	87	56		

SPS-2421

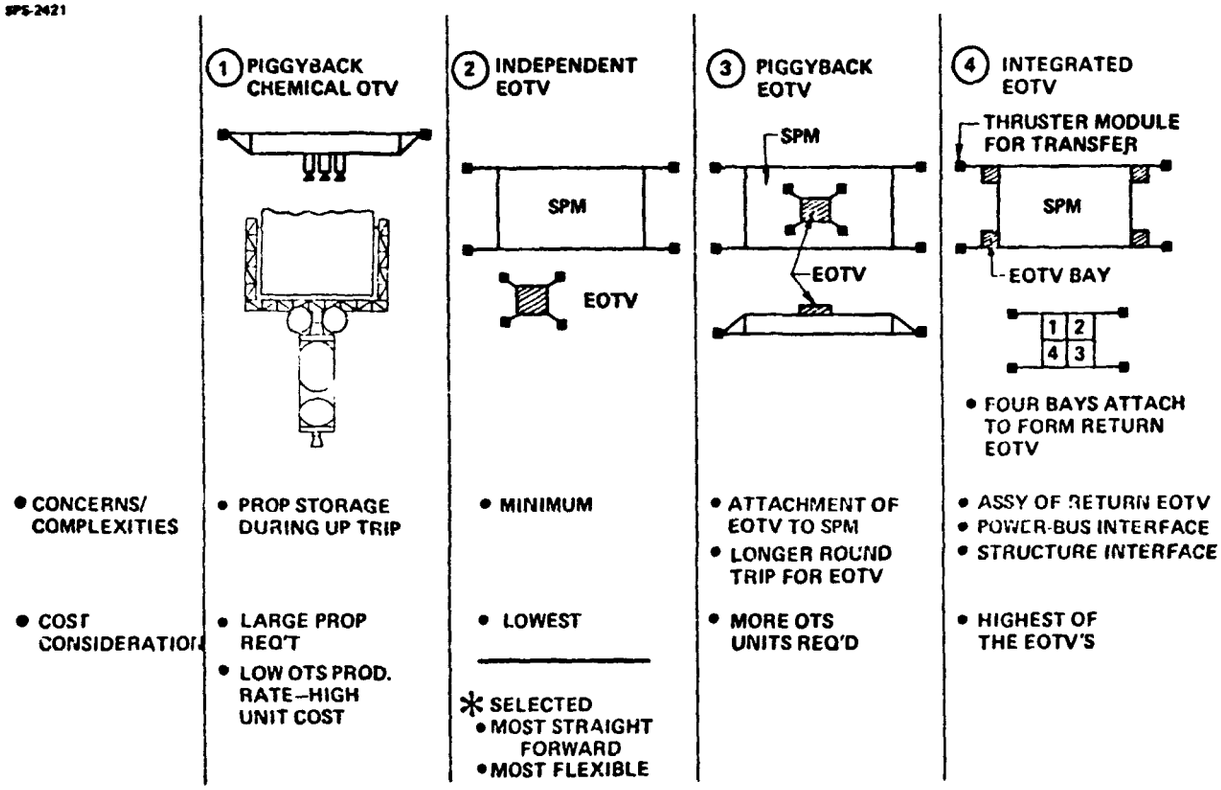

Figure 1.3.2-44 Recovery System Options

propellant requirements for this type of system resulting in excessive launch cost. Another method of recovery is the use of small electric orbit transfer vehicles. Three different methods employing this concept have been analyzed. The first of these is called the independent EOTV and consists simply of sending up a small EOTV independent of the self-power module. The second option has the EOTV sent up piggyback on the self-power module. Once GEO is reached, the components are placed on the EOTV and transferred back to LEO for refurb and reuse. The third method employs an EOTV concept that is more tightly integrated into the self-power module. In the case illustrated, the thruster modules of the EOTV would actually be used to propel the module to GEO. The thruster modules would be larger than that normally required for the EOTV operations by itself. The array of the EOTV would be used as well as a portion of the array of the self-power modules. Once GEO is reached, the four separate sectors of the EOTV must be reassembled to form an EOTV that can be transferred back down to LEO. The method selected for the recovery is that of the independent electric OTV, since it provides the most straightforward concept and the most flexibility at this point in time.

Several options exist in terms of the size of the EOTV. These options are brought about by several different payload requirements associated with the modules. As noted in Table 1.3.2-14, six of the eight modules have a recovery payload mass of approximately 550 metric tons, while two of the eight modules have OTS components that total 1650 metric tons. A detailed analysis has not been conducted on the three options indicated, but Option 2 which sizes the EOTV to return the largest payload appears to be a reasonable choice and was used in the remainder of the OTS recovery analysis.

1.3.2.3.2.2 Recovery EOTV Design and Operations

The configuration for the independent electric orbit transfer vehicles used to recover the self-power module OTS components is shown in Figure 1.3.2-45. This configuration is generally the same as that for the EOTV used in the GEO construction concept. The primary difference has been that the payload requirements are smaller resulting in about 1/3 the power requirements and about 1/2 the solar array requirements resulting in a dry mass of 760 metric tons.

The flight operations schedule associated with use of independent electric orbit transfer vehicles for recovery of OTS systems is illustrated in Figure 1.3.2-46. This

SPS-2420

Table 1.3.2-14 EOTV Sizing Options

• REQUIREMENTS

Module	OTS mass (10^6kg) to be recovered
1	0.55
2	0.55
3	0.55
4	1.65
5	0.55
6	0.55
7	0.55
8	1.65

• OPTIONS

1. Size for 0.55×10^6 kg
   - 1.65×10^6 kg payload required three EOTV's
   - Large number of EOTV's

√ 2. Size for 1.65×10^6 kg
   - Can bring down three 0.55×10^6 kg payloads

3. Have two sizes of EOTV:
   - One for 0.55×10^6 kg
   - One for 1.65×10^6 kg

√ SELECTED

SPS 2423

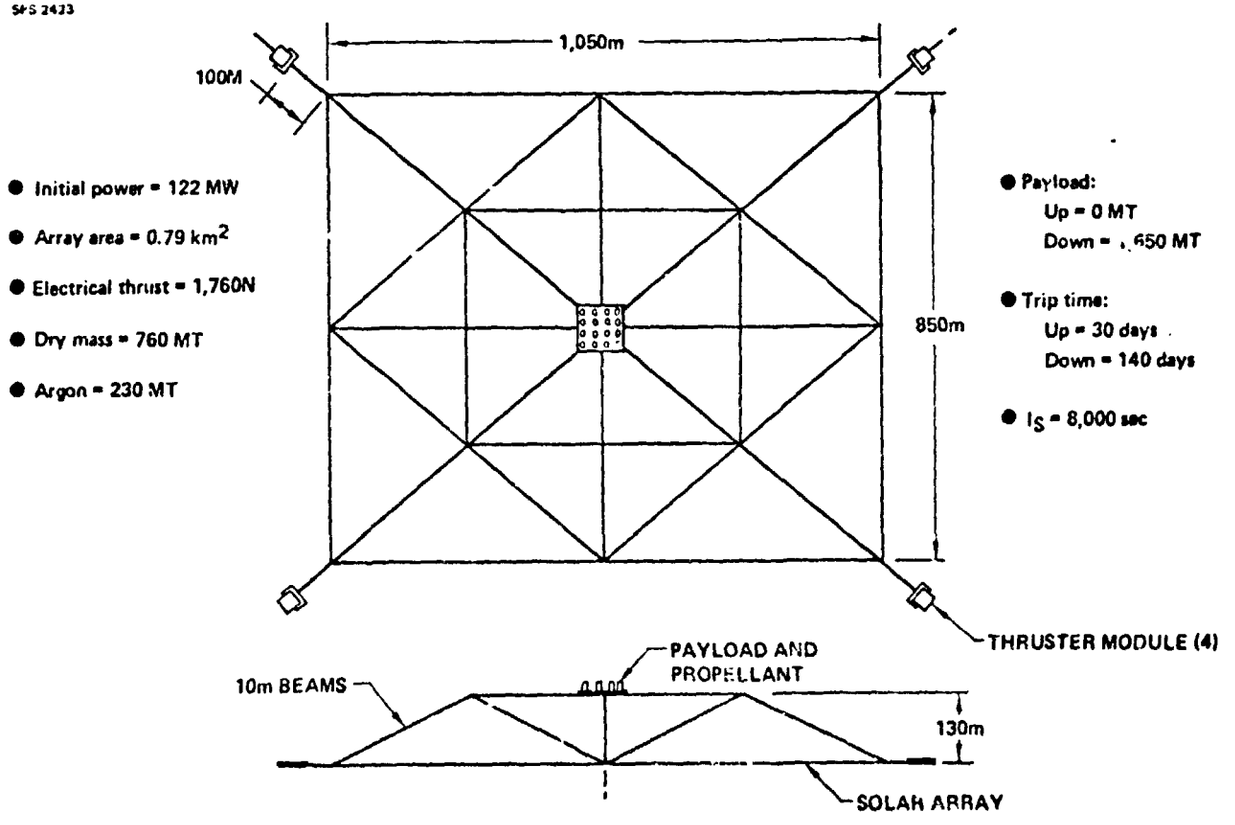

Figure 1.3.2-45 Independent EOTV for Self-Power OTS Recovery

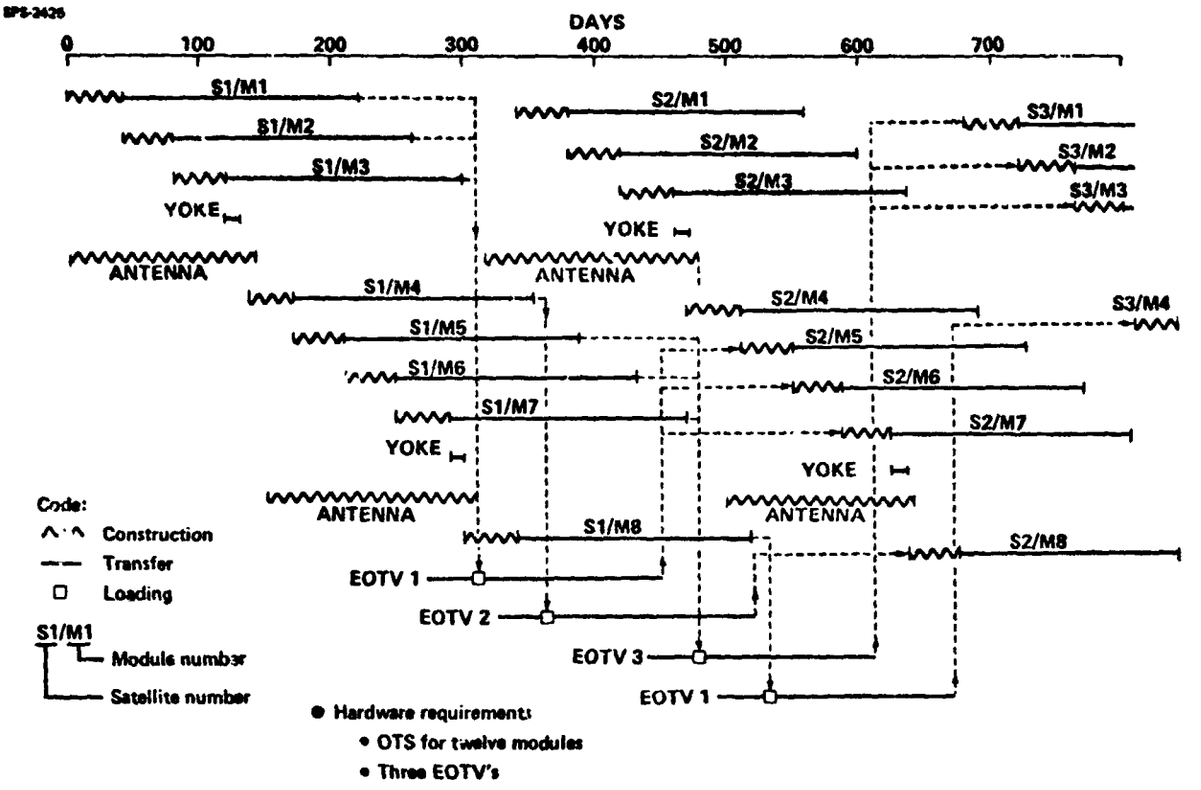

Figure 1.3.2-46 Flight Operations OTS Recovery

schedule includes that associated with the construction of the modules, the transfer of the modules and then at certain times the storage of the OTS requirements that are to be recovered. For example, components for the first three modules of the first satellite are removed from their modules and stored at the GEO base. Prior to the arrival of the third module at GEO, the first electric orbit transfer vehicle is sent to GEO. Once the EOTV reaches GEO, the components are loaded to form the full 1650 metric ton payload. That EOTV then returns the components back to LEO where they are removed and taken to the LEO base for refurbishment and subsequent reuse. The fourth module of each satellite also transfers an antenna and consequently the recovered electric propulsion components constitute a 1650 metric ton payload in itself. This requires a dedicated EOTV such as #2 to perform the recovery operations. The OTS units of satellite modules 5, 6, and 7 are also collected at GEO to form one payload package and are returned using the third electric orbit transfer vehicle. The OTS components of the eighth satellite module which also takes up an antenna is brought back through the use of the first EOTV. As can be seen from this schedule, module 1, 2, 3 and 4 of the second satellite cannot use any of the propulsion systems used on the first satellite modules. Consequently, they must also be provided with their own separate dedicated orbit transfer systems. As a result, the LEO construction concept using self power and recovery of the OTS components requires 12 modules of OTS equipment and three independent electric orbit transfer vehicles.

The primary operations associated with the recovery of the orbit transfer system elements at GEO are shown in Figure 1.3.2-47. Following the docking of the module with the already present modules, component recovery vehicles are flown out from the GEO base to the thruster module of the self-power module. The complete thruster modules including gimbals are removed and flown back to GEO final assembly base where an OTS pallet vehicle is stationed. Propellant tanks and avionics are also removed, loaded on the transfer orbit pallet vehicle and flown to the EOTV which has been stationkeeping at a location near the GEO base.

The recovery and refurb operations performed at LEO are shown in Figure 1.3.2-48. The EOTV returns to LEO at a location near the LEO construction base. The OTS pallet vehicle is then flown from EOTV over the LEO base where components are removed and taken to the refurbishment facility. The empty OTS pallet is flown back to the EOTV for a subsequent trip to GEO. Meanwhile, maintenance vehicles from the LEO base are flown to the EOTV to perform maintenance on the thruster modules of that vehicle.

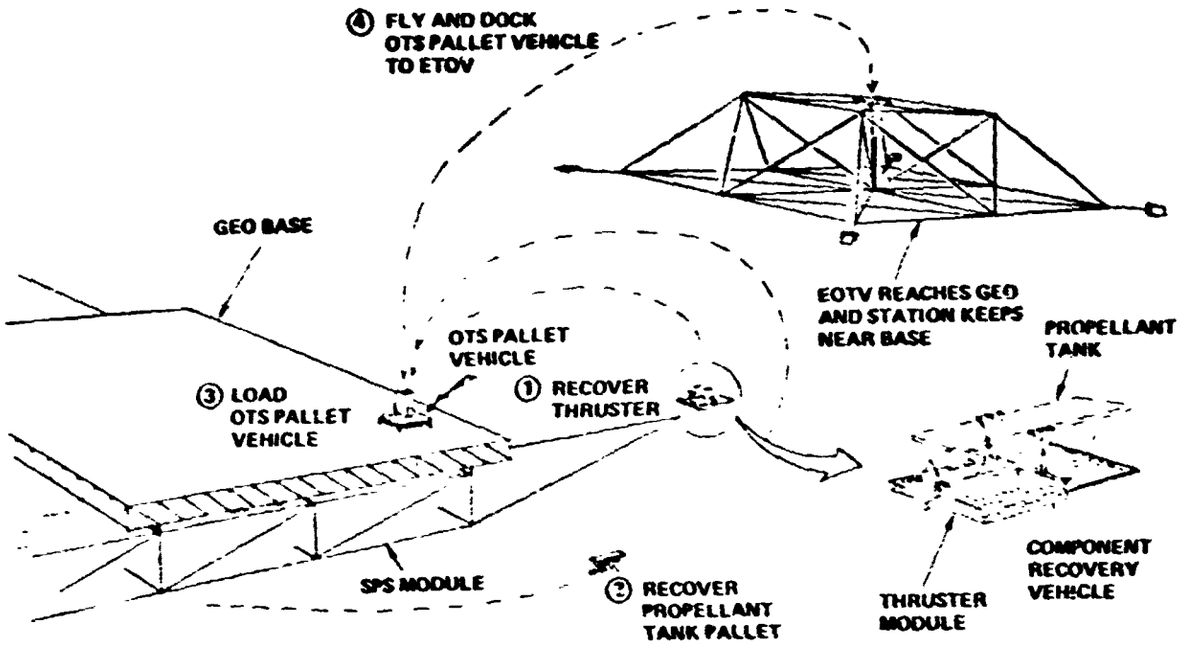

Figure 1.3.2-47 GEO OTS Recovery Operations

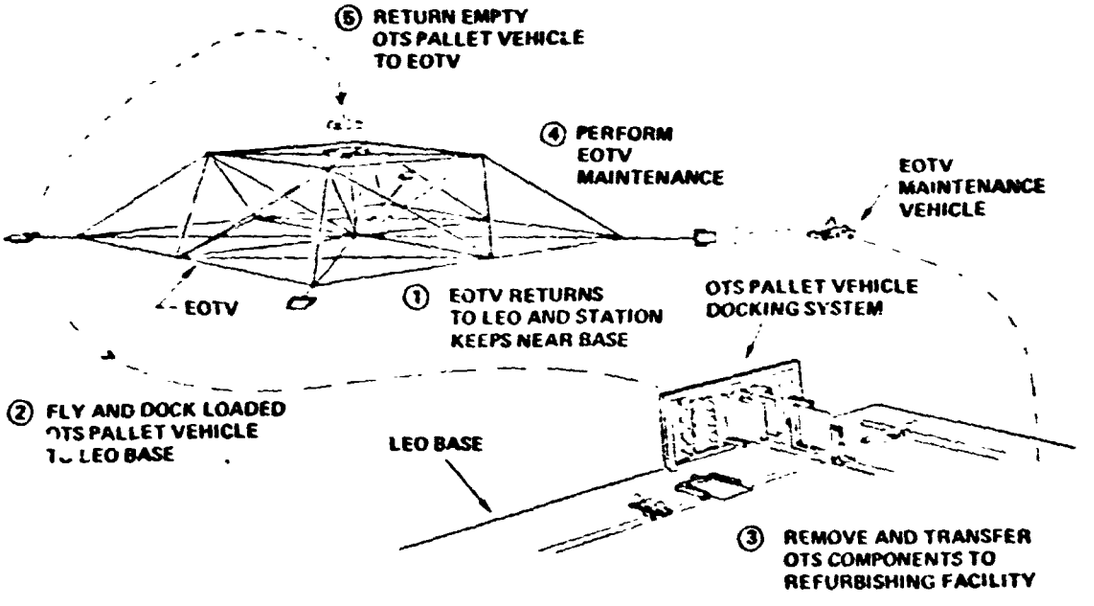

Figure 1.3.2-48 LEO OTS Recovery Operations

1.3.2.4 CONSTRUCTION LOCATION COMPARISON

The parameters to be used comparing GEO construction using electric orbit transfer vehicles for SPS cargo delivery with LEO construction that uses self-power transfer of satellite modules will use the parameters shown in Table 1.3.2-15.

1.3.2.4.1 Construction Preparation

Initially it was thought that GEO construction using EOTV's for cargo delivery would require a longer preparation time in terms of when the first SPS could be put on line. Data presented in Figure 1.3.2-49, however, indicates this method can have its system elements arranged in a manner that results in the first satellite coming on line at the same time as the LEO construction method. The only difference between these two options at this point in time appears to be the time when the chemical orbit transfer vehicle must be available. For the case of the LEO construction concept, the chem (LO_2/LH_2) OTV is not required until approximately 1½ years after the first system element payload is launched and is used to support the construction of the GEO final assembly base.

In the case of GEO construction, the chem OTV must be available at the end of the first half year in order to provide the capability to deliver components of the satellite construction base which will be assembled at GEO. In addition to the difference in the availability date for the chem OTV, the GEO construction chem OTV will also be about twice as large in terms of propellant capacity.

1.3.2.4.2 Satellite Design Impact Summary

The key differences between a satellite that would be constructed in LEO using a modular approach with one that would be constructed at GEO and be monolithic are indicated in Table 1.3.2-16. For the LEO construction case, an additional mass penalty will result in terms of the solar array due to the oversizing for the radiation degradation on that solar array which is deployed for the self-power transfer. The mass indicated reflects about a 3% oversizing penalty. The structural penalty reflects both the fact that the array will be oversized because the radiation degradation as well as the modularity which means redundant additional members in additional strength in the structure. Finally, because of the oversizing of the solar array there will be a small power distribution penalty for a total mass penalty of approximately 3 million kilograms for a 10 GWe satellite built at LEO versus GEO. This mass penalty has been included in all transportation cost analysis.

Table 1.3.2-15 Construction Location Comparison Parameters

SPS-2685

PARAMETER

- CONSTRUCTION PREPARATION TIME
- SATELLITE DESIGN IMPACT
- ORBITAL BASES/CONST EQUIP
- CONSTRUCTION OPERATIONS
- CREW REQUIREMENTS
- ENVIRONMENTAL FACTORS
- ORBIT TRANSFER OPERATIONS
- LAUNCH OPERATIONS
- RISK/UNCERTAINTY
- COST
  - CONST PREPARATION
  - FIRST SATELLITE TRANSP.
  - AVERAGE PER SATELLITE

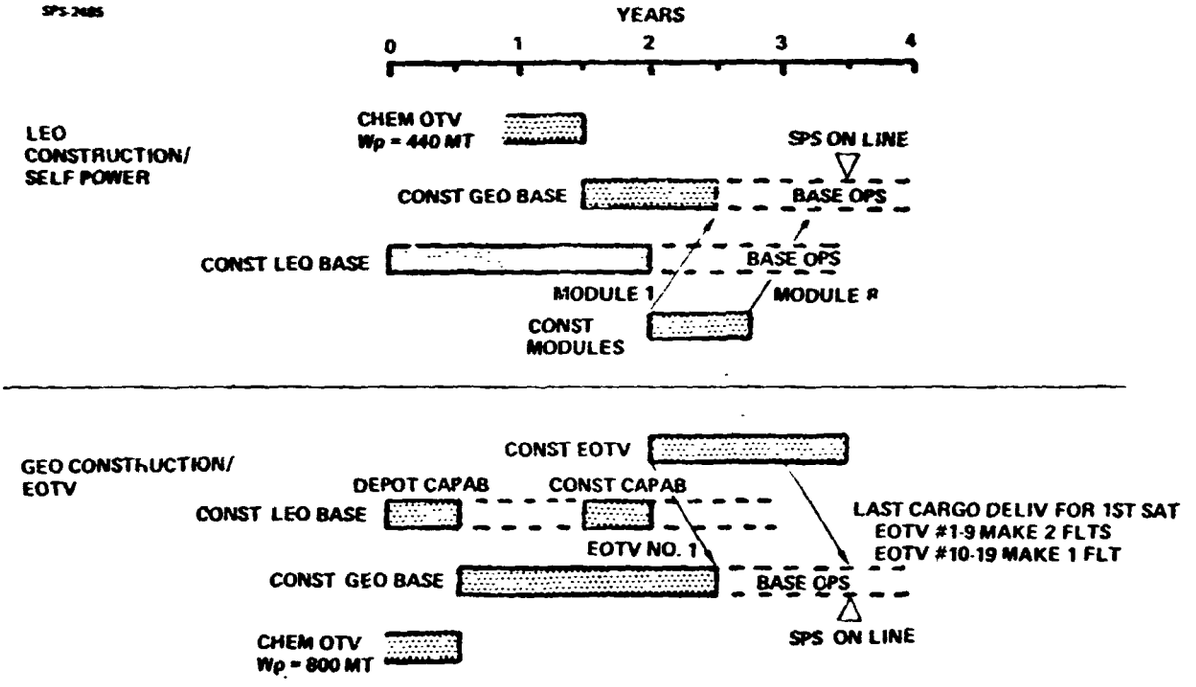

Figure 1.3.2-49 Construction Preparation

Table 1.3.2-16 Satellite Design Impact Summary LEO Construction

SFS-1620

SELF POWER TRANSFER

IMPACT	REASON	PENALTY
• SOLAR ARRAY	• OVERSIZING FOR RADIATION DEGRADATION	• 1.75M Kg (1)
• STRUCTURE	• MODULARITY	• 1.07M Kg
	• OVERSIZING	• 0.25M Kg (1)
• POWER DISTRIBUTION	• EXTRA LENGTH DUE TO OVERSIZING	• 0.07M Kg (1)

≈ 3M Kg PENALTY OVER GEO CONST

(1) FUNCTION OF SELF POWER PERFORMANCE CHARACTERISTICS

1.3.2.4.3 Orbital Bases

Primary characteristics of the orbital bases associated with LEO construction are indicated in Figure 1.3.2-50. The LEO base is used for the construction of the self-power module. It has a mass of approximately 5,550 metric tons and requires a construction crew of 407. The overall dimensions of the base are approximately 5.9 kilometers by 1.8 kilometers. A GEO final assembly base is also required and has a mass of approximately 850 metric tons and a crew size of 65.

The orbital bases for the GEO construction concept are shown in Figure 1.3.2-51. The LEO support base has a mass of approximately 1300 metric tons and requires a crew size of around 200 during the construction phase of the EOTV. Once the program is underway, the crew size can be reduced to 130 people since only depot type operations are performed. The GEO construction base has the task of constructing a monolithic 5 gigawatt or 10 gigawatt satellite. The mass at this base is 6,250 metric tons with the increase over the LEO satellite construction base being primarily that related to additional radiation shelters for the crew.

1.3.2.4.4 Construction Operations

As indicated earlier, the GEO construction concept has been associated with the construction of a monolithic satellite. LEO construction, however, uses a modular satellite design which means modules are constructed at LEO and use self-power electric propulsion transfer to GEO. Consequently, the LEO construction option has several additional construction requirements and are indicated in Figure 1.3.2-52. The first of these is the docking of the modules once GEO is reached. Another requirement is that on both the 4th and 8th modules the antenna is transferred in a position underneath the module in order to improve the moment of inertia characteristics and as a result, once the modules are docked the antenna must be rotated up into its operating position. The final difference in the LEO construction approach is that those solar arrays not deployed for the self-power transfer must be deployed through the use of deployment machines at the final assembly base.

1.3.2.4.5 Environmental Factors Summary

The environmental factors indicated in Table 1.3.2-17 are those that influence the construction of the satellite. In the case of radiation, all crew modules located at GEO will have a substantial mass penalty for protection against solar flares. A shielding density of 20 to 25 grams per square centimeter is required in the radiation

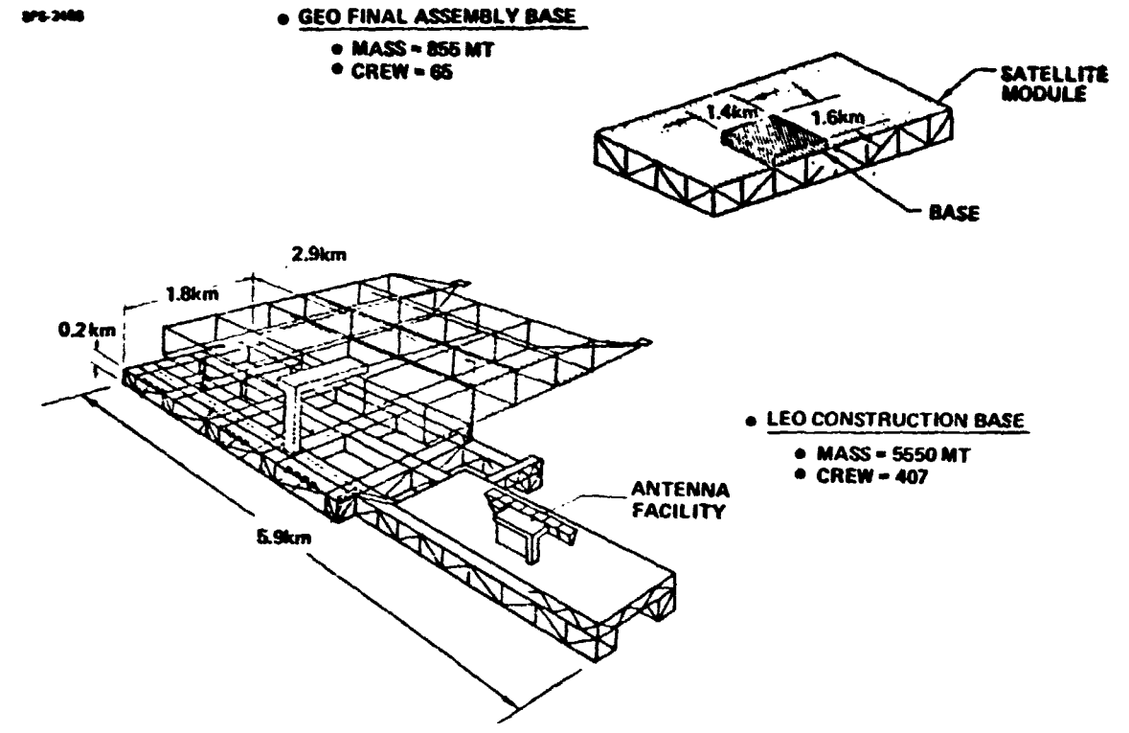

Figure 1.3.2-50 Orbital Bases LEO Construction Concept

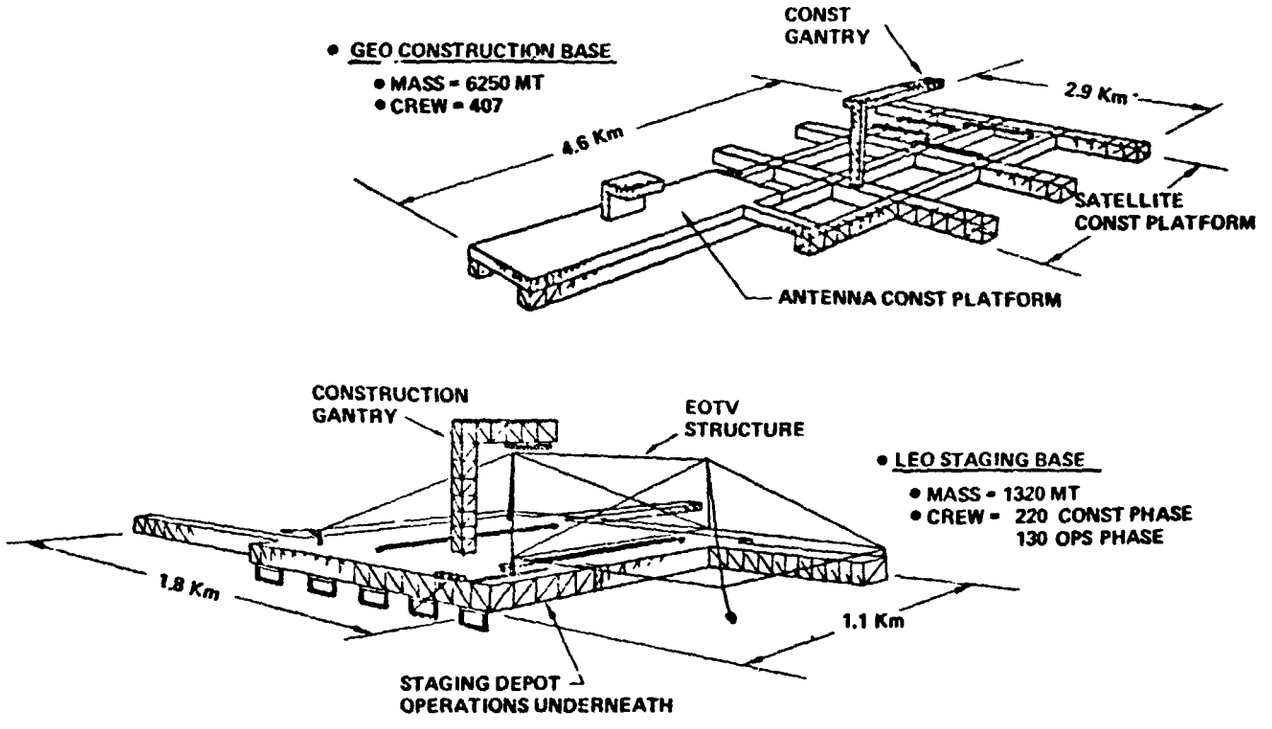

Figure 1.3.2-51 Orbital Bases GEO Construction

SPS-2816

- GEO CONSTRUCTION ALLOWS MONOLITHIC SATELLITE
- LEO CONSTRUCTION UTILIZES A MODULAR DESIGN AND REQUIRES THE FOLLOWING GEO OPERATIONS:

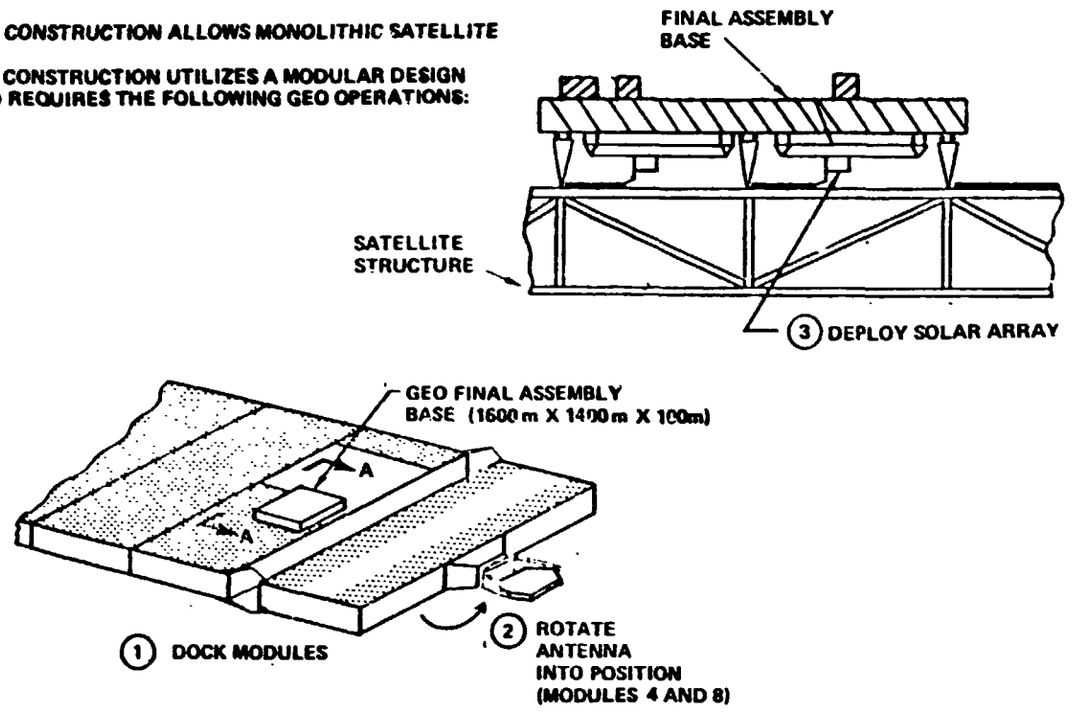

Figure 1.3.2-52 Construction Operations

Table 1.3.2-17 Environmental Factors Summary

SPS-1611

FACTOR	LEO BASE	GEO BASE
• RADIATION		
• SOLAR FLARE	2-3 GM/CM^2	20-25 GM/CM^2 (115 000 KG/100 PEOPLE)
• EVA	SO. ATLANTIC ANOMALY RESTRICTION	STEADY STATE IS WORSE
• OCCULTATION		
• BASE POWER REQ'TS:	3600 KW	2500 KW
• LIGHTING:	• REQ'D AT BOTH LOCATIONS (Δ OF 100-150 KW)	
• THERMAL EFFECTS:	• NO SIGNIFICANT DIFFERENCE IF GRAPHITE TYPE STRUCTURE IS USED	
• GRAVITY GRADIENT & DRAG:	• GRAVITY GRADIENT CONST MODE USED FOR BOTH LOCATIONS • LEO CONST PROPELLANT IS GREATER BY 600-700 KG/DAY	
• COLLISION WITH MAN-MADE OBJECTS	• POTENTIAL GREATER FOR LEO CONST (SEE ORBIT TRANSFER FLIGHT OPERATIONS) BUT AVOIDANCE MANEUVERS CAN REDUCE PROBABILITY TO NEAR ZERO	

shelters. EVA operations if required would be worse at GEO. EVA operations in LEO should be restricted to time periods when the construction base is not passing through the South Atlantic anomaly. Occultation of the construction bases has several impacts with one being in terms of the base power generation system. The GEO construction base requires the same amount of operational power but requires less total power because of nearly continuous sunlight on the solar array that is used to generate power for the base. Lighting will be required at both locations either due to the base being occulted by the earth or the construction base itself will cast shadows so that lighting will be required. Should graphite structure be used, the thermal effects on the structure should be minimum in both cases. Gravity gradient and drag penalties associated with LEO construction are larger although the difference of 600-700 kilograms a day is less than one HLLV flight per year. Collision with manmade objects is judged to be greater for the LEO construction concept during the satellite (module) construction phase. However, the total collision probability must also include collisions that may occur during the transfer between LEO and GEO; this comparison is presented as part of the orbit transfer operations discussion which follows.

1.3.2.4.6 Orbit Transfer Operations

Flight mechanics associated with the self-power module method and the electric orbit transfer vehicle are essentially the same. There are some factors, however, which will differ between the two approaches; one being the collision with manmade debris, another being the potential of interrupting the power beams coming down from operating satellites. The comparison of these factors is presented in Table 1.3.2-18. The key inputs into these two factors are the size of the modules being transferred and the amount of time that they are exposed to the environment. In the case of the potential collisions per year (with no avoidance maneuvers), the LEO construction concept is predicted to have 18 collisions while the GEO construction approach would have only one during satellite construction. However, in terms of the transfer of vehicles from low orbit to high orbit, the GEO construction approach with the large fleet of 23 vehicles has an (area) times (time) exposure value approximately 3 times that of the self-power module concept, resulting in approximately 3 times as many potential collisions. As a result, the GEO construction concept has approximately 50% more potential collisions if no avoidance is done. It should be emphasized, however, that prior study has indicated that practical avoidance maneuvers can prevent any collisions with manmade debris.

Table 1.3.2-18 Orbit Transfer Operations

SPS-2484

- FACTORS
  - COLLISION WITH MAN-MADE DEBRIS
  - SATELLITE POWER BEAM INTERRUPTIONS
- KEY DATA
  - SELF POWER MODULES ..... 8 FLIGHT PER YEAR
    2.75 KM^2 PER MODULE
    0.5 YR EXPOSURE PER MODULE
  - GEO EOTV'S ..... 22 VEHICLES
    1.5 KM^2 PER VEHICLE
    1.0 YR EXPOSURE PER VEH.
- POTENTIAL COLLISIONS PER YEAR (WITH NO AVOIDANCE MANEUVERS)

	LEO/SPM	GEO/ETOV
CONST	18	1
TRANSIT	22	66
TOTAL	40	67

- POTENTIAL POWER BEAM INTERRUPTIONS PER YEAR
  (QUANTITY NOT AVAILABLE BUT WILL BE PROPORTIONAL TO NO. OF REV'S)
  - LEO/SPM - - - 8 FLIGHTS @ 800 REV/FLT = 6400 REV
  - LEO/EOTV - EQUIV TO 21 FLTS UP @ 1200 REV
    16 FLTS DOWN @ 200 REV
    } = 28400 REV

The second item to be compared is that dealing with potential interruptions of power beams originating from operating power satellites. The problem occurs since the modules or vehicles transporting cargo depart from a 30 degree inclination orbit and have a destination of 0 degrees at GEO. These interruptions will be proportional to the number of revolutions that the vehicles make in the transfer from low orbit to high orbit (See Section 1.1.2.7). Again, the total number of flights plays a key part in this estimate. The LEO construction concept using self-power modules is estimated to require a total of 6,400 revolutions to get one 10 gigawatt satellite to GEO. In the case of GEO construction using 23 EOTV's flying 28 flights per year, a total of 28,000 revolutions is required or approximately 4 times revolutions per year, which should indicate approximately 4 times as many interruptions of the power beams coming down as for the LEO construction option.

1.3.2.4.7 Risk/Uncertainty

As stated previously, the LEO construction concept uses self-power and as such the orbit transfer system may be used only once although recovery and reuse is possible as discussed previously. The construction concept using EOTV's, however, requires multiple use for each EOTV. Concerns for the multiple use EOTV's are indicated in Figure 1.3.2-19. In the case of the solar arrays, the cost optimum transfer time for each flight will result in degradations as low as 40 to 45% as compared with 30 years of satellite operation which will degrade approximately 10%. The impact of this deep degradation is not known in terms of overall power generation capability nor in terms of the number of anneals which can be made nor the level of recovery. Cell to cell mismatch occurs even though annealing has been performed since each cell has its own unique characteristics. With excessive cell to cell mismatch there would be non-optimum power characteristics from the solar array. The impact on the solar array resulting from the large number of thermal cycles associated with occultations and annealing is unknown. Finally, as the power output degrades during the missions, so will the voltage degrade which will present some complication in terms of power conditioning equipment. The other components indicated also offer some concern, however they are judged to be less significant. In the case of avionics, one typical 180 day transfer presents a dose of approximately 10^4 rads. This radiation level will require use of radiation hardened electronics particularly when 10 flights (10^5 rads) are planned. The impact of radiation hardened electronics is twofold. One, the system will be slightly more expensive than standard avionics, and two, the number of design solutions will be restricted. The final item to be considered is that of the

SPS-2402

- LEO CONSTRUCTION
  - SELF POWER SYSTEM IS USED ONLY ONCE
- GEO CONSTRUCTION
  - SOTV IS A MULTI USE SYSTEM IN A HOSTILE LEO-GEO ENVIRONMENT
- KEY FACTORS OF ONE LEO-GEO-LEO TRIP
  - RADIATION IS MORE SEVERE
    - 10 TIMES THAT OF 30 YRS AT GEO FOR SOLAR ARRAY
  - NUMBER OF THERMAL CYCLES (OCCULTATIONS) IS THE SAME AS 18 YRS GEO OPS
- COMPONENT CONCERNS
  - SOLAR ARRAY
    - DEEP DEGRADATION
    - RECOVERY
    - CELL TO CELL MISMATCH
    - THERMAL/ANNEALING CYCLES
    - VOLTAGE FLUCTUATIONS
  - AVIONICS
  - STRUCTURE

Figure 1.3.2-19 Risk/Uncertainty Orbit Transfer System

structure. For a typical transfer of 180 days, approximately 5×10^9 rads will be experienced at the surface of the graphite type structure. Previous data has indicated that decomposition will occur beginning with about 10^9 rads. This decomposition results from the outgassing and constitutes a form of contamination which may have an impact on the solar cells performance. The extent of this impact is not known at this time.

1.3.2.4.8 Construction/Transportation Cost Comparison

The final parameter to be compared in the LEO vs GEO construction trade is that of cost associated will all elements of the construction and transportation systems. This comparison is presented in Figure 1.3.2-53. Several categories of cost are indicated with each category including cost for three construction options: 1) LEO construction with self-power modules and no recovery 2) LEO construction with self-power modules in conjunction with recovery of the electric transportation system elements and 3) the GEO construction concept using electric orbit transfer vehicles. All costs are plotted as a function of total transportation and construction cost. In summary, for the construction preparation portion of the program which includes placement of the construction bases and buying any necessary ground manufacturing facilities for the orbit to orbit transportation elements, the LEO construction concept using recovery of the electric components provides the least cost. The procurement of the first set of orbit transfer hardware, however, gives a considerable advantage to the LEO construction concept with self-power and no recovery. Flight operations associated with the first satellite, namely that of launching of the propellant to perform the delivery of the first satellite is approximately equal. When all three of these increments are added together, one gets the cumulative cost through the first satellite. At this point, the LEO construction concept with self-power transfer and no recovery provides approximately a $3 billion savings over the LEO concept with recovery of the electric system and approximately a $7 billion savings over that of the GEO construction concept. When the capital costs are amortized the total operating cost of all three concepts is quite comparable with the LEO construction using recovery of the electric propulsion systems providing a slight margin.

Costs presented in Figure 1.3.2-53 are shown in more detail in Table 1.3.2-20. During the construction preparation period, the chief difference between the options is that associated with the placement of the orbital bases including the unit cost of the bases. The second difference is that of the amount of ground production facilities for the

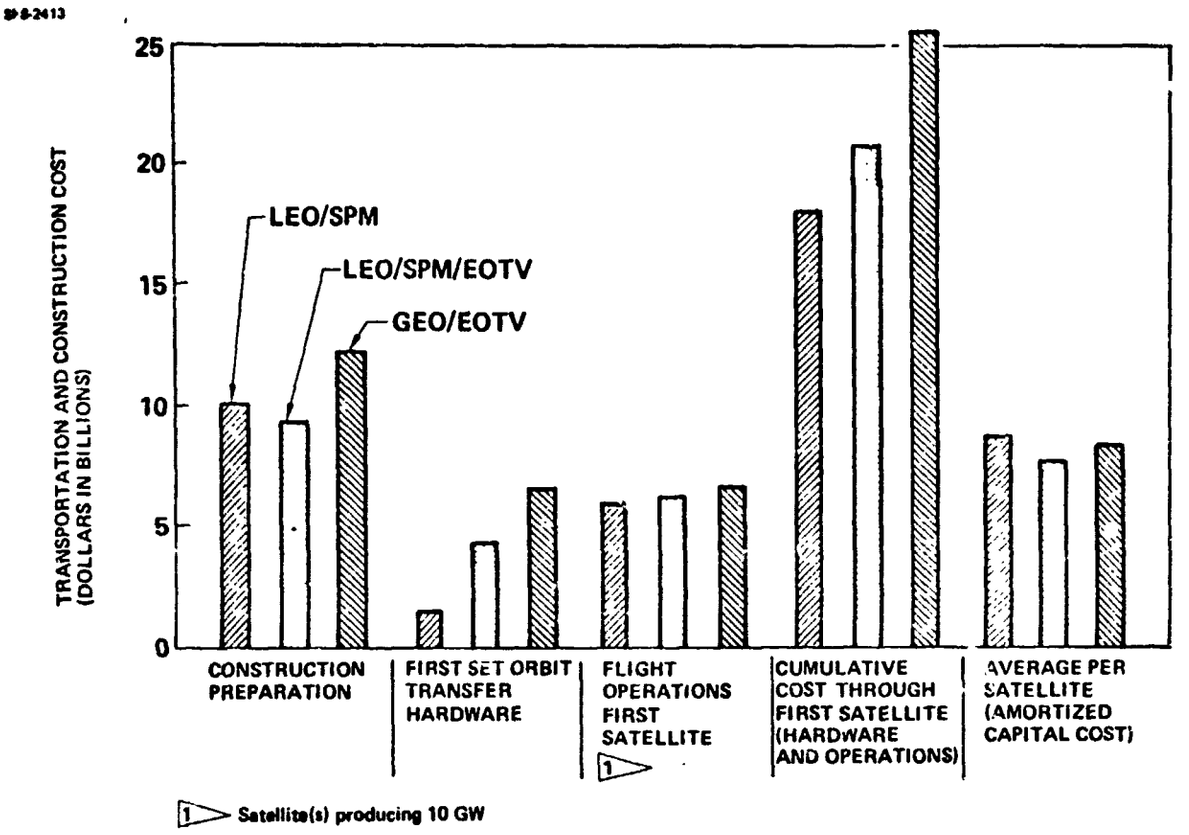

Figure 1.3.2-53 Construction/Transportation Cost Comparison

Table 1.3.2-20 Detail Cost Comparison Construction/Transportation

SPS-2480 NR = NO RECOVERY OF OTS R = RECOVERY OF OTS

ITEM	CONSTRUCTION PREPARATION			TRANSPORT THRU FIRST SATELLITE (HRDW + OPS)			AVG PER SATELLITE (AMORTIZED CAPITAL)		
	LEO/NR	LEO/R	GEO	LEO/NR	LEO/R	GEO	LEO/NR	LEO/R	GEO
CAPITAL COST	(9795)	(9015)	(11185)	(2010)	(5615)	(7830)	(2715)	(1565)	(2290)
SAT OTV LAUNCH	–	–	–	560	840	1310	560	120	1450
SAT OTV HRDW	–	–	–	1450	4350	6520	1450	830	
RECOV OTV LAUNCH	–	–	–	–	75	–	–	20	–
RECOV OTV HRDW	–	–	–	–	350	–	–	85	–
ORB BASE HRDW	7895	8035	9300	–	–	–	705	710	840
ORB BASE TRANS.	360	350	675	–	–	–			
OTV PROD. FACIL	1450	630	1210	–	–	–	–	–	–
DIRECT	(430)	(450)	(750)	(5515)	(5440)	(5315)	(5515)	(6020)	(5315)
SAT LAUNCH	–	–	–	3880	3765	3850	3880	3765	3850
SAT OTV PROPL.	–	–	–	1045	1015	535	1045	1015	535
SAT Δ HRDW	–	–	–	160	160	–	160	160	–
SAT OTV REFURB	–	–	–	–	–	180	–	570	180
RECOV OTV REFURB & PROP LAUNCH	–	–	–	–	50	–	–	50	–
CREW/SUPPLY	430	450	750	430	450	750	430	450	750
CONST TIME DELAY				(380)	(380)	(490)	(380)	(380)	(490)
TOTAL	10225	9465	11935	7905	11435	13635	8610	7965	8095
$/KG OF SATELLITE				79.8	115.5	137.7	86.9	80.4	81.8

orbit transfer hardware. The cost penalty reflects $1 for each $1 of recurring OTV hardware costs that show up under the average per satellite column. In terms of direct cost during the construction preparation period, the numbers reflect approximately half the crew size used in the normal construction operation but spread out over a two year time period. The GEO construction case has the majority of the orbital crew at GEO thus resulting in the highest cost. Total cost for the construction preparation period indicates that the LEO construction approach with recovery of the electric transportation system to be the lowest cost.

The second major cost comparison covers the transportation cost associated with placement of the first satellite. In terms of capital costs, the LEO construction approach with no recovery of the electric transportation system provides the least cost primarily because it has a very small OTV investment. A LEO construction case with recovery reflects a somewhat higher cost primarily as a result of low production rate on the electric propulsion components. The GEO construction case, with a fleet of 23 vehicles results in the highest capital cost. In terms of the direct cost for this period, the LEO construction case with no recovery has sightly higher costs although not significant. The propellant required for the transfer of each satellite in the LEO case is approximately twice that of the GEO construction concept, however, such factors as lower costs, associated crew rotation and resupply, and no refurbishment during the first year, offset this to some degree resulting in the small difference between the concept in terms of direct cost. Construction delay time primarily reflects the fact that for LEO construction, the trip is optimized at around 140 days of transfer while the GEO construction is more optimum at 180 days of transfer resulting in slightly larger interest payment. The total cost during this phase shows that LEO construction without recovery being nearly $3 billion cheaper than the LEO construction with recovery and approximately $5.5 billion cheaper than the GEO construction concept.

The final comparison of these concepts deals with the average per satellite cost which amortizes all capital costs. In the case of LEO construction with no recovery, the cost indicated is the same as that for the first satellite since a complete set of orbit transfer systems is needed for each satellite. The LEO construction with recovery concept and GEO construction using EOTV's both amortize the unit cost of the electric propulsion equipment and its placement. The total average per satellite cost shows that approximately $130 million savings per satellite for the LEO construction with

recovery of OTS over the GEO construction case and approximately $700 million over the construction with no recovery.

The total transportation and construction costs can be plotted as a function of the number of 10-gigawatt satellites placed online, as shown in Figure 1.3.2-54. In the case indicated, one 10-gigawatt satellite is added per year. The initial point on the cost curves reflect the procurement of the construction bases followed by the procurement of the first set of orbit transfer hardware to deliver the first 10 gigawatt SPS. Cost thereafter essentially reflects recurring cost per satellite for each of the construction options except in those cases where the orbit transfer fleet must be replenished. From this plot it can be seen that there is a relatively narrow band of cost for all three construction options and possibly it is not until approximately 150 gigawatts of capacity has been procured that the LEO construction concept using self-power transfer of the modules with recovery of the electric systems starts to provide an advantage.

Another cost comparison that can be shown deals with the uncertainty associated with the electric OTV concept and particularly to the cost sensitivity to the amount of radiation damage that can be removed with annealing. Previous analysis has assumed 95% of the damage is removed with each annealing. A limit case occurs if one assumes that no recovery is possible in terms of annealing. The results of this analysis are presented in Table 1.3.2-21. In the case of the LEO construction concept, this will result in a cost penalty of approximately $740 million per satellite which is a result of having to oversize by approximately 8%. For the GEO construction concept using EOTV's, there must be an assumption regarding the number of uses possible for each EOTV. In this analysis it is assumed that once the power output falls to 50% of initial power output, sufficient damage has been done to the array and probably to supplemental systems that further use is not possible. The 50% level is reached after 4 EOTV trips if no annealing recovery is possible. The average trip time during these four trips will be 280 days resulting in an amortization period of 3.5 years rather than 7.1 years in the baseline EOTV case that uses radiation damage removal. As a result, the cost penalty per satellite will be 1230 million which is approximately 70% greater than the LEO construction concept using self-power. Consequently, it is judged that the GEO construction EOTV concept is much more sensitive to the understanding of radiation and its damage removal through the use of annealing.

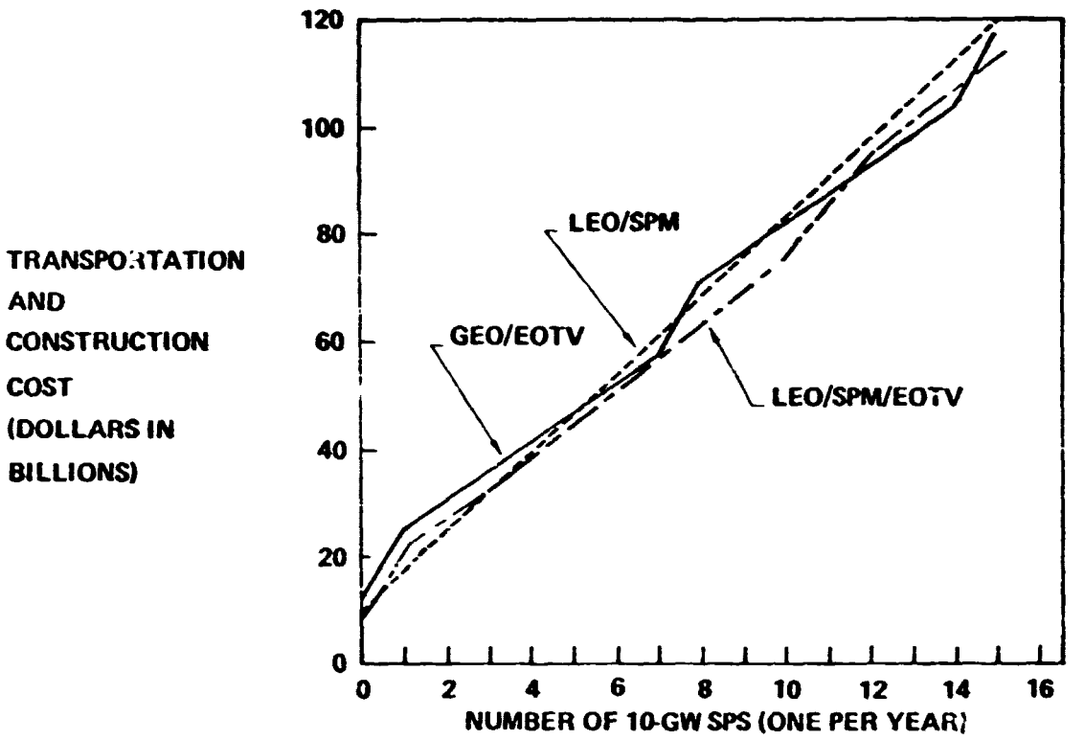

Figure 1.3.2-54 Cumulative Cost Comparison

Table 1.3.2-21 Cost Sensitivity No Recovery from Radiation Damage

- LEO CONSTRUCTION/SELF POWER (NO RECOVERY)
  - 22% OF SATELLITE SOLAR ARRAY DEPLOYED FOR TRANSFER
  - RADIATION LOSS IS 40%
  - RESULTS IN 8.8% OVERSIZING
  - Δ COST/SATELLITE (AVG) = $740 MILLION

- GEO CONSTRUCTION/EOTV
  - ASSUME EOTV DISGARDED WHEN $P/P_O < 50\%$
  - NUMBER OF EOTV TRIPS = 4
  - AVERAGE TRIP TIME = 280 DAYS
  - AMORTIZATION PERIOD = 3.5 YRS
  - PRINCIPAL IS $7,800 MILLION PER FLEET
  - Δ COST/SATELLITE (AVG) = $1,230 MILLION

1.3.2.4.9 Construction Location Summary

A summary of all the comparison parameters used in the construction location comparison is presented in Table 1.3.2-22. Some of these parameters have indicated little or no difference between the construction option. The GEO construction option using EOTV's has an advantage in terms of impact on the satellite design and also in terms of the construction operation. LEO construction with no recovery of the electric transportation system is judged to be better in terms of orbit transfer operations and uncertainties associated with orbit transfer hardware design. In terms of construction cost, the LEO construction approach has an advantage while the LEO construction concept with no recovery has a cost advantage through placement of the first satellite. On a recurring cost basis, LEO construction with recovery of the orbit transportation system and the GEO construction concepts are approximately equal in cost.

1.3.2.5 CONCLUSIONS AND RECOMMENDATIONS

The LEO construction concept using self-power transfer of the modules and no recovery is recommended for the initial stages of the operational program for the reasons tabulated in Table 1.3.2-23. The dominating reason for this recommendation is that it has significantly lower front end cost with recurring cost being competitive out to at least 150 gigawatts of installed power. In addition, this concept does not require repeated exposure of the power generation system to the environment between LEO and GEO. Finally, this concept allows natural evolution to the recovery of the electric propulsion system, which would result in the lowest recurring costs of any of the concepts evaluated.

1.3.2.6 EFFECTS OF ION JETS ON THE MAGNETSPHERE.

This task was originally directed to investigate effects on the ionosphere. The investigator quickly concluded, however, that these effects would be minimal and that effects on the magnetosphere were of more substantive concern. The effort was redirected accordingly.

Electric orbit transfer operations will consume roughly 10,000 tons of argon per 10,000 megawatts of SPS's emplaced. Although this consumption rate is entirely negligible in terms of resource availability, 10,000 tons of argon represents more than 10^{32} ions and neutrals injected into the Earth's magnetosphere during orbit transfer operations.

Table 1.3.2-22 Construction Location Summary

SPS-2406

COMPARISON PARAMETER	① LEO/SPM	② LEO/SPM/EOTV	③ GEO/EOTV	RATIONALE
• CONST PREPARATION	• NO SIGNIF DIFF			• SAME TIME FOR FIRST SATELLITE
• SATELLITE DESIGN IMPACT			✓	• NO MODULARITY • SMALLER LOADS
• ORBITAL BASES/CONST EQUIP	• NO SIGNIF DIFF			• SAME CONST BASE • STAGING DEPOT VS FINAL ASSY BASE
• CONSTRUCTION OPS			✓	• NO MODULE BERTHING OR ANTENNA HINGING
• CREW REQ'TS	✓			• SAME SIZE BUT MAJORITY AT LEO
• ENVIRONMENTAL FACTORS	• NO SIGNIF DIFF			• ALL CAN BE HANDLED WITH ACCEPTABLE SOLUTIONS
• ORBIT TRANSFER OPS	✓			• FEWER POTENTIAL COLLISIONS AND BEAM PENETRATIONS
• LAUNCH OPS	• NO SIGNIF DIFF			• APPROX SAME NO. LAUNCHES
• RISK/UNCERTAINTY	✓			• MULTI USE IN HOSTILE ENVIRONMENT NOT REQ'D
• CONST COST	✓	✓		• CHEAPER ≈ $2B
• FIRST SAT. TRANS COST	✓			• CHEAPER $3B OVER ② $7B OVER ③
• AVG. COST PER SAT		✓	✓	• CHEAPER ($0.6B)

✓ INDICATES MOST PROMISING

Table 1.3.2-23 Construction Location Conclusions to Date

SPS-2406

- LEO CONSTRUCTION WITH SELF POWER TRANSFER IS RECOMMENDED.
  - FRONT-END COSTS ARE $2 AND $7 BILLION (13% & 29%) CHEAPER
  - CUMULATIVE COST REMAINS COMPETITIVE OUT TO 150 GW_E OF INSTALLED SATELLITE POWER
  - OPERATIONS NOT DEPENDENT ON MULTIPLE REUSE OF HARDWARE EXPOSED TO SEVERE LEO-GEO ENVIRONMENT
  - ALLOWS EVOLUTION TO THE LOWEST RECURRING COST CONCEPT WHICH IS LEO CONSTRUCTION WITH SELF POWER AND RECOVERY OF THE PROPULSION SYSTEMS THROUGH USE OF EOTV'S

A brief investigation of possible effects on the magnetosphere indicated that this is problably not an environmental risk. Significant questions remain, and an analytical investigation adequate to give high assurance of no risk will require roughly two years.

The motion of a charged particle trapped in the Earth's magnetic field follows a reflected helical path within a curved flux tube as illustrated in Figure 1.3.2-54. The Earth's field is a magnetic mirror configuration that will cause the particles to be trapped with long lifetimes provided certain conditions are met. The particle trajectories migrate around the Earth in longitude also, as illustrated in Figure 1.3.2-55.

The argon ions produced by the electric propulsion system will be singly positively ionized and most will have energies of about 1.5 kev. corresponding to the acceleration voltage of 1,500 volts. Some thermal ions will be produced as a result of charge exchange between accelerated ions and the thermal neutrals that escape from the ion thruster without being ionized. These low energy ions will have energies less than 1 ev. Key characteristics of the 1.5 kev argon ion trap orbits as a function of altitude are given in Table 1.3.2-24 and plotted in Figure 1.3.2-56

The trapped ions will interact with the ambient magnetosphere constituents, primarily neutral hydrogen above about 1,500 kev altitude, as shown in Figure 1.3.2-57. The principal interaction will be charge-exchange in which the argon ion will be neutralized (and hence released from magnetic confinement). The estimated charge-exchange lifetimes for argon ions are shown in Figure 1.3.2-58. Note that the lifetimes range from a few seconds at LEO to about a year at GEO. It should be recognized that an argon ion released from magnetic confinement by charge exchange can be re-trapped if another charge exchange reaction re-ionizes it.

This analysis was highly exploratory and not at all complete, but reached certain preliminary conclusions.

1. Argon beam from thrusters travel intact for long distances tangential to orbit (at injection angle).

2. Transition from beam to single ion injection into geomagnetic field is a major unsolved problem in plasma physics.

3. Below 2.5 earth radii geocentric, all of the beam argon is temporarily captured by the geomagnetic field.

4. Above 2.5 earth radii (10,000 km altitude) most of beam argon escapes in a jet of plasma (86.6 km/sec); a small fraction is peeled off into trapped orbits.

5. A small fraction of the thruster beam charge exchanges at the thruster exit plane and escapes as neutral gas.

6. Inefficiencies in the present thruster systems allow 10-20% of the fuel to escape from the exit plan as thermal (0.1-1.0 eV) argon ions and neutrals.

7. At low altiudes (below 1000 km) this thermal argon diffuses back into the upper atmosphere.

8. At higher altitudes this thermal argon populates the magnetosphere.

9. The primary interaction between resident plasma and argon from the thruster is charge exchange between ions and neutrals.

Below 1000 km	$A^+ + 0$ and $A + 0^+$
Above 1000 km	$A^+ + H$ and $A + P^+$

10. The random walk diffusion of neutral and charges species is a second major unsolved problem, complicated by the infulence of geomagnetic field orbit effects on ions.

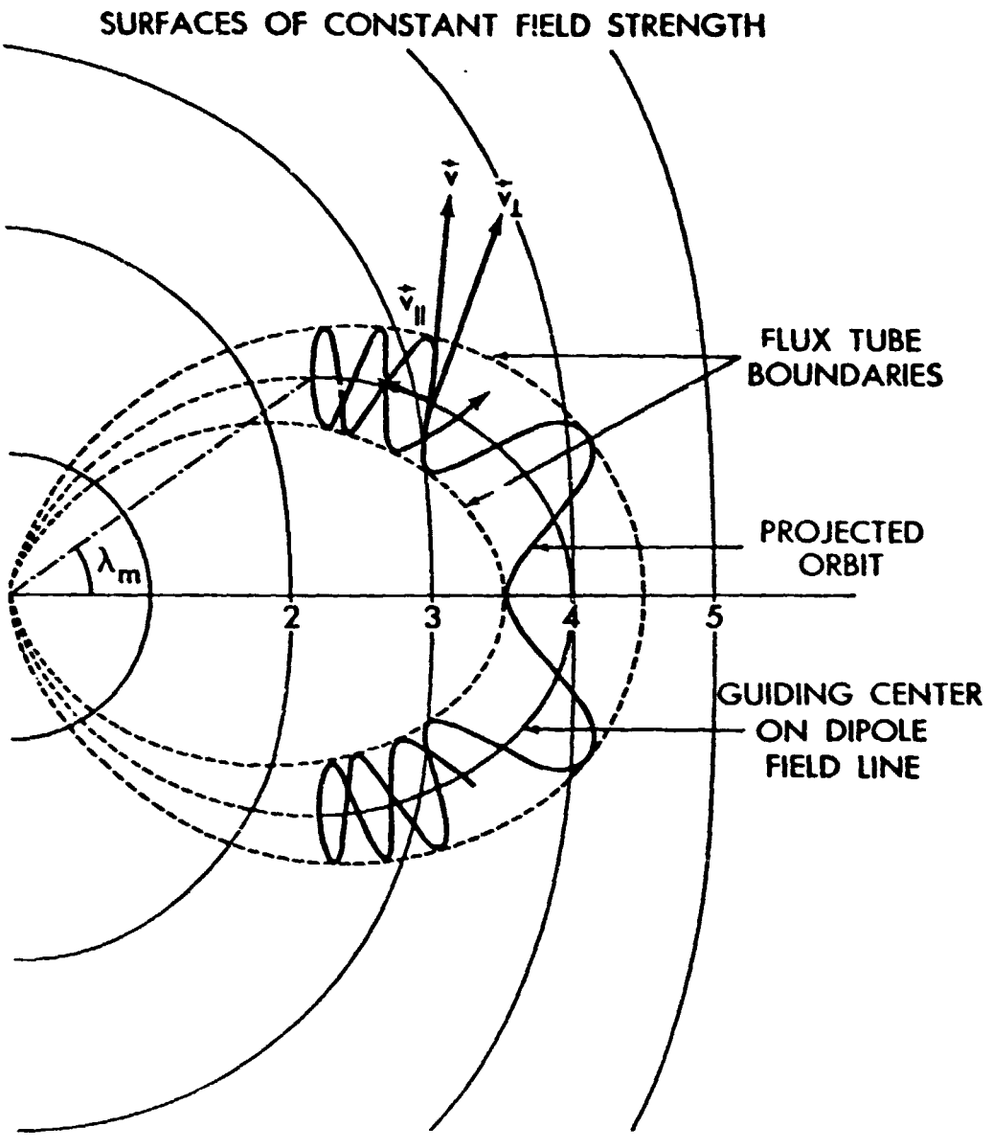

Figure 1.3.2-54 Meridian Plane Projection of a Particle Orbit

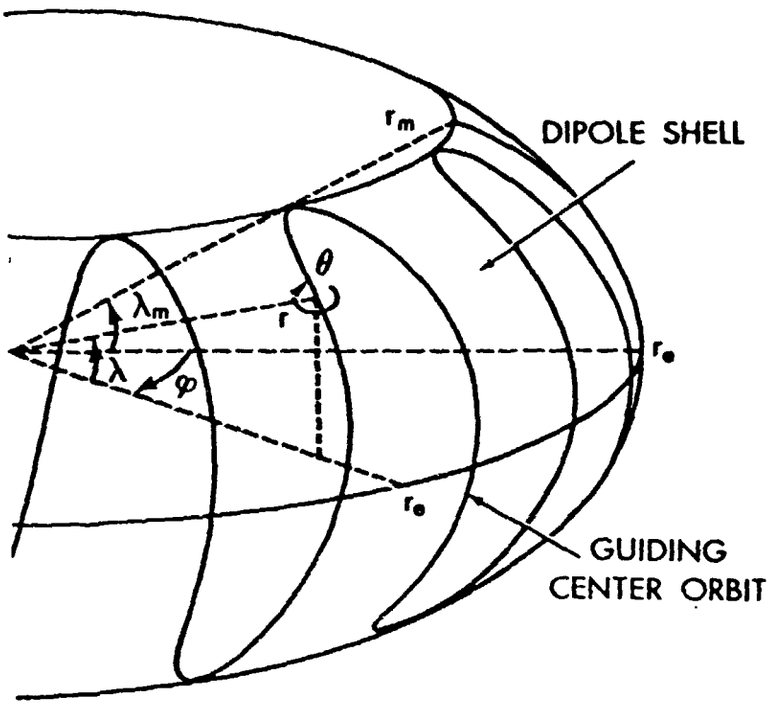

Figure 1.3.2-55 The Guiding Center Orbit

SPS-2632

Table 1.3.2-24 Argon Ion Orbit Characteristics

R/R_0 EARTH RADII	1.5	2	3	4	5	6
B (EQTR) GAUSS	0.927	0.0392	0.0116	0.0049	0.0025	0.00145
λ MAX MICRON DEGREES	35.4	45.0	54.5	60.0	63.5	66.9
α MIN EQTR DEGREES	27.1	16.3	8.4	5.3	3.8	2.4
$T_\perp$ (EQTR) SECONDS	0.28	0.67	2.3	5.3	11	18
1.5 KE V ARGON						
ρ (GYRO) KM	3.6	8.4	28.4	67.4	132	228
T_{11} (BOUNCE) MINUTES	2.95	4.0	5.9	8.0	9.9	12.0
T_D DRIFT) DAYS)	15.7	11.8	7.9	5.9	4.7	3.9

SPS-2636

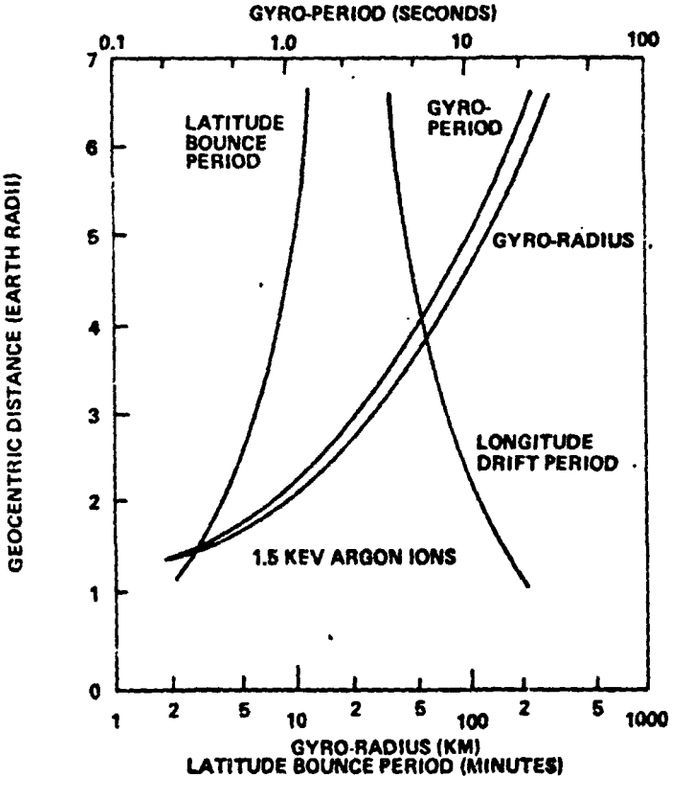

Figure 1.3.2-56 Argon Ion Orbit Characteristics

SPS-2634

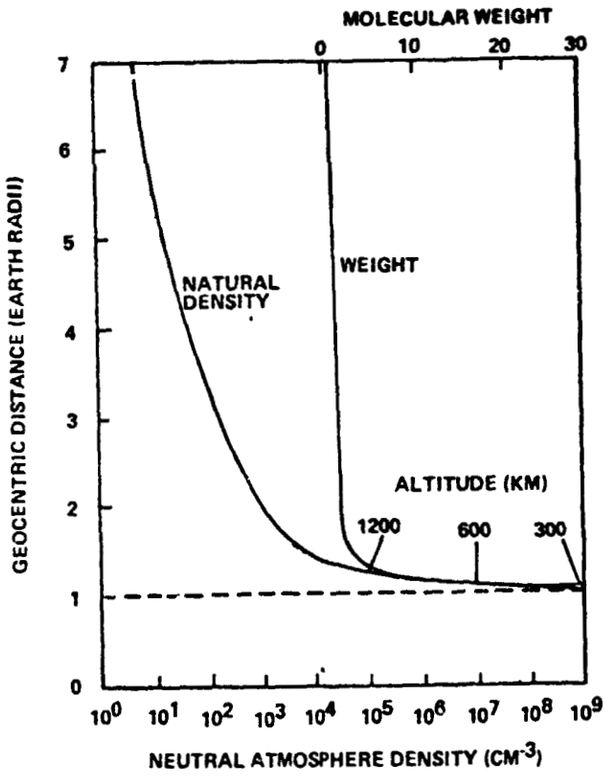

Figure 1.3.2-57 Mass and Density of Neutral Geomagnetosphere Constituents

SPS-2637

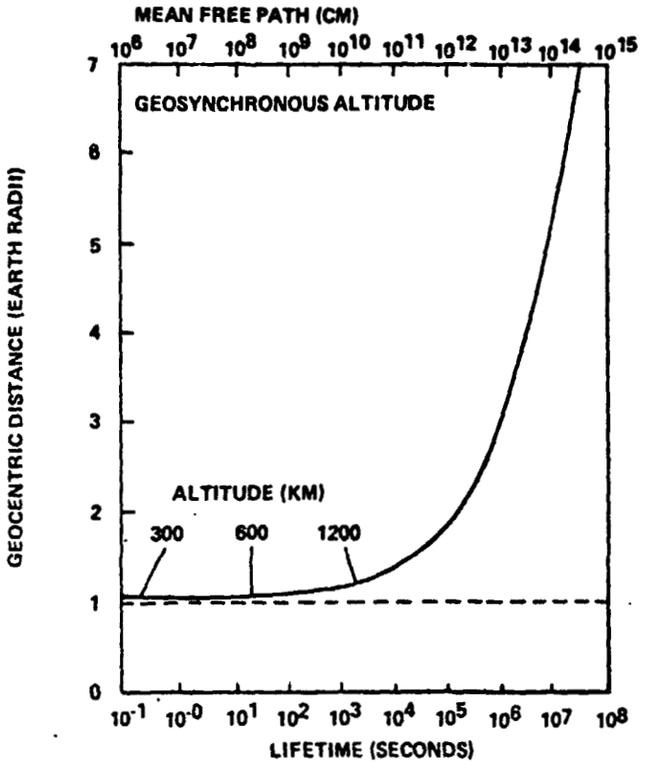

Figure 1.3.2-58 Charge Exchange Lifetime for 1.5 kev Argon Ions

WBS 1.3.7 Ground Support Facilities: Launch Site Analyses

Problem Statement

The construction and emplacement of SPS's in geosynchronous orbit at a nominal rate of 10,000 megawatts per year will require launches of a large heavy lift launch vehicle (HLLV) at rates approaching once per day.

The number of launch pads that can be provided at KSC, observing noise and pad separation constraints, will be limitd to 2 or 3. Figure 1.3.7-1 illustrates a concept for placement of pads offshore on causeways. The design of the causeways and breakwaters would have to reflect environmental considerations. As an example, it would probably be necessary to employ piling instead of riprap so that drift currents parallel to the shoreline would not be interrupted.

One way to relieve these concerns would be to employ remote launch sites fo operations. Several approaches have been discussed.

A. An inland site, such as in the desert southwest of the U.S. This would allow downrange landings of boosters, improving performance by elimination of flyback fuel requirements. These sites are, however, further from the equator than KSC and incur added orbit transfer delta V penalties. Further, the environmental issues associated with inland sites have seemed more and more intractable as time goes on. Inland sites were therefore dropped from further analysis in this study.

B. Seacoast sites similar to KSC but remotely located.

C. Sea-based sites, either floating or construction on the sea bed using Texas tower structures.

If a remote site is to be used, a motivation exists to go to equatorial sites. The orbit transfer delta V from a zero inclination low Earth orbit to geosynchronous orbit is reduced from about 4200 m/sec to about 3800 m/sec (a reduction of 400 m/sec), for high-thrust transfer. In the case of low-thrust transfers, the delta V is reduced from about 5,800 m/sec to about 4,550 m/sec (a reduction of 1,300 m/sec).

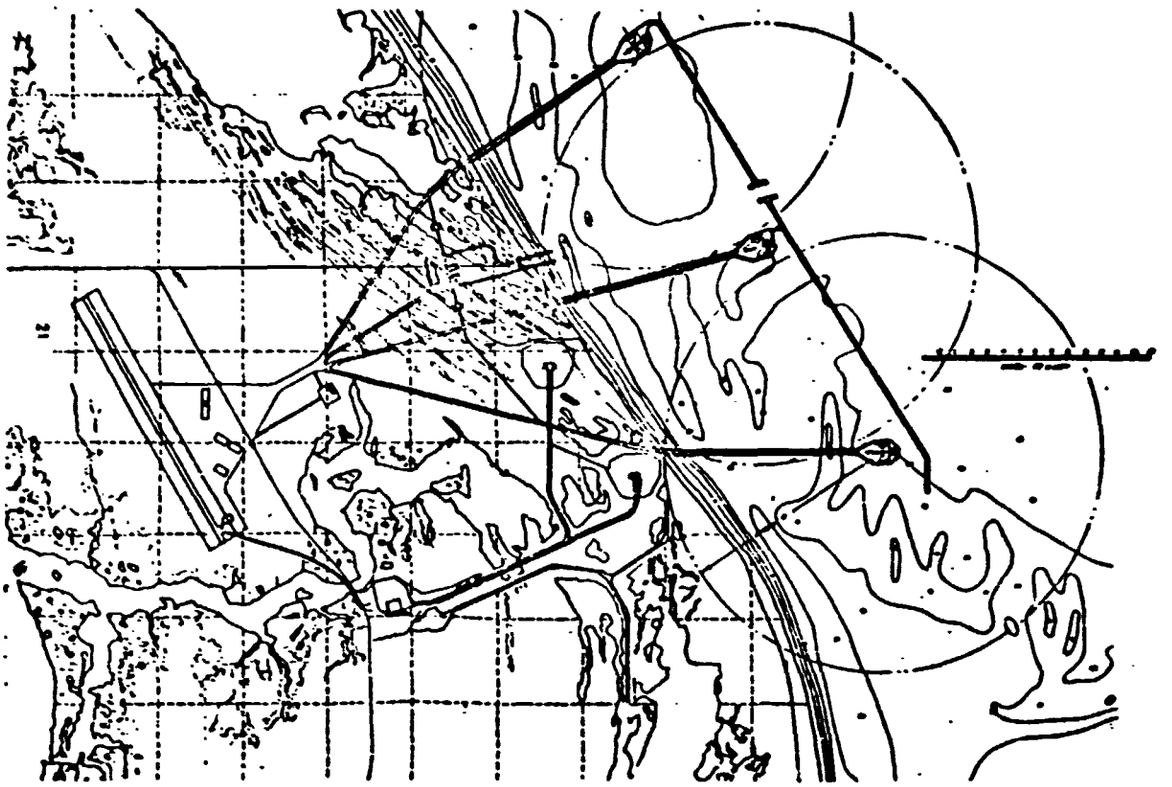

Figure 1.3.7-1. Overlay of HLLV Pads on KSC Map

Further, the radiation environment in low Earth orbits below about 5^{o} inclination, and up to about 600 km altitude, is much less severe than for higher inclination orbits that pass through the South Atlantic anomaly. (The transfer environment is more severe for low inclination starting orbits.)

Therefore, this task was established to address the feasibility and desirability of remote launch sites for SPS with emphasis on low-latitude sites.

Launch Site and Vehicle Options

The coastal launch sites are compatible with either the two-stage ballistic or two-stage winged vehicle. Being a coastal site, use of water transportation provides flexibility to move large amounts of bulk materials and propellant or raw materials readily. The total population required to support the launch rate equivalent to place one satellite in orbit per year will be in the range of 250,000 to 500,000 people. This amount is an approximation of the total number of people involved to provide all the sevices for launch site employees and includes their families. This approach will eliminate a number of small islands which could only be operated as remote sites, with premium pay and a split work schedule of two weeks a the site and one week home.

Potential seacost equatorial sites are identified in Figure 1.3.7-2. Distances to these locations from primary seaports are shown in Figure 1.3.7-3. A tentative ranking of these sites is given in Table 1.3.7-1.

A prime candidate location for a sea-based site is in the western Pacific Ocean, about 300 km north of the Galapagos Islands. This area enjoys a mild climate, experiences very infrequent tropical storms, has a mild sea state nearly all of the time, and the sea bed is at depths that would allow mooring of a floating launch site.

Cost Deltas for Equatorial Sites

Orbit Transfer Savings

An initial attempt at performance simulation for a low latitude transfer from 5^{o} inclination to geosynchronous orbit actually exhibited reduced performance as compared to the ref rence 30^{o} case. Increased loss due to sun occulations apparently more than offset the reduction in delta V and in gravity gradient losses. In fact, the variations in solar-electric orbit transfer performance due to variations in orbit geometry and season are greater than performance differences between low latitude

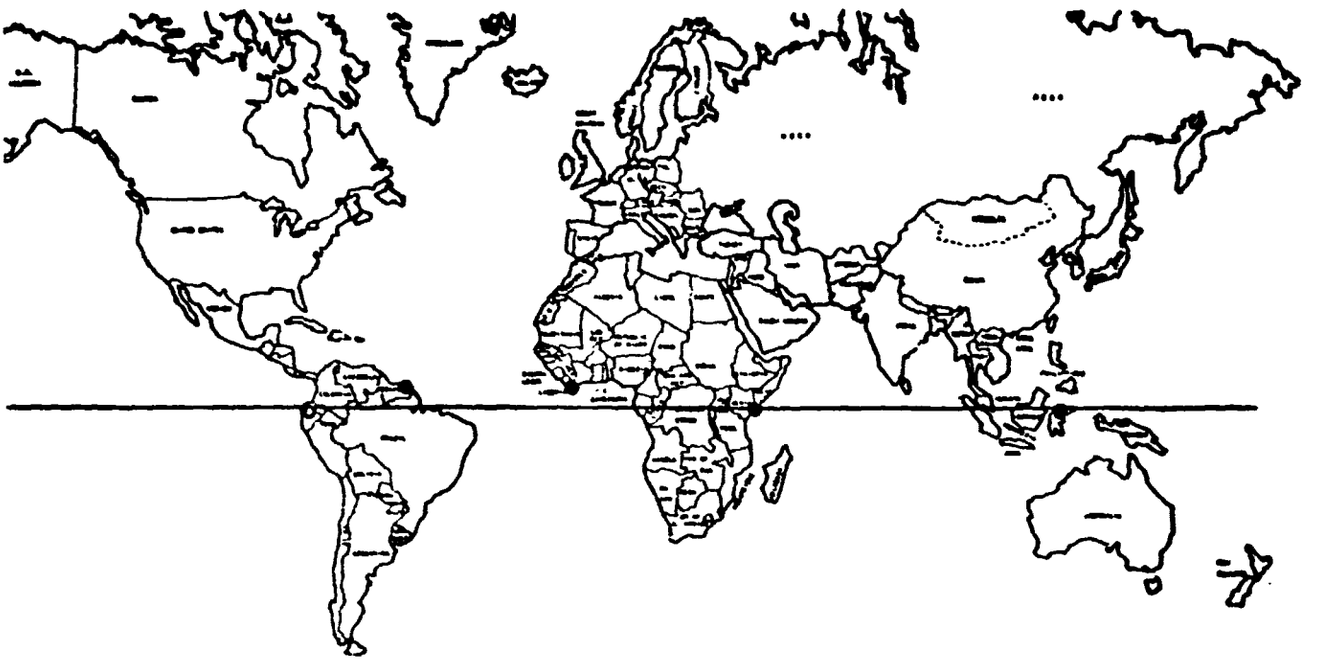

Figure 1.3.7-2. Potential Equatorial Launch Sites

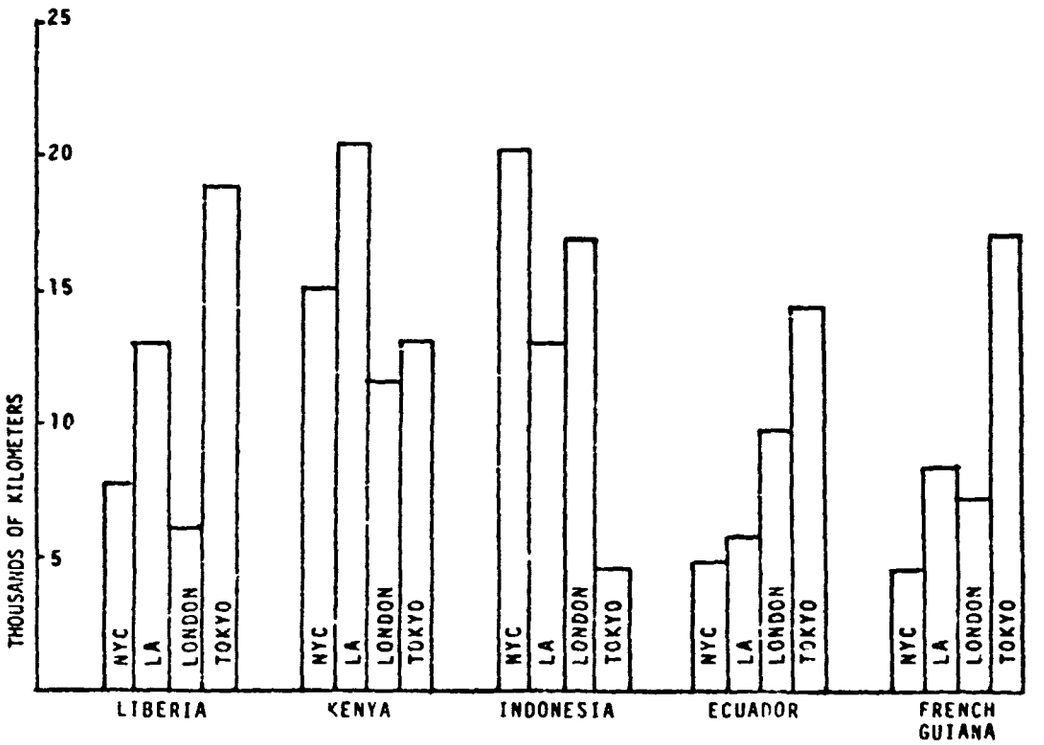

Figure 1.3.7-3. Distances by Sea to Potential Equatorial Sites

Table 1.3.7-1. Rankings of Potential Equatorial Launch Sites (Tentative)

	Liberia	Kenya	Indonesia	Ecuador	French Guiana
Existing Launch Facilities	3	2	3	3	1
Overwater Range, East	2	1	1	-	1
Access to Inclined Orbits	2	1	1	?	1
Access to Oil/Gas Field	3	2	2	1	3
Downrange Tracking Sites	1	3	1	2	4
Industrial Base, Energy, etc.	3	2	1	2	4
Logistics, Port Facilities, etc.	2	1	3	2	4
Sea Route Distance	3	5	4	1	2
Climate	4	2	3	1	5
High Mountains	-	2	2	1	-

and 30^{o} inclination starting orbits. Therefore, in determining the cost benefits from performance improvement between low inclination and high inclination orbits an upper bound analysis was adopted. This analysis is summarized in Table 1.3.7-2 and shows that cost advantages for the low latitude transfer are minimal.

Although it is not likely that this small cost advantage can overcome the cost increases associated with departing from an existing facility, such as KSC, other reasons may exist for setting up a new launch site for SPS operation. These reasons include the likelihood that the scale of SPS transportation operations will eventually outgrow KSC as well as potential desirability of an international launch site for what could eventually become an international project.

Transportation Cost

Representative costs for transportation of SPS hardware to remoe sea coast sites are enumerated in Table 1.3.7-3.

Sea-Based Sites and Facility Requirements

An overall concept of a sea-based launch facility was also developed. Figures 1.3.7-4 through 1.3.7-7 are descriptive diagrams. Figures 1.3.7-8 and 1.3.7-9 show additional details and Figure 1.3.7-10 summarizes the activity flow for this site concept.

Preliminary cost estimates have been developed for the launch complex facilities at KSC and for the facilities (exclusive of the floating structures themselves) for the sea-based launch complex. These are presented in Tables 1.3.7-4 and 1.3.7-5.

Construction costs for a land-based remote site will be higher than those for KSC due to two factors: (1) the remote construction cost delta. Boeing experience in this indicates that remote cost delta factors range from 1.5 to 2 depending on circumstances. (2) Replication of existing KSC facilities (tracking, computing, etc.) that can support HLLV operations.

Thus a remote land site would probably cost roughly $8 to $10 billion.

The sea-based site can be fabricated in sections in U.S. or other shipbuilding facilities, towed in sections to the final location, and joined together. Thus remote site construction deltas would be largely eliminated but a very large floating structure

Table 1.3.7-2. Upper Bound Performance Delta Summary Low Latitude Versus KSC

- MASS RATIO FOR 30° PLANE CHANGE FROM LEO TO GEO (1.25 SELF-POWER; ABOUT 1.1 FOR IEOTV)
- MASS RATIO FOR NO PLANE CHANGE FROM LEO TO GEO = 1.20
- DELTA NUMBER OF HLLV FLIGHTS = 17 (400 RATHER THAN 417)
- DELTA TRIP TIME–20 DAYS (LESS FOR NO PLANE CHANGE)
- VALUE OF DELTA TRIP TIME ≈ 35 MILLION
- COST FOR REFERENCE CASE 5,570 MILLION NOT INCLUDING TRIP TIME COST
- INCLUDING DELTA TRIP TIME, 400 FLIGHTS FROM 0° CAN COST 5,605 MILLION OR $14 MILLION PER FLIGHT, COMPARED TO $13.35 MILLION AT KSC

Table 1.3.7-3. Transportation Costs to Equatorial Site (One 5GW SPS)

Distance to Launch Site	4600	20500	km
SHIP			
Freight Cost	$ 4.2	$ 18.7	million
Time in Transit (@ 15 knots)	165	738	hours
Lost Revenues	$24.8	$110.7	million
Total Cost	$29.0	$129.4	million
AIR			
Freight Cost	$61.3	$273.2	million
Time in Transit	7	31	hours
Lost Revenues	$ 1.1	$ 4.7	million
Total Cost	$62.4	$277.9	million

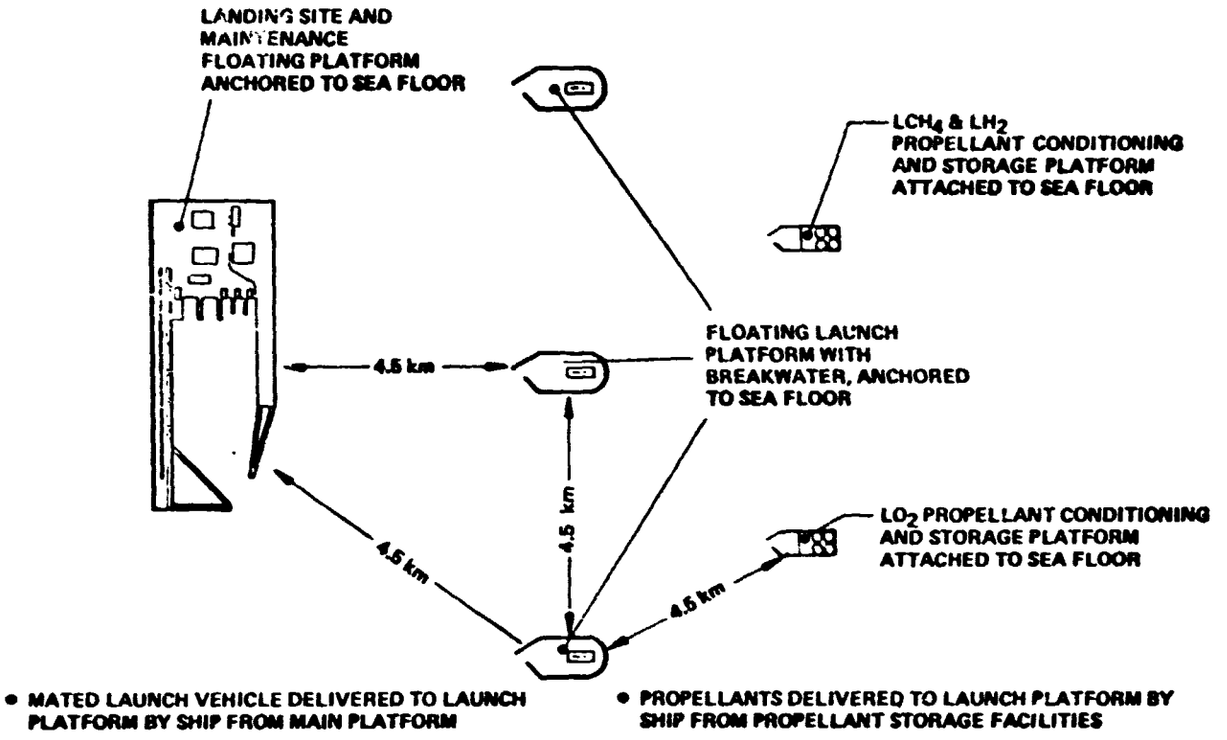

Figure 1.3.7-4. Sea Based Launch Site Concept

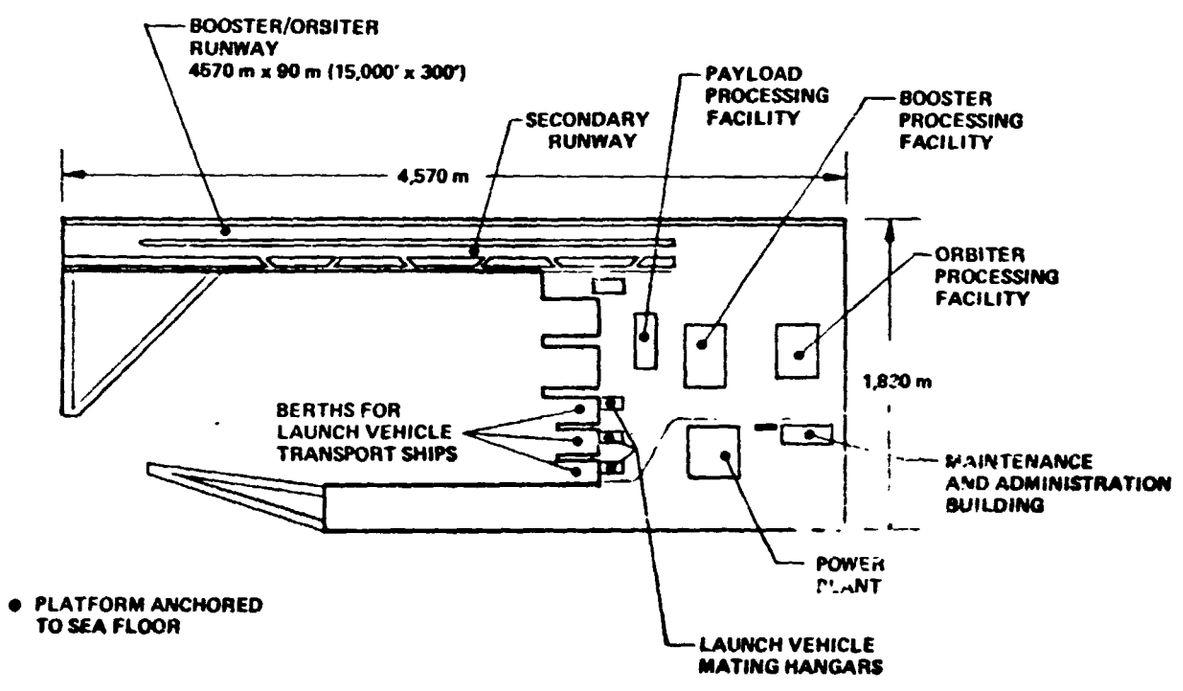

Figure 1.3.7-5. Landing Site and Maintenance Facility Floating Platform

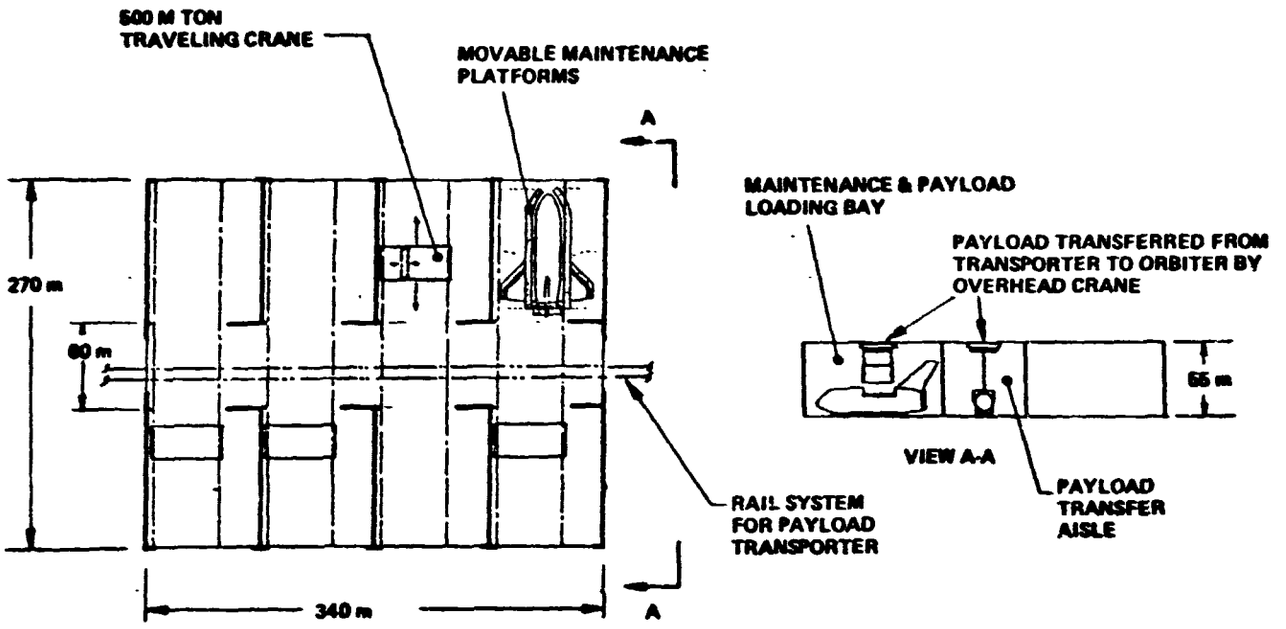

Figure 1.3.7-6. Oribter Processing Facility

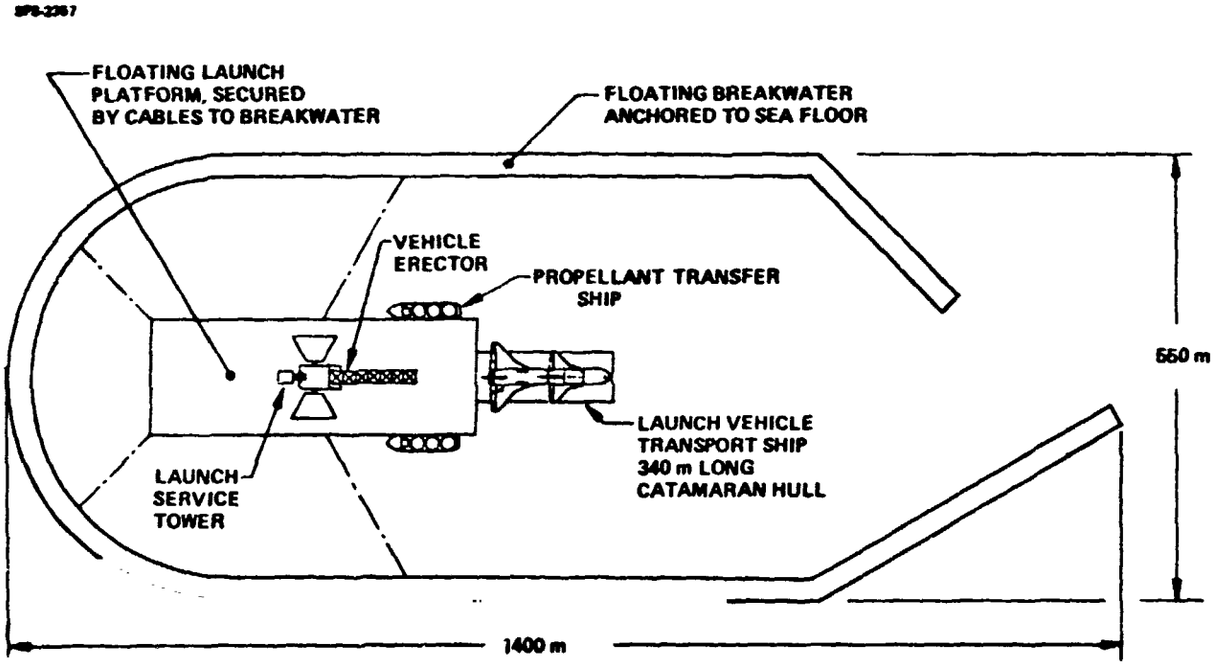

Figure 1.3.7-7. Floating Launch Platform

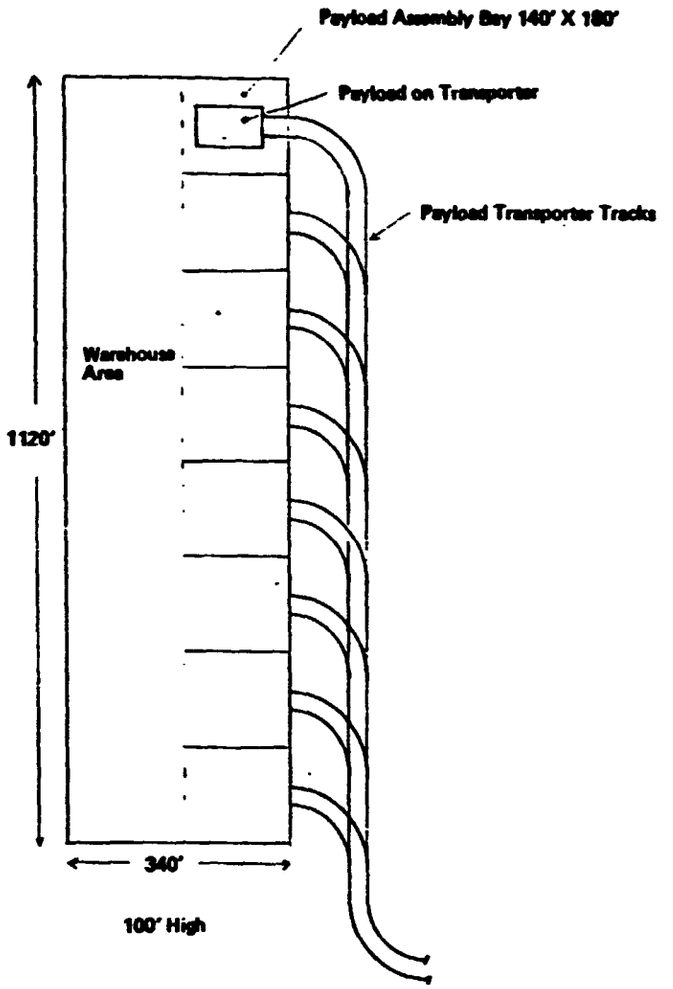

Figure 1.3.7-8. Payload Assembly and Storage Facility

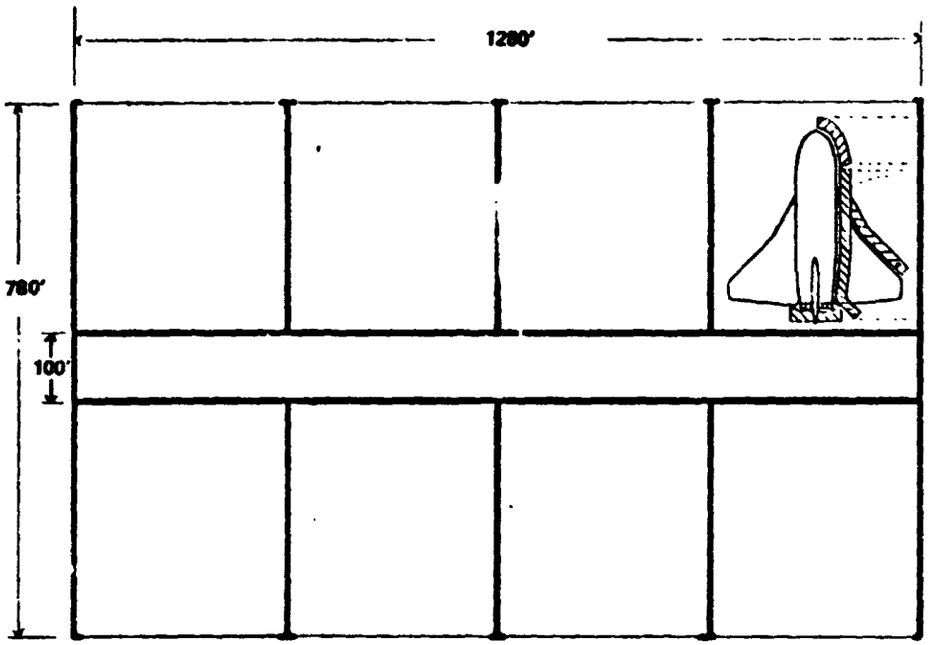

Figure 1.3.7-9. Booster Processing Facility

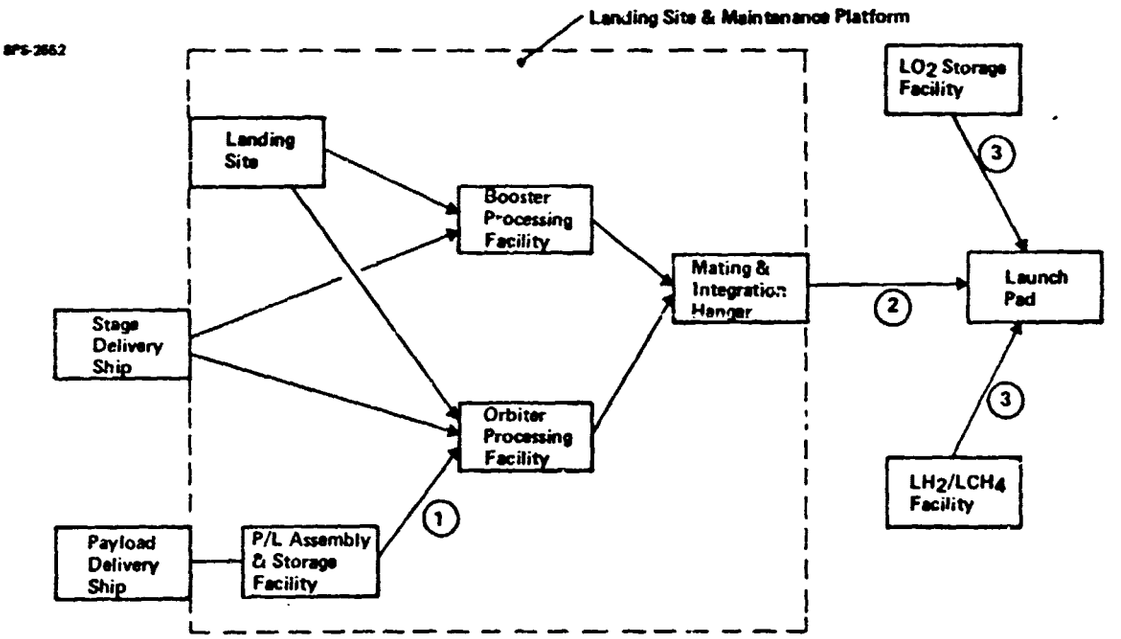

1. Assembled payload delivered to OPF VIA fixed rail transporter.
2. Stages mated on mobile strongback. Strongback transported to launch pad by ship.
3. Propellants for each launch delivered to launch pad in propellant transfer barges.

Figure 1.3.7-10. Sea Based Launch Site Concept Activity Flow

Table 1.3.7-4. SPS Launch Complex Facilities Costs
KSC Location

	ITEM	Quantity	Unit Cost	Total Cost
1.	Launch Pads	3	201.75	605.25
2.	Mating & Integration Hangars	3	44.61	133,83
3.	Propellant Storage Facilities	2	96.00	192.00
4.	Launch Control Center	1		78.30
5.	Orbiter Processing Facility	1		422.48
6.	Booster Processing Facility	1		244.59
7.	Payload Assembly Facility	1		62.20
8.	Maint./Admin. Building	1		15.00
9.	Mated VEhicle Transporters	3	74.85	224.55
10.	GSE	-		169.05
11.	Railroads, Misc. Sup. Vehicles & Equip	-		50.00
	Total			$2,197.25 M
	Estimated Land Prep. Cost:	$2,657.41 M		
	TOTAL LAUNCH COMPLEX COST:			$4,854.66 M

Table 1.3.7-5. Sea-Based SPS Launch Complex Facilities Summary

	Item	Quantity	Unit Cost	Total Cost
1.	Launch Pads	3	162.23	486.69
2.	Vehicle Transfer Ships	2	40.00	80.00
3.	Mating and Integration Hangars	3	44.61	133.83
4.	Propellant Storage Facilities	2	96.00	192.00
5.	Propellant Transfer Barges	4	18.00	72.00
6.	Launch Control Center	1		78.30
7.	Orbiter Processing Facility	1		422.48
8.	Booster Processing Facility	1		244.59
9.	Payload Assembly Facility	1		62.20
10.	Maint./Admin. Building	1		15.00
11.	Mated Vehicle Transporters	3	74.85	224.55
12.	GSE			169.05
13.	Railroads, Misc. Sup. Vehicles and Equipment			50.00
	*TOTAL			$2230.69M

*Does not include platform costs

Platform Area = 49.88 x 10^6 ft^2

must be built. The area of this structure is roughly 5 million square meters; the break-even cost allowable for its construction is roughly $5 billion or $1000/M^2 ($100 per square foot). Whether or not this large structure can be built for such a figure remains unanswered.

It has recently been reported that the Japanese are planning a floating airport for Osaka. This would indicate they believe acceptable costs can be achieved.

The following conclusions were reached regarding remote equatorial sites:

- Terrestrial transportation costs are modest but not negligible.
- Loss of revenues due to time in transit may be cost driver for sea freight.
- Air freight to close site may be cheaper overall than sea freight to remote site.
- Freight mode faster than sea but cheaper than air should be used if available (hovercraft, hydrofoil, dirigible?)
- Ecuador, Guiana/Brazil, Liberia preferable sites.
- Terrestrial transportation costs and delays will probably not be offset by reduction in EOTV costs and delays
- Use of international equatorial site may be ultimately justified for reasons other than cost
- Sea-based siting merits further analysis

1.3.8 TRANSPORTATION TO EQUATORIAL LAUNCH SITES

1.3.8.1 Terrestrial Transportation Issues

The scale and characteristics of the Solar Power Satellite require that much more attention be paid to problems of logistics than in previous space projects. The choices made in connection with fabrication of the components of the SPS (and of the launch vehicle, fuel, etc.), warehousing, inspection, and transportation to the launch site can have a significant effect, not only on the cost of the system, but on decisions which are fundamental to the SPS systems design (for example, the choice between LEO and GEO assembly). As the cost of launch to orbit is reduced, the costs of terrestrial transportation become more important; as the cost of space hardware is reduced, means for reducing handling and inspection costs must be found. On the other hand, the total required investment and the necessary lead time before the SPS can be operational are such that it may be cost-effective to construct new factories, launch facilities, etc., optimized for the SPS, rather than relying on existing institutions.

There are many uncertainties about the best organization of the industrial infrastructure to support the SPS program. In general, the questions which arise can usefully be divided into two categories: those which depend critically on the technology used for fabrication of the SPS, and those whose answers may remain valid if the technology changes.

As an example of a question of the first type, consider the manufacture of solar cell blankets (which is discussed in more detail in the next Chapter). Although the baseline reference SPS design retains only two photovoltaic options (single-crystal silicon and gallium aluminum arsenide), there are numerous other contenders (e.g., amorphous silicon or multijunction cells) which may become more attractive as development continues. Even if it were possible to agree on a specific cell type, the techniques which might be used for mass production, on the scale required for building one or more solar power satellites per year, are presently quite speculative. Issues relating to manufacturability should be regarded as an important part of the development program for various photovoltaic cells, but iw ould be premature to base a detailed analysis of manufacturing logistics on a particular choice of cell and a fabrication technique which, in most cases, has not yet been demonstrated except at laboratory scale.

On the other hand, it may be possible to draw conclusions of some general validity about the transportation and warehousing of solar cell blankets. If the cost goals of the SPS are to be met, the solar cell cost must be of order \$50-\$100/m^2 (in '977 dollars), and the substrate must be very thin (~100 μm). The inspection, transportation and warehousing costs must be not more than a few dollars per square meter, but it is clear that these cells may not be easy to handle in quantity, especially if the substrate is brittle. How should the cells be packed for shipping from the factory to the launch site? Can the same shipping container be used for launch? If so, should the cells be unpacked and inspected at the launch site to cull out breakages during terrestrial transportation? Where should assembly of cells into blankets take place? What degree of shipping damage is acceptable?

It is possible that transportation problems may be influential in the choice of substrate materials for the solar cells -- a roll of flexible cells would be much easier to handle (during assembly in space as well as during transportation) than would thin glass sheets. The type of packaging

used for transportation may have a significant impact on launch costs. For example, if cells of thickness y are separated by lightweight packing material of thickness x, the density of the package will be less than that of the cell material by a factor (1 + x/y). Although solar arrays are ordinarily regarded as high-density, packaging considerations could reduce this density substantially.

It should be noted that, packed for launch, solar cell panels will be a relatively high-value cargo. Packed as above, a cubic meter would contain about 900 square meters of solar cells, with a value of order $100,000 and a mass of about 250 kg. Since the cargo volume would also be high (tens of thousands of cubic meters for each SPS), it is probably economically feasible to design special terrestrial transportation systems for delivery of solar cells to the launch site -- for example, trucks in which launch containers are mounted in fairly elaborate shock isolation systems.

In order to discuss terrestrial transportation problems, it is of course necessary to make an assumption about where the launch site is located. It is not obvious that the best site is Kennedy Space Center (KSC): apart from problems such as the noise in the vicinity from frequent launches of the Heavy Lift Launch Vehicle (HLLV), the magnitude of the SPS program and the changes which would be needed in KSC facilities are such that the penalty to be incurred by moving to another site, may be acceptable, if one with preferable characteristics could be found.

In Phase I of the present study, a preliminary analysis was undertaken of the costs of transportation to potential launch sites at low latitudes. The objective was to determine whether the benefits to be obtained from low-latitude launch (discussed in Section 3.4) would be sufficient to offset the additional costs and difficulties which would be incurred by launch from a site remote from the areas where most SPS components would most probably be manufactured.

1.3.8.2 Potential Equatorial Launch Sites

There have been several studies to date of possible low-latitude launch sites[1,2]. Launch facilities exist at the Kouru range in French Guiana, the San Marco platform (Italian) off the coast of Kenya, the Thumba sounding rocket site in India, and the range in Zaire belonging to the West German company OTRAG. None of these facilities are in any way sufficient to support a program of the magnitude of the SPS.

The search for potential low-latitude sites may be greatly simplified by imposing the following simple conditions: (i) The site should be as close to the equator as possible, certainly within 10° latitude (the penalty in launch vehicle performance due to latitude is discussed below). (ii) There should be an extensive region to the east which is essentially uninhabited, where the sonic footprint of the booster and perhaps spent stages may fall. (iii) The site should be on or near a seacoast with good harbor facilities. As shown by the map **Fig. 1.3.8-1, there are basically** six areas meeting these requirements:

1. East Coast, South America: Venezuela, Guyana, Surinam, French Guiana or Brazil.
2. West Africa: A vehicle launched due east from Cape Palmas, Liberia, would be over water for about 1800 km, before reaching the Cameroon coast; and Cape Three Points in Ghana affords about 750 km over water to the Nigerian coast. All other sites in West Africa require overland launches.
3. East Africa: Somali Republic, Kenya or Tanzania.
4. India, on the coast south of Madras, or on the eastern coast of Sri Lanka.
5. Far East: Malaysia, Indonesia, Philippines (Mindanao), Papua New Guinea, or perhaps Australia (Cape York).
6. West Coast, South America: Colombia, Ecuador or Peru. All sites in this area require launch over the Andes and the Amazon basin, which is very sparsely inhabited.

D180-25037-2

Figure 1.3.8-1: POSSIBLE LOW-LATITUDE LAUNCH SITES

In addition to these sites, there are a number of oceanic islands which might be considered:

7. Indian Ocean: Seychelles, Chagos Archipelago (Diego Garcia), and the Maldives.
8. Pacific Ocean: Bismarck Archipelago (New Ireland), Solomons, Carolines, Marshalls, Gilberts, Nauru, Christmas Island, Galapagos Islands, and many others, mostly small.

There are no suitable islands in the Atlantic Ocean.

Finally, a floating launch facility could be built and located wherever is convenient, in international waters.

Although most equatorial nations may be classed as less developed or emerging countries, there are of course substantial differences between them, in the political climate, industrial base, gross national product, population, level of education, culture, etc., all of which should be taken into account in choosing a potential launch site. In the present study, however, the focus of interest was launch site logistics (in particular, terrestrial transportation costs): the objective is not to recommend an equatorial launch site, but to find out whether the probable costs incurred by operations at such sites exceed the benefits. For these purposes, it is sufficient to choose, more or less arbitrarily, a particular nation in each of the restricted geographical areas listed above. To make the comparison definite, the following nations were therefore considered:

1. French Guiana, because of the existing French range.
2. Liberia, which has a longer overwater range than Ghana, and which has expressed interest[3] in setting aside an area as a possible spaceport.
3. Kenya, because of the existing San Marco facility.
4. Sri Lanka, which has a latitude advantage over India.
5. Indonesia, which has been investigating the feasibility of a launch site on Sulawesi (Celebes)[3].
6. Ecuador.

1.3.8.2.1 Sea Route Distances and Transportation Costs

In order to compare transportation costs, sea route distances to major p[illegible] in the above nations were calculated from New York City, Los Angeles, London and Tokyo. These ports were taken as representative transshipment points for SPS components from factories in the eastern and western United States, Europe and Japan, respectively. The Suez and Panama Canals were used to minimize distances, wherever appropriate.

The results are shown in Fig. 1.3.8-2. From the present point of view, the South American sites appear to be preferable if the SPS factories are in the United States or Western Europe, with Ecuador providing the best compromise if a substantial fraction of the freight to the launch site comes from Japan.

It is not easy to obtain a reliable estimate of shipping costs over these distances without a detailed breakdown of the cargo. Freight costs depend on the mass and volume of the cargo, special handling procedures which may be needed, the value of and probability of damage to the items shipped, and several other factors. Even though, for the SPS, a dedicated transport fleet may be assumed, the cost will not be accurately proportional to the distance, in part because of fixed turnaround costs. For preliminary comparisons, however, the following simple cost model was used:

$$C = (k_1 + k_2/v)x \qquad [3.1]$$

where C is the cost of shipping for a single 5 GW SPS, k_1 is the direct cost/km, v is the average speed (in km/h) of the transport, k_2 is the revenue which would be obtained from one hour of operation of the SPS, and x is the shipping distance in kilometers. The second term in this equation represents revenues lost because the time spent in transit from the factory to the launch site delays initial operation of the SPS -- in other words, it assumes that terrestrial transportation lies on the critical path in the PERT chart governing launch and assembly of the system. This assumption will probably be true for an efficient operation, with minimum movements in and out of warehouses.

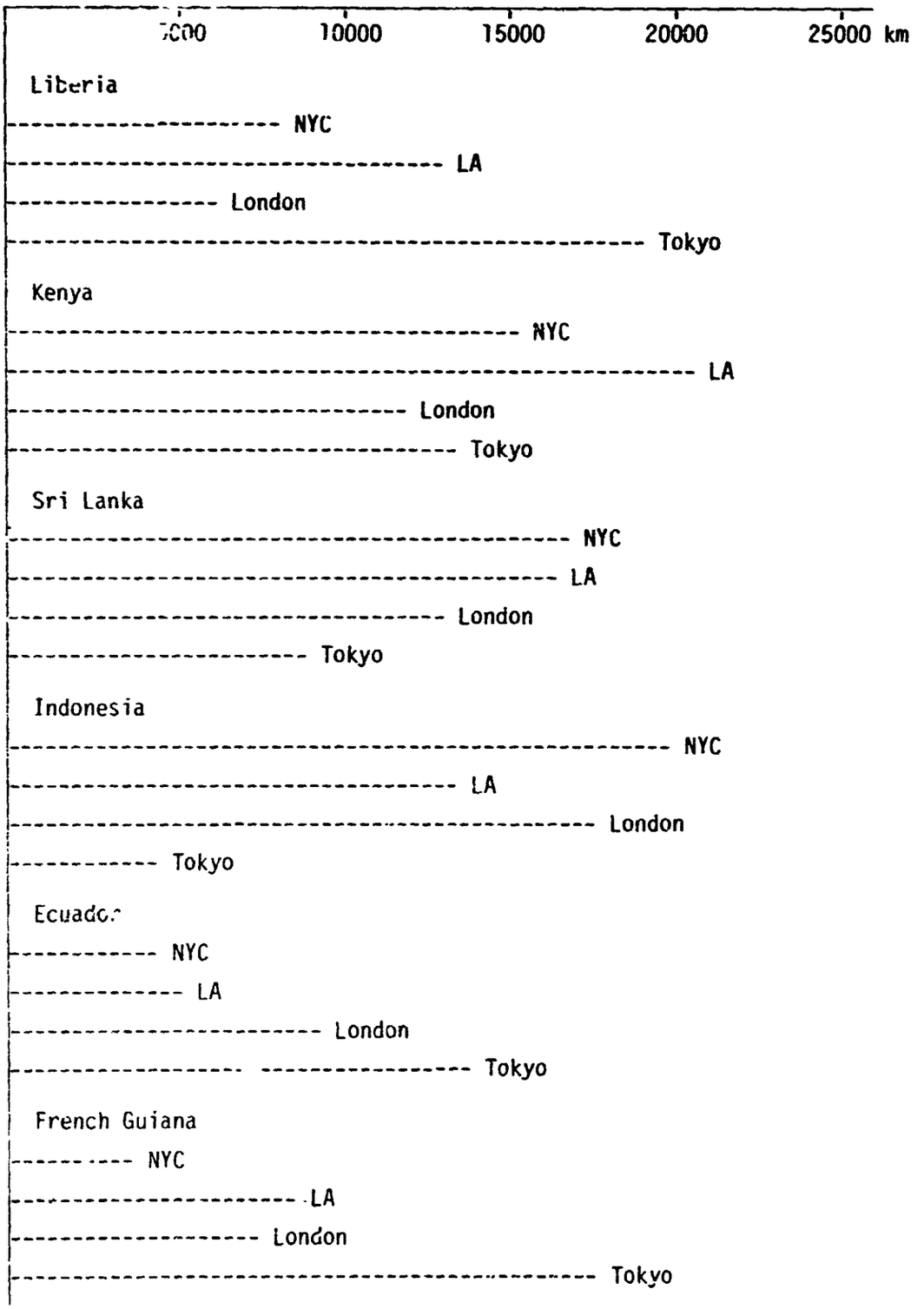

Figure 1.3.8-2: SEA ROUTE DISTANCES

Table 1.3.8-1: Shipping Costs

	Sea	Air
Mass to be shipped	50,000 metric tons	50,000 metric tons
Average density of cargo	0.3 gm/cm^3	N/A
Shipping cost	\$0.016/m^3/km*	\$0.27/ton/km**
Average speed	28 km/hr	830 km/hr
SPS revenues (5×10^6 kwh/hr @ 3¢/kwh)	\$150,000/hr	\$150,000/hr
k_1	\$2670/km	\$13,500/km
k_2/v	\$5360/km	\$181/km
$(k_1 + k_2/v)$	\$8030/km	\$13,700/km

Estimates of the costs of shipment by sea and by air are given in Table 1.3.8-1, and the cost as a function of distance is shown in Fig. 1.3.8-3. It is interesting to note that, for shipment by sea, lost revenues due to the time in transit are the dominant cost, and that it may be cheaper to ship by air to closer sites than by sea to distant ones.

The shipping costs obtained from this simple model are only of order \$10/kw, a small component of the overall SPS cost. A more accurate model would thus be of doubtful utility at the present stage of development of the system. The absolute costs for shipment of each SPS to a low-latitude site are however of order \$100 million, so that optimization of shipping may be absolutely worth while, even if it is relatively unimportant.

It is possible that the total cost of shipment might be minimized by using a freight mode which is faster than a ship but slower than an aircraft. If it were decided to use a low-latitude launch site for the SPS, the possibilities of employing hovercraft, hydrofoils or dirigibles for shipment should be investigated.

*This figure is an average of quotes from shippers for long-haul sea freight of machinery in quantity. If the cargo has a density much less than that of water, the cost typically depends on the volume rather than the mass.

**This figure was obtained from quoted prices for bulk air freight from New York City to Rio de Janeiro.

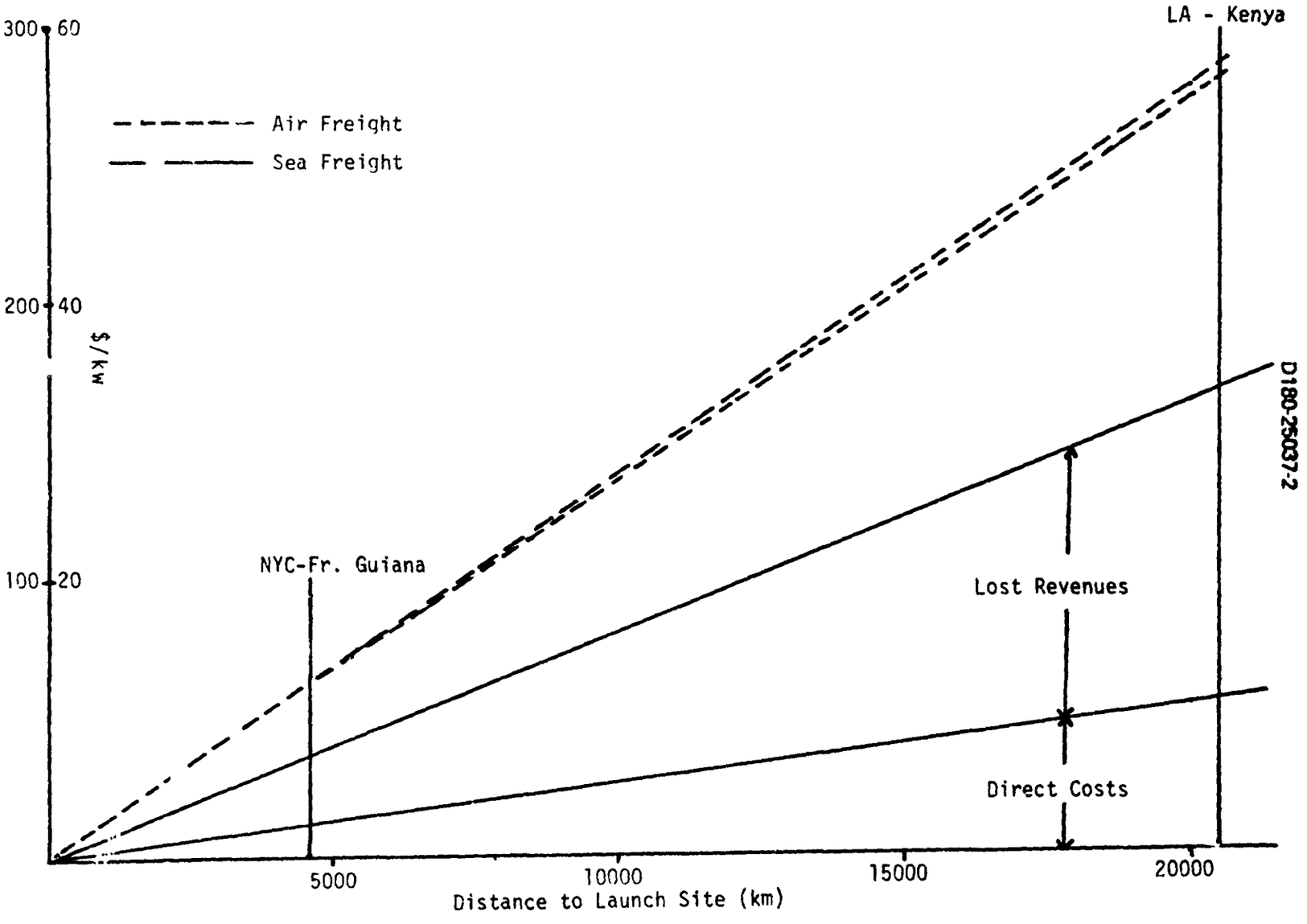

Figure 1.3.2-3: TRANSPORTATION COSTS

1.3.8.2.2 Advantages of Low-Latitude Sites

Even if the SPS is assembled in geosynchronous orbit (GEO), there will be a requirement for a manned facility in low orbit (LEO), providing warehousing and transshipment to the electric orbital transfer vehicle (EOTV) of cargo from Earth, refuelling of the EOTV and other OTV's, etc. It is highly desirable that this facility be in equatorial orbit, in order to avoid the radiation shielding required if the orbit penetrates the South Atlantic Anomaly. Moreover, from a given launch site the launch window to an inclined LEO opens twice per day, at most. Launch to equatorial LEO from a site at latitude L requires a plane change through an angle L at the equator, and generally a phasing maneuver as well for rendezvous with the SPS facility (so as to avoid launch window restrictions).

The ΔV required for the plane change is easily seen to be

$$\Delta V = 2v_1 \sin \frac{1}{2} L \simeq v_1 L \qquad [3.2]$$

where L is in radians. The approximation given is accurate within about one per cent for $L < 30°$. The expression is valid for orbits at any altitude, with circular velocity v_1.

If the plane change is required, the upper stage of the launch vehicle must carry additional propellants. For a given booster, the burnout mass is reduced by the plane-change mass ratio

$$R = \exp(\Delta V/c) \qquad [3.3]$$

Assuming the upper stage uses LOX/LH_2 (with a vacuum specific impulse $I_{sp} \simeq 420$ seconds), the expression [3.3] is plotted in Fig. 1.3.8-4 as a function of the launch site latitude. The orbit altitude is taken to be 500 km, so that $v_1 = 7.62$ km/sec. The mass ratio penalty for launch to equatorial LEO can be quite substantial, amounting to a factor of 2.5 at $L = 28.5°$ (KSC).

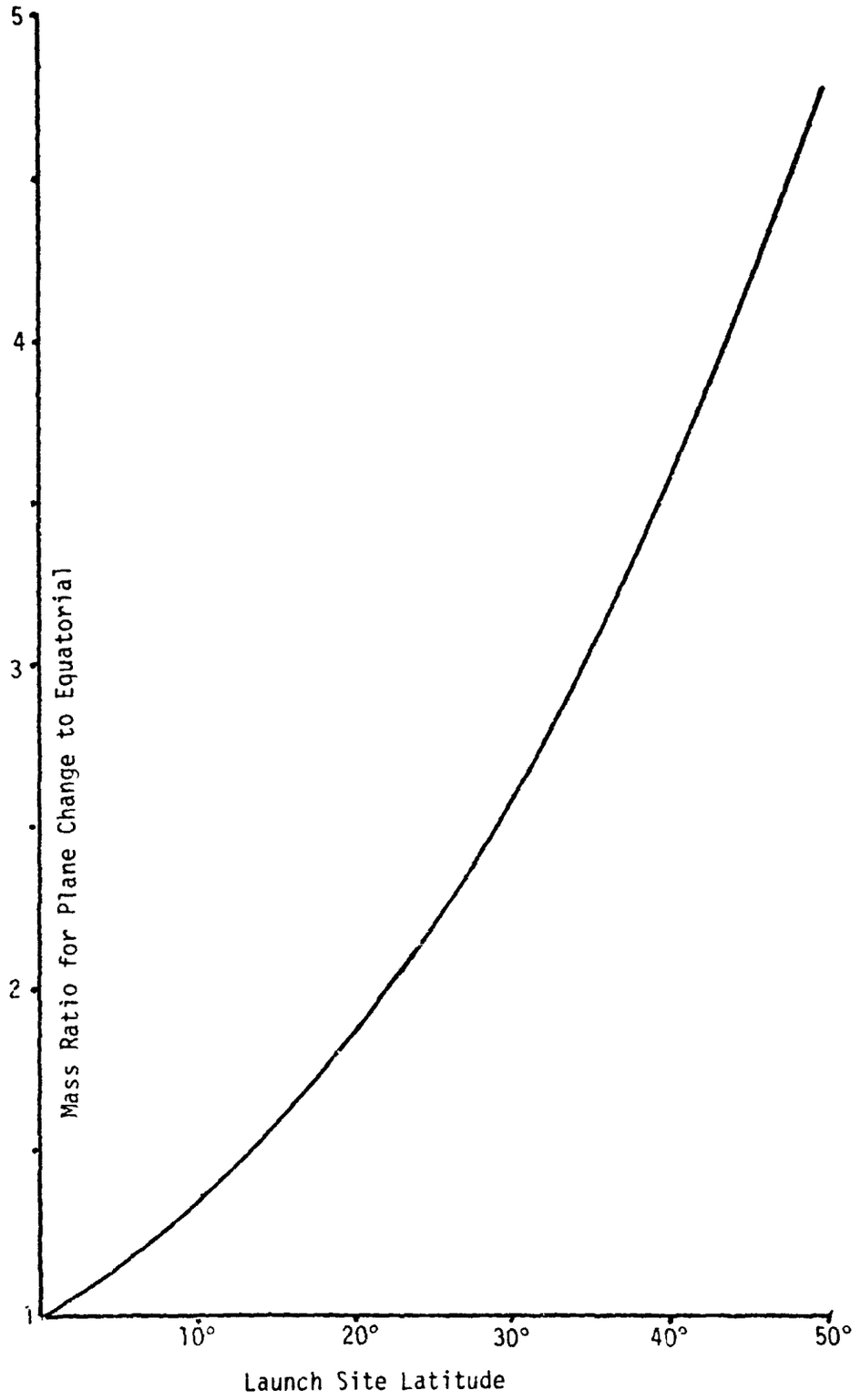

Figure 1.3.8-4: LEO PLANE-CHANGE PENALTY

The effect on launch costs per unit mass will actually be larger than is shown in the figure, because of the cost of additional propellants and, more importantly, because part of the burnout mass must be used for additional structure, especially tankage Furthermore, if the upper stage is reuseable, it must deorbit to an equatorial recovery area, or else have the capability of changing planes again when empty, so as to pass over the launch site. In practice, it may be necessary to use a separate kick stage for the plane change maneuvers, further increasing costs and complicating reuseability.

It is interesting to compare the ΔV for LEO plane change, Eq.[3.2], with that for ascent to GEO. If the vehicle is initially in a circular orbit of radius r_1 and inclination L, the velocity increment required to inject to a transfer ellipse with apogee at geosynchronous radius r_s, without plane change, is given by the vis viva integral[4] as

$$\Delta V_1 = v_1\left[\left(\frac{2r_s}{r_1+r_s}\right)^{1/2} - 1\right] \qquad [3.4]$$

The velocity at apogee is then

$$v_a = v_1 r_1 \left(\frac{2}{r_s(r_1+r_s)}\right)^{1/2} \qquad [3.5]$$

and the velocity increment from the "kick in the apogee" to change plane and circularize in equatorial GEO is given by

$$(\Delta V_2)^2 = v_a^2 + v_s^2 - 2v_a v_s \cos L \qquad [3.6]$$

where $v_s = v_1(r_1/r_s)^{1/2}$ is the GEO circular velocity.

The total velocity increment $(\Delta V_1 + \Delta V_2)$ for this maneuver is plotted in Fig. 1.3.8-5, along with the LEO plane-change ΔV, assuming that the altitude of the initial orbit is 500 km. The surprising fact is that, if $L > 32°$, it is cheaper to make a direct ascent to equatorial GEO than it is to stay in LEO and merely change the orbital plane to equatorial.

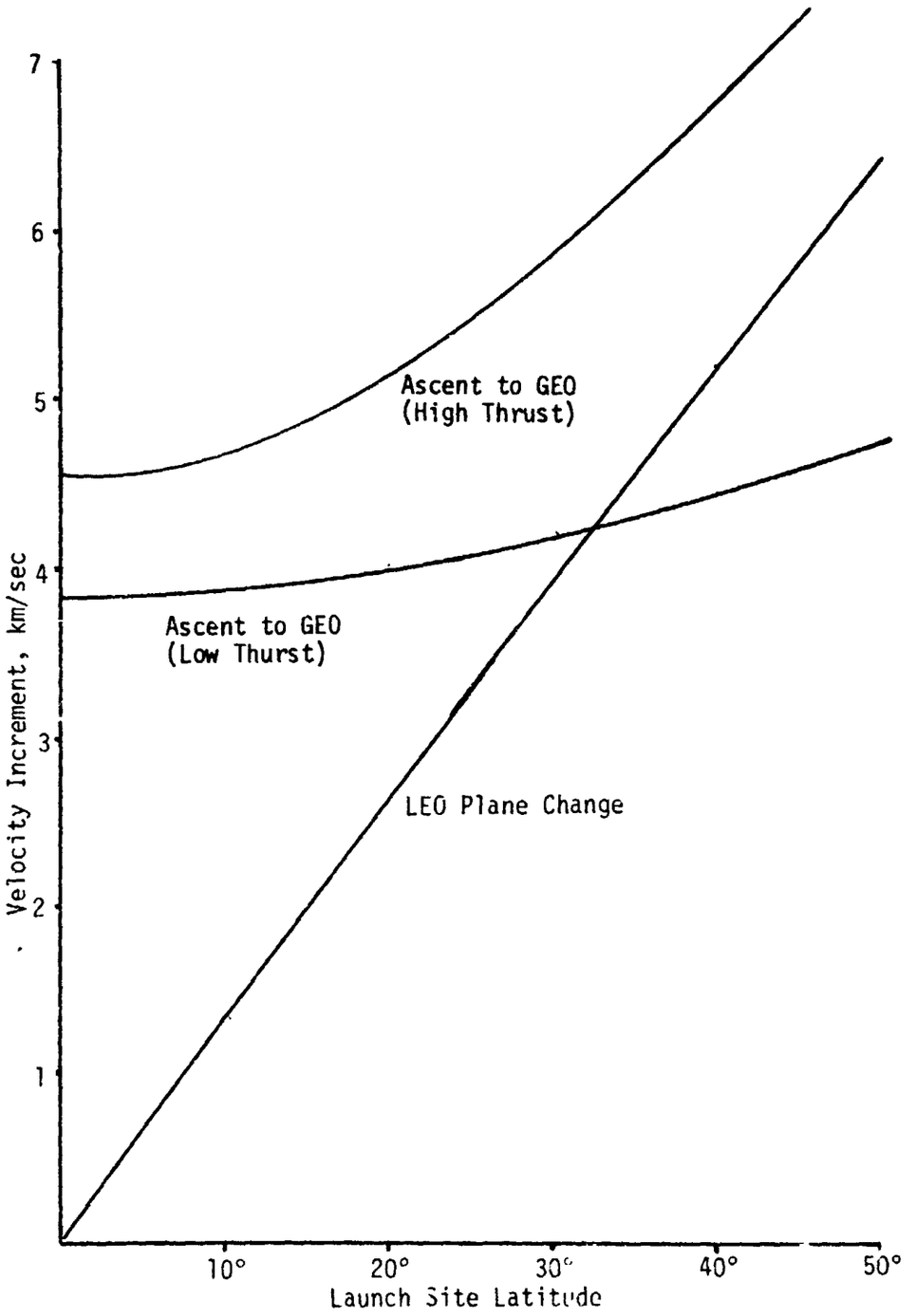

Figure 1.3.8-5: LEO PLANE CHANGES AND ASCENT TO GEO

The conclusion to be drawn from this analysis is that launch from KSC to a staging base in equatorial LEO, with subsequent low-thrust transfer to GEO, is not a practical approach to construction of the SPS. Direct ascent from KSC to GEO, with no facilities in LEO, would provide performance advantages, but a third chemical stage for the HLLV would be needed in either case. If launch must be from KSC (or other high-latitude site), the best approach is probably to use a staging base in LEO at an inclination equal to the latitude, accepting the radiation shielding penalties and launch window restrictions which this implies. The benefits of equatorial LEO are obtainable only with a low-latitude launch site.

One other possible advantage of a staging base in equatorial LEO is that the ΔV requirements (defined as the time integral of the acceleration due to thrust) for low-thrust transfer to GEO are somewhat reduced, because no plane change is involved. The variation of low-thrust delta V with inclination of the initial orbit is also shown in Figure 1.3.8-5 . For an ion engine of given I_{sp}, reduction in ΔV can lead to a reduced transfer time or reduced power levels as well as reduced propellant requirements.

For a solar EOTV, however, increased occultation of the sun by the Earth in equatorial low-thrust transfer may offset the ΔV reductions by reducing the average available power. The total nightside time in a spiral low-thrust orbit clearly depends on the orientation of the orbital plane to the ecliptic, not the equator. The equator is inclined E = 23½ degrees to the ecliptic. An orbit inclined at an angle i to the equator can be inclined from i = E to abs(i=E) to the ecliptic, depending on the orientation of the orbit line of nodes relative to the intersection of the equator and ecliptic. Thus the shadowing effects vary not only with inclination and season, but also with orbit nodal regression. This problem was analyzed in depth during the Boeing FSTSA study for JSC. A representative variation in solar-electric orbit transfer performance is shown in Figure 1.3.8-6.

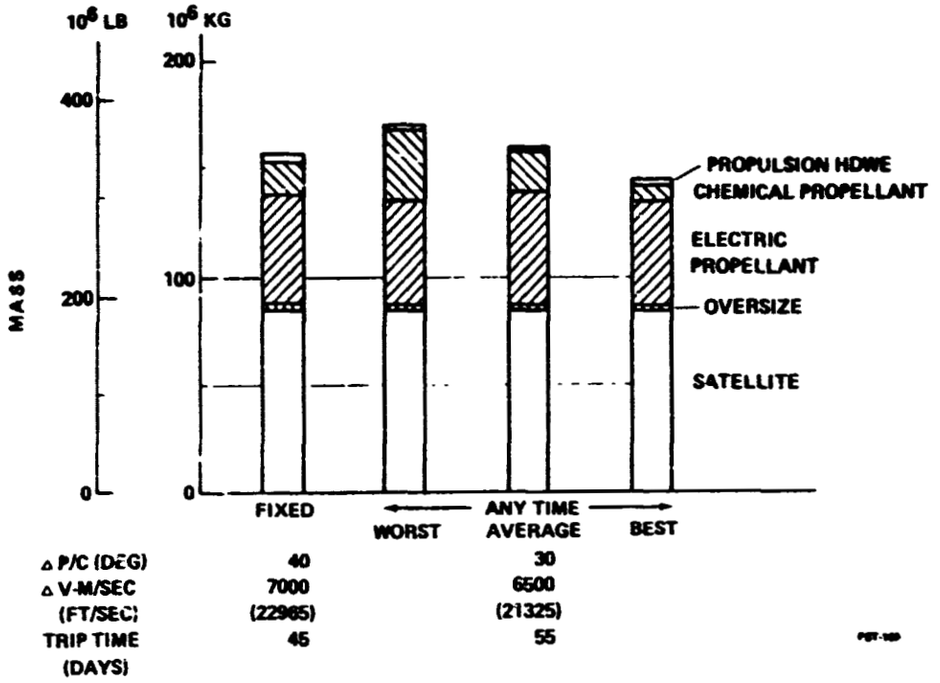

Figure 1.3.8-6 Fixed vs Anytime Departure Mass Comparison Arc Jet Propulsion

1.3.8.3 Ranking of Potential Low-Latitude Launch Sites

The six potential launch sites listed at the end of Section 3.2 have been compared so far only on the basis of the sea route distances and shipping costs to them from the United States, Europe and Japan. Although these characteristics are of primary concern in the present study, it would not be appropriate to form opinions about the relative merits of these areas on the basis of these data alone. This Section therefore presents several other types of data about each site. In the following paragraphs, the number in parentheses following each site is a tentative ranking of the site in comparison to the others, with respect to the characteristic under discussion, with the lowest ranking assigned to the best site. Where there are little grounds for choosing between sites, they are given the same ranking.

I. Existing launch facilities.

1. French Guiana (1): The Kouru range is the best developed equatorial launch facility.
2. Liberia (3): No existing launch facilities.
3. Kenya (2): The San Marco platform.
4. Sri Lanka (3): No existing facilities.
5. Indonesia (3): No existing facilities.
6. Ecuador (3): No existing facilities.

II. Over water range, east.

1. French Guiana (1): 7000 km
2. Liberia (2): 1800 km
3. Kenya (1): 6700 km
4. Sri Lanka (2): 1500 km
5. Indonesia (1): 17800 km (some islands).
6. Ecuador (3): None (Andes and Amazon basin).

III. Available launch azimuths.

1. French Guiana (1): 0° to 135°
2. Liberia (1): 90° to >180°
3. Kenya (1): 45° to 180°.

4. Sri Lanka (2): 0° to 180°, but limited overwater range to northeast.
5. Indonesia (2): 0° to 180°, but range limited by islands in some directions, and by Australia (but sparsely inhabited areas) to southeast.
6. Ecuador (3): Easterly azimuths probably limited to narrow corridor. Polar orbits (south) also possible.

This characteristic is not of great significance directly to the SPS, but it may affect the utility of the site for other missions and hence limit cost-sharing possibilities.

IV. Access to Oil and Gas Fields and Refinery Facilities. Assuming that petroleum-based hydrocarbons (kerosene, LNG, etc.) are used as fuel in the first stage of the HLLV, the equivalent of several million barrels of oil will be required annually to support the SPS build-up scenario. If a deepwater port is available, this fuel could be imported by tanker at acceptable cost. However, if LH_2 is used as fuel in the upper stage of the HLLV, several tens of thousands of tons of hydrogen will be required annually. Liquid hydrogen has a very low density (0.07 gm/cm^3) and is requires specially-designed equipment and facilities to handle in quantity. It would be possible to manufacture it on site by electrolysis of water, but a pipeline to a nearby oil and gas field, where it can be obtained cheaply, would be highly desirable.

1. French Guiana (5): Venezuela (c.2000 km) is the closest major source.
2. Liberia (4): Nigeria (c. 1300 km) is the closest source.
3. Kenya (3): Indigenous, but limited.
4. Sri Lanka (6): Import probably required.
5. Indonesia (2): Indigenous (Borneo, across Makassar Straits from Sulawesi).
6. Ecuador (1): Indigenous, ample reserves.

For French Guiana and Liberia, pipelines from oilfields across intervening nations may cause problems.

V. Availability of Downrange Tracking Sites (Boost Phase).

1. French Guiana (4): Poor; ship probably required.
2. Liberia (1): Excellent.
3. Kenya (3): Fair; ship or Amirante Islands.
4. Sri Lanka (5): Poor; ship required.

Table 1.3.7-2: Selected National Statistics

Nation	Ranking	Population (millions)	GNP $U.S.[1] (billions)	GNP per capita $U.S.	Education[2]
Brazil[3]	1	107.1	41.9	391	5.0
Liberia	6	1.75	0.64	363	1.7
Kenya	5	13.4	2.17	162	1.8
Sri Lanka	4	13.6	2.41	177	3.8
Indonesia[4]	3	138.1	22.5	163	2.0
Ecuador	2	6.7	3.5	516	4.6
France		52.9	269.3	5090	8.9
U.S.		215.1	1516.3	7048	11.4

Notes:

(1) Converted from local currency at free exchange rate (1976 data)

(2) This is the percentage of the population which is enrolled in secondary and tertiary education.

(3) French Guiana is an overseas département of France, with a population of only 55,000. Brazil is a more likely source of personnel.

(4) Although Indonesia's per capita GNP is low, the country is large enough to have significant industrial resources. Singapore and perhaps Australia are sources of skilled workers.

V. Availability of Downrange Tracking Sites (continued).

5. Indonesia (1): Excellent.

6. Ecuador (2): Good, although mountain and jungle terrain may cause difficulties.

VI. National Statistics: Wealth and Education.

Table 3.2 gives some statistics which are intended to be representative of the industrial base and availability of skilled labor in the six equatorial areas. For comparison, figures for France and the United States

are included. Although the discrepancy between the advanced and emerging nations is of course very pronounced, care is needed in interpreting the average values given. For example, the emerging nations generally have much higher birthrates than the advanced countries, which means that a higher percentage of their populations are of school age; if adjusted for this effect, the difference between the education levels would be even more pronounced. On the other hand, especially in larger nations, a low value of the GNP per capita does not preclude the existence of a substantial class of educated and relatively affluent people who could provide skilled workers at a launch site. The rankings given to the various sites thus involve a considerable amount of judgment.

VI. Climate: Availability of High Mountains

Climate can have a strong effect on the desirability of a launch site, affecting operations there and influencing personnel changeovers. Mountains in the area modify the climate and provide attractive areas for vacations etc. In addition, there is a possibility that high mountains may eventually prove of significance to launch technology; in particular, a launch site for boosters employing laser propulsion[5] must be above the freezing level (at least, if CO_2 lasers are used).

1. Ecuador (1): Rainfall 40 - 60 in/yr, depending on elevation. Cool summers, mild winters. Mountain elevations to 6000 meters.
2. French Guiana (4): Rainfall 120 in/yr, hot and rainy all year, near sealevel.
3. Liberia (4): Rainfall 100 in/yr, mostly hot and rainy, near sealevel.
4. Kenya (2): Rainfall 50 in/yr, hot all year but short rainy season. Mt Kenya (5200 m) and Mt Kilimanjaro (5900 m) nearby.
5. Sri Lanka (3): Rainfall 40 in/yr, hot all year but fairly short rainy season. Maximum elevation 2600 m.
6. Indonesia (4): Rainfall 120 in/yr, mostly hot and rainy, near sealevel. Nearest mountains on Borneo, to 4000 m, and in West Irian, to 5000 m.

Table 1.3.8-3: Tentative Launch Site Rankings

	French Guiana	Liberia	Kenya	Sri Lanka	Indonesia	Ecuador
Existing launch facilities	1	3	2	3	3	3
Overwater range, east	1	2	1	2	1	3
Available launch azimuths	1	1	1	2	2	3
Access to oil/gas fields	5	4	3	6	2	1
Downrange tracking sites	4	1	3	5	1	2
National Statistics	1*	6	5	4	3	2
Climate; High Mountains	4	4	2	3	4	1
Sea Route Distance	2	3	6	4	5	1

*Brazil

The rankings obtained with respect to these various characteristics are tabulated in Table 1.3.8-3, along with a ranking on sea route distance from Figure 1.3.8-2 These data of course do not provide an unequivocal basis for choosing the "best" equatorial site, which clearly depends on the weight given to the different characteristics. Moreover, the analysis here can be regarded only as a preliminary cut at the site-selection problem, and many important factors (e.g., the political climate) have been ignored entirely. Nevertheless, it does appear that the South American sites are generally preferable, with the West Coast sites (Ecuador, Colombia, or Peru) preferred if it proves acceptable to launch over the Andes and the Amazon basin.

Conclusions

The analysis presented in this chapter leads to the following conclusions:

1. Equatorial orbit provides significant advantages for a LEO staging base for the SPS, but this orbit is not practically accessible except from a low-latitude launch site.
2. If a low-latitude site is desired, attention should be given first to potential locations in South America. The West Coast may be preferable if it is possible to launch over (largely uninhabited) land.
3. Transportation costs to these sites are modest but not negligible.
4. Loss of revenues due to time in transit may be cost driver for sea freight.
5. Freight modes faster than sea but cheaper than air freight (hovercraft, hydrofoils, dirigibles, etc.) should be investigated to minimize overall costs.
6. Further work is needed to determine whether possible cost savings in space operations (e.g., from reduced EOTV transit time to GEO) due to equatorial launch offset terrestrial transportation costs and other costs arising from launch operations at a remote site.

REFERENCES

1. Chapman, P.K., & Searcy, J.B.: A Proposal for an Equatorial Launch Facility, The Chippewa Corporation, Lexington, Mass., 1964
2. Frazier, M., et al: Earthport - A Launch Pad for Industry Into Space, The Sabre Foundation, Santa Barbara, California, 1977.
3. Frazier, M., The Sabre Foundation, private communication.
4. Battin, R.H.: Astronautical Guidance, McGraw-Hill, NY, 1964, p.37.
5. Douglas-Hamilton, D.H., Riley, D., & Chapman, P.K.: Studies in Laser Propulsion, Avco Everett Research Laboratory, Inc., Everett, Mass., 1978.

1.4 GROUND RECEIVING STATION

Five tasks related to the ground receiving station were conducted:

Rectenna siting reported below under paragraph 1.4.1.

Rectenna construction reported below under paragraph 1.4.2.

Rectenna failure rates reported under system failure rates and effects tasks under paragraph 1.0.

Rectenna power collection reported under paragraph 1.4.3 in Voilume III.

Rectenna grid interface reported under paragraph 1.4.5 in Volume III.

1.4.1 Rectenna Siting

Approach. A siting analysis was conducted to develop information on siting criteria and make a preliminary assessment of siting problems. Related to this task, an informal information exchange agreement was made with the three utility regions shown in Figure 1.4-1:

- Bonneville Power Administration (BPA) (Pacific Northwest)
- Mid-Continent Area Power Pool (MAPP) (North Central USA)
- Southern California Edison

Additional ground rules employed in the siting investigation are as follows: Most of these can be regarded as candidate site selection criteria.

- Two "beam + buffer" region wideth (East-West dimension)
  - 13.18 km (corresponds to 5,000 mw output)
  - 9.32 km (corresponds to 2,500 mw output)
- SPS on the longitude of the site
- North-South dimension a function of latitude
  - Examples: 48° latitude, 23.05 km
  - 35° latitude, 17.37 km
- No encroachment upon:
  - Game preserves

SPS-2319

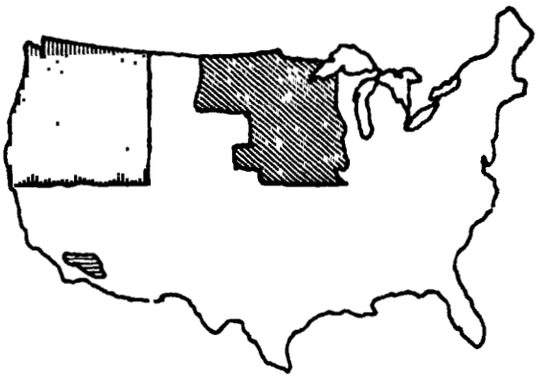

Figure 1.4-1. Regions for Siting Investigation

  - Bird refuges
  - National monuments
  - National and state parks
  - Indian reservations
- Maximum and minimum elevations in site to be within 1,000 feet of each other
- Minimum displacement of persons and property
- National forest and existing farmland use o.k.

The siting analysis employed a manual map search employing aeronautical charts, contour plots, and road maps.

Population counts were derived from the "Atlas of the United States."

The approach was comprised of five steps:

1. Identification of promising areas
2. Check for agreement with ground rules
3. Check for fit of 5,000 mw rectenna
4. If fit o.k., 5,000 mw assigned
5. If 5,000 mw did not fit, 2,500 mw was tried

The relative sizes of 5,000 megawatt and 2,500 megawtt sites are ilustrated in Figure 1.4-2.

Results. Preliminary studies of rectenna siting have indicated that the number of potential sites is considerably greater than presently-estimated requirements. Specific sites were identified in the three areas indicated with total numbers of sites as summarized in Table 1.4-1.

It was found beneficial to have available in the inventory two sizes of receiving antenna. The two sizes utiilzed correspond to the power transmission link capacities, 2,500 and 5,000 megawatts. If both 2,500 and 5,000 megawatts receiving sites could be employed, the total amount of power that could be sited was much greater than that for either size of receiving antenna alone.

Table 1.4-1. Rectenna Siting Potential Sites Identified

UTILITY REGION	5000 MW SITES [1]	2500 MW SITES
BONNEVILLE POWER ADMINISTRATION	25	27
MID-CONTINENT AREA POWER POOL	51	34
SOUTHERN CALIFORNIA EDISON	8	9
TOTALS	84	70

[1] > ALSO SUITABLE FOR 2500 MW

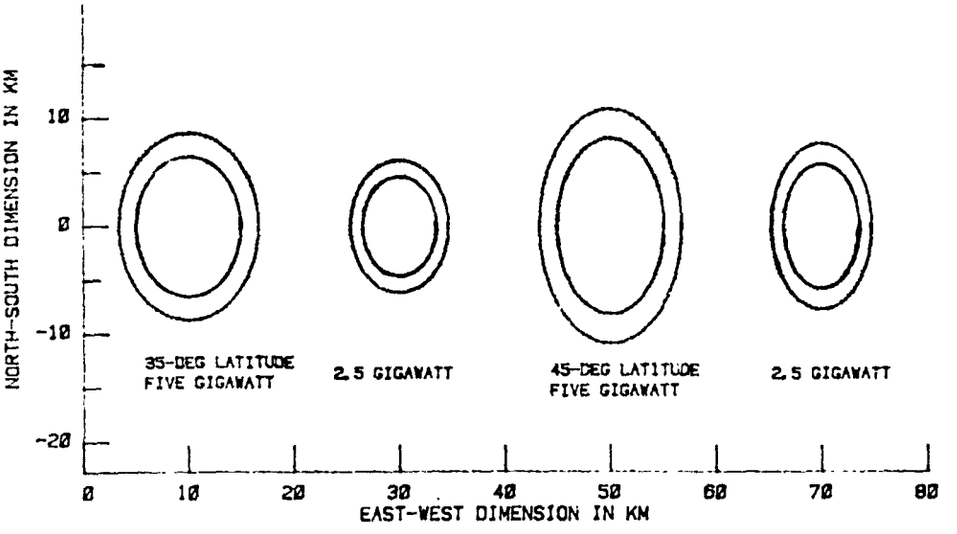

Figure 1.4-2 Rectenna Dimensions

Specifically, if only 2,500 mw rectennas were sited, 385 gw of capacity could be installed. If only 5,000 mw rectennas were sited, 420 gw of capacity could be installed (9% more than with 2,500 mw alone). However, if both 2,500 mw and 5,000 mw rectennas are available, 595 gw could be sited (42% more than with 5,000 mw alone). This preliminary analysis indicates that potential sites exist for at least four times the 2,000 A.D. requirements. Siting in the energy-intensive Northeast was not investigated, but demands for that area might be met by modest interties from rectennas in the north central U.S. Alternatively, offshore rectennas may be possible.

A number of sites in each utility region was selected at random for closer investigation of slope and other features which might presumably cause rejection. In general, most of the sites were quite flat. That is, the average slopes were less than 5 parts in 100; however, most of sites had small regions of local slope which might be considered to be excessive (slopes of 30 degrees or more).

As shown in Figure 1.4-3, the microwave beam from space ultimately falls on some ground area. It is possible in this concept to locate rectenna panels so as to receive all of the beam area even in regions of very extreme slope, but diffraction effects may cause some loss of performance for panels positioned fan downbeam from adjacent panels as a result of steep slopes. Consequently, it appears that rejection of cites on the basis of slope mut be decided individually, with economics as the criterion.

In investigation of specific individual sites it might be decided to merely reject any site with localized slope. Alternatively, large scale landscaping would be used. Also it might be desirable, in some cases, to allow holes in the rectenna. That is, in the area of either excessive slope, or some other terrain features, to merely not construct panels in that area, and allow the microwave beam to fall (wasted) directly on the natural or somewhat modified terrain. The consequences of reflection of the microwave power from such unused area need closer examination.

Conclusions. This siting effort indicated that, in the three utility areas investigated, "potential" sites exist to more than fill the requirements for electrical power for those regions in the year 2000. Due to the potential of excess sites, it might be possible to feed energy to the northeast from rectenna sites in the north central area, using modest interties. The benefits of having two rectenna and SPS sizes (in this case 5,000 and 2,500 megawatts) were obvious. Far more "energy from space" can be sited by having two sizes

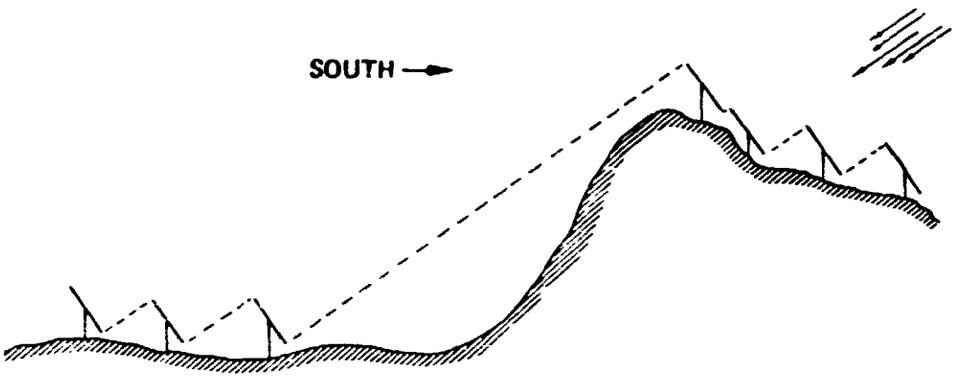

- **Rejection on basis of slope will be a function of construction economics.**

Figure 1.4-3. Even Extreme Slopes Do Not Block The Beam

rather than with either size alone. Further, the siting of SPS rectennas will obviously require individual site investigation. Each site selected will be a compromise. That is, no site can be expected to be perfectly flat, with the most desired terrain, type of soil, drainage, etc. No site will be immediately adjacent to the required energy use point. Thus, each siting will be an engineering and economic compromise.

Recommendations. The siting data developed in this study should be correlated with that produced in the exclusion area study of SPS rectennas accomplished at Rice University. If possible, this effort should be extended to cover not only the three contributing utility regions but the entire United States. As stated under groundrules, sites were not rejected which involve either national forests or farms currently in use. The impact of changing this groundrule to preclude use of national forests or land currently in use for farming should be investigated. Tests should be conducted on rectenna panels to determine the effect of precipitation particularly as regards to water sheet build-up during heavy rain, and the consequence of snow on the rectenna.

1.4.2 Rectenna Construction Analysis

General Electric conducted an analysis of rectenna structure and construction processes. This section presents a synopsis of their results. They will issue a full report on this subject under separate cover.

Task Description. For purposes of analysis, the overall project is divided into tasks, which are completed in serial fashion, i.e., task 1 must be complete before task 2 can be started, etc. Within each task, all jobs are conducted in parallel, paced by the "slowest machine" in the task. This is a simple artifice to assure that we do not try to place superstructure into footings not yet dug, or make panel assemblies without enough parts yet made. Task allocations are given in Table 1.4-2.

Figure 1.4-4 shows a preliminary concept for a 10 km by 12 km rectenna site. The east-west road is about 7 km, from staging area to the west lateral. The east and west lateral (north-south) roads are taken to be 6 km long, and the center lateral is 9 km long. Based on these distances, we have used, as an eyeball average, an average travel distance for all construction 'move' tasks an on-road distance of 10 km, and off-road move distance of 1 km. This is almost certainly a high estimate, and the total hauling cost for the construction task is only $24 million.

Table 1.4-2. Task Description

TASK ONE — INITIAL SITE PREPARATION
(3 MONTHS, 239 WORKERS)

TASK TWO — COMPLETE SITE PREPARATION
(5 MONTHS, 306 WORKERS)

TASK THREE — STRUCTURE CONSTRUCTION
(8 MONTHS, 706 WORKERS)

TASK FOUR — RECTENNA PANEL MANUFACTURE AND INSTALLATION
(9 MONTHS, 327 WORKERS)

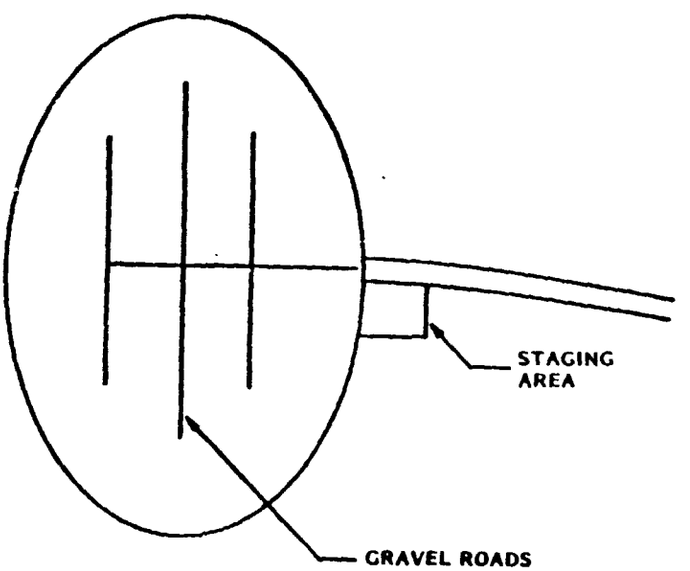

Figure 1.4-4. Site Plan

Figure 1.4-5 is a simple illustration of the "module" of a rectenna which will be repeated 1,238,350 times. It contains the equivalent of six of the 3.3 by 3 meter panels.

Our concept is to do as little site preparation as possible. We will have to cut down the trees on the site, and move the logs back to the staging area, where they are sold. Stumps will be left in place, unless they happen to be just hwere we want to make a footing hole. In that case, assumed to happen once every fifty modules, the stump is removed with a bulldozer. The bulldozer also backfills the cavity, and compacts it so it will permit a footing hole to be drilled there.

Except for grading and graveling roads, and removing trees and underbrush, nothing is done to the site. We will be able to build a rectenna wherever we can drive a bulldozer.

Figure 1.4-6 shows the main active rf configurations we considered. At the mid-term briefing we talked about the "printed honeycomb" and the "low drag" configuration concepts. However, when the time came to start doing actual construction and manufacturing cost analysis, it was concluded that there was too limited a design basis to support a costing exercise. We then briefly considered the low drag version of the baseline, until we noticed that the rf shield effectively blocks the lower dipole from receiving microwave radiation, so we returned to the original baseline.

Note that all three concepts impose substantial lifting forces on their supporting structures.

Figure 1.4-7 shows our baseline superstructure. We need to use several metric tons of mass to avoid upward loads on our footings.* Given that we must use tons of materials, the cheapest choise is concrete reinforced or prestressed as necessary to support the applied loads. Using an automated factory that is shown below, these piers can be made for about $26 assumed for reinforcing bar. No stress analysis has yet been done to support these estimates.

---

*The mass required to resist lift loads appears to have been overestimated by as much as a factor of 10. This is being reviewed and will be corrected as appropriate in the detailed GE report.

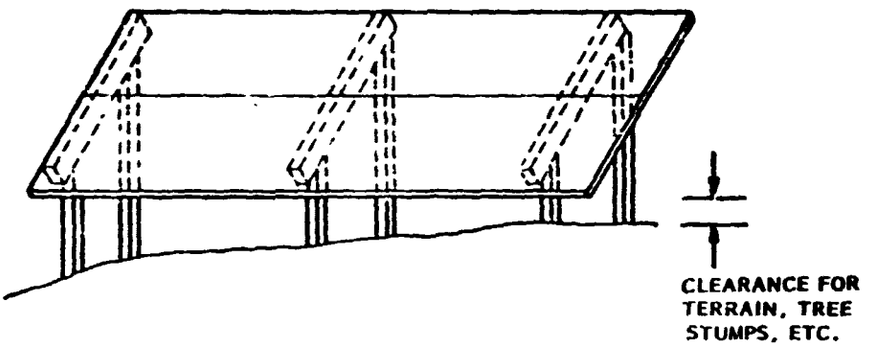

Figure 1.4-5. Rectenna Module

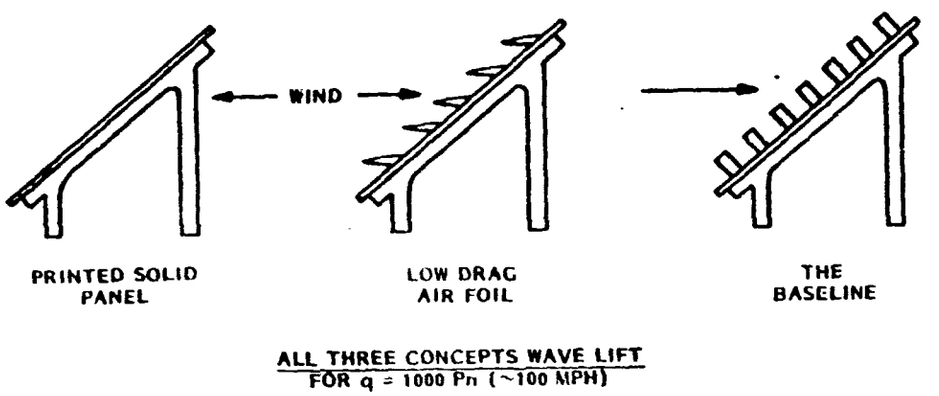

Figure 1.4-6. Three Panel Concepts

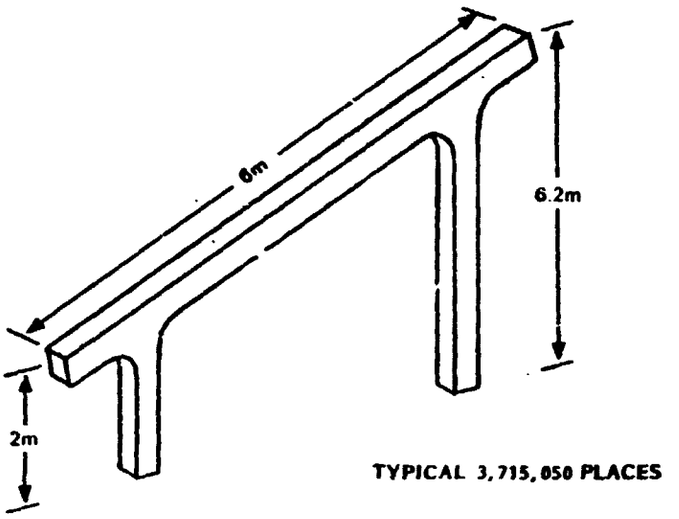

Figure 1.4-7. Pre-Stressed Concrete in Baseline Structure

Dipole Machine. Figure 1.4-8 shows the operation of a multi-station transfer machine simultaneously making the baseline dipole/diode assembly. The machine illustrated is part of a complex of three machines making foreplane assemblies. Each set of machines is assumed to cost 1.0M and be capable of manufacturing 150 ten meter foreplane strips every hour. The total cost for the 120 sets of machines, not including material, is $161.6M. The cost of material, which we will examine more closely later, is the driving factor in total rectenna cost.

Figure 1.4-9 illustrates the flow needed to assembly a rectenna panel, 3 meters by 10 meters, from all of the component parts. The process is assumed to be highly automated, with only two machine tenders for each panel assembly machine. The cost of this assemby machine is 3.3M.

Figure 1.4-10 artist's concept of an automated plant to produce the concrete support structure for the rectenna panels. The sketch shows only two conveyor belts carrying forms past the pouring chutes, but in our overall concept each machine would have five such belts, each casting an arch every minute, for a total of 250 arches produced every hour. Each machine costs about $2M, and has four operators. Ten such machines are used to produce the 3,750,000 arches needed in nine months. The equipment amortization for this equipment is 3.3M, and the total cost to make all of the arches for one rectenna is $177M, of which $139M is materials, including $100M of reinforcing bar.

This is a good place to mention that two kinds of arches are used; "regular" and "special." The "regular" one was shown earlier. It supports the rectenna panels with the lower edge two meters above the ground. This is not high enough to permit trucks to pass under the rectenna on the north-south roads, so "special" arches are used over north-south roads to increase the clearance to four meters.

Several specialized construction machine concepts were developed. These machines incorporate a design philosophy generally similar to that used for road-building equipment but are tailored for the rectenna construction task. An example is the concept shown in Figure 1.4-11 for a machine to drill footings. This concept implies that we will be working on soils that are reasonably cohesive and do not have much rock near the surface. Small rocks are broken by the jack hammer action of the tip (when needed) so that boring is not interrupted too often. Another machine is called in to handle large rocks, assumed to occur once for every hundred modules constructed.

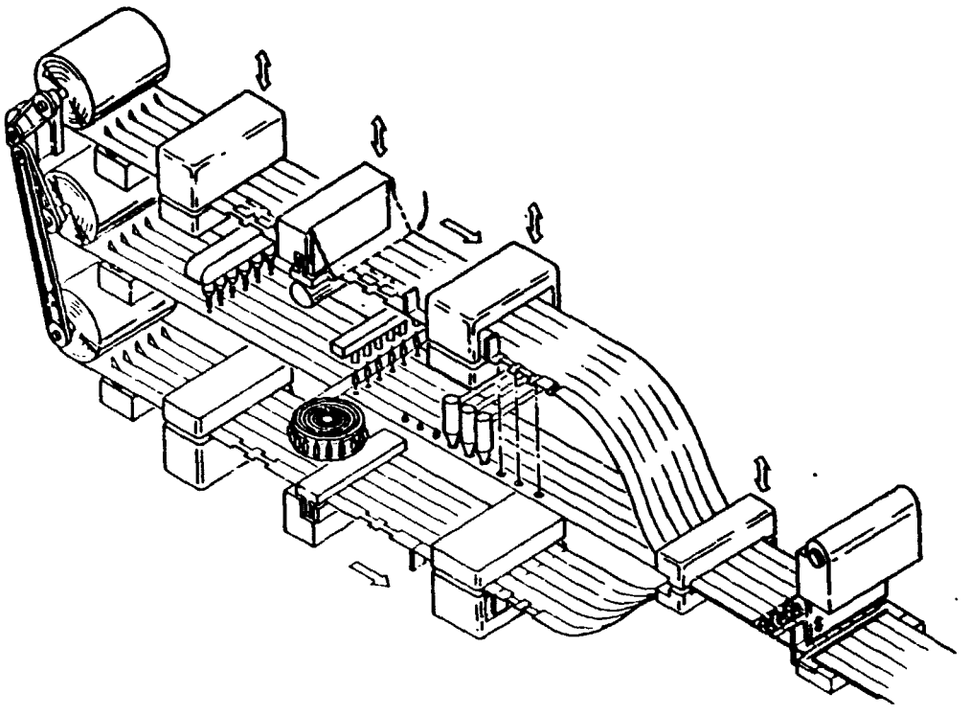

Figure 1.4-8. Dipole Machine

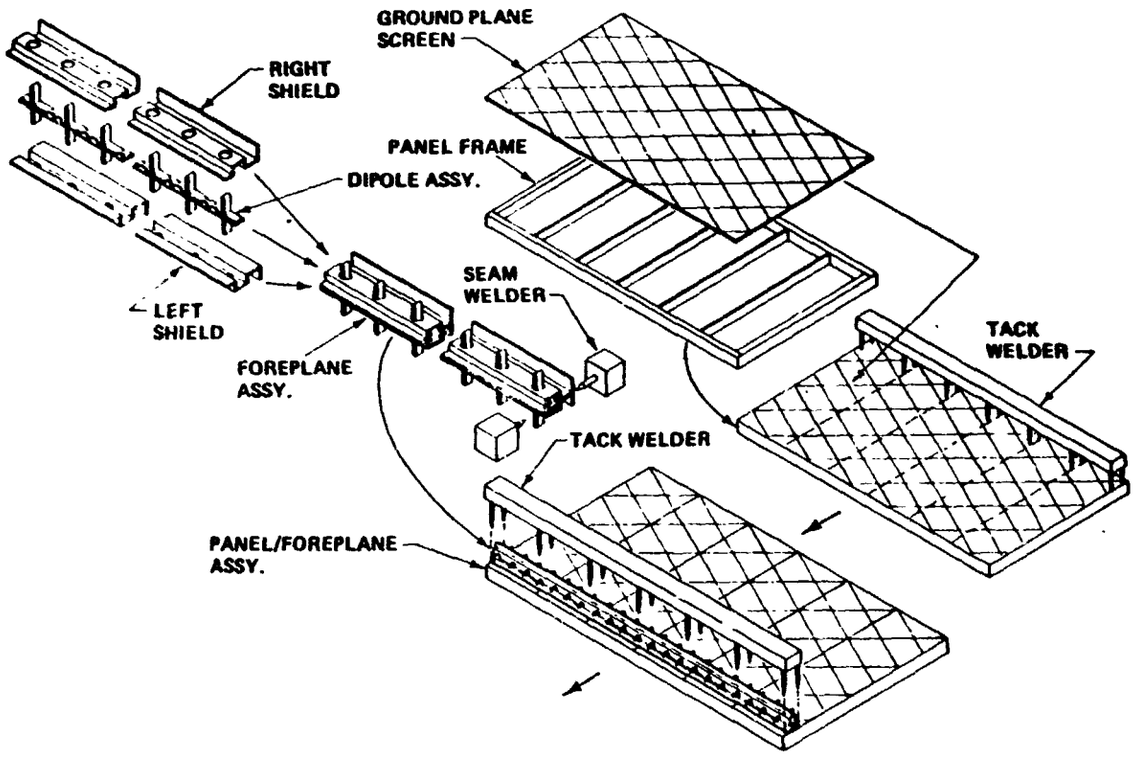

Figure 1.4-9. Rectenna Panel Fabrication Sequence

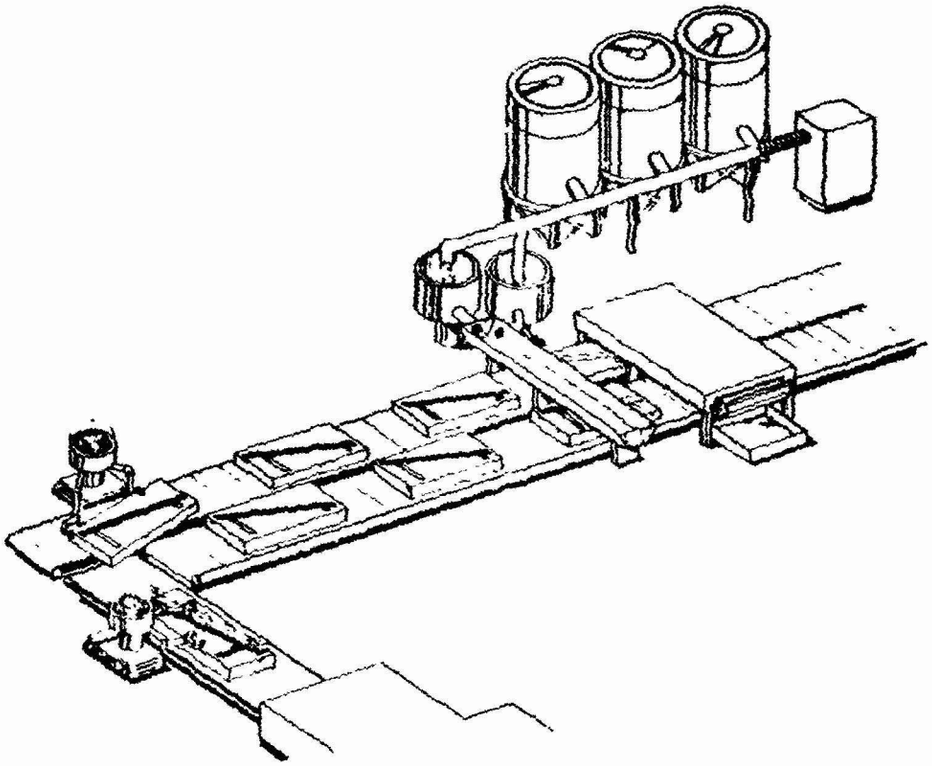

Figure 1.4-10. Arch Casting Factory

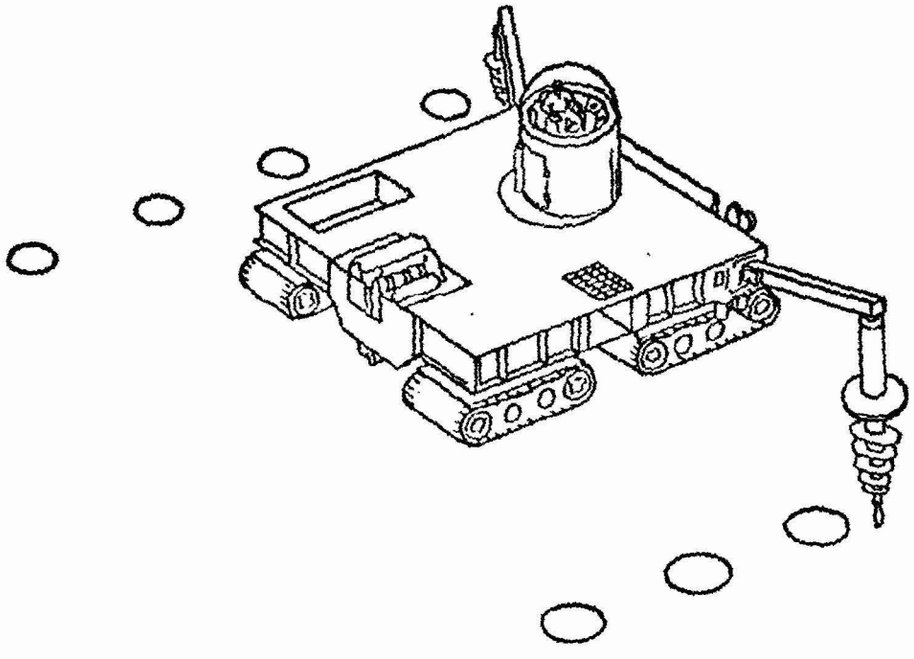

Figure 1.4-11. Foundation Machine

The machine shown here is assumed to cost $250,000, and is able to drill ten pairs of holes in an hour. The capital cost charged to one rectenna for this machine is $10.4 million. The total cost to drill all of the footings with this machine is $23.7 million.

Figure 1.4-12 shows the rectenna panels being delivered to the field and installed.

Five GW Rectenna Construction Concept. Figure 1.3-13 shows an artist's concept of the entire rectenna construction approach, using automated equipment for field erection of the many rectenna modules. Each "module" has three prestressed concrete "piers" or "arches" supporting two rectenna panels three meters wide and ten meters long. This panel size was selected as being the largest panel that could be conveniently moved over off-site roads. Our concept would build the initial panels at a staging and manufacturing area at the site, and so could be made larger. However, panels needed to replace any damaged by accident would have to be moved by highway to the damaged rectenna.

The six meter width of these panels was derived by using a double width version of the design described in the final briefing. This width is adequate to provide a roadway between rectenna rows of about four meters (13.12 feet) width and a clearance of over five meters (16.4 feet).

A "grass-roots" (detailed estimating) computer cost model was developed for the cost analysis. At the time we started it, it was not apparent which cost elements would be major and which would be minor. So it seemed that the best approach would be to divide the whole job into a number of pieces small enough to be amenable to analysis, and for which we could develop an opinion about the cost of doing that job, and then to estimate all of the kinds of costs involved in doing each small job thousands or millions of times.

The input data is stored in several data files. It takes over 1675 pieces of input data to run the program, and they must be in order, formatted exactly, and so on. However, using a text editor, any piece of data can be quickly changed.

The model flow is shown in Figure 1.4-14. The cost matrix has 12,375 cost bins to hold intermediate results. Most of the bins are empty, since only a few jobs are active at any time, and not every task generates every category of cost. This matrix is printed, so that detail data is available to permit trade-offs to be done at any level of cost accumulation.

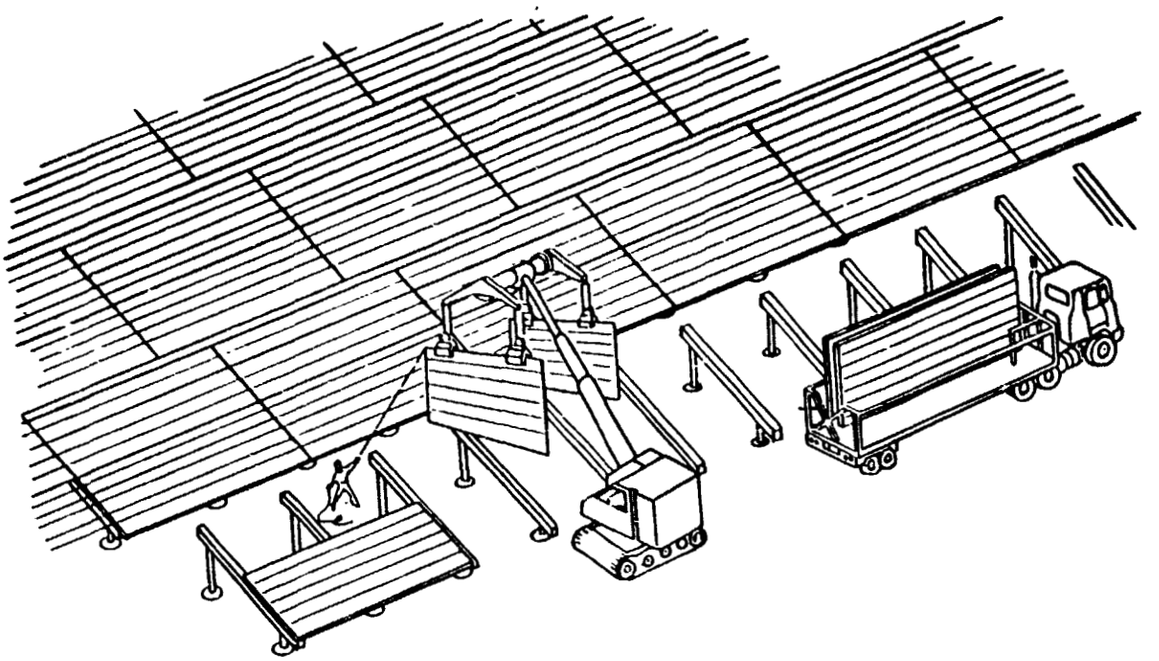

Figure 4.1-12. Panel Installer

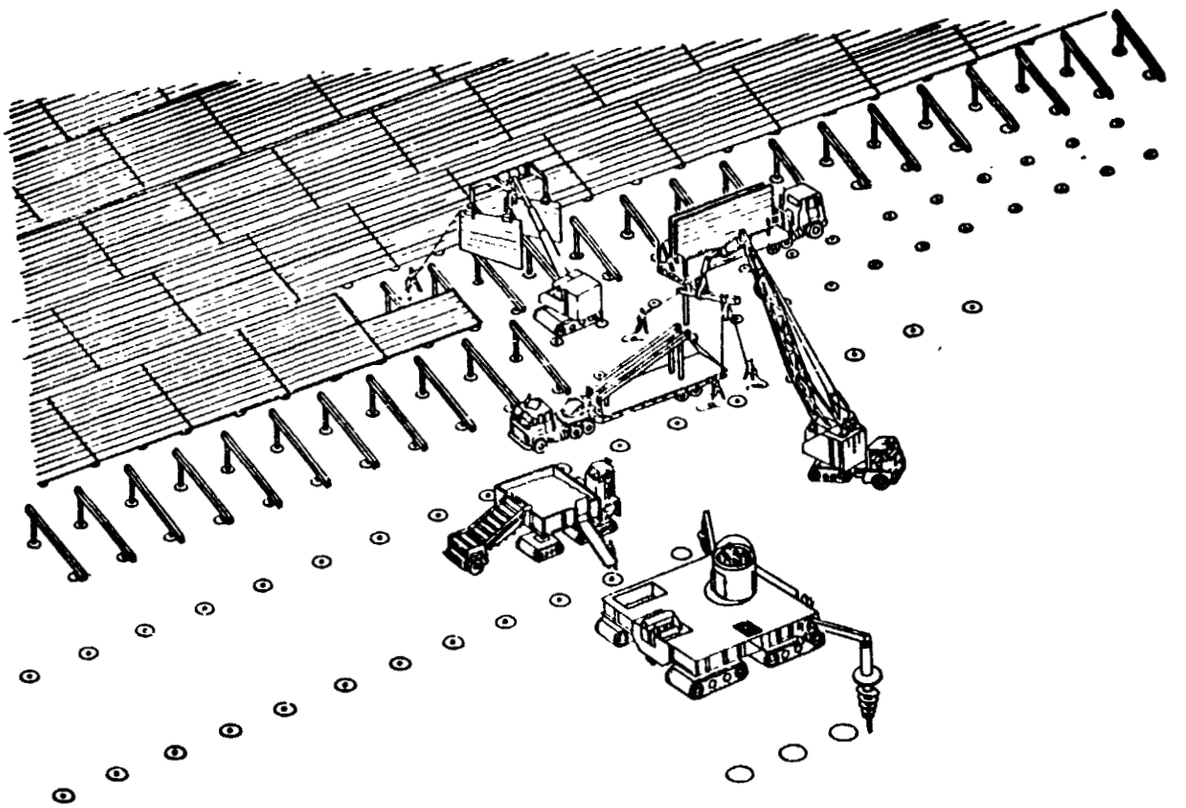

Figure 1.4-13. GW Rectanna Construction Concept

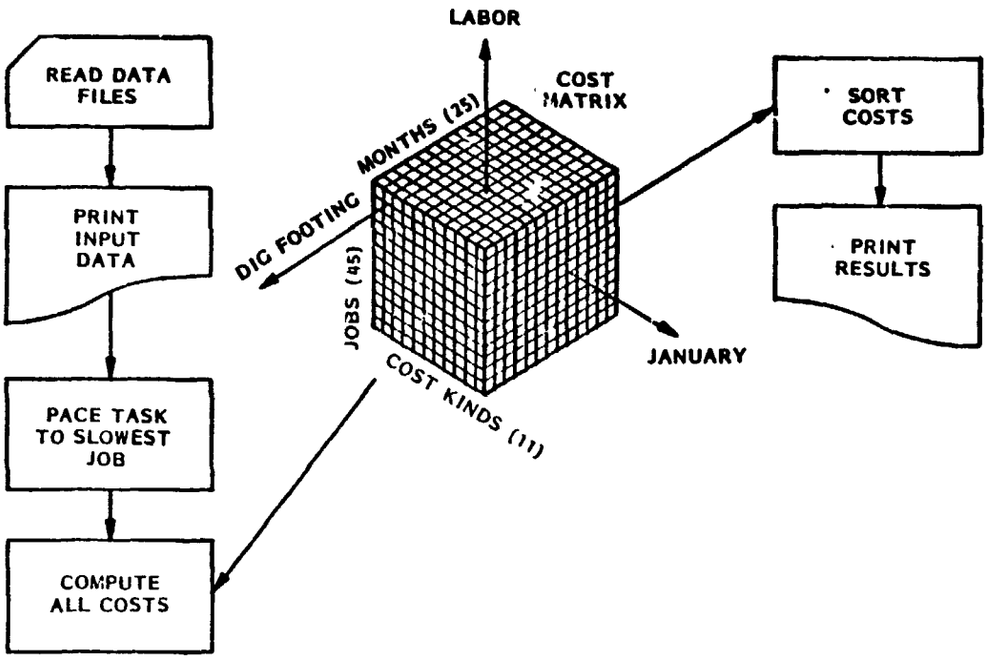

Figure 1.4-14. Operation of the Cost Model

Cost results are summarized in Table 1.4-3 and Figure 1.4-15. The total SPS ground system cost is about $2 billion. This cost excludes land and development of the rectenna and associated special purpose equipment.

About one-third of the ground system cost is in the ground power distribution and transmission. The other two-thirds of the cost are in the rectenna itself; this includes the cost from the dipole elements up to the wiring of the converter stations.

The bulk of the rectenna cost is in three materials:

(A)	Diodes	$298M
(B)	Steel	449M
(C)	Aluminum	267M
		$1,014M

Labor and capital costs are very low by comparison.

Table 1.4-3. SPS Ground System Cost (Summary of Major Equipment, Buildings, Material and Labor)

TYPE	SENSITIVITY	TOTAL COST (M$) (1977 DOLLARS)
RECTENNA		
MATERIAL:		
DIODES	4¢/DIODE	298
STEEL IN PANELS	15.8 Kg/m²	349
ALUMINUM BUSBARS (.02" x 0.5")	165,000 METRIC TONS	267
STRUCTURE		
CONCRETE (6 x 10 METER MODULE)	9 METRIC TONS/MODULE	81
STEEL (REINFORCING)	300 Kg/MODULE (100 Kg/ARCH; 3 ARCHES/MODULE)	100
LABOR		50
CAPITAL COST	(TYPICAL MACHINE LIFE IS 5 YEARS, COST TO PROJECT ONLY DURING USE)	40
MISCELLANEOUS		175
	TOTAL RECTENNA COST	1360
GROUND POWER DISTRIBUTION AND TRANSMISSION (PER SPS PHASE III FINAL REVIEW)		630
	TOTAL SPS GROUND SYSTEM COST (EXCLUDING LAND AND DEVELOPMENT COST)	1990

SPS-2609

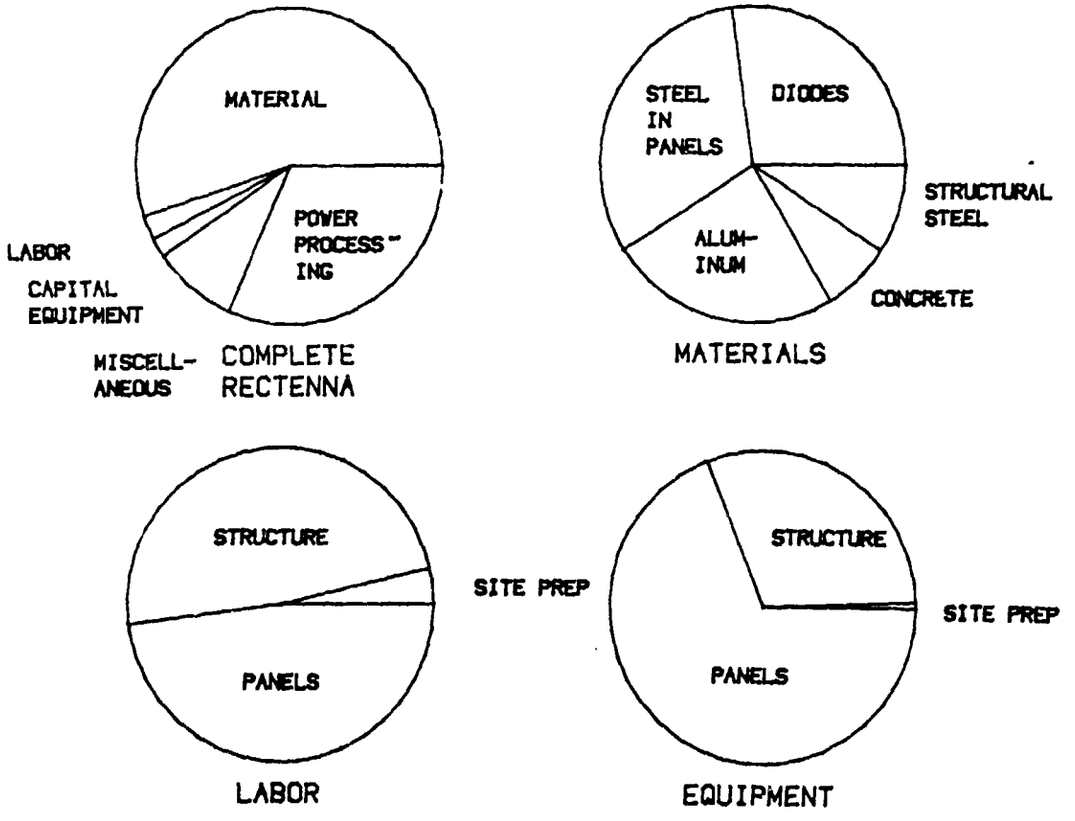

Figure 1.4-15. Rectenna Cost Distribution

1.5 Management and Integration

A comprehensive study of management and integreation was not conducted. A preliminary examination was made of mission operations; this item was assigned WBS #1.5.1.1

WBS 1.5.11 Mission Operations: Command and Control

The mission operations task assigned to TRW was to develop a representative set of command and control options for the SPS system, together with a proposed set of evaluation criteria for these options. In subsequent discussions it was decided that the way to present the options concisely and with the greatest clarity was to present a strawman concept and the options of interest to that concept.

In order to assure a common basis for communication in this discussion of a somewhat complex subject, a definition of some of the principal terms is provided in Table 1.5.11-1. Throughout this report the abbreviation "C&C" is used for the term "command and control."

The following is a summary of the work accomplished and of the results:

A. A preliminary analysis was made to define mission operations during construction of the first and subsequent Solar Power Satellites.

B. The C&C functions required for each major mission operation were enumerated and examined in some detail.

C. Next an assessment was made as to which element of the SPS system should have C&C authority for the various mission operation functions. As a result of this analysis and assessment five types of C&C centers were established as shown in Table 1.5.11-2. Four of these are located in system segments which will have control centers for their internal operations and the mission operations C&C will be an additional task for that control center. The fifth center, the Mission Control Center (MCC), is an independent center created specifically for control of mission operations. This center will be the central authority for mission operations and will coordinate the efforts of the other centers. In the case of the Rectenna Command and Control Center there will be a center for each rectenna (and its corresponding SPS).

D. The following ground rules were utilized in allocating C&C responsibility to the various control centers.

Table 1.5.11-1. Definitions

- MISSION OPERATIONS – OPERATIONS OF ALL ORBITAL ELEMENTS OF THE SPS SYSTEM INCLUDING THE TRANSPORTATION VEHICLES WHICH TRAVEL AMONG THESE ELEMENTS

- MISSION OPERATION COMMAND AND CONTROL – THE COMMAND AND CONTROL OF MISSION OPERATIONS. THIS INCLUDES THE RECEPTION AND INTERPRETATION OF STATUS DATA (PREDOMINANTLY TELEMETRY DATA) TO DETERMINE ANY NECESSARY COMMANDS AND THE IMPLEMENTATION OF THESE COMMANDS. ORBITAL AND TRAJECTORY TRACKING IS ALSO INCLUDED IN THIS TASK

- COMMAND AND CONTROL CENTERS – CENTERS WHICH HAVE BEEN DELEGATED AUTHORITY FOR COMMAND AND CONTROL OF SELECTED MISSION OPERATIONS

- MISSION CONTROL CENTER (MCC) – THE COMMAND AND CONTROL CENTER WHICH HAS CENTRAL COMMAND AND CONTROL AUTHORITY FOR MISSION OPERATIONS

Table 1.5.11-2. Command and Control Centers

1. LAUNCH AND RECOVERY COMMAND AND CONTROL CENTER
2. LEO BASE COMMAND AND CONTROL CENTER
3. GEO BASE COMMAND AND CONTROL CENTER
4. RECTENNA COMMAND AND CONTROL CENTER
5. MISSION CONTROL CENTER

1. To the extent practical, cor rol authority was delegated to provide local autonomy. For example, the LEO Base Control will not only be responsible for all construction opeations on the base, but also for such mission related tasks as docking, unloading, and relaunch of the HLLV orbiter stage. The latter tasks would, of course, be coordinated with the MCC.

2. The MCC as well as the other control centers will be elemen*s of an organization which tiers down from a central authority that controls the total program and delegates authority to the various elements. The MCC will depend on the other elements to perform their functions such as provide payloads, crews, propellant, etc., on schedule.

3. This central organization will probably be a matrix type, i.e., although one element may be responsible for all LEO base operations, it may have to depend on another element for recruiting, training and scheduling the crews which will operate the base.

4. The MCC will be located on the ground. Since all the functions assigned to it can be performed on the ground as well as from an orbital location, the expense of transporting equipment and crews to an orbital location is not warranted.

E. Table 1.5.11-3 is a summary of the command and control functions defined and of their assignment to the control centers using the ground rules listed above.

F. Upon completion of the definition and allocation of C&C responsibilities to the control centers, a review was made of the many diverse responsibilities (functions) assigned to the MCC. The objective of this review was to organize and categorize these functions to make efficient use of resources. The functions were divided into the six categories shown in Figure 1.5.11-1 by grouping together those functions having similar requirements for the following resources; type of information required, technical expertise, equipment and software.

Four of these categories (i.e., Transportation Vehicle C&C, SMIT C&C, Operational SPS C&C, and Communication Satellite C&C) each require the information, expertise, etc. to operate these space vehicles. However, the space vehicles are

Table 1.5.11-3. Command and Control Functions Required During Mission Operations

SYSTEM ELEMENT	LOCAL COMMAND AND CONTROL CENTERS AND FUNCTIONS	MISSION CONTROL CENTER FUNCTIONS
LAUNCH AND RECOVERY SITE – HLLV AND PLV	LAUNCH AND RECOVERY C&C CENTER – PREPARE AND LAUNCH VEHICLES, PAYLOADS AND CREW – LANDING AND/OR RECOVERY	– LAUNCH AND RANGE COORDINATION – MIDCOURSE CONTROL TO LEO – BOOSTER STAGE SEPARATION AND CONTROL
LEO BASE – HLLV AND PLV – OTV – EOTV	LEO BASE C&C CENTER – BASE AND SPS MODULE CONSTRUCTION MANAGEMENT – HLLV; PLV; OTV – DOCKING AND UNLOADING – PREPARE AND LAUNCH VEHICLES, PAYLOADS, CREWS – EOTV – LAUNCH PREPARATION AND LAUNCH	– HLLV; PLV; OTV – RENDEZVOUS COORDINATION – LAUNCH COORDINATION – MIDCOURSE CONTROL – OTV BOOSTER SEPARATION AND CONTROL – EOTV – LAUNCH COORDINATION – MIDCOURSE CONTROL – LEO BASE – TRACKING, STATIONKEEPING, CONTINGENCY RESOLUTION
GEO BASE – OTV – EOTV – SPS – MAINTENANCE VEHICLES	GEO BASE C&C CENTER – BASE AND SPS CONSTRUCTION MANAGEMENT – OTV – DOCKING AND UNLOADING – PREPARE AND LAUNCH VEHICLES, PAYLOADS AND CREWS – EOTV – RENDEZVOUS AND BERTHING – SPS – MAINTENANCE OPERATIONS – MAINTENANCE VEHICLES – PREPARE AND LAUNCH VEHICLES, CREWS AND PAYLOADS – DOCKING AND UNLOADING	– OTV; MAINTENANCE VEHICLES – RENDEZVOUS COORDINATION – LAUNCH COORDINATION – MIDCOURSE CONTROL – EOTV – RENDEZVOUS COORDINATION – SPS – ACTIVATION AND COORDINATION – MAINTENANCE COORDINATION – GEO BASE – TRACKING, STATIONKEEPING, CONTINGENCY RESOLUTION
OPERATIONAL SPS	RECTENNA C&C CENTER – MONITOR SPS POWER PERFORMANCE	– C&C, TRACKING, STATIONKEEPING – POWER SUBSYSTEM C&C – ECLIPSE SCHEDULES/ANTENNA POINTING – MAINTENANCE VEHICLES DOCKING AND LAUNCH
COMMUNICATIONS SATELLITES		– C&C, TRACKING, STATIONKEEPING

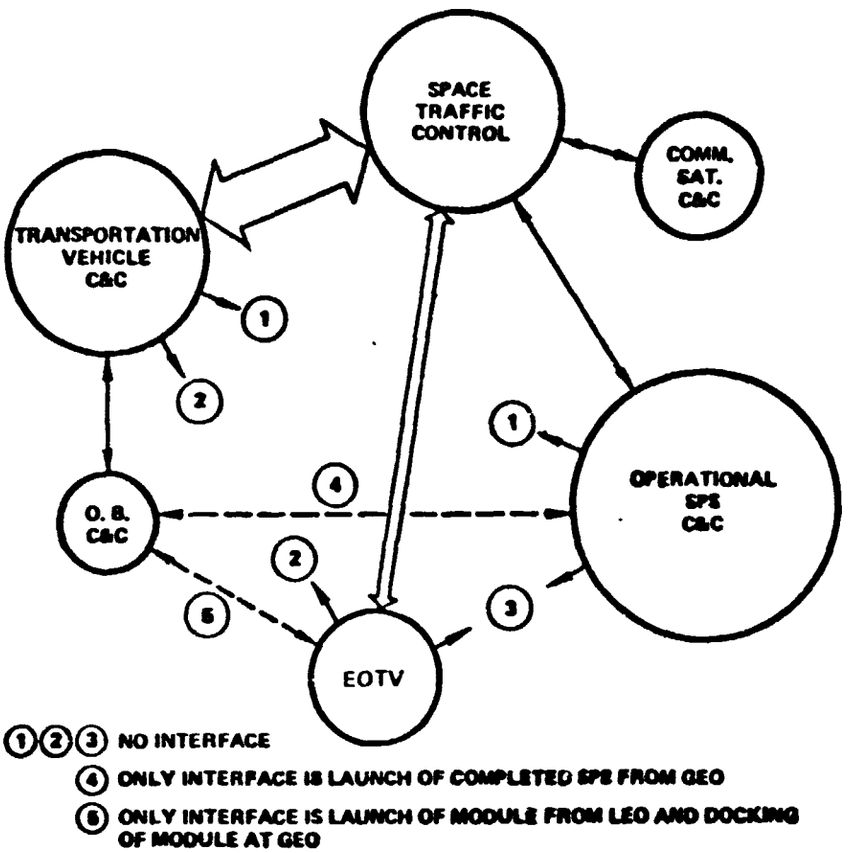

Figure 1.5.11-1. Categories of C&C Functions Assigned to Mission Control Center

so widely different (i.e., attitude control, propulsion, power, etc.) that specially trained crews, widely different software unique procedures will be required. Hence, separate categories were established.

Space Traffic Control has the responsibility to insure that the movements of all space vehicles and other space elements are coordinated and controlled such that they do not interfere with each other or with other space traffic and are not impacted by space debris or meteors. This requires tracking information plus personnel and software capable of projecting this information into future traffic situations.

Orbital Base C&C - It is anticipated that the orbital bases (which may be considered as a type of spacecraft) will be autonomous, however, the Mission Control Center may be called upon to perform tracking, stationkeeping, resposi-tioning, anomaly support and other selected functions in a back-up mode.

The size of the circles indicates a preliminary estimate of the relative magnitude of the effort required for accomplishing the tasks in each category. Similarly the thickness of the arrows indicates the magnitude of the interface between each category.

G. Figure 1.5.11-2 summarizes the results of the analyses and illustrates the relationships within the SPS system C&C strawman concept. The local C&C areas which are collocated with major system elements are shown by shaded circles. For clarity each of the six categories of MCC functions are shown separately as cross-hatched circles. The clear circles represent satellites and the large clear arrows represent transportation vehicles, all of which are parts of the SPS system. The annotated line arrows indicate the principal type of interface among the control centers and elements. Space Traffic Control will interface with all other centers and elements, however, these interfaces are not shown in order to simplify the figure.

H. The strawman C&C concept is further defined by the following configuration of the MCC facilities:

1. One facility which includes the Transportation Vehicle C&C and Space Traffic Control function categories. These are the first two facilities needed

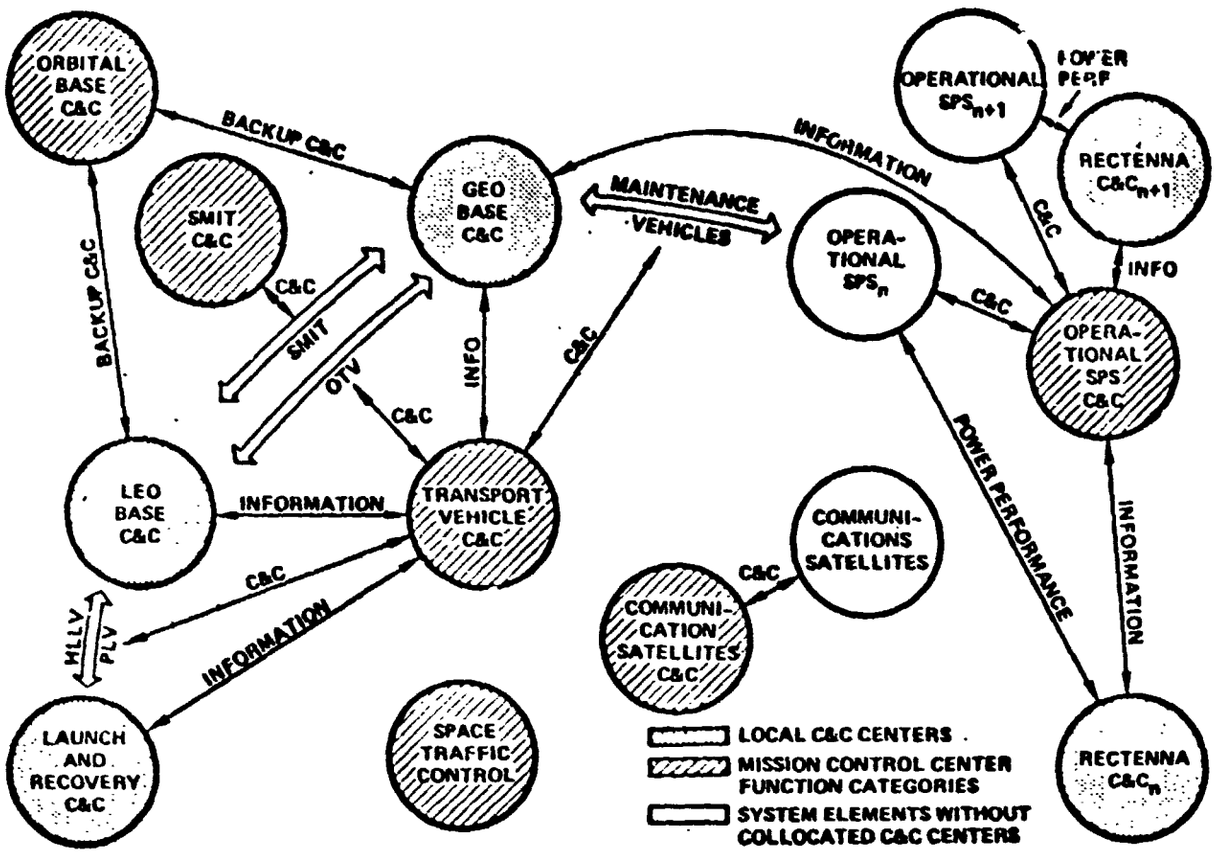

Figure 1.5.11-2. C&C Center Relationships to Major System Elements and to Each Other

during the construction of LEO, GEO and the first SPS modules. Also as shown in Figure 1.5.11-2 they have the busiest interface.

2. A second facility which contains the other function categories Orbital Base C&C, SMIT C&C, Communication Satellite C&C and the Operational SPS C&C. Facilities for these functions can be constructed in sequence as needed by the program.

3. As the number of operational SPS increases, capability for their control will also be provided at the first facility with the possibility that a third facility will be added which is dedicated to this function. Another possibility will exist when all SPS have been built, i.e., the SMIT control facility may be converted to this function also.

I. Various options to the strawman C&C concept will be evaluated during Phase II. These options are summarized as follows:

1. Assign C&C responsibilities differently among the local control centers and the Mission Control Center. Examples of this are:

   - HLLV and PLV midcourse trajectory control performed by Launch and Recovery C&C.

   - SMIT midcourse trajectory control performed by the LEO Base C&C.

   - Each Rectenna C&C Center have complete responsibility for C&C of its corresponding SPS instead of a power monitoring function with communication to the MCC for SPS C&C as in the strawman concept.

2. Eliminate the Orbital Base C&C function category in the MCC and make the bases completely autonomous, without ground back-up.

3. Modify the number of MCC facilities/locations. Due to the necessity for provision of continuous, reliable, power by the SPS system, redundant SPS command and control capability is provided in the present concepts. This includes two geographical locations as well as internal redundancy. The

magnitude of the SPS control tasks, with the resultant large numbers of crews and amounts of equipment involved were reasons for the recommendation of dual locations.

However, options to this preliminary configuration are:

- More or less redundancy
- Single location
  - Collocate with a local C&C centr such as Launch and Recovery C&C Center or a Rectenna C&C Center
  - Separate location
- Multiple locations
  - Collocate with local C&C centers
  - Modify the number of facilities and their locations as well as the groupings of the six categories of MCC functions within those facilities

4. The ground rule in item D3 of this report assumes that a central program authority has delegated mission operations responsibilities as defined herein to the MCC and local C&C centers. The definition of mission operations may be considered to encompass other responsibilities related to orbital operations and to assuring that these operations will be performed on schedule. This definition could include such responsibilities as orbital construction, as well as the logistics associated with providing cargo, propellants and crews on time. Therefore, another option to be considered is a redefinition of the responsibilities which are included in mission operations.

J. The options enumerated in Item I. will be evaluated during phase II using the following criteria:

1. Technical suitability - assurance that mission operations will be performed satisfactorily by the selected concept.

2. Cost - the total cost including hardware, software, personnel, real-estate, etc. will be a factor.

3. Schedule - the concept selected should be such that it can be provided in compliance with the total system schedule. Other schedule considerations include how well the concept lends itself to grouping the functions required

early in the program into the same facilities, also to conversion of facilities from functions which are no longer required to other functions (e.g., SMIT C&C to operational SPS C&C).

4. Interfaces - interfaces should be minimized by proper grouping of functions.

5. Redundancy/backup capability - the concept must provide assurance of control capability in the event catastrophic events disable a C&C facility. This factor should include consideration of providing back-up facilities at separae geographical locations.

2.0 SPS PROGRAM PLANNING ANALYSES

The SPS program is presently in a feasibility study and evaluation phase. Many program steps and activities will be needed to achieve successful program function. One of the tasks in this study was directed to identification and planning for the potential future of an SPS program. The analysis followed two converging paths as illustrated in Figure 2-1.

2.1 PROGRAMMATIC STUDIES

Analyses of the programmatic structure of an SPS program have resulted in the multi-step approach illustrated in Table 2-1. Each step will provide knowledge and technical confidence leading to a program decision to initiate the next step. If the appropriate technical confidence from any step is not achieved, then the approach would be modified or possibly the program terminated if major difficulties were encountered.

The purpose of the technology research phase is to develop confidence in the achievable technology performance in all the critical areas so that a much firmer assessment of SPS economics and environmental impact can be made. Listed in Table 2-2 are the principal objectives of a technology research program designed to obtain the necessary information.

Many of the technological advances needed for SPS are of an engineering nature, where the performance of the technology can be reasonably well forecast, but significant developments are still required in order to be able to construct SPS's at some meaningful rate and at an economic cost. These areas were termed engineering developments and cost verification. Certain of these, listed in Table 2-3, may present calendar time issues.

Many types of activities will be required to get from today's state of knowledge to a commercially acceptable SPS. Figure 2-2 presents a representative schedule.

The development test article must be initiated relatively early in order to support design of a prototype SPS. During the prototype design period, development of the production technology and production capability will continue. Space operations systems including launch vehicles and a prototype production space construction

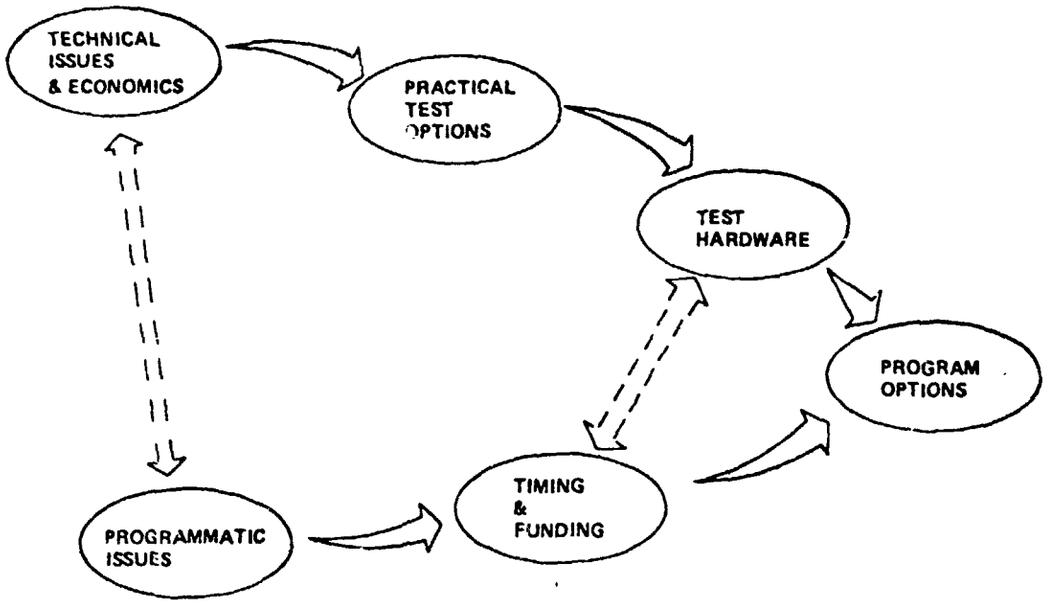

Figure 2-1 Program Option Definition

Table 2-1 SPS Development Phases

SPS 2478

STEP	KNOWLEDGE GAINED	TECHNICAL CONFIDENCE	PROGRAM DECISION
EXPLORATORY STUDIES (COMPLETE)	SYSTEMS CONCEPT OPTIONS	THERE ARE NO FIRST-ORDER TECHNICAL OR ECONOMIC BARRIERS TO EVENTUAL SUCCESS	PROCEED WITH SYSTEMS AND EVALUATION STUDIES
SYSTEMS STUDIES	CONCEPTUAL DESIGN CHARACTERIZATIONS OF SELECTED BASELINES; TECHNOLOGY PERFORMANCE OBJECTIVES	DESIGN APPROACHES EXIST THAT CAN PROBABLY ACHIEVE TECHNICAL AND ECONOMIC OBJECTIVES	INITIATE TECHNOLOGY RESEARCH AND CONTINUE EVALUATION STUDIES
TECHNOLOGY RESEARCH	ACTUAL TECHNOLOGY PERFORMANCE	TECHNOLOGY PERFORMANCE SUPPORTS SPS DESIGN APPROACHES	INITIATE ENGINEERING DEVELOPMENT AND COST VERIFICATION
ENGINEERING DEVELOPMENT AND COST VERIFICATION	SUBSYSTEMS AND SYSTEMS ENGINEERING PERFORMANCE AND PRODUCTION COST; ADEQUATE BASIS FOR SPECIFICATIONS	SPS DESIGN APPROACHES VALIDATED; PREFERRED APPROACHES SELECTED; SPS COST CONFIDENCE	INITIATE FULL-SCALE DEVELOPMENT
FULL SCALE DEVELOPMENT	SPS IS OPERATIONALLY SUITABLE AND ECONOMICALLY VIABLE	SPS CAN BE SUCCESSFULLY COMMERCIALIZED	ENTER COMMERCIAL PRODUCTION

SPS-2503

Table 2-2 SPS Technology Research—Priority Objectives

● DEVELOP SOLAR ARRAY TECHNOLOGIES INCLUDING ANNEALING	● DEVELOP INTEGRATED STRUCTURAL/ ELECTRICAL POWER DISTRIBUTION TECHNOLOGY FOR LONG-LIFE VACUUM OPERATION WITHOUT ELECTRICAL BREAKDOWN
● DEVELOP SOLAR CELL/ARRAY PRODUCIBILITY APPROACHES	● DEVELOP HIGH-EFFICIENCY, HIGH-SPECTRAL-PURITY RF GENERATION AND RADIATION TECHNIQUES
● DEVELOP SWITCHGEAR AND POWER PROCESSOR TECHNOLOGY	● DEVELOP PRECISION PHASE CONTROL TECHNOLOGIES
● DEFINE PLASMA EFFECTS OF HIGH-VOLTAGE SOLAR ARRAY OPERATION AND ELECTRIC PROPULSION OPERATION; DEVELOP SYSTEM DESIGN APPROACHES ACCORDINGLY	● DEFINE EFFECTS OF IONOSPHERE AND SPACE PLASMAS ON POWER TRANSMISSION AND PHASE CONTROL; DEVELOP DESIGN APPROACHES ACCORDINGLY
	● DEVELOP HIGH-EFFICIENCY POWER RECEPTION AND COLLECTION TECHNIQUES
● DEVELOP PRACTICAL, LOW-COST MATERIALS TECHNOLOGIES FOR SPS APPLICATIONS	● DEVELOP SPACE FABRICATION AND ASSEMBLY TECHNOLOGIES

Table 2-3 Engineering Development and Cost Verification—Long-Lead Items

SPS-2504

- DEVELOPMENT TEST ARTICLE
- SPACE VEHICLE ENGINES: BOOSTER; ORBIT TRANSFER CHEMICAL & ELECTRIC; SSME IMPROVEMENTS
- THERMAL SYSTEMS: VEHICLE TPS; THERMAL COATINGS; ACTIVE THERMAL CONTROL
- SOLAR ARRAY PRODUCTION SYSTEMS
- RF AMPLIFIER & SUBARRAY PRODUCTION SYSTEMS
- SPACE CONSTRUCTION: CREW HABITATS & CREW SUPPORT SYSTEMS; CONSTRUCTION EQUIPMENT; BASE LOGISTICS SYSTEMS

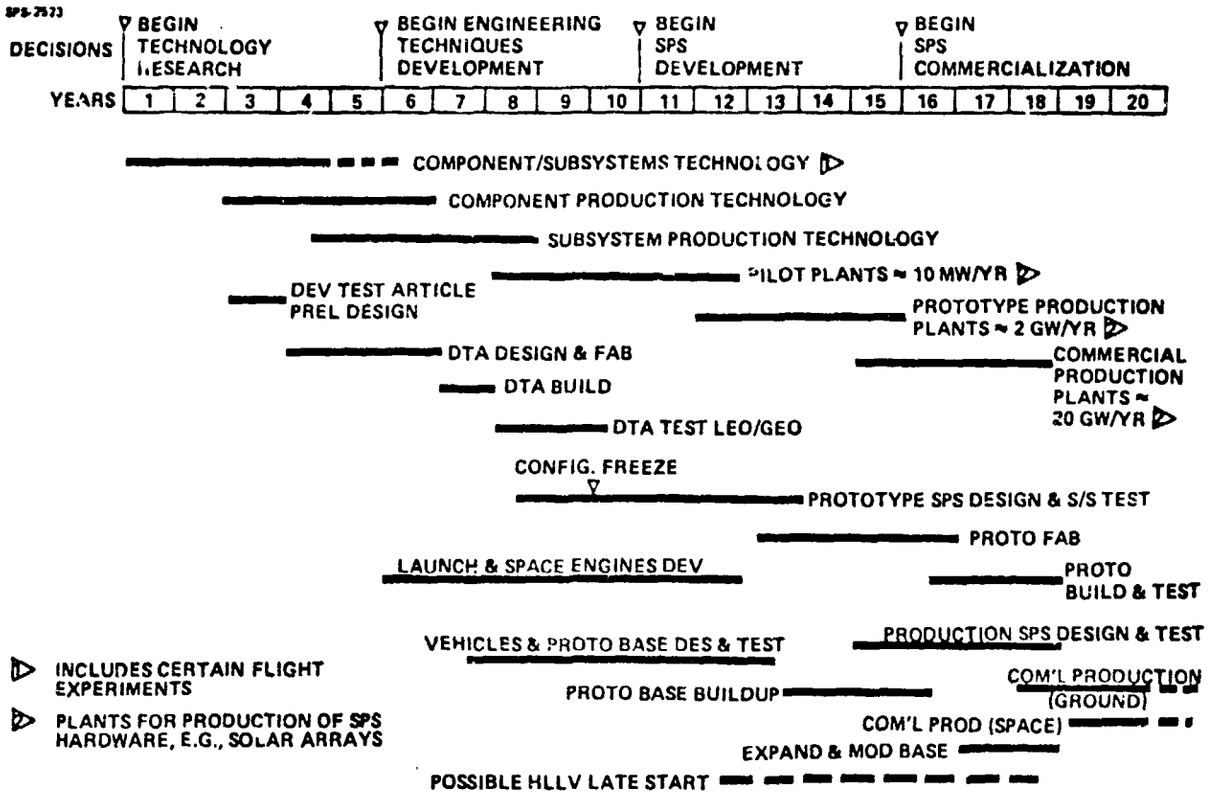

Figure 2-2 SPS Development Program Structure (Early Commercialization)

base must be developed in order to support the prototype program. Depending on the size of the prototype, it may be possible to have a late start on the heavy lift launch vehicle to spread out the space vehicle systems development costs. Shown on the lower righthand portion of the schedule is the initiation of a commercial production program.

The principal activities shown on the schedule chart are represented in Figure 2-3 in a preliminary estimate of funding requirements. It is clear that the major funding requirements occur when beginning the development of space vehicles and space construction bases.

There are a number of options available to smooth or reduce the funding peak shown in the previous figures. Some of the principal ones are tabulated in Table 2-4. The cost deferrals have consequences that may not be particularly desirable, but do offer the potential of reducing funding peaks.

The programmatics analysis reached the following principal conclusions:

- A development test article is needed early to provide design data for the SPS prototype design. It should be of the size to permit early funding; 1 megawatt or less. It is possible that the development test article will be constrained by photovoltaic's production capability, but it does not appear important that the development test article represent a final solar blanket configuration.

- We have identified the need for an SPS prototype, but there is still a major uncertainty in how large the prototype should be. It seems clear that whatever size prototype is selected, it should provide efficient power transfer. If it is a low power system it will still have a large transmitter aperture.

- The major funding requirements arise from development from space bases and heavy lift launch vehicles. Some cost deferral options exist to reduce the peak funding to a degree, but their benefits in an economic sense are quite dubious unless it is expected that the completion of the prototype would result in a decision not to proceed with commercialization of SPS'. If commercialization proceeds, then the economic cost of these deferrals tends to exceed their value.

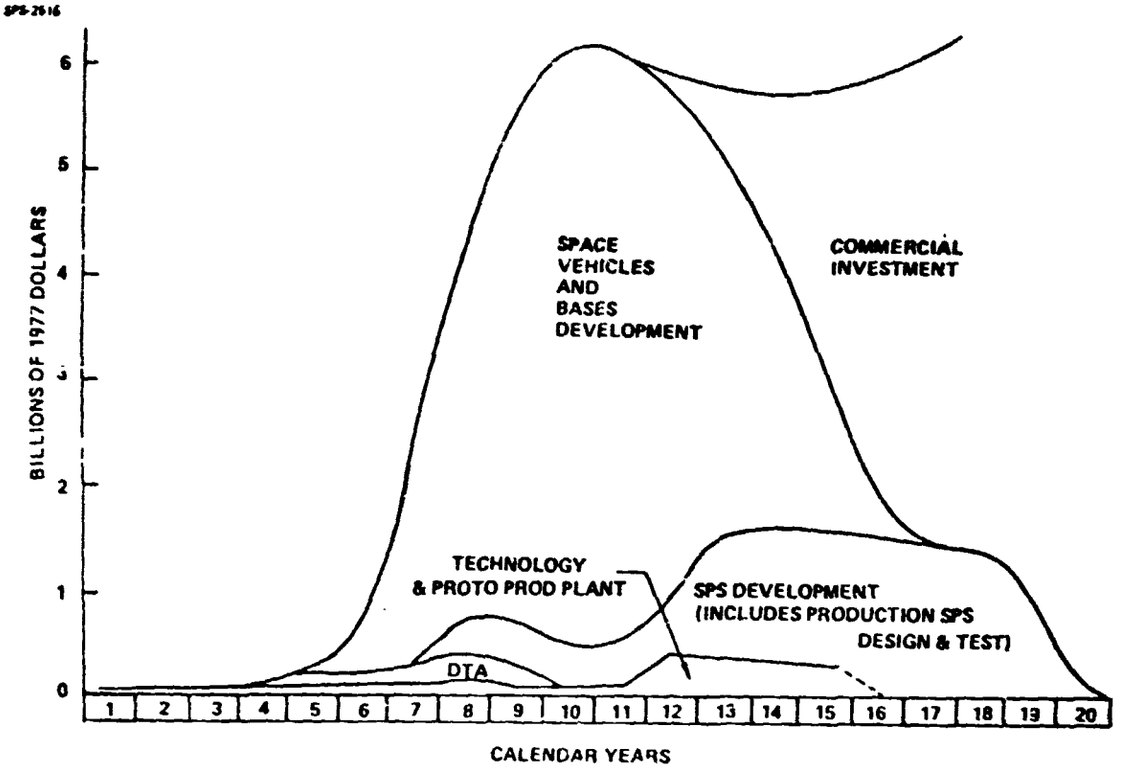

Figure 2-3 General Nature of Non-Recurring SPS Funding

SPS-2501

Table 2-4 Cost Deferral Options

ITEM	AMOUNT DEFERRED (ROM)	COST OF DEFERRAL	CONSEQUENCE OF DEFERRAL
DEFER MAIN COMMERCIALIZATION BUILDUP UNTIL PROTOTYPE TESTS COMPLETE	$30-$40B; 5 YEARS, SOME IS COMMERCIAL	$3 TO $5B	PRODUCTION SPS PROGRAM DELAYED 5 YEARS
DEFER HLLV TO SUPPORT ONLY COMMERCIAL PROGRAM; DO PROTOTYPE WITH SHUTTLE DERIVATIVE	$20B; 5 YEARS	$2 TO $5B; DEPENDS ON PROTOTYPE SIZE	HLLV COST CHARACTERISTICS NOT DEMONSTRATED WHEN COMMERCIAL INVESTMENTS REQUIRED
INITIALLY COMMERCIALIZE TO 5 GW/YR RATE	$5-$10B; UNTIL HIGHER RATE IMPLE-MENTED	UNIT COST SOMEWHAT HIGHER AT REDUCED PRODUCTION	SLOWER SPS CAPACITY BUILDUP

2.2 TEST-HARDWARE ANALYSIS

A schedule by which the previous developmental flight project elements could lead to a potential decision either to preceed with a large (2000 to 10,000 megawatt) SPS or to a smaller "commercial demonstrator" is shown in Figure 2-4. This schedule is generally compatible with the programmatically-derived schedule shown earlier.

Figure 2-5 expands on the overall developmental test program. Again, it leads to a potential decision point whereafter construction base and solar power satellite phase C/D might begin. Essential for this decision point are accomplishment of the large aperture test satellite, shuttle sortie flights, developmental test article, etc. In addition, SPS environmental standards must be set. It is also recommended that a high efficiency, 70 kilowatt (full size) klystron be tested on the ground, and that a prototype of the production line intended to produce high volume, low cost solar cells and arrays should have been demonstrated. Near the end of the "SPS and construction base phase C/D", qualification flight of actual SPS and construction base parts should take place. Two years are allowed for build up of the construction base before construction of SPS #1, transfer to geosynchronous orbit, a make-operable period, etc. Again, at the decision point shown it might be decided to proceed instead with a large commercial demonstrator or some other SPS percursor unit. However, it is felt that at the decision point, insofar as technical confidence is concerned, a full size unit could be required and built.

Figure 2-6 shows a path for the developmental test effort related to a shuttle size microwave power transmitter subarray. By selecting a size of 3.0 meters per side, the subarray will fit the shuttle bayload bay in a position normal to the acceleration vector. The subarray would be tested in a microwave anechoic chamber and a vacuum chamber, where phenomena such as multipactor, heat rejection, etc. could be investigated. It would be used in a microwave power transmission ground-to-ground test range, shown here as 30 meters on a side (hence with 100 subarrays) under the control of a pilot transmitter located on a rectenna panel oriented normal to the beam some distance away. The subarray would fly on a high power element sortie test flight which could include test of electric thruster panels requiring approximately the same power level as the subarray. Finally, the subarray would be the transmitting element of a solar

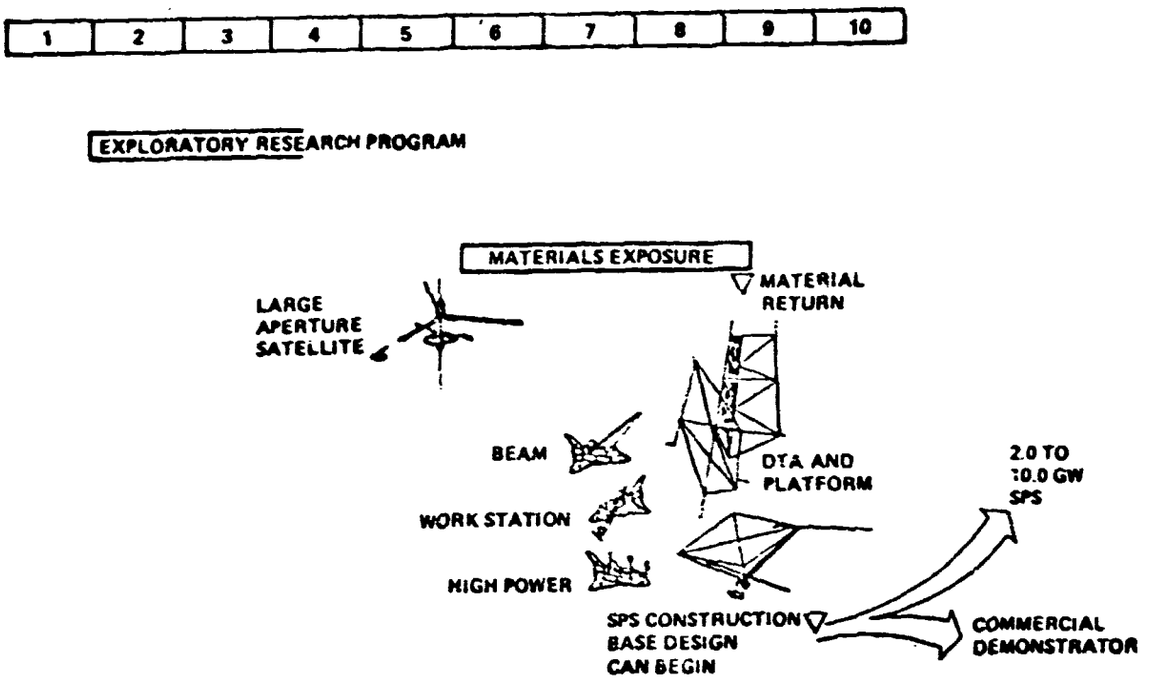

Figure 2-4 Development Program—Provides Decision Basis

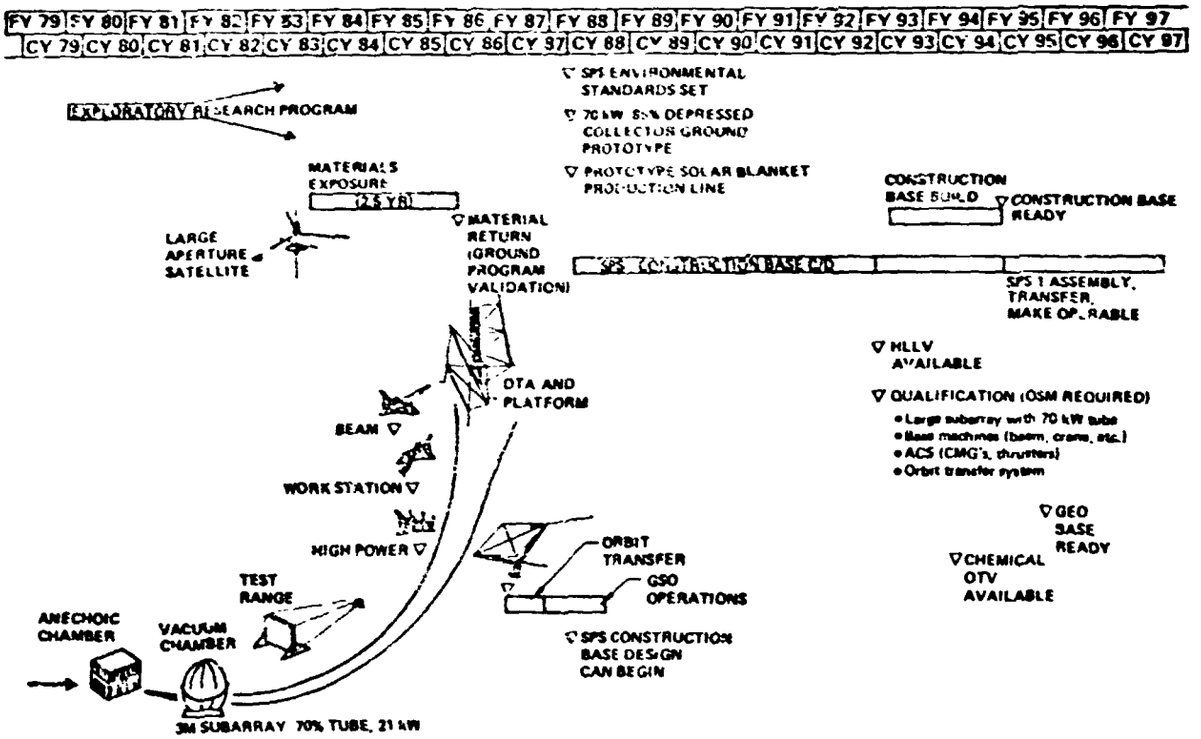

Figure 2-5 Overall Development Program

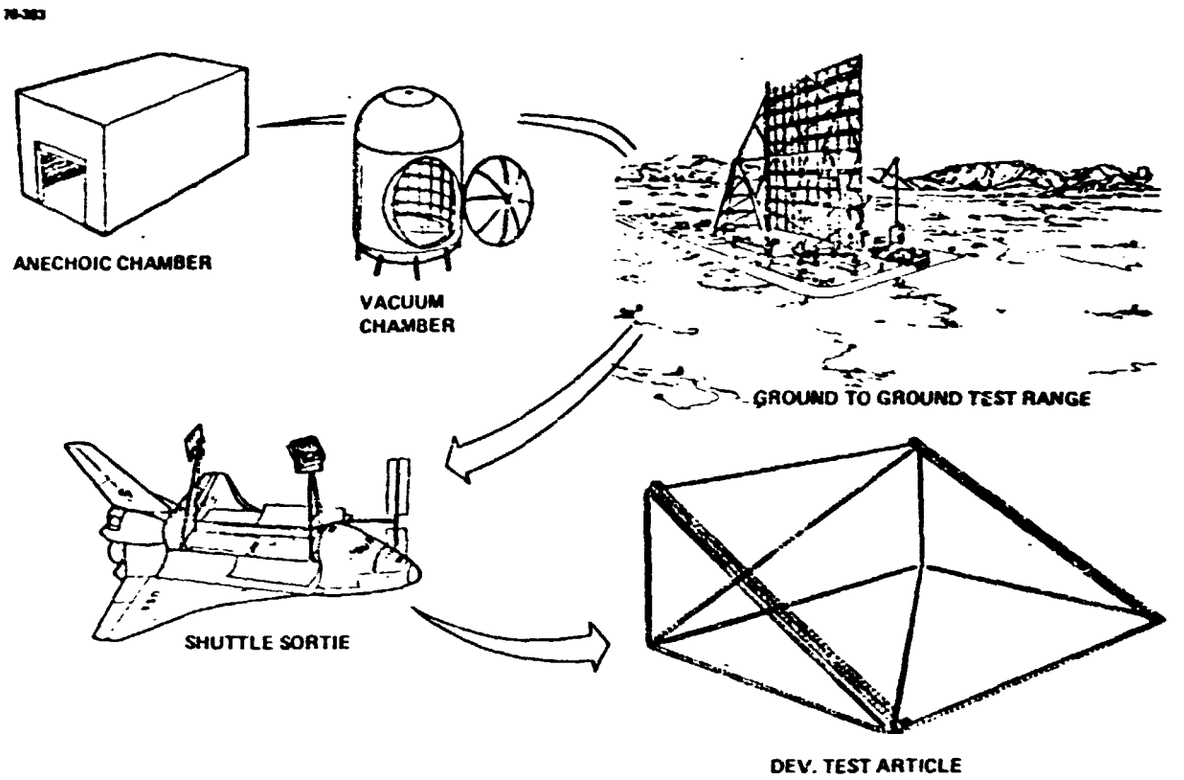

Figure 2-6 3.0 Meter Subarray

power satellite developmental test article. In the DTA shown, four subarrays are located at the corners of the array, mounted upon extendable/deployable secondary structure, which is in turn mounted upon a primary structure.

Shown in Figure 2-7 is installation of a 3.0 meter subarray into the transmitting group of the microwave ground-to-ground test range. The structure of the microwave test range transmitter supports the subarray elements and allows for tilt. In test, a tilt angle might be used such that the difference in distance from the subarray which is closest to the rectenna panel and that which is furthest from the rectenna panel would be the same as that anticipated in a full scale solar power satellite. That is, the angle would be much larger than the angle in a full size satellite but the distance difference would be the same. Trunnions are provided for this tilt. The framework includes power distribution, phase control distribution, etc. The run of coaxial cable or optical fiber between subarrays and to the central reference subarray, might use coils so as to equal the total distance involved in phase distribution aboard the full size satellite.

Figure 2-8 shows two potential methods of utilization for a "large aperture test satellite." On the left a test array such as the 30 meter square array of 100 subarrays, shown previously, transmits to space under control of the 9.0 meter dish of the large aperture test satellite. That is, the large dish on the satellite provides the pilot beam for phase control of the test array. The test array was provided with trunnions to permit tilt to the required near-vertical orientation. Operation could be accomplished through ionospheric strata heated by a transmitter such as that Arecibo. If frequency scaling was employed, and the power level at that transmitter was increased, andother possible utilization is to act as a pilot transmitter for a large array of SPS similar transmitter elements placed horizontally on the ground (as shown on the right). Here the test array is sufficiently large to directly heat the ionisphere without frequency scalling.

To position the four transmit/receive elements indicated on the previous chart, a geosynchronous satellite employing large extendable booms is shown in Figure 2-9. The number of booms is somewhat arbitrary. Two or four might be preferred. The transmit/receive dishes at the ends of the arms are baselined as being 2.0 meters in diameter. A 2.0 meter diameter transmit/receipt element is also located in the center of the satellite just below a 9.0 meter diameter antenna. This

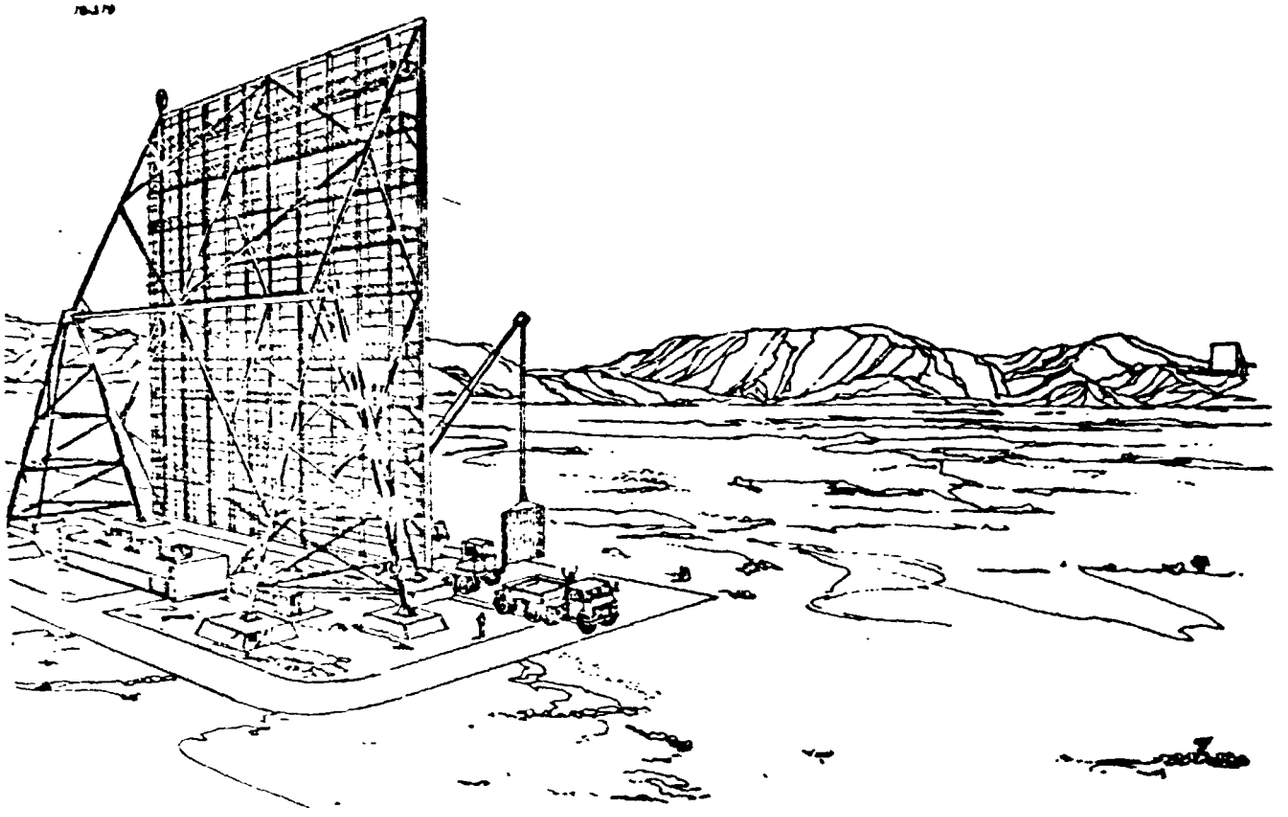

Figure 2-7 Ground-To-Ground Microwave Range

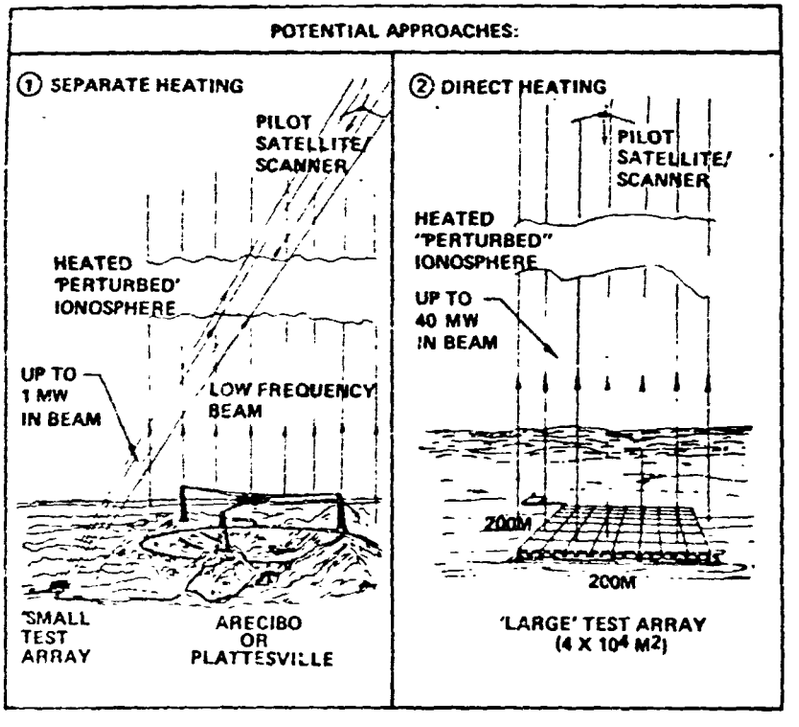

Figure 2-8 Ground-To-Ground MPTS Test System

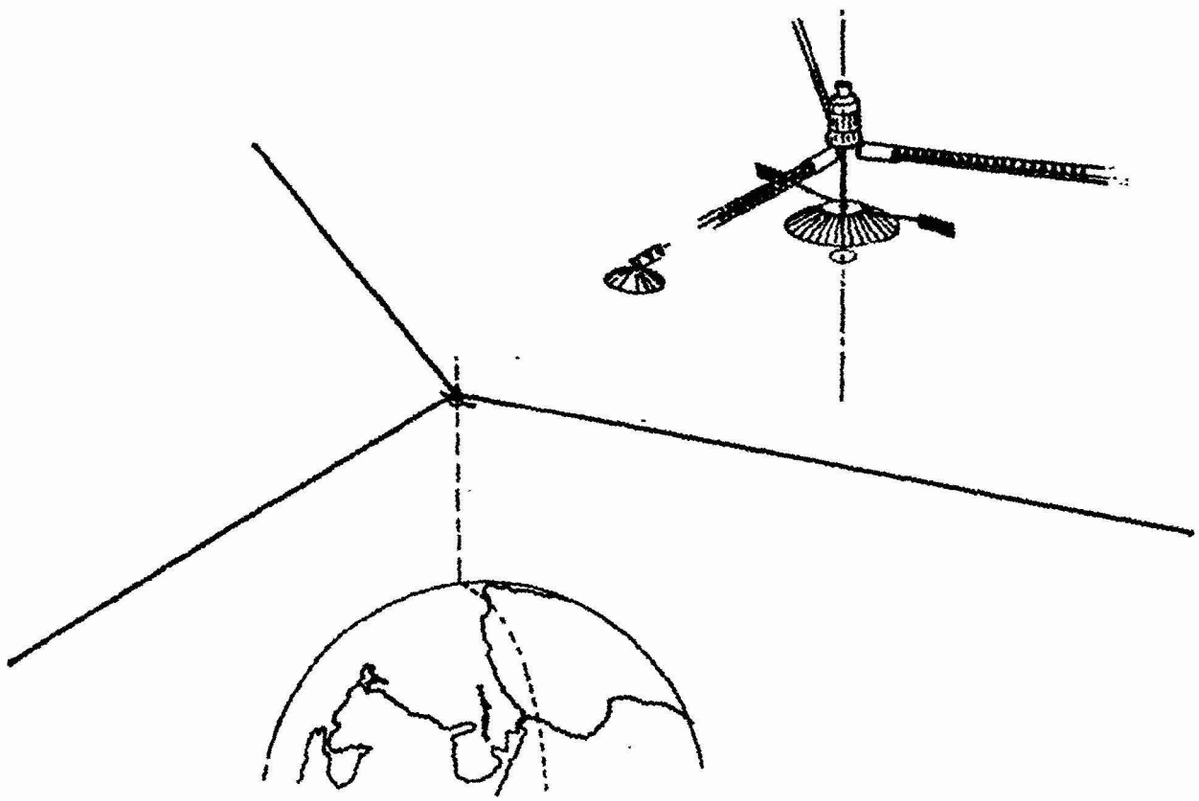

Figure 2-9 Large Aperture Satellite

larger antenna would be used for pilot control of a ground transmitter subarray group. The large aperture satellite would be launched to geosynchronous orbit by a shuttle and inertial upper stage. After arrival in geosynchronous orbit the cannisters for the extendable booms would be swung out and then the booms extended to locate the transmit/receive elements. The satellite would include solar power supply, attitude and stationkeeping control systems, command and control systems, etc. It would be advantageous to have a design lifetime of serveral years for this satellite. The transmitter tubes used for the 2.0 meter dishes might be 10 to 20 watts traveling wave tube of the type currently flying in many satellites and space probes.

The large aperture test satellite could also provide years of stable orientation in geosynchronous orbit. In the concept shown in Figure 2-10, samples of potential SPS components would be extended and deployed aboard that satellite by an accordian pull-out and lanyard system. These samples might include solar cells of various types, potential structural elements and materials such as composites, metals, plastics, etc. After the desired exposure period the samples would be drawn within the reentry body and hatches closed. The entire system, including the solid rocket return motor would be spun up upon a turntable; after reaching the required spin rate, springs would be used to kick the system free of the large aperture transmission satellite and achieve a save separation before firing the solid rocket motor. Approximately 5 1/2 hours later the reentry body would enter the earths' atmosphere. Here it would be recovered using proven space recovery techniques. The SPS candidate material samples could then be tested to determine the resultant degradation due to their exposure. During the exposure period in space, analyses should have been carried out to predict degradation mechanisms, ground test including radiation exposure should have taken place, so that the space operation provides a correlation and calibration of the ground test program.

Charging of spacecraft elements to high voltages during operation in geosynchronous orbit has been observed. Actual failures of some components have been observed. The solar power satellite with its large dimensions and high voltage power transmission systems may have additional problems resulting from the energetic plasma occurring during geomagnetic substorms. To investigate this phenomena a test satellite of large dimensions should be provided in geosynchronous orbit. The large aperture test satellite could serve this purpose since its extendable booms

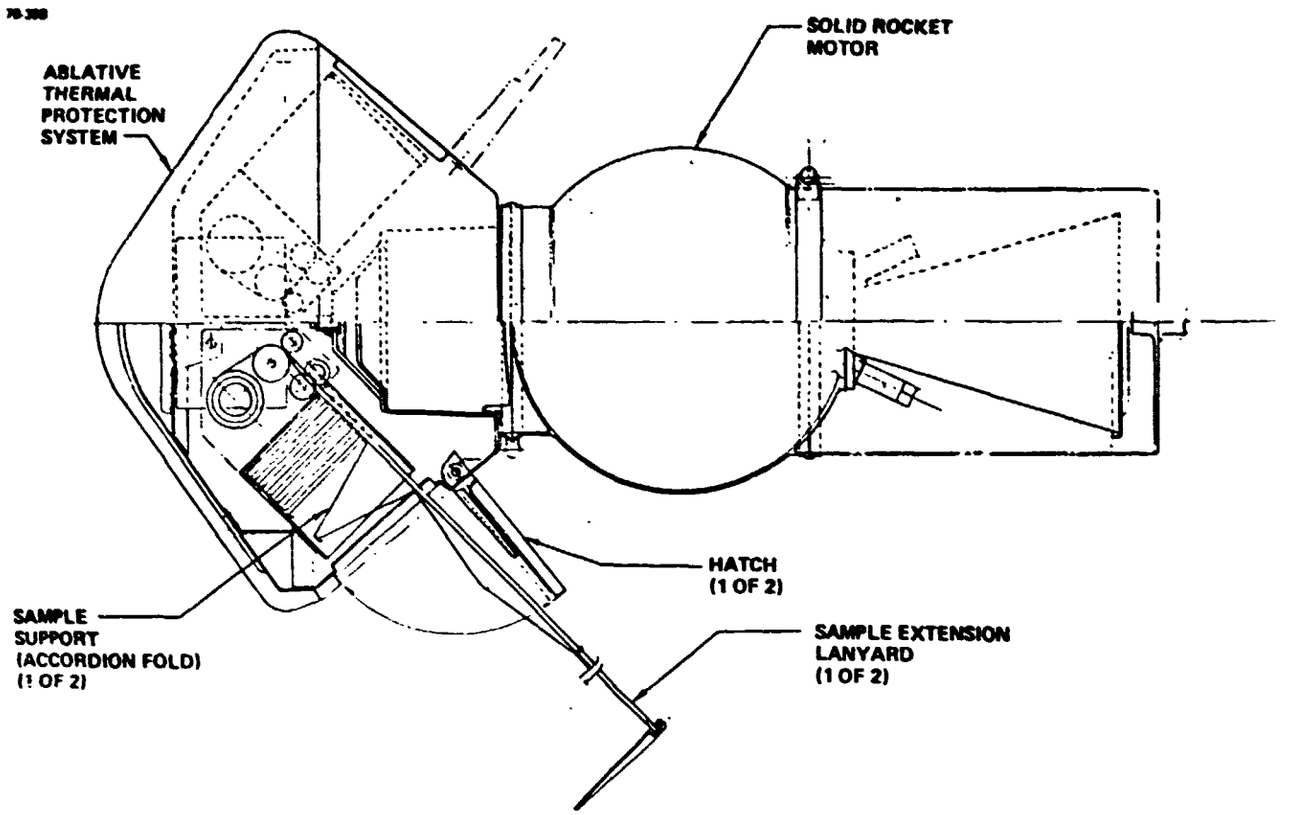

Figure 2-10 Sample Expose/Return System

might be up to three hundred meters or more in length. By providing a high voltage power supply, for example at forty thousand volts, and distributing this charge to the test panels located at the end of the arms, plasma interaction phenomena could be observed. Test instrumentation would be used to search out currents induced by the external plasma, arc discharges (potentially a source of electromagnetic interference), etc. Representative changing test provisions are shown in Figure 2-11.

The engineering development issues summarized in Table 2-5 were drawn from analyses of specialists who have been involved wth construction concepts for solar power satellites. They identify these as primary issues. The issues have been assigned to either analysis, ground test, shuttle sortie flights, or to (in most cases) a major flight project, such as the developmental test article.

The large aperture test satellite, launched by an IUS, serves to address the major questions of the "will SPS work?" type. That is, questions related to microwave transmission, susceptability of the SPS to the geosynchronous environment, and suitability of selected materials. The second category of developmental flights of the space shuttle would be those to ensure that a precursor major flight project succeeds. Finally, during actual design of the solar power satellite and its construction base, qualification flights for specific SPS components will take place. These might involve, for large components, the heavy lift launch vehicle.

Early flight tests will employ shuttle sorties.

Shown in Figure 1-12 is the first of three shuttle sorties flights which preceed the developmental test article. The beam builder shown extended from the payload bay incorporates not only provisions for the construction of the triangular beam but also for the attachment of rails which, on the developmental test article construction platform, allow modules of the DTA, after construction, to be moved to the side of the construction platform.

On the flight, depicted in Figure 2-13, either a 3.0 meter microwave transmitter subarray or an electric thruster module used to elevate the developmental test article to geosynchronous orbit would be tested. Power capability and physical arrangement of the system would allow either of these to be tested, but not

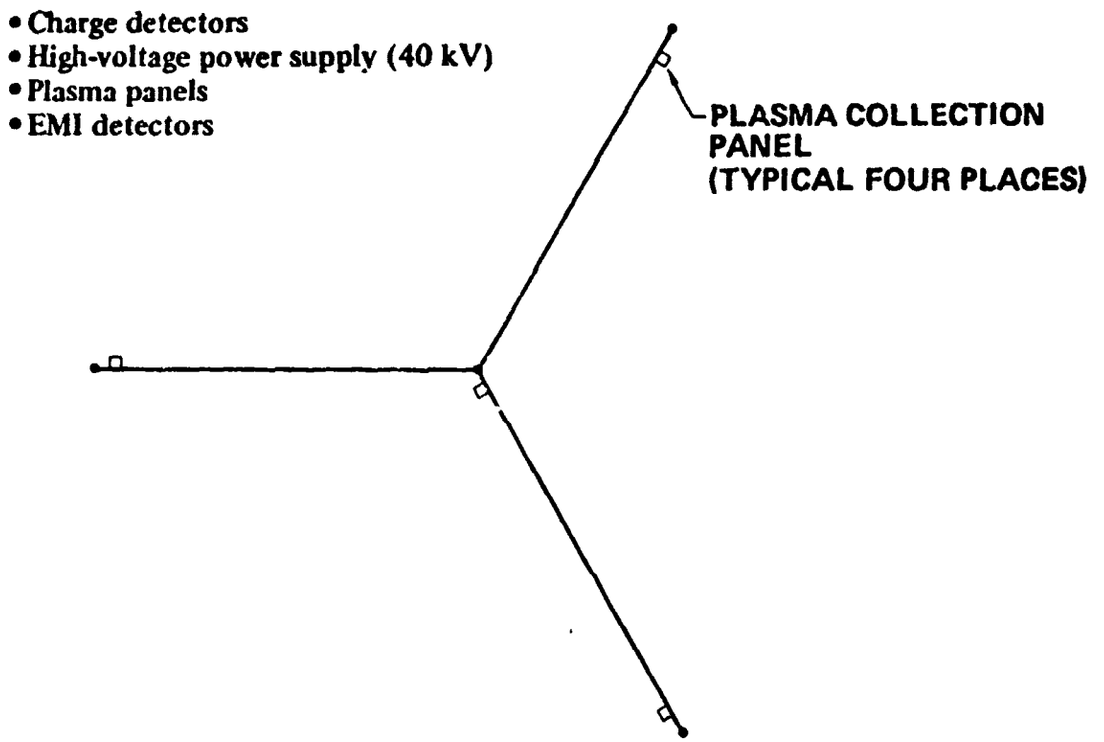

Figure 2-11 Charging Test Provisions: Concept

Table 2-5 Development Issue Assignment

78-344

(Construction)

ISSUE	ANALYSIS/GND. TEST	SHUTTLE SORTIE	MAJOR FLT. PROJECT
1. BEAM MACHINE RATE, RELIABILITY	ONE G UNITS	SHUTTLE SORTIE	INTEGRATION WITH "BASE"
2. JOINTS, BEAM HANDLING	NEUTRAL BOYANT	WORK STATION SORTIE	INTEGRATED OPS.
3. SOLAR ARRAY DEPLOYMENT		COMBINE WITH BEAM SORTIE (SMALL SCALE)	INTEGRATION WITH "BASE"
4. BUSBAR INSTALLATION			DEPLOY BUSBAR (DUMMY)
5. MODULE INDEXING			DEMONSTRATE
6. ANTENNA SECONDARY STRUCTURE			DEPLOYMENT, MOUNTING
7. SUBARRAY INSTALLATION			MOUNT ON SECONDARY STRUCTURE

(Maintenance)

KLYSTRON CHANGEOUT	NEUTRAL BOUYANT	POSSIBLE CHANGEOUT ON SORTIE	"ADVANCED" DTA COULD INCLUDE GANTRY

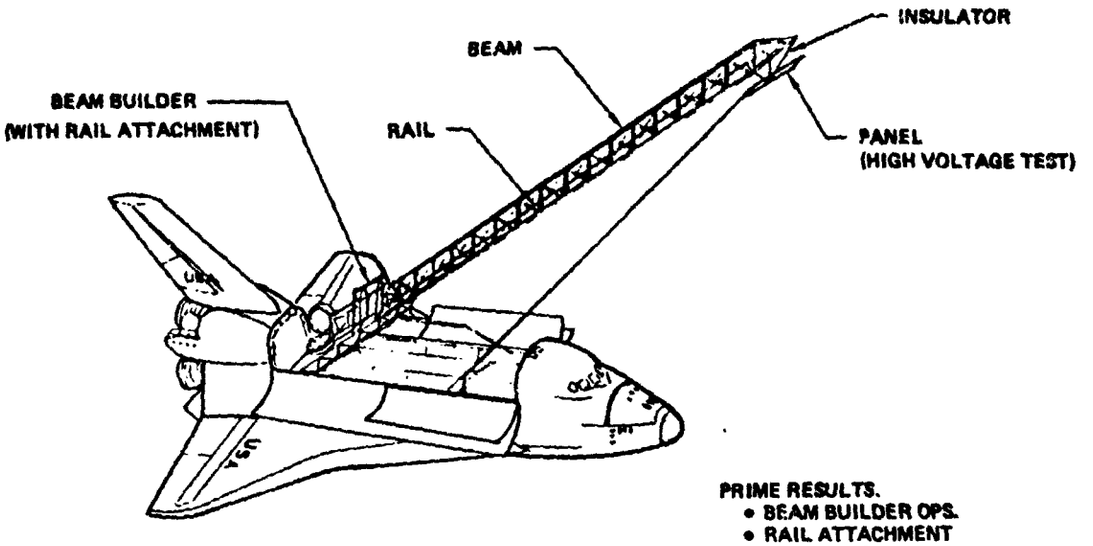

PRIME RESULTS.
- BEAM BUILDER OPS.
- RAIL ATTACHMENT
- TIMELINES

ADDITIONAL RESULTS:
- LARGE OBJECT CHARGING IN EARTH'S MAGNETIC FIELD
- BEAM DYNAMICS
- END FITTING INSTALLATION

Figure 2-12 Beam Builder Sortie

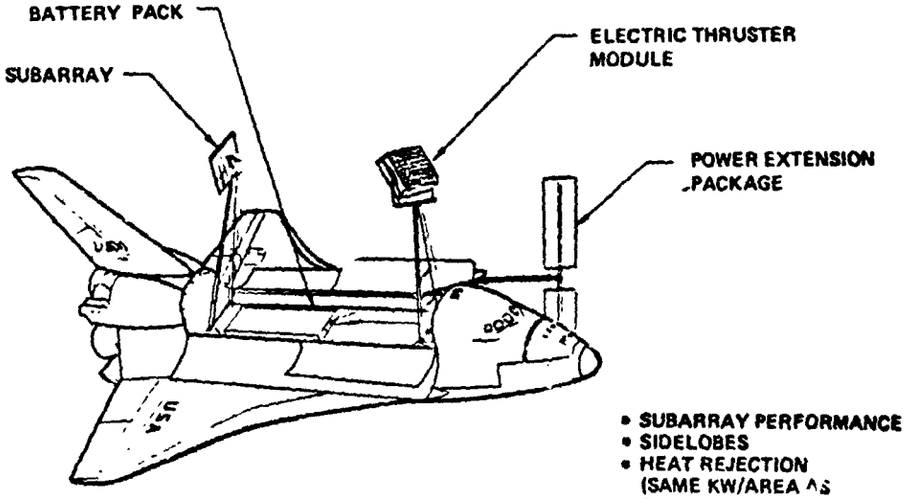

- SUBARRAY PERFORMANCE
- SIDELOBES
- HEAT REJECTION (SAME KW/AREA AS FULL SCALE) –START-UP
- TUBE START-UP PLUME FORM
- FROM THRUSTERS

- (SUBARRAY AND THRUSTER MODULE ARE NOT SIMULTANEOUSLY ERECTED, AS SHOWN)
- ALTERNATIVE APPROACH: POWER WITH OSM.

Figure 2-13 High Power Element Sortie

simultaneously. An alternative to the use of a power extension package and battery pack, as shown, would be the use of an Orbital Service Module.

Another shuttle sortie flight, depicted in Figure 2-14, will test the crane turret and a mobile work station with 1 or 2 crewmen. The work station would be verified by this test flight. That is timelines, manipulator capability, etc. would be investigated.

Figure 2-15 illustrates a potential sequence of developmental efforts ranging from ground test (ground exploratory research program) to a very large commercial demonstrator which would be built before an operational solar power satellite. Also shown are shuttle sortie flights such as those discussed on the previous chart, a large power module (which might not be directly relevant to solar power satellites), a small developmental test article and its construction platform or base, and a proof-of-concept/productivity satellite and its construction base. The commercial demonstrator is sufficiently large to have a ground output of at least 1 megawatt. If all of the elements shown here were to take place prior to a full-size SPS, the date of significant solar power satellite energy availability might be as far off as the year 2020 or 2030. It would therefore be prudent not to construct each of the precursor units shown.

Figure 2-16 is a rough estimate of SPS and SPS development article costs vs. power output. It shows a basic phenomena involved with microwave power transmission: essentially no useful ground power output is obtained until relatively large expenditures have taken place. The commercial demonstrator, which might have 1 to 10 megawatts of ground output, is estimated to require approximately 17 billion dollars for its accomplishment. A 2500 megawatt SPS constructed in space with shuttle derived launch vehicles and minimum facilitization (for contruction of solar cells, etc.) is estimated to cost 43 billion dollars. If a heavy lift launch vehicle is used instead, it saves some money for space transportation but requires that the heavy lift launch vehicle development cost, fleet costs, launch pads costs, etc. be expended, raising the total approximate cost to just over 50 billion dollas. A 10,000 megawatt SPS plus facilitization to produce a similar unit every year (including the heavy lfit launch vehicle) has been estimated at somewhat

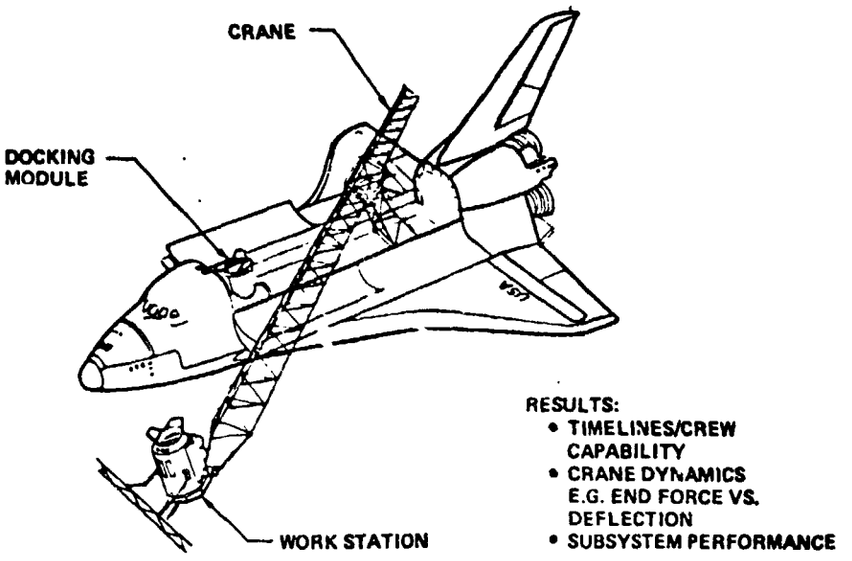

Figure 2-14 Work Station/Crane Sortie

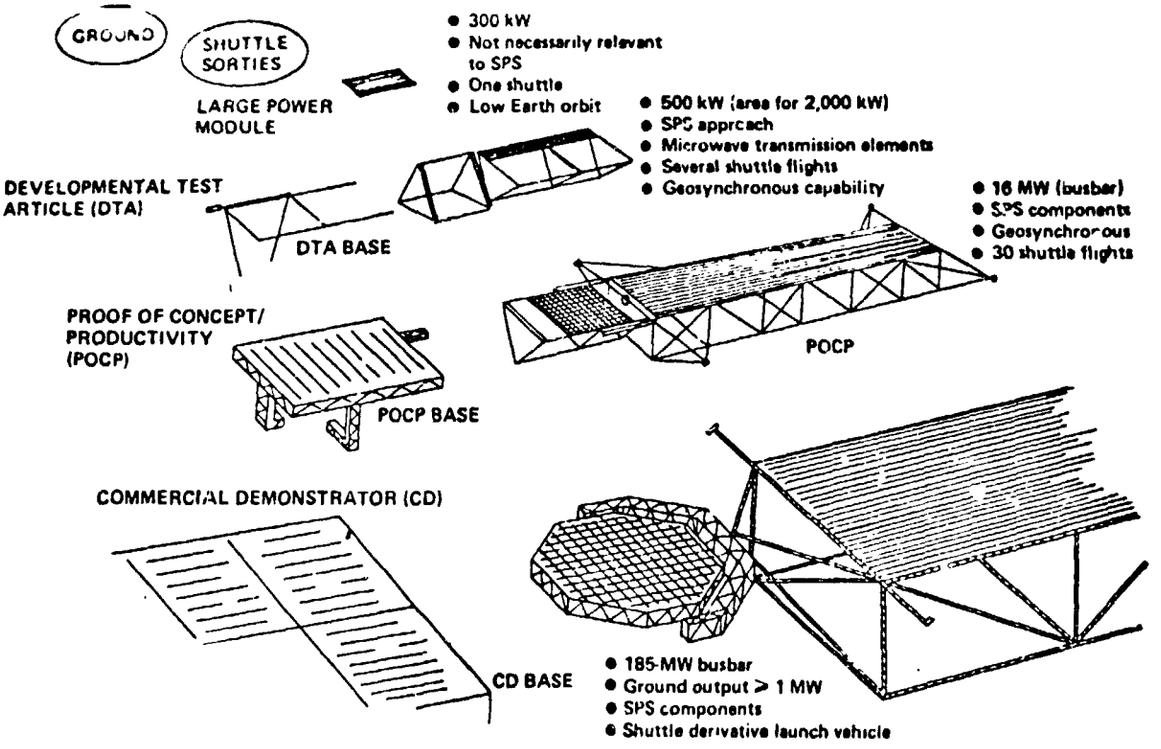

Figure 2 15 Potential SPS Precursory Elements

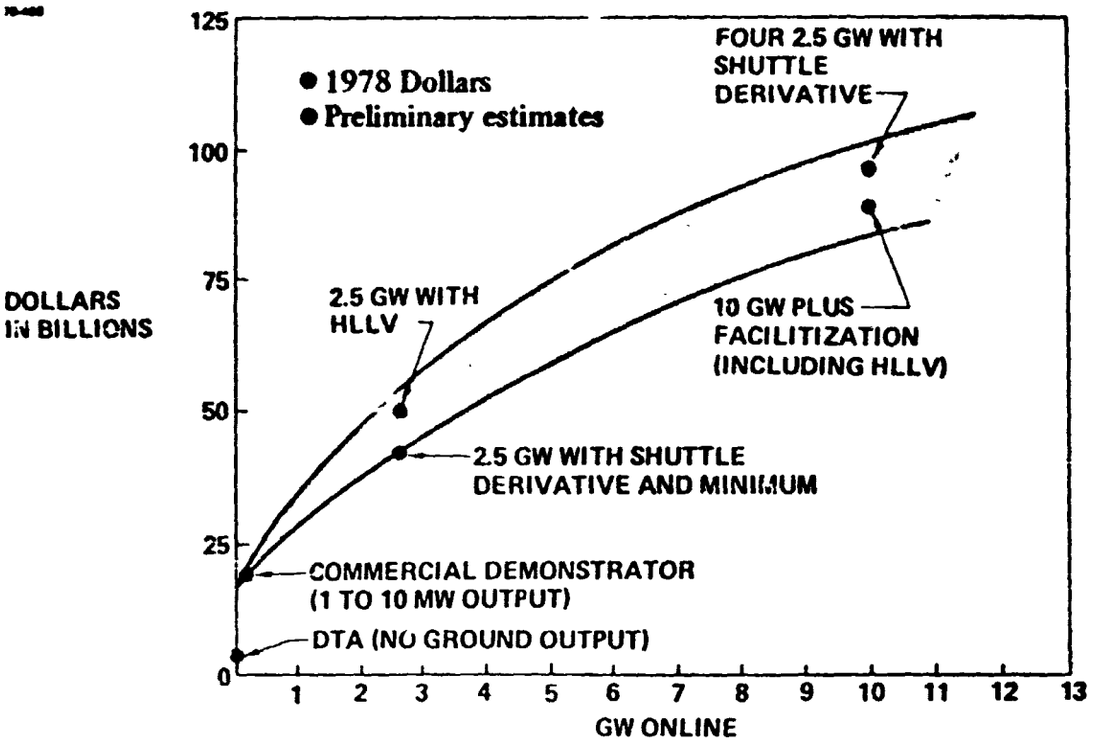

Figure 2-16 SPS Output Versus Investment

over $90B (for 1978 dollars). If four 2500 megawatt units were built with shuttle derivatives, the expenditure would be greater, due to higher transportation cost, even though no costs for the heavy lift launch vehicle are included.

The developmental test article configuration shown in Figure 2-17 incorporates two power collection modules and one power transmission module. This system would be constructed in low Earth orbit on a platform or base and then moved to geosynchronous orbit by means of electric thrusters located at the four corners. During this transfer the transmitter would be rotated on its turntable so as to be in alignment with the two power collection bays. The transmitter incorporates four subarrays (of the type shown in previous charts as being used for ground and shuttle sortie tests) at its corners. Solar blanket area is provided to energize these transmitters and to allow for degradation on the way to geosynchronous orbit. The power busbars and other parts of the full size system concept are also incorporated so as to thoroughly investigate the construction issues shown on the previous chart.

The "commercial demonstrator" system was analyzed in part III of the previous JSC study (Contract NAS9-15196). It is shown in Figure 2-18. The power output level from the microwave transmitter was 185 megawatts. If approximately 10% of the project budget was involved with ground reception (rectenna) about 1 megawatt of useful power would be produced. The system is also sufficiently large to use full size SPS power generation bays, full length solar cell strings, etc.; it can be made, essentially, of full scale SPS components.

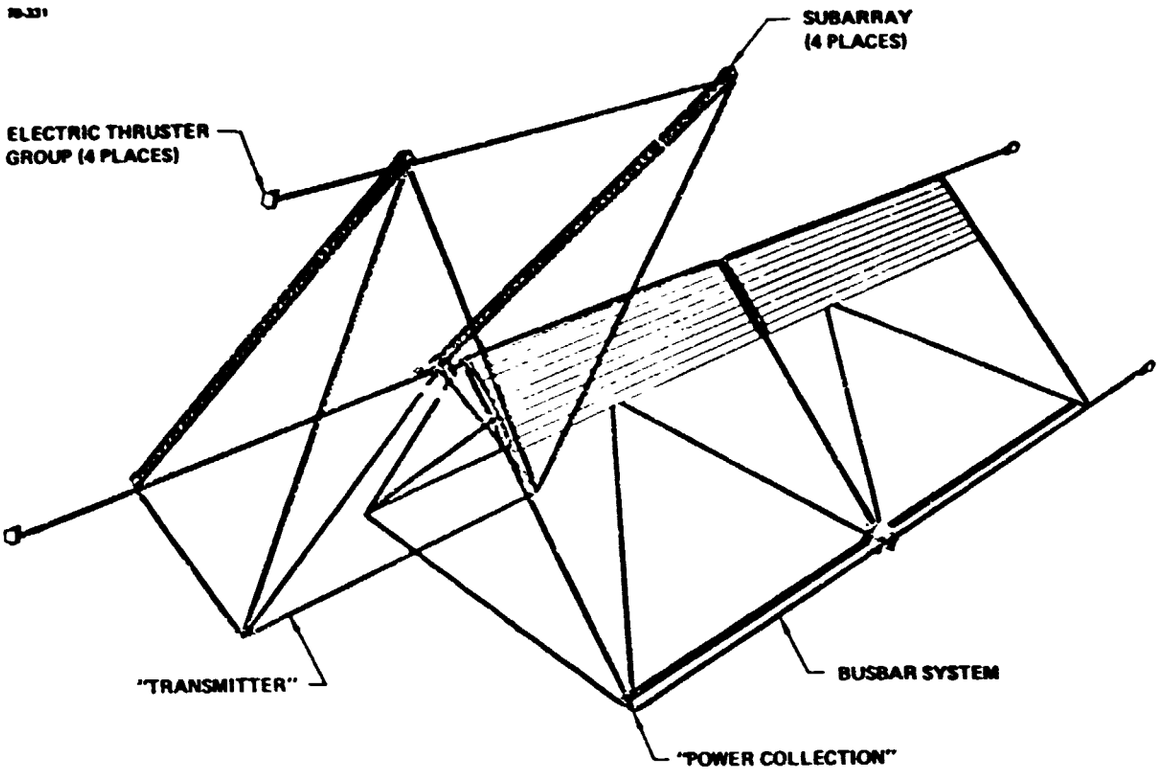

Figure 2-17 DTA General Arrangement

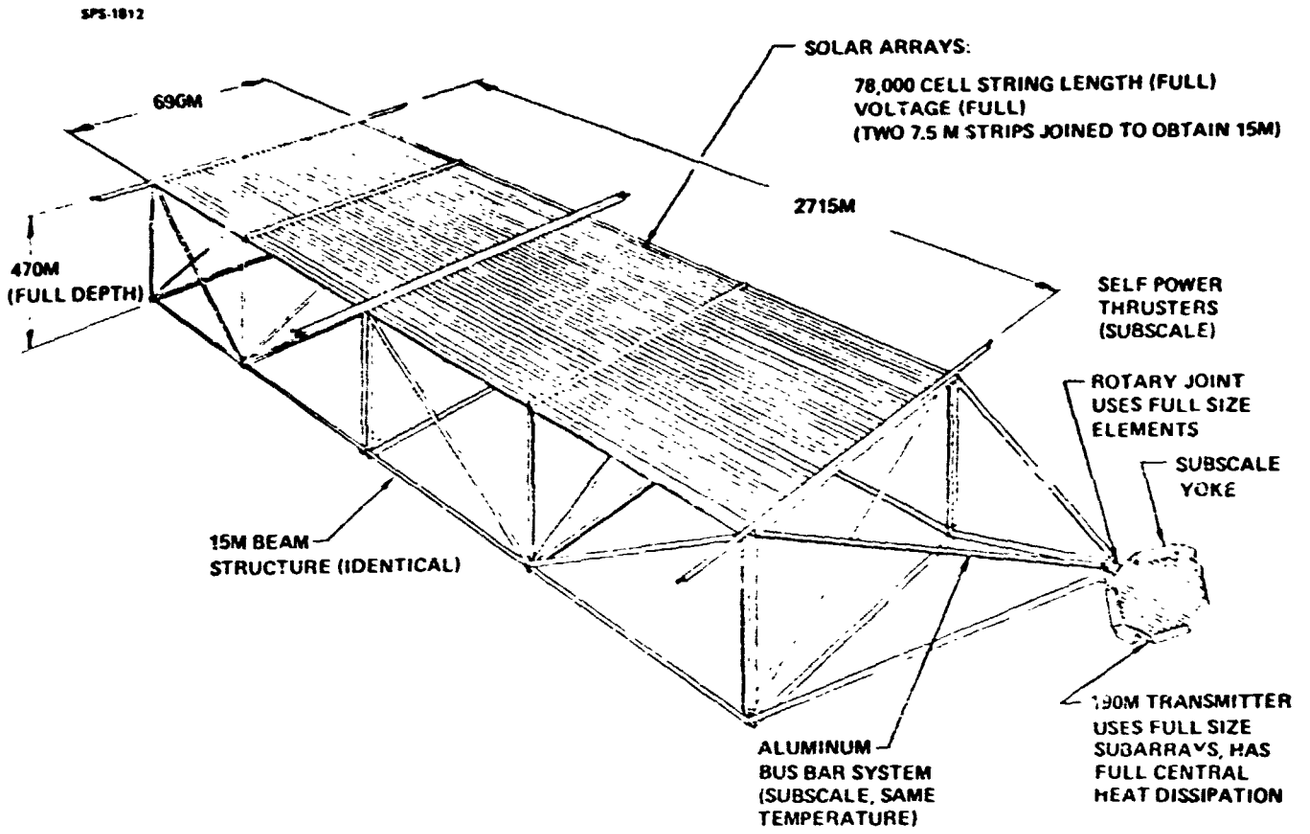

Figure 2-18 Commercial Demonstrator

In summary, the SPS program planning analyses have concluded that:

- A research program should first ascertain the performance that can be obtained from SPS technologies, emerging and alternative technologies as well as those represented in the DOE/NASA baselines. During this period SPS systems studies should provide a suitable evaluation and planning overview. Environmental research should evaluate environmental effects impact potentials, and mitigating strategies for system design that can reduce or eliminate environmental concerns. Process technologies with potential of achieving SPS economic goals should be explored.

- Given a successful conclusion of this program phase, the next program phase should be devoted to engineering developments at the subsystem prototype level, and system cost verification and risk management planning. Examples of the cost-risk activities include (a) Construction and operation of prototype or pilot production lines for hardware with identified cost risks; (b) Updating of space transportation system designs and re-evaluation of transportation costs in light of Shuttle operating experience; (c) Definition of an integrated development plan with the necessary system design, hardware option and schedule flexibility to ensure successful risk management. Successful conclusion of this program phase would result in high confidence in system cost and economics.

- If, at this point, the economics assessment is favorable, SPS development would commence, resulting in an operational prototype. The appropriate size for this prototype has yet to be determined.

- The final phase of the program is commercial production, in which SPS's would be built and installed at a rate appropriate to the demand for new baseload electrical generating capacity.

These program phases can be overlapped to a greater or lesser degree; the amount of overlap must be determined by a tradeoff of risk versus need.

The next phase of the present study, now underway, will include a major task devoted to defining the content, schedule, and cost of the research phase in considerable

detail, with later phases defined in somewhat less detail. Analysis of the development phase will include a cost benefit assessment of the appropriate size for an SPS prorotype.